Study of Solvation Dynamics in Micelles and Interactions of Gemini Surfactants with β-Cyclodextrin and Biomolecules in Aqueous Media

THESIS

Submitted in partial fulfillment of the requirements for the degree of

DOCTOR OF PHILOSOPHY

by

Sunita Kumari
(2013PHXF0016P)

Under the supervision of

Prof. Subit Kumar Saha
Professor, Department of Chemistry
Birla Institute of Technology & Science Pilani, Pilani Campus
Pilani - 333 031 (Rajasthan)

and

Prof. G. Sundar
Senior Professor, Department of Chemistry
Birla Institute of Technology & Science Pilani, Hyderabad Campus
Jawahar Nagar, Hyderabad - 500 078 (Telangana)

BITS Pilani
Pilani | Dubai | Goa | Hyderabad

BIRLA INSTITUTE OF TECHNOLOGY & SCIENCE
PILANI – 333 031 (RAJASTHAN) INDIA

2018

BIRLA INSTITUTE OF TECHNOLOGY & SCIENCE

PILANI – 333 031 (RAJASTHAN) INDIA

CERTIFICATE

This is to certify that the thesis entitled **"Study of Solvation Dynamics in Micelles and Interactions of Gemini Surfactants with *β*-Cyclodextrin and Biomolecules in Aqueous Media"** submitted by **Sunita Kumari**, **ID.No. 2013PHXF0016P** for award of Ph.D. Degree of the Institute embodies original work done by her under our supervision.

Signature in full of the Supervisor _____

Name : **Prof. Subit Kumar Saha**
Designation : Professor, Department of Chemistry
Birla Institute of Technology & Science Pilani, Pilani Campus
Pilani – 333 031 (Rajasthan)

Date : _____

Signature in full of the Co-Supervisor _____

Name : **Prof. G. Sundar**
Designation : Senior Professor, Department of Chemistry
Birla Institute of Technology & Science Pilani, Hyderabad Campus
Jawahar Nagar, Hyderabad – 500 078 (Telangana)

Date : _____

Dedicated to My Parents

Acknowledgements

An endeavor in any field needs spirit, inspiration, guidance and moral support at every step. So, I must preface my thesis by expressing sincere and deep gratitude to those who all made possible for me to complete my research work. I devote all my achievements to "*The Almighty*" for instilling in me strength, perseverance and spirit needed to accomplish my research work.

Exploring deep into the field of research as a Scholar in the Department of Chemistry, BITS, was in fact, a glorious as well as challenging experience to investigate and accumulate some comprehension and conception in Chemistry. In all these years, the role of many accomplished people in and out of the laboratory was directly or indirectly influential, decisive and supportive in powering up my academic career over and above social career. Here is an opportunity to honor and shell out my tributes and hearty complements to all these personalities whose precious support made it possible for me to blossom in my work of philosophy.

First and foremost, I feel the honor to express my profound thanks to my supervisor *Prof. Subit Kumar Saha*, Professor, Department of Chemistry, BITS Pilani, Pilani campus, who gave me the essence of the scientific approach. It was his encouragement and valuable advice that provided me with the confidence, which has been the pivot for my progress in these studies. I have been extremely lucky to have a supervisor who cared so much about my work, and who responded to my questions and queries so promptly. I express my thanks to *Prof. S. K. Saha* for his friendly approach in discussion and valuable help for my research work.

I owe my special sincere thanks to my co-supervisor *Prof. G. Sundar*, Senior Professor, Director, BITS Pilani, Hyderabad campus, for his valuable suggestions, support, and encouragement that he has showered upon me during my research work. I am very appreciative of the time and effort that he devoted in guiding me with his profound knowledge of subjects ranging from research to career direction.

I express my sincere gratitude to *Prof. S. C. Sivasubramanian* and *Prof. Inamur R. Laskar*, for serving as my Doctoral Advisory Committee (DAC) members and giving constructive feedback and comments to shape my research work. I am also thankful to the members of the Doctoral research committee (DRC) for their comments which immensely aided me to improve the quality of this thesis. I am extremely grateful to Head Department of Chemistry, *Prof. Saumi Ray* and all faculty members of Department of Chemistry, BITS

Pilani, for their priceless suggestions, constant inspiration, excellent teaching and enthusiastic cooperation throughout my doctoral study.

. I am immensely thankful to the Vice-Chancellor, Director and Deans of Birla Institute of Technology & Science (BITS), Pilani for granting me the opportunity to pursue my doctoral studies by providing necessary facilities and financial assistance.

I express my gratitude to *Prof. Srinivas Krishnaswamy*, Dean, Academic-Graduate Studies & Research (AGSR) Division, BITS Pilani, Goa Campus, and *Prof. Jitendra Panwar*, Associate Dean, Academic-Graduate Studies & Research (AGSR) Division, BITS Pilani, Pilani Campus and office staff of AGSR Division, whose secretarial assistance helped me in submitting the various evaluation documents in time. I thank *Prof. Inamur R. Laskar*, Convenor, Departmental Research Committee (DRC), Department of Chemistry, BITS Pilani, Pilani Campus for his official support and encouragement and members of DRC, Department of Chemistry, BITS Pilani, Pilani Campus for their cooperation and constant guidance during each of the past few years.

I wish to convey my thanks to Heads of Department of Pharmacy, Physics, Biology, Chemical Engineering during my tenure for providing necessary laboratory facilities for the accomplishment of this work. I am also thankful to the librarian, *Mr. Giridhar Kunkur* and other technical and non-teaching members for their co-operative and healthy attitude and valuable assistance.

I heartily express my thankfulness to the AIRF, JNU, New Delhi for helping me with the instrument facility to support my doctoral research.

Every effort is motivated by ambition; all ambitions have inspiration behind them. So I bestow my unbound gratitude and a deep sense of respect for my Papa, *Mr. Chiman Lal* and Mummy, *Mrs. Badami Devi* for their affection, encouragement and emotional support. I feel my life short to count their struggles to make me reach up to this level. I am also eternally grateful to my Chacha, *Mr. Maru Ram*, and Mosi, *Mrs. Sumitra Devi*, for their myriad of support, they are only for me after my parents in my life, who deserve this respect. I feel short of words in expressing my wholehearted appreciation to my Brothers and Sisters, *Dr. Surendra Singh, Mr. Vijendra Poonia, Mr. Balvir Singh, Manju Poonia, Dr. Omveer Singh* and *Anita* for standing beside me through thick and thin of my life, especially, *Dr. Surendra Singh*, my brother, he always stands between me and my life's

hurdles. I extend my wholehearted appreciation to *Dr. Santosh Kasnia*, *Mrs. Sarita* and *Mrs. Usha* and rest family members for their love, support, care and understanding.

Special thanks to God to blossom my life with kids, *Manav Poonia, Parithika Poonia, Pareen Sheoran*, and *Ivan Poonia*, their cute innocent faces, talks, and smiles which give me hundreds of refreshment booster.

I am thankful to my seniors *Dr. M. Sowmiya, Dr. Amit Kumar Tiwari*, and *Dr. Sonu* and my juniors, *Mr. Sayantan Halder* and *Ms. Rishika Aggrawal* who always supported me, whenever I am in need of any help along with all research scholars of the Department of Chemistry, BITS Pilani.

With all zeal and cheers, I express my thankfulness to my friends *Dr. Pragati Fageria, Mrs. Rajinder Kaswan, Ms. Saroj*, and *Ms. Mamta Devi Sharma*. They are always with me in all vicissitudes of my research as well as in personal life. Apart from these, I am also thankful to all Ph.D. colleagues for helping, supporting, inspiring and encouraging me during the research work.

My thanks are duly acknowledged to UGC-BSR, New Delhi and BITS Pilani for their valuable financial support during my research tenure.

Last but not the least I would love to extend warm thanks to everyone who is related to me either in a direct or indirect way.

Finally, I would like to conclude acknowledgement with the special quote:

"The starting point of all achievement is desire"

– Napoleon Hill (Founder of the science of success)

Date: / / 2019

Place: BITS, Pilani *Sunita Kumari*

Table of Contents

Abstract

The thesis entitled "**Study of Solvation Dynamics in Micelles and Interactions of Gemini Surfactants with *β*-Cyclodextrin and Biomolecules in Aqueous Media**" deals with several spectroscopic tools such as UV-visible absorption, steady-state and time-resolved fluorescence and circular dichroism (CD) and dynamic light scattering (DLS), ^{1}H NMR and field emitting scanning electron microscopy (FESEM) to explore various aspects of the thesis work. Present thesis demonstrates the solvation dynamics and rotational relaxation of Coumarin 480 (C-480) in the different aqueous micellar systems and micelles in presence of urea. It also illustrates the interactions of cationic gemini surfactants with bovine serum albumin (BSA) to unfold the BSA and further refolding of unfolded BSA using cationic surfactant stripping agents *β*-cyclodextrin (*β*-CD) and anionic surfactant, sodium dodecyl sulfate (SDS). The binding interactions of gemini surfactants with nanotubes of *β*-CD induced by guest molecule, Coumarin 485 (C-485) and binding of guest molecule with Calf thymus DNA (ctDNA) after being released from the nanotubes of the *β*-CD have also been explored.

The effect of an organic counterion, *p*-toluenesulphonate (*p*-TS^-) and a Hofmeister series of inorganic counterions, NO_3^-, Br^- and SO_4^{2-} on the solvation dynamics and rotational relaxation of C-480 in the Stern layer of aqueous micelles of hexadecyltrimethylammonium surfactants ($C_{16}TAX$) has been studied. The rate of solvation increases in the order $C_{16}TABr < C_{16}TANO_3 < (C_{16}TA)_2SO_4 < C_{16}TA$*p*-TS. Effectively, the solvation process is controlled by the extent of release of water molecules during the formation of micelles which depends on the nature of counterion. Counterions indirectly contribute to the slow solvation by the formation of clusters of water molecules. The decreasing order of the average rotational relaxation time of C-480 in the micelles of surfactants is $C_{16}TA$*p*-TS >> $C_{16}TABr > C_{16}TANO_3 > (C_{16}TA)_2SO_4$, which is the same as the decreasing order of microviscosity of micelles.

Solvation dynamics and rotational relaxation of C-480 in aqueous micelles of cationic gemini surfactants with diethyl ether (EE) spacer group (*m*–EE–*m*) and tails with varying tail lengths (*m* = 12, 14 and 16) have been studied. Effects of hydrocarbon tail length and hydrophilicity of spacer group on solvation dynamics and rotational relaxation processes at inner side of the Stern layer of micelles have been studied. With increasing hydrophobicity of tails of surfactants water molecules in Stern layer become progressively more rigid resulting in decrease in the rate of solvation process with slow solvation as a

major component. With increasing hydrophilicity of the spacer group of gemini surfactant the extent of free water molecules is decreased thereby making the duration of solvation process longer. Rotational relaxation time increases with increasing tail length of surfactant as a result of increasing microviscosity of micelles. With increasing hydrophilicity of the spacer group the anisotropy decay becomes slower due to the formation of more compact micelles.

The effect of urea on solvation dynamic and the rotational relaxation of C-480 in the Stern layer of aqueous micelles of cationic gemini surfactants, 12-4(OH)$_n$-12 (n = 0, 1, 2) has been explored. The formation of micelles becomes disfavored in presence of urea at high concentration. Solvation dynamics is bimodal in nature. Average solvation time increases, reaches a maximum and then decreases with increasing concentration of urea because the degree of counterion dissociation also follows the same order with the addition of urea in the micellar solution. With increased degree of counterion dissociation the extent of clustering of water molecules is increased resulting in slower solvation process. The –OH group present in the spacer group of gemini surfactant controls the rate of solvation. The microviscosity of micelles is decreased with increasing concentration of urea as a result of it rotational relaxation process becomes faster. In presence of –OH group in the spacer group the microviscosity of micelles is enhanced resulting in longer rotational relaxation time.

The interactions between protein, bovine serum albumin (BSA) and cationic gemini surfactants, 12-n-12 with varying number of –CH_2- group (n = 3, 6, 8, 12) in the spacer has been demonstrated. At low concentration range of surfactants, the decrease in secondary structure (α-helix) of the protein is more with decreasing chain length of the spacer group due to the interaction of larger-sized pre-micellar aggregates with the protein. However, the unusual decrease in α-helix found in case of 12-12-12 is because of the greater extent of hydrophobic interactions between its long spacer chain and the protein. Present study also demonstrates the step-by-step refolding of protein present in the form of protein-gemini surfactant complex using β-CD)/SDS as stripping agents. This method is in contrast to the refolding of protein via artificial chaperone protocol. The mechanisms of interactions between β-CD/SDS and protein-gemini complex have been described. It has been observed that a gemini surfactant molecule with a long flexible spacer chain can more easily be stripped off by β-CD molecules forming simple inclusion complexes or

nanotubes/rods depending on the concentration of *β*-CD. Gemini surfactant induced unfolded proteins are also refolded by SDS molecules through the formation of catanion (mixed micelles, vesicles etc.).

The formation of guest molecule (C-485) induced nanotubes by *β*-cyclodextrin (*β*-CD) and their interactions with cationic gemini surfactants (12-*n*-12, where *n* = 3, 6, and 12) have been explored. *β*-CD at high concentrations forms extended nanotubes and secondary aggregates of nanotubes. A gemini surfactant has a role on binding between C-485 and nanotubes of *β*-CD. At a low concentration range, surfactant molecules are co-associated with the guest molecules, C-485, however at high concentrations they are capable of pushing C-485 out of the nanotubular cavities. A gemini molecule with a comparatively longer spacer chain is more efficient in removing the guest molecules out of the nanotubular cavities. Also, rate of release of guest molecules increases with increasing concentration of surfactants. Guest molecules after coming out of the nanotubular cavities, get solubilized in the micelles formed by surfactant molecules in the solution.

The binding interactions of C-485 with ctDNA have been described by means of UV-visible absorption and fluorescence studies. Ethidium bromide displacement assay and iodide ion quenching experiment confirm that C-485 binds with ctDNA through the groove binding mode. The binding of C-485 with *β*-CD is reduced in presence of ctDNA. *β*-CD molecules in presence of C-485 form the nanotubes and secondary aggregates of nanotubes, which has been explored as the carrier for C-485. Gemini surfactants, *m*-4-*m* induced the release of C-485 from the cavity of nanotubes of the *β*-CD. After being released from the cavity, C-485 molecules interact with ctDNA at the low concentration of the gemini surfactants. The releasing efficiency of gemini surfactants increases in the order as 12-4-12 < 14-4-14 < 16-4-16, which is according to the increasing order of hydrophobicity of their tails.

List of Figures

List of Figures

List of Figures

List of Figures

List of Figures

List of Figures

List of Figures

List of Figures

List of Figures

List of Figures

List of Figures

List of Schemes

Chapter 6

List of Tables

List of Tables

List of Tables

List of Tables

List of Tables

List of Tables

List of Symbols and Abbreviations

Symbol	Abbreviation
DO	1,4-dioxane
DPH	1,6-diphenyl-1,3,5-hexatriene
4-AP	4-aminopthalimide
$\lambda^{abs}{}_{max}$	Absorption peak maximum
A	Adenine
ADC	Analog-to-digital converter
Å	Angstrom
K	Association constant
$<\tau_f>$	Average fluorescence lifetime
$<\tau_r>$	Average rotational relaxation time
$\langle \tau_s \rangle$	Average solvation time
BSA	Bovine serum albumin
ctDNA	Calf thymus deoxyribonucleic acid
CPC	Cetylpyridinium chloride
CTAB	Cetyltrimethylammonium bromide
CT	Charge Transfer
θ_o	Cone angle
C-153	Coumarin 153
C-311	Coumarin 311
C-480	Coumarin 480
C-485	Coumarin 485
C-490	Coumarin 490
C-522	Coumarin 522
Cmc	Critical micellar concentration
C	Cytosine
DSE	Debye–Stokes–Einstein
DAS	Decay analysis software

List of Symbols and Abbreviations

Symbol	Abbreviation
α	Degree of counterion dissociation
DMSO	Dimethyl sulfoxide
DMABN	Dimethylaminobenzonitrile
DTAB	Dodecyltrimethylammonium bromide
DLS	Dynamic light scattering
λ_{em}	Emission wavelength
$E_T(30)$	Empirical solvent polarity parameter
EB	Ethidium bromide
λ_{ex}	Excitation wavelength
μ_e	Excited state dipole moment
τ_f	Excited state fluorescence lifetime
$\mathcal{E}^{fl}_{max}$	Fluorescence energy peak maxima
r	Fluorescence anisotropy
$I(t)$	Fluorescence intensity decay
F_o/F	Fluorescence intensity ratio
λ_{max}^{flu}	fluorescence peak maxima
ϕ_f	Fluorescence quantum yields
FT-IR	Fourier transform infrared spectroscopy
FCE state	Frank-Condon excited state
FCG state	Frank-Condon ground state
μg	Ground state dipole moment
G	Guanine
IC	Internal conversion
τ_e	Internal motion of the probe
ISC	Intersystem crossing
ICT	Intramolecular charge transfer
τ_D	Lateral diffusion of the fluorophores
r_o	limitting anisotropy

List of Symbols and Abbreviations

Symbol	Abbreviation
η_m	Microviscosity
K^{mic}	Mole fraction partition coefficient
k_{nr}	Non-radiative rate constant
NMR	Nuclear magnetic resonance
ORD	Optical rotatory dispersion
$\|S\|$	Order parameter
Phe	Phenylalanine
PMT	Photomultiplier tube
PICT	Planar Intramolecular Charge Transfer
PCM	Polarized continuum model
Brij 58	Polyoxyethylene-(20)-cetyl-ether
Brij 35	Polyoxyethylene-(23)-lauryl-ether
Tween 80	Polyoxyethylene-sorbitan monooleate
a	Pre-exponential factor
Kq	Quenching constant
k_r	Radiative rate constant
R	Regression Coefficient
RICT	Rehybridization by Intramolecular Charge Transfer
RMs	Reverse micelles
τ_R	Rotational correlation times
τ_m	Rotational motion of the micelle
SDS	Sodium dodecyl sulfate
AOT	Sodium salt of dioctyl sulfosuccinic acid
$C(t)$	Solvent correlation function
κ	Specific conductivity
$\Delta G^{o,\,mic}$	Standard molar Gibbs free energy of micellization
K_{SV}	Stern-Volmer quenching constant
TTAB	Tetradecyltrimethylammonium bromide

List of Symbols and Abbreviations

Symbol	Abbreviation
THF	Tetrahydrofuran
T	Thymine
TDDFT	Time dependent density functional theory
TCSPC	Time-correlated single photon counting
TRES	Time-resolved emission spectra
r(t)	Time-resolved fluorescence anisotropy
TAC	Time-to-amplitude converter
TX-100	t-Octylphenoxypolyethoxyethanol
DMASBT	Trans-2-[4-(dimethylamino)styryl]benzothiazole
Trp	Tryptophan
TICT	Twisted intramolecular charge transfer
Tyr	Tyrosine
D_w	Wobbling diffusion coefficient
τ_w	Wobbling motion time
α-CD	α-Cyclcodextrin
β-CD	β-Cyclcodextrin
γ-CD	γ-Cyclcodextrin

Chapter 1

Introduction

Key Concepts:

- *This chapter covers the generalized introduction of surfactants, cyclodextrin, protein and deoxyribonucleic acid (DNA), which are different aspects of the thesis work.*

- *The chapter highlights the different fluorescence spectroscopic tools, which were essential to carry out the thesis work.*

- *The zeal to the thesis work has been offered in the chapter.*

Chapter 1

Introduction

1.1 Fluorescence spectroscopy: An overview

Principles and applications of fluorescence spectroscopy deliver essential information to the users in order to assist them to perceive and use the technique positively in various applications. Fluorescence is a spectrochemical technique used for analysis, in which the molecules of interest are excited by a specific short wavelength and emit radiation of a longer wavelength. The fluorescence spectrum offers details of both qualitative and quantitative analysis. Fluorescence is widely accepted and is an imperative investigational technique in countless applications in the areas of environmental, industrial, forensics, medical diagnostics, DNA sequencing, genetic analysis, and biotechnology, due to its exceptionally great sensitivity, high selectivity, simplicity, and low cost as compared to other analytical techniques. In the present scenario, this technique is highly used for chemical, biochemical, pharmaceutical, and medical research, providing detailed information about the real-time observation of the structure and dynamics of intact biological systems and dynamics of molecules in complex self-assembled amphiphilic systems with an extremely high resolution. Steady-state and time-resolved fluorescence methods are frequently cast off to characterize emissive belongings of fluorophores. Time-resolved fluorescence measurements are superior to steady-state fluorescence measurements as it provides the information regarding the changes in the molecular surroundings of the fluorophore because of the competing or perturbing kinetic processes such as collisional quenching, energy transfer, solvent relaxation, and rotational reorientation, which disturb the fluorescence. These processes are very fast as compared to the fluorescence (10^{-9} s). Therefore, time-resolved fluorescence spectroscopy can be applied to quantify these processes and gain insight into the chemical surroundings of the fluorophore. This thesis explores different microheterogeneous systems and process, which can be positively studied by means of fluorescence spectroscopy, in precise: steady-state fluorescence and fluorescence anisotropy, excited state fluorescence lifetime, time-resolved fluorescence anisotropy, and solvation dynamics.

1.2 Surfactants

Surfactants, surface-active agents, are decent soaking agents. They reduce the surface tension or interfacial tension of polar and non-polar liquids at their surface and therefore lay at the heart of interfacial chemistry. Surfactant molecules belong to the

colloid and interface science. The term 'colloid' is signified as glue-like materials appearing in one phase system under the microscope. The boundary between the two phases is designated as an interface. Most of the surfactants have a long hydrocarbon tail that can be linear/branched and interacts very weakly with the water molecules in an aqueous media. The hydrophilic head is a rather small polar or ionic group that interacts strongly with water through ion-dipole or dipole-dipole interactions. Hence, a surfactant is said to have a split personality, as it is composed of two parts with entirely different characteristics. Surfactants are denoted as amphiphiles too, due to the presence of both hydrophobic and hydrophilic parts in its structure.

In general, the surfactants are organic molecules, which have polar hydrophilic headgroup and a non-polar hydrophobic tail. Polar headgroup helps to interact with the aqueous/polar solvent and the hydrophobic tails with the non-aqueous/non-polar solvents. The basic properties of surfactants depend on its structural features. The headgroups can be ionic (cationic and anionic) or non-ionic type and hydrophobic tails can consist of hydrocarbon, fluorocarbon, or siloxane. The basic structural sketches of different types of surfactants are shown in Figure 1.1. Surfactants have the tendency to be absorbed at the surface and interface (the boundary between any two immiscible phases, *i.e.* gas, liquid and solid). A very little amount of surfactant molecules reduces the surface tension of water at the water-air interface up to a noticeable level.

The surfactants have entropy driven self-assembling tendency in the aqueous or aqueous-organic mixed medium and they try to reduce the contact of hydrophobic tails with the aqueous phase. This is the way by which surfactant molecule reduces the surface tension (the energy required to create the interface per unit area). The aggregation properties of surfactants and physicochemical properties of solution can be tuned by tuning the structural features of surfactant. The self-assemblies of surfactants can either be called micelles or reverse micelles depending on the polarity of the medium. Self-assembled molecular systems of surfactants have received intense attention among the scientific society. These self-assembled microstructures of surfactants can be micelles, reverse micelles, vesicles etc., which have many similarities with the biological membrane. Hence, the physicochemical properties of surfactants systems mimics the properties of biological membrane.

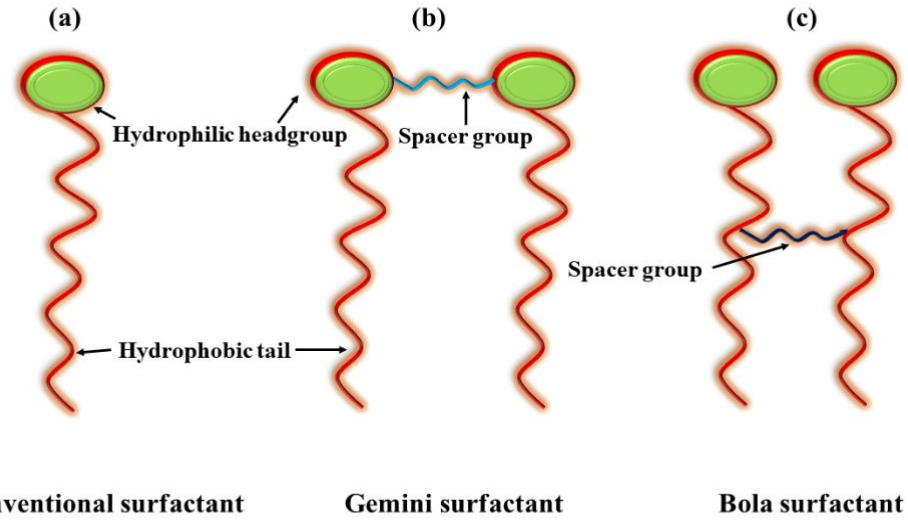

Figure 1.1. Schematic representation of (a) Conventional surfactant, (b) Gemini surfactant, and (c) Bola surfactant.

1.2.1 Applications of the surfactants

Surfactants are the most versatile chemicals, being key components in a diverse range of products and technologies. Surfactants are extensively used in our day-to-day lives in countless ways and are existing essentially in the areas like food, water, drinks, household and personal care products, foams, agriculture, pesticides, pharmaceuticals, oil recovery, and particle synthesis etc.[1-7] In addition to these applications, surfactants possess bacteriostatic and bactericidal properties, and thus, they can be used as antimicrobial agents in biocatalysis and bioprocessing.[8]

The widespread use of surfactants in various fields makes it an important research material for further modification and safer use. Surfactant assemblies for instance micelles, reverse micelles, vesicles etc. are vastly used in different biological aspects because of their extraordinary ability to solubilize the membrane proteins. They are tremendously important in simulating the complex environmental conditions present in larger bioaggregates such as biological membranes. Thus, these systems are mimicking the physicochemical properties of biological systems. Several times newly developed active pharmaceutical drugs are facing water solubility problem that can be vanquished by surfactants. Many efforts to increase the solubility of drugs using a suitable carrier for enclosing hydrophobic drugs, like inclusion complexes with cyclodextrins, microemulsions, and liposome formulations have been well developed. However, all these systems have some drawbacks.[9, 10] Therefore, nowadays numerous articles appear on the

surfactant chemistry. Modern research is based on the new application of these surfactants in various fields such as biotechnology, analogous processes in biological membranes, a drug carrier, solubilization of drugs, and gene therapy.[11-13]

1.2.2 Types (classes) of surfactants

Surfactants are sorted into four categories based on the nature and the type of the surface-active moiety that exists in the molecule, which are given below:

1. Anionic surfactants
2. Cationic surfactants
3. Nonionic surfactants
4. Zwitterionic/Amphoteric surfactants

1.2.2.1 Anionic surfactants

The headgroup of anionic surfactants is negatively charged. Anionic surfactants are comparatively less expensive and are used extremely in a wide variety of applications. The most commonly used anionic surfactants contain sulfates, sulfonates, carboxylates, or phosphates moiety as hydrophilic anionic headgroup and sodium, potassium, ammonium, calcium and various protonated alkyl amines as a counterpart.[14] Mostly, anionic surfactants are effective in cleaning oily soil and oil/clay soil suspension. Anionic surfactants are also used to remove the hardness of water, especially, the positively charged ions such as calcium and magnesium. Examples of anionic surfactants are: sodium stearate [$CH_3(CH_2)_{16}COO^-Na^+$], sodium dodecyl sulfate [$CH_3(CH_2)_{11}SO_4^-Na^+$], sodium dodecyl benzene sulphonate [$CH_3(CH_2)_{10}\ CH_2C_6H_4SO_3^-Na^+$].

1.2.2.2 Cationic surfactants

The headgroup of cationic surfactants is positively charged. The most frequently used cationic surfactants contain amine or ammonium groups but some other sulfonium, phosphonium, and sulfoxonium moieties also act as hydrophilic cationic headgroup and Cl^-, Br^- as counterions. Cationic surfactants reduce the surface tension and are active wetting agents in the acidic medium. However, these surfactants do not have detergent property in the alkaline medium due to the formation of quaternary ammonium salts.[15] Examples of cationic surfactants are: cetyltrimethyl ammonium bromide (CTAB)

$[C_{16}H_{33}N^{+}(CH_3)_3Br^{-}]$, cetylpyridinium chloride (CPC) $[C_6H_5N^{+}C_{16}H_{33}Cl^{-}]$, tetradecyltrimethylammonium bromide (TTAB) $[CH_3(CH_2)_{13}N^{+}(CH_3)_3Br^{-}]$, taurylamine hydrochloride $[CH_3(CH_2)_{11}NH_3^{+}Cl^{-}]$.

1.2.2.3 Nonionic surfactants

The headgroup of non-ionic surfactants does not carry any electrical charge, which makes them resistant to deactivation of water hardness. They are lesser irritant than the anionic or cationic surfactants. Non-ionic surfactants generally have ethylene oxide chains or hydroxyl groups as a polar center and are less reactive compared to the ionic ones. The most common hydrophilic part consists of the polyoxyethylene, polyoxypropylene or polyol derivatives. The hydrophobic part is made up of saturated or unsaturated fatty acids or fatty alcohols. These surfactants can be classified as polyol esters, polyoxyethylene esters poloxamers. Normally used non-ionic surfactants are ethers of fatty alcohols.[16] Examples of the non-ionic surfactants are: Triton X-100, Brijs, Tweens, PEGs [Polyoxyethylene (4) dodecanol ($CH_3(CH_2)_{11}$-O-$(CH_2$-$CH_2O)_4H$).

1.2.2.4 Zwitterionic/Amphoteric surfactants

Amphoteric surfactants have both positive (cationic) and negative (anionic) charges on the same molecule. Since the zwitterionic surfactants contain both cationic and anionic parts, so its ionic behavior depends on the pH of the solvent. These surfactants are good in household cleaning and personal care products because of the excellent dermatological properties of the surfactants. The cationic part can be primary, secondary, or tertiary amines or quaternary ammonium cations and the anionic part can include variables such as sulfonates, as in CHAPS 3-[(3-Cholamidopropyl)dimethylammonio]-1-propanesulfonate). Some common zwitterionic surfactants are N-alkyl and C-alkyl betains and sultains as well as phosphatidyl amino alcohols and acids. Examples of the zwitterionic surfactants are: Dodecyl betaine $C_{12}H_{25}N^{+}(CH_3)_2CH_2COO^{-}$, Dodecyldimethylammonium acetate $CH_3(CH_2)_{11}(CH_3)_2N^{+}CH_2COO^{-}$, 3-(dimethyldodecylamino)-propane-1-sulphonate $[CH_3(CH_2)_{11}N^{+}(CH_3)_2CH_2CH_2CH_2SO_3^{-}]$.

Two monomer units of surfactants connected by a spacer group comprise a special type of surfactant depending on their connection position, which can be divided into two types: first, the spacer groups connected at their headgroups, are called gemini surfactant [17] (Figure 1.1), and the spacer groups connected at their hydrophobic tails, are called bola

surfactants.[18] (Figure 1.1). The nature of the spacer group of surfactants can be varied. The present research work has been carried out with gemini surfactants, hence the details of the gemini surfactants are given below:

1.2.3 Gemini surfactants

The word "gemini" signifies twins and the gemini or dimeric surfactant is an amphiphilic molecule containing two hydrophobic tails united by a spacer group at their hydrophilic headgroups. A schematic representation of a gemini surfactant is given in Figure 1.1. Gemini surfactants have three structural parts namely, hydrophilic headgroup, hydrophobic tails, and the spacer group. The hydrophobic tail can be short or long and the spacer group of gemini surfactants can be rigid, flexible, hydrophilic or hydrophobic in nature.[19, 20] The polar headgroups can be cationic, non-ionic, anionic, or zwitterionic. Properties of gemini surfactants depend on its various parts.[21-24] Hence, properties of gemini surfactants are advanced as compared to their conventional surfactants.[19] Gemini surfactants were first identified by Bunton *et al*.[25] and named as bis-surfactants in 1991 by Menger and Littau.[17] In 1971, Bunton *et al*.[25] have first studied the catalytic role of gemini surfactants in the nucleophilic substitutions reactions. Bis-quaternary ammonium gemini surfactants with a variation in its structures are synthesized by the Devinsky *et al*.[4] Similarly, Okahara *et al*.[26, 27] have synthesized anionic gemini surfactants with different variation in its structures. Many kinds of gemini surfactants have been synthesized and explored which contain anionic, cationic, zwitterionic, and non-ionic gemini surfactants with different kinds of spacer groups and a variety of structural types: alkylglucoside-based,[28] arginine-based,[29] glucamide-based,[30] sugar-based,[31] with unsaturated linkages,[32] hydrolysable,[33] and with nonidentical headgroups.[34]

The revolutionary and passionate exploration of the gemini surfactants are mainly done by research groups of Zana,[35, 36] Menger,[37, 38] Rosen,[39, 40] Okahara,[26, 27] Oda,[41, 42] Engberts,[43] and others. Mostly, the explored gemini surfactants are the *m*-*s*-*m* type with quaternary ammonium headgroups, where, *s* and *m* symbolize the number of carbon atoms of the spacer group and the hydrophobic tail, respectively.[44, 45] Gemini surfactants have attracted the attention of academic researchers and field experts because of their unique properties such as low critical micelle concentration, better wetting ability, low Kraft temperature, good water solubility, unusual micelle structures and aggregation behavior, high efficiency in reducing oil/water interfacial tension, and interesting rheological

properties.[46-50] Some gemini surfactants have strong electrostatic interactions with a charged surface, especially with the lipid membrane, thus, surfactants show a toxic effect on the aquatic lives by the hemolytic activity. Gemini surfactants are adsorbed quickly at cellular membranes of microorganisms and provide high antimicrobial activity.[51] Gemini surfactants have been used in potential drug delivery system,[52] synthetic vectors for gene transfection,[13] drug and vitamin solublization,[53] antibacterial and antifungal formulations,[54] personal care products[55] etc. Interactions of gemini surfactants with conventional surfactants,[56] cyclodextrins,[57] DNAs,[58] proteins,[59] room temperature ionic liquids[60] and nanoparticles[61] have importance in real-world life.

1.2.4 Micellization of surfactants

Surfactants have the most interesting property of self-aggregation in aqueous solution to form the association colloids known as micelles, accompanied by an overall decrease in the free energy of the system.[62] At very low concentration, the surfactants are adsorbed at the water-air interface in such a way that its hydrophobic tail directs away from the water surface thereby dropping the interfacial tension.[63] As the concentration increases, the number of absorbed molecules increases and strongly condensed monolayer is formed at the surface, is called Gibb's monolayer. With further increasing the concentration of the surfactant, the surfactant molecules remain in the aqueous phase.[62] After a certain concentration of surfactant, they start self-assembling and try to keep the hydrophobic tails away from the water phase. This concentration of surfactants is called critical micellar concentration (*cmc*). These self-assemblies or self-aggregates are known as micelles and this whole process of micelle formation is called micellization. After the *cmc*, the physicochemical properties of surfactant solution change abruptly. A schematic representation of the micellization process of gemini surfactants in aqueous solution is shown in Figure 1.2.

For the estimation of *cmc* of surfactants, many methods are being used *viz.* surface tension, conductance, fluorescence, viscosity, calorimetry, dynamic light scattering, sound velocity, dye solubilization etc. Out of them, the conductometric method is limited for the ionic surfactants; it is not applicable for the non-ionic or zwitterionic surfactants. The physicochemical properties of surfactant solutions before the *cmc* are entirely different from that after the *cmc*. Hence, a breakpoint in the plot of appropriate physicochemical property with the surfactant concentration will provide the *cmc* of that surfactant. The

sharpness of the break in the physical properties depends on the nature of the micelle and on the method, which is used for the *cmc* determination.[64]

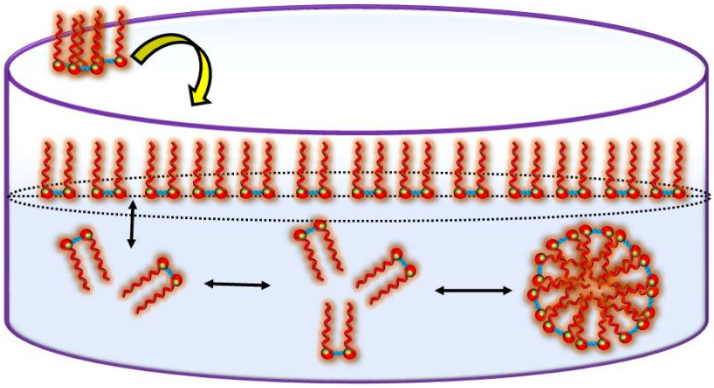

Figure 1.2. Schematic representation of the micellization process of gemini surfactants.

1.2.5 Structure and shape of the micelles

The first model proposed by Hartely[65] stated that the micelles have globular structures with hydrocarbon core surrounded by a highly hydrophilic zone created by the surfactant headgroups, counterions and water molecules, as given in Figure 1.3. The radius of the sphere is almost equal to the extended length of the hydrocarbon chain of the surfactant. The spherical aggregate comprises 50-200 monomer units, sometimes less than 50 (for gemini surfactants). If we see the micelles on the macroscopic level then micelles are described as a mixed aqueous-organic solvent.[66] The ionic headgroups of the surfactants and some of the counterions form a compact "Stern" layer at the micellar surface, in which about 60-75% of the micellar charge is believed to be neutralized.[67] Rest of counterions take part in the formation of a diffused Gouy-Chapman layer, where, they are dissociated from the micellar region and are free to exchange with ions distributed in the bulk aqueous phase. The inner hydrophobic region made up by hydrocarbon chain is known as the core of the micelle. In the core, the hydrocarbon portion of the micelle cannot have an open space at middle and therefore, micelle size does not go beyond the maximum stretched out length of the hydrocarbon chain.[68] Many experiments such as ^{1}H NMR, ^{13}C NMR, and other spectroscopic studies support that water cannot be strictly-excluded from the micellar core.[67] According to the proposed Menger's model, the micelles have open structures with a series of microchannels, which allow the deeper penetration of water towards the core.[68] But according to the "Reef" model, water does not penetrate beyond the ionic group, whereas "Fjord" model states that water penetrates closely to the center

of the micelle. Menger *et al*.[69] proposed that water cannot go to the very center of the micellar core, but can penetrate up to seven carbon atoms of tail away from the headgroup.

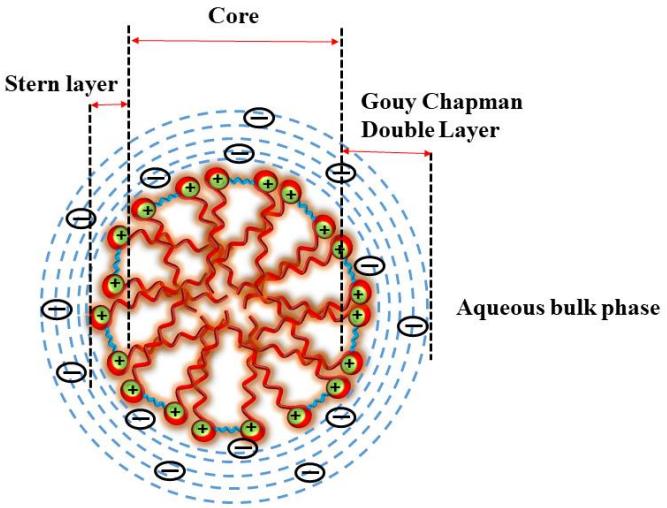

Figure 1.3. Cross-section of spherical micelle of cationic gemini surfactant.

Micelles always show structural dynamics and there is an equilibrium between monomers and other forms of aggregates in solution. Micelles can be spherical, ellipsoidal, disk-like or rod-shaped and bilayers in shape depending on the temperature, concentration, and other experimental conditions. The micellar shape can also vary with the structure of surfactant, and headgroups and charge on the headgroups. The ionic surfactants can form the spherical, rod-shaped micelle throughout the entire concentration range or spherical at a low concentration and rod-shaped at the higher concentration according to the structure of their headgroups. The micellar shape depends on the length of tail (l), headgroup area (a), and the molecular volume (v) of the molecule.[70] Israelachvili *et al*.[71] observed that on the basis of the value of packing parameter p ($p = v/al$), the surfactant aggregates could grow in different shapes given in Table 1.1.

Table 1.1 The relationship between critical packing parameter and shapes of the micelle.

Critical packing parameter *p*, (*v*/*al*)	**< 1/3**	**1/3 –1/2**	**1/2 -1**	**~1**	**>1**
Critical packing shape	Cone	Truncated Cone	Truncated Cone	Cylinder	Inverted truncated cone
Structure of the micelle	Spherical micelles	Cylindrical micelles	Flexible bilayers, Vesicles	Planar bilayers	Inverted micelle

The spacer of gemini surfactants has great influences on the shape of the micelles. Therefore, the shape of gemini surfactant can't be explained only by packing parameter because the link between headgroups can modify both the spontaneous curvature and the bending modulus. For a fixed tail length, the morphology in aqueous solutions depends strongly on the spacer. For the series with $m = 12$ and $2 \leq s \leq 16$, it was detected that the surfactant aggregated into spherical micelles, cylindrical micelles or vesicles, depending on the value of *s*. Measurement of *a* at the air/water interface represents that this parameter changes in non-monotonic fashion. *a* increases rapidly for short spacers, reaches a maximum for medium spacers of 10 to 12 methylene groups, and after that again decreases for larger spacers. Determination of *p* depends on the two parameters *a* and *l*. If *l* is constant and the number of carbon is enhanced then it's expected to have a slow monotonic increase, except for very long spacers ($s \geq 14$). Therefore, the spacer group of gemini surfactant has a strong impact on the morphology of micelle.

1.2.6 Factors affecting micellization of surfactant

Many factors influence the micellization process of surfactant in an aqueous medium. The most important factors are given below:

1. The chemical structure of surfactants
2. Presence of electrolytes
3. Presence of organic additives
4. Experimental conditions for instance temperature, pH, pressure, solvent, etc.

1.2.6.1 The chemical structure of the surfactant

The architecture of surfactants such as headgroups, hydrophobic tails, counterions and the spacer groups (applicable for gemini surfactant) has a strong impact on the c*mc* of the surfactants and are discussed below:

1.2.6.1.1 Effect of headgroups

During the micelle formation, headgroup-headgroup repulsion has an impact on the stabilization of formed micelles. For the formation of stable micelles, headgroup-headgroup repulsion should be less. Non-ionic surfactants do not have any charge on the headgroup, hence, the *cmc* of non-ionic surfactants is much lower as compared to ionic surfactants. Anionic gemini surfactants with sulfonate, phosphate, sodium sulfate or

carboxylate headgroups have been synthesized.[72-74] The *cmc* of gemini surfactant is highly influenced by the size of headgroups and charge as compared to their counterpart, monomeric surfactants. The surfactants with same alkyl tail length and with different size of headgroups have difference in their *cmc*.[75] It is also reported that the *cmc* does not get altered with the replacement of CH_3-group by CH_3CH_2- of the gemini surfactants.[76] A series of cationic gemini surfactants have been synthesized but with replacement of the CH_3- with $HOCH_2CH_2$- and found that these surfactants form dimers below their *cmc*.[77] But above their *cmc*, they form micelles as well as vesicles by the micelle-to-vesicle transition. The hydrogen bonding between the water molecules and -OH groups of headgroups as well as the strong hydrophobic interaction among the hydrocarbon side chains should be the main reason for the special type of aggregation behavior of these gemini surfactants.[78]

1.2.6.1.2 Effect of hydrophobic tails

The *cmc* of surfactant decreases effectively with increasing the hydrophobic tail length of surfactant. However, after the chain length of 16 carbon, decreasing order of *cmc* is ruled out because the coiling of the tail happens in the solution.[75] Generally, the *cmc* of ionic surfactants drops by factor 2 and *cmc* of non-ionic surfactants drops by factor 3 on increasing the one methylene group in the unbranched hydrophobic tail. If phenyl group is present in the alkyl chain then it is considered to be approximately 3.5 methylene group. Whereas, in the branched alkyl chain, the carbon atom on which branching occurs appears to exhibit one-half of an effect than that on an unbranched chain. In presence of unsaturated hydrophobic carbon chain, the *cmc* exhibits increasing tendency despite the decreasing tendency of *cmc* on the increasing alkyl chain of sp^3 hybridized carbon.[75, 79]

In the symmetric gemini surfactants (*m*-*s*-*m*), the variation in the *cmc* with *m* is in line up to *m* = 16 (with *s* = 2, 3, 5 and 6) and up to *m* = 18 (with *s* = 4), but the series, *m*-8-*m* shows a deviation from linearity starting at *m* =14, as given in the review of Zana.[80] The other groups have also reported the similar type of effect of alkyl tail.[81, 82] In the dissymmetric gemini surfactants (*m*-2-*n)*, the hydrophobic chains affect the aggregation behavior hugely. Oda and co-workers explored *m*-2-*n* series with equal values of *m* + *n* and found that these dissymmetric gemini surfactants exhibit almost same *cmc* values.[41, 50, 83] Han *et al*. detected that as the m/n ratio enhances, the *cmc* decreases for the *m*-*s*-*n* series in a linear fashion.[78]

1.2.6.1.3 Effect of counterions

Counterions also have a huge impact on the aggregation behavior of the surfactants by altering the ionic strength of the surfactant solution.[84, 85] Moreover, the valency of the counterion also influences the *cmc* largely. In the micelle formation, the degree of the counterion binding is due to the balance between the electrostatic forces, which pull the counterion towards the oppositely charged head group of micelles, and the hydration forces, which limit the binding.[86] Normally, the *cmc* value decreases as counterion binding increases. Counterions or ions with opposite charge to that of the surface-active moiety of the surfactant are recognized to have a supplementary effect. Unlike sodium bromide which induced the growth of micelles of the cationic surfactant, cetyl pyridinium bromide, sodium chloride did not.[87] Aromatic counterions such as benzoate, tosylate, salicylate, show strong binding at the micellar surface and lower the *cmc* with increasing the counterion binding.[88] Mainly, salicylate ion is effective in prompting micellar growth. The counterion binding also increases with increasing its hydrophobicity enhancing the micelle formation.[23] Hydrophobic counterions are interesting as charge carrier or quencher in biomembranes and membrane photochemistry.[89] Addition of the cationic surfactant into the anionic is a special case of counterion interaction. The *cmc* of the mixture of anionic and cationic surfactant in aqueous solution is considerably lower than that of the individual surfactants due to the synergistic interaction between the surfactant molecules and they exhibit properties superior to their constituent single surfactant in many surfactant applications.[90, 91] The nature of the counterion significantly affects the micellization process. Both *cmc* as well as counterion dissociation increase in the sequence $SO_4^{2-} < NO_3^- < Br^- < Ac^- < Cl^- < F^-$. The results are related to the difference in the hydration of these counterions and match with the extent of the bare ions to the dimensions of the gemini headgroup region.[78] Salts can effectively influence the behavior of macromolecules such as proteins in the aqueous solution.[92] Franz Hofmeister discovered the series of ions based on their ability to salt-out and salt-in proteins.[93] Later on, the series of ions is named as Hofmeister series and are given below:

Strongly hydrated anions — Weakly hydrated anions

$F^- \approx SO_4^{2-} > HPO_4^{2-} > \text{Acetate} > Cl^- > NO_3^- > Br^- > ClO_3^- > I^- > ClO_4^- > SCN^-$

Weakly hydrated cations — Strongly hydrated cations

$NH_4^+ > K^+ > Na^+ > Li^+ > Mg^{2+} > Ca^{2+} > \text{Guanidinium}$

Anions have a greater effect than the cations.[94] It is believed that ions affect the structure and dynamics of water.[95] However, the extent of such effect needs to be further explored. The ions on the left and right hand side are also called kosmotropes (structure makers) and chaotropes (structure breakers), respectively.[96] The Hofmeister series has been growing as an active research area.[97] Counterions stabilize the micelle by screening the electrostatic repulsive interactions between the ionic headgroup.[98] Both *cmc* and α decrease in the order $F^- > Cl^- > Br^- > NO_3^- > SO_4^{2-}$ which can be rationalized in terms of Hofmeister series,[99] and an increase in the binding ability of counterion except for the bivalent SO_4^{2-} ion. The more negative value of ΔH_{mic} follows the order $SO_4^{2-} < F^- < Cl^- < Br^- < NO_3^-$ with even positive value for SO_4^{2-} ion. The unusual behaviour of SO_4^{2-} ion is due to its bivalency and degree of dehydration. The microenvironmental properties of micelles such as micropolarity and microviscosity have been studied by probing with electron spin resonance of 5-doxylstearic acid (5-DSA).[98] The dependence of micellar properties on the valencies of counterions is also reported by Nicoli *et al*.[100] Aggregation properties of gemini surfactants and growth of micelles are also influenced by the aromatic and inorganic counterions.[101] The observation is that micellization of surfactant follows the Hofmeister series of ions except for SO_4^{2-} ion as mentioned above.[99] Matsubara *et al.*[102] have recently reported that the Kraft temperature decreases sharply from 25 ºC to 2 ºC when counterion, Br^- of cetyltrimethylammonium bromide is replaced by Cl^-. Shah *et al.*[103] have studied the foam stability of dodecyl sulfate (DS) with Li^+, Na^+, Cs^+ and Mg^{2+} as counterions at a concentration below and above the *cmc*. While there is no significant change in foam stability at a concentration below the *cmc*, but at a concentration above the *cmc*, CsDS and $Mg(DS)_2$ surfactants form more stable foams as compared to LiDS and NaDS surfactants. The surface activity order of these dodecyl sulfates follows LiDS < NaDS < CsDS < $Mg(DS)_2$.

As mentioned above, micellar properties are controlled by the hydrophobic character of counterions as well.[104] Paz *et al.*[105] observed that the interaction of inorganic counterions with micellar surface depends on the hydrated size of the ions (smaller hydrated ions favor the interactions). However, for quaternaryammonium counterions, it depends on the hydrocarbon exterior (more hydrophobicity is more effective in micellization). Puig *et al.*[106] have reported that the shear thickening intensity of micellar solution of CTAX (where X = tosylate (T^-), 3-fluorobenzoate ($3FB^-$) and 4-fluorobenzoate ($4FB^-$), vinylbenzoate (VB^-) and salicylate (S^-) can be rationalized by the hydrophobicity

of counterions in the Hofmeister series $S^- < VB^- < T^- < 3FB^- < 4FB^-$. Micelle architecture is changed to vesicle as a function of the counterion hydrophobicity of perfluorodecanoate surfactants with different counterions, ammonium, tetramethylammonium, butyltrimethylammonium, dimethyldibutylammonium and tetrabutylammonium.[107]

1.2.6.1.4 Effect of the spacer group of gemini surfactants

Spacer group is a connector between two amphiphilic moieties at the headgroups of gemini surfactants. The spacer group of gemini surfactant can vary in nature: hydrophilic or hydrophobic, rigid or flexible. The appearance of the spacer group (chemical structure, length, flexibility) has been shown to be of the utmost significance in the estimation of properties of the gemini surfactants in the aqueous solution. The spacer groups cause the conformational changes in the gemini surfactant which have great influence on the *cmc* of that surfactant. The number of the methylene group in the spacer group affects the aggregation properties as well as the shape of the aggregates.[80, 108, 109] Gemini surfactant with shorter spacer group (12-2-12, $2Br^-$) form the worm-like micelles and also displays concentration-dependent micellar growth. Similarly, gemini surfactant, 12-3-12, with Br^- form spheroidal micelles at higher concentration. Zana *et al*.[18] have studied the morphology of aggregates of gemini surfactants, 12-*n*-12 (with $n = 2, 3, 4$) in aqueous medium and they have observed that the gemini surfactants with a short spacer ($s = 2, 3$) form thread like, long and entangled micelles at low concentration, whereas gemini with $s = 4$ form spherical micelles. These results exhibit that the length of a spacer affects the morphology of formed micelles and the short spacer promotes less spontaneous curvature in the self-assemblies. It is well documented[109-111] that the *cmc* of *m*-*s*-*m* gemini surfactants change with the change in the value of *s*. When the value of *s* increases from 2 to 5 or 6 ($s \leq 6$) the *cmc* of a surfactant increases and after the $s > 6$ *cmc* of surfactant decreases but when $s \geq 10$ *cmc* of surfactant drastically decreases. The increase in *cmc* for $s \leq 6$ of *m*-*s*-*m* surfactants is due to the other conformational change in the surfactant molecule[109] and a decrease in *cmc* for $s \geq 10$ is due to the formation of loop by the spacer group towards the hydrophobic core of the micelle. The change in conformation of gemini surfactant molecule followed by progressive penetration of the spacer towards the core of micelles with increasing *s* is expected to disturb the number of water molecules interacting with each spacer group at the Stern layer or micelle-water interface. It is also noticed that hydrophilic, flexible spacer favors micellization and that is why the *cmc* of surfactants

decreases.[56, 112] The aggregation behavior of the gemini surfactants with partially fluorinated spacer has also been studied[113] and observed that the *cmc* does not change significantly. If the fluorine atom is present in the spacer, the surfactant is less soluble in water because of the increased hydrophobicity and rigidity of the spacer. Fluorinated spacer may make the spacer hard to loop and prevent the surfactant molecules to aggregate with each other, resulting in larger *cmc*.

1.2.6.2 Presence of electrolytes

The effect of electrolyte on the *cmc* of the surfactants is more pronounced for the ionic surfactants than that for zwitterionic and non-ionic surfactants in the aqueous solution. The addition of electrolyte in the solution of non-ionic and zwitterionic surfactants causes the salting-out and salting-in of the hydrophobic part of surfactant, as a result of which the *cmc* values of surfactants are changed.[114] The capacity of the ions to cause the salting-in or salting-out is chiefly depended on the ion whether it is water structure maker or breaker. The ions, which have a high ionic charge/radius ratio, are highly hydrated and are water structure maker such as F^- ion. These types of ions salt-out the hydrophobic part of the surfactant resulting in the decrease in the *cmc* values. Apart from this, the ions with small ions charge/radius ratio are water breakers such as CNS^- ion. These type of ions salt-in the hydrophobic part of the surfactant and *cmc* of the surfactant is increased.[79]

1.2.6.3 Presence of organic additives

The presence of an organic compound has an impact on the micellization behavior of the surfactants in the aqueous solution depending on their chemical nature. Mainly, these compounds are divided into two categories based on how they are interacting and influencing the micellization of surfactants.

1.2.6.3.1 First category compounds

Mainly the polar organic molecules like alcohols and amides fall in this category. These compounds reduce the *cmc*. They only affect the *cmc* at their lower concentration. If the chain length of these compounds is short, they are adsorbed mostly at the water-micelle interface whereas comparatively longer chain compounds are adsorbed mainly in the outer portion of the core, between the surfactant molecules. Therefore, these

compounds reduce the work required for the micellization by their pattern of adsorption. Dioxane and ethanol type compounds with a very short chain also decrease the *cmc* at the low concentration, although the effect is not that much pronounced.[115] The probable location of these compounds is at the surface of the micelle near to the headgroups, hence, they reduce the headgroup-headgroup repulsion. The reduction in the *cmc* is lesser in presence of the branched compounds than the unbranched compounds.

1.2.6.3.2 Second category compounds

These compounds affect the *cmc* of surfactant at the higher concentration. Mainly, Urea, formamide, N-methylacetamide, guanidinium salts, short-chain alcohols, water-soluble esters, dioxane, ethylene glycol, and other polyhydric alcohols such as fructose, xylose etc. fall into this category. These compounds alter the structure of water, or dielectric constant, or solubility parameter (cohesive energy density). Urea, formamide, and guanidinium salts are supposed to increase the *cmc* by disturbing the water structure.[116] Therefore, these compounds may increase the degree of hydration of the hydrophilic group, subsequently, hydration of the hydrophilic group opposes micellization, causing an enhancement in the *cmc*. Apart from this, these water structure breakers may also increase the *cmc* by reducing the entropy effect accompanying micellization.

Presence of urea in water affects the structure of water by disturbing hydrogen bonding. Although Frank model describes that urea act as a water structure breaker,[117] neutron scattering study does not show any evidence in favor of this effect after addition of urea in water.[118] Two different types of mechanisms have been suggested to explain the effect of urea on water structure: In first indirect mechanism, urea acts as a water "structure breaker" facilitating the solvation of nonpolar solutes and in second direct mechanism, urea participates in the solvation of hydrophobic solutes in water by replacing some water molecules in the hydration shell of solute.[119-121] Xylose or fructose are the water structure maker as they reduce the *cmc* of the surfactant.[122] Ethylene glycol, dioxane, water-soluble esters, and short-chain alcohols at high bulk phase concentrations may increase the *cmc* by reducing the cohesive energy density, or solubility parameter of the water, hence, they increase the solubility of the surfactant and *cmc*.[116] Moreover, these compounds reduce the dielectric constant of water, thus, increases the repulsion between the headgroups of the surfactants. Hence, the process of micellization is disfavoured and *cmc* of surfactant increases.[123]

1.2.6.4 Experimental conditions (temperature, pH, pressure, solvent, etc.)

1.2.6.4.1 Effect of temperature

With an increase in the temperature, first, *cmc* of the surfactant decreases up to a certain point and then starts increasing. Rosen *et al.*[79] have explained that the rise in temperature reduces the hydration of the hydrophilic headgroups, therefore, *cmc* of surfactant decreases. The increase in temperature also disturbs the water structure around the hydrophobic tail, resulting in increase in *cmc* of surfactant. Hence, temperature influences the micellization of surfactant in a little complex way. For the ionic surfactants, Akhtar *et al.* explained temperature effect based on the decrease in the degree of hydration and increase in the degree of dehydration of the hydrophilic and hydrophobic parts of surfactants, which favors and disfavors the micellization of surfactants, respectively. Partial dehydration of hydrophilic headgroups causes the increase in the headgroup-headgroup repulsion, because of which micellization process is disfavored. The relative extents of these two opposite factors will elect whether *cmc* will increase or decrease in a certain temperature range. The lowest value of *cmc* for ionic surfactant is observed around 298 K, whereas, the same for non-ionic surfactant is 323 K. Effect of temperature on the micellization of gemini surfactants is also well explored by various groups.[124, 125]

1.2.6.4.2 Effect of pH

The degree of dissociation of the polar groups of the amphiphile depends on the pH of the solution if the molecules have ionizable groups such as $-NH_2$, $-(CH_3)_2N\rightarrow O$ and –COOH etc.[126] The value of *cmc* will be high at that pH where the groups do have charges and low when groups do not have charges. The $-NH_2$, $-(CH_3)_2N\rightarrow O$ groups have the charge at low pH whereas -COOH has the charge at high pH. Similarly, zwitterionic surfactants also become cationic at low pH, *cmc* of surfactant rises rapidly[127] or more modestly depending on the structure of the zwitterionic form.[128]

1.2.6.4.3 Effect of pressure

Several reports are available on the effect of pressure on the micellization of ionic surfactants.[129, 130] The *cmc* of ionic surfactants increases with increase in pressure up to 1000 atm and after that *cmc* decreases.[131, 132] Such behavior has been simplified in terms of solidification of the micellar interior, the amplified dielectric constant of water[131], and

other features which are associated with water structure.[133] For non-ionic surfactants, the *cmc* value enhances tediously and then levels off with increasing pressure.

1.2.6.4.4 Effect of solvents

In the ethylene glycol, the *cmc* of surfactants decreases with an increase in the hydrophobic tail length, but the change is much lesser than that in water.[134] For polyoxyethylenated non-ionic solutions in benzene and carbon tetrachloride, the micellization is favored with an increase in the length of the polyoxyethylene group at fixed hydrophobic chain length. For alkylammonium carboxylates in the benzene solvent, the *cmc* increases with an increase in chain length of alkyl of an anion but decreases with an increase in the chain length of alkyl of a cation. Whereas, in carbon tetrachloride, there is an insignificant alteration in the *cmc* with these structural variations. The *cmc* of various surfactants is observed to be lower in D_2O as compared to H_2O[135], but the size of a micelle is bigger[136] because the hydrophobic interactions are expected to be stronger in D_2O than H_2O.[137] The micelle formation of ionic surfactant in the polar non-aqueous solution such as *N*-methylacetamide, formamide, dimethyl sulfoxide, and *N, N'*- dimethylformamide depend on the dielectric constant of the medium, intermolecular hydrogen bonding, and on the bulk structuredness.

1.2.7 Types of micelles

Micelles are of two types depending on the nature of the used solvents:

1.2.7.1 Normal or aqueous micelles

Micelles are formed when the surfactant molecules dispersed in polar solvents. The structure of the aggregates in water as solvent is such that the interior of the micelles consists of the hydrophobic core and the hydrophilic residues are located on the surface and are in contact with water (Figure 1.4).

1.2.7.2 Inverted or reverse micelles

Reverse micelles (RMs) are formed when surfactant molecules are dispersed in nonpolar solvents such as hexane, heptane, benzene etc. (Figure 1.4). In the RMs, the hydrophobic tails of surfactants projected towards the nonpolar solvent phase and the polar headgroups of surfactants are pointed towards the nanoscale droplet of the polar solvent.[138]

Generally, RMs are defined by the ratio of the polar solvent to the amount of surfactant present, which is represented by the following formula, w_o = [polar solvent]/[surfactant]. Size of RMs depends upon w_o values.

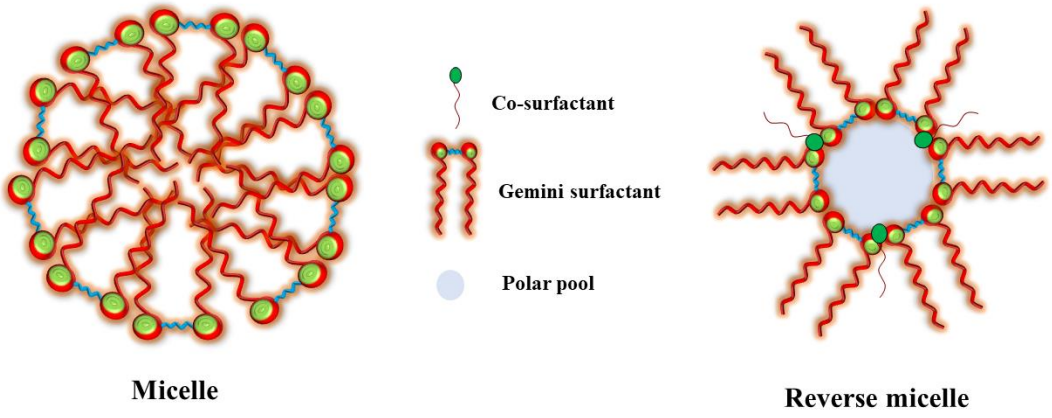

Figure 1.4. Diagrammatic representation of micelle and reverse micelle formed by gemini surfactants.

In typical RMs, water acts as a polar solvent.[139] Apart from water, other solvents such as acetonitrile, propylene glycol (PG), ethylene glycol (EG), formamide (FA) etc. also act as polar solvent, due to their immiscible nature in a nonpolar solvent. If the polar solvent is water or other organic solvent then the formed RMs are called aqueous or non-aqueous reverse micelles, respectively.[139] Different types of surfactants like anionic, cationic, nonionic, and zwitterionic surfactants can form a reverse micelle. Various scattering techniques such as small-angle neutron scattering (SANS) and small-angle X-ray scattering (SAXS) are used to determine the shape and size of RMs.[140, 141]

1.2.8 Site of solubilization in the micelle

The exact site of solubilization depends on nature (extent of hydrophilicity or hydrophobicity) of material as well as on the type of interaction between the solute and surfactant. It is observed that solubilization can occur at a number of different sites in micelle such as (Figure 1.5):

1. On the micellar surface.
2. Between the hydrophilic headgroups.
3. In the outer core of micellar interior (between hydrophilic headgroups and first few carbon atoms in the hydrophobic portion).
4. In the core of the micelles.

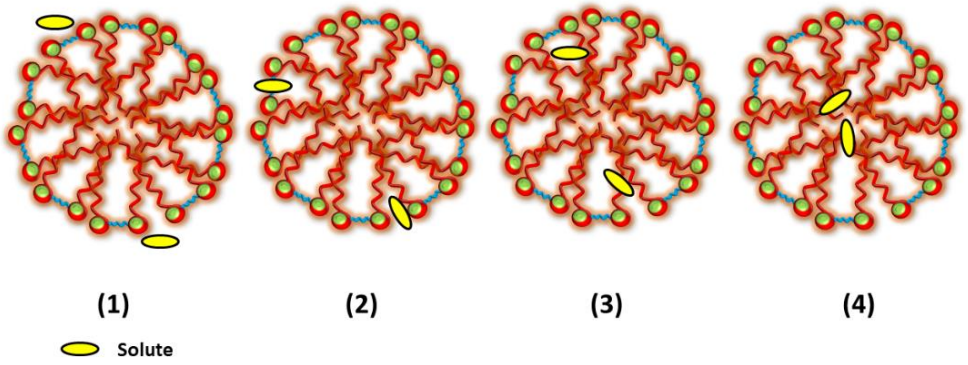

Figure 1.5. Possible location for the solubilized the solute molecule.

1.2.9 Mixed micelles

The addition of additive into micelle results in the formation of a mixed micelle. Thus, solubilization is closely associated with mixed micelle formation as usually used. However, the mixed micelle means a micelle composed of surfactants capable of forming micelles themselves. By this practice, mixed micellization is a special instance of solubilization (Figure 1.6). Currently, the mixed micelles are gaining attention because the aqueous solutions with two surfactants display sharp alterations in their physical properties such as surface tension or the intensity of scattered light as a function of concentration. These variations are associated with the formation of micelles in solutions of a single surfactant. Mixed micellar systems are novel models to study the molecular interactions on complex supramolecular aggregates[142-144], which are mimicking the biological systems and to perform functions such as ion transport, drug delivery, and so on,[75] and their use in pharmaceutical, detergency, food and cosmetic industries, micellar solubilisation etc.[145] than those consisting of only one type of surfactant.

Various types of molecular interactions are possible in mixed surfactant systems e.g.: (1) electrostatic interaction between ionic hydrophilic groups, (2) ion-dipole interaction between ionic and nonionic hydrophilic groups, (3) steric interactions between bulky groups, (4) van der Waals interactions between hydrophobic groups, and (5) hydrogen bonding between component surfactant molecules. If there is no interaction between surfactant's molecules in the mixed surfactants system, then it shows an ideal nature. If attractive interactions are present then it is called synergism and if repulsive interactions are present then it is known as antagonism. Zana *et al*.[146, 147] worked on mixed systems of cationic gemini surfactants and conventional surfactants.

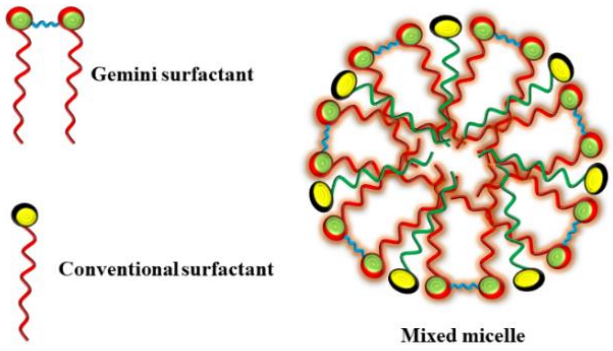

Figure 1.6. Formation of mixed micelles of a conventional surfactant with a gemini surfactant.

1.3 Cyclodextrin

Cyclodextrins (CDs) are a family of macrocyclics of oligosaccharides in which glucose units are associated by α-1,4 glycosidic linkage. Generally, CDs are semi-natural products in which 6, 7, 8-glucose units are present in a ring and called α- β-, and γ-CDs, respectively.[148] CD is also known as doughnut-shaped molecule because it comprises a truncated conical structure with a hollow space in the centre (Figure 1.7). CDs have inner hydrophobic (or non-polar) cavity and polar hydrophilic exterior (or outside surface). It also consists of the primary hydroxyl group on the narrow side and secondary hydroxyl group at the wide side of the ring. The diameter of the cavity is smaller on the primary face and wider on the secondary face. This is because the free rotation of the primary hydroxyl groups reduces the effective diameter of the cavity. Due to their toroid geometry, and relatively hydrophobic character of the internal cavity and the hydrophilic character of external hydroxyl groups, CD molecules can easily form inclusion complexes with a huge range of molecules. This property of inclusion complex formation is the reason for the prevalent application of CD in various aspect of chemistry.

CD is a supramolecule and its interaction with other molecule do not involve covalent bonds, so, it acts as a potential host in a host-guest type complexation. CDs are semi-natural products formed from starch and are renewable natural substances. Apart from this, CDs are cost effective and highly produced from the natural sources. CDs also have the ability to eliminate the toxic effect of cyclodextrins itself by choosing the appropriate derivatives and can be consumed by humans in a form of drugs, foods, and cosmetics. Due to all these properties that have been stated above, CDs have been used to form the host-guest type of inclusion complexes and act as host molecules. Inclusion

complex is formed when a guest compound is inserted into the cavity of the host compound as shown in Figure 1.7. Inclusion complexation with a variety of organic or inorganic guest molecules can occur via various interactions like hydrogen bonding, van der Waals, hydrophobic and dipole-dipole interaction without any covalent bond. Water molecules leave the CDs cavity and contribute to the stability of the CD complexes with these interactions.[149] Most of the current interest with CDs arises from their ability to form host-guest complexes with a wide range of guest species.[150, 151] Their ability to form host-guest complexes has led to the use of CDs in a number of industrial applications.[152]

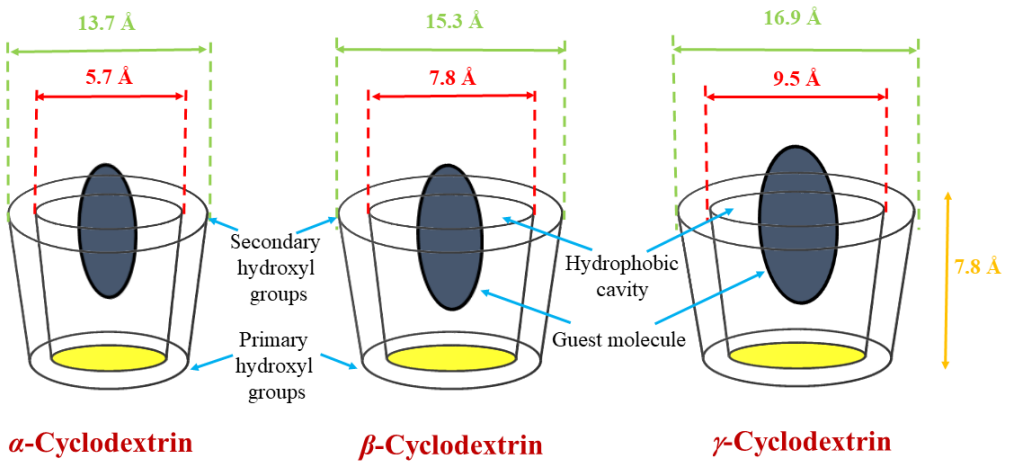

Figure 1.7. Structures of α, β, and γ-cyclodextrins.

1.3.1 Inclusion complex formation of cyclodextrin

The most outstanding property of CDs is their ability to form the inclusion complexes with widespread of solid, liquid and gaseous compounds by a molecular complexation.[153] Inclusion complex is a complex of two compounds, one chemical compound called "host" having a cavity and second compound called "guest" is located or trapped inside the cavity of the host.[154] In the process of inclusion complexation, the physicochemical properties of the guest molecule are altered such as solubility of hydrophobic molecule is increased, chemical stability is improved, toxicity is reduced and so forth.[155] From an analytical viewpoint, formation of inclusion complexes in certain cases allows improvement in the performance of the methods used for the determination of different analytes using spectrophotometry technique.[156]

Benesi–Hildebrand equations are used to know the stoichiometry of the inclusion complex at a low concentration of CD.[157, 158] Benesi–Hildebrand Equations 1.1 and 1.2

given below to see whether the inclusion complex of guest and host has 1:1 or 1:2 stoichiometry, respectively:

$$\frac{1}{F - F_0} = \frac{1}{F_m - F_0} + \frac{1}{K[CD](F_m - F_0)} \quad (1.1)$$

$$\frac{1}{F - F_0} = \frac{1}{F_m - F_0} + \frac{1}{K'[CD]^2(F_m - F_0)} \quad (1.2)$$

where, F and F_o are the fluorescence intensities in presence and absence of CD, respectively. F_m is the limiting intensity of fluorescence. $[CD]$ is the experimental concentration of CD. K and K' are the association constants. The formation of a 1:1 inclusion complex of host and guest is an equilibrium process between the dissociated and associated species in solution, which is characterized by the stability constant, *K*. This is the simplest and is more frequent. However, 2:1, 1:2 or 2:2 stoichiometries also exist for CD host-guest complexes.[148] At a low concentration of CD, small inclusion complexes with a stoichiometric ratio of either 1:1 or 1:2 are reported.[159-161] But at the high concentration of CD, nanotubes are formed because of van der Waals, hydrophobic and hydrogen bonding interactions between the guest and host molecules.[159, 160, 162-165] By the internanotubular hydrogen bonding, the secondary aggregates of nanotubes in the form of micrometer-sized rods have also been well documented.[159-161] Secondary aggregates of nanotubes can be grown in 2D fashion and 3D fashion.[166] The formation of guest molecule induced nanotubes and secondary aggregates of nanotubes are shown in Figure 1.8.[167]

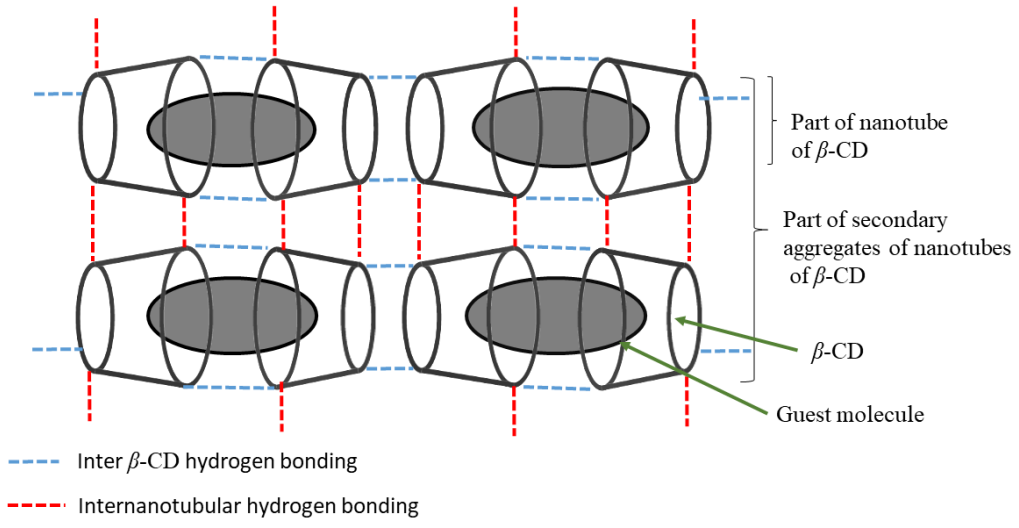

Figure 1.8. Representative structure of guest induced nanotubes of cyclodextrin and their secondary aggregates.

Considerable interest has been centered on the nature of interaction during the host-guest complexation as well as the structure of the CD complexes.[149] CDs have found a range of applications in drug delivery because of their unique characteristic of possessing a hydrophobic interior and hydrophilic exterior.[168] Molecular modeling, simulation, X-ray crystallography, NMR spectroscopy, optical spectroscopy (UV-Vis, fluorescence, circular dichroism) and thermal characterization methods have been frequently used to determine the molecular structure of inclusion complexes.

1.4 Proteins

Proteins are the building blocks of life. Proteins are polymers of 20 different amino acids attached by peptide bonds in various sequential manner. Primary structure of the protein is a polypeptide chain of different amino acids. The secondary structure of a protein is made by systematic hydrogen bonding interactions between N-H and C=O groups in the invariant parts of the amino acids in the polypeptide chain. It is of two types, namely, the alpha helices and beta sheets. The tertiary structure of a protein is a three-dimensional structure of it. In the tertiary structure of the protein, four types of interactions are present: 1. Hydrogen bonding, 2. Ionic interactions between oppositely charged groups, 3. Hydrophobic interactions, and 4. Disulfide cross-linkages. The first three types of interactions are non-covalent and are weaker than the fourth covalent interaction.[169] A protein, in its active form, has a specific three-dimensionally folded structure. Serum albumins are a particular class of well-studied proteins because of their great importance in biological functions.

1.4.1 Importance of serum albumins

Serum albumins are the most abundant proteins in blood plasma; providing about 80% of the osmotic pressure of blood. The most important function of serum albumin is to transport fatty acids, a great variety of metabolites and drugs such as anti-coagulants, tranquilizers, and general anesthetics.[170] These proteins have interesting properties of binding with a variety of hydrophobic ligands such as hematin, metals ions, surfactants, fatty acids, lysolecithin, bilirubin, warfarin, tryptophan, steroids, anesthetics and several dyes.[171, 172] In recent years, recombinant proteins and antibodies are widely used in the treatment and prevention of diseases.[173] Hence, there is a need for analytical techniques to detect and analyze the protein samples apart from the characterization techniques to

monitor the conformational variants. These changes in the conformation of proteins can be due to environmental stress, chemical changes of protein such as oxidation due to environmental and various types of aggregate formation etc.[174, 175] Fluorescence spectroscopy can be applied to characterize the protein conformation. Among serum albumins, bovine serum albumin (BSA) is the most used protein for the spectroscopic studies.

1.4.2 Bovine Serum Albumin (BSA)

BSA is a globular serum protein highly soluble in water. BSA contains 583 amino acids in its primary structure. Primary structure of BSA consists of nine loops, which are held together by 17 disulfide bonds. The secondary structure is composed of 67% of the helix of six turns. The tertiary structure consists of three domains, I, II and III with each domain constituted by subdomains IA, IB, IIA, IIB, IIIA and IIIB. Domains II and III share a common interface, binding of a ligand with domain III results in the conformation changes to domain II also. BSA contains two tryptophan residues, one is Trp-134 located near the surface of the albumin molecule in the second helix of subdomain IB, while the other one is Trp-213 in a hydrophobic subdomain IIA. The molecular weight of BSA is 66 kD.[176]

1.4.3 Intrinsic fluorescence of BSA

Structural changes in the native form of BSA can be studied by fluorescence spectroscopy (discussed in the respective chapter). BSA contains three aromatic amino acid residues such as tryptophan (Trp), tyrosine (Tyr), and phenylalanine (Phe). The tryptophan (Trp) residues of BSA largely contribute to the intrinsic fluorescence, with only an insignificant contribution by the tyrosines (Tyr). The fluorescence properties of Trp change more significantly than that of Tyr and Phe. The fluorescence of Phe can be ignored due to the low value of quantum yield. The intensity, quantum yield, and fluorescence peak position of Trp depend upon the environment of Trp. Hence, alterations in the fluorescence properties of Trp are used to study any sort of structural changes in BSA caused by external environment.[177-179] However, the fluorescence of Tyr and Phe are not much sensitive towards the external environment.

1.4.4 Interaction of BSA with surfactants

BSA has both hydrophobic and hydrophilic part in their structure. Because of this property, surfactant molecules interact with BSA easily. Interactions of proteins with surfactants have been well documented.[177, 178, 180] These interactions are of great significance in a wide range of industrial, biological, pharmaceutical, and cosmetic applications.[181-183] Surfactants cause the denaturation and make changes in the conformation of protein. The nature of the protein-surfactant interaction can be studied in terms of the binding isotherms. With the increase in surfactant concentration, the binding isotherms exhibit four characteristic regions. These regions are as follow:

1. Specific binding region: At a lower concentration of a surfactant, it binds to the specific sites (high-energy site) of protein and these interactions are electrostatic in nature.
2. Non-cooperative binding region: The binding of surfactant with protein occurs gradually.
3. Cooperative binding region: The binding affinity of surfactant to protein increases drastically. Most of the protein unfolds in the cooperative binding region and significant numbers of hydrophobic binding sites, previously covered in the interior of BSA, are uncovered.[184]
4. Saturation binding region: Binding of the surfactant on the protein does not occur and there will be a formation of normal micelle as the excess of surfactant is added. A variety of models have been proposed to mimic how surfactant interacts with protein such as rod-like particle model, flexible-cylindrical micelle model, and necklace-bead model.[185, 186] Out of these models, the necklace-bead model is the most accepted one.

Interactions of protein with a single chain surfactant have been widely studied.[178, 179, 187] Nowadays study on the interaction of gemini surfactant with protein is an area of interest. Interaction of cationic gemini surfactants has been studied with BSA.[177, 188] and gelatin.[177] It has been observed that binding of gemini surfactant induces changes in the microenvironment around the aromatic amino acid residues and disulfide bonds of BSA at the higher concentration of surfactants. Gao *et al*.[189] have studied the effect of tail length of anionic gemini surfactant on the interaction with BSA. Faustino *et al*.[190] have reported the effect of temperature, pH, and stereochemistry of surfactant on gemini surfactant-

protein interactions. Recently, Rather *et al*. [191] have observed the refolding of BSA by using gemini surfactant and reported that gemini surfactant, at very low concentration, refolds the denatured BSA. Protein-surfactant interactions have been a subject of extensive study over the past few decades because they play an important role in many industrial, biological, pharmaceutical, cosmetics and detergent actions.[180, 192]

Nowadays, refolding of the denatured proteins has been garnering attraction due to its biological importance. Non-native, aggregated and misfolded proteins are required to get native conformation of proteins to get rid from some human diseases.[193] Aggregation of proteins occurs due to the association of the hydrophobic surface which are exposed during the refolding process of protein.[194, 195] Artificial chaperone method is used to control the aggregation of proteins during the refolding process. In this method, surfactant and cyclodextrin has been sequentially added into the diluted denatured protein as described by the Rozema *et al.*[196, 197] In this refolding process, the surfactants act as a capturing agent and cyclodextrin act as a stripping agent of surfactant from the surfactant-protein complex.[196, 198] Refolding of protein assisted by the artificial chaperone method is well explored.[196, 198, 199] The effect of cyclodextrin on the interaction between BSA and the anionic surfactants has been also studied.[200, 201] The presence of cyclodextrin hinders the strong interactions between BSA and surfactant by the combined effect of electrostatic and hydrophobic interactions between them. The hydrophobic interaction between cyclodextrin and surfactant is stronger than that between BSA and surfactant. The refolding of BSA by the use of gemini surfactants and β-CD via artificial chaperone method and a comparison with a conventional surfactant have also been studied.[191]

1.5 Deoxyribonucleic acid (DNA)

Deoxyribonucleic acid (DNA) is a storehouse of genetic information in the form of the genome of an organism as a double-stranded DNA. Watson and Crick gave the first double helix model for the DNA structure. A nucleotide unit consists of any one of nitrogen bases (includes cytosine (C), guanine (G), adenine (A), and thymine (T)), a sugar (deoxyribose), and a phosphate group. The DNA consists of two polynucleotides with backbones made by phosphate groups joined via ester bonds. The two strands of polynucleotides are connected by the hydrogen bonding between the bases according to the base-pairing rule (A forms two hydrogen bonds with T, and C forms three hydrogen bonds with G). These two strands move in opposite directions with each other and are

therefore anti-parallel.[202] The gene is the functional unit of the genome, which is a particular segment of DNA that transcripts and translates into a specific functional protein.[203] The basic double helical structure of DNA is given in Figure 1.9.

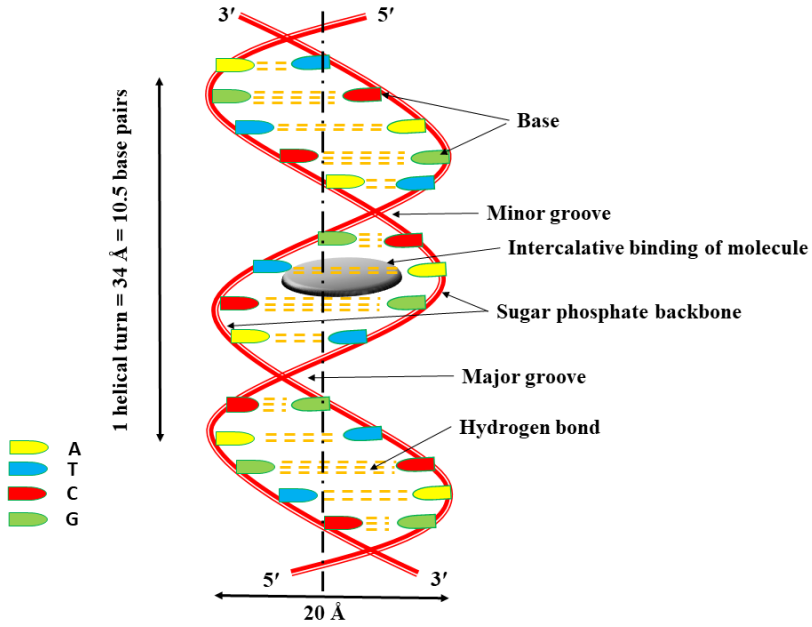

Figure 1.9. The basic structure of the DNA double helix.

1.5.1 Calf thymus DNA (ctDNA)

Calf thymus DNA (ctDNA) has been used as a model DNA for various studies, is extracted from the thymus gland of the calf. The thymus gland is very large gland in immature mammals. Since many white blood cells are present in the thymus gland with large nuclei, hence, it is the part of the immune system. Large numbers of thymus cells are used for the extraction of ctDNA. ctDNA is natural DNA and largely used in the various drug-DNA interaction studies such as DNA binding with anticancer agents, and DNA binding agent which can alter the structure and function of the DNA. ctDNA has great resemblance with the mammalian DNA and can be easily extracted from the natural sources with a great abundance which could be the reason for its high usage in the research purpose.

1.5.2 DNA-drug interactions

In the world, millions of people are suffering from mortal diseases such as cancers of numerous types including lungs, brain, liver, bladder, breast, kidney, skin, ovarian, prostate, etc. Several therapeutic drugs are available to target these cancers, but after a

certain stage again a problem to cure these cell lines arises.[204] At present, chemotherapy is widely used for the most of cancer treatment out of various offered treatment options. In the chemotherapy, the use of the drug has displayed binding with the DNA and altered the DNA-protein interaction followed by the apoptosis of cancer cells. Hence, the DNA-drug binding interactions are the epicenter of numerous research investigations. In pharmaceutical applications like new drug development, drug carrier in the way of drug loading, drug releasing and their effectiveness, various molecules showing fluorescence are broadly used. The fluorescent molecule acts as a drug showing various changes in their fluorescence properties after binding with DNA, which has a significant impression on the physiological functionality of DNA.

As discussed above that DNA is a carrier of genetic information and is a major target for drug interaction because of the ability to interfere with transcription and replication, which are major steps in cell growth and division. To design the effective therapeutic drug, the knowledge of the mechanism of DNA-drug binding is important for a better understanding of the DNA-drug interactions.[205] Because of the binding interaction, changes occur in the properties of the DNA and drug as well. Most of the time, the conformational changes happen in the DNA, which leads to the alteration in the functionality of DNA.[205] Several techniques, such as nuclear magnetic resonance (NMR), light scattering studies, viscometry, and electric linear and circular dichroism (ELD, CD), have been applied to provide insight into binding modes, DNA affinity and base pair selectivity of DNA-binding drugs. In last few decades, enormous research has been done on ligand-DNA interactions. Most of the drugs currently used interact with the DNA by three general binding modes: DNA intercalation, groove binding, and covalent binding.[205] The kind of interactions between small molecules and DNA is an essential tool for the prediction of potential physiological and/or therapeutic consequences of such interactions. The DNA interactions with small aromatic molecules can be classified as covalent and non-covalent, where non-covalent interactions can be further classified as intercalation and groove binding.[206]

1.5.1.1 Intercalative binding mode

When a planner aromatic molecular system is inserted between the base pairs of DNA double helix and their interactions are non-covalent type then this type of binding is called intercalative binding mode. Intercalative binding is generally independent of the

base pair sequence. Generally, condensed aromatic ring molecular systems provide the stacking force to the ligands to stack between base pairs of DNA. To accommodate the aromatic molecule between the base pairs also require variations in the sugar-phosphate torsional angles along with other modifications such as unwinding and bending of helical structure. Electrostatic, van der Waals and hydrophobic forces stabiliz the binding of the drug with DNA.[206] Intercalators introduce the strong structural perturbations in the DNA. The drugs that intercalate to DNA are used as anti-cancer drugs.[207] Furthermore, the most widely used intercalative binders are ethidium bromide, nogalamycin, etc.

1.5.1.2 Groove binding mode

In the DNA structure, there are two type of grooves, major and minor grooves. They are opposite to each other and run continuously along the whole length of the DNA because they arise by the antiparallel arrangement of both the strands. The major groove is wide and deep, whereas the minor groove is narrow and shallow. Details of major and minor grooves binding are given below:

1.5.1.2.1 Major-groove binding mode

Major-groove binding arises due to the hydrogen bonding between the DNA and drug molecule. This type of binding depends on the nitrogenous base pair sequence. The proteins mainly bind with this groove of the DNA after recognition and reading of the sequence information. However, some non-peptidyl compounds bind with the minor-groove allowing simultaneous major groove recognition by proteins. Hence, major groove binder blocks the binding of protein, which recognizes the same groove, and it has fundamental importance.[208]

1.5.1.2.2 Minor-groove binding mode

Minor groove binding includes greater binding affinity and higher sequence specificity than that of intercalative binding mode. This type of groove binding is mainly exhibited by the neutral and charged molecules. The driving forces behind this binding are electrostatic interactions, van der Waals forces, hydrophobic interactions and hydrogen bonding. It is a kind of spatial fitting of the drug in the targeted groove such that they are in maximum contact with each other for the best binding. The hydrogen bonding between the drug and DNA strands is responsible for the required sequence specificity in this type

of binding. Most of the minor groove binding drugs bind at the A/T rich sequences because A/T rich grooves have larger electrostatic potential, narrow and deeper dimension of groove site as compared to the G/C rich grooves. Apart from this, the topology at A/T sites allows easier filling and better van der Waals contacts by small drug molecules, while the amino group of G in G/C locations stick out into the groove, thus prohibiting van der Waals contacts as compared to the A/T sites.[206] Minor-groove binding molecules are the main current research concern for their pharmaceuticals, and biotechnology applications. Minor-groove binders can act as an inhibitor or activator for the transcription and gene expression, which is entirely new and great method for the treatment of particular diseases.[209] Minor-groove binders possess some special features such as positively charged species, bent shape or the ability to adopt a curved shape, H-bond donating ability, and a relatively flat conformation. The minor groove in A/T sequences can more easily take on the narrow width that is required for tight binding of the heterocyclic-amidine system of the dictions than the groove in G/C or mixed base pair sequences. The extra H-bond of the G/C base pairs typically leads to a wider minor groove and presents a steric block to the deep penetration of compounds into the groove.[210]

1.5.1.3 Covalent-cross linking binding mode

In this type of binding specific metal binds with the DNA by the coordination or recognition of specific binding site. The platinum metal complex is a most important example of this type of binding, in which cisplatin is a well-known anticancer drug and its show the covalent cross-linking binding mechanism. Due to the formation of covalent bond in the DNA after binding with the cisplatin, the separation of the two strands of DNA is blocked, which prevents the transcription of the DNA and synthesis of that particular protein. This mechanism causes mismatching of base pairs of the nucleotides leading to mutations.[211] The discovery of cisplatin lead in a new period of DNA-interactive anticancer agents based upon coordination chemistry.[212]

1.6 Fluorescence spectroscopy

In recent times, several sophisticated spectroscopic tools or techniques are applied for analytical applications. Out of them fluorescence spectroscopy is rapidly growing and is thus highly used for the last couples of decades due to its greater sensitivity and selectivity towards the microenvironment. Fluorescence spectroscopy has vast

applications in different fields such as biochemistry, biophysics, environmental sciences, nuclear chemistry, cell biology, forensic sciences, medical diagnostics etc. Nowadays, fluorescence spectroscopy has turned out to be a very potent technique in DNA sequencing, immunoassays, flow cytometry and genetic analysis.[213, 214] The extensive use of this spectroscopy is due to advances in time resolution, methods of data analysis, and improved instrumentation.

The fluorescence is a photophysical process of a molecule in the excited electronic state. When a molecule absorbs the light and goes to an electronically excited state, it comes back from completely relaxed excited state to the ground state by two mechanisms. First is a non-radiative de-excitation mechanism, in which, molecule comes to the ground state by loss of energy in the form of heat. The second is a radiative de-excitation mechanism, in which molecule comes to the ground state by emission of the photons. The radiative mechanism further can be of two types: if the excited molecule comes from the singlet-excited state to the ground state, then, it is called fluorescence and if the excited molecule comes from the triplet-excited state to the ground state, then, it is called phosphorescence. The fluorescencent photons have various informations at a given wavelength such as energy (wavenumber), intensity (number of photons), time and polarization. These fluorescencent photons provide information regarding the microenvironment of the fluorophore. Therefore, fluorescence intensity, wavelength, spectrum, polarization and their time dependence are the main parameters that can be used for the characterization of molecular systems.[214] The mechanisms for de-excitation process of electronically excited molecules to ground state are given by the Jablonski diagram demonstrated in Figure 1.10.[215]

The lowest electronic state is the most populated one at the room temperature that can be explained by Boltzmann distribution. S_o denotes the lowest singlet electronic ground state with multiplicity one. S_1 and S_2 represent the first and second singlet electronic excited states, respectively. After interacting with incident light of UV-range, the molecules undergo an electronic transition in ~ 10^{-15} seconds from the ground state (S_o) to a higher excited state (say S_2) accompanied by a vibrational transition. Molecule present in a higher vibrational level of the higher excited electronic state (say S_2) dissipates its excess vibrational energy as thermal energy and goes to zero vibrational level (v = 0) of the S_2 state. Generally, the energy gap between the higher electronic states is lesser than

the energy gap between S_1 state and S_o state. Therefore, the molecule reaches the S_1 state quickly by internal conversion (IC) or quantum mechanical tunneling, followed by vibrational relaxation to v = 0 level of the S_1 state. Here, if there is an overlap between the zero vibrational level of S_1 state and higher vibrational level of S_o state, then the molecule comes to the S_o state by internal conversion.

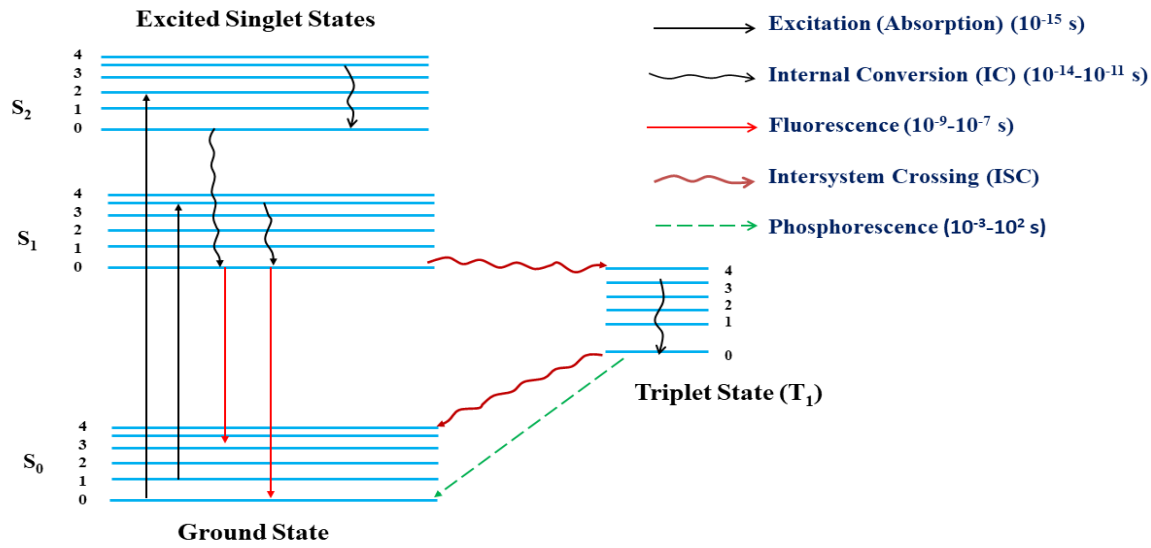

Figure 1.10. Fortunes of polyatomic molecules after photoexcitation presented by Jablonski diagram.

When the molecule gets de-excited through the release of its excitation energy as photon then this radiative deactivation process of the molecule from S_1 state to S_o state is known as fluorescence. However, there is also the possibility that the zero vibrational level of S_1 state couples with the higher vibrational levels of the triplet state say, T_1. In this situation, the molecule in the S_1 state undergoes a spin-conversion to the first triplet state T_1. This process is known as intersystem crossing (ISC). The molecule at the higher vibrational level of T_1 state rapidly losses its vibrational energy and reaches the v = 0 level of T_1 state. The molecule can also return from T_1 state to S_o state either by the non-radiative process, i.e. intersystem crossing or by radiative process i.e. phosphorescence. Since T_1 to the singlet ground state (S_o) transition is forbidden, hence, the rate constants for triplet emission are several orders of magnitude lesser than those of fluorescence. Both radiative processes leave the molecule to the Frank-Condon ground (FCG) state, from where molecule goes to zero vibrational level of S_o state by collisional deactivation process. Phosphorescence spectrometry lacks sensitivity when applied in a liquid solution at

ambient room temperature. Phosphorescence is observed either occasionally or with weak signal due to the forbidden (triplet-to-singlet transition) transition. Fluorescence is a fast process (in picoseconds to nanoseconds) as compared to the phosphorescence (in microseconds to milliseconds). Many factors affect the electronic spectrum of a molecule such as substituents, pH, nature of solvents and so forth, are discussed below:

1.6.1 Effect of the substituent on the fluorescent molecule

Absorption and fluorescence properties of the molecule are highly influenced by the substituents present on it. The peak maxima of absorption and fluorescence are shifted towards longer wavelength on enhancing the conjugation for example benzene, naphthalene, and anthracene. According to Kasha's rule fluorescence occurs if the $\pi \rightarrow \pi^*$ is the lowest energy transition, and phosphorescence is possible if $n \rightarrow \pi^*$ is the lowest energy transition.[216] Substitution of electron donating group on the benzene ring such as –OH, $-NH_2$, $-N(CH_3)_2$, causes the large red shift, but halogens reduce the fluorescence intensity as well as quantum yield due to the heavy atom effect on moving from top to bottom in the periodic table.[217] Substitution of the alkyl group on the aromatic ring has little effect, only small shifts in the absorption and fluorescence spectra towards the red. Alkyl side chain, as substituents, increases the vibrational degrees of freedom and thus increases internal conversion, consequently the fluorescence quantum yield decreases. Fluorescence quantum yield thus depends upon the rate of non-radiative processes with respect to the rate of the radiative process. Sometimes, the presence of heteroatom in the ring system increases the rate of non-radiative process, consequently fluorescence quantum yield decreases.[218]

1.6.2 Effect of solvents

The absorption and fluorescence spectra of the molecule are greatly influenced by the polarity of the solvent system in the aspect of peak position and intensity. Usually, an absorption and emission spectra of a probe are observed differently in different solvents like non polar, polar, aprotic, protic *etc.* because of both solute-solute and solute-solvent interactions. Thus, the spectral characteristics of the molecules depend on the nature of the solvent as well as on the solute. The effect of solvents on the spectral properties of the solute molecules is explained below:

1.6.2.1 Dispersive or general solvent interactions

These interactions are involved the electrostatic forces and the observed spectral shifts can be linked with the refractive index (n) and dielectric constant (ε) of the solvents. These interactions are of following types:

1.6.2.1.1 Dipole-Dipole interaction: Solute and solvent molecules have a permanent dipole moment.

1.6.2.1.2 Dipole-Induced dipole interaction: One molecule is having a permanent dipole moment that induces a dipole into the other.

1.6.2.1.3 Induced Dipole-Induced Dipole interaction (London Dispersion forces): Solute and solvent molecules do not have a permanent dipole moment.

These interactions are decreasing as follows: dipole-dipole > dipole-induced dipole > induced dipole-induced dipole.

1.6.2.2 Specific interactions

Hydrogen bonding and complex formation between solute and solvent are coming in the specific interactions. These interactions are comparatively stronger than the non-specific interaction between solute and solvent, which causes the drastic changes in absorption and fluorescence spectra of probe molecules. Electronic transitions can be divided into three different types, (i) $\pi \rightarrow \pi^*$, (ii) $n \rightarrow \pi^*$, and (iii) charge transfer. The interactions of solute with solvent are different in different transitions due to the different dipole moment. The hydrogen bonding changes the spectral characteristics of molecules largely. The hydrogen bonding properties between solvent and solute in the ground state are generally different from that in the first excited singlet state.

According to Frank-Condon principle, absorption of light is a too rapid process as compared to the period of nuclear motion and occurs within 10^{-15} s. At the instant of its formation of a Frank-Condon excited state (FCE) (Figure 1.11), the excited solute molecule is shortly surrounded by a solvent cage whose size and orientation is similar to those that are present in the ground state. The molecule, which is present in the FCE state gets relaxed vibrationally to the lowest vibrational level of the first excited singlet state within the time scale of 10^{-13} s. After the excitation and vibrational relaxation, the solvent cage reorganizes according to the new environment due to change in charge distribution

and thus the dipole moment upon excitation, within the time scale of 10^{-11} and 10^{-12} s. Therefore, this kind of solvent reorganization or reorientation is known as "solvent relaxation". The combination of all vibrational, solvent, and geometry relaxations is called thermal relaxation. By these processes, an equilibrium excited state is formed in which solvent configuration is optimal for the geometry and electron distribution of the excited molecule. Emission takes place from the equilibrium excited state to the metastable Frank-Condon ground (FCG) state. The molecule in the FCG state is still in the environments that are similar to the excited state due to rapid transition. Vibrational and solvent relaxation further bring it to equilibrium ground state. Since the thermally relaxed excited state is lower in energy than FCE state and FCG state is higher in energy than the thermally relaxed ground state, hence, fluorescence occurs at a longer wavelength than absorption. The loss of energy between absorption and fluorescence is known as Stokes-shift [($\bar{\upsilon}_{ab}$ - $\bar{\upsilon}_{fl}$), in cm^{-1}], where $\bar{\upsilon}_{ab}$ and $\bar{\upsilon}_{fl}$ signify the peak frequencies of absorption and fluorescence, respectively.

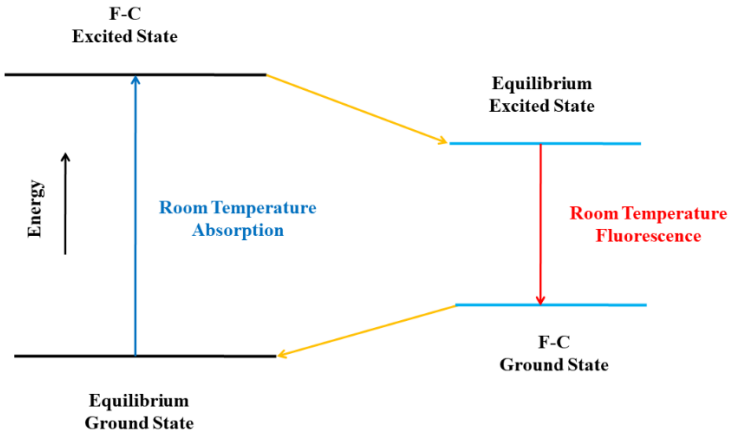

Figure 1.11. Demonstration of equilibrium and Frank-Condon (F-C) electronic states.

The n → π* transitions are weak and blue shifted in the protic solvents due to the de-excitation of the excited state. Whereas, both π → π* and charge transfer (CT) bands are strong, red shifted with an increase in the polarity of proton donor capacity of solvent. In the charge transfer transitions the solvatochromic shift is more prominent than π → π* transitions. These various types of transitions are differentiated by the molar extinction coefficient, and the effect of solvents on spectral characteristics and emission properties. Many reports are available which shows the linear dependence of the solvent polarity with the peak maxima of fluorescence that is correlated with solvatochromic plots.[219] However,

in some solvents, which have strong hydrogen bonding like water, alcohol, *etc.* deviation has been found from the linear correlation.[220, 221] The significant effect of hydrogen bonding in the solvent has been reported by Pimental,[222] Mataga *et al.*[223]. The effect of the solvents on the emission spectra of aromatic molecules was systematically explored by the Pringsheim[224] and Forster.[225]

Lippert[226], McRae[227] and Suppan[228] have estimated the quantitative treatment of the effect of solvents on the absorption and fluorescence spectra. Oshika[229], Lippert[226] and Mataga *et al.*[230] first derived the equations which represent the relation between variations in the dipole moments on excitation and spectral changes. Later on, these equations were modified by incorporating the polarizability of the fluorophores and dispersive interactions by Liptay[231], Bilot and Kawaski.[232] Again correction was made by the Lippert and Mataga in the equation by neglecting the polarizability effects of the fluorophore.[226, 230] The equation given by the Lippert-Mataga is extensively used to analyze the solvatochromic effect.[233-235] Lippert-Mataga equation is expressed by the Equation 1.3:

$$\left(\bar{\upsilon}_{ab} - \bar{\upsilon}_{fl}\right) = \left[\frac{2\left(\mu_e - \mu_g\right)^2}{hca^3}\right]\Delta f + \text{constant} \tag{1.3}$$

where Δf expressed by the following Equation 1.4:

$$\Delta f = \frac{(\varepsilon - 1)}{(2\varepsilon + 1)} - \frac{\left(n^2 - 1\right)}{\left(2n^2 + 1\right)} \tag{1.4}$$

Here, μ_g and μ_e are the ground state and excited state dipole moments of the fluorophore, respectively, and *h*, *c*, *a*, ε and *n* represent Planck's constant, velocity of light, Onsager cavity radius, the dielectric constant of a particular solvent, and the refractive index of a particular solvent, respectively. The excited state dipole moment of the fluorophore can be determined with the help of this equation. This equation is limited to the interaction of fluorophore in the nonpolar and polar aprotic solvents. However, the term polarity is loosely used to describe both types of interactions, specific as well as non-specific. Several polarity scales were established for the fluorescent molecules including all type of interactions. Various dyes are considered and studied for different polarity scales in the reports.[236] Reichardt's empirical scale of solvent polarity is one of them and named as $E_T(30)$. $E_T(30)$ scale includes approximately 360 solvents and is used for many compounds. This scale is analogous to Kosower's Z-values.[237, 238] $E_T(30)$ values are

estimated by the negatively solvatochromic pyridinium *N*-phenolate betaine dye (Figure 1.12) as probe molecule and defined as the molar electronic transition energies (E_T) of dissolved betaine dye, determined in kilocalories per mole (kcal mol^{-1}) at room temperature (25°C) and normal pressure (1 bar) using the following Equation 1.5:

$$E_T(30)(\text{kcal mol}^{-1}) = hc\bar{\upsilon}_{max} N_A = (2.8591\times10^{-3})\bar{\upsilon}_{max}(\text{cm}^{-1}) \quad (1.5)$$

$$= 28591/\lambda_{max}(\text{nm})$$

where $\bar{\upsilon}_{max}$ and λ_{max} signify the frequency of maximum absorption and wavelength of the maximum of the longest wavelength band, respectively. This is the intramolecular charge-transfer $\pi \rightarrow \pi^*$ absorption band of the dye. In the first report,[239] the betaine dye had by chance the formula number 30. Thus, the number 30 was added in order to avoid misperception with 'E_T', which is commonly used in photochemistry as an abbreviation for triplet energy. This betaine dye displays a remarkable high solvatochromic band shift. Its negatively solvatochromic, intramolecular charge transfer absorption band is blue shifted by 357 nm on moving from diphenyl ether (λ_{max} = 810 nm) to water (λ_{max} = 453 nm).[236]

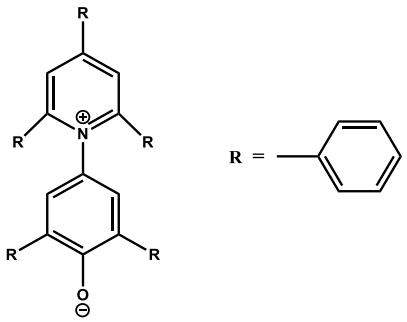

Figure 1.12. Structure of betaine dye.

1.6.3 Intramolecular charge transfer (ICT)/ twisted intramolecular charge transfer (TICT) in the context of Coumarin derivatives

Coumarin derivatives have been getting attention due to their emission in blue-green band.[240] The photophysical properties of coumarins are vastly dependent on the nature of substituents and solvents in which coumarins are present.[241, 242] 7-aminocoumarins are good examples of the ICT/TICT probes and the conversion in the different states of aminocoumarins can be explained by Scheme 1.1.[241]

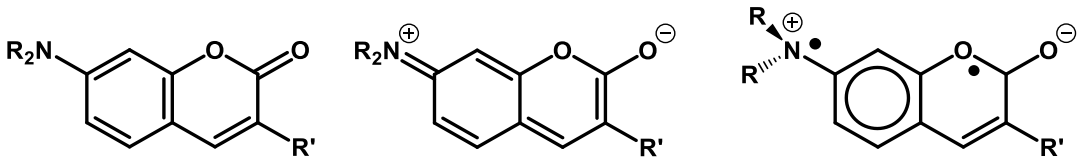

I II III
ICT TICT

Scheme 1.1: Different states of aminocoumarins.

The structure I represents the ground state of aminocoumarin. The Structure II resembles with the lowest excited state (S_1) which is mostly contributed by the polar ICT state with high value of dipole moment. Nature of the substituents influences the dipole moments of excited states. Later on, the polar ICT excited state converts to more polar TICT state (structure III) through a nonradiative rotatory decay mechanism.[243] In most of the cases the TICT excited state is non-fluorescent.[242] The fluorescent states of coumarin are ICT in character and follows the ICT→TICT ground state de-excitation pathway in highly polar solvents.[244, 245] The extent of formation and stabilization of TICT excited state are highly dependent on the polarity of the solvents and electron donating and electron withdrawing properties of the substituents present on it.[242, 243, 246] In the more polar solvents the non-radiative rotatory decay (ICT→ TICT) is very fast and forms the more stable TICT state as compared to the that of in less polar solvent[242] as shown in Figure 1.13. Viscosity can also disturb the rate of ICT→TICT conversion either by restricting the twisting motion or by enhancing the dielectric relaxation time.[247, 248]

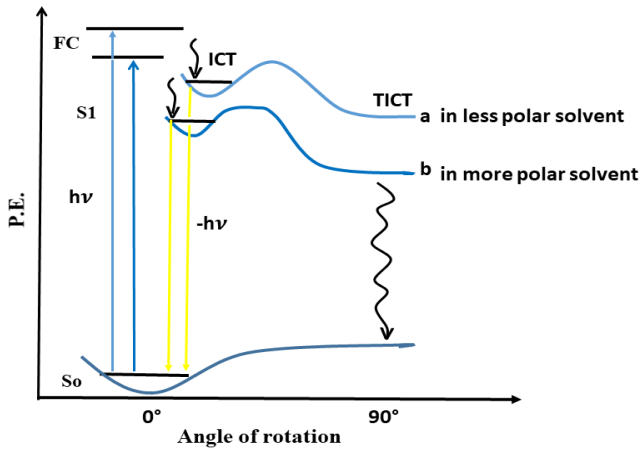

Figure 1.13. Potential energy surfaces for rotation at the amine function of coumarin, depicting a Franck-Condon (FC) transition, relaxation involving coordinates for solvation, and evolution of the planar emissive ICT to TICT state.

1.6.4 Fluorescence intensity decay and lifetime

Time-resolved fluorescence spectroscopic techniques provide the information about the kinetics of the various processes, which are involved in the deactivation of the excited state.[214] The fluorescence intensity decay is a plot of fluorescence intensity as a function of time. The single exponential fluorescence intensity decay, *I(t)*, for a system having single fluorescent species is expressed by the following Equation 1.6:[214]

$$I(t) = I_o e^{-t/\tau} \tag{1.6}$$

where, I_o and τ signify the initial intensity and fluorescence lifetime, respectively. If the studied system has more than one fluorescent species, then the fluorescence intensity decay has to be fitted with a multi-exponential function instead of a single exponential function. The fluorescence intensity decay of a multi-exponential function is given as follow:

$$I(t) = \sum_{i=1}^{n} a_i e^{-t/\tau_i} \tag{1.7}$$

where a_i and τ_i are ith pre-exponential factor and lifetime in the multiexponential decay, respectively. The average lifetime, $\langle \tau_f \rangle$, for the multiexponential decays is expressed by the Equation 1.8:

$$\langle \tau_f \rangle = \sum_i a_i \tau_i \tag{1.8}$$

The fluorescence lifetime is also related to the radiative and the nonradiative rates. The relations between the fluorescence quantum yield (ϕ) and rate constants, and fluorescence lifetime (τ) and ϕ are expressed by the Equations 1.9-1.11:

$$\phi = \frac{k_r}{k_r + k_{nr}} \tag{1.9}$$

$$\phi = \frac{1}{k_r + k_{nr}} \tag{1.10}$$

$$\phi = k_r \tau \tag{1.11}$$

where k_r and k_{nr} are the rate constants for radiative and non-radiative processes, respectively. The ratio of the number of photons emitted to the number of photons absorbed is expressed as fluorescence quantum yield (ϕ).

1.6.5 Fluorescence anisotropy

Some of the fluorophore molecules are preferentially excited when fluorophore molecules are exposed under the polarized light. The obtained fluorescence from the excited fluorophores is also polarized. The extent of polarization of the fluorescence emission is defined in terms of anisotropy (r). Fluorescence anisotropy measurements have been used to quantify protein denaturation and for measurement of dynamics of proteins. In the field of biochemical and biophysical research, the fluorescence anisotropy measurement is very important because very little change in microenvironment such as alteration in size, shape, or segmental flexibility of a molecule will also change the anisotropy.[249, 250] In the microheterogeneous environment, fluorescence anisotropy is useful to find out the probable location of the probe molecule.[214, 251] Saha *et al.* observed that the steady-state fluorescence anisotropy measurement is a good method to monitor the formation of premicellar aggregates of conventional and gemini surfactants.[252, 253]

1.6.5.1 Steady-state fluorescence anisotropy

The steady-state fluorescence anisotropy[213] is expressed by the Equation 1.12:

$$r = \frac{I_{VV} - GI_{VH}}{I_{VV} + 2GI_{VH}} \tag{1.12}$$

where I_{VV} and I_{VH} represent the fluorescence intensities obtained from the excitation polarizer oriented vertically and the emission polarizer oriented in vertical and horizontal orientations, respectively. G is the correction factor and is determined by the following Equation 1.13:

$$G = \frac{I_{HV}}{I_{HH}} \tag{1.13}$$

where I_{HV} and I_{HH} are fluorescence intensities obtained from the excitation polarizer oriented horizontally and the emission polarizer oriented vertically and horizontally, respectively.

1.6.5.2 Time-resolved fluorescence anisotropy (Rotational relaxation time)

In molecular assemblies, the time-dependent fluorescence anisotropy measurement provides further information about the rotational relaxation of the fluorophores. In the time domain, the sample is excited with a short pulse of polarized light and the time-dependent parallel $(I_{\parallel}(t))$ and perpendicular $(I_{\perp}(t))$ components of the fluorescence are used to form the time-resolved fluorescence anisotropy, *r(t)*:

$$r(t) = \frac{I_{\parallel}(t) - I_{\perp}(t)}{I_{\parallel}(t) + 2I_{\perp}(t)} \tag{1.14}$$

To compensate the polarization biased of the detection system and monochromator efficiency, the above equation is revised as Equation 1.15:

$$r(t) = \frac{I_{\parallel}(t) - GI_{\perp}(t)}{I_{\parallel}(t) + 2GI_{\perp}(t)} \tag{1.15}$$

where *G* expresses the correction factor for the detector sensitivity to the polarization detection of emission.

For a single isotropic rotor, *r(t)* decays with a single rotational correlation time (τ_r), defined by the following Equation:[213]

$$r(t) = r_o \exp\left(-\frac{t}{\tau_r}\right) \tag{1.16}$$

For the more complicated systems, *r(t)* becomes multi-exponential and given by the Equation:

$$r(t) = r_o \sum_i a_{ir} \exp\left(-\frac{t}{\tau_{ir}}\right) \tag{1.17}$$

where a_{ir} and τ_{ir} represent the fractional contribution of total depolarization and rotational correlation times attributed to reorientational motion *i*, respectively. r_o is the inherent anisotropy. The relation of τ_r with the medium is expressed by the Stoke-Einstein Equation:

$$\tau_r = \frac{\eta V}{kT} = \frac{1}{6D} \tag{1.18}$$

where η, V, k, T, and D represent the viscosity of the medium, molecular volume, Boltzmann's constant, absolute temperature and rotation diffusion coefficient, respectively.

1.6.6 Solvation dynamics

The dynamics of solvents and its influence on various chemical processes have great importance in the area of physical chemistry and biology.[254-256] The reorientation of the solvent dipoles around an immediately created solute dipole originating from photoexcitation is defined as solvation dynamics. The solvation dynamics study is now a renowned technique to get the idea about the response of the solvent molecule at the molecular level. A probe molecule whose dipole moment is approximately zero in the ground state and is increased to a large extent in the electronically excited state, gives solvent polarity dependent fluorescence emission spectra. An instant dipole can be created by exciting such a molecule with light radiation. In the ground state, the dipoles of polar solvent molecules are randomly oriented around the weakly polar probe molecule. Immediately after photoexcitation the polar solvent molecules stay randomly oriented around the dipole because the solvent relaxation process is very much slower compared to the photoexcitation process. Afterwards, the dipoles of polar solvent molecules reorient around the newly created dipole. The process of reorientation of dipoles of polar solvent molecules around the immediately created dipole after photoexcitation is known as solvation dynamics (Figure 1.14). The time taken for the solvent molecules ongoing from the Frank-Condon (F-C) excited state to relaxed excited state (R) is denoted as the average solvation time $<\tau_s>$. With increase in time, the energy of the dipole of the probe molecule decreases and the fluorescence maxima gets red shifted. This phenomenon is termed as time-dependent Stokes shift (TDSS).

Emission wavelength dependent decays are being collected in solvation dynamics process. At shorter wavelength, the most of the fluorescence decays are from the unsolvated dipole. At a longer wavelength, the time-resolved fluorescence spectra show a growth in the decay followed by a slow decay with a negative pre-exponential factor. Hence, the most fashionable evidence of solvation dynamics is TDSS and emission wavelength-dependent time-resolved fluorescence spectra (TRES). Time is required for the F-state molecules to reach the R state. Even if the F and R states have the same intrinsic decay time, the long-wavelength decay will appear to be slower.

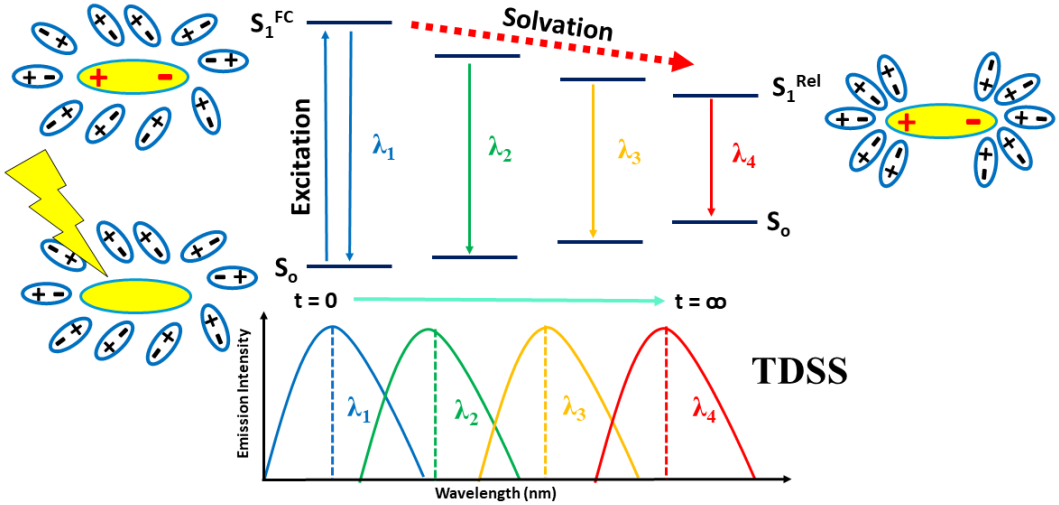

Figure 1.14. Schematic diagram showing the mechanism of solvation dynamics.

If the emission spectrum is observed immediately after excitation, then a blue-shifted or unrelaxed emission will be observed. If the time of observation is more, then large number of the molecules would have been relaxed to longer wavelengths, resulting in emission spectra being progressively shifted to longer wavelengths at longer times. These emission spectra representing discrete times following excitation are called the time-resolved emission spectra (TRES). The solvation dynamics is monitored by the decay of solvent correlation function *C(t)* and represented by Equation 1.19:

$$C(t) = \frac{\bar{\upsilon}(t) - \bar{\upsilon}(\infty)}{\bar{\upsilon}(0) - \bar{\upsilon}(\infty)} \qquad (1.19)$$

where, $\bar{\upsilon}(t)$, $\bar{\upsilon}(\infty)$ and $\bar{\upsilon}(0)$ are the peak wavenumbers in cm^{-1} at time t, infinity and zero, respectively acquired from TRES.

1.6.6.1 Coumarin as a probe for the study of solvation dynamics

As discussed above, a specific type of fluorescent molecules is required for the solvation dynamics study. Fluorescencent molecules should have nonpolar or weakly polar ground state and highly polar excited state. Mostly, 7-amino coumarin dyes have all these basic requirements and are used as a probe to explore the solvation study. Coumarins are the derivatives of 1,2-benzopyrone. Representative chemical structures of some coumarin derivatives are given in Scheme 1.2. Coumarins are well explored laser dyes, which emit a strong fluorescence with significant charge transfer (CT) character.[257, 258]

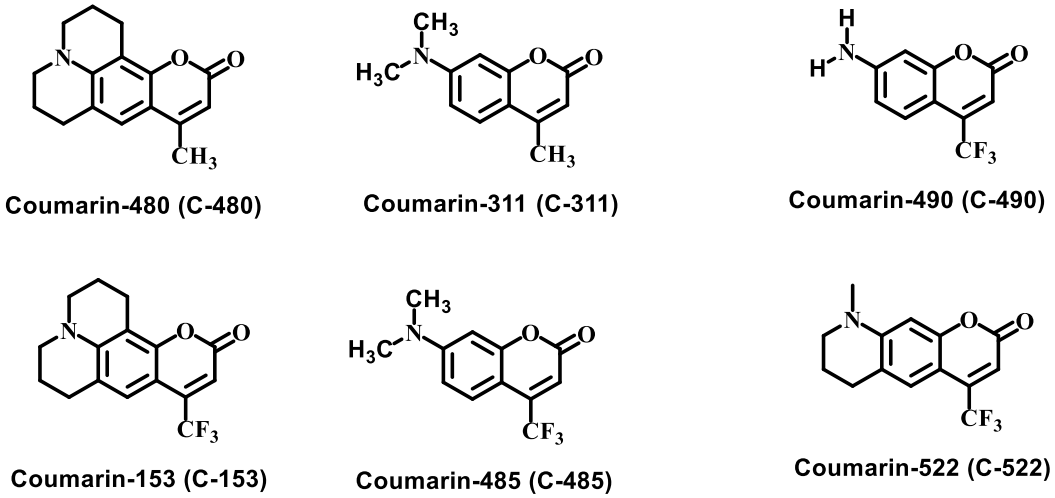

Scheme 1.2: Some derivatives of Coumarin.

Coumarin-480 is highly used as a solvation probe in the solvation dynamics studies. The reported ground state and excited state dipole moment for Coumarin-480 are 1.36 D and 4.17 D, respectively.[259] Furthermore, there is no report on the occurrence of any excited state reaction in most of the solvents. Due to such properties, Coumarins are used for solvation dynamics studies and structures of some Coumarins are given below:

1.7 Application of solvation dynamics and rotational relaxation

1.7.1 Solvation dynamics: In the context of biological water

Water is the most important lubricant of life. The biological water called "bound" water is different from the "free" bulk water in a number of ways.[260, 261] The dynamic exchange between the bound and the free water molecules is an important process from the biological point of view.[262] The dynamics of water molecules in the bulk is much different from that in biological systems.[260, 263-269] The study of dynamics in biological systems is important because it controls various processes in those systems.[270] Because of this importance, a substantial amount of work on the dynamics of water has been carried out in various confined media such as micelles,[111, 264, 271, 272] reverse micelles,[139, 273, 274] mixed micelles[275-278] and cyclodextrin[265, 279] those mimic the biological systems. Water molecules in these confined media behave as "free" and "bound" water molecules those are in dynamic exchange with each other.[261, 262] Various techniques like dielectric relaxation,[280] NMR relaxation dispersion[281] and time-dependent fluorescence Stokes' shift or solvation dynamics[214, 260, 282, 283] are available to study the properties of water molecules in these organized assemblies.[139, 264, 273,,271, 284-287,265-269, 277] Solvation dynamics is one of

the best techniques because of its high sensitivity towards time and length scale.[260,214, 282, 283] In most of the cases, the solvation dynamics has been studied by the time-dependent fluorescence Stokes' shift method.[260, 263, 264, 270, 271, 274, 284, 288]

Several techniques such as Fluorescence up-conversion[289, 290, 265, 291, 292] three-photon echo peak shift,[293, 294] and optical Kerr effect[295, 296] are applied to the study of the solvation dynamics using the probe molecule in the pure solvent systems but the fluorescence up-conversion technique is the best one and is mostly used to explore the solvation dynamics in the pure solvents. The solvation dynamics is faster in water as compared to the other polar solvents. Jimenez *et al*.[289] reported a Gaussian component of the time constant of less than 50 fs and a slower biexponential decay with a time constant 126 and 880 fs. The solvation dynamics was observed to be bimodal in nature for the probe 7-(dimethylamino) Coumarin-4-acetate with the time constants of 0.160 ps (33%) and 1.200 ps (67%) and for Coumarin-343 with time constants of 0.250 ps (50%) and 0.960 ps (50%) in the pure water.[297, 298] After that, Vajda *et al*.[265] also reported the bimodal nature of solvation dynamics of Coumarin-102 in water with solvation times as 0.310 ps (74%) and 50 ps (26%). The three-photon echo peak shift method was applied by the Fleming *et al*.[293] to determine the solvation time (30 fs). The observed solvation time constants are 0.180 ps (20%) and 1.1 ps (80%) for the amino acid, tryptophan in the pure water.[267] The solvent relaxation time of 1-anilinonapthalene-8-sulfonate is also bimodal in nature[299] with time constants as 0. 185 ps (22%) and 1.2 ps (78%).[300]

Apart from water, other pure solvents are also used to explore the solvation dynamics. The observed average solvation times were 0.28 ps, 6.2 ps and 8.3 ps for the Coumarin-153, Coumarin-152, and anionic Coumarin-343, respectively in the methanol.[301-303] Not only the Coumarins, but also some other probe molecules such as 2-(p-dimethylaminostyryl) pyridylmethyl iodide and 4-dicyanomethylene-2-methyl-6-(p-(dimethylamino) styryl)-4H-pyran are also used for the solvation dynamics study in the methanol.[304, 305] Acetonitrile is a frequently used solvent for the solvation dynamics study of the probes such as Coumarin-153, Coumarin-311, Coumarin-480, LDS-750, thiopyrilium dye, IR 1061, a cyanine dye, and IR 1048.[306-310] The rate of solvation is very fast in the pure solvent as compared to the rigid microheterogeneous systems.[304] Detailed methods of solvation dynamics study have been applied in Chapter 2 (Section 2.2.10)

1.7.2 Rotational relaxation or time-resolved anisotropy

Anisotropy deals with the depolarization of the fluorescence emission. The depolarization of the fluorophore happens due to the transfer of energy to the other molecule by the molecular rotation as a result of the Brownian motion. The molecular motion is directly related to the molecular confinement such as microviscosity and size of the fluorophore. Hence, the determination of the fluorescence anisotropy is helpful to get the deep idea about the location of the probe in the target environment by comparing the fluorometric properties in the bulk phase to the microheterogeneous phase. Sometimes this type of comparison is not effective because the conditions of the bulk phase analogs to the environments in the microheterogeneous system might be quite different. Time-resolved techniques, more proficient than steady-state measurements, gives intense knowledge about complex microheterogeneous systems. Depolarization of the fluorescence of probes is one of the most powerful techniques to reveal the dynamic behavior of the fluorophore in the complex microheterogeneous environments such as biological systems (proteins, lipids, DNA etc.) and mimicking systems (micelles, reverse micelles, cyclodextrin, etc.).[214, 276, 311-313] Dynamic behavior includes the rotational and/or tumbling motion of the bound fluorophore within the microheterogeneous environments on the picosecond/nanosecond timescale.[314] Development of pico- and femtosecond lasers has enabled the researchers to directly probe into the ultrafast relaxation processes in micellar environments by time-resolved fluorescence depolarization techniques or rotational relaxation process.[314-317] The time-dependent decay of the fluorescence anisotropy provides additional information about the rotational motion/rotational relaxation of the fluorophore in organized assemblies. The rotational relaxation dynamics of the probe is faster in bulk solvent as compared to the micellar environments. Detailed methods of rotational relexation study have been discussed in Chapter 2 (Section 2.2.11).

1.7.3 Solvation dynamics and rotational relaxation in microheterogeneous systems

Solvation dynamics and rotational relaxation have been studied in various microheterogeneous systems like micelles, mixed micelles, RMs, vesicles etc. These self-organized molecular assemblies have resemblance with biological lipid membranes. Solvation dynamics and rotational relaxation in these systems is found to be many folds slower than that in pure solvents. The bimodal nature of solvation dynamics has been reported in presence of ionic and nonionic conventional surfactants by Bhattacharyya e*t*

al.[264] which was explained by Bagchi *et al*. in presence of microheterogeneous systems.[262] They proposed a dynamic exchange model based on free and bound water molecules and the strength of the hydrogen bonds. According to dynamic exchange model, a dynamic equilibrium between the "free" and "bound" water molecules is responsible for the bimodal nature solvation dynamics. The slow component and fast component of solvation dynamics correspond to the bound water and free water, respectively. Maroncelli and co-workers observed very fast solvation process (< 1 ps) of bulk water with single solvation time using Coumarin-343 as a probe[318] and solvation processes of various solvents probing with number of Coumarins[289, 301, 319] Similarly, rotational relaxation of Coumarin-480 is reported as 125 ps in the pure water, which is very fast as compared to the rotational relaxation time in the micelles.[276] Bhattacharyya *et al.*[264] first reported that the solvation dynamics of water molecules at the Stern layer of micelles of conventional surfactants was much slower than that of ordinary bulk water. Free and bound water molecules contribute to the fast and slow components of solvation dynamics, respectively.[262] Hydrogen bonding interaction between the water molecules and surfactant headgroups is responsible for the slower component of solvation dynamics of water in the micelles.[320, 321] The bimodal behavior of solvation dynamics of water molecules in the micelles of surfactants[111, 264, 271, 278, 322] and even solvation dynamics with three solvation components in the amphiphilic starlike macromolecular (ASM) system are well studied.[323]

Sarkar *et al.* have studied the solvation dynamics and rotational relaxation in various systems e.g., micelles of Brij 35 and Brij 58,[272] CTAB micelles,[324] the mixed micelles of surfactants (TX-100, Tween 80 and CTAB) with bile salt,[275, 276] and also the mixed micelles of different cationic conventional surfactants,[277] and ionic liquids.[325] Samanta *et al.* have reported the dynamics of different types of Coumarins in various types of room temperature ionic liquids.[326, 327] Shirota *et al*.[328, 329] have demonstrated the effect of surfactant concentration and the effect of solvent isotope on the dynamics of Coumarin-102 and Coumarin-153. They have also reported the solvation dynamics in the micelles of cationic and anionic surfactants. They have found that the solvation dynamics in the aqueous micelles of anionic surfactant is slower than that in the aqueous micelles of the cationic surfactant. The slow solvation dynamics in anionic micelles as compared to that in cationic micelles is due to stronger hydrogen bonding interaction between the water molecule and headgroup in the former than that in the latter.

Recently it was established that added salts such as LiCl, KCl, NaCl and CsCl affect solvation dynamics and rotational relaxation of C-153 in Triton X-100 (TX-100) micellar medium. These added salts enhance the trapped water content in the palisade layer of micelles causing clustering of water molecules, which results in a slow solvation process. However, the clustering of the water molecules near to the ions will act in opposite to the increased micellar hydration to estimate the microviscosity and relaxation dynamics. All used salts influence the clustering of water slightly higher than that of the increased hydration, resulting in an effective increase in the microviscosity for the palisade layer, which reduced the rate of relaxation dynamics with the addition of salts.[330] Levinger *et al*.[331] have reported that as compared to NH_4^+ ion, Na^+ ion acting as a counterion of Aerosol-OT (AOT) reduces a large fraction of the water motion resulting in an increase in solvation time. These reports show that the clustering of water molecules induced by counterions or added salts has an effect on the solvation dynamics in the reverse micelles.

Bhattacharyya *et al*.[264, 332] investigated the solvation dynamics of C-480 and 4-aminopthalimide (4-AP) in the micelles of various types of conventional surfactants such as cetyltrimethylammonium bromide (CTAB), sodium dodecyl sulfate (SDS) and Triton X-100 (TX-100) and concluded that with different probe molecules solvation time remained the same in similar environment. Hazra *et al.*[333] have reported the solvation dynamics and rotational relaxation of Coumarin-153 (C-153) in SDS dispersed single-walled carbon nanotubes (SWNTs). They have found that the rates of both solvation and rotational relaxation processes become slower in this system as compared to bulk water.

Sarkar *et al.*[277] have noticed that both rotational relaxation and solvation times increase with increasing hydrocarbon tail length of conventional surfactants. This is happened because of increasing microviscosity of micelles with increasing tail length of surfactants as a result of the formation of more closely packed micelles. Earlier, the direct correlation between rotational relaxation time and microviscosity of micelles was observed by Maroncelli and co-workers.[334] The effect of the ionic liquid on the solvation dynamics as well as on the rotational relaxation of C-153 in the aqueous micelles of Triton X-100 has been studied by Sarkar and co-workers.[335] They have found that the presence of ionic liquid increases the microfluidity of micelles that causes faster solvation and rotational relaxation processes.

Studies have also been carried out by Sarkar *et al*.[336] to see the effect of tail length of ionic liquids on the rotational motions of C-153 and Rhodamine 6G (R6G) in micelles. It has been observed that the rotational relaxation process becomes slower in the micelles of C_{16}mimCl as compared to C_{12}mimCl ionic liquid as the rotational motions are more restricted in the former system due to the longer alkyl chain length. Also, in their another study they have seen the decrease in the rates of solvation and rotational relaxation processes in the neat micelles and microemulsions of each of ionic liquids, [C_2mim][C_4SO_4], [C_2mim][C_6SO_4] and [C_2mim][C_8SO_4].[337] Samanta and co-workers[338] have reported the effect of alkyl tail length on the rotational dynamics of polar and nonpolar solutes in a series of N-alkyl-N-methylmorpholinium ionic liquids. Studies have revealed the location of these probes in a distinct environment of the ionic liquids from their contrasting rotational dynamics.

Many techniques have been used to study the dynamics of water in the water-urea mixture. Infra-red pump-probe spectroscopy has been used to study the effect of urea on structure and dynamics of water and it was found that even at high concentration of urea, dynamics of water has not been altered.[339] Only a small fraction of water molecules displays slower dynamics than bulk water molecules by forming specific water-urea complex. Idrissi *et al*. have studied the short time dynamics of the water-urea mixture and the results have shown that addition of urea leads to an overall isotropy and stiffening of the short time dynamics of both the species. Many of these studies concentrated on the study of water dynamics in water-urea mixtures.[339, 340] Few reports are available on the study of urea dynamics as a function of urea concentration in water-urea mixture.[341, 342] Hazra *et al*. have studied the dynamics of water, urea and water-urea mixture inside the reverse micelles of anionic surfactant.[284] Chattopadhyay *et al.* have studied the effect of urea on the organization and dynamics of TX-100 micelles.[343] Ruiz *et al*. have studied the microenvironmental properties of sodium dodecyl sulfate in the aqueous urea solution.[344] Recently, Saha *et al*. studied the solvation dynamics in presence of mixed micelles of gemini surfactant and conventional surfactants.[278]

1.8 The scope of the present thesis work

Surfactants molecules are the flagship of surface and colloidal chemistry. Inspired by vast application of the surfactants in the biological, chemical, pharmaceutical, and industrial fields and each aspect of life, these surfactant systems still need to get insight,

which would be exciting fundament challenges. Change in the structure of the surfactant creates quite interesting changes in its surface activity as well. Micellar properties of a surfactant such as the critical micelle concentration (*cmc*), the degree of ionization (α), micelle size and microenvironment depend not only on the surfactant structure but also on types of counterions and their hydration.[345, 346] The formation of micelles of ionic surfactants is stabilized by the binding of the counterions to the headgroups of surfactant molecules.[347] The binding ability of an inorganic counterion depends upon its size and valency.[98] Micellar behavior depends on the hydrophobic nature of counterions as well.[104] The interaction of inorganic counterions with the micellar surface is influenced by the hydration diameter of the ions (smaller hydrated ions favor their interactions). But, for quaternary ammonium counterions, it depends on the hydrocarbon exterior (more hydrophobicity is more effective in micellization).[105]

Various properties of gemini surfactants depend on various parts of surfactants such as hydrophobic tails, hydrophilic headgroups, counterions and spacer groups.[21, 23, 24, 348-351] Spacer groups and hydrophobic tail length play a very important role in the aggregation behavior of gemini surfactants. Studies with gemini surfactants with rigid, flexible, hydrophilic or hydrophobic spacer groups have been investigated well.[19, 112, 352] The micelles of surfactant and gemini surfactants mimic biological systems such as lipid bilayer membrane and have applications in the synthesis of nanoparticles, food industries, cosmetic industries and most importantly in pharmaceuticals industries. A detailed study on the aggregation behavior of the synthesized gemini surfactants is very important. The spacer group and hydrophobic tail of the gemini surfactant plays a very crucial role in the micellar behavior.

Apart from this, an effort has been made to get complete information about the physicochemical properties of gemini surfactant in the presence of an additive such as urea keeping in view of the aim that the urea disturb the water structure. Urea, a well-known protein denaturant, increases the critical micellar concentration (*cmc*) values of surfactants,[343, 353, 354] and reduces the aggregation number of micelles.[355, 356] Presence of urea increases the solubility of the surfactant, resulting in delaying the micellization process. Urea and surfactant mixtures are used in the field of membrane-protein research.[357, 358] Presence of urea in water affects the hydrogen bonding of water structure. Two different types of mechanisms are proposed to explain the effect of urea on the water structure. To comprehend the properties of the urea-water system many studies have been

carried out and according to them urea acts as water "structure breaker"[359, 360] or water "structure maker".[361, 362] whereas some studies show the combined effect.[363, 364]

After being inspired by above-made discussions, the motive of the first part of the present thesis work is to provide details about how the features of surfactant, as well as the presence of additives in the aqueous micelles, influence the solvation dynamics of Coumarin-485. In the second part, gemini surfactant induced denaturation of the protein followed by renaturation by appropriate refolding agents have been discussed. Lastly, in third part, gemini surfactant and cyclodextrin-based controlled drug releasing systems have been developed and its application in the interaction of the drug with DNA after being released from the carrier system has been highlighted. With the application of fluorescence to investigate problems at the forefront of biochemistry and pharmaceutical fields, this work is intended to fill the void and yet provide sufficient details to the experts to keep abreast of recent developments in such areas. To accomplish these objectives, the present work has been distributed in four chapters (Chapter 3, 4, 5, and 6), which are preceded by a detailed introduction (Chapter 1) and experimental (Chapter 2) including materials, methods, and instrumentation, employed to carry out the study with above discussed motives. The brief discussion of each chapter is as given below:

Chapter 3 deals with the studies of solvation dynamics and rotational relaxation of Coumarin 480 in the aqueous micelles of surfactant, which are influenced by the chemical structure of the surfactant and presence of an additive, urea. This chapter has three parts, Chapter 3a, Chapter 3b, and Chapter 3c.

Water is a very important part of all biological systems. In these systems, water may exist in free and bound states.[260] The dynamic exchange between the bound and the free water molecules is an important process from the biological point of view.[262] The study of water dynamics in organized assemblies possesses immense significance. It is known that the properties of solvent surrounding the reactants present in different biological systems and biomimicking organized assemblies significantly control various chemical reactions, such as charge transfer, electron transfer, etc.[365] Thus, the study of the physicochemical properties of a confined medium surrounding probe molecules needs to be carried out to understand and control various processes. The study of solvation dynamics provides us with information regarding the behavior of water molecules surrounding probe molecules, giving in-depth knowledge about the microenvironment. Pure water exhibits very fast solvation dynamics. In organized assemblies, solvation

dynamics get retarded with many folds compared to that in the bulk.[260] The values of anisotropy and time-resolved fluorescence anisotropy provide the deep information about the microheterogeneous systems such as micelles, reverse micelles, proteins, DNA, which would be helpful to understand the real biological microenvironment around the fluorescent molecule.

Chapter 3a describes the effect of counterions (NO_3^-, Br^-, SO_4^{2-}, and *p*-TS^-) on the solvation dynamics and rotational relaxation of the C-480 molecule in aqueous micelles of hexadecyltrimethylammonium surfactant. The increasing order of rate of solvation is $C_{16}TABr < C_{16}TANO_3 < (C_{16}TA)_2SO_4 < C_{16}TA$*p*-TS. The order for solvation time is similar to the order for *cmc*. SO_4^{2-} ions behave differently than from the monovalent ions. Effectively the solvation process is controlled by the extent of release of water molecules during the formation of micelles. The release of water molecules during the formation of micelles depends on effective binding of counterions to the headgroups. *p*-TS^- ions are more tightly bound to the headgroups because of the added effect of its hydrophobic part. Counterions can indirectly contribute to the slow solvation by causing clustering of water molecules. The decreasing order of average rotational relaxation time of C-480 in the micelles of surfactants is $C_{16}TA$*p*-TS >> $C_{16}TABr > C_{16}TANO_3 > (C_{16}TA)_2SO_4$ which is same as the decreasing order of microviscosity. It is expected that the solvation dynamics and rotational relaxation would be dependent upon the binding ability of these counterions to the micelles due to the difference between their sizes, valencies, and hydrophobicities**.**

Chapter 3b describes the effect of hydrophobicity of tails and hydrophilicity of the spacer group of gemini surfactants on the rates of solvation dynamics and rotational relaxation of C-480 in micelles of diethyl ether spacer group containing gemini surfactants with varying hydrocarbon tail lengths, C_{12}, C_{14} and C_{16}. We have also compared our present dynamics data with that in the micelles of gemini surfactant containing C_{12} tails and tetramethylene spacer group studied earlier. Micelles become gradually more compact with increasing hydrocarbon tail length which results in the lesser extent of penetration of water molecules thereby increasing microviscosity of micelles. Stern layer of micelles and water molecules become gradually more rigid with increasing compactness of micelles. Micelles with hydrophilic spacer group are more compact as compared to the hydrophobic spacer. Moreover, the hydrophilic spacer group gets easily hydrated. Therefore, the microviscosity of micelles of a gemini surfactant with hydrophobic spacer group is lower as compared to hydrophilic spacer group. The extent of free water molecules at the Stern

layer of micelles control the rate of solvation dynamics. The rate of rotational relaxation process is also affected by hydrocarbon tail length of surfactants as a result of the change in microviscosity of micelles.

Chapter 3c investigates the effect of urea concentration on aggregation properties of gemini surfactants with different spacer groups (with and without –OH group(s)) and also its effect on solvation dynamics and rotational relaxation of C-480 in aqueous micelles of those surfactants. Urea reduces the hydrophobic interactions between surfactant molecules and disfavors the formation of micelles. Average solvation time increases reaching a maximum and then decreases with increasing concentration of urea. It has also been noticed that the degree of counterion dissociation also follows the same trend. With increasing concentration of free counterions, the extent of clustering of water molecules is expected to increase resulting in longer solvation times. Thus the rate of solvation process can be correlated with the degree of counterion dissociation. The presence of –OH group in the spacer group has an effect on the rate of solvation process. The microviscosity of micelles decreases with increasing concentration of urea as a result of which its rotational relaxation process becomes faster. At a given concentration of urea, the rotational relaxation process slows down with the introduction of –OH group in the spacer group due to enhanced microviscosity of micelles. Results of the present study could be useful to understand the water dynamics in biological systems in presence of urea. Seeing the importance of gemini surfactants over conventional surfactants and urea in the protein denaturation process, it would be valuable to study the effect of urea on solvation dynamics and rotational relaxation in aqueous micelles of gemini surfactant.

Chapter 4 describes the binding interaction of the protein, bovine serum albumin (BSA), with the gemini surfactants, 12-*n*-12 with varying number of $–CH_2-$ group (n = 3, 6, 8, 12) in the spacer. Since proteins are important molecules and are involved in all life processes, hence, the studies have been done to get knowledge about the role of the spacer group of the gemini surfactant on unfolding as well as on refolding of unfolded BSA by gemini surfactant. The unfolding of BSA using the surfactants are well explored but a study using gemini surfactants especially the effect of the spacer group is not explored much. Moreover, we have worked on refolding of denatured protein by using cationic gemini surfactant with capturing agents such as cyclodextrin (hydrophobic interaction between the cavity of CD and tail of surfactant) and anionic sodium dodecyl sulfate (SDS) (driving force is the formation of mixed micelles i.e. catanion). Gemini surfactant is a very effective denaturing agent for protein at the very low concentration. Renaturation of any

proteins has great importance in the aspect of proteins engineering. Protein has to adopt specific 3D conformation to perform a certain function. A slight change in the protein structure will affect the functionality of protein that causes some serious neurodegenerative diseases such as Alzheimer, Perkinson etc. in humans. The refolding of protein using the formation of catanion approach is a new method. Catanion forms the vesicle type structure, which can be further explored as a carrier system for the protein itself. Refolding of the proteins using an artificial chaperon method is widely used in protein refolding process but the present method is somehow different from that chaperone method. In the artificial chaperon method, some external denaturation agents such as guanidinium hydrochloride, temperature have been used and after the dilution of this solution, surfactants have been added to prevent the aggregation of the denatured protein. To strip off the surfactant from this solution cyclodextrin has been added in the last step. But in the present method, gemini surfactant itself do the denaturation as well as the prevention of the aggregation of protein, which stripped off by cyclodextrin as well as an anionic surfactant. Therefore, this refolding approach can be applied in the proper refolding (active protein) of the misfolded or aggregated protein. Apart from this, we have noticed the role of the spacer group of gemini surfactants on the unfolding as well as refolding of BSA which is a new rising area of research, and useful to understand the effect of hydrophobicity of the spacer on BSA-surfactant interaction, surfactant-cyclodextrin, and cationic-anionic surfactant interactions.

Chapter 5 deals with the interactions of the gemini surfactants with the nanotubes of the β-CD. Guest molecules, C-485 induce the formation of nanotubes of β-CD and secondary aggregates of nanotubes of CDs. Gemini surfactants are used as a releasing agent for the guest molecule due to the more favorable interactions in between CD and surfactant as compared to the interaction between guest and CD. Currently, research is focused on that how to get control over the toxicity of the drug itself, if it reaches in excess at the target site because most used drugs are organic/inorganic in nature and have some toxicity for the biological system. To overcome this toxicity problem of the drug itself, the controlled releasing system of the drug has been developing rapidly.[366-368] Keeping this problem in mind, we have designed new β-CD based drug carrier system, which releases the guest molecule (that can be a drug) by the gemini surfactants. We can control the releasing capacity of the of gemini surfactant by using different spacer chain length of gemini surfactant in the context of time as well as the concentration. The effectiveness of any drug carrier also depends on many factors such as: the site where the drug has to be

release, which stimuli are responsive to releases, how long drug has to be released. Generally, stimuli to release the drug can be exogenous (thermoresponsive, magnetically responsive, ultrasound triggered, photoresponsive, electroresponsive etc.) or endogenous (pH-sensitive systems, enzyme sensitive systems, redox-sensitive systems etc), but how is the body of individuals respond to these stimuli also creates some hurdles to use these system in *in vitro* and *in vivo* condition. Moreover, sometimes in pharmaceutical process reproducibility and modification in the drug itself could happen that will affect the safety and quality of the drug. CDs are well known and widely applicable in the drug delivery system due to the complex formation with the variety of guest molecules. Therefore, the present system can be applied to develop an effective drug delivery system.

Chapter 6 explores the binding interaction of the C-485 with ctDNA after being released from the cavity of a nanotube of *β*-CD. The mode of binding of the drug with DNA is a key factor for targeting the DNA with therapeutic drugs or fluorophores.[369] C-485 bind with the DNA in the groove binding mode, which has been confirmed by the ethidium bromide displacement experiment. The tail length of gemini surfactant controls the release of the C-485 from the cavity. Gemini surfactants also interact with the ctDNA that causes the compaction and decompaction of the DNA molecule by the electrostatic interaction between the positively charged head group of surfactants and negatively charged phosphate backbone of DNA. Decompaction/compaction of DNA can be further used to carry the gene through the cell membrane. The main goal of this part of the thesis is to develop novel drug carrier system and the controlled release of drug using gemini surfactants by studying the drug-DNA interaction with the help of spectroscopic tools. The study of drug and DNA interactions is important for targeting antifungal, antiviral, antibacterial, and antitumor drugs in fields of science such as life, medicine, and chemistry. Observation of the drug DNA interaction using a fluorescent molecule, that can be a drug, leads to drugs development field of pharmaceutics. The release of the drug is also stimuli free. Therefore, the system can be effectively used to carry and release the drug in biomedical science.

References

1. I. Kralova and J. Sjöblom, *J. Disper. Sci. Technol.*, 2009, **30**, 1363-1383.
2. M. Exner and H. Färber, *Environ. Sci. Pollut. Res.*, 2006, **13**, 299-307.
3. J. Zeng, X. Xu, X. Chen, Q. Liang, X. Bian, L. Yang and X. Jing, *J. Control. Release*, 2003, **92**, 227-231.

4. F. Devinsky, Ľ. Masárová and I. Lacko, *J. Colloid Interface Sci.*, 1985, **105**, 235-239.
5. D. V. Moreno, Z. S. Ferrera and J. J. S. Rodríguez, *J. Chromatogr. A*, 2006, **1104**, 11-17.
6. I. M. Banat, *Bioresour. Technol.*, 1995, **51**, 1-12.
7. N. R. Jana, L. Gearheart and C. J. Murphy, *Adv. Mater*, 2001, **13**, 1389-1393.
8. C. M. Dvoracek, G. Sukhonosova, M. J. Benedik and J. C. Grunlan, *Langmuir*, 2009, **25**, 10322-10328.
9. V. P. Torchilin, *J. Control. Release*, 2001, **73**, 137-172.
10. A. N. Lukyanov and V. P. Torchilin, *Adv. Drug Deliv. Rev.*, 2004, **56**, 1273-1289.
11. A. Singh, J. D. Van Hamme and O. P. Ward, *Biotechnol. Adv.*, 2007, **25**, 99-121.
12. C. O. Rangel-Yagui, A. Pessoa Jr and L. C. Tavares, *J. Pharm. Pharm. Sci*, 2005, **8**, 147-163.
13. A. J. Kirby, P. Camilleri, J. B. Engberts, M. C. Feiters, R. J. Nolte, O. Söderman, M. Bergsma, P. C. Bell, M. L. Fielden and C. L. García Rodríguez, *Angew. Chem. Int. Edit.*, 2003, **42**, 1448-1457.
14. B. Kronberg, K. Holmberg and B. Lindman, *Surface chemistry of surfactants and polymers*, John Wiley & Sons, 2014.
15. A. Ali, M. Tariq, R. Patel and F. A. Ittoo, *Colloid Polym. Sci.*, 2008, **286**, 183-190.
16. W. Zhang, X. Dai, Y. Zhao, X. Lu and P. Gao, *Langmuir*, 2009, **25**, 2363-2368.
17. F. M. Menger and C. Littau, *J. Am. Chem. Soc.*, 1991, **113**, 1451-1452.
18. R. Zana and Y. Talmon, *Nature*, 1993, **362**, 228.
19. F. M. Menger and J. S. Keiper, *Angew. Chem. Int. Edit.*, 2000, **39**, 1906-1920.
20. R. Zana, *Adv. Colloid Interface Sci.*, 2002, **97**, 205-253.
21. P. X. Li, C. C. Dong, R. K. Thomas, J. Penfold and Y. Wang, *Langmuir*, 2011, **27**, 2575-2586.
22. M. Borse, V. Sharma, V. Aswal, P. Goyal and S. Devi, *J. Colloid Interface Sci.*, 2005, **284**, 282-288.
23. S. Manet, Y. Karpichev, D. Bassani, R. Kiagus-Ahmad and R. Oda, *Langmuir*, 2010, **26**, 10645-10656.
24. X. Wang, J. Wang, Y. Wang, H. Yan, P. Li and R. K. Thomas, *Langmuir*, 2004, **20**, 53-56.
25. C. A. Bunton, L. B. Robinson, J. Schaak and M. Stam, *J. Org.Chem.*, 1971, **36**, 2346-2350.

26. Y. p. Zhu, A. Masuyama and M. Okahara, *J. Am. Oil Chem. Soc.*, 1991, **68**, 268-271.
27. Y.-P. Zhu, A. Masuyama, Y. Kobata, Y. Nakatsuji, M. Okahara and M. J. Rose, *J. Colloid Interface Sci.*, 1993, **158**, 40-45.
28. M. J. Castro, J. Kovensky and A. Fernández Cirelli, *Langmuir*, 2002, **18**, 2477-2482.
29. A. Pinazo, X. Wen, L. Pérez, M.-R. Infante and E. I. Franses, *Langmuir*, 1999, **15**, 3134-3142.
30. J. Eastoe, P. Rogueda, A. M. Howe, A. R. Pitt and R. K. Heenan, *Langmuir*, 1996, **12**, 2701-2705.
31. M. Johnsson, A. Wagenaar, M. C. Stuart and J. B. Engberts, *Langmuir*, 2003, **19**, 4609-4618.
32. F. Menger, J. Keiper and V. Azov, *Langmuir*, 2000, **16**, 2062-2067.
33. E. Alami, K. Holmberg and J. Eastoe, *J. Colloid Interface Sci.*, 2002, **247**, 447-455.
34. D. Jurašin, I. Habuš and N. Filipović-Vinceković, *Colloids Surf. A Physicochem. Eng. Asp.*, 2010, **368**, 119-128.
35. R. Zana, M. Benrraou and R. Rueff, *Langmuir*, 1991, **7**, 1072-1075.
36. R. Zana, *J. Colloid Interface Sci.*, 2002, **246**, 182-190.
37. F. M. Menger and V. A. Migulin, *J. Org. Chem.*, 1999, **64**, 8916-8921.
38. F. M. Menger and B. N. Mbadugha, *J. Am. Chem. Soc.*, 2001, **123**, 875-885.
39. L. D. Song and M. J. Rosen, *Langmuir*, 1996, **12**, 1149-1153.
40. J. H. Mathias, M. J. Rosen and L. Davenport, *Langmuir*, 2001, **17**, 6148-6154.
41. R. Oda, S. J. Candau and I. Huc, *Chem. Commun.*, 1997, 2105-2106.
42. R. Oda, I. Huc, M. Schmutz, S. Candau and F. MacKintosh, *Nature*, 1999, **399**, 566.
43. M. Johnsson, A. Wagenaar and J. B. Engberts, *J. Am. Chem. Soc.*, 2003, **125**, 757-760.
44. A. Bhadani, R. G. Shrestha, S. Koura, T. Endo, K. Sakai, M. Abe and H. Sakai, *Colloids Surf. A Physicochem.Eng. Asp.*, 2014, **461**, 258-266.
45. Y. Li, X. Wang and Y. Wang, *J. Phys. Chem. B*, 2006, **110**, 8499-8505.
46. X. Wu, J. Zhao, E. Li and W. Zou, *Colloid Poly. Sci.*, 2011, **289**, 1025-1034.
47. G. Liu, D. Gu, H. Liu, W. Ding and Z. Li, *J. Colloid Interface Sci.*, 2011, **358**, 521-526.

48. S. Zhu, L. Liu and F. Cheng, *J. Surfactants Deterg.*, 2011, **14**, 221-225.
49. M. S. Bakshi and K. Singh, *J. Colloid Interface Sci.*, 2005, **287**, 288-297.
50. R. Oda, I. Huc, J.-C. Homo, B. Heinrich, M. Schmutz and S. Candau, *Langmuir*, 1999, **15**, 2384-2390.
51. J. Łuczyński, R. Frąckowiak, A. Włoch, H. Kleszczyńska and S. Witek, *Cell. Mol. Bio.Lett.*, 2013, **18**, 89.
52. B. C. Stephenson, C. O. Rangel-Yagui, A. P. Junior, L. C. Tavares, K. Beers and D. Blankschtein, *Langmuir*, 2006, **22**, 1514-1525.
53. K. Sakai, E. Nakajima, Y. Takamatsu, S. C. Sharma, K. Torigoe, T. Yoshimura, K. Esumi, H. Sakai and M. Abe, *J. Oleo Sci.*, 2008, **57**, 423-429.
54. E. Obłąk, A. Gamian, R. Adamski and S. Ułaszewski, *Cell. Mol. Bio. Lett.*, 2010, **15**, 215.
55. M. Macian, J. Seguer, M. R. Infante, C. Selve and M. P. Vinardell, *Toxicology*, 1996, **106**, 1-9.
56. N. Azum, M. A. Rub, A. M. Asiri, A. A. P. Khan and A. Khan, *J. Surfactants Deterg.*, 2013, **16**, 77-84.
57. V. I. Martín, P. López-Cornejo, M. López-López, D. Blanco-Arévalo, A. J. Moreno-Vargas, M. Angulo, A. Laschewsky and M. L. Moyá, *Arab. J. Chem.*, 2018.
58. S. M. Shortall and S. D. Wettig, *J. Phys. Chem. B*, 2017, **122**, 194-199.
59. Sonu, S. Halder, S. Kumari, R. Aggrawal, V. K. Aswal and S. K. Saha, *J. Mol. Liq.*, 2017, **243**, 369-379.
60. J. Łuczak, C. Jungnickel, M. Markiewicz and J. Hupka, *J. Phys. Chem. B*, 2013, **117**, 5653-5658.
61. S. Yan, Z. Gao, Y. Xia, X. Liao, J. Han, C. Pan, Y. Zhang and W. Zhai, *Eur. J. Inorg. Chem.*, 2018, **2018**, 1891-1901.
62. Y. Moroi, *Micelles: theoretical and applied aspects*, Springer Science & Business Media, 1992.
63. L. L. Schramm, *Surfactants: fundamentals and applications in the petroleum industry*, Cambridge University Press, 2000.
64. P. Mukerjee and K. J. Mysels, *Critical micelle concentrations of aqueous surfactant systems*, National Standard reference data system, 1971.
65. G. Hartley, B. Collie and C. Samis, *Trans. Faraday Soc.*, 1936, **32**, 795-815.
66. M. D. Garcia and A. Sanz-Medel, *Talanta*, 1986, **33**, 255-264.

67. K. Kalyanasundaram, *Photochemistry in microheterogeneous systems*, Elsevier, 2012.
68. H. Tartar, *J. Phys. Chem.*, 1955, **59**, 1195-1199.
69. F. Menger, H. Yoshinaga, K. Venkatasubban and A. Das, *J. Org. Chem.*, 1981, **46**, 415-419.
70. P. Goyal and V. Aswal, *Curr. Sci.*, 2001, **80**, 972-979.
71. J. N. Israelachvili, D. J. Mitchell and B. W. Ninham, *J. Chem. Soc. Faraday Trans. 2 Mol. Chem. Phys.*, 1976, **72**, 1525-1568.
72. Y.-p. Zhu, A. Masuyama and M. Okahara, *J. Am. Oil Chem.*, 1990, **67**, 459-463.
73. Y. p. Zhu, A. Masuyama, Y. i. Kirito and M. Okahara, *J. Am. Oil Chem.*, 1991, **68**, 539-543.
74. Y. p. Zhu, A. Masuyama, Y. i. Kirito, M. Okahara and M. J. Rosen, *J. Am. Oil Chem. Soc.*, 1992, **69**, 626-632.
75. D. Attwood and A. Florence, *Chapman and Hall, London*, 1985.
76. T. Lu, F. Han, G. Mao, G. Lin, J. Huang, X. Huang, Y. Wang and H. Fu, *Langmuir*, 2007, **23**, 2932-2936.
77. X. Huang, Y. Han, Y. Wang, M. Cao and Y. Wang, *Colloids Surf. A Physicochem. Eng. Asp.*, 2008, **325**, 26-32.
78. Y. Han and Y. Wang, *Phys. Chem. Chem. Phys.*, 2011, **13**, 1939-1956.
79. M. J. Rosen and J. T. Kunjappu, *Surfactants and interfacial phenomena*, John Wiley & Sons, 2012.
80. R. Zana and J. Xia, *Gemini surfactants: synthesis, interfacial and solution-phase behavior, and applications*, CRC Press, 2003.
81. M. H. Alimohammadi, S. Javadian, H. Gharibi, A. reza Tehrani-Bagha, M. R. Alavijeh and K. Kakaei, *J. Chem. Thermodyn.*, 2012, **44**, 107-115.
82. S. Wettig and R. Verrall, *J. Colloid Interface Sci.*, 2001, **235**, 310-316.
83. R. Oda, I. Huc, D. Danino and Y. Talmon, *Langmuir*, 2000, **16**, 9759-9769.
84. A. Goldsipe and D. Blankschtein, *Langmuir*, 2005, **21**, 9850-9865.
85. B. Lindman and H. Wennerstrom, *Micelles Amphiphile Aggregation in Aqueous Solution. Springer Verlag, Heidelberg*, 1980, 1-83.
86. S. Berr, R. R. Jones and J. S. Johnson Jr, *J. Phys. Chem.*, 1992, **96**, 5611-5614.
87. G. Porte, J. Appell and Y. Poggi, *J. Phys. Chem.*, 1980, **84**, 3105-3110.
88. K. Bijma and J. B. Engberts, *Langmuir*, 1997, **13**, 4843-4849.
89. M. Almgren and S. Swarup, *J. Phys. Chem.*, 1983, **87**, 876-881.

90. S. Puvvada and D. Blankschtein, *J. Phys. Chem.*, 1992, **96**, 5567-5579.
91. P. Parekh, D. Varade, J. Parikh and P. Bahadur, *Colloids Surf. A Physicochem. Eng. Asp.*, 2011, **385**, 111-120.
92. P. Jungwirth and B. Winter, *Annu. Rev. Phys. Chem.*, 2008, **59**, 343-366.
93. F. Hofmeister, *Arch. Exp. Pathol. Pharmacol.*, 1888, **24**, 247-260.
94. Z. Yang, *J. Biotechno.*, 2009, **144**, 12-22.
95. W. J. Xie and Y. Q. Gao, *J. Phys. Chem. Lett.*, 2013, **4**, 4247-4252.
96. Y. Marcus, *Chem. Rev.*, 2009, **109**, 1346-1370.
97. T.-M. Chang and L. X. Dang, *Chem. Rev.*, 2006, **106**, 1305-1322.
98. N. Jiang, P. Li, Y. Wang, J. Wang, H. Yan and R. K. Thomas, *J. Colloid Interface Sci.*, 2005, **286**, 755-760.
99. N. Jiang, P. Li, Y. Wang, J. Wang, H. Yan and R. K. Thomas, *J. Phys. Chem. B*, 2004, **108**, 15385-15391.
100. G. Biresaw, D. C. McKenzie, C. A. Bunton and D. F. Nicoli, *J. Phys. Chem.*, 1985, **89**, 5144-5146.
101. D. Yu, X. Huang, M. Deng, Y. Lin, L. Jiang, J. Huang and Y. Wang, *J. Phys. Chem. B*, 2010, **114**, 14955-14964.
102. Y. Tokiwa, H. Sakamoto, T. Takiue, M. Aratono and H. Matsubara, *J. Phys. Chem. B*, 2015, **119**, 6235-6241.
103. S. Pandey, R. P. Bagwe and D. O. Shah, *J. Colloid Interface Sci.*, 2003, **267**, 160-166.
104. M. Benrraou, B. L. Bales and R. Zana, *J. Phys. Chem. B*, 2003, **107**, 13432-13440.
105. P. Mukerjee, K. Mysels and P. Kapauan, *J. Phys. Chem.*, 1967, **71**, 4166-4175.
106. F. Bautista, N. Tepale, V. Fernández, G. Landázuri, E. Hernández, E. Macías, J. Soltero, J. Escalante, O. Manero and J. Puig, *Soft matter*, 2016, **12**, 165-170.
107. O. Regev, M. Leaver, R. Zhou and S. Puntambekar, *Langmuir*, 2001, **17**, 5141-5149.
108. D. Ke, Q. Yang, M. Yang, Y. Wu, J. Li, H. Zhou and X. Wang, *Colloids Surf. A Physicochem. Eng. Asp.*, 2013, **436**, 80-86.
109. R. Zana, *J. Colloid Interface Sci.*, 2002, **248**, 203-220.
110. T. Okano, N. Egawa, M. Fujiwara and M. Fukuda, *J. Am. Oil Chem. Soc.*, 1996, **73**, 31-37.
111. Sonu, S. Kumari and S. K. Saha, *J. Phys. Chem. B*, 2015, **119**, 9751-9763.
112. A. K. Tiwari, M. Sowmiya and S. K. Saha, *J. Mol. Liq.*, 2012, **167**, 18-27.

113. Y. Li, P. Li, C. Dong, X. Wang, Y. Wang, H. Yan and R. K. Thomas, *Langmuir*, 2006, **22**, 42-45.
114. A. Ray, *Nature*, 1971, **231**, 313.
115. K. Shirahama and R. Matuura, *Bull. Chem. Soc. Jpn.*, 1965, **38**, 373-378.
116. M. Schick and A. Gilbert, *J. Colloid Sci.*, 1965, **20**, 464-472.
117. H. S. Frank and F. Franks, *J. Chem. Phys.*, 1968, **48**, 4746-4757.
118. A. Soper, E. Castner Jr and A. Luzar, *Biophys. Chem.*, 2003, **105**, 649-666.
119. T. Yamazaki, A. Kovalenko, V. V. Murashov and G. N. Patey, *J. Phys. Chem. B*, 2009, **114**, 613-619.
120. A. Das and C. Mukhopadhyay, *J. Phys. Chem. B*, 2009, **113**, 12816-12824.
121. M.-E. Lee and N. F. van der Vegt, *J. Am. Chem. Soc.*, 2006, **128**, 4948-4949.
122. M. Schwuger, *Ber Bunsen-Gen Phys Chem*, 1971, **75**, 167.
123. H. Singh, S. M. Saleem, R. Singh and K. Birdi, *J. Phys. Chem.*, 1980, **84**, 2191-2194.
124. P. A. Koya and K. Ismail, *J. Solution Chem.*, 2012, **41**, 1271-1281.
125. B. Kumar, D. Tikariha, K. K. Ghosh, N. Barbero and P. Quagliotto, *J. Chem. Thermodyn.*, 2013, **62**, 178-185.
126. F. Tokiwa, *Adv. Colloid Interface Sci.*, 1972, **3**, 389-424.
127. J. Corkill, K. Gemmell, J. Goodman and T. Walker, *Trans. Faraday Soc.*, 1970, **66**, 1817-1824.
128. M. J. Rosen, *Structure/performance relationships in surfactants*, American chemical society, 1984.
129. S. Kaneshina, M. Tanaka, T. Tomida and R. Matuura, *J. Colloid Interface Sci.* , 1974, **48**, 450-460.
130. Y. Ikawa, S. Tsuru, Y. Murata, M. Ōkawauchi, M. Shigematsu and G. Sugihara, *J. Solution Chem.*, 1988, **17**, 125-137.
131. M. Tanaka, S. Kaneshina, S. Kuramoto and R. Matuura, Chem. Soc. Jpn. 1975.
132. S. Hamann, *J. Phys. Chem.*, 1962, **66**, 1359-1361.
133. S. Rodriguez and H. Offen, *J. Phys. Chem.*, 1977, **81**, 47-50.
134. A. Ray, *J. Am. Chem. Soc.*, 1969, **91**, 6511-6512.
135. P. Mukerjee, P. Kapauan and H. G. Meyer, *J. Phys. Chem.*, 1966, **70**, 783-786.
136. N. J. Chang and E. W. Kaler, *J. Phys. Chem.*, 1985, **89**, 2996-3000.
137. G. C. Kresheck, H. Schneider and H. A. Scheraga, *J. Phys. Chem.*, 1965, **69**, 3132-3144.

138. J. H. Fendler, *Membrane mimetic chemistry: characterizations and applications of micelles, microemulsions, monolayers, bilayers, vesicles, host-guest systems, and polyions*, John Wiley & Sons Inc, 1982.
139. N. M. Correa, J. J. Silber, R. E. Riter and N. E. Levinger, *Chem. Rev.*, 2012, **112**, 4569-4602.
140. L. K. Shrestha, T. Sato and K. Aramaki, *Phys. Chem. Chem. Phys.*, 2009, **11**, 4251-4259.
141. B. A. Simmons, C. E. Taylor, F. A. Landis, V. T. John, G. L. McPherson, D. K. Schwartz and R. Moore, *J. Am. Chem. Soc.*, 2001, **123**, 2414-2421.
142. R. Sharma, S. Mahajan and R. K. Mahajan, *Colloids Surf. A Physicochem. Eng. Asp.*, 2013, **427**, 62-75.
143. R. Sanan and R. K. Mahajan, *Ind. Eng. Chem. Res.*, 2011, **50**, 7319-7325.
144. M. S. Bakshi, I. Kaur, R. Sood, J. Singh, K. Singh, S. Sachar, K. J. Singh and G. Kaur, *J. Colloid Interface Sci.*, 2004, **271**, 227-231.
145. S. D. Christian and J. F. Scamehorn, *Solubilization in surfactant aggregates*, CRC Press, 1995.
146. R. Alargova, I. Kochijashky, M. Sierra, K. Kwetkat and R. Zana, *J. Colloid Interface Sci.*, 2001, **235**, 119-129.
147. F. Schosseler, O. Anthony, G. Beinert and R. Zana, *Langmuir*, 1995, **11**, 3347-3350.
148. J. Szejtli, *Cyclodextrin and their inclusion complexes*, Akedemiai Kiado, Budapest, 1982.
149. K. A. Connors, *Chem. Rev.*, 1997, **97**, 1325-1358.
150. J. Szejtli, in *Cyclodextrin technology*, Kluwer, Dordrecht, 1988, pp. 79-185.
151. C. J. Easton and S. F. Lincoln, *Scaffolds and Templates for Supramolecular Chemistry*, World Scientific, 1999.
152. A. R. Hedges, *Chem. Rev.*, 1998, **98**, 2035-2044.
153. A. Villiers, *Compt Rendu*, 1891, **112**, 536.
154. S. Muñoz-Botella, B. Del Castillo and M. Martyn, *Ars Pharm*, 1995, **36**, 187-198.
155. J. Li, M. Zhang, J. Chao and S. Shuang, *Spectrochim. Acta A* , 2009, **73**, 752-756.
156. J. L. Manzoori, H. Abdolmohammad-Zadeh and M. Amjadi, *Il Farmaco*, 2005, **60**, 575-581.
157. H. A. Benesi and J. Hildebrand, *J. Am. Chem. Soc.*, 1949, **71**, 2703-2707.
158. J. Dey, E. L. Roberts and I. M. Warner, *J. Phys. Chem. A*, 1998, **102**, 301-305.

159. A. Wu, X. Shen and Y. He, *J. Colloid Interface Sci.*, 2006, **297**, 525-533.
160. A. Wu, X. Shen and Y. He, *J. Colloid Interface Sci.*, 2006, **302**, 87-94.
161. M. Sowmiya, P. Purkayastha, A. K. Tiwari, S. S. Jaffer and S. K. Saha, *J. Photochem. Photobiol. A Chem.*, 2009, **205**, 186-196.
162. G. Pistolis and A. Malliaris, *J. Phys. Chem.*, 1996, **100**, 15562-15568.
163. R. A. Agbaria and D. Gill, *J. Phys. Chem.*, 1988, **92**, 1052-1055.
164. K. A. Agnew, T. D. McCarley, R. A. Agbaria and I. M. Warner, *J. Photochem. Photobiol. A Chem.*, 1995, **91**, 205-210.
165. C. Zhang, X. Shen and H. Gao, *Chem. Phys. Lett.*, 2002, **363**, 515-522.
166. B. J. Ravoo, R. Darcy, A. Mazzaglia, D. Nolan and K. Gaffney, *Chem. Commun.*, 2001, 827-828.
167. M. Sowmiya, P. Purkayastha, A. K. Tiwari, S. S. Jaffer and S. K. Saha, *J. Photochem. Photobiol. A Chem.*, 2009, **205**, 186-196.
168. S. Aggarwal, P. Singh and B. Mishra, *Die Pharmazie*, 2002, **57**, 191-193.
169. C. I. Branden, *Introduction to protein structure*, Garland Science, 1999.
170. S. Curry, H. Mandelkow, P. Brick and N. Franks, *Nat. Struct. Mol. Bio.*, 1998, **5**, 827.
171. B. Mishra, A. Barik, K. I. Priyadarsini and H. Mohan, *J. Chem. Sci.*, 2005, **117**, 641-647.
172. D. C. Carter and J. X. Ho, in *Advances in protein chemistry*, Elsevier, 1994, vol. 45, pp. 153-203.
173. G. Walsh, *Nature biotechnology*, 2006, **24**, 769.
174. W. Wang, S. Singh, D. L. Zeng, K. King and S. Nema, *J. Pharma. Sci.*, 2007, **96**, 1-26.
175. A. Hawe, M. Sutter and W. Jiskoot, *Pharma. Res.*, 2008, **25**, 1487-1499.
176. A. Chakrabarty, A. Mallick, B. Haldar, P. Das and N. Chattopadhyay, *Biomacromolecules*, 2007, **8**, 920-927.
177. D. Wu, G. Xu, Y. Sun, H. Zhang, H. Mao and Y. Feng, *Biomacromolecules*, 2007, **8**, 708-712.
178. E. Gelamo, C. Silva, H. Imasato and M. Tabak, *Biochimica et Biophysica Acta Protein Struct. Mol. Enzymol.*, 2002, **1594**, 84-99.
179. S. De, A. Girigoswami and S. Das, *J. Colloid Interface Sci.*, 2005, **285**, 562-573.
180. N. Gull, P. Sen and R. H. Khan, *Langmuir*, 2009, **25**, 11686-11691.
181. A. Sułkowska, *J. Mol. Struct.*, 2002, **614**, 227-232.

182. B. Kamat and J. Seetharamappa, *J. Pharm. Biomed. Anal.*, 2004, **35**, 655-664.
183. C. La Mesa, *J. Colloid Interface Sci.*, 2005, **286**, 148-157.
184. R. Das, D. Guha, S. Mitra, S. Kar, S. Lahiri and S. Mukherjee, *J. Phys. Chem. A*, 1997, **101**, 4042-4047.
185. K. Ibel, R. P. May, K. Kirschner, H. Szadkowski, E. Mascher And P. Lundahl, *Eur. Jo. Biochem.*, 1990, **190**, 311-318.
186. N. J. Turro, X.-G. Lei, K. Ananthapadmanabhan and M. Aronson, *Langmuir*, 1995, **11**, 2525-2533.
187. C. C. Ruiz, J. Hierrezuelo, J. Aguiar and J. Peula-García, *Biomacromolecules*, 2007, **8**, 2497-2503.
188. Y. Pi, Y. Shang, C. Peng, H. Liu, Y. Hu and J. Jiang, *Biopolymers*, 2006, **83**, 243-249.
189. Y.-S. Ge, S.-X. Tai, Z.-Q. Xu, L. Lai, F.-F. Tian, D.-W. Li, F.-L. Jiang, Y. Liu and Z.-N. Gao, *Langmuir*, 2012, **28**, 5913-5920.
190. C. M. Faustino, A. R. Calado and L. Garcia-Rio, *Biomacromolecules*, 2009, **10**, 2508-2514.
191. N. Gull, M. A. Mir, J. M. Khan, R. H. Khan, G. M. Rather and A. A. Dar, *J. Colloid Interface Sci.*, 2011, **364**, 157-162.
192. S. Veeralakshmi, S. Nehru, S. Arunachalam, P. Kumar and M. Govindaraju, *Inorg. Chem. Front.*, 2014, **1**, 393-404.
193. T. K. Chaudhuri and S. Paul, *FEBS J.*, 2006, **273**, 1331-1349.
194. P. Horowitz and N. Criscimagna, *J. Biolog. Chem.*, 1986, **261**, 15652-15658.
195. F. U. Hartl, *Nature*, 1996, **381**, 571.
196. D. Rozema and S. H. Gellman, *J. Am. Chem. Soc.*, 1995, **117**, 2373-2374.
197. D. Rozema and S. H. Gellman, *J. Biol. Chem.*, 1996, **271**, 3478-3487.
198. D. Rozema and S. H. Gellman, *Biochemistry*, 1996, **35**, 15760-15771.
199. R. Yazdanparast, M. A. Esmaeili and F. Khodagholi, *Int. J. Biol. Macromol.*, 2007, **40**, 126-133.
200. Y. Liu, Y. Liu and R. Guo, *J. Solution Chem.*, 2011, **40**, 1140-1152.
201. Y. Liu, Y. Liu and R. Guo, *J. Colloid Interface Sci.*, 2010, **351**, 180-189.
202. L. A. Marky, H. T. Lee and A. Garcia, *Encycl. Life Sci*, 2001.
203. H. Lodish, A. Berk, S. Zipursky, P. Matsudaira, D. Baltimore and J. Darnell, *Mol. Cell Biol.*, 2000, **4**.
204. C. Wang, B. Carter-Cooper, Y. Du, J. Zhou, M. A. Saeed, J. Liu, M. Guo, B.

Roembke, C. Mikek and E. A. Lewis, *Eur. J. Med. Chem.*, 2016, **118**, 266-275.

205. A. Erdem and M. Ozsoz, *Electroanalysis*, 2002, **14**, 965-974.
206. W. Denny, *Anti-cancer Drug Des.*, 1989, **4**, 241-263.
207. S. Neidle, *Nat. Prod. Rep.*, 2001, **18**, 291-309.
208. A. K. Jain and S. Bhattacharya, *Bioconjugate Chem.*, 2010, **21**, 1389-1403.
209. C. Bailly and M. J. Waring, *Nucleic Acids Res.*, 1998, **26**, 4309-4314.
210. H. S. Rye, S. Yue, D. E. Wemmer, M. A. Quesada, R. P. Haugland, R. A. Mathies and A. N. Glazer, *Nucleic Acids Res.*, 1992, **20**, 2803-2812.
211. L. H. Hurley, *Nat. Rev. Cancer*, 2002, **2**, 188.
212. C. O. Pabo and R. T. Sauer, *Ann. Rev. Biochem.*, 1992, **61**, 1053-1095.
213. B. Valeur, *Molecular Fluorescence: Principles and Applications*, 2001, **2**.
214. J. R. Lakowicz, in *Principles of fluorescence spectroscopy*, Springer, New York, 2006.
215. A. Jabłoński, *Z. Phys.*, 1935, **94**, 38-46.
216. M. Kasha, *Discuss. Faraday Soc.*, 1950, **9**, 14-19.
217. S. G. Schulman, *Fluorescence and phosphorescence spectroscopy: physicochemical principles and practice*, Elsevier, 2017.
218. N. Mataga, T. Okada and N. Yamamoto, *Chem. Phys. Lett.*, 1967, **1**, 119-121.
219. W. Rettig, *J. Mol. Struct.* , 1982, **84**, 303-327.
220. P. Suppan, *Chem. Phys. Lett.*, 1986, **128**, 160-161.
221. W. Baumann, H. Bischof, J. C. Fröhling, C. Brittinger, W. Rettig and K. Rotkiewicz, *J. Photochem. Photobiol. A Chem.*, 1992, **64**, 49-72.
222. G. C. Pimentel, *J. Am. Chem. Soc.*, 1957, **79**, 3323-3326.
223. N. Mataga and S. Tsuno, *Bull. Chem. Soc. Jpn*, 1957, **30**, 368-374.
224. P. Pringsheim, *Interscience, New York*, , 1949.
225. T. Forster, *Gottingen, Germany*, 1951.
226. E. Lippert, *Z. Naturforsch. A*, 1955, **10**, 541-545.
227. E. McRae, *J. Phys. Chem.* , 1957, **61**, 562-572.
228. P. Suppan, *J. Chem. Soc. A Inorg.c, Phys., Theoret.*, 1968, 3125-3133.
229. Y. Ooshika, *J. Phys. Soc. Jpn*, 1954, **9**, 594-602.
230. N. Mataga, Y. Kaifu and M. Koizumi, *Bull. Chem. Soc. Jpn*, 1955, **28**, 690-691.
231. W. Liptay, *Zeitschrift für Naturforschung A*, 1965, **20**, 1441-1471.
232. v. L. Bilot and A. Kawski, *Z. Naturforsch. A*, 1962, **17**, 621-627.
233. M. Shaikh, J. Mohanty, P. Singh, A. Bhasikuttan, R. Rajule, V. Satam, S. Bendre,

V. Kanetkar and H. Pal, *J. Phys. Chem. A*, 2010, **114**, 4507-4519.

234. N. Dash, F. Chipem, R. Swaminathan and G. Krishnamoorthy, *Chem. Phys. Lett.*, 2008, **460**, 119-124.
235. S. K. Saha, P. Purkayastha and A. B. Das, *J. Photochem. Photobiol. A Chem.*, 2008, **195**, 368-377.
236. C. Reichardt, *Chem. Rev.*, 1994, **94**, 2319-2358.
237. E. M. Kosower, *J. Am. Chem. Soc.*, 1958, **80**, 3253-3260.
238. E. M. Kosower, J. A. Skorcz, W. M. Schwarz Jr and J. W. Patton, *J. Am. Chem. Soc.*, 1960, **82**, 2188-2191.
239. K. Dimroth, C. Reichardt, T. Siepmann and F. Bohlmann, *Justus Liebigs Ann. Chem.*, 1963, **661**, 1-37.
240. G. Jones II, W. R. Jackson, S. Kanoktanaporn and A. M. Halpern, *Opt. Commun.*, 1980, **33**, 315-320.
241. B. Raju B and T. Varadarajan, *J. Phys. Chem.*, 1994, **98**, 8903-8905.
242. G. Jones, W. R. Jackson, C. Y. Choi and W. R. Bergmark, *J. Phys. Chem.*, 1985, **89**, 294-300.
243. G. Jones, *J. Phys. Chem*, 1974, **89**, 294.
244. S. Nad, M. Kumbhakar and H. Pal, *J. Phys. Chem. A*, 2003, **107**, 4808-4816.
245. P. Dahiya, M. Kumbhakar, T. Mukherjee and H. Pal, *Chem. Phys. Lett.*, 2005, **414**, 148-154.
246. T. Lopez Arbeloa, F. Lopez Arbeloa, M. J. Tapia and I. Lopez Arbeloa, *J. Phys. Chem.*, 1993, **97**, 4704-4707.
247. B. Bagchi, *Ann. Rev. Phys. Chem.*, 1989, **40**, 115-141.
248. K. Tamm, *Theory of Electric Polarization.* Elsevier Scientific Publication Company, Seiten. Preis, 1973.
249. B. Sengupta and P. K. Sengupta, *Biochem. Biophys. Res. Commun.*, 2002, **299**, 400-403.
250. S. Muthusubramanian and S. K. Saha, *J. Lumin.*, 2012, **132**, 2166-2177.
251. A. Mallick, B. Haldar, S. Maiti and N. Chattopadhyay, *J. Colloid Interface Sci.*, 2004, **278**, 215-223.
252. M. Sowmiya, A. K. Tiwari and S. K. Saha, *J. Colloid Interface Sci.*, 2010, **344**, 97-104.
253. S. S. Jaffer, M. Sowmiya, S. K. Saha and P. Purkayastha, *J. Colloid Interface Sci.*, 2008, **325**, 236-242.

254. N. E. Levinger, *Curr. Opin. Colloid Interface Sci.*, 2000, **5**, 118-124.
255. N. Sarkar, K. Das, A. Datta, S. Das and K. Bhattacharyya, *J. Phys. Chem.*, 1996, **100**, 10523-10527.
256. D. K. Sasmal, S. Ghosh, A. K. Das and K. Bhattacharyya, *Langmuir*, 2013, **29**, 2289-2298.
257. X. Liu, J. M. Cole and K. S. Low, *J. Phys. Chem. C*, 2013, **117**, 14723-14730.
258. K. Khemakhem, H. Ammar, S. Abid, R. El Gharbi and S. Fery-Forgues, *Dyes Pigm.*, 2013, **99**, 594-598.
259. S. Kumar.
260. K. Bhattacharyya, *Chem. Commun.*, 2008, 2848-2857.
261. N. Nandi, K. Bhattacharyya and B. Bagchi, *Chem. Rev.*, 2000, **100**, 2013-2046.
262. N. Nandi and B. Bagchi, *J. Phys. Chem. B*, 1997, **101**, 10954-10961.
263. R. Jimenez, G. R. Fleming, P. Kumar and M. Maroncelli, *Nature*, 1994, **369**, 471-473.
264. N. Sarkar, A. Datta, S. Das and K. Bhattacharyya, *J. Phys. Chem.*, 1996, **100**, 15483-15486.
265. Š. Vajda, R. Jimenez, S. J. Rosenthal, V. Fidler, G. R. Fleming and E. W. Castner, *J. Chem. Soc. Faraday Trans.*, 1995, **91**, 867-873.
266. S. K. Pal, D. Mandal, D. Sukul, S. Sen and K. Bhattacharyya, *J. Phys. Chem. B*, 2001, **105**, 1438-1441.
267. S. K. Pal, J. Peon and A. H. Zewail, . *Proc. Natl. Acad. Sci.*, 2002, **99**, 1763-1768.
268. E. B. Brauns, M. L. Madaras, R. S. Coleman, C. J. Murphy and M. A. Berg, *Phys. Rev. Lett.*, 2002, **88**, 158101.
269. L. A. Gearheart, M. M. Somoza, W. E. Rivers, C. J. Murphy, R. S. Coleman and M. A. Berg, *J. Am. Chem. Soc.*, 2003, **125**, 11812-11813.
270. D. Zhong, S. K. Pal and A. H. Zewail, *Chem. Phys. Lett.*, 2011, **503**, 1-11.
271. A. K. Tiwari and S. K. Saha, *J. Phys. Chem. B*, 2014, **118**, 3582-3592.
272. D. Chakrabarty, P. Hazra, A. Chakraborty and N. Sarkar, *Chem. Phys. Lett.*, 2004, **392**, 340-347.
273. P. Hazra and N. Sarkar, *Phys. Chem. Chem. Phys.*, 2002, **4**, 1040-1045.
274. T. Sonu, Amit K, S. Kumari and S. K. Saha, *RSC Advances*, 2014, **4**, 25210-25219.
275. D. Chakrabarty, P. Hazra, A. Chakraborty and N. Sarkar, *J. Phys. Chem. B*, 2003, **107**, 13643-13648.
276. D. Chakrabarty, P. Hazra and N. Sarkar, *J. Phys. Chem. A*, 2003, **107**, 5887-5893.

277. D. Chakrabarty, A. Chakraborty, D. Seth, P. Hazra and N. Sarkar, *J. Chem. Phys.*, 2005, **122**, 184516.
278. S. Kumari and S. K. Saha, *Phys. Chem. Chem. Phys.*, 2016, **18**, 1551-1563.
279. P. Sen, D. Roy, S. K. Mondal, K. Sahu, S. Ghosh and K. Bhattacharyya, *J. Phys. Chem. A*, 2005, **109**, 9716-9722.
280. T. Telgmann and U. Kaatze, *J. Phys. Chem. A*, 2000, **104**, 1085-1094.
281. V. P. Denisov, J. Peters, H. D. Hörlein and B. Halle, *Nat. Struct. Mol. Biol.*, 1996, **3**, 505-509.
282. M. A. Kahlow, T. J. Kang and P. F. Barbara, *J. Chem. Phys.*, 1989, **90**, 151-158.
283. C. Silva, P. K. Walhout, K. Yokoyama and P. F. Barbara, *Phys. Rev. Lett.*, 1998, **80**, 1086.
284. A. Sengupta, R. V. Khade and P. Hazra, *J. Phys. Chem. A*, 2011, **115**, 10398-10407.
285. P. Sen, D. Roy, S. K. Mondal, K. Sahu, S. Ghosh and K. Bhattacharyya, *J. Phys. Chem. A*, 2005, **109**, 9716-9722.
286. P. Hazra, D. Chakrabarty and N. Sarkar, *Langmuir*, 2002, **18**, 7872-7879.
287. P. Hazra, D. Chakrabarty and N. Sarkar, *Chem. Phys. Lett.*, 2003, **371**, 553-562.
288. S. Dey, A. Adhikari, U. Mandal, S. Ghosh and K. Bhattacharyya, *J. Phys. Chem. B*, 2008, **112**, 5020-5026.
289. R. Jimenez, G. R. Fleming, P. Kumar and M. Maroncelli, *Nature*, 1994, **369**, 471.
290. P. F. Barbara and W. Jarzeba, *Adv. Photochem.*, 1990, **15**, 1-68.
291. M. Maroncelli, *J. Mol. Liq.*, 1993, **57**, 1-37.
292. A. Szemik-Hojniak, I. Deperasińska, K. Oberda, Y. Erez, D. Huppert and Y. P. Nizhnik, *Phys. Chem. Chem. Phys.*, 2013, **15**, 9914-9923.
293. M. Lang, X. Jordanides, X. Song and G. Fleming, *J. Chem. Phys.*, 1999, **110**, 5884-5892.
294. T. Joo, Y. Jia, J. Y. Yu, M. J. Lang and G. R. Fleming, *J. Chem. Phys.*, 1996, **104**, 6089-6108.
295. B. Zolotov, A. Gan, B. Fainberg and D. Huppert, *Chem. Phys. Lett.*, 1997, **265**, 418-426.
296. M. Cho, S. J. Rosenthal, N. F. Scherer, L. D. Ziegler and G. R. Fleming, *J. Chem. Phys.*, 1992, **96**, 5033-5038.
297. M. Glasbeek and H. Zhang, *Chem. Rev.*, 2004, **104**, 1929-1954.
298. W. Jarzeba, G. C. Walker, A. E. Johnson, M. A. Kahlow and P. F. Barbara, *J. Phys.*

Chem., 1988, **92**, 7039-7041.

299. S. K. Pal, J. Peon and A. H. Zewail, *Proc. Natl. Acad. Sci.*, 2002, **99**, 15297-15302.
300. S. K. Pal, J. Peon and A. H. Zewail, *Chem. Phys. Lett.*, 2002, **363**, 57-63.
301. M. Horng, J. Gardecki, A. Papazyan and M. Maroncelli, *J. Phys. Chem.*, 1995, **99**, 17311-17337.
302. M. A. Kahlow, W. o. Jarzęba, T. J. Kang and P. F. Barbara, *J. Chem. Phys.*, 1989, **90**, 151-158.
303. K. Tominaga and G. C. Walker, *J. Photochem. Photobiol. A Chem.*, 1995, **87**, 127-133.
304. S. Kovalenko, N. Ernsting and J. Ruthmann, *Chem. Phys. Lett.*, 1996, **258**, 445-454.
305. A. Jonkman, P. v. d. Meulen, H. Zhang and M. Glasbeek, *Chem. Phys. Lett.*, 1996, **256**, 21-26.
306. E. W. Castner Jr, M. Maroncelli and G. R. Fleming, *J. Chem. Phys.*, 1987, **86**, 1090-1097.
307. S. Kovalenko, N. Ernsting and J. Ruthmann, *J. Chem. Phys.*, 1997, **106**, 3504-3511.
308. M. A. Kahlow, T. J. Kang and P. F. Barbara, *J. Chem. Phys.*, 1988, **88**, 2372-2378.
309. P. Van der Meulen, H. Zhang, A. Jonkman and M. Glasbeek, *J. Phys. Chem.*, 1996, **100**, 5367-5373.
310. P. Prosposito, M. Casalboni, F. De Matteis, M. Glasbeek, A. Quatela, E. Van Veldhoven and H. Zhang, *J. Lumin.*, 2001, **94**, 641-644.
311. A. Mallick, M. C. Mandal, B. Haldar, A. Chakrabarty, P. Das and N. Chattopadhyay, *J. Am. Chem. Soc.*, 2006, **128**, 3126-3127.
312. S. D. Choudhury, M. Kumbhakar, S. Nath, S. K. Sarkar, T. Mukherjee and H. Pal, *J. Phys. Chem. B*, 2007, **111**, 8842-8853.
313. P. Dutta, P. Sen, S. Mukherjee and K. Bhattacharyya, *Chem. Phys. Lett.*, 2003, **382**, 426-433.
314. A. Mahata, D. Sarkar, D. Bose, D. Ghosh, P. Das and N. Chattopadhyay, *J. Colloid Interface Sci.*, 2009, **335**, 234-241.
315. P. Das, A. Mallick, A. Chakrabarty, B. Haldar and N. Chattopadhyay, *J. Chem. Phys.*, 2006, **125**, 044516.
316. N. C. Maiti, M. Krishna, P. Britto and N. Periasamy, *J. Phys. Chem. B*, 1997, **101**, 11051-11060.

317. S. Matzinger, D. M. Hussey and M. Fayer, *J. Phys. Chem. B*, 1998, **102**, 7216-7224.
318. C. Chapman, R. Fee and M. Maroncelli, *J. Phys. Chem.*, 1995, **99**, 4811-4819.
319. M. Maroncelli and G. R. Fleming, *J. Chem. Phys.*, 1987, **86**, 6221-6239.
320. S. Balasubramanian and B. Bagchi, *J. Phys. Chem. B*, 2001, **105**, 12529-12533.
321. S. Balasubramanian, S. Pal and B. Bagchi, *Phys. Rev. Lett.*, 2002, **89**, 115505.
322. D. Mandal, S. Sen, K. Bhattacharyya and T. Tahara, *Chem. Phys. Lett.*, 2002, **359**, 77-82.
323. L. Frauchiger, H. Shirota, K. E. Uhrich and E. W. Castner, *J. Phys. Chem. B*, 2002, **106**, 7463-7468.
324. A. Chakraborty, D. Chakrabarty, P. Hazra, D. Seth and N. Sarkar, *Chem. Phys. Lett.*, 2003, **382**, 508-517.
325. A. Chakraborty, D. Seth, D. Chakrabarty, P. Setua and N. Sarkar, *J. Phys. Chem. A*, 2005, **109**, 11110-11116.
326. R. Karmakar and A. Samanta, *J. Phys. Chem. A*, 2002, **106**, 4447-4452.
327. R. Karmakar and A. Samanta, *J. Phys. Chem. A*, 2003, **107**, 7340-7346.
328. H. Shirota, Y. Tamoto and H. Segawa, *J. Phys. Chem. A*, 2004, **108**, 3244-3252.
329. Y. Tamoto, H. Segawa and H. Shirota, *Langmuir*, 2005, **21**, 3757-3764.
330. B. O. Roos, R. Lindh, P.-Å. Malmqvist, V. Veryazov and P.-O. Widmark, *J. Phys. Chem. A*, 2005, **109**, 6575-6579.
331. R. E. Riter, E. P. Undiks and N. E. Levinger, *J. Am. Chem. Soc.*, 1998, **120**, 6062-6067.
332. A. Datta, D. Mandal, S. K. Pal, S. Das and K. Bhattacharyya, *J. Mol. Liq.*, 1998, **77**, 121-129.
333. A. Sengupta and P. Hazra, *Chem. Phys. Lett.*, 2010, **501**, 33-38.
334. M.-L. Horng, J. Gardecki and M. Maroncelli, *J. Phys. Chem. A*, 1997, **101**, 1030-1047.
335. R. Pramanik, S. Sarkar, C. Ghatak, V. G. Rao, S. Mandal and N. Sarkar, *J. Phys. Chem. B*, 2011, **115**, 6957-6963.
336. R. Dutta, S. Ghosh, P. Banerjee, S. Kundu and N. Sarkar, *J. Colloid Interface Sci.*, 2017, **490**, 762-773.
337. S. Ghosh, C. Banerjee, S. Mandal, V. G. Rao and N. Sarkar, *J. Phys. Chem. B*, 2013, **117**, 5886-5897.
338. D. C. Khara, J. P. Kumar, N. Mondal and A. Samanta, *J. Phys. Chem. B*, 2013,

117, 5156-5164.

339. Y. Rezus and H. Bakker, *Proc. Natl. Acad. Sci.*, 2006, **103**, 18417-18420.
340. A. Idrissi, F. Sokolić and A. Perera, *J. Chem. Phys.*, 2000, **112**, 9479-9488.
341. J. Reimers, R. Watts and M. Klein, *Chemical Physics*, 1982, **64**, 95-114.
342. L. J. Gosting and D. F. Akeley, *J. Am. Chem. Soc.*, 1952, **74**, 2058-2060.
343. H. Raghuraman, S. K. Pradhan and A. Chattopadhyay, *J. Phys. Chem. B*, 2004, **108**, 2489-2496.
344. C. C. Ruiz, *Colloids Surf. A Physicochem. Eng. Asp.*, 1999, **147**, 349-357.
345. J. D. Morgan, D. H. Napper and G. G. Warr, *J. Phys. Chem.*, 1995, **99**, 9458-9465.
346. V. Soldi, J. Keiper, L. S. Romsted, I. M. Cuccovia and H. Chaimovich, *Langmuir*, 2000, **16**, 59-71.
347. K. Maiti, D. Mitra, S. Guha and S. P. Moulik, *J. Mol. Liq.*, 2009, **146**, 44-51.
348. M. Borse, V. Sharma, V. Aswal, N. K. Pokhriyal, J. V. Joshi, P. S. Goyal and S. Devi, *Phys. Chem. Chem. Phys.*, 2004, **6**, 3508-3514.
349. M. S. Borse and S. Devi, *Adv. Colloid Interface Sci.*, 2006, **123**, 387-399.
350. M. Pisárčik, J. Jampílek, F. Devínsky, J. Drábiková, J. Tkacz and T. Opravil, *J. Surfactants Deterg.*, 2016, **19**, 477-486.
351. S. Zhang, J. Yu, J. Wu, W. Tong, Q. Lei and W. Fang, *J. Chem. Eng. Data*, 2014, **59**, 2891-2900.
352. R. Zana, *Adv. Colloid Interface Sci.*, 2002, **97**, 205-253.
353. C. C. Ruiz and F. G. a. Sánchez, *J. Colloid Interface Sci.*, 1994, **165**, 110-115.
354. S. Causi, R. De Lisi, S. Milioto and N. Tirone, *J. Phys. Chem.*, 1991, **95**, 5664-5673.
355. M. Almgren and S. Swarup, *J. Colloid Interface Sci.*, 1983, **91**, 256-266.
356. E. Caponetti, S. Causi, R. De Lisi, M. Floriano, S. Milioto and R. Triolo, *J. Phys. Chem.*, 1992, **96**, 4950-4960.
357. J. L. Baneres, J.-L. Popot and B. Mouillac, *Trends Biotechnol.*, 2011, **29**, 314-322.
358. S. Fiedler, J. Broecker and S. Keller, *Cell. Mol. Life Sci.*, 2010, **67**, 1779-1798.
359. E. Finer, F. Franks and M. Tait, *J. Am. Chem. Soc.*, 1972, **94**, 4424-4429.
360. X. Hoccart and G. Turrell, *J. Chem. Phys.*, 1993, **99**, 8498-8503.
361. F. Vanzi, B. Madan and K. Sharp, *J. Am. Chem. Soc.*, 1998, **120**, 10748-10753.
362. R. Chitra and P. E. Smith, *J. Phys. Chem. B*, 2000, **104**, 5854-5864.
363. B. J. Bennion and V. Daggett, *Proc. Natl. Acad. Sci.*, 2003, **100**, 5142-5147.
364. A. Caflisch and M. Karplus, *Structure*, 1999, **7**, 477-S472.

365. M. Grätzel, *Heterogeneous photochemical electron transfer*, CRC Press, 1989.

366. Q. He and J. Shi, *J. Mater. Chem.*, 2011, **21**, 5845-5855.

367. O. Tacar, P. Sriamornsak and C. R. Dass, *J. Pharm. Pharmacol.*, 2013, **65**, 157-170.

368. F. Masood, *Mater. Sci. Eng. C*, 2016, **60**, 569-578.

369. P. H. Doan, D. R. Pitter, A. Kocher, J. N. Wilson and T. Goodson III, *J. Am. Chem. Soc.*, 2015, **137**, 9198-9201.

Chapter 2

Materials, Methods and Instrumentation

Key Concepts:

- *This chapter covers details of chemicals required for the synthesis of surfactants, and their characterization methods.*
- *Preparation methods of different solutions for the spectroscopic studies, and instruments used for their characterization.*

Chapter 2

Materials, Methods and Instrumentation

The material section includes chemicals required for the synthesis of the surfactants and the spectral studies used. The method section includes synthesis and characterization of surfactants, preparation of different solutions for the studies, and their characterization techniques. Instrumentation section includes various techniques involved in the studies *viz*. UV-visible spectroscopy, steady-state fluorescence and time-resolved fluorescence spectroscopy, circular dichroism spectroscopy, and dynamic light scattering.

2.1 Materials

Table 2.1. List of compounds used for this work with their purchasing source.

Sr. No.	Compounds	Purchased from
For the synthesis of convention surfactant with different counterions		
1.	Cetyltrimethylammonium bromide (C_{16}TABr)	Aldrich Chemical Company, USA
2.	Amberlyst A26 OH	SD Fine-Chem Limited. Mumbai, India
3.	*p*-Toluenesulfonic acid (*p*-TSA)	Spectrochem Chemical Company, India
4.	HNO_3	SD Fine-Chem Limited Mumbai, India
5.	H_2SO_4	SD Fine-Chem Limited Mumbai, India
6.	$AgNO_3$	SD Fine-Chem Limited. Mumbai, India
For the synthesis of gemini surfactants		
1.	1,4-dibromodiethylether	Alfa Aesar, a Johnson Matthey Company
2.	1,3-dibromopropane	Spectrochem Company, India
3.	1,4-dibromobutane	Spectrochem Company, India
4.	1,6- dibromohexane	Spectrochem Company, India
5.	1,8-dibromoctane	Spectrochem Company, India
6.	1,12-dibromododecane	Spectrochem Company, India
7.	1,4-dibromo-2,3-butanediol	Sigma Chemical Company, WI, USA
8.	1,4-dibromo-2-butanol	Sigma Chemical Company, WI, USA
9.	*N*, *N*-dimethyldodecylamine	Alfa Aesar, USA
10.	*N*, *N*-dimethyltetradecylamine	Alfa Aesar, USA
11.	*N*, *N*-dimethylhexadecylamine	Alfa Aesar, USA

Fluorescent molecules		
1.	C-480	Exciton (laser grade), USA
2.	C-485	Exciton (laser grade), USA
3.	1,6-Diphenyl-1,3,5-hexatriene (DPH)	Aldrich Chemical Company, WI, USA
4.	Quinine sulfate	Aldrich Chemical Company, WI, USA
Other compounds		
1.	Urea	SD Fine-Chem Limited Mumbai, India
2.	*β*-cyclodextrin	Aldrich Chemical Company, USA
3.	Ludox	Aldrich Chemical Company, WI, USA
4.	Glycerol	Alfa Aesar, USA
5.	Standard KCl solution	Merck, India
Biomolecules		
1.	Bovine serum albumin (BSA)	Sigma Chemical Company, WI, USA
2.	Deoxyribonucleic acid sodium salt from calf thymus fibers type (ctDNA)	Sigma Chemical Company, WI, USA
For pH adjustment of water and buffer solution		
1.	Disodium hydrogen orthophosphate (Na_2HPO_4)	SD Fine-Chem Limited Mumbai, India
2.	2-[4-(2-hydroxyethyl)piperazin-1-yl]ethanesulfonic acid (HEPES)	SRL, Pvt. Ltd. Mumbai, India
3.	NaOH	Spectrochem Company, India
4.	H_2SO_4	Spectrochem Company, India
4.	H_3PO_4	Spectrochem Company, India
Solvents		
1.	Methanol (UV grade)	Spectrochem Company, India
2.	Cyclohexane (UV grade)	Spectrochem Company, India
3.	*n*-Hexane (UV grade)	Spectrochem Company, India
4.	Diethylether (UV grade)	Spectrochem Company, India
5.	Ethylacetate (UV grade)	Spectrochem Company, India
6.	Ethanol	Changshu Yangyuan Chemical Company, China

7.	1,4-dioxane (UV grade)	Spectrochem Company, India
8.	Tetrahydrofuran (THF) (UV grade)	Spectrochem Company, India
9.	Acetone (UV grade)	Spectrochem Company, India

Fluorescence probes

Highest purity grade fluorophores are used without any further purification for the spectroscopic studies. The molecular structures of these probes are shown below as Scheme 2.1.

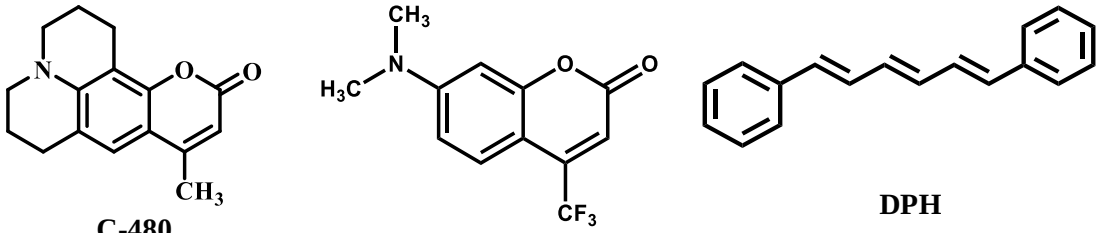

Scheme 2.1: Molecular structures of fluorescence probes.

2.2 Methods

2.2.1 Synthesis and characterization of conventional surfactant with different counterions

Cetyltrimethylammoniumbromide (C_{16}TABr), was used for the synthesis of C_{16}TAX (X= SO_4^{2-}, NO_3^- and *p*-toluenesulfonate (*p*-TS^-)) surfactant with various counterions. Counterion, Br^-, of C_{16}TABr surfactant was exchanged by SO_4^{2-}, NO_3^- and *p*-toluenesulfonate (*p* -TS^-) using the reported method.[1] In this method, C_{16}TABr was taken in the round bottom flask and dissolved in the minimum quantity of Milli-Q water; if it was not dissolved then dissolved by heating with continuous stirring. After that, (4-5 times excess of C_{16}TABr) strongly basic anion exchange resin (Amberlyst A26 OH) was added to replace bromide with hydroxide from the C_{16}TABr surfactants. Complete exchange of Br^- ion by the OH^- ion was confirmed by the $AgNO_3$ test. While filtering, the resin was washed three to four times with water. The filtrate was the aqueous solution of a surfactant with the OH^- ions, as the counterions. After that, this solution was neutralized by the appropriate acid as precisely as possible to get the desired counterions in the surfactant. Water content was removed by heating. The obtained white solid powder was recrystallized in a mixture of ethyl acetate and methanol. Chemical structure of surfactants

with their abbreviations is given in Scheme 2.2. FT-IR and ^{1}H NMR data for the synthesized conventional surfactants are given in Table 2.2.

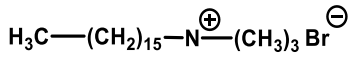 Hexadecyltrimethylammonium bromide [C_{16}TABr]	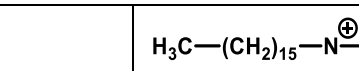 Hexadecyltrimethylammonium sulfate [$(C_{16}TA)_2SO_4$]
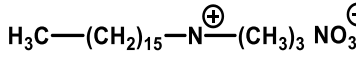 Hexadecyltrimethylammonium nitrate [C_{16}TANO_3]	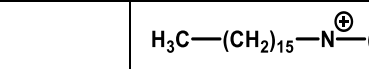 Hexadecyltrimethylammonium *p*-toluenesulfonate [C_{16}TA*p*-TS]

Scheme 2.2: Chemical structure of conventional surfactants with their abbreviations.

Table 2.2. FT-IR and ^{1}H NMR data for the synthesized conventional surfactants.

Surfactants	FT-IR (ν/cm^{-1})	^{1}H NMR
C_{16}TABr	2917, 2847 (CH_3), 1488, 1467 (CH_2)	**(400 MHz, $CDCl_3$) δ:** 0.88 (t, *J* = 6.8 Hz, 3H, CH_3), 1.32-1.21 (m, 22H, CH_2), 1.46- 1.32 (m, 4H, CH_2), 1.84-1.65 (m, 2H, CH_2), 3.48 (s, 9H, CH_3), 3.65-3.55 (m, 2H, CH_2).
$C_{16}TANO_3$	2917, 2847 (CH_3), 1488, 1467 (CH_2), 1328 (N=O)	**(400 MHz, $CDCl_3$) δ:** 0.89 (t, *J* = 6.8 Hz, 3H, CH_3), 1.51-1.19 (m, 26H, CH_2), 1.82-1.66 (m, 2H, CH_2), 3.28 (s, 9H, CH_3), 3.46-3.38 (m, 2H, CH_2).
$(C_{16}TA)_2SO_4$	2917, 2847 (CH_3), 1488, 1467 (CH_2), 1064 (S=O)	**(400 MHz, $CDCl_3$) δ:** 0.89 (t, *J* = 6.8 Hz, 3H, CH_3), 1.26 (s, 22H, CH_2), 1.39-1.32 (m, 4H, CH_2), 1.80-1.67 (m, 2H, CH_2), 3.28 (s, 9H, CH_3), 3.44-3.36 (m, 2H, CH_2).
C_{16}TA*p*-TS	2917, 2847 (CH_3), 1488, 1467 (CH_2), 1196(S=O)	**(400 MHz, $CDCl_3$) δ:** 0.89 (t, *J* = 6.8 Hz, 3H, CH_3), 1.27 (s, 24H, CH_2), 1.71-1.60 (m, 2H, CH_2), 2.12 (s, 2H, CH_2), 2.35 (s, 3H, CH_3), 3.33 (s, 9H, CH_3), 3.43-3.37 (m, 2H, CH_2), 7.16 (d, *J* = 7.9 Hz, 2H, CH), 7.76 (d, *J* = 8.1 Hz, 2H, CH).

2.2.2 Synthesis and characterization of gemini surfactants

The procedure of synthesis of gemini surfactants are reported earlier.[2-4] In short, combined synthesis procedure is given here. For the synthesis of gemini surfactants, the required reactants are given in Table 2.3. Reactant A (1 molar equivalent) and reactant B (2 molar equivalent with 10% extra) were mixed. This reaction mixture was refluxed in dry ethanol for 72 hours. After completion, the reaction mixture was cooled down, and the solvent was vaporized under vacuum pump. The obtained solid product was washed several times with a mixture of ethyl acetate and hexane. Recrystallization of the

surfactants was done by a mixture of ethyl acetate/methanol (10:1 v/v). The structures of synthesized compounds were confirmed by ^{1}H-NMR spectroscopy. The data are documented in Table 2.4. ^{1}H-NMR spectrum Gemini-X is shown in Figure 2.1 as a representative one. The molecular structures of the synthesized gemini surfactants are given by Scheme 2.3.

Table 2.3. Reactants for the synthesis of gemini surfactants.

Sr. No.	Gemini surfactants	Denoted as	Reactant A	Reactant B
1.	1,4-bis(dodecyl-N,N-dimethylammonium bromide)diethylether	12-EE-12 (Gemini-X)	Bis(2-bromoethyl) ether	*N*,*N*-dimethyl dodecyl amine
2.	1,4-bis(tetradecyl-N,N-dimethylammonium bromide)diethylether	14-EE-14 (Gemini-Y)	Bis(2-bromoethyl) ether	*N*,*N*-dimethyltetra decyl amine
3.	1,4-bis(hexadecyl-N,N-dimethylammonium bromide)diethylether	16-EE-16 (Gemini-Z)	Bis(2-bromoethyl) ether	*N*,*N*-dimethyl hexadecyl amine
4.	1,4-bis(dodecyl-*N*,*N*-dimethylammoniumbromide)-butane	12-4-12 (Gemini-A)	1,4-dibromobutane	*N*,*N*-dimethyl dodecyl amine
5.	1,4-bis(dodecyl-*N*,*N*-dimethylammoniumbromide)-2-butanol	12-4(OH)-12 (Gemini-B)	1,4-dibromo-2-butanol	*N*,*N*-dimethyl dodecyl amine
6.	1,4-bis(dodecyl-*N*,*N*-dimethylammoniumbromide)-2,3-butanediol	12-4(OH)$_2$-12 (Gemini-C)	1,4-dibromo-2,3-butanediol	*N*,*N*-dimethyl dodecyl amine
7.	1,3-bis(dodecyl-*N*,*N*-dimethylammoniumbromide)-propane	12-3-12	1,3-dibromopropane	*N*,*N*-dimethyl dodecyl amine
8.	1,6-bis(dodecyl-*N*,*N*-dimethylammoniumbromide)-hexane	12-6-12	1,6- dibromohexane	*N*,*N*-dimethyl dodecyl amine
9.	1,8-bis(dodecyl-*N*,*N*-dimethylammoniumbromide)-octane	12-8-12	1,8-dibromoctane	*N*,*N*-dimethyl dodecyl amine
10.	1,12-bis(dodecyl-*N*,*N*-dimethylammoniumbromide)-dodecane	12-12-12	1,12-dibromododecane	*N*,*N*-dimethyl dodecyl amine
11.	1,4-bis(tetradecyl-*N*,*N*-dimethylammoniumbromide)-butane	14-4-14	1,4-dibromobutane	*N*,*N*-dimethyl tetradecyl amine
12.	1,4-bis(hexadecyl-*N*,*N*-dimethylammoniumbromide)-butane	16-4-16	1,4-dibromobutane	*N*,*N*-dimethyl hexadecyl amine

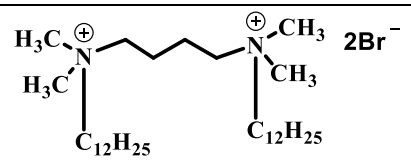 **12-4-12 (Gemini-A)**	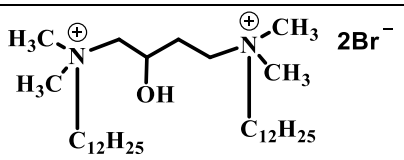 **12-4(OH)-12 (Gemini-B)**
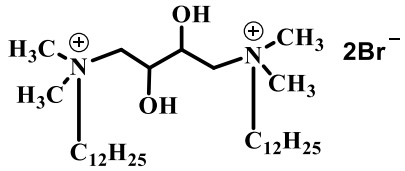 **12-4(OH)$_2$-12 (Gemini-C)**	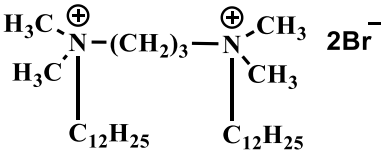 **12-3-12**
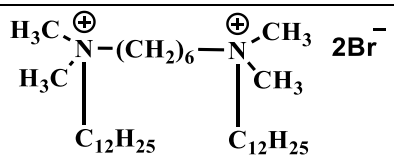 **12-6-12**	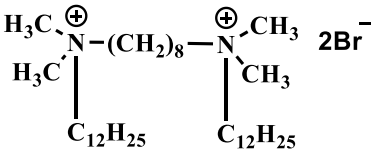 **12-8-12**
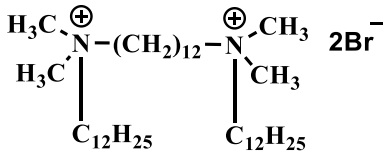 **12-12-12**	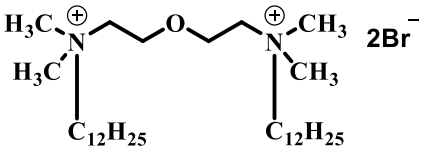 **Gemini-X**
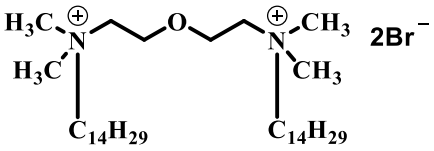 **Gemini-Y**	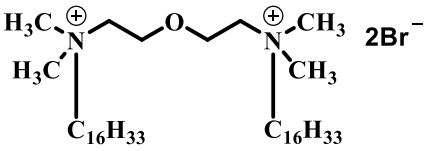 **Gemini-Z**
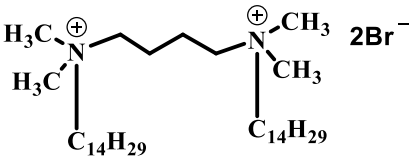 **14-4-14**	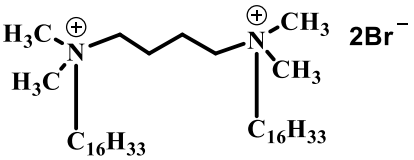 **16-4-16**

Scheme 2.3: Molecular structures of synthesized gemini surfactants.

Table 2.4. Empirical formula, molar mass, and ^{1}H-NMR data of synthesized gemini surfactants.

Compounds	Empirical Formula	Molar mass	^{1}H-NMR
12-EE-12 Gemini-X	$C_{32}H_{70}N_2Br_2O$	658.73	**(400 MHz, $CDCl_3$) δ:** 0.88 (t, *J* = 6.9 Hz, 6H, CH_3), 1.29-1.23 (m, 24H, CH_2), 1.37-1.30 (m, 8H, CH_2), 1.78-1.66 (m, 4H, CH_2), 2.24 (br s, 4H, CH_2), 3.45 (s, 12H, CH_3), 3.67-3.58 (m, 4H, CH_2), 4.02 (t, 4H, CH_2), 4.34 (t, 4H, CH_2).
14-EE-14 Gemini-Y	$C_{36}H_{78}N_2Br_2O$	714.83	**(400 MHz, $CDCl_3$) δ:** 0.88 (t, *J* = 6.9 Hz, 6H, CH_3), 1.29-1.22 (m, 32H, CH_2), 1.42-1.31 (m, 8H, CH_2), 1.83-1.63 (m, 4H, CH_2), 2.24 (br s, 4H, CH_2), 3.45 (s, 12H, CH_3), 3.68-3.57 (m, 4H, CH_2), 4.02 (t, 4H, CH_2), 4.34 (t, 4H, CH_2).
16-EE-16 Gemini-Z	$C_{40}H_{86}N_2Br_2O$	770.94	**(400 MHz, $CDCl_3$) δ:** 0.88 (t, *J* = 6.9 Hz, 6H, CH_3), 1.29-1.22 (m, 40H, CH_2), 1.37-1.31 (m, 8H, CH_2), 1.79-1.66 (m, 4H, CH_2), 2.12 (br s, 4H, CH_2), 3.44 (s, 12H, CH_3), 3.67-3.57 (m, 4H, CH_2), 4.02 (t, 4H, CH_2), 4.32 (t, 4H, CH_2).
12-4(OH)-12 Gemini-B	$C_{32}H_{70}N_2Br_2O$	658.73	**(500 MHz, $CDCl_3$) δ:** 0.85 (t, *J* = 6.9 Hz, 6H, CH_3),1.31-1.23 (m, 36H, CH_2), 1.74 (t, 4H, CH_2), 2.57 (t, 4H, CH_2), 3.26 (s, 6H, N-CH_2), 3.33 (s, 6H, N-CH_2), 3.49-3.43 (m, 2H, CH), 3.61-3.60 (m, 1H, CH), 3.75-3.73 (m, 1H, CH), 3.90 (t, 1H, CH), 4.17 (t, 1H, CH), 4.59 (s, 1H, O-CH), 5.72 (s, 1H, OH).
12-4$(OH)_2$-12 Gemini-C	$C_{32}H_{70}N_2Br_2O_2$	674.73	**(400MHz, DMSO) δ:** 0.86 (t, *J* = 6.9 Hz, 6H, CH_3), 1.24-1.23 (m, 44H, CH_2), 1.71-1.68 (t, 4H, CH_2), 3.08 (s, 12H, CH_3), 4.12 (s, 2H, OH), 5.79-5.78 (t, 2H, CH).
12-3-12	$C_{31}H_{68}N_2Br_2$	628.73	**(400 MHz, $CDCl_3$) δ:** 0.85 (t, *J* = 6.9 Hz, 6H, CH_3), 1.35-1.19 (m, 36H, CH_2), 1.80-1.69 (m, 4H, CH_2), 2.72-2.58 (m, 2H, CH_2), 3.39 (s, 12H, CH_3), 3.56-3.45 (m, 4H, CH_2), 3.85-3.72 (m, 4H, CH_2).

12-4-12 Gemini-A	$C_{32}H_{70}N_2Br_2$	642.73	(**400 MHz, $CDCl_3$) δ:** 0.88 (t, *J* = 6.8 Hz, 6H, CH_3), 1.30-1.22 (m, 24H, CH_2), 1.40-1.31 (m, 8H, CH_2), 1.84-1.66 (m, 4H, CH_2), 2.18-2.01 (m, 4H, CH_2), 2.73 (br s, 4H, CH_2), 3.30 (s, 12H, CH_3), 3.46-3.38 (m, 4H, CH_2), 3.84 (t, 4H, CH_2).
12-6-12	$C_{34}H_{74}N_2Br_2$	670.73	**(400 MHz, $CDCl_3$) δ:** 0.84 (t, *J* = 6.8 Hz, 6H, CH_3), 1.34-1.18 (m, 36H, CH_2), 1.57-1.45 (m, 4H, CH_2), 1.73-1.62 (m, 4H, CH_2), 2.00-1.89 (m, 4H, CH_2), 3.36 (s, 12H, CH_3), 3.50-3.43 (m, 4H, CH_2), 3.72-3.60 (m, 4H, CH_2).
12-8-12	$C_{36}H_{78}N_2Br_2$	698.73	**(400 MHz, $CDCl_3$) δ:** 0.80 (t, *J* = 6.8 Hz, 6H, CH_3), 1.37-1.16 (m, 44H, CH_2), 1.69-1.58 (m, 4H, CH_2), 1.85-1.69 (m, 4H, CH_2), 3.28 (s, 12H, CH_3), 3.47-3.37 (m, 4H, CH_2), 3.61-3.48 (m, 4H, CH_2).
12-12-12	$C_{40}H_{86}N_2Br_2$	754.73	**(400 MHz, $CDCl_3$) δ:** 0.82 (t, *J* = 6.8 Hz, 6H, CH_3), 1.36-1.17 (m, 52H, CH_2), 1.74-1.59 (m, 8H, CH_2), 3.32 (s, 12H, CH_3), 3.51-3.44 (m, 4H, CH_2), 3.58-3.51 (m, 4H, CH_2).
14-4-14	$C_{36}H_{78}N_2Br_2$	698.83	**(400 MHz, $CDCl_3$) δ:** 0.88 (t, *J* = 6.8 Hz, 6H, CH_3), 1.30-1.21 (m, 32H, CH_2), 1.40-1.31 (m, 8H, CH_2), 1.84-1.66 (m, 4H, CH_2), 2.18-2.01 (m, 4H, CH_2), 2.73 (br s, 4H, CH_2), 3.30 (s, 12H, CH_3), 3.46-3.38 (m, 4H, CH_2), 3.84 (t, 4H, CH_2).
16-4-16	$C_{40}H_{86}N_2Br_2$	754.94	**(400 MHz, $CDCl_3$) δ:** 0.88 (t, *J* = 6.8 Hz, 6H, CH_3), 1.30-1.21 (m, 40H, CH_2), 1.40-1.31 (m, 8H, CH_2), 1.84-1.66 (m, 4H, CH_2), 2.18-2.01 (m, 4H, CH_2), 2.73 (br s, 4H, CH_2), 3.30 (s, 12H, CH_3), 3.46-3.38 (m, 4H, CH_2), 3.84 (t, 4H, CH_2).

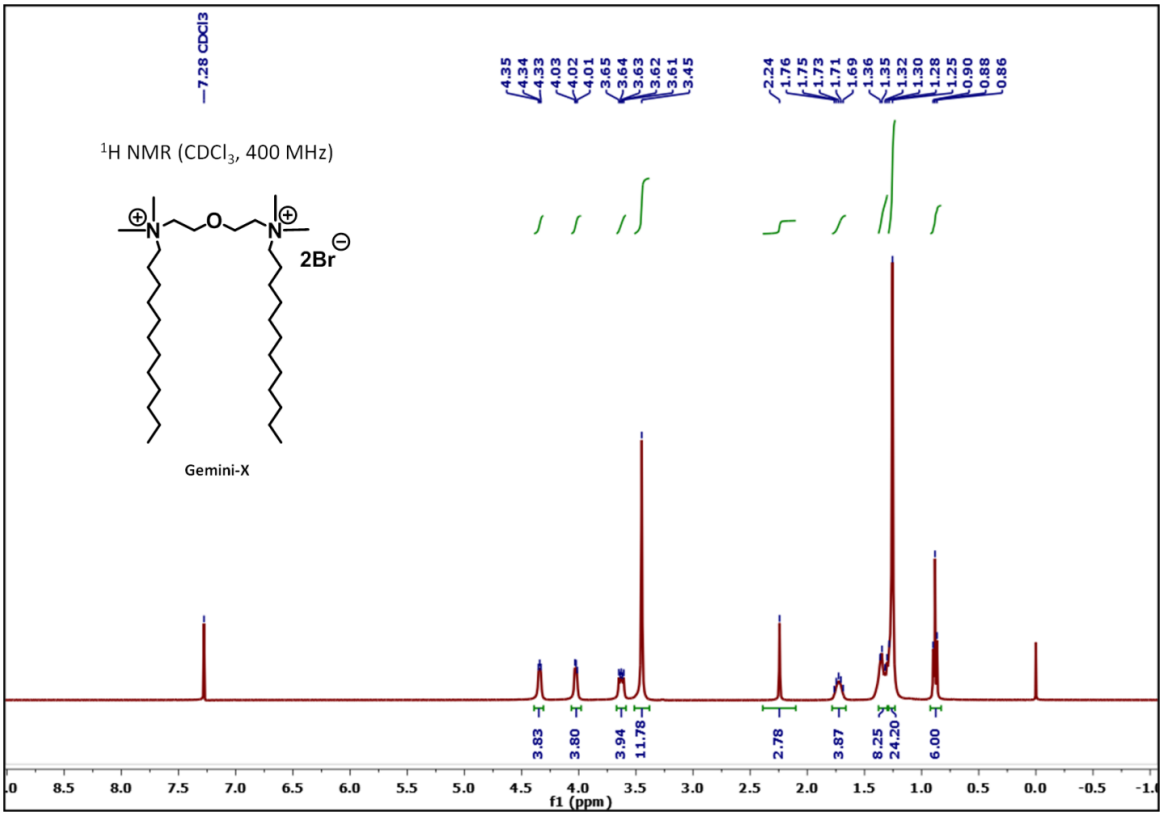

Figure 2.1. ^{1}H-NMR spectrum of Gemini-X.

2.2.3 Preparation of various solutions

Milli-Q water is ions free water, obtained from the Millipore water filtration system and was used for the preparation of the aqueous solutions.

2.2.3.1 Preparation of solutions for solvation dynamic and rotational relaxation studies

(i) For the solvatochromic studies, C-480 and C-485 were used as the fluorophore or probe. A stock solution of probes (1 mM) was prepared in pure methanol. The final concentration of probes in all the experimental solutions used for spectroscopic measurements was 5 μM. The required amount of probe (in ml from a stock solution of 1 mM) was added in different test tubes and kept for some time to air-dry the methanol. After drying off the methanol, the required volume of respective solvent was added into it. For the solvatochromic study, spectra were taken immediately after preparation of the solution.

(ii) For the preparation of the solutions of different concentrations of hexadecyltrimethylammonium, $C_{16}TAX$ (X= Br^-, SO_4^{2-}, NO_3^- and *p*-TS^-), the addition of C-480 was same, the only difference is that the amount of surfactant was added from their respective aqueous stock solutions according to their final concentration ten times of their

respective *cmc*. Make up of final volumes was done using the Milli-Q water. The final concentration of C-480 in all solutions was 5 μM. Solutions were then kept for 5–6 h to attain equilibrium.

(iii) The solution preparation method was same for the solvation dynamics and rotational relaxation of C-480 in the aqueous micelles of Gemini-A, Gemini-X, Gemini-Y, and Gemini-Z at the concentration ten times of their respective *cmc* and 5 μM concentration of C-480. The stock solution of C-480 (1 mM) was prepared in pure methanol and was added, dried and after addition of surfactants, its final volume was adjusted to 5 mL with Milli-Q water. Solutions were then kept for 5–6 h to attain equilibrium.

(iv) For the study of the effect of urea concentrations on solvation and rotational relaxation of C-480 in the 10 mM concentration of aqueous micelles of Gemini-A, Gemini-B, and Gemini-C, solutions were prepared in similar fashion as discussed above. Concentration of C-480 was kept at 5 μM throughout the study. DPH solution was prepared in THF. After preparation of surfactant solutions in presence of DPH, the test tubes were kept in dark prior to the spectral measurements. Solutions were then kept for 5–6 h to attain equilibrium.

2.2.3.2 Preparation of *β*-cyclodextrin solution

In order to prepare *β*-cyclodextrin solution for the spectral analysis, all aqueous solution has been prepared in the Milli-Q water, and pH was adjusted to the value of 7.4 by using the $NaOH/H_2SO_4$. pH adjusted water was used for the preparation of all aqueous solutions of surfactants and *β*-CD to maintain the pH at 7.4. The concentration of C-485 (5 μM) was fixed for all the experimental studies. Standard solution of C-485 was prepared in methanol. From the standard solution, the required amount of C-485 was added to the experimental solutions. Vaporization of methanol has not done, studies were performed in presence of 0.5% of methanol.

2.2.3.3 Preparation of BSA solution

Disodium hydrogen orthophosphate (Na_2HPO_4), was used to prepare buffer solution. The buffer of 10 mM was prepared in Milli-Q water. pH of the buffer was adjusted at 7.4 using $NaOH/H_3PO_4$. BSA (5 μM) and gemini surfactants solutions were prepared in the same buffer solution. Solutions of gemini surfactants with varying concentrations were also prepared in the same buffer.

2.2.3.4 Preparation of ctDNA solution

2-[4-(2-hydroxyethyl)piperazin-1-yl]ethanesulfonic acid (HEPES), was used to prepare buffer solution. HEPES buffer of 10 mM was prepared in Milli-Q water. pH of the

buffer was adjusted at 7.4 using $NaOH/H_2SO_4$. The buffer was used for the preparation of the ctDNA and gemini surfactants solutions. A stock solution of ctDNA was prepared by dissolving fibrous solid ctDNA in prepared HEPES buffer and stored at 4 °C to swell it. The purity of ctDNA was confirmed by monitoring the ratio of absorbance at 260 nm to that at 280 nm, which was in the range of 1.8-1.9. The concentration of ctDNA stock solution was determined spectrophotometrically using ε_{DNA} = 6,600 mol^{-1} dm^3 cm^{-1} at 260 nm. Freshly prepared (stored for maximum 4-5 day at 4 °C) stock solutions were used for the preparation of all spectral solutions.

2.2.3.5 Preparation of solution for measurement of the specific conductance

Concentrated stock solutions of conventional, as well as gemini surfactants, were prepared by dissolving required amounts of surfactants in Milli-Q water. The stock solution was then added progressively using a micropipette to a beaker containing water and kept in a thermostat (Julabo, F25) to maintain the temperature with an accuracy of ± 0.01 °C. Before the measurement of specific conductance (κ), proper mixing and equilibration of solutions were ensured.

2.2.3.6 Preparation of solution for determination of *cmc* by fluorescence method

A set of aqueous solutions of gemini surfactants with various concentrations of surfactant at a constant concentration of C-480 (5 μM) were prepared. A fixed amount of C-480 from the stock solution (prepared in methanol) was transferred into the test tubes and then methanol was evaporated. The required amount of surfactant solution was then added into these test tubes to prepare the solution of desired concentration.

2.2.4 Conductivity measurement

The conductance or specific conductance of an electrolyte solution is the measurement of its capability to conduct electricity. The electrical conductivity is reciprocal of electric resistance (R) and similarly, specific conductivity (κ) is of specific resistance (ρ):

$$\kappa = \frac{1}{\rho} = \frac{1}{R} \times \frac{l}{A} \tag{2.1}$$

Here, l/A denotes cell constant, which is 1.0 cm^{-1} for the used conductometer. The SI unit of specific conductance is Siemens per meter (Sm^{-1}). The conductivity dip cell was calibrated prior to the measurement with a standard KCl solution of specific conductivity 1413 $\mu S.cm^{-1}$.

2.2.4.1 Critical micellar concentration (*cmc*) by conductivity method

This method is only applicable for the ionic surfactants for determination of their *cmc*. The variation in the specific conductance of ionic surfactants depends on the concentration of the surfactants, either it's lower or higher than their *cmc*. Below the *cmc*, surfactant monomers behave as a strong electrolyte, consequently, with increasing concentration of surfactant, number of ions increases, so specific conductance also increases. Above the *cmc*, when the micelles are formed, surfactants molecules come closer and there is repulsion between the headgroups, which makes the micelles unstable. Therefore, to reduce the headgroup-headgroup repulsion, some of counterions bind to the surface of the micelles, which gives stability to the micellar system and reduces the rate of increase in the specific conductance. The *cmc* of ionic surfactants can be estimated by the breakpoint of two straight lines of specific conductivity (κ) versus surfactant concentration plot in premicellar and post-micellar region using the William *et al*.[5] method.

2.2.4.2 The degree of counterion dissociation

The degree of counterion dissociation (α) can be estimated from the ratio of post-micellar slope to pre-micellar slope of the plot of specific conductance (κ) versus surfactant concentration according to Williams' method.[5]

2.2.4.3 Critical micellar concentration (*cmc*) by fluorescence method

This method is used for all ionic and nonionic surfactants to determine their *cmc*.[6] In the fluorescence method, the *cmc* of surfactant is estimated by monitoring the change in fluorescence intensity of probe molecule with increasing concentration of surfactant. At concentrations below the *cmc*, the fluorescence intensity is very low, and a lesser enhancement in intensity with increasing surfactant concentration in the solution is observed. However, just above the *cmc*, there is an abrupt increase in the fluorescence intensity associated with blue shifts in the peak maximum. At the very high concentrations of surfactant, fluorescence intensity is saturated. These changes in the fluorescence intensity happen due to the transfer of probe molecule from the bulk polar aqueous environment to the more hydrophobic environment i.e. probe molecules are trapped inside the micelles. Later on, at the high concentrations of surfactant, all probe molecules get micellized.

2.2.5 Determination of micropolarity of the microenvironment around C-480

The micropolarity is symbolized in terms of empirical solvent polarity parameter, $E_T(30)$, developed by Reichardt *et al.*,[7] which represents the resemblance in the fluorescence behavior of probe molecule in microheterogeneous systems to that in a mixture of homogeneous solvents of different composition.[8-10] The procedure reported by Saha *et al.*[11] was used for the estimation of the micropolarity in the equivalent scale of $E_T(30)$ for the microenvironment of C-480 in the different micelles. First fluorescence spectra of C-480 were recorded in a mixture of dioxane-water, and then the fluorescence peak maxima in the form of wavenumbers were plotted against $E_T(30)$ and is given as a Figure 2.2 . After getting the $E_T(30)$, this plot data was compared with the peak maxima in wavenumber of different micellar system, which provides the micropolarity around the probe molecule. Figure 2.2 has been used to calculate the $E_T(30)$ values in the respective chapters.

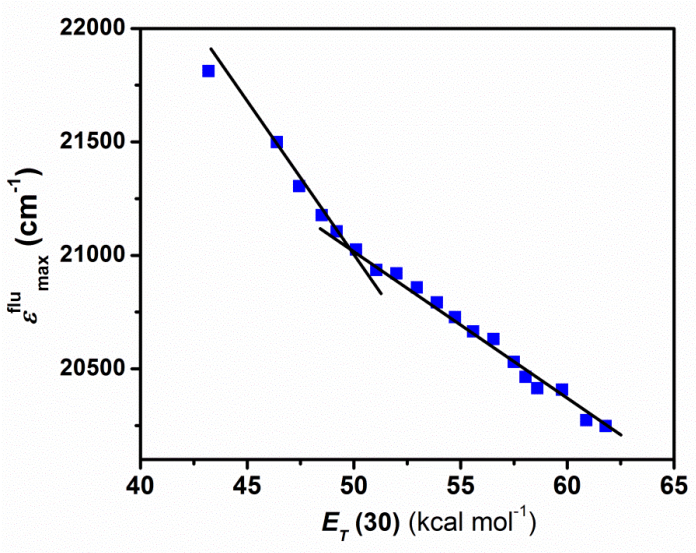

Figure 2.2. Variation of the fluorescence energy at peak maximum (ε_{max}^{fl}) of C-480 with $E_T(30)$ of various dioxane-water mixtures at 298.15±1 K.

2.2.6 Determination of microviscosity of microenvironment around C-480 and DPH

The steady-state fluorescence anisotropy measurement gives information regarding the microenvironment around the probe molecule. Minute modification in the shape, size, and medium of biological molecules are noticeable by an alteration in the fluorescence anisotropy. This could be the reason for the vast use of fluorescence anisotropy in biophysical and biochemical research.[12] The restriction in the motion of probe by the microenvironment is clearly visible through the values of fluorescence

anisotropy, which is related to the viscosity of microenvironment felt by molecule. Hence, microviscosity is determined using the comparison method, in which the fluorescence anisotropy of probe molecule in the microenvironment is compared with anisotropy of the same probe molecule in different environments of known viscosities.[9, 13-15]

In this method, the fluorescence anisotropy of C-480 has been measured in different percentages (v/v) of glycerol in glycerol-water mixtures and in the different micellar system. Later on, microviscosity has been estimated by correlation of both anisotropy data with viscosity, which are given by Figure 2.3 and Figure 2.4, respectively.

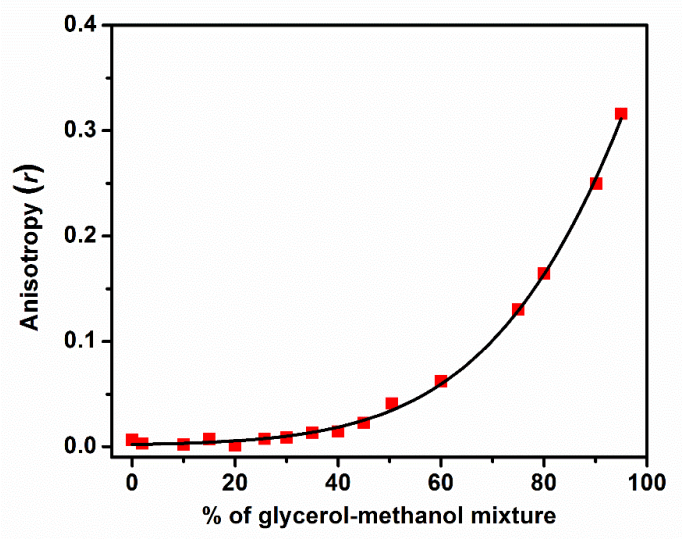

Figure 2.3. Fluorescence anisotropy of C-480 as a function of volume percentages of glycerol-methanol mixture at 298.15±1 K.

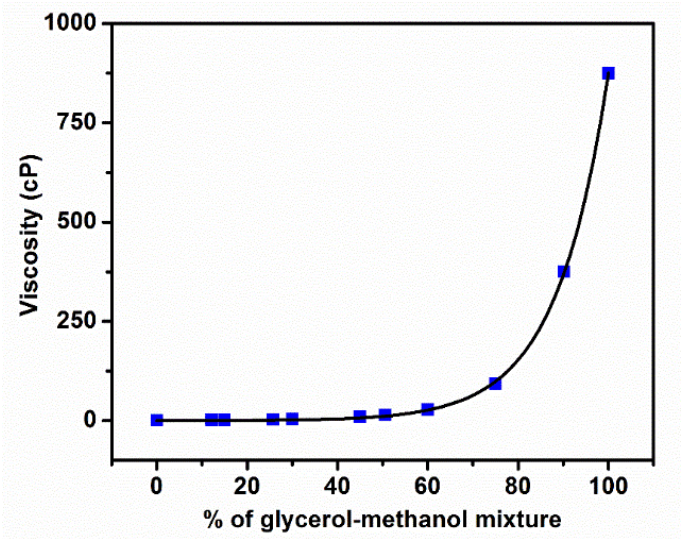

Figure 2.4. Viscosity as a function of volume percentage of glycerol-methanol mixture at 298.15±1 K.

In the other method, we explored 1,6-diphenyl-1,3,5-hexatriene (DPH), which is a well-known viscosity-sensitive fluorescence probe molecule.[2] The absolute values of

microviscosity of micelles, η_m, using DPH have been calculated following the Debye-Stokes-Einstein relation (Equation 2.2):[16]

$$\eta_m = k\,T\tau_r / \upsilon_h \tag{2.2}$$

where k is the Boltzmann constant, T is the Kelvin scale temperature, υ_h represents the hydrodynamic volume of DPH (313 Å)[16] and τ_r signify rotational correlation time of DPH. The rotational correlation time, τ_r can be calculated by the following Perrin Equation:[12]

$$\tau_r = \tau / \left[\left(r_o / r\right) - 1\right] \tag{2.3}$$

where r_o signify the steady-state fluorescence anisotropy in an extremely viscous solvent, whose value is taken as 0.362[16], r and τ represent steady-state fluorescence anisotropy and excited singlet state lifetime in the surfactant solution, respectively.

2.2.7 Steady-state fluorescence anisotropy measurements

The steady-state fluorescence anisotropy, r can be determined using the following Equation:[12]

$$r = \frac{I_{VV} - GI_{VH}}{I_{VV} + 2GI_{VH}} \tag{2.4}$$

where I_{VH} and I_{VV} represent the fluorescence intensities collected from the excitation polarizer aligned vertically and the emission polarizer aligned in horizontal and vertical positions, respectively. The factor G is represented by the following Equation:

$$G = \frac{I_{HV}}{I_{HH}} \tag{2.5}$$

where I_{HV} and I_{HH} represent the fluorescence intensities collected from the excitation polarizer aligned in a horizontal position and emission polarizer aligned in vertical and horizontal positions, respectively.

2.2.8 Fluorescence quantum yield

The relative fluorescence quantum yields (ϕ) of fluorescent molecules in different microheterogeneous systems were determined using the quinine sulphate[17] (ϕ = 0.55, in 0.1N H_2SO_4) as a standard fluorescence reference. First absorption spectra were recorded (absorbance less than 0.1 at the excitation wavelength for quinine sulfate) and after that corrected fluorescence spectra were recorded for reference as well as for samples at fixed

excitation wavelength, emission range, and slit widths. Generally, the longer wavelength band was used for selecting the excitation wavelength. Quantum yield of a sample was estimated using the Equation:

$$\phi_{\text{unknown}} = \frac{F_{\text{unknown}}}{F_{\text{standard}}} \times \frac{A_{\text{standard}}}{A_{\text{unknown}}} \times \phi_{\text{standard}} \tag{2.6}$$

where ϕ, *A, F* signify the fluorescence quantum yield, an absorbance at the excitation wavelength, and the area under the curve of corrected fluorescence spectra, respectively.

2.2.9 Determination of mole fraction partition coefficient

The mole fraction partition coefficient of gemini surfactants from the aqueous phase to micellar phase (K^{mic}) was determined by using the following Equation, 2.7 for required all micellar systems:[18]

$$\mathrm{K^{mic}} = \frac{55.5\mathrm{M}}{\mathrm{CMC}} \tag{2.7}$$

where 55.5 M is the molar concentration of the water. The values of standard molar Gibbs free energy of micellization were calculated by the given Equation 2.8:[18]

$$\Delta \mathrm{G^{o,mic}} = -\mathrm{RT\ln K^{mic}} \tag{2.8}$$

2.2.10 Solvation dynamics

For the quantitative measurement of solvation dynamics, the solvent response function (SRF), *C(t)* (eq 2.9) given by Fleming and Maroncelli[19] was used:

$$C(t) = \frac{\bar{\upsilon}(t) - \bar{\upsilon}(\infty)}{\bar{\upsilon}(0) - \bar{\upsilon}(\infty)} \tag{2.9}$$

where $\bar{\upsilon}(0)$, $\bar{\upsilon}(t)$ and $\bar{\upsilon}(\infty)$ are the peak wavenumbers at time zero, *t* and infinity, respectively. $\bar{\upsilon}(\infty)$ can be taken as the maximum of the steady-state fluorescence spectrum if solvation is more rapid than the population decay of the probe and $\bar{\upsilon}(t)$ can be determined by taking the maximum from the log-normal fits as the emission maximum.[19, 20] The *C*(*t*) function can be estimated using "spectral reconstruction" method. This method involves reconstruction of time-resolved emission spectra (TRES) from wavelength-dependent time-resolved decay data.[21] The fluorescence decays were collected at the different wavelength with 10-15 nm intervals across the fluorescence spectrum. All decays are fitted to mono/bi/tri-exponential as per the cases. The TRES were constructed by

following the procedure of Fleming and Maroncelli.[19] The impulse response function, $I(\lambda,t)$ is given by Equation 2.10:

$$I(\lambda,t) = \sum a_i(\lambda) \exp\left[\frac{-t}{\tau_i(\lambda)}\right] \tag{2.10}$$

where $a_i(\lambda)$ represents the pre-exponential factor, and $\tau_i(\lambda)$ represents the decay time at that wavelength with $\Sigma a_i(\lambda) = 1$.

A TRES is constructed after calculations of $H(\lambda)$ values, which is given by Equation 2.11:

$$H(\lambda) = \frac{F(\lambda)}{\sum a_i(\lambda)\tau_i(\lambda)} \tag{2.11}$$

where $F(\lambda)$ represents the steady-state intensity. The TRES at different times were constructed from the appropriately normalized intensity decay functions, $I'(\lambda,t)$ for various wavelengths and at various times using the following Equation 2.12:

$$I'(\lambda,t) = H(\lambda) \times I(\lambda,t) = H(\lambda)\sum a_i(\lambda) \exp\left[\frac{-t}{\tau_i(\lambda)}\right] \tag{2.12}$$

Each time-resolved emission spectrum (TRES) was fitted by "log-normal line shape function", which is given by the Equation:

$$g(\nu) = g_o \exp\left[-\ln 2\left(\frac{\ln[1+2b(\nu-\nu_p)/\Delta]}{b}\right)\right] \tag{2.13}$$

where g_o, b, ν_p, and Δ are signifying the peak height, asymmetric parameter, peak frequency, and width parameter, respectively. The peak frequency in wavenumber calculated from this log-normal fitting of TRES was then used to construct the decay of the solvent correlation function, $C(t)$. In generating $C(t)$, the first point was obtained from the zero time spectrum. The second point was taken at the maximum of the instrument response function. Finally, the time dependence of the estimated $C(t)$ values were fitted as bi/tri-exponential function using the Equation 2.14:

$$C(t) = \sum_i a_{is} \exp\left(-\frac{t}{\tau_{is}}\right) \tag{2.14}$$

Finally, the average solvation time is calculated using the Equation:

$$\langle \tau_s \rangle = \sum_i a_{is} \tau_{is} \tag{2.15}$$

where a_{is} represents the contribution of respective solvation component, τ_{is}.

2.2.11 Time-resolved fluorescence anisotropy

The time-resolved fluorescence anisotropy, $r(t)$[12] has been determined using Equation 2.16:

$$r(t) = \frac{I_{\parallel}(t) - GI_{\perp}(t)}{I_{\parallel}(t) + 2GI_{\perp}(t)} \tag{2.16}$$

where $I_{\parallel}(t)$ and $I_{\perp}(t)$ represent fluorescence decays polarized parallel and perpendicular to the polarization of the excitation light, respectively. G represents the correction factor for the detector sensitivity to the polarization detection of emission and the value of G factor is ~ 0.6 for the used instrument.

Typically, the fluorescence anisotropy decay of the fluorescence probe molecule residing in micelles is having two components, fast and slow components. The bi-exponential behavior of the anisotropy decay is not due to the different location of the probe molecule in the micelles but due to the different types of rotational motions.[22] The theoretical model, the two-step and wobbling-in-a-cone mode are generally used to explain the bi-exponential behavior of anisotropy decay because of different types of rotational motions.[23] The applicability of these models is limited to spherical micelles.

2.2.12 Two-step model

In the two-step model, both rotational motion *viz.* fast and slow are assumed to be distinguishable. If both of these motions are independent, then the bi-exponential anisotropy decay was fitted to the decay function as represented by the following Equation 2.17:

$$r(t) = r_o[a_{1r}e^{-t/\tau_{1r}} + a_{2r}e^{-t/\tau_{2r}}] \tag{2.17}$$

where r_0 is the limiting value of anisotropy in order to represent the inherent depolarization of the probe molecule, τ_{1r} and τ_{2r} are the time constants for the fast and slow rotational relaxation components, respectively, and, a_{1r} and a_{2r} are relative amplitudes for these two

components, respectively. The rotational relaxation times for fast and slow components were calculated from the fitted decay. The following equation (Equation 2.18) was used to estimate the average rotational relaxation time:

$$\langle \tau_r \rangle = a_{1r}\tau_{1r} + a_{2r}\tau_{2r} \tag{2.18}$$

where, τ_{1r} and τ_{2r} are the rotational relaxation times, and, a_{1r} and a_{2r} are the corresponding amplitudes. The two-step model explains that the slow relaxation time (τ_{2r}) can be related to the times corresponding to the tumbling motion of the micelle as a whole (τ_m) and the lateral diffusion (τ_D) of the probe along the micelle surface following the relation (eq 2.19):

$$\frac{1}{\tau_{2r}} = \frac{1}{\tau_D} + \frac{1}{\tau_m} \tag{2.19}$$

τ_m is calculated following Debye-Stokes-Einstein equation using the value of the hydrodynamic radius of the micelle and assuming that the spherical micelle is rotating in the solvent with sticking boundary conditions[24] as follows:

$$\tau_m = \frac{4\pi\eta r_h^3}{3kT} \tag{2.20}$$

where η, r_h, k, and T represent the shear viscosity of water, the hydrodynamic radius of the micelle, the Boltzmann constant and the temperature in Kelvin scale, respectively. After getting the values of τ_{2r} and τ_m, τ_D can be estimated using Equation 2.19.

2.2.13 Wobbling in a cone model

The restricted motion of a rod-like rotor with the transition moment parallel to the long axis is explained by the wobbling-in-a-cone model.[22] The schematic demonstration of the wobbling-in-a-cone model is represented in Figure 2.5. This model relates the internal motion of the probe (τ_e) with cone angle (θ_o) and wobbling diffusion coefficient (D_w). To measure the spatial restrictions of motion of the probe molecule, the order parameter, $|S|$ is calculated. The value of the order parameter varies from 0 to 1, where 0 reflects no restriction and 1 means complete restriction of the rotational motion of the probe molecule. The order parameter is associated with the recovery decay of anisotropy by the following Equation:

$$r(t) = r_o\left[S^2 \exp\left(-\frac{t}{\tau_{2r}}\right) + (1-S^2)\exp\left(-\frac{t}{\tau_{1r}}\right)\right] \tag{2.21}$$

From a comparison of Equations 2.23 and 2.26, we can calculate *S* using the Equation:

$$S^2 = a_{2r}. \tag{2.22}$$

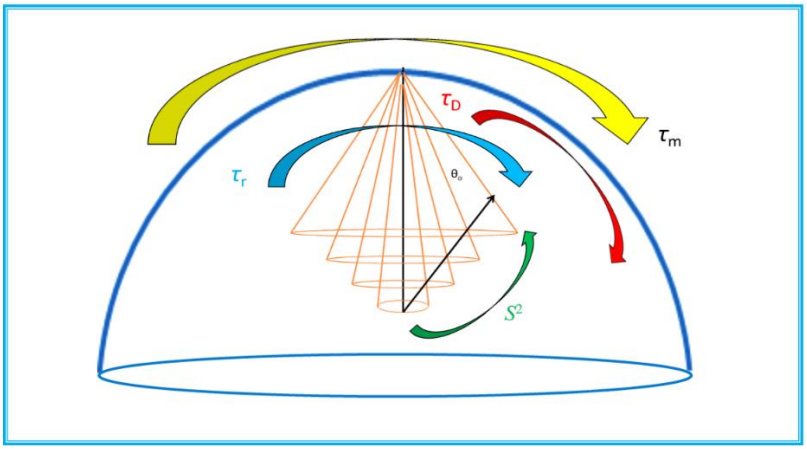

Figure 2.5. Schematic representation of a wobbling-in-a-cone model of rotational dynamics.

The order parameter is a measurement of the equilibrium orientational distribution of the probe. If the value of order parameter is zero that means the fluorophore tumbles without obstruction and the equilibrium orientational distribution is arbitrary. For the micellar solution, the value of order parameter mostly varies between 0.55-0.88, which shows that the equilibrium orientational distribution is highly constrained due to the aqueous or non-aqueous interface in the micelles. If the value of order parameter is less than 0.5 in micelles then the spinning-in-equatorial-band model is used for explanation.[25] The order parameter does not enclose any data regarding the dynamical properties of the probe. The dynamics are reflected by the faster rotational correlation time, which is described by the wobbling motion of the probe. In the wobbling-in-a-cone model, the order parameter is correlated to the cone angle, θ_o by the following Equation 2.23:

$$\theta_o = \cos^{-1}\left[\frac{1}{2}\left((1+8S)^{1/2} - 1\right)\right] \tag{2.23}$$

In the spinning-in-equatorial-band model, the order parameter is correlated to the cone angle, θ_o by the following Equation 2.24:

$$S^2 = \left[\frac{1}{2}\left(1-\cos^2\theta_o\right)\right]^2 \tag{2.24}$$

The wobbling motion time, (τ_w) corresponding to the restricted rotational diffusion is correlated to the fast relaxation time (τ_{1r}) and slow relaxation time (τ_{2r}) by the following Equation 2.25:

$$\frac{1}{\tau_{1r}} = \frac{1}{\tau_w} + \frac{1}{\tau_{2r}} \tag{2.25}$$

The wobbling diffusion coefficient, D_w is determined using Equation 2.26:

$$D_w = \frac{7\theta^2}{24\tau_e} \tag{2.26}$$

where θ signifies the cone angle in radian. The lateral diffusion coefficient (D_L) is determined using Equation 2.27:

$$D_L = r_h^2 / 4\,\tau_D \tag{2.27}$$

where r_h signifies hydrodynamic radius of the micelle.

2.2.14 Determination of binding isotherm of BSA

Binding isotherm study gives a better understanding of interaction between BSA and surfactants by giving an idea about the availability of binding positions in the protein, where the surfactants molecule can actually interact. Suppose, a protein has total binding positions, n_o, and at a particular concentration of surfactant, surfactants bind to positions of protein, n, then the fraction of binding (α) of surfactant with protein was given by the following Equation 2.28:[8, 26, 27]

$$\alpha = \frac{n}{n_0} \tag{2.28}$$

At the saturated binding condition, the fractional alteration in the fluorescence of BSA (α) caused by the binding of gemini surfactant has been determined by following Equation 2.29:[8, 27, 28]

$$\alpha = \left(\frac{I-I_0}{I_{min}-I_0}\right) \tag{2.29}$$

where I_o, I and I_{min} are signified the fluorescence intensities in absence, presence, and saturated concentration of surfactant. Based on the variation in α values with surfactant concentration, mainly, four binding regions are reported earlier:[8, 29] (1) specific binding, (2) non-cooperative binding, (3) co-operative binding and (4) saturation region.

2.3 Instrumentation

The various characterization techniques used for the present work are discussed below:

2.3.1 UV-Visible spectrophotometer

UV-visible absorption spectroscopy is a good spectroscopic tool, which provides the information regarding the interaction of UV-vis radiation with absorbing materials. This spectroscopy gives the information about the change in polarity of the environment, which can change the energy of the ground and excited states and is observed by a shift in spectra. The UV-visible spectroscopy works on the Beer-Lambert's law. The fraction of a parallel beam of light absorbed by a sample is independent of the intensity of the incident beam, which has relation with the concentration of the absorbing samples by the Beer-Lambert's law, and is given by the following Equation 2.30:

$$A = \log\left(\frac{I_o}{I}\right) = \varepsilon_\lambda Cl \tag{2.30}$$

Where ε_λ is molar extinction coefficient at wavelength λ, A is absorbance or optical density, I_o and I signify the intensity of the incident and transmitted light, C is the concentration of the light absorbing sample and l is the path length of the light absorbing medium.

The absorption spectra were recorded using a Jasco V-650 UV-Visible spectrophotometer (image is given as Figure 2.6) at room temperature. Quartz cuvettes of Hellma, 1 cm light path, capacity 3.5 ml, Model: 100-QS were used for the spectral recording.

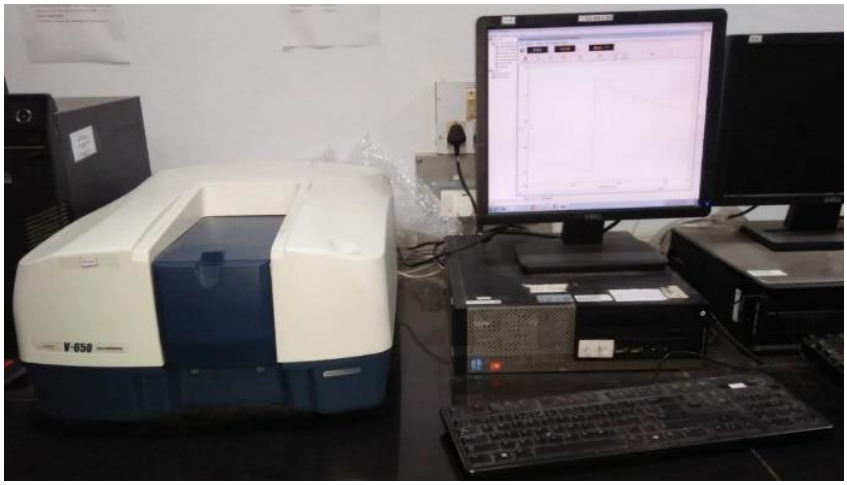

Figure 2.6. Image of the Jasco V-650 UV-visible spectrophotometer.

2.3.2 Steady-state spectrofluorimeter

Steady-state fluorescence spectroscopy explores the long-range average fluorescence of a sample after irradiation with UV, visible or near-IR Light. The fluorescence emission spectrum provides information for both qualitative and quantitative analysis in the form of fluorescence intensity as well as wavelength. Horiba Jobin Yvon Fluoromax-4 scanning spectrofluorimeter was used to perform all the fluorescence experiments (image is given as Figure 2.7). In this spectrophotometer, at first the sample is irradiated with a light of fixed wavelength, called excitation wavelength. Sample upon absorption of light, get excited and emits the lights of higher wavelengths in all direction. The detector detects this emitted light. Spectrofluorimeter is made up of various components; details of components are given below: The schematic diagram of the instrument is shown in Scheme 2.4

Present spectrofluorimeter is equipped with the light source of 1905-OFR 150-W Xenon lamp. The lamp housing is given with ozone self-decomposition. The instrument has Czerny-Turner monochromators for excitation and emission. The main portion of the monochromator is a reflection grating. A grating disperses the incident light by its vertical grooves. The gratings in present instrument have 1200 grooves mm^{-1} and are blazed at 330 nm (excitation) and 500 nm (emission). Blazing means etching of the grooves at a particular angle, to optimize the grating's reflectivity in a particular spectral region. The instrument uses a direct drive for each grating to scan the spectrum up to 200 nm s^{-1}, with

more than 0.5 nm accuracy and 0.3 nm repeatability. The scan range of the present instrument is 240-850 nm.

Figure 2.7. Image of the Horiba Jobin Yvon Fluoromax-4 scanning spectrofluorimeter.

The sample holder holds a cuvette filled with sample. The emission monochromator selectively collects fluorescence emitted from the sample and the photomultiplier tube (PMT) detects the fluorescence intensity. The monochromator has a diffraction grating of the same size as of the excitation monochromator for the collection of the maximum light. The detector of the present instrument comprises photomultiplier tube for both photometry and monitor sides. In general, the Xenon lamps used in spectrofluorimeter are characterized by very high emission intensity and an uninterrupted radiation spectrum. However, their tendency to unstable light emission will result in a greater signal to noise ratio if no countermeasure is added. Apart from this, the non-uniformity in the radiation spectrum of the Xenon lamp and in spectral sensitivity characteristics of the photomultiplier tube (known as instrument functions) produces distortion in the spectrum. To solve these problems, the photomultiplier tube monitors a portion of excitation light and feeds the resulting signal back to the photomultiplier tube for fluorescence scanning. This procedure is known as light-source compensation system. By using the computer slits widths can be controlled in the units of nanometers. The steady-state fluorescence anisotropy has been measured with the same instrument fitted with a polarizer attachment (105UV polarizers), manufactured by POLACOAT Co., USA. The measurements were recorded by keeping one set of two polarizer, which contains the polarizer for both the excitation and emission sides. Quartz cuvette (Hellma, 1 cm light path, capacity 3.5 ml, Model: 101-QS) with all transparent walls was used to record the excitation and emission spectra of the samples.

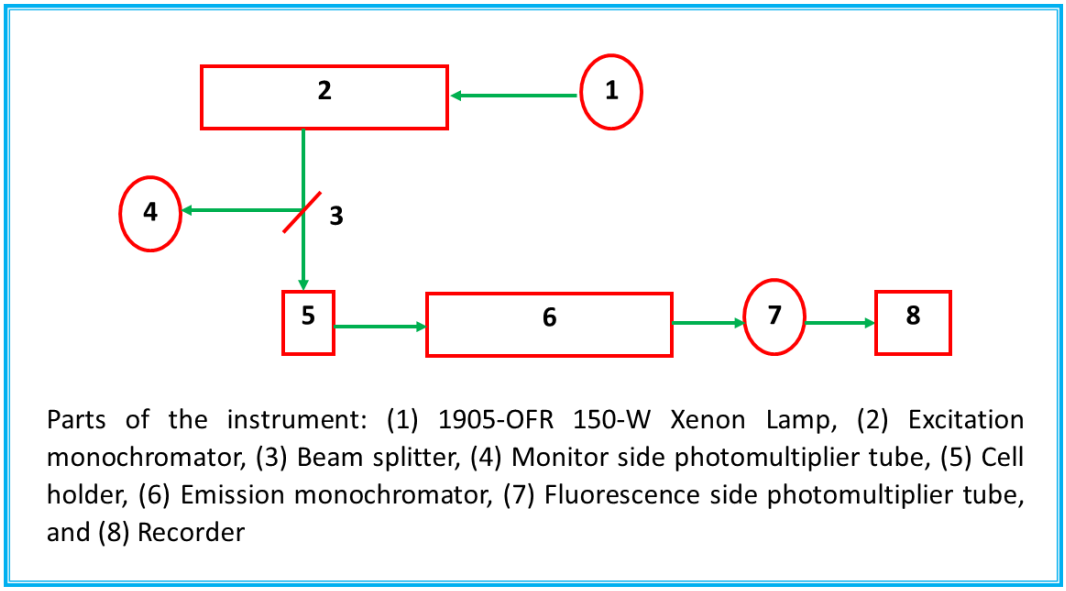

Parts of the instrument: (1) 1905-OFR 150-W Xenon Lamp, (2) Excitation monochromator, (3) Beam splitter, (4) Monitor side photomultiplier tube, (5) Cell holder, (6) Emission monochromator, (7) Fluorescence side photomultiplier tube, and (8) Recorder

Scheme 2.4: Schematic diagram of a steady-state spectrofluorimeter.

2.3.3 Time-resolved spectrofluorimeter

Steady-state and time-resolved fluorescence spectroscopy are rife and dominant tools to study of various systems viz. physical, chemical and biological systems. In the present thesis, these technologies are used to study important processes taking place on timescales from picoseconds (10^{-12} s) to nanoseconds (10^{-9} s). Particularly, the time-correlated single photon counting fluorescence techniques was used, which is described below in detail. The solvation dynamics is mainly addressed with this technology in various micellar systems.

Horiba Jobin Yvon Fluorocube-01-NL picosecond time-correlated single-photon counting (TCSPC) experimental setup was used to determine the excited singlet state lifetimes from intensity decays (image is given as Figure 2.8). Picosecond diode laser of 375 nm (NanoLED 375L, IBH, UK), and 300 nm NanoLED ((NanoLED 300 nm, IBH, UK) were used as light sources. Fluorescence signals were collected at magic angle (54.7^{o}) polarization using a TBX photon detection module (TBX-07C). The instrument response functions (IRF) of used diode laser and NanoLED are ~165 ps and ~900 ps, respectively. A basic schematic diagram of the instrument is given in Scheme 2.5.

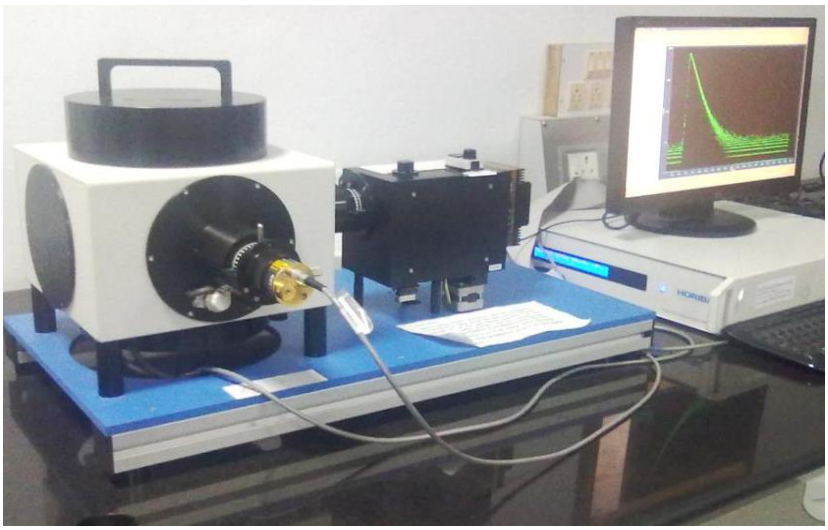

Figure 2.8. Image of the Horiba Jobin Yvon Fluorocube-01-NL picosecond time-correlated single-photon counting (TCSPC) spectrofluorimeter.

2.3.3.1 Time-correlated single photon counting (TCSPC) technique

The TCSPC is well established and commonly used for the fluorescence lifetime measurements. TCSPC technique is based on the detection of single photons and measurement of their arrival times with respect to a reference signal, which is generally the light source. This is a statistical sampling technique with single photon detection sensitivity, and capable of picosecond timing resolution. This technique trusts on the theory that the probability distribution for emission of a single photon after an excitation event yields the actual intensity versus time distribution of all the photons emitted as a result of the excitation. By sampling, the single photon emission following a large number of excitation events, the experiment constructs the probability distributions.

Time-to-amplitude converter (TAC) is the central part of this technique. It measures elapsed time between the initial rise in intensity of the pulse light source and the detection of an emitted photon from the sample. In procedure, an electrical pulse is produced at a time exactly correlated with the time of production of the optical pulse by the trigger. Once trigger pulse is received, TAC starts the charging of a capacitor plate, which is directed to the TAC start input through a discriminator. The fluorescent sample is excited by the same optical pulses (which trigger the TAC). Only one stop photon is detected from 100-200 excitations. The signal resulting from the detected photon stops the charging ramp in the TAC, which transmits a pulse. The amplitude of this pulse is proportional to the charge in the capacitor, and hence to the time difference between the

start and stop pulses. The TAC output pulse is given a numerical value within the analog-to-digital converter (ADC) and a count is stored in the data storage in an address corresponding to that number. This process of excitation and data storage is repeated continuously until the decay curve of the sample is not achieved

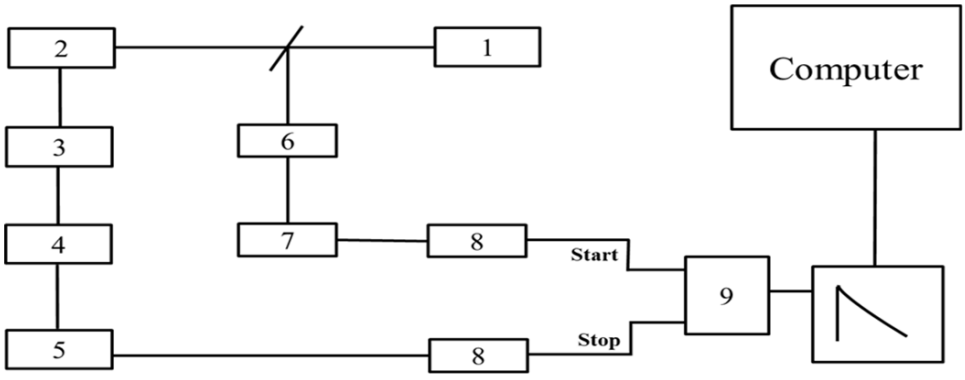

Parts of the instrument: (1) Diode laser, (2) Sample holder, (3) Fluorescence, (4) Monochromator, (5) Micro-channel plate-photomultiplier tube, (6) Photodiode, (7) Delay, (8) Constant fraction discriminator, and (9) Time-to-amplitude converter.

Scheme 2.5: Schematic diagram of time-resolved spectrofluorimeter.

2.3.3.2 Procedure of deconvolution

When the sample is excited with an infinitely short pulse of light, the time domain decay profile will be acquired. But generally, the excitation pulses are on the identical timescale as the fluorescence process. Therefore, the fluorescence response becomes the convolution of the measured instrumental prompt response, $P(t')$ and the theoretical fluorescence response function $F(t)$ of the form:

$$R(t) = \int_0^t P(t')F\left(t - t'\right)dt' \tag{2.31}$$

where t' describes the variable time delays or channel numbers of the infinitesimally small widths dt' (i.e. channel widths) of which the $P(t')$ is composed. Many methods are available to extract $P(t')$ from $F(t)$ but the most used method is a least-square method in concert with an iterative reconvolution scheme. After that convolution integral is determined using the test model (Equation 2.32):

$$F(t) = \sum_i a_i e^{t/\tau_i} \tag{2.32}$$

and using the initial set of a_i and τ_i values and the recorded instrument response function. Calculated and observed data are matched and a_i and τ_i terms are tuned until the best fit is acquired. The excellence of the fit is confirmed by the chi-square value (χ^2):

$$\chi^2 = \sum_{i=1}^{n} \omega_i \left[R(t) - R_c(t) \right]^2 \tag{2.33}$$

where $R_c(t)$ is determined by assuming the functional form of $F(t)$. ω_i and i represent the weighting factor [$\omega_i = 1/R(t)$], and the number of data points in the decay file, respectively. ω_i follows the Poisson statistics. The value of χ^2 is close to 1.0 which represents the good fitting. The goodness of fit was also confirmed visualization of residuals.

2.3.3.3 Analysis of fluorescence lifetime and anisotropy decays

The recorded fluorescence lifetime and anisotropy decays were analyzed via commercially available lifetime analysis software, decay analysis software (DAS 6) of IBH (UK).

2.3.4 Circular dichroism spectrophotometer

Circular dichroism (CD) spectroscopy is a type of light absorption spectroscopy that measures the difference in absorbance of right- and left-circularly polarized light by the substances. Far-UV circular dichroism spectroscopy is extensively used to study chiral molecules of all kinds and sizes, while it has huge applications in large biological molecules such as proteins, nucleic acids. It can be used to monitor the alteration in the secondary structure of protein due to change in the microenvironment. Structural, thermodynamic and kinetic information about macromolecules can be identified from this spectroscopy.

Circular dichroism is usually recorded by the differential absorbance of the left (ALCP) and right circularly polarised (ARCP) light, and so can be noted as, ΔA= ALCP - ARCP. If we consider cell pathlength and compound concentration, then the molar circular dichroism ($\Delta\varepsilon$) is given by Equation 2.34:

$$\Delta\varepsilon = \varepsilon LCP - \varepsilon RCP = \Delta A/(C \times l) \tag{2.34}$$

where εLCP and εRCP are the molar extinction coefficients for LCP and RCP light, respectively. C and l are molar concentration and path length (cm), respectively. Another important unit is mean residue molar circular dichroism, $\Delta\varepsilon$MR. This unit is specific for proteins and reports the molar circular dichroism for individual protein residues instead of

entire protein molecules. It makes ease of comparison of different proteins with greatly different molecular weights. CD is also noted as degrees of ellipticity (θ), which is an inheritance of polarimetry, and these units are regularly used in the literature.

The far-UV circular dichroism (CD) spectra have been recorded using Chirascan CD spectropolarimeter (Applied Photophysics Ltd.) in the range of wavelength 190–260 nm (image is given as Figure 2.9). A cuvette of the path length of 1 mm was used for the spectral measurements. Average CD spectrum was taken from consecutive five scans with the scan speed of 200 nm min^{-1} and with a 10 nm spectral bandwidth. The spectrum of Na-phosphate buffer was subtracted prior to the measurements to reduce the noise of the background.

Figure 2.9. Image of the Chirascan CD spectropolarimeter.

2.3.4.1 Analysis of CD spectra

CD spectra were analyzed for the calculation of various components of the secondary structures of BSA using CDNN 2.1 software in the range of 200-260 nm. In the software, we fed the CD spectral data as an input file (circular dichroism in millidegree) along with molecular mass (Dalton) of protein, concentration of the protein (mg/ml), pathlength (cm) and number of amino acids present in the protein. Distribution of α-helical, β-sheet and the random coil contents of the secondary structure of BSA was obtained by deconvolution of the CD spectra. These provide detailed information regarding helical and sheet structures in the secondary structure of BSA.

2.3.5 Other instruments

To establish the size of micelles of synthesized surfactants, the dynamic light scattering (DLS) measurements were done using a Zeta Sizer, model Nano ZS (ZEN 3600,

Malvern instrument, UK) (image is given as Figure 2.10). Before doing the measurements of size, and to avoid detection of the large dust particles, samples were centrifuged at 13000 rpm for 1 hour and later on, filtered with 0.22-µM pore size filter (Durapore, PVDF, and Micropore). The wavelength of the laser light and scattering angle were fixed at the 632.8 nm, and 173^{o}, respectively throughout the measurements. The instrument was auto-optimized to perform the number of scans of measurements for an individual sample at ambient conditions. The signal of scattering intensity of the sample is transferred to a digital signal processing board, known as correlator, which compares the scattering intensity at successive time intervals to derive the rate at which the intensity is changing. The correlator informations are transferred to the computer and the data were analyzed by using the Zetasizer software and provide the information about the size. To judge the size distribution the corresponding G function is considered carefully.

Figure 2.10. Image of the Zeta Sizer, model Nano ZS (ZEN 3600, Malvern) instrument.

Conductivity measurements and adjustment of the pH of the solution have been done using the direct reading Eutech Instruments combined pH and conductometer, model PC 510 and Systronics conductivity meter 304. *Cmc* measurements have been done at 25 °C, for that, a thermostat, model Julabo, F25 was used to regulate the temperature.

^{1}H-NMR spectra were recorded in $CDCl_3$, D_2O and DMSO solutions with a Bruker-Avance instrument at Department of Chemistry, BITS, Pilani, Pilani Campus.

The FT-IR spectra were recorded with a Shimazu (IRAffinity-1S) instrument by directly keeping the surfactant sample in the sample holder.

A field emitting scanning electron microscopy (FESEM), FEI Teneo LV 450 instrument (at BITS Pilani, Pilani campus) was utilized to observe the morphology of sample surface. Thin films of liquid samples were prepared on the glass cover slip. Samples were drop cast on the cover slip and were air dried. Samples were sputtered with gold for 30 seconds prior to the measurements. All measurements were performed at 298.15 ± 1 K temperature.

References

1. N. Jiang, P. Li, Y. Wang, J. Wang, H. Yan and R. K. Thomas, *J. Colloid Interface Sci.*, 2005, **286**, 755-760.
2. Sonu, S. Kumari and S. K. Saha, *J. Phys. Chem. B*, 2015, **119**, 9751-9763.
3. A. K. Tiwari, Sonu and S. K. Saha, *J. Phys. Chem. B*, 2014, **118**, 3582-3592.
4. A. K. Tiwari, Sonu and S. K. Saha, *J. Chem. Thermodyn.*, 2014, **70**, 24-32.
5. R. Williams, J. Phillips and K. Mysels, *Trans. Faraday Soc.*, 1955, **51**, 728-737.
6. A. Domínguez, A. Fernández, N. González, E. Iglesias and L. Montenegro, *J. Chem. Edu.*, 1997, **74**, 1227.
7. C. Reichardt, *Chem. Rev.*, 1994, **94**, 2319-2358.
8. R. Das, D. Guha, S. Mitra, S. Kar, S. Lahiri and S. Mukherjee, *J. Phys. Chem. A*, 1997, **101**, 4042-4047.
9. A. Mallick, B. Haldar, S. Maiti and N. Chattopadhyay, *J. Colloid Interface Sci.*, 2004, **278**, 215-223.
10. R. B. Macgregor and G. Weber, *Nature*, 1986, **319**, 70.
11. S. M. Dennison, J. Guharay and P. K. Sengupta, *Spectrochim. Acta A Mol. Biomol. Spectrosc.*, 1999, **55**, 1127-1132.
12. J. R. Lakowicz, *Principles of Fluorescence Spectroscopy*, Kluwer Academic, Plenum Press, New York, 1999.
13. A. Mallick, B. Haldar and N. Chattopadhyay, *J. Phys. Chem. B*, 2005, **109**, 14683-14690.
14. A. Mallick, B. Haldar, S. Maiti, S. C. Bera and N. Chattopadhyay, *J. Phys. Chem. B*, 2005, **109**, 14675-14682.
15. X. Wang, J. Wang, Y. Wang, H. Yan, P. Li and R. K. Thomas, *Langmuir*, 2004, **20**, 53-56.
16. S. Roy, A. Mohanty and J. Dey, *Chem. Phys. Lett.*, 2005, **414**, 23-27.
17. G. G. Guilbault, *Practical fluorescence*, CRC Press, 1990.

18. J. Broecker and S. Keller, *Langmuir*, 2013, **29**, 8502-8510.
19. M. Maroncelli and G. R. Fleming, *J. Chem. Phys.*, 1987, **86**, 6221-6239.
20. A. Maciejewski, J. Kubicki and K. Dobek, *J. Phys. Chem. B*, 2003, **107**, 13986-13999.
21. C. Hirose and L. Sepulveda, *J. Phys. Chem.*, 1981, **85**, 3689-3694.
22. K. Kinoshita, *Biophys. J*, 1977, **20**, 289.
23. N. C. Maiti, M. Krishna, P. Britto and N. Periasamy, *J. Phys. Chem. B*, 1997, **101**, 11051-11060.
24. E. L. Quitevis, A. H. Marcus and M. D. Fayer, *J. Phys. Chem.*, 1993, **97**, 5762-5769.
25. L. B. Johansson and A. Niemi, *J. Phys. Chem.*, 1987, **91**, 3020-3023.
26. Sonu, S. Halder, S. Kumari, R. Aggrawal, V. K. Aswal and S. K. Saha, *J. Mol. Liq.*, 2017, **243**, 369-379.
27. J. Hierrezuelo and C. C. Ruiz, *Mater. Sci. Eng. C*, 2015, **53**, 156-165.
28. J. M. Andreu and J. A. Munoz, *Biochemistry*, 1986, **25**, 5220-5230.
29. S. Sinha, D. Tikariha, J. Lakra, T. Yadav, S. Kumari, S. K. Saha and K. K. Ghosh, *J. Mol. Liq.*, 2016, **218**, 421-428.

Chapter 3

Solvation Dynamics and Rotational Relaxation of Coumarin 480 (C-480) in the Aqueous Micelles: Effect of the Chemical Structure of Surfactants and Additive

---

Key Concepts:

- *This chapter is divided into three parts 3a, 3b, and 3c.*
- *Solvation dynamics and rotational relaxation of the C-480 in the aqueous micelles of conventional and gemini surfactants are influenced by:*
  - *Counterions of surfactants.*
  - *Hydrophilicity of spacer group and hydrophobicity of the tails of gemini surfactants.*
  - *Addition of urea in the micelles of gemini surfactants.*

Chapter 3a

Effect of Organic and a Hofmeister Series of Inorganic Counterions on the Solvation Dynamics and Rotational Relaxation in Aqueous Micelles of Hexadecyltrimethylammonium Surfactants

Abstract: *The effect of an organic counterion, p-toluenesulphonate (p-TS$^-$) and a Hofmeister series of inorganic counterions, NO_3^-, Br^- and SO_4^{2-} on the solvation dynamics and rotational relaxation of Coumarin 480 (C-480) in the Stern layer of aqueous micelles of hexadecyltrimethylammonium surfactants ($C_{16}TAX$) has been studied. Studies have been carried out by means of UV-Vis absorption, steady-state fluorescence and fluorescence anisotropy, time-resolved fluorescence and fluorescence anisotropy, and dynamic light scattering measurements. The rate of solvation increases in the order $C_{16}TABr$ < $C_{16}TANO_3$ < $(C_{16}TA)_2SO_4$ < $C_{16}TAp$-TS. Effectively, the solvation process is controlled by the extent of release of water molecules during the formation of micelles which depends on the nature of counterion. p-TS$^-$ counterions are more tightly bound to the headgroups because of added effect of its hydrophobic part. Counterions indirectly contribute to the slow solvation by the formation of clusters of water molecules. The decreasing order of the average rotational relaxation time of C-480 in the micelles of surfactants is $C_{16}TAp$-TS >> $C_{16}TABr$ > $C_{16}TANO_3$ > $(C_{16}TA)_2SO_4$, which is the same as the decreasing order of microviscosity of micelles. The rotational relaxation time is shorter in the micelles of $(C_{16}TA)_2SO_4$ as compared to $C_{16}TAp$-TS as the former micelles have less tightly packed structure than the latter. The slow rotational relaxation is mainly contributed by the lateral diffusion of C-480 along the surface of the micelle. The rotational motion is the slowest for the micelle of $(C_{16}TA)_2SO_4$, and the same is the fastest for the micelle of $C_{16}TABr$. There is an indication of different orientation of C-480 molecules in viscous micelles of $C_{16}TAp$-TS as compared to other less viscous micelles. The fact of counterion dependent solvation processes might help us for various studies on physicochemical properties of surfactants in solutions.*

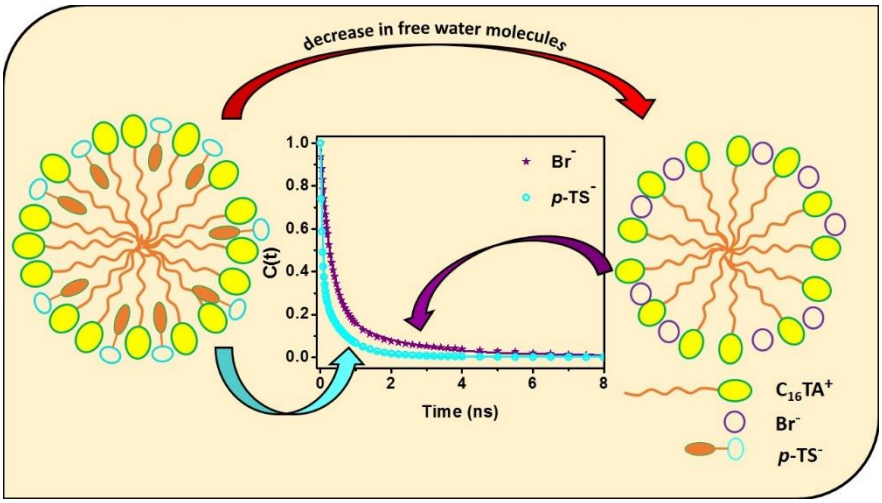

*Sunita Kumari, Sonu, G. Sundar and Subit K. Saha, *J. Photochem. Photobiol. A Chem.*, **2017**, *345*, 98-108.

3a.1 Introduction

Surfactants are amphiphilic molecules having a hydrophilic headgroup and a hydrophobic tail. Headgroups may be ionic or non-ionic. Exclusion of the non-polar part of the surfactant from the polar solvent phase to the micellar phase and repulsion between the ionic parts of surfactant molecules are two competitive processes. The former process supports the formation of aggregates and the latter process opposes the same. The formation of micelles of ionic surfactants is stabilized by the binding of the counterions to the headgroups of surfactant molecules.[1, 2] Micellar properties of a surfactant such as the critical micelle concentration (*cmc*), the degree of ionization (α), micelle size and microenvironment not only depend upon the surfactant structure but also on counterions and their hydration.[3-5]

Both cationic and anionic counterions affect the micellar properties and the thermodynamics of micellization.[2, 5-7] Jiang *et al*.[2] have studied *cmc*, α, enthalpies of micellization (ΔH_{mic}), Gibbs free energies of micellization (ΔG_{mic}) and entropies of micellization (ΔS_{mic}) of hexadecyltrimethylammonium surfactants, $C_{16}TAX$ with different counterions, X = F^-, Cl^-, Br^-, NO_3^-, and SO_4^{2-}. Both *cmc* and α decrease in the order $F^- > Cl^- > Br^- > NO_3^- > SO_4^{2-}$ which can be rationalized in terms of Hofmeister series[8], and an increase in the binding ability of counterion except for the bivalent SO_4^{2-} ion. The more negative value of ΔH_{mic} follows the order $SO_4^{2-} < F^- < Cl^- < Br^- < NO_3^-$ with even positive value for SO_4^{2-} ion. The unusual behavior of SO_4^{2-} ion is due to its bivalency and degree of dehydration.[2] Reports are available on the micellar properties depending upon the hydrophobicity, valency, and hydrated size of counterions.[5, 6, 8-14] Interaction of inorganic counterions with micellar surface depends upon the hydrated size of the ions (smaller hydrated ions favor the interactions). However, for quaternary ammonium counterions, it depends upon the hydrocarbon exterior (more hydrophobicity is more effective in micellization).[6] Counterions are reported to influence the stability of the foam.[12] Externally added electrolytes also control the micellization of surfactants.[15-20] Various reports on the formation of worm-like micelles and rheological behavior of hexadecyltrimethylammonium surfactant with *p*-toluenesulfonate counterion are available in the literature.[7, 13, 21-23]

Looking into a large number of reports of the significant effect of inorganic and organic counterions on the aggregation behavior of surfactants and a very few reports on

solvation dynamics in the micelles, this chapter aims to study how these counterions affect the solvation dynamics and rotational relaxation of the probe molecule in aqueous micelles. A Hofmeister series of counterions, NO_3^-, Br^- and SO_4^{2-} along with an organic counterion, *p*-toluenesulfonate (*p*-TS^-) with a hydrophobic part in it for hexadecyltrimethylammonium surfactant have been chosen for the present study (structures are given in Scheme 3a.1). It is expected that the solvation dynamics and rotational relaxation would be dependent upon the binding ability of these counterions to the micelles due to the difference between their sizes, valencies, and hydrophobicities. The well-known C-480 (Scheme 3a.1) has been taken to probe the solvation dynamics and rotational relaxation in the micelles. UV-visible absorption spectroscopy, steady-state fluorescence spectroscopy, time-correlated single photon counting (TCSPC) fluorescence spectroscopy, and dynamic light scattering (DLS) measurements have been carried out.

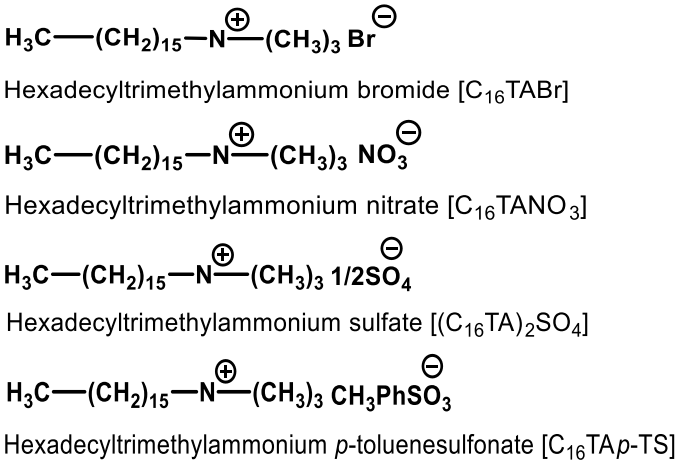

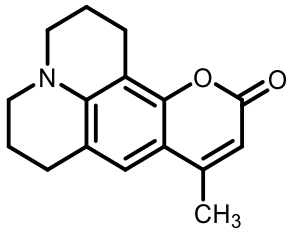

Coumarin 480 (C-480)

Scheme 3a.1: Chemical structure of surfactants and Coumarin 480.

3a.2 Results and discussion

3a.2.1 Conductivity measurements

Specific conductivity measurements were carried out to determine the *cmc* of surfactants, $C_{16}TAX$ with various counterions (X = Br^-, NO_3^-, SO_4^{2-} and *p*-TS^-) in aqueous solution, following Williams' method.[24] Figure 3a.1 represents the variation of specific conductivity (κ) with the concentration of solutions of surfactant, [$C_{16}TAX$] at 298.15 K. A clear break point has been noted in each case. This break point is indicative of the binding of some of the counterions once the micelles are formed. As a result of this binding, the slope of the plot is decreased in post micellar region. The break point

corresponds to *cmc*. Estimated *cmc* values are given in Table 3a.1 along with the values reported in the literature in parentheses. There is good agreement between the present and reported values.

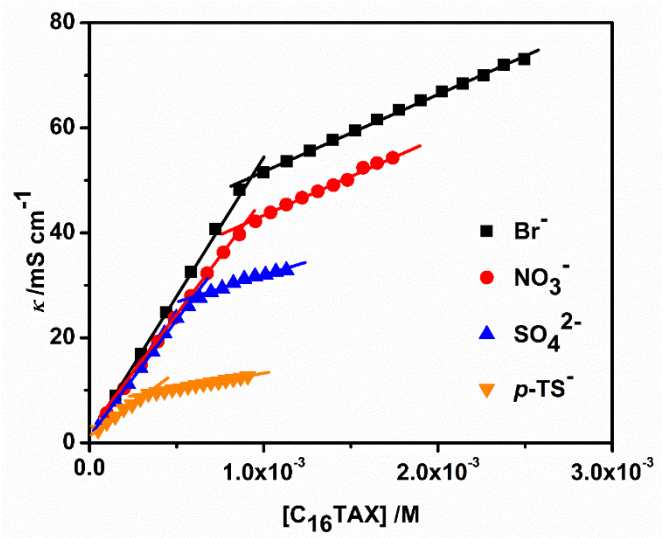

Figure 3a.1. Variation of specific conductivity (κ) of aqueous solutions of $C_{16}TAX$ (X = Br^-, NO_3^-, SO_4^{2-} and *p*-TS^-) with the concentration of [$C_{16}TAX$] at 298.15 K.

The decreasing order of *cmc* values of $C_{16}TAX$ with different counterions is as follows: $Br^- > NO_3^- > SO_4^{2-} >$ *p*-TS^-. All counterions are monovalent except sulfate ion, SO_4^{2-}. The Hofmeister series based on increasing order of hydrated radius is $NO_3^- < Br^- < SO_4^{2-}$.[7, 25] The NO_3^- ions with smaller hydrated radius as compared to Br^- ions have higher ability to bind at the micellar surface resulting in lowering of electrostatic repulsive interaction between the headgroups of surfactant molecules. Because of this reason, the process of micellization is favored and hence *cmc* of $C_{16}TANO_3$ is lower than that of $C_{16}TABr$. In this line, degree of counterion dissociation (α) of the former is expected to be lower than that of the latter. Although this trend has been noted by Jiang *et al.*[2], but it is not so in the present case and also the results reported by Sepulveda *et al.*[26]

Table 3a.1. Cmc of surfactants, $C_{16}TAX$ (X = Br^-, NO_3^-, SO_4^{2-} and *p*-TS^-) in aqueous solutions and degree of counterion dissociation (α) at 298.15 K.

Systems	*Cmc* (mM)	α
$C_{16}TABr$	0.92(0.95)[a]	0.26(0.33)[a](0.22)[c]
$C_{16}TANO_3$	0.89(0.89)[a]	0.34(0.31)[a](0.30)[c]
$(C_{16}TA)_2SO_4$	0.59(0.61)[a]	0.24(0.29)[a](0.26)[c]
$C_{16}TA$*p*-TS	0.32(0.26)[b]	0.24

[a]Reference[2], [b]Reference[21] and [c]Reference.[26]

The higher value of α in case of $C_{16}TANO_3$ as compared to $C_{16}TABr$ might indicate that the fewer NO_3^- ions can effectively stabilize the micelles. The divalent sulfate ions behave differently as compared to monovalent ions. Although due to the large hydrated radius it may be difficult for the sulfate ion to bind effectively with the micelle, it could be that due to its bivalency, the ion is able to neutralize the micellar charge very effectively. That is perhaps why lower values of *cmc* and α for $(C_{16}TA)_2SO_4$ as compared to other two surfactants with monovalent counterions are observed than expected from the Hofmeister series.[2, 8] Jiang *et al.*[2] also noticed the same trend. According to them, the divalency and the greater distance of the hydration water from the centre of the sulfate ion help the ion to bind with the headgroups very effectively resulting in decrease in *cmc* and α. Stronger interaction of sulfate ions with the headgroups and a greater release of water molecules result in an endothermic contribution to the enthalpy and an increase in entropy. There is also a smaller decrease in entropy from the binding of a single bivalent ion rather than two monovalent ions to the micelle.[2] They have observed higher entropy of micellization for the sulfate system because of the contribution of these two factors. The decreasing order of hydrodynamic radii of the micelles discussed later is $(C_{16}TA)_2SO_4$ > $C_{16}TA$*p*-TS > $C_{16}TANO_3$ > $C_{16}TABr$. This order can be correlated with the *cmc* values except for $(C_{16}TA)_2SO_4$. The greater hydrodynamic radius of $(C_{16}TA)_2SO_4$ as compared to $C_{16}TA$*p*-TS (Table 3a. 6) is due to less packing structure of the former than the latter.[2] As far as *p*-TS^- counterion is concerned, its hydrophobic part is aligned towards the core of the micelles and the hydrophilic part is protruded towards the bulk aqueous phase. The *p*-TS^- ions bind more tightly to the micelles as compared to other three counterions discussed above as a result of added hydrophobic interactions. That is why *p*-TS^- ions can screen the electrostatic repulsions between the ionic headgroups more effectively resulting in lower values of *cmc* and α (Table 3a.1).

3a.2.2 UV - visible absorption spectra

3a.2.2.1 Study with C-480

The UV-visible absorption spectra of C-480 have been recorded in the presence of micelle of different surfactants, $C_{16}TAX$ (X = Br^-, NO_3^-, SO_4^{2-} and *p*-TS^-) and are shown in Figure 3a.2. The spectral data are given in Table 3a.2. The concentration of each surfactant is chosen to be ten times of the respective *cmc* to ensure the complete micellization of the probe molecules. It was further confirmed by the fact that the

fluorescence peak maximum in each case was independent of the excitation wavelength. The λ_{max}^{abs} of C-480 is found to be 394 nm in the presence of surfactants with Br^-, NO_3^- and SO_4^{2-} as conterions. However, in case of *p*-TS^- as counterion, the λ_{max}^{abs} is 391 nm. It is noteworthy that the λ_{max}^{abs} is 392 nm in pure water which is in good agreement with the literature value.[27] An absorption band at ~ 321 nm (Figure 3a.2) with very low absorbance could be because of the formation of complex between C-480 and water molecules in the Stern layer.[28] A detailed discussion on this aspect is available in section 3a.1.4.

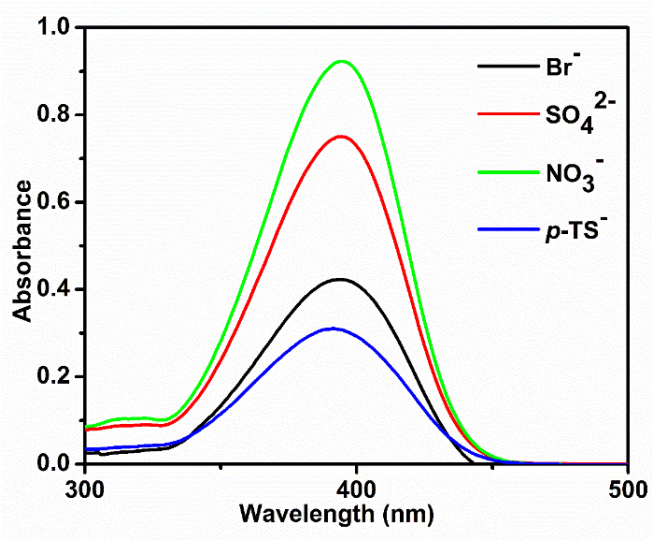

Figure 3a.2. UV-visible absorption spectra of C-480 in the micelles of different surfactants, $C_{16}TAX$ (X = Br^-, NO_3^-, SO_4^{2-} and *p*-TS^-), [C-480] = 5 μM.

Table 3a.2. Concentration of surfactants taken for spectral study, absorption peak maxima (λ_{max}^{abs}), fluorescence peak maxima (λ_{max}^{flu}), and $E_T(30)$ (empirical solvent polarity parameter) values of C-480 in micelles of $C_{16}TAX$.

Systems	Exper. conc. (mM)	λ_{max}^{abs} (nm)	λ_{max}^{flu} (nm)	$E_T(30)$ (kcal mol^{-1})
$C_{16}TABr$	9.50	394	475	52.8
$C_{16}TANO_3$	9.00	394	475	52.8
$(C_{16}TA)_2SO_4$	6.00	394	475	52.8
$C_{16}TA$*p*-TS	3.50	391	480	55.6

3a.2.3 Steady-state fluorescence spectra

3a.2.3.1 Study of microenvironment of micelles

The steady-state fluorescence spectra of C-480 in the micelles of surfactants, $C_{16}TAX$ (X = Br^-, NO_3^-, SO_4^{2-} and *p*-TS^-) have been recorded (Figure 3a.3) and fluorescence data obtained are also tabulated in Table 3a.2. The λ_{max}^{flu} value of C-480 in

the micelles of C_{16}TABr is available in the literature[29] which is same as that observed by us. Fluorescence spectra of C-480 in different pure solvents were recorded earlier[30] and peak maxima noted were 489 nm, 475 nm and 408 nm in water, methanol and cyclohexane, respectively. It can be seen from the data in Table 3a.2 that the λ_{max}^{flu} of C-480 is 475 nm in the presence of micelles of C_{16}TABr, C_{16}TANO_3 and $(C_{16}TA)_2SO_4$ surfactants, however, it is 480 nm in the case of micelles of C_{16}TA*p*-TS surfactants. Therefore, comparing the fluorescence data of C-480 in the micelles of different surfactants to that in various pure solvents one can conclude that the micropolarity of environment of micelles where C-480 molecules are located is similar to that of methanol. This result suggests that the C-480 molecules are located at the Stern layer of micelles.[29, 31] The peak maximum of C-480 in the micelles of C_{16}TA*p*-TS is red shifted by 5 nm with respect to that in the micelles of other three surfactants because in this case the number of bound water molecules with the surfactant headgroups would be less than that of hydrogen bonded free water molecules.

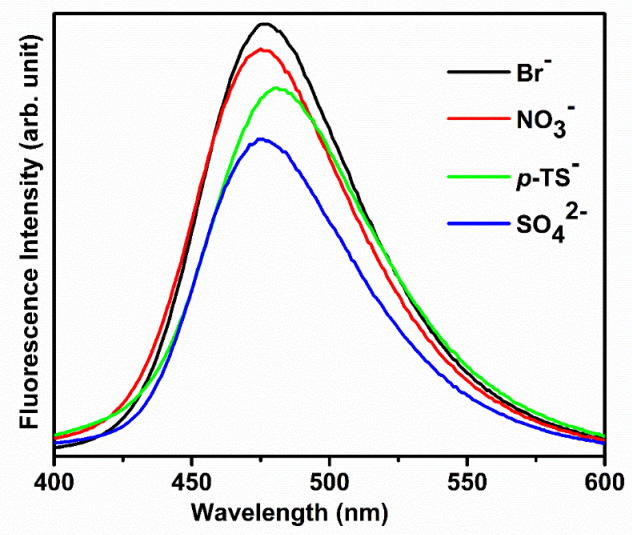

Figure 3a.3. Steady-state fluorescence spectra of C-480 in the micelles of C_{16}TAX (X = Br^-, NO_3^-, SO_4^{2-} and *p*-TS^-) surfactants. λ_{ex} = 375 nm, [C-480] = 5 μM.

It is known that the polarity of hydrogen bonded water molecules is higher than that of bound water molecules as the former kind of water molecules undergo mutual polarization which results in an increase in the dipole moment and dielectric constant.[32, 33] That is why C-480 molecules feel more polar microenvironment in C_{16}TA*p*-TS micelle as compared to the micelles of other three surfactants. To support these results of micropolarity, the $E_T(30)$ values of micelles have been determined according to method given in Chapter 2, Section no. 2.2.5.[30] The data listed in Table 3a.2 show that the $E_T(30)$

of micelles of C_{16}TA*p*-TS is higher than that of other three surfactants supporting the fact of more polar nature of the Stern layer of the former micelles than that of the latter micelles. Although Jiang *et al.*[2] noticed the difference in micropolarity among the surfactants, C_{16}TAX with X = Br^-, NO_3^-, and SO_4^{2-} using ESR experiments with a probe, 5-doxylstearic acid (5-DSA), but that has not been observed in the present fluorescence experiments. It could be because of use of two different kinds of probe molecules with difference in their locations in the micelles. It might in particular, be due to the attachment of a C_{13} carbon chain with 5-DSA which pulls the hydrophilic part of the molecule towards the core of the micelles. In fact Kevan *et al.*[34] in their study have reported that the 5-DSA probe molecules are located in the inner part of the Stern layer of micelles. On the other hand, C-480 molecules are comparatively more exposed to the bulk water.

Table 3a.3. Steady-state fluorescence anisotropy (r), fluorescence lifetime $<\tau_f>$, rotational correlation time (τ_R) of DPH and microviscosity (η_m) of micelles at 298.15 K.

Systems	r	$<\tau_f>$ (ns)	τ_R (ns)	η_m (mPa s)
C_{16}TABr	0.065	5.66	1.24	16.4
C_{16}TANO_3	0.060	5.85	1.16	15.3
$(C_{16}TA)_2SO_4$	0.055	6.05	1.08	14.2
C_{16}TA*p*-TS	0.071	6.24	1.52	20.0

To estimate the microviscosity of micelles we have used 1,6-diphenyl-1,3,5-hexatriene (DPH) as a viscosity probe molecule.[35, 36] The microviscosity of micelles, η_m have been determined by using Debye-Stokes-Einstein[35, 37] and Perrin's Equations[38, 39] (Chapter 2, Section no. 2.2.6, Equation 2.2, and 2.3, respectively) Although in our case the differences between the microviscosity values for these surfactants are very less (Table 3a.3), but considering the fact that DPH is a quite sensitive viscosity probe the experimental errors are expected to below. The estimated η_m values along with other fluorescence parameters are given in Table 3a.3. The data listed in Table 3a.3 show that while there is not much difference in the microviscosity values of micelles of C_{16}TABr, C_{16}TANO_3 and $(C_{16}TA)_2SO_4$ surfactants, the microviscosity value is comparatively higher for the micelles of C_{16}TA*p*-TS surfactant. This could be because of very tight association of the latter surfactant molecules in the micelles. Jiang *et al.*[2] based on their ESR experiments with 5-DSA have found that the microviscosity increases in the order $(C_{16}TA)_2SO_4 < C_{16}TABr \approx C_{16}TANO_3$ same as Hofmeister series. Even though in our case

the variations in microviscosities are very small, the trend is same as that reported by Jiang *et al.*[2] Low microviscosity for $(C_{16}TA)_2SO_4$ micelle is due to its less packing structure.[2]

3a.2.4 Solvation dynamics

The fluorescence decays of C-480 have been recorded in the micelles of each of the surfactants, $C_{16}TAX$ with different counterions, X = Br^-, NO_3^-, SO_4^{2-} and *p*-TS^- at several wavelengths across the range of its emission spectrum (430 - 530 nm). The emission wavelength dependent fluorescence decays of C-480 in the micelles of $(C_{16}TA)_2SO_4$ surfactant have been shown in Figure 3a.4 as a representative one. In each case the emission at lower wavelength is very fast with tri-exponential decay. This fast decay is due to the decay of unsolvated dipoles of the probe molecules created after the excitation. Of course, there would be a small contribution from the solvated dipoles as well which is beyond the control due to the limitation of our instrument (the instrument response function of our laser system is ~ 165 ps). However, at higher wavelength shows bi-exponential decay with clear growth has been observed. The growth with a negative pre-exponential factor is the manifestation of the solvation of the dipole of the C-480 molecule created in the excited state. On complete solvation the decay comes from the fully relaxed energy state at the red edge of fluorescence spectrum which is delayed by the relaxation time.[32, 40]

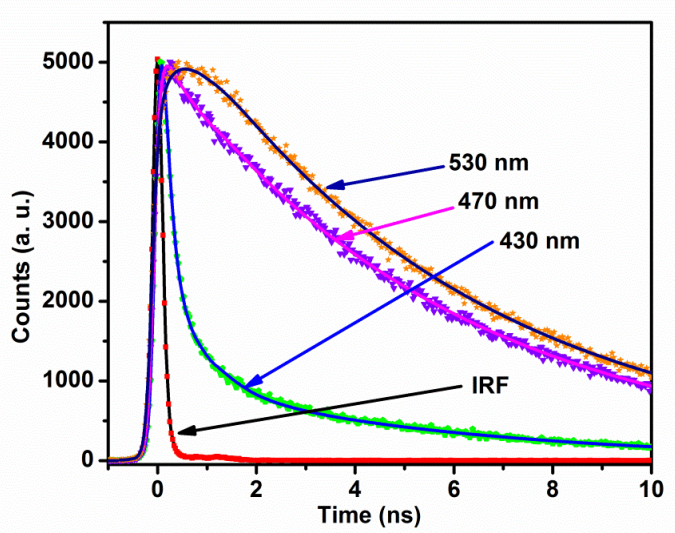

Figure 3a.4. Fluorescence decays of C-480 in the micelles of $(C_{16}TA)_2SO_4$ at various wavelengths. λ_{ex} = 375 nm.

It is to be noted here that all decays are for the neutral C-480 only. A small absorption due to the protonated species of C-480 is observed at ~321 nm; however, to record a decay the sample was excited at 375 nm where there is no existence of the

protonated species (a single steady-state fluorescence band from λ_{ex} = 375 nm is shown by Figure 3a.3). On the basis of above mentioned discussion about the location of the probe molecules, C-480, one can conclude that the solvation is taking place at the Stern layer of the micelles. Moreover, wavelength dependent decays in bulk water are difficult to observe because it requires high time resolution of instrument and the probe molecules present in the hydrocarbon core of the micelles do not show wavelength dependent decays.[29] The time-resolved emission spectrum (TRES) have been constructed using the procedure given by Fleming and Maroncelli [30, 41] Decay profiles were fitted to a bi- or tri-exponential function to have χ^2 value in between 1-1.2 using decay analysis software (DAS 6). The impulse response function, $I(\lambda,t)$ was calculated using those best fitted decay profiles. The TRES have been constructed according to method discussed in Chapter 2 (Section no. 2.2.10) [30 30 30 30 11] . The wavenumber at maximum emission at a time t, $\bar{\upsilon}(t)$ was then obtained after fitting the spectrum to a log-normal function.[41, 42] The TRES of C-480 in the micelles of all four types of surfactants are shown in Figure 3a.5.

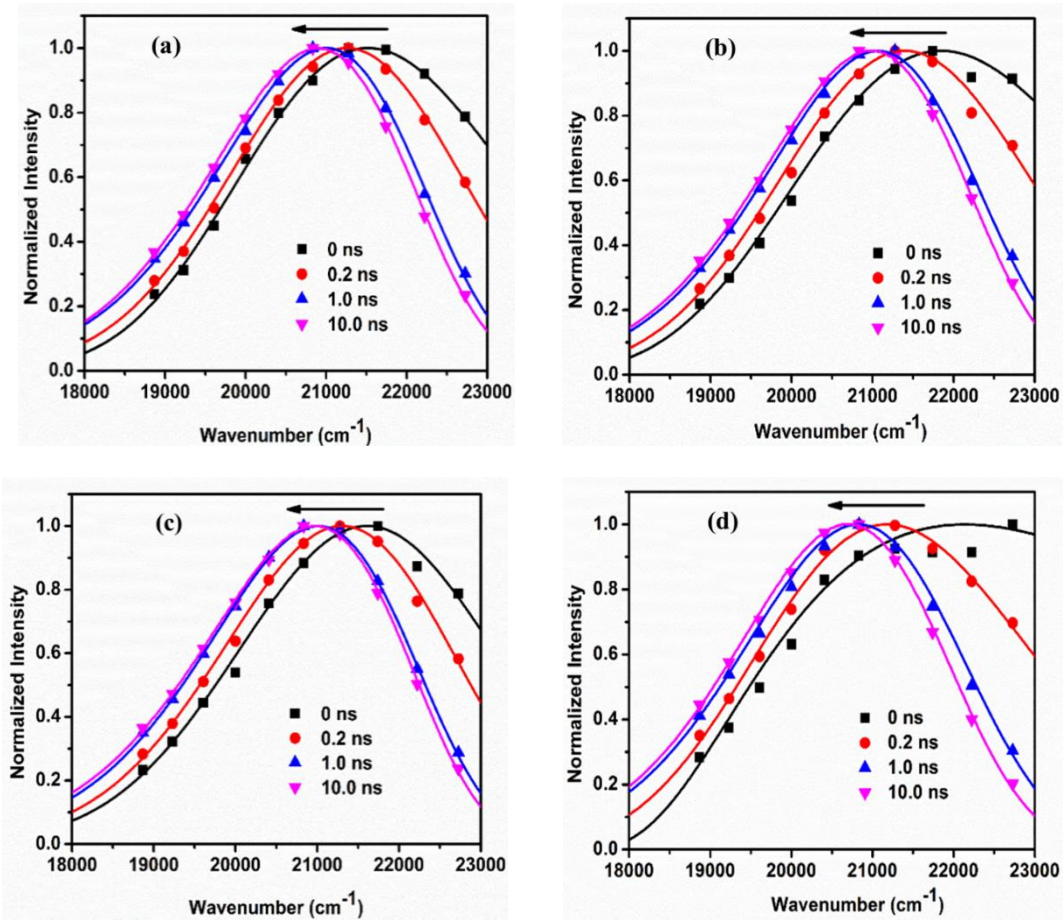

Figure 3a.5. Time-resolved emission spectra (TRES) of C-480 in the micelles of surfactants, $C_{16}TAX$ with X = (a) Br^-, (b) NO_3^-, (c) SO_4^{2-} and (d) *p*-TS^-.

The time constants of the solvation have been calculated by the use of decays of solvent response functions, *C*(*t*) (Equation 2.9) which is explained by Fleming and Maroncelli[41] (Chapter 2, Section no. 2.2.10) The peak wavenumbers $\bar{\upsilon}(t)$, $\bar{\upsilon}(\infty)$ and $\bar{\upsilon}(0)$ at time *t*, infinity and zero, respectively have been calculated from the time resolved emission spectra (TRES). The decays of solvent correlation function, *C(t)* of C-480 in the micelles of each of four different surfactants have been shown in Figure 3a.6. The time constants of the observable solvation are obtained after fitting the plot of solvent correlation function, *C(t)* versus time. A bi-exponential function which is written as Equation 2.14 (Chapter 2) , has been used to obtain the solvent relaxation time constants. The decay parameters of C-480 in different micelles are listed in Table 3a.4.

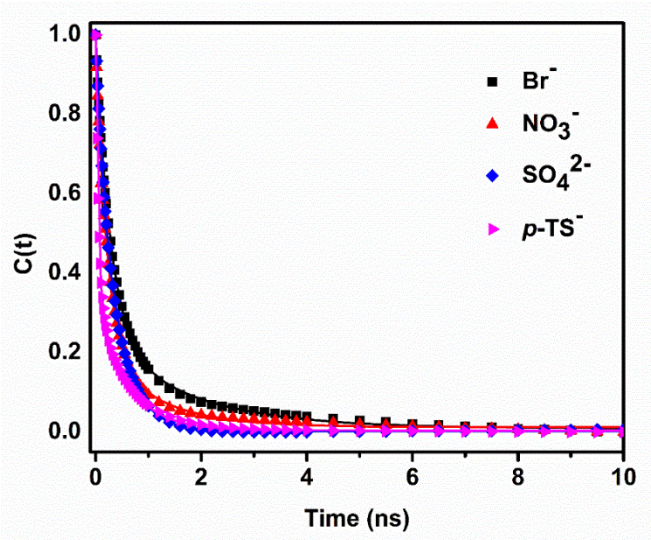

Figure 3a.6. Decays of solvent correlation function, *C(t)* of C-480 in micelles of surfactants, $C_{16}TAX$ (X = Br^-, NO_3^-, SO_4^{2-} and *p*-TS^-).

Table 3a.4. Decay characteristics of *C(t)* of C-480 in different micelles.

Systems	a_1	τ_1 (ps)	a_2	τ_2 (ps)	$<\tau_s>$ (ps)	$\bar{\upsilon}(0)$ (cm^{-1})	$\bar{\upsilon}(\infty)$ (cm^{-1})	$\Delta\bar{\upsilon}^a$ (cm^{-1})	%Missing component
$C_{16}TABr$	0.79	292	0.21	2167	685	21521	20901	620	44
$C_{16}TANO_3$	0.83	226	0.17	1852	502	21846	20985	861	14
$(C_{16}TA)_2SO_4$	0.32	170	0.68	425	343	21608	20971	637	39
$C_{16}TAp$-TS	0.73	80	0.27	670	239	22095	20699	1396	3

[a] $\Delta\bar{\upsilon} = \bar{\upsilon}(0) - \bar{\upsilon}(\infty)$

It can be seen from the data given in Table 3a.4 that the solvation dynamics is bimodal in nature and the average solvation time in each micellar system is much longer

than that in bulk water (310 fs) reported by Fleming *et al.*[43] Therefore, solvation dynamics in the Stern layer of the present micelles is approximately three orders of magnitude slower than that in bulk water. Bhattacharyya *et al.*[29] also noticed the solvation dynamics of same order in the micelles of various surfactants, CTAB, SDS and Triton X-100. Free and bound water molecules are responsible for the fast and the slow components, respectively in the bimodal behavior of solvation dynamics. As far as micelles are concerned, water molecules interacting with the polar headgroups of the surfactant molecules are more restricted (bound water), compared to water molecules hydrogen bonded among themselves (free water).[32, 44, 45] Apart from water molecules, various other factors responsible for the solvation of the dipoles are counterions and polar headgroups of the surfactant molecules. However, a headgroup being attached to the long molecular tail experiences restriction in the mobility and is expected to contribute to a slow solvation process. It is reported that the dynamics of polymer chain occur on very slow time scale (~ 100 ns).[29, 46] Therefore, water molecules and counterions are mostly responsible for the solvation dynamics.

From the data given in Table 3a.4 one can see that the increasing order of solvation time for the surfactants, C_{16}TAX follows the order C_{16}TA*p*-TS < $(C_{16}TA)_2SO_4$ < $C_{16}TANO_3$ < C_{16}TABr. *p*-TS^- ions bind so strongly that the repulsive interactions between the headgroups of surfactant molecules are screened very effectively. As a result, the majority of water molecules that are released, are hydrogen bonded among themselves, and can be considered to be free water that contributes to the fast solvation. Among other three counterions, larger number of water molecules is released due to stronger interaction of SO_4^{2-} ions with the headgroups as compared to NO_3^- and Br^- ions. Although the SO_4^{2-} ions are bivalent but there is lesser extent of release of water molecules as compared to that of *p*-TS^- ions could be because of two reasons: (i) micelles with SO_4^{2-} ions might have less tightly packed structure, and (ii) *p*-TS^- ions are more tightly bound to the headgroups could be because of added effect of its hydrophobic part. NO_3^- ions bind with the surfactant headgroups less strongly than SO_4^{2-} ions but more strongly than Br^- ions. Thus the increasing order of release of water molecules during the formation of micelles is expected to be C_{16}TABr < $C_{16}TANO_3$ < $(C_{16}TA)_2SO_4$ < C_{16}TA*p*-TS which is same as the increasing order of rate of solvation (Table 3a.4). The more the number of water molecules released as free water during the formation of micelles, the greater would be the contribution towards the fast solvation process. The number of free water molecules might be the

dominating factor responsible for the ease of solvation of C-480 in the micelles of C_{16}TA*p*-TS rather than the effect of its more viscous environment. The greater extent of release of water molecules during the formation of the micelles of C_{16}TA*p*-TS is also supported by significant higher value of Stokes' shift, $\Delta\bar{\upsilon}$ (Table 3a.4) estimated from time resolved fluorescence data in this case as compared to other micellar systems. Hessz *et al*.[28] have reported that C-480 can form two types of complexes with H_2O molecules: either oxo complex (complexation through H-bonding between keto oxygen atom of C-480 and H_2O) or amino complex (complexation through H-bonding between nitrogen atom of C-480 and H_2O). An absorption band at ~ 321 nm (Figure 3a.2) in each case of micelles of all four surfactants indicates the formation of either of these complexes. However, the data in Table 3a.2 shows that there is a blue shift in absorption band and a red shift in fluorescence band in case of micelles of C_{16}TA*p*-TS with respect to that for other three surfactants. This phenomenon could be because of the formation of amino complex in the ground state and oxo complex in the excited state in the Stern layer of micelles of C_{16}TA*p*-TS. Although the complexes are formed in all cases of micelles, but the effects of complexation on the absorption and fluorescence spectra are more prominent in the case of micelle of C_{16}TA*p*-TS as there is a greater extent of availability of free water molecules surrounding the C-480 molecules in the Stern layer of this micelle. Thus, greater extent of release of water molecules during the formation of C_{16}TA*p*-TS micelles as compared to other micelles is sufficiently evidenced.

It has been reported that counterions also indirectly contribute to the solvation process.[35, 36, 47, 48] The increasing order of α observed in the present case is C_{16}TA*p*-TS ≈ $(C_{16}TA)_2SO_4$ < C_{16}TABr < $C_{16}TANO_3$. Water molecules can interact with anions through hydrogen bonds. More the number of dissociated counter ions greater would be the clustering of water molecules and lesser would be the contribution towards the fast solvation by free water molecules.[36] As per the value of α, the clustering of water molecules would be greater in case of $C_{16}TANO_3$ as compared to C_{16}TABr. However, the observed solvation time is faster in case of the former than that of the latter. It is known that the aggregation number of micelles of $C_{16}TANO_3$ is greater than that of C_{16}TABr.[49] In fact the hydrodynamic radius of a micelle of $C_{16}TANO_3$ (0.80 nm) is found to be greater than that of C_{16}TABr (0.67 nm) (Table 3a.6). Thus, the faster solvation in $C_{16}TANO_3$ as compared to C_{16}TABr is due to greater extent of release of water molecules in the former than the latter. α values of C_{16}TA*p*-TS and $(C_{16}TA)_2SO_4$ are smaller than that of the

micelles of other two surfactants. So, the extent of clustering of water molecules in the former two micelles is expected to be lesser than the latter two micelles which is also in support to the fact of faster solvation. It is to be noted in Figure 3a.5 that the full width at half the maximum of TRES decreases on longer time scale in case of each type of micelles. This indicates that there is a possibility of self-diffusion of the probe, C-480 which can contribute towards the slower component of solvation.[50]

3a.2.5 Missing component

As our TCSPC set-up has some time resolution limitation, so some part of dynamic Stokes' shift must have been missed. Fee[51] and Maroncelli[41] proposed a method to calculate the missing component. Using their method we have calculated the missing components for all the studied micellar systems and the values are listed in Table 3a.4. Missing component found in case of C_{16}TABr micelle is in agreement with that reported before.[31]

3a.2.6 Rotational relaxation or time-resolved fluorescence anisotropy

For further exploration of the location of the probe molecules in the micellar media, time-resolved fluorescence anisotropy measurements have been carried out. The time resolved fluorescence anisotropy, *r(t)* has been calculated by using the Equation 2.16 (Chapter 2, Section no. 2.2.11). Anisotropy decay is mono-exponential in pure water, however, it is bi-exponential in all micellar media. The bi-exponential anisotropy decay function can be represented as Equation 2.17 (Chapter 2, Section no. 2.2.12). The average rotational relaxation time for the bi-exponential decay in micelles is calculated using the fluorescence anisotropy decays of C-480 in the micelles of each type of the syrfactants at 10 times of respective *cmc* are represented by Figure 3a.7. The rotational relaxation parameters i.e. fast and slow relaxation components (τ_{1r} and τ_{2r}, respectively) along with average rotational relaxation time ($<\tau_r>$) of C-480 in different micelles are given in Table 3a.5. The rotational relaxation time in pure water is found to be 132 ps which is very close to the reported value, i.e., 125 ps.[31] The average relaxation time in micellar media is higher than that in pure water, which indicates that the random motions of the probe molecules in the former media are restricted more than in the latter media. The decreasing order of average rotational relaxation time of C-480 in the micelles of surfactants is C_{16}TA*p*-TS >> C_{16}TABr > C_{16}TANO_3 > $(C_{16}TA)_2SO_4$. The decreasing order of microviscosity found in

the present study is $C_{16}TAp$-TS >> $C_{16}TABr$ > $C_{16}TANO_3$ > $(C_{16}TA)_2SO_4$ within a very low limit of experimental errors. Thus, more the microviscosity of the environment around the probe molecules harder is their random motions. Loose packing micelle structure in case of $(C_{16}TA)_2SO_4$ is the cause for its low microviscosity. Pal *et al.*[52] have also reported that the rotational relaxation times correlate well with the viscosity values. It is noteworthy that although the solvation process is faster, but the rotational relaxation process is slower in case of micelles of $C_{16}TAp$-TS as compared to that in the micelles of other surfactants. It is inferred that viscosity has very less effect to slow down the solvation dynamics. It is also indicated that rotational relaxation and solvation are two independent processes. Unlike simple solution, the solvation dynamics and rotational relaxation in micelle-like complex solutions are not related.

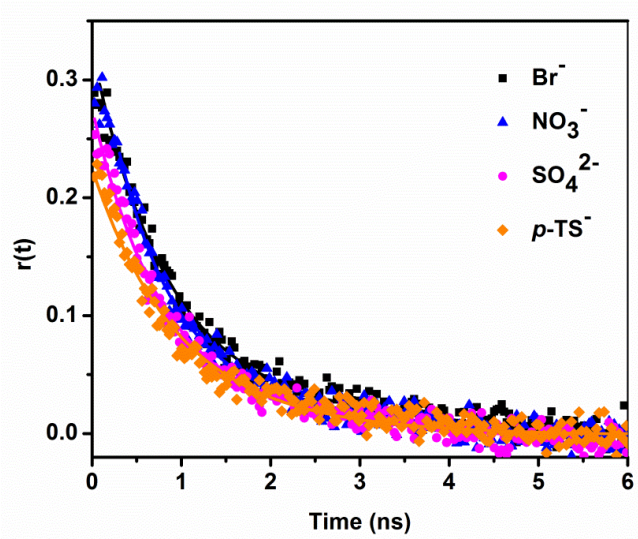

Figure 3a.7. Fluorescence anisotropy decays of C-480 in the micelles of surfactants, $C_{16}TAX$ (X = Br^-, NO_3^-, SO_4^{2-} and *p*-TS^-).

Table 3a.5. Rotational relaxation parameters for C-480 in different micelles.

Systems	a_{1r}	τ_{1r} (ps)	a_{2r}	τ_{2r} (ps)	$<\tau_r>$ (ps)	χ^2
$C_{16}TABr$	0.81	392	0.19	2030	706	1.03
$C_{16}TANO_3$	0.68	294	0.32	1308	614	1.00
$(C_{16}TA)_2SO_4$	0.80	364	0.20	1518	590	1.00
$C_{16}TAp$-TS	0.93	477	0.07	7436	952	1.00

The fluorescence anisotropy decay of C-480 in the micellar media is bi-exponential in nature. This bi-exponential anisotropy decay is generally not because of the fact that probe molecules are present at the different locations in the micelles, but due to their

various kinds of rotational motions.[52] The data in Table 3a.5 shows that the time scale for fast rotational relaxation lies in the range of ~ 294 ps to ~ 477 ps. Thus the longer time scale for fast relaxation process as compared to that in water (132 ps) and complete solubilization of C-480 molecules in micelles infer that rotational relaxation of C-480 molecules takes place only in micellar environment. The bi-exponential behavior of anisotropy decay usually is explained using the two-step and wobbling-in-a-cone model (Chapter 2, Section no. 2.2.12 and 2.2.13, respectively).[31, 53-56] These models are applicable for spherical micelles. In our case the hydrodynamic radius data given in Table 3a.6 suggest that all the micelles are spherical in shape.

According to the two-step model,[30, 35, 55] the slow rotational relaxation process is related to the lateral diffusion of the fluorophore and rotational motion of the micelle as a whole. The slow rotational relaxation time, τ_{2r} is calculated from the fitted decay. The method of calculation of τ_m using hydrodynamic radius of micelle has been described in Chapter 2, Equation 2.20. The estimated values of hydrodynamic radii (r_h) and size distribution plots of all four micelles are given in Table 3a.6 and Figure 3a.8, respectively. The values of τ_m calculated by using the Equation 2.20 and τ_D calculated using the values of τ_m and Equation 2.19 at 298.15 K temperature. Calculated values of τ_m and τ_D are given in Table 3a. 6. From the data in Tables 3a.5 and 6 one can see that the slow rotational relaxation time (τ_{2r}) of C-480 in each type of micelle is same as the time of lateral diffusion (τ_D) of C-480 along the surface of the micelle. Thus, the slow rotational relaxation is mainly due to the lateral diffusion. The τ_D values obtained are mostly the function of the microviscosity of the micelles. The rotational motion of the micelle as a whole containing C-480 molecule is a much slower process than lateral diffusion of C-480 molecule. τ_m values are found to be the function of the size of the micelles. With increasing size of the micelle, τ_m increases. The rotational motion is the slowest for the micelle of $(C_{16}TA)_2SO_4$, and the fastest for the micelle of $C_{16}TABr$.

The time constant for the wobbling motion (τ_w) of the probe molecule, C-480 has been calculated by the method given in Chapter 2, Equation 2.25. The calculated τ_w values are also given in Table 3a.6. The decreasing order of τ_w values of C-480 in the micelles of surfactants is $C_{16}TA$*p*-TS > $C_{16}TABr \approx (C_{16}TA)_2SO_4 > C_{16}TANO_3$. The decreasing order of microviscosity is $C_{16}TA$*p*-TS >> $C_{16}TABr > C_{16}TANO_3 > (C_{16}TA)_2SO_4$. The difference between these two orders suggests that in addition to microviscosity the nature of local structure of the micelle also affects the wobbling motion. It is known that τ_w is a measure

of the relaxation of the local structure of the micelle.[55] The differences between the local structures as a result of different packing structures of micelles due to variable counterions are expected.

Table 3a.6. Hydrodynamic radius (r_h)[a], time for overall rotational motion of the micelle (τ_m), lateral diffusion time (τ_D), wobbling motion time (τ_w), wobbling diffusion coefficient (D_w), cone angle (θ_o) and order parameter ($|S|$) obtained from the anisotropy decays of C-480 in different micelles.

Systems	r_h (nm)	τ_w (ps)	τ_m (μs)	τ_D (ps)	$D_w \times 10^{-8}$ (s^{-1})	θ_o (deg)	$\|S\|$
$C_{16}TABr$	0.67	486	0.273	2045	5.74	55.7	0.44
$C_{16}TANO_3$	0.80	379	0.464	1312	5.29	47.2	0.57
$(C_{16}TA)_2SO_4$	1.75	479	4.861	1518	5.67	55.1	0.45
$C_{16}TAp$-TS	1.09	510	1.175	7483	7.94	68.8	0.26

[a]Standard deviation: ± 0.02

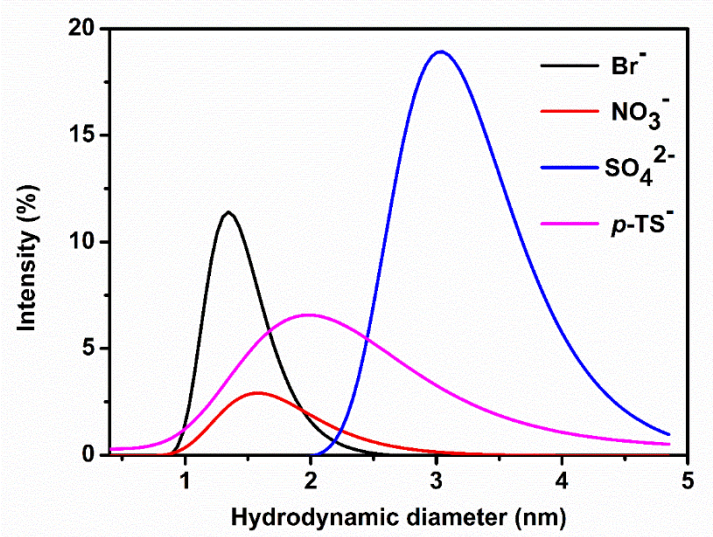

Figure 3a.8. The Size distribution graph for the micelle of the $C_{16}TAX$ (X = Br^-, NO_3^-, SO_4^{2-} and *p*-TS^-) surfactants obtained from dynamic light scattering (DLS) measurement.

Further information about the motional restriction of the probe molecules within the micelles can be obtained using the wobbling-in-a-cone model.[30, 55] For this purpose the generalized order parameter, S (Equation 2.22), the wobbling cone angle (θ_o) (Equation 2.23) and wobbling diffusion coefficient (D_W) (Equation 2.26) have been calculated and values obtained are also given in Table 3a.6. S values higher than zero indicate restricted motion of C-480 in the micelles. It has been discussed above that the microviscosity of $C_{16}TAp$-TS is greater than that of other three micelles. However, lower value of S, and

higher values of θ_o and D_w for the former as compared to the latter have been observed. This might be indicating that the wobbling-in-a-cone model is not suitable for the micelles of C_{16}TA*p*-TS. Saha *et al*.[30] earlier made a similar observation in case of rotational relaxation of the same probe, C-480 in micelles with high microviscosity and another reported model called spinning-in-equatorial-band model[55, 57] was used to resolve this apparent discrepancy. In fact this model is applicable for S < 0.5 which is the case for C_{16}TA*p*-TS. According to this model, $S^2 = [(1/2)(1- cos^2\theta_o)]^2$. After applying this model, the θ_o value is coming out to be 46.1°. In spinning-in-equatorial-band model, the rod-like probe molecule is aligned in such a way that the emission moment is perpendicular to the long axis unlike the wobbling-in-a-cone model. This result indicates that the orientation of C-480 in viscous micelles of C_{16}TA*p*-TS is different from that in other three comparatively less viscous micelles. It is to be mentioned here that the D_w values are almost the same in the micelles of C_{16}TAX with X = Br^-, NO_3^- and SO_4^{2-}.

3a.3 Conclusions

The effects of an organic and a Hofmeister series of inorganic counterions on the solvation dynamics and rotational relaxation of C-480 in the Stern layer of aqueous micelles of hexadecyltrimethylammonium surfactants have been studied. C-480 molecules feel more polar microenvironment in C_{16}TA*p*-TS micelles as compared to the micelles of other three surfactants. Solvation dynamics in the Stern layer of the present micelles is approximately three orders of magnitude slower than that in the bulk water. The increasing order of rate of solvation is C_{16}TABr < C_{16}TANO_3 < $(C_{16}TA)_2SO_4$ < C_{16}TA*p*-TS. The repulsive interactions between the headgroups of surfactant molecules are screened very effectively due to the stronger binding ability of *p*-TS^- ions. The majority of water molecules are hydrogen bonded among themselves, resulting in comparatively more polar microenvironment of C_{16}TA*p*-TS micelles. These water molecules, considered to be free water, contribute to the fast solvation. The order for solvation time is similar to the order for *cmc*. SO_4^{2-} ions behave differently than from the monovalent ions. Effectively the solvation process is controlled by the extent of release of water molecules during the formation of micelles. More the number of water molecules released as free water, greater would be the contribution towards the fast solvation process. Release of water molecules during the formation of micelles depends on effective binding of counterions to the headgroups. *p*-TS^- ions are more tightly bound to the headgroups because of added effect

of its hydrophobic part. Counterions can indirectly contribute to the slow solvation by causing clustering of water molecules. However, not only the number of dissociated counterions, but also the effective number of surfactant molecules participating in micelles formation could be a function of net amount of free water molecules. NO_3^- ions bind more strongly to the micelles as compared to Br^- ions promoting more number of surfactant molecules to form micelles. NO_3^- ions contribute to greater number of free water molecules as compared to Br^- ions resulting in faster solvation in $C_{16}TANO_3$ as compared to $C_{16}TABr$ micelles. α values of $C_{16}TA$*p*-TS and $(C_{16}TA)_2SO_4$ are smaller than that of the micelles of other two surfactants. The extent of clustering of water molecules in the former two micelles is expected to be lesser than the latter two micelles. The effective binding of counterions forming larger micelles and resulting in release of greater number of free water molecules, and the lesser extent of clustering of water molecules in the micelles of $C_{16}TA$*p*-TS and $(C_{16}TA)_2SO_4$ contribute to fast solvation. The decreasing order of average rotational relaxation time of C-480 in the micelles of surfactants is $C_{16}TA$*p*-TS >> $C_{16}TABr$ > $C_{16}TANO_3$ > $(C_{16}TA)_2SO_4$ which is same as the decreasing order of microviscosity. The rotational relaxation time is shorter in the micelles of $(C_{16}TA)_2SO_4$ as compared to $C_{16}TA$*p*-TS is because of less tightly packed structure of the former. The slow rotational relaxation is mainly due to the lateral diffusion of C-480 along the surface of the micelle. The rotational motion of the micelle as a whole containing C-480 molecule is a much slower process than lateral diffusion. The rotational motion is the slowest for the micelle of $(C_{16}TA)_2SO_4$, and the same is the fastest for the micelle of $C_{16}TABr$. There is an indication of different orientation of C-480 in viscous micelles $C_{16}TA$*p*-TS as compared to other less viscous micelles. The fact of counterion dependent solvation processes might help us in studying physicochemical properties of surfactants in solutions.

References

1. K. Maiti, D. Mitra, S. Guha and S. P. Moulik, *J. Mol. Liq.*, 2009, **146**, 44-51.
2. N. Jiang, P. Li, Y. Wang, J. Wang, H. Yan and R. K. Thomas, *J. Colloid Interface Sci.*, 2005, **286**, 755-760.
3. J. D. Morgan, D. H. Napper and G. G. Warr, *J. Phys. Chem.*, 1995, **99**, 9458-9465.
4. V. Soldi, J. Keiper, L. S. Romsted, I. M. Cuccovia and H. Chaimovich, *Langmuir*, 2000, **16**, 59-71.
5. M. Benrraou, B. L. Bales and R. Zana, *J. Phys. Chem. B*, 2003, **107**, 13432-13440.
6. P. Mukerjee, K. Mysels and P. Kapauan, *J. Phys. Chem.*, 1967, **71**, 4166-4175.

7. J. W. Larsen and L. J. Magid, *J. Am. Chem. Soc.*, 1974, **96**, 5774-5782.
8. N. Jiang, P. Li, Y. Wang, J. Wang, H. Yan and R. K. Thomas, *J. Phys. Chem. B*, 2004, **108**, 15385-15391.
9. G. Biresaw, D. C. McKenzie, C. A. Bunton and D. F. Nicoli, *J. Phys. Chem.*, 1985, **89**, 5144-5146.
10. D. Yu, X. Huang, M. Deng, Y. Lin, L. Jiang, J. Huang and Y. Wang, *J. Phys. Chem. B*, 2010, **114**, 14955-14964.
11. Y. Tokiwa, H. Sakamoto, T. Takiue, M. Aratono and H. Matsubara, *J. Phys. Chem. B*, 2015, **119**, 6235-6241.
12. S. Pandey, R. P. Bagwe and D. O. Shah, *J. Colloid Interface Sci.*, 2003, **267**, 160-166.
13. F. Bautista, N. Tepale, V. Fernández, G. Landázuri, E. Hernández, E. Macías, J. Soltero, J. Escalante, O. Manero and J. Puig, *Soft matter*, 2016, **12**, 165-170.
14. O. Regev, M. Leaver, R. Zhou and S. Puntambekar, *Langmuir*, 2001, **17**, 5141-5149.
15. L. Abezgauz, K. Kuperkar, P. A. Hassan, O. Ramon, P. Bahadur and D. Danino, *J. Colloid Interface Sci.*, 2010, **342**, 83-92.
16. V. Aswal, P. Goyal, S. Menon and B. Dasannacharya, *Physica B Condens. Matter*, 1995, **213**, 607-609.
17. S. Kumar, D. Bansal and Kabir-ud-Din, *Langmuir*, 1999, **15**, 4960-4965.
18. C. Oelschlaeger, P. Suwita and N. Willenbacher, *Langmuir*, 2010, **26**, 7045-7053.
19. L. Wattebled and A. Laschewsky, *Langmuir*, 2007, **23**, 10044-10052.
20. V. Aswal and P. Goyal, *Chem. Phys. Lett.*, 2002, **364**, 44-50.
21. M. Truong and L. Walker, *Langmuir*, 2000, **16**, 7991-7998.
22. A. Müller, M. Torres and A. Saez, *Langmuir*, 2004, **20**, 3838-3841.
23. M. R. Rojas, A. J. Müller and A. E. Sáez, *J. Colloid Interface Sci.*, 2010, **342**, 103-109.
24. R. Williams, J. Phillips and K. Mysels, *Transact. Faraday Soc.*, 1955, **51**, 728-737.
25. E. Nightingale Jr, *J. Phys. Chem.*, 1959, **63**, 1381-1387.
26. L. Sepulveda and J. Cortes, *J. Phys. Chem.*, 1985, **89**, 5322-5324.
27. D. Chakrabarty, P. Hazra, A. Chakraborty and N. Sarkar, *J. Phys. Chem. B*, 2003, **107**, 13643-13648.
28. D. Hessz, B. Hégely, M. Kállay, T. Vidóczy and M. Kubinyi, *J. Phys. Chem. A*, 2014, **118**, 5238-5247.

29. N. Sarkar, A. Datta, S. Das and K. Bhattacharyya, *J. Phys. Chem.*, 1996, **100**, 15483-15486.

30. A. K. Tiwari and S. K. Saha, *J. Phys. Chem. B*, 2014, **118**, 3582-3592.

31. D. Chakrabarty, A. Chakraborty, D. Seth, P. Hazra and N. Sarkar, *V*, 2005, **122**, 184516.

32. K. Bhattacharyya, *Chem. Commun.*, 2008, 2848-2857.

33. S. W. Rick, S. J. Stuart and B. J. Berne, *J. Chem. Phys.*, 1994, **101**, 6141-6156.

34. E. Szajdzinska-Pietek, R. Maldonado, L. Kevan, R. R. Jones and M. J. Coleman, *J. Am. Chem. Soc.*, 1985, **107**, 784-788.

35. S. Kumari and S. K. Saha, *J. Phys. Chem. B*, 2015, **119**, 9751-9763.

36. S. Kumari and S. K. Saha, *Phys. Chem. Chem. Phys.*, 2016, **18**, 1551-1563.

37. S. Roy, A. Mohanty and J. Dey, *Chem. Phys. Lett.*, 2005, **414**, 23-27.

38. A. K. Tiwari, S. Kumari and S. K. Saha, *RSC Adv.*, 2014, **4**, 25210-25219.

39. M. Shinitzky and Y. Barenholz, *J. Biol. Chem.*, 1974, **249**, 2652-2657.

40. J. R. Lakowicz, *Principles of Fluorescence Spectroscopy*. Kluwer Academic, Plenum Press, New York, 1999.

41. M. Maroncelli and G. R. Fleming, *J. Chem. Phys.*, 1987, **86**, 6221-6239.

42. A. Maciejewski, J. Kubicki and K. Dobek, *J. Phys. Chem. B*, 2003, **107**, 13986-13999.

43. Š. Vajda, R. Jimenez, S. J. Rosenthal, V. Fidler, G. R. Fleming and E. W. Castner, *J. Chem. Soc. Faraday Trans.*, 1995, **91**, 867-873.

44. N. Nandi and B. Bagchi, *J. Phys. Chem. B*, 1997, **101**, 10954-10961.

45. N. Nandi and B. Bagchi, *J. Phys. Chem. A*, 1998, **102**, 8217-8221.

46. A. Datta, S. K. Pal, D. Mandal and K. Bhattacharyya, *J. Phys. Chem. B*, 1998, **102**, 6114-6117.

47. M. Kumbhakar, T. Goel, T. Mukherjee and H. Pal, *J. Phys. Chem. B*, 2005, **109**, 14168-14174.

48. R. E. Riter, E. P. Undiks and N. E. Levinger, *J. Am. Chem. Soc.*, 1998, **120**, 6062-6067.

49. S. Berr, R. R. Jones and J. S. Johnson Jr, *J. Phys. Chem.*, 1992, **96**, 5611-5614.

50. B. Roy, S. Satpathi, K. Gavvala, R. K. Koninti and P. Hazra, *J. Phys. Chem. B*, 2015, **119**, 11721-11731.

51. R. Fee and M. Maroncelli, *Chem. Phys.*, 1994, **183**, 235-247.

52. M. Kumbhakar, T. Goel, T. Mukherjee and H. Pal, *J. Phys. Chem. B*, 2004, **108**, 19246-19254.

53. K. Kinosita Jr, S. Kawato and A. Ikegami, *Biophysical J.*, 1977, **20**, 289.

54. D. Chakrabarty, D. Seth, A. Chakraborty and N. Sarkar, *J. Phys. Chem. B*, 2005, **109**, 5753-5758.

55. E. L. Quitevis, A. H. Marcus and M. D. Fayer, *J. Phys. Chem.*, 1993, **97**, 5762-5769.

56. N. C. Maiti, M. Krishna, P. Britto and N. Periasamy, *J. Phys. Chem. B*, 1997, **101**, 11051-11060.

57. L. B. Johansson and A. Niemi, *J. Phys. Chem.*, 1987, **91**, 3020-3023.

Chapter 3b

Effect of Hydrophobicity of Tails and Hydrophilicity of Spacer Group of Cationic Gemini Surfactants on Solvation Dynamics and Rotational Relaxation of Coumarin 480 in Aqueous Micelles

Abstract: *Solvation dynamics and rotational relaxation of Coumarin 480 (C-480) in aqueous micelles of cationic gemini surfactants with diethyl ether (EE) spacer group (m–EE–m) and tails with varying tail lengths (m = 12, 14 and 16) have been studied. Studies have been carried out by measuring UV-vis absorption, both steady-state and time-resolved fluorescence with fluorescence anisotropy,* ^{1}*H NMR and dynamic light scattering. Effects of hydrocarbon tail length and hydrophilicity of spacer group on solvation dynamics and rotational relaxation processes at inner side of the Stern layer of micelles have been studied. With increasing hydrophobicity of tails of surfactants water molecules in Stern layer become progressively more rigid resulting in decrease in rate of solvation process with slow solvation as a major component. With increasing hydrophilicity of the spacer group of gemini surfactant the extent of free water molecules is decreased thereby making the duration of solvation process longer. Solvation times in the micelles of gemini surfactants with hydrophilic spacer are almost four times longer as compared to micelles of their conventional counterpart. Rotational relaxation time increases with increasing tail length of surfactant as a result of increasing microviscosity of micelles with fast relaxation as a major component. With increasing hydrophilicity of the spacer group the anisotropy decay becomes slower due to the formation of more compact micelles. Rotational relaxation in gemini micelles is also slower as compared to micelles of conventional counterpart. The anisotropy decay is found to be bi-exponential with lateral diffusion of the probe along the surface of the micelle as a slow component. Rotational motion of micelle as a whole is a very slow process and the motion becomes further slower with increasing size of the micelle. The time constants for wobbling motion and lateral diffusion of the probe become longer with increasing microviscosity of micelles.*

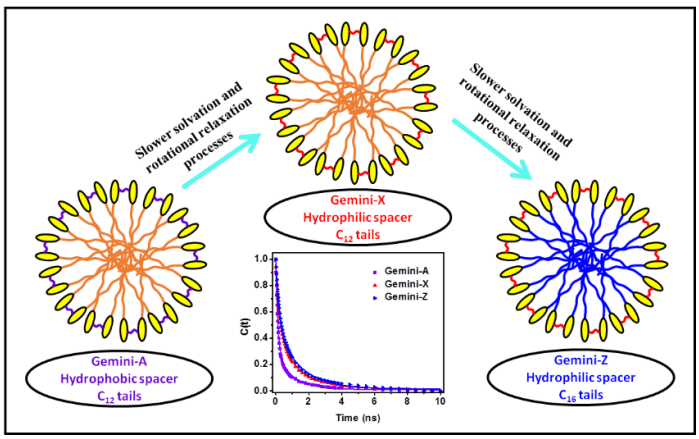

*Sunita Kumari, Rishika Aggrawal, Sonu, Sayantan Halder, G. Sundar and Subit K. Saha, *ACS Omega*, **2017**, *9*, 5898-5910.

3b.1 Introduction

In recent time gemini surfactants have attracted attention because of their countless applications in the nanotechnology, biotechnology, material science, supramolecular chemistry and pharmaceutical application such as drug delivery, gene delivery etc.[1-5] Gemini surfactants are made up of two hydrophobic tails and two hydrophilic headgroups, covalently connected by a spacer group at their headgroups. Gemini surfactants are more surface active than their conventional counterparts.[6] Aggregation properties of a gemini surfactant are dependent upon the various parts of the surfactant such as headgroups,[7-9] spacer group,[10-15] counterions,[16] and alkyl chain lengths.[17, 18] Gemini surfactants are reported to have different types of spacer groups like hydrophilic, hydrophobic, rigid and flexible.[6, 19, 20] The spacer part plays a significant role in the aggregation properties of a gemini surfactant. The critical micelle concentration (*cmc*), counterion binding, thermodynamic properties, microviscosity and micropolarity, rheological behavior and aggregation number of gemini surfactants vary with any change in the spacer part.[1, 6, 14, 21-25] Not only the spacer group but also the hydrophobic tails of the gemini surfactant have an intense effect on the aggregation properties of the surfactants [26, 27]

Polymethylene spacer chain length of a series of cationic gemini surfactants influences the solvation dynamics and rotational relaxation of C-153 in aqueous micelles.[28] The value of α increases with increasing the spacer chain length which induces more and more clustering of water molecules at the Stern layer of micelles. Thus solvation dynamics becomes slower with increasing spacer chain length of the surfactant. Saha *et al*. studied the solvation dynamics in presence of gemini surfactants.[29] Effect of hydroxyl group present at spacer group of gemini surfactant on solvation dynamics has been monitored. Solvation dynamics becomes slow with increasing the number of the hydroxyl group in the spacer part of gemini surfactant. The increase in the solvation time could be due to the formation of hydrogen bonds between water molecules and hydroxyl group(s) of spacer group which results in protection of the probe molecule from its contact with some of the water molecules. Moreover, hydrogen bonding interactions between hydroxyl group(s) of the spacer group and water molecules may restrict the mobility of water molecules as well. Saha *et al.* have studied the effect of hydroxyl group substituted[29] and polymethylene[28] spacer groups on the solvation dynamics and rotational relaxation processes in aqueous micelles. They have demonstrated that hydrogen bonding through hydroxyl groups on the spacer group has a significant effect on retardation of the solvation process in aqueous

micelles. Also, average solvation time increases with increasing polymethylene spacer chain length as a result of increasing degree of counterion dissociation.

Observing into the fact of interesting aggregation behavior of gemini surfactants and effects of chemical nature of its spacer groups and also the effect of hydrocarbon tail length of conventional surfactants on solvation dynamics and rotational dynamics, the chapter aims to see how these dynamics depend on the hydrophobicity of the tails of gemini surfactants using C-480 as a probe. In this chapter, we have selected a series of diethyl ether spacer group containing gemini surfactants with varying hydrocarbon tail lengths, C_{12} (Gemini-X), C_{14} (Gemini-Y) and C_{16} (Gemini-Z) [Scheme 3b.1]. We have also compared our present dynamics data with that in the micelles of gemini surfactant containing C_{12} tails and tetramethylene spacer group (Gemini-A) [Scheme 3b.1] studied earlier.[29] With these compounds, we could simultaneously demonstrate how the rates of solvation and rotational relaxation processes in aqueous micelles depend on increasing tail length of gemini surfactants i.e. increasing hydrophobicity of tails and also how these rates change with increasing hydrophilicity of spacer group with similar tails. We have also shown how these rates in gemini micelles with hydrophobic spacer group as well as with hydrophilic spacer group differ from that in the micelles of their conventional counterparts, dodecyltrimethylammonium bromide (DTAB), tetradecyltrimethylammonium bromide (TTAB) and cetyltrimethylammonium bromide (CTAB) reported earlier.[30]

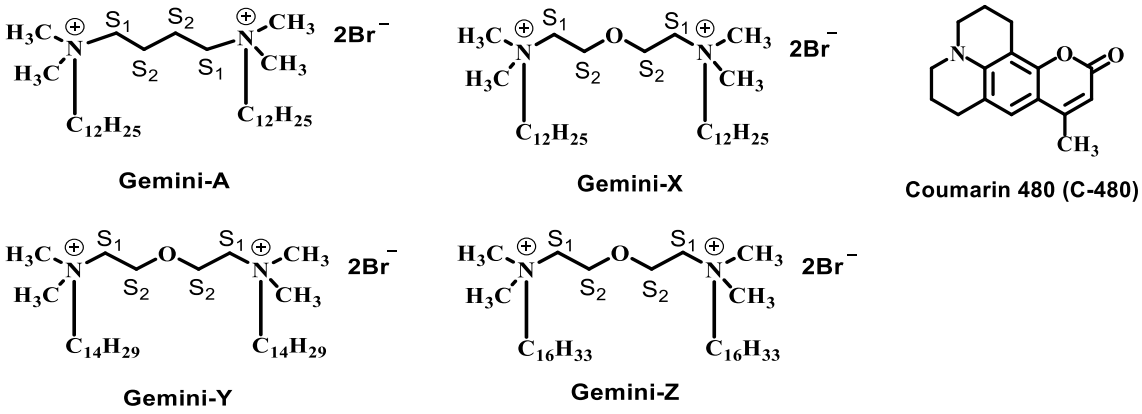

Scheme 3b.1: Chemical structures of gemini surfactants with numbering of spacer protons and Coumarin 480 with their names in short form.

3b.2 Results and discussion

3b.2.1 UV-visible absorption and steady-state fluorescence study

The UV-visible absorption and steady-state fluorescence spectra of C-480 have been recorded in the aqueous micelles of Gemini-X, Gemini-Y, and Gemini-Z surfactants (Figure 3b.1). To ensure complete solubilization of C-480 molecules in the micelles, the concentration of each surfactant was chosen to be fifteen times of respective *cmc*. To see the effect of spacer group of gemini surfactants, we have also compared our present results with that for Gemini-A studied earlier.[29] The peak maxima of absorption and fluorescence bands of C-480 in all these micellar systems are tabulated in Table 3b.1. The *cmc* values of all gemini surfactants determined using conductometric method are given in Table 3b.1.[27]

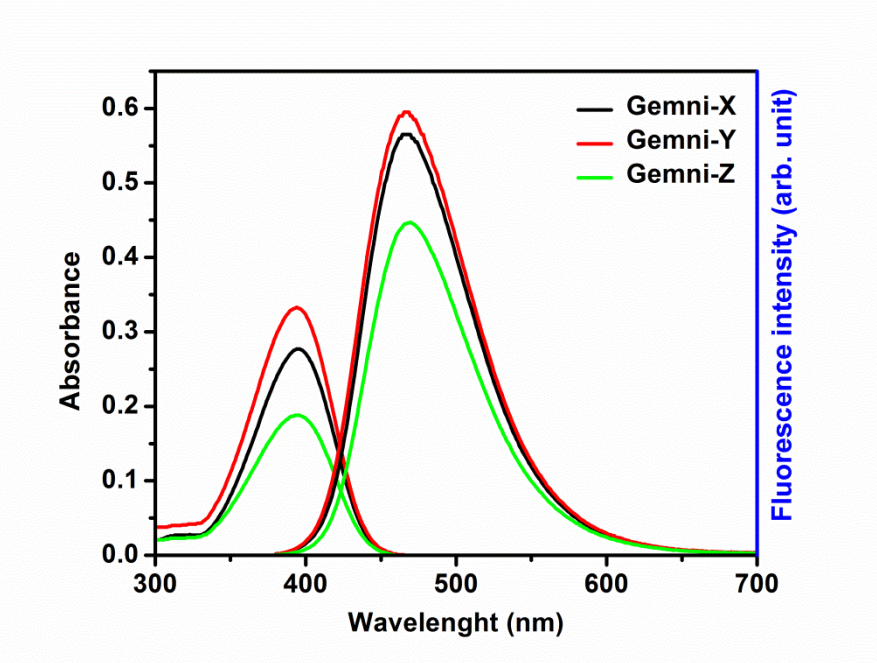

Figure 3b.1. UV-visible absorption and steady-state fluorescence spectra of C-480 in aqueous micellar media of Gemini-X, Gemini-Y and Gemini-Z surfactants. λ_{ex} = 375 nm, slit width = 3 nm (both excitation and emission).

To support those values the *cmc* values have also been determined by fluorescence method in the present study (Figure 3b.2). The solubilization of C-480 in the micelles is evidenced by the change in fluorescence intensity with increasing concentration of a surfactant (Figure 3b.2). The *cmc* values determined by these two different methods corroborate very well which further supports the purity of the synthesized surfactants. The peak positions of absorption and fluorescence bands of C-480 in each of the micellar media of Gemini-X, -Y and -Z are found to be at 394 nm, and 482 nm, respectively. Although

there is a change in the absorption and fluorescence intensity, but no change in peak position has been noted with the change in hydrophobic tail length of these surfactants. It could be due to constrained structure of C-480.[29-31] With changing the tail length of surfactants there may not be significant change in the polarity of the microenvironment, but motional restriction is increased.

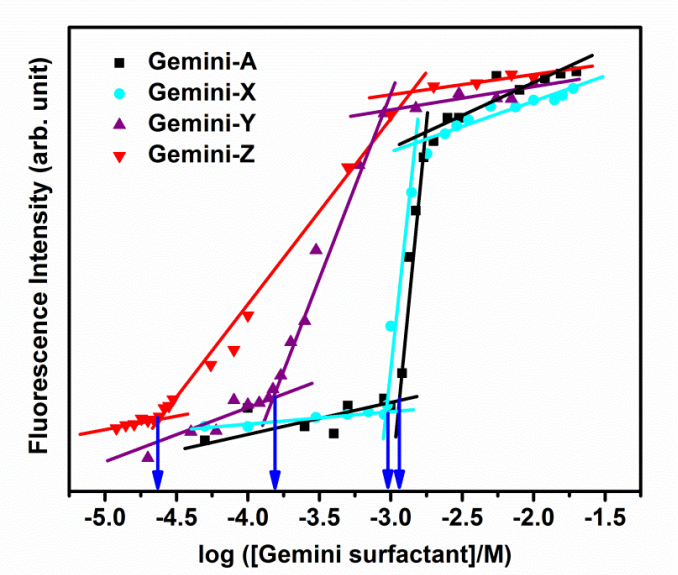

Figure 3b.2. Plot of variation of fluorescence intensities with increasing concentration of gemini surfactants. λ_{ex} = 375 nm, slit width = 3 nm (both excitation and emission).

It has been documented that C-480 molecules show fluorescence peak maxima at 494 nm, 473 nm, 417 nm, and 408 nm in the pure water, methanol, hexane, and cyclohexane, respectively.[32] By comparison of fluorescence peak maxima of C-480 in studied micellar systems to that in all pure solvents, one can say that the polarity of microenvironment around C-480 is similar to that of methanol. Therefore, the C-480 molecules are mostly located in the Stern layer of micelles.[32, 33] To further support this, the micropolarity expressed in the form of empirical solvent polarity parameter, $E_T(30)$ has been estimated by the reported method and is given in Chapter 2, Section no. 2.2.5.[29, 34-36] The value of $E_T(30)$ for the micelles of each of Gemini-X, -Y and -Z is found to be 56.5 kcal mol^{-1} which is close to that of methanol (55.4 kcal mol^{-1}).[29] Absorption and fluorescence peak maxima of C-480 appear at 390 nm, and 477 nm, respectively in the micelles of Gemini-A.[29] It implies that there is a blue shift in the fluorescence peak position of C-480 in the micelles of Gemini-A as compared to that in the present micellar systems. Different values of both λ_{max}^{Abs} and λ_{max}^{fl} of C-480 in the micelles of Gemini-X, -Y and -

Z as compared to micelles of Gemini-A (Table 3b.1) show the effect of hydrophilic spacer on the location of probe molecules. The solvent polarity parameter, $E_T(30)$ for the micelles of Gemini-A is found to be 53.2 kcalmol^{-1} which is lesser than that for the present micellar systems. Li *et al.*[17] have described that the hydrophilic spacer group can easily be located at the Stern layer of micelles favoring the formation of micelles. The data in Table 3b.1 show that the *cmc* value (Table 3b.1) of each of Gemini-X, -Y and -Z is lesser than that of Gemini-A.[29] These results infer that C-480 molecules feel comparatively more polar environment in the micelles of surfactants, Gemini-X, -Y and -Z with hydrophilic diethyl ether spacer group as compared to the micelles of surfactant, Gemini-A with hydrophobic tetramethylene spacer group.

Table 3b.1. *Cmc* of gemini surfactants, experimental concentration of surfactants, absorption and steady-state fluorescence peak maxima and average excited singlet state lifetime and fluorescence anisotropy of C-480 in micelles of Gemini-X, Gemini-Y, Gemini-Z and Gemini-A[a] (λ_{ex} = 375 nm and λ_{em} = 475 nm), microviscosity and micropolarity [$E_T(30)$] of micelles.

System	Cmc^b (mM)	Cmc^c (mM)	Conc. (mM)	λ_{max}^{abs} (nm)	λ_{max}^{flu} (nm)	$\langle\tau_f\rangle$ (ns)	χ^2	r	Microviscosity (cP)	$E_T(30)$ kcal mol^{-1}
Gemini-A[a]	1.170	1.145	18.00	390	477	5.05	1.01	0.022	15.1±0.5	53.2
Gemini-X	0.966	0.950	14.49	394	482	5.29	1.03	0.026	19.2±0.5	56.5
Gemini-Y	0.158	0.154	2.37	394	482	5.31	1.06	0.028	23.3±0.6	56.5
Gemini-Z	0.024	0.023	0.36	394	482	5.35	1.07	0.041	27.3±0.5	56.5

[a]All data for Gemini-A are taken from the reference.[29] [b]*cmc* determined by conductometric method, [c]*cmc* determined by fluorescence method.

3b.2.2 Excited singlet state lifetime

Excited singlet state lifetime values (τ_f) of C-480 molecule in the aqueous micelles of each of gemini surfactant at ~ 15*cmc* have been determined using time-correlated single photon counting (TCSPC) method. All decays were fitted bi-exponentially. The average lifetime has been calculated by using the Equation 1.8 , (Chapter 1). The average lifetime of C-480 in the all studied micelles along with the χ^2 values are given in Table 3b.1. The lifetime values of all components along with corresponding pre-exponential factors are separately given in Table 3b.2. The lifetime values of C-480 molecules in pure solvent have been reported earlier[29] and the values are 5.89, 4.90, and 3.13 ns in water, methanol and cyclohexane, respectively. Comparing the lifetime value in a particular micellar

system to that in pure solvents one can conclude that the microenvironment around C-480 is similar to that of methanol.

Table 3b.2. Excited state lifetime of C-480 in the different pure solvents and micelles.

System	a_1	τ_1 (ns)	a_2	τ_2 (ns)	a_3	τ_3 (ns)	$<\tau_f>$ (ns)	χ^2
Water	1.00	5.89	-	-	-	-	5.89	1.09
Cyclohexane	1.00	3.13	-	-	-	-	3.13	1.12
Methanol	1.00	4.90	-	-	-	-	4.90	1.01
Gemini-A	0.03	2.60	0.84	5.69	0.13	1.48	5.05	1.01
Gemini-X	0.11	0.73	0.89	5.86	-	-	5.29	1.03
Gemini-Y	0.11	1.02	0.89	5.85	-	-	5.31	1.06
Gemini-Z	0.12	1.10	0.90	5.80	-	-	5.35	1.07

λ_{ex} = 375 nm, λ_{em} = 475 nm. Lifetime data of C-480 in water, cyclohexane, methanol and Gemini-A are taken from reference.[29]

3b.2.3 Steady-state anisotropy and microviscosity

The steady-state fluorescence anisotropy of C-480 in the micelles of Gemini-X, -Y and -Z have been determined and the values obtained along with the same in the micelles of Gemini-A reported earlier[29] are given in Table 3b.1. Using these values the microviscosities of environment around C-480 in all micelles have been estimated by the method described before (Chapter 2, Section no. 2.2.6).[29, 37, 38] The data given in Table 3b.1 show that the microviscosity increases with increasing tail length of the surfactants. One can also see that the microviscosity of micelles of Gemini-X, -Y and -Z are greater than that of Gemini-A. It is true that with increasing tail length of the surfactants the formation of micelles become favored due to enhanced hydrophobic interactions and as a result of that the compactness of surfactant molecules in the micelles increases.[27] In fact, it is supported by the decrease in *cmc* values with increasing tail length (Table 3b.1). The fact of increase in microviscosity has been probed by C-480 which however, is located at the Stern layer of micelles. Thus, this result infers that the C-480 molecules penetrate up to a certain depth at the Stern layer of micelles. They feel comparatively more viscous environment with increasing tail length of the surfactants as more compact micelle structure inhibits the penetration of water molecules deep inside the Stern layer. Thus compact micelle structure has indirect effect on the microviscosity at the Stern layer of micelles. The microviscosity of micelles of Gemini-A is lower than that of other three gemini is due to the less compact structure of the former than that of the latter. Formation

of a micelle is favored by hydrophobic attractive interactions between the tails of surfactant molecules and disfavored by the repulsive interactions between the hydrophilic headgroups of surfactants. These repulsive interactions are reduced by the solvation of headgroups by the water molecules in aqueous micelles. Therefore, in the present case when a micelle is stabilized by greater extent of hydrophobic interactions between the longer tails, then the requirement of solvation of headgroups becomes less important. In addition, the water molecules near to hydrophilic spacer group are more restricted than that to hydrophobic spacer group. These could be the reasons for why microviscosity of micelles of Gemini-X, -Y and -Z are greater as compared to Gemini-A. The greater micropolarity of the micelles of Gemini-X, -Y and -Z as compared to that of Gemini-A is because of the presence of hydrophilic spacer groups in the former.

3b.2.4 Solvation dynamics

In the micelles of all gemini surfactants, C-480 molecule exhibits wavelength-dependent fluorescence decay. Fluorescence decays of C-480 have been recorded at different intervals in the whole wavelength range of fluorescence spectrum. A decay at a shorter wavelength corresponds to the fluorescence from the unsolvated dipole created at the excited state. However, as mentioned before due to the limitation of our TCSPC setup in the present case also there is a possibility that a high % of solvated dipoles contribute to the fast decays observed at shorter wavelength range. But at a longer wavelength, the fluorescence decay is from a solvated dipole which is delayed by solvent relaxation process showing a clear growth in the decay.[39, 40] Figures 3b.3a-c represent the wavelength-dependent decays of C-480 in the micelles of Gemini-X, Gemini-Y and Gemini-Z, respectively. For the quantitative measurement of solvation dynamics, the solvent response function (SRF), *C(t)* given by Fleming and Maroncelli[41] has been used (Equation 2.9 Chapter 2).

Time-resolved emission spectra (TRES) have been constructed to determine the peak wavenumbers following the method proposed by Fleming and Maroncelli (Chapter 2, Section no. 2..2.10).[41] TRES for Gemini-X, -Y and -Z are shown by Figure 3b.4. The peak wavenumber, $\bar{\upsilon}(t)$ for each TRES at different times was obtained after the fitting of TRES to a log-normal function.[41, 42] After calculating solvent response function, *C(t)* using Equation 2.9, (Chapter 2) the decays of *C(t)* have been shown by Figure 3b.5. The bi-exponential fitting of the decay of *C(t)* with time has been done using Equation 2.14 (Chapter 2). The values of solvation times obtained from the fitted data are given in Table

3b.3. The average solvation time, $\langle \tau_s \rangle$ for a bi-exponential decay, was calculated by the Equation 2.15 and are also given in Table 3b.3.

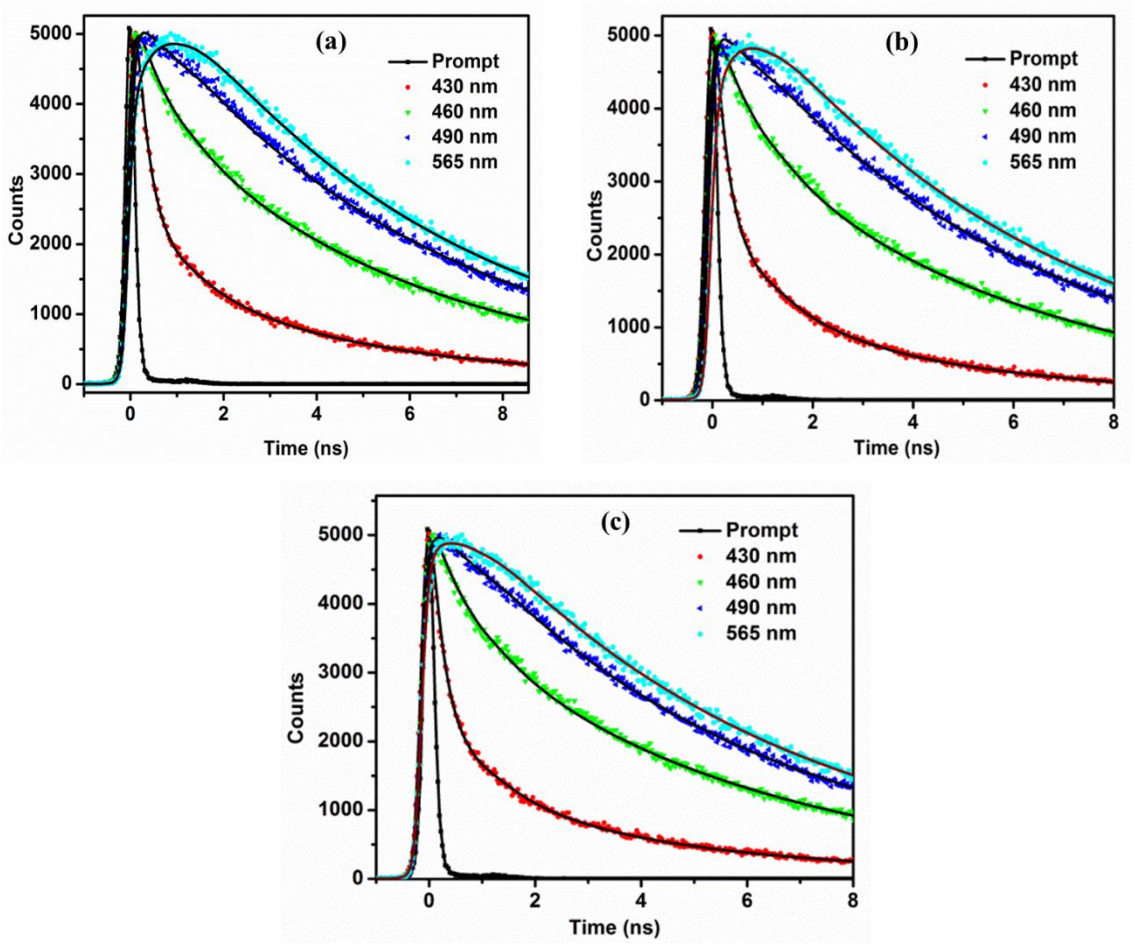

Figure 3b.3. Fluorescence decays of C-480 in the micelles of (a) Gemini-X (b) Gemini-Y and (b) Gemini-Z, respectively at λ_{em} = 430 nm, 460 nm, 490 nm and 565 nm along with instrument response function. λ_{ex} = 375 nm.

The time-dependent Stokes' shift occurring is because of the probe molecules present at the Stern layer of the micelles,[43] neither for the probes those exist in the core of the micelles (no solvation),[29, 32] nor for the probes present in the bulk water (too fast to be detected by the present set-up).[44] The bimodal behavior of solvation dynamics i.e. fast and slow solvation components (Table 3b.3) are due to the free and bound water molecules, respectively.[45] Apart from water molecules polar headgroups, spacer groups and counterions may also be responsible for the solvation of the probe molecule in the Stern layer of aqueous micelles. However, polar headgroups are directly attached with the tails and spacer group is indirectly attached with the tails which restrict their mobility. Therefore, the solvation process contributed by the headgroups and the spacer group is

very slow because it has been reported that dynamics of polymer chains occurs in ~100 ns time scale.[32, 46] Thus water molecules and counterions are mainly responsible for the present solvation process.

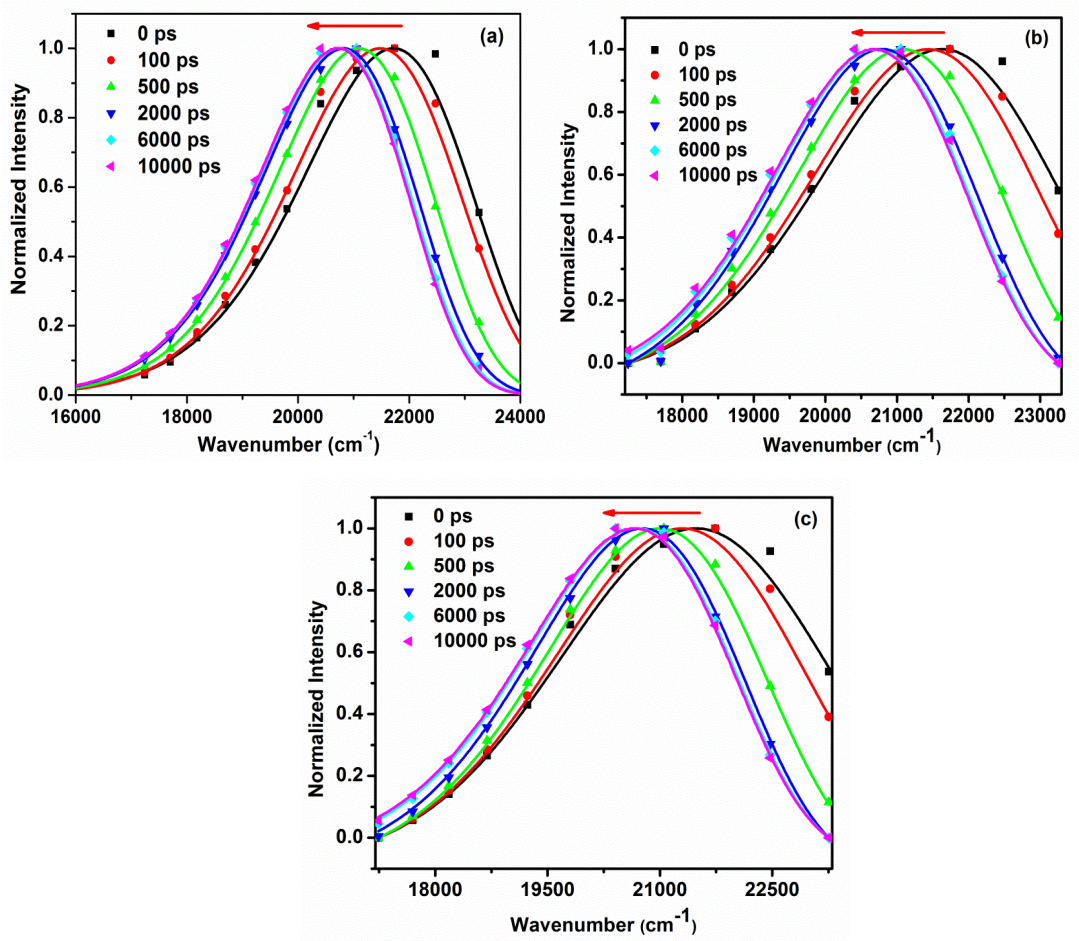

Figure 3b.4. Time-resolved emission spectra (TRES) of C-480 in the micelles of (a) Gemini-X, (b) Gemini-Y and (c) Gemini-Z at different times (0 ps -10000 ps).

It has been reported that the strength of a hydrogen bond between water and polar headgroup is much stronger than that between two water molecules.[32, 47, 48] Thus those water molecules interacting with the polar headgroups contribute to the slow component of solvation and the water molecules hydrogen bonded among themselves contribute to the fast component of solvation. The data in Table 3b.3 show that fast and slow solvation times as well as average solvation time increase with increasing tail length from C_{12} to C_{16} in Gemini-X, -Y and -Z, respectively. In all cases the slow components have major contribution to the solvation than the fast component. Reason behind this could be that water molecules taking part in this solvation process are present deep inside the Stern layer and are quite rigid. Rigidness of water molecules increases with increasing tail length

which is evidenced by decrease in Stokes' shift, $\Delta\bar{\upsilon}$ (Table 3b.3). Chattopadhyay *et al.*[49] have reported that water can penetrate the micelles up to a certain depth depending upon the compactness of the micelle. Although the increase in solvation time is not very significant for increase in tail length from C_{14} to C_{16}, but it is comparatively more significant for increasing tail length from C_{12} to C_{14} which is unlike conventional surfactants studied by Sarkar *et al.*[30] They have noticed average solvation times, 273 ps, 286 ps and 341 ps for conventional surfactants with tails C_{12}, C_{14} and C_{16}, respectively.

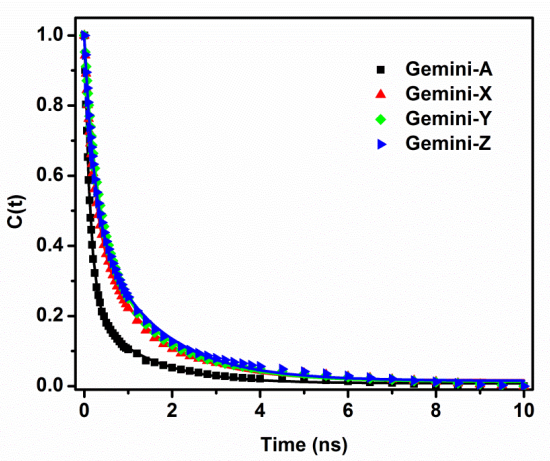

Figure 3b.5. Decays of solvent response function, *C(t)* of C-480 in the micelles of Gemini-A, -X, -Y and -Z.

Table 3b.3. Decay characteristics of *C(t)* of C-480 in different micelles.

System	a_{1s}	τ_{1s} (ps)	a_{2s}	τ_{2s} (ps)	$<\tau_s>^a$ (ps)	$\Delta\bar{\upsilon}^b$ (cm^{-1})	Missing component (%)
Gemini-A	0.34	233	0.66	574	458	1354	16
Gemini-X	0.40	254	0.60	1742	1147	1005	16
Gemini-Y	0.43	331	0.57	1834	1188	955	29
Gemini-Z	0.45	359	0.55	1895	1204	819	39

$^a\langle\tau_s\rangle = a_1\tau_1 + a_2\tau_2$, $^b\Delta\bar{\upsilon} = \bar{\upsilon}(0) - \bar{\upsilon}(\infty)$. All data for Gemini-A are taken from reference.[29]

From these results it can be suggested that there is a little effect of increasing tail length on the solvation time and this effect is not linearly proportional to the increase in the number of carbon atoms in the tail. On the other hand, when one compares these results with that of Gemini-A, it can be seen that solvation process is much faster in Gemini-A with a larger value of Stokes' shift, $\Delta\bar{\upsilon}$ (Table 3b.3) as compared to other three gemini

surfactants. Even it is faster as compared to Gemini-X which has tails of same length as Gemini-A. This difference must be due to the difference in the chemical nature of their spacer group. Results depict that solvation process at the Stern layer is faster in case of micelles of gemini surfactants with comparatively hydrophobic spacer group. Gemini-A micelle has less compact structure (hydrodynamic radius = 1.92 nm) as compared to that of other three surfactants (hydrodynamic radius = 0.52 - 0.63 nm). Moreover, hydrophobic spacer group in Gemini-A is not hydrated whereas the hydrophilic diethyl ether spacer group in other surfactants is easily hydrated. Therefore, due to the presence of greater extent of free water molecules the solvation dynamics in the micelles of Gemini-A is faster than that in the micelles of other three surfactants. It is noteworthy that although the contribution of slower component in Gemini-A is similar to that in other three micelles, but bound water molecules contributing to the slow solvation is expected to be less rigid in the micelles of the former than that in the latter. The average solvation times noted in the present micelles are almost four times longer than that in the micelles of conventional surfactants with same tail length.[30] This difference could be due to two reasons. First, formation of micelles by gemini surfactants having two tails is thermodynamically more feasible; *cmc* of Gemini-X, -Y and -Z are much smaller than their conventional counterparts,[30] DTAB (15 mM), TTAB (3.5 mM) and CTAB (0.8 mM), respectively, therefore, micelles of gemini surfactants are expected to be more compact as compared to micelles of conventional surfactants. Second, the hydrophilic spacer groups present in the present gemini surfactants easily get hydrated and protect a significant amount of water molecules from their contact with the probe molecules. It can be mentioned here that Shirota and co-workers[50] have also found that solvation dynamics in the micelles of anionic surfactant, sodium alkyl sulfate (C_n = 8, 10, 12, and 14), and cationic surfactant, alkyltrimethylammonium bromide (C_n = 10, 12, 14, and 16) become slower with increasing alkyl chain length.

As there is a limitation of time resolution of our TCSPC setup (instrument response function = 165 ps), we are unable to detect a percentage of ultrafast solvation. The quantification of these missing components has been done following the method proposed by Fee and Maroncelli[41, 51] and the values are listed in Table 3b.3. To further support the fact that the hydrophilic spacer groups present in the gemini surfactants protect a certain amount of water molecules from their contact with the probe molecule, C-480, we have carried out a fluorescence experiment by forming micelles in the water-methanol mixture.

In our previous study[20] and also study carried out by other groups,[52] it has been observed that significant change in *cmc* values or the change in size of micelles is occurred when the percentage of an organic co-solvent especially hydrogen bond donating solvent in water-organic solvent mixture is above 20%. Keeping this in mind, we have recorded fluorescence spectra of C-480 in pure water and also in presence of various % of organic co-solvent not exceeding 20%. In this experiment we wanted to see the extent of interactions between the -OH group of methanol and C-480. Figure 3b.6(a) shows that in presence of 15*cmc* of Gemini-A the fluorescence peak maximum gets red-shifted from 477 nm to 480 nm on increasing % of methanol up to 20%. On the other hand, Figure 3b.6(b) shows that there is no change in fluorescence peak maximum for same % of increase in methanol in case of 15*cmc* of Gemini-X. This result is a clear evidence of protection of molecules containing -OH groups by hydrophilic spacer group from their contact with the probe molecule.

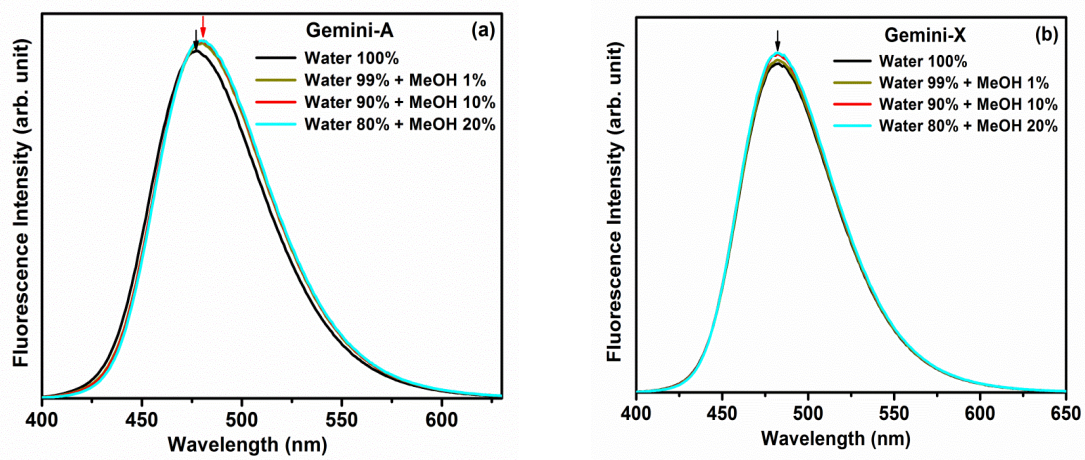

Figure 3b.6. Fluorescence spectra of C-480 in (a) 15*cmc* Gemini-A and (b) 15*cmc* Gemini-X in presence of various % of methanol in water-methanol mixture. λ_{ex} = 375 nm.

We have also carried out ^{1}H NMR study to demonstrate the interactions between spacer part of gemini surfactants and water molecules. The ^{1}H NMR spectra of Gemini-A, -X, -Y and -Z have been recorded in D_2O as solvent. A detailed discussion in this regard is given below for Gemini-A and Gemini-X. The same is true for Gemini-Y and Gemini-Z as well. The chemical shifts for the S_1 protons and S_2 protons (Scheme 1) of Gemini-A are observed to be at δ 3.34 and 1.81, respectively in D_2O, while that for Gemini-X are found to be at δ 3.59 and at δ 3.95, respectively in D_2O. Both S_1 and S_2 protons are more deshielded in Gemini-X as compared to Gemini-A. The ^{1}H NMR spectra for Gemini-A,

Gemini-X, Gemini-Y and Gemini-Z in D_2O are given in Figure 3b.7 (a), (b), (c) and (d), respectively and data are given below:

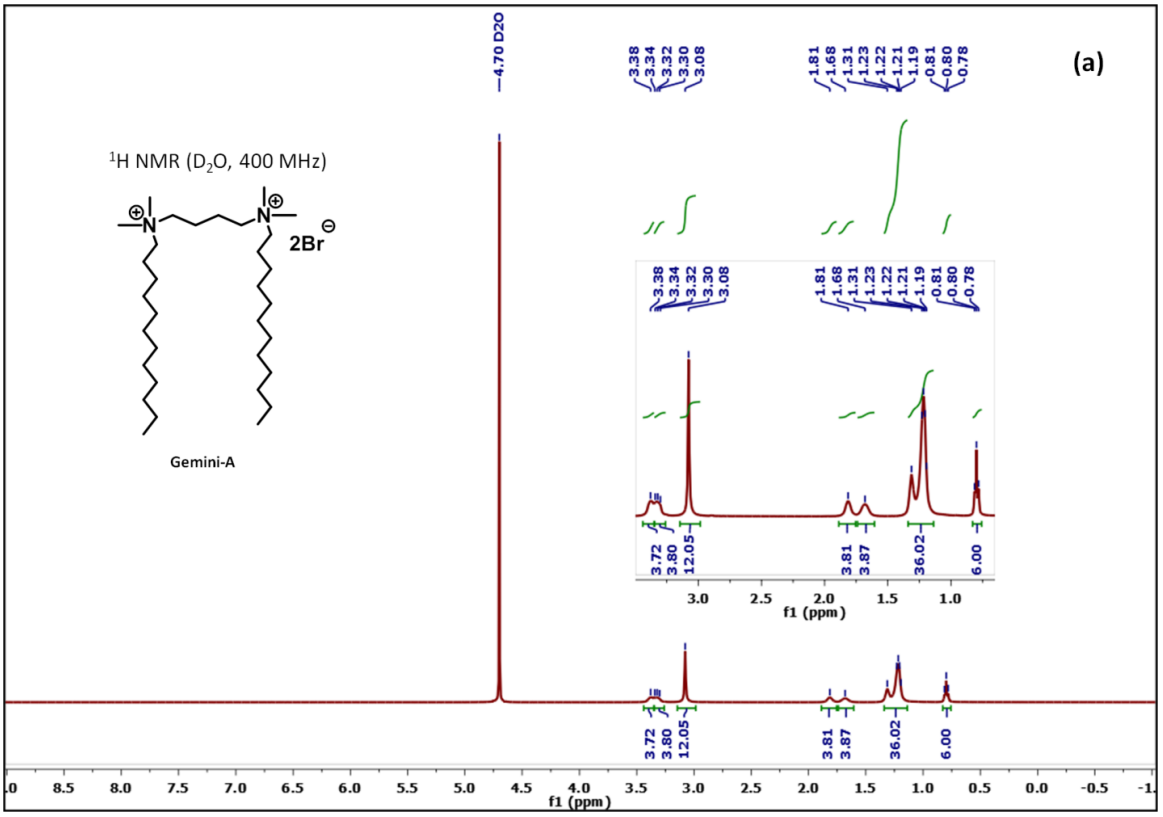

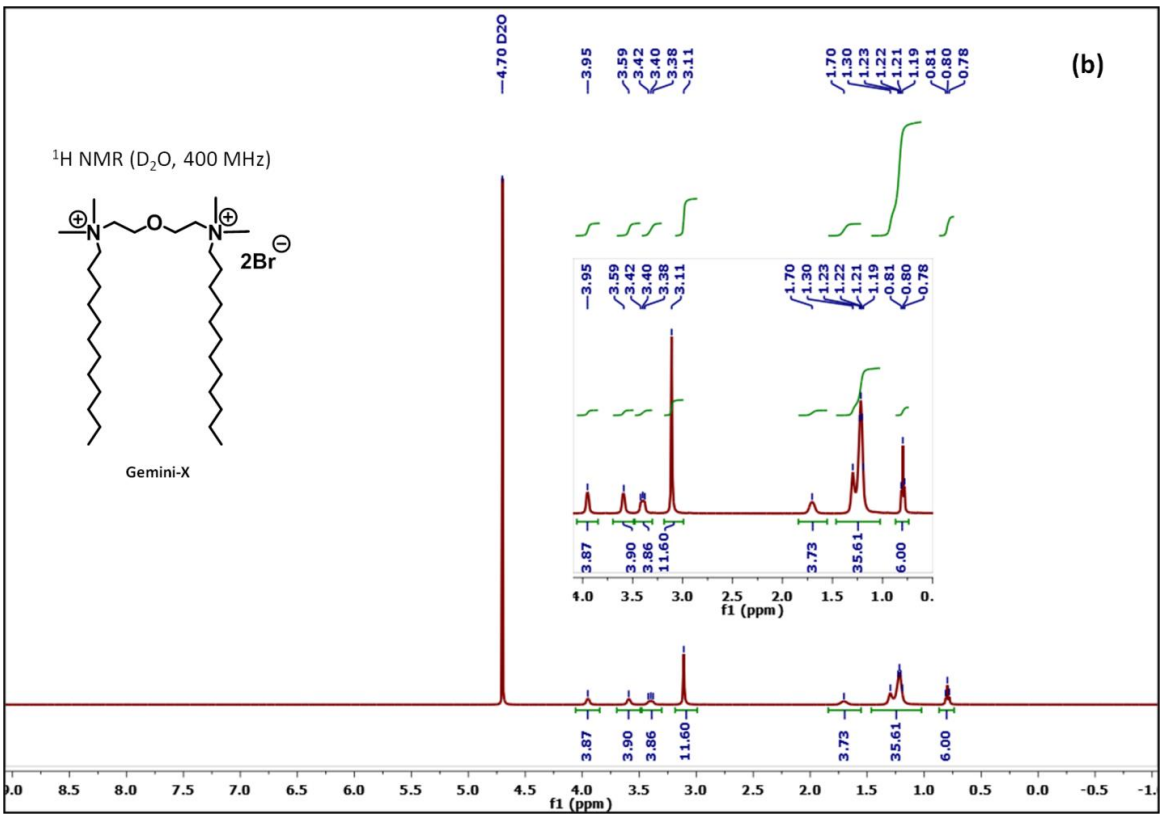

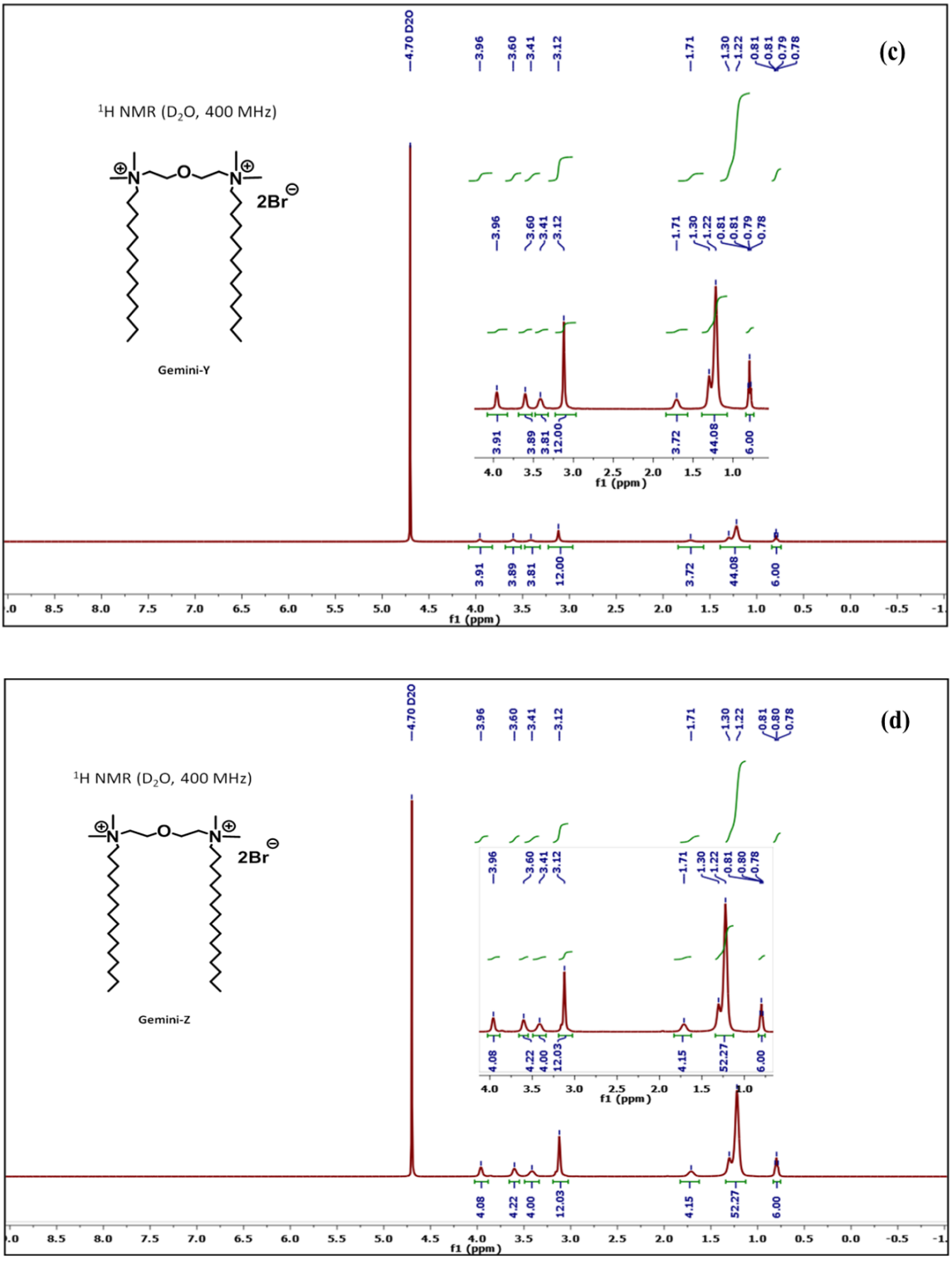

Figure 3b.7. ^{1}H NMR spectra of (a) Gemini-A (18.0 mM), (b) Gemini-X (14.5 mM), (c) Gemini-Y (5.0 mM) and (d) Gemini-Z (5.0 mM) in D_2O.

Gemini-A: ^{1}H NMR (400 MHz, D_2O) δ 3.34 (t, 4H), 3.30 (t, 4H), 3.08 (s, 12H), 1.81 (br s, 4H), 1.68 (br s, 4H), 1.34-1.14 (m, 36H), 0.80 (t, 6H).

Gemini-X: ^{1}H NMR (400 MHz, D_2O) δ 3.95 (br s, 4H), 3.59 (br s, 4H), 3.46-3.30 (m, 4H), 3.11 (s, 12H), 1.70 (br s, 4H), 1.48-1.03 (m, 36H), 0.80 (t, 6H).
Gemini-Y: ^{1}H NMR (400 MHz, D_2O) δ 3.96 (br s, 4H), 3.60 (br s, 4H), 3.41 (br s, 4H), 3.12 (s, 12H), 1.71 (br s, 4H), 1.39-1.07 (m, 44H), 0.79 (t, 6H).
Gemini-Z: ^{1}H NMR (400 MHz, D_2O) δ 3.96 (br s, 4H), 3.60 (br s, 4H), 3.41 (br s, 4H), 3.12 (s, 12H), 1.71 (br s, 4H), 1.34-1.12 (m, 52H), 0.80 (t, 6H).

It has been reported in the literature[53, 54] that in presence of an electronegative atom in a molecule close to a proton the latter becomes more acidic resulting in showing downfield ^{1}H NMR signal which is observed in the present case as well. It is also noteworthy that while S_1 protons are more deshielded as compared to S_2 protons in case of Gemini-A, but for Gemini-X, S_2 protons are more deshielded as compared to S_1 protons. Because of the presence of an oxygen atom in between two carbon atoms in the spacer of Gemini-X, S_2 protons are acidic in nature making those protons highly deshielded. Therefore, it is expected that extent of H-bonding between a proton in the spacer and water molecule would be more in case of Gemini-X as compared to Gemini-A. Thus the presence of oxygen atom in the spacer group of Gemini-X can protect the water molecules from their contact with the probe molecules present in inner side of the micelles to a greater extent as compared to Gemini-A. The ^{1}H NMR data for Gemini-Y and -Z in D_2O are also in the same line as Gemini-X. Thus ^{1}H NMR results support our above mentioned discussion that the hydrophilic spacer has effect on the rate of solvation dynamics in the micelles.

3b.2.5 Time-resolved fluorescence anisotropy

To have better idea about the microenvironment of micelles, the time-resolved fluorescence anisotropy measurements of C-480 have been carried out in micellar media. The time-resolved fluorescence anisotropy, *r(t)* values have been calculated by using the Equation 2.16 in Chapter 2. The anisotropy decays in the micelles of Gemini-A, -X, -Y and -Z are shown by Figure 3b.8. While the anisotropy decay of C-480 is found to be single exponential in water, but it is bi-exponential in micellar media. Earlier we have reported that the anisotropy decay of C-480 in pure water is single exponential with rotational relaxation time of 132 ps.[29] The bi-exponential anisotropy decay has been fitted to the decay function represented by the Equation 2.17 in Chapter 2. The rotational

relaxation times for first and slow components have been calculated from the fitted decay. The Equation 2.18 has been used to estimate the average rotational relaxation time.

The values of rotational relaxation times for the first and slow components along with average rotational relaxation time have been given in Table 3b.4. Longer rotational relaxation time in a micellar environment as compared to pure water represents that the free rotational motions of C-480 in water get restricted in micelles. The rotational relaxation data for C-480 in the micelles of Gemini-A obtained in our previous study[29] have also been given in Figure 3b.8 and Table 3b.4 for the purpose of comparison.

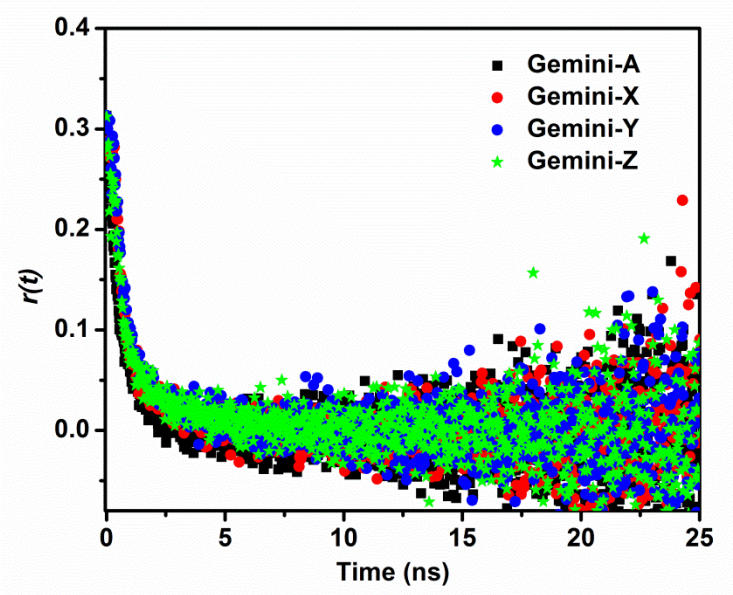

Figure 3b.8. Fluorescence anisotropy decays of C-480 in the micelles of gemini surfactants. λ_{ex} = 375 nm. λ_{em} = 470 nm.

Table 3b.4. Rotational relaxation data of C-480 in the different system.

System	a_{1r}	τ_{1r} (ps)	a_{2r}	τ_{2r} (ps)	$\langle\tau_r\rangle$ (ps)	χ^2
Gemini-A[a]	0.64	372	0.36	1663	837	1.04
Gemini-X	0.61	304	0.39	1853	908	1.00
Gemini-Y	0.65	375	0.35	2174	1005	1.00
Gemini-Z	0.71	407	0.29	2856	1117	1.08

[a]All data for Gemini-A are taken from reference.[29]

Data in Table 3b.4 show that both fast and slow relaxation times along with average relaxation time increase with increasing tail length of surfactants. This result can be corroborated with the increase in microviscosity of micelles with increasing tail length. Recently, Samanta *et al.*[55] have found that the rotational dynamics of 4- aminopthlimide

(4-AP) slows down when the chain length of cationic part of N-alkyl-N-methylmorpholiniumionic liquid (ionic liquid) increases. It can be noted that the fast component has major contribution (61-71%) to the fluorescence depolarization than that of the slow component (29-39%) in each of micellar system. Although C-480 is apparently present in a rigid environment, but the presence of fast motions responsible for the loss of anisotropy is evidenced by the values of time-zero anisotropy, r_o = 0.30, 0.31 and 0.31 for Gemini-X, -Y and -Z, respectively which are less than the maximum possible value of r_o = 0.40.[40] One can note that the change in average relaxation time is more for increasing tail length from C_{14} to C_{16} than that for C_{12} to C_{14} which is unlike solvation time. As expected the relaxation time is lower in case of micelles of Gemini-A as compared to micelles of other surfactants due to lower microviscosity of the former than that of the latter.[14] It has been discussed above that slow solvation component has major contribution to the solvation dynamics of C-480 in the Stern layer. Thus, these results infer that although solvation dynamics is a slow process, but C-480 molecules are quite freely movable deep inside the Stern layer of micelles. In a complex micellar environment, rate of rotational relaxation process may be directly correlated with the microviscosity, but it may not be true for rate of solvation process. Sarkar *et al.*[30] have reported that the average rotational relaxation times for C-480 in the micelles of conventional surfactants with C_{12}, C_{14} and C_{16} tails are 481, 687 and 812 ps, respectively. However, in the present surfactant systems with hydrophilic spacer groups these values are almost 1.5 times longer. It is even longer in presence of hydrophobic spacer group as well. Thus, the presence of spacer group in a gemini surfactant makes the rotational relaxation process slower in more compact micelles with higher microviscosity as compared to their conventional counterparts.

The observed bi-exponential behavior of the anisotropy decay is not due to the different location of the probe molecule in the micelles but due to the different types of rotational motions.[56, 57] This type of bimodal anisotropy decay is well explained by two-step and wobbling-in-a-cone model[57, 58] According to this model, wobbling motion of the probe in a cone, translational motion or lateral diffusion of the probe along the surface of the micelle, and overall tumbling motion of the micelles are responsible for fluorescence depolarization in a micelle.[16, 73, 74] The two-step model explains that the slow relaxation time (τ_{2r}) can be related to the times corresponding to the tumbling motion of the micelle as a whole (τ_m) and the lateral diffusion (τ_D) of the probe along the micelle surface following the relation given by Equation 2.19 in Chapter 2.

The time corresponding to the rotational motion of the micelle as a whole (τ_m) has been calculated using Debye-Stokes-Einstein equation (Equation 2.20) using the value of hydrodynamic radius of micelle. The hydrodynamic radii (r_h) estimated in the present study and size distribution plots of all three micellar media are given in Table 3b.5 and Figure 3b.9, respectively. The τ_m values have been calculated by using the Equation 2.20 and τ_D values have been calculated using the values of τ_m and Equation 2.19 at 298.15 K temperature and are tabulated in Table 3b.5. By comparing the values of τ_D (Table 3b.5) with the values of slow rotational relaxation time (τ_{2r}) (Table 3b.4), one can see that these values are almost same. Therefore, the slow rotational relaxation is mainly due to the lateral diffusion of the probe along the surface of the micelle. The time constant for the lateral diffusion of the probe increases with increasing tail length of the gemini surfactants i.e. with increasing microviscosity of micelles. The tumbling motion of the micelle as a whole is much slower than the lateral diffusion of the probe in the micelle. As expected the time constant for the overall motion of micelle increases with increasing size of micelle. The time constant for the wobbling motion (τ_w) of C-480 in the micelles has been calculated by using the Equation 2.25. The calculated τ_w values are also tabulated in Table 3b.5. The wobbling motion time (τ_w) is a measurement of relaxation of local structure in a micelle. The value of τ_w increases with increasing microviscosity of micelles.

Table 3b.5. Hydrodynamic radius (r_h), wobbling motion time (τ_w), time for overall rotational motion of the micelle (τ_m), lateral diffusion time (τ_D), wobbling diffusion coefficient (D_w), cone angle (θ_o), and order parameter ($|S|$) obtained from the anisotropy decay of C-480 in the different micelles**.**

System	r_h (nm)	τ_w (ps)	τ_m (ns)	τ_D (ps)	$D_w \times 10^{-8}$ (s^{-1})	θ_o (deg)	$\|S\|$
Gemini-X	0.52	364	126	1880	4.64	43.6	0.62
Gemini-Y	0.61	453	208	2200	4.11	45.8	0.59
Gemini-Z	0.63	475	226	2890	4.55	49.3	0.54

Applying wobbling-in-a-cone model[57], the values of wobbling diffusion coefficient (D_w), order parameter ($|S|$) and cone angle (θ_o) have been calculated using Equations 2.26, 2.22 and 2.23, respectively to have further information about the motional restriction of C-480 molecules within the micelles. The values obtained are summarized in Table 3b.5. A large value (greater than 0.5) of spatial restriction parameter ($|S|$) shows that the probe molecules are located in a restricted environment. The higher values of θ_o

and lower values of (|*S*|) for Gemini-Y and -Z as compared to Gemini-X might be indicating that wobbling-in-a-cone model is not suitable for micelles with high microviscosity. To resolve this apparent discrepancy, often spinning-in-equatorial-band model[59, 60] is used. However, in the present case it is not applicable as for this model the value of |*S*| should be less than 0.5. The possible reason could be that the probe molecule is aligned in such a way that the emission moment is neither perpendicular to the long axis like that in spinning-in-equatorial-band model, nor parallel to the long axis like that in the wobbling-in-a-cone model, but oriented in between these two possibilities. More importantly, the orientation of C-480 molecules in more viscous Gemini-Y and Gemini-Z micelles are possibly different from that in Gemini-X micelles.

It is noteworthy that hydrodynamic radii data show the micelles are spherical in nature and that is why we could use Two-step and Wobbling-in-a-cone model those are applicable for spherical micelles. Data also show that size variation is not very large. So there is no chance of effect of aggregation states i.e. change in micellar shapes from spherical to worm-like or so on the solvation dynamics or rotational relaxation. Also concentration of surfactant taken is much higher than *cmc*, so there would be hardly any chances of existence of premicellar aggregates.

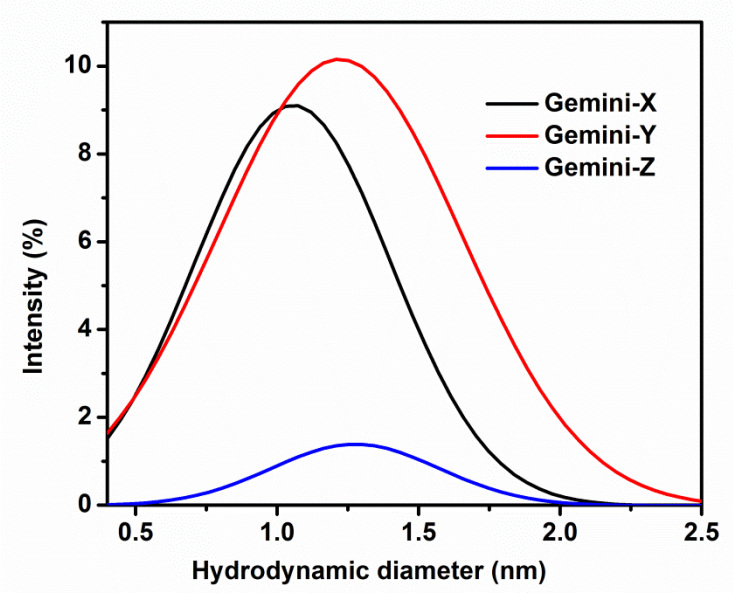

Figure 3b.9. The size distribution graph for the micelles of the surfactants, Gemini-X, -Y and -Z obtained from dynamic light scattering (DLS) measurement.

3b.3 Conclusions

Present study demonstrates the effect of hydrophobicity of tails and hydrophilicity of the spacer group of gemini surfactants on the rates of solvation and rotational relaxation processes of C-480 in aqueous micelles. Study shows that C-480 molecules are located in the Stern layer. Micelles become progressively more compact with increasing hydrocarbon tail length which results in lesser extent of penetration of water molecules thereby increasing microviscosity of micelles. The rate of solvation process becomes slower with increasing microviscosity of micelles with slow solvation as a major component. It infers that C-480 molecules are located inside the Stern layer of micelles and water molecules become progressively more rigid with increasing compactness of micelles. Micelles with hydrophilic spacer group like diethyl ether in the present case are more compact as compared to hydrophobic spacer. Moreover, hydrophilic spacer group gets easily hydrated. Therefore, the microviscosity of micelles of a gemini surfactant with hydrophobic spacer group is lower as compared to hydrophilic spacer group. Also the extent of free water molecules is more at the Stern layer of micelles of the former than that of the latter. As a result, solvation dynamics is faster in case of micelles of gemini surfactants with hydrophobic spacer. The rate of rotational relaxation process also slows down with increasing hydrocarbon tail length of surfactants as a result of increased microviscosity of micelles. However, unlike solvation process the fast rotational motion is a major component for depolarization. Thus although solvation process is slow, but the rotational motion of C-480 is quite feasible inside the Stern layer of a compact micelle. More compact micelles are formed with increased hydrophilicity of the spacer group of gemini surfactants which results in slowing down the rate of rotational relaxation process. The hydrophilic spacer group of gemini molecules protects the water molecules from their easy contact with the probe molecules present inside the Stern layer and also favors the formation of compact micelle. That is why solvation and rotational relaxation processes are almost 4 and 1.5 times longer in case of present micelles of surfactants with hydrophilic spacer groups as compared to micelles of their conventional counterparts, respectively. Thus the spacer group of a gemini surfactant has an effect on the rates of solvation and rotational relaxation processes in the micelles and the effect is more pronounced in the case of solvation process. The slow rotational component is mainly due to the lateral diffusion of the probe along the surface of micelle. The tumbling motion of micelles as a whole is a very slow process as compared to the lateral diffusion of the probe and the time

constant for the former motion increases with increasing size of the micelle. Both wobbling motion and lateral diffusion of the probe become slower with increasing microviscosity of micelles. There is an indication of different orientation of probe molecules in the micelles of high microviscosity.

References

1. Y. Han and Y. Wang, *Phys. Chem. Chem. Phys.*, 2011, **13**, 1939-1956.
2. S. He, H. Chen, Z. Guo, B. Wang, C. Tang and Y. Feng, *Colloids Surf. A Physicochem. Eng. Asp.*, 2013, **429**, 98-105.
3. S. Bhattacharya and J. Biswas, *Nanoscale*, 2011, **3**, 2924-2930.
4. C. McGregor, C. Perrin, M. Monck, P. Camilleri and A. J. Kirby, *J. Am. Chem. Soc.*, 2001, **123**, 6215-6220.
5. L. Caillier, E. T. de Givenchy, R. Levy, Y. Vandenberghe, S. Geribaldi and F. Guittard, *J. Colloid Interface Sci.*, 2009, **332**, 201-207.
6. F. M. Menger and J. S. Keiper, *Angew. Chem. Int. Ed.*, 2000, **39**, 1906-1920.
7. M. Borse, V. Sharma, V. Aswal, N. K. Pokhriyal, J. V. Joshi, P. S. Goyal and S. Devi, *Phys. Chem. Chem. Phys.*, 2004, **6**, 3508-3514.
8. M. Borse, V. Sharma, V. Aswal, P. Goyal and S. Devi, *J. Colloid Interface Sci.*, 2005, **284**, 282-288.
9. M. S. Borse and S. Devi, *Adv. Colloid Interface Sci.* , 2006, **123**, 387-399.
10. D. Danino, Y. Talmon and R. Zana, *Langmuir*, 1995, **11**, 1448-1456.
11. R. Oda, P. Panizza, M. Schmutz and F. Lequeux, *Langmuir*, 1997, **13**, 6407-6412.
12. D. Shukla and V. Tyagi, *J. Oleo Sci.*, 2006, **55**, 381-390.
13. P. Ajmal Koya, *Langmuir*, 2010, **26**, 7905-7914.
14. X. Wang, J. Wang, Y. Wang, H. Yan, P. Li and R. K. Thomas, *Langmuir*, 2004, **20**, 53-56.
15. M. Pisárčik, J. Jampílek, F. Devínsky, J. Drábiková, J. Tkacz and T. Opravil, *J. Surfactants Deterg.*, 2016, **19**, 477-486.
16. S. Manet, Y. Karpichev, D. Bassani, R. Kiagus-Ahmad and R. Oda, *Langmuir*, 2010, **26**, 10645-10656.
17. P. X. Li, C. C. Dong, R. K. Thomas, J. Penfold and Y. Wang, *Langmuir*, 2011, **27**, 2575-2586.
18. S. Zhang, J. Yu, J. Wu, W. Tong, Q. Lei and W. Fang, *J. Chem. Eng. Data*, 2014, **59**, 2891-2900.

19. R. Zana, *Adv. Colloid Interface Sci.*, 2002, **97**, 205-253.
20. A. K. Tiwari, M. Sowmiya and S. K. Saha, *J. Mol. Liq.*, 2012, **167**, 18-27.
21. R. Zana, *Langmuir*, 1996, **12**, 1208-1211.
22. R. Zana, *J. Colloid Interface Sci.*, 2002, **248**, 203-220.
23. X. Wang, J. Wang, Y. Wang, J. Ye, H. Yan and R. K. Thomas, *J. Colloid Interface Sci.*, 2005, **286**, 739-746.
24. A. K. Tiwari, M. Sowmiya and S. K. Saha, *J. Photochem. Photobiol. A Chem.*, 2011, **223**, 6-13.
25. A. K. Tiwari, Sonu and S. K. Saha, *Ind. Eng. Chem. Res.*, 2013, **52**, 5895-5905.
26. F. Menger and C. Littau, *J. Am. Chem. Soc.*, 1993, **115**, 10083-10090.
27. A. K. Tiwari, Sonu and S. K. Saha, *J. Chem. Thermodyn.*, 2014, **70**, 24-32.
28. S. Kumari and S. K. Saha, *J. Phys. Chem. B*, 2015, **119**, 9751-9763.
29. A. K. Tiwari, Sonu and S. K. Saha, *J. Phys. Chem. B*, 2014, **118**, 3582-3592.
30. D. Chakrabarty, A. Chakraborty, D. Seth, P. Hazra and N. Sarkar, *J. Chem. Phys.*, 2005, **122**, 184516.
31. R. Yip, Y. Wen and A. Szabo, *J. Phys. Chem.*, 1993, **97**, 10458-10462.
32. N. Sarkar, A. Datta, S. Das and K. Bhattacharyya, *J. Phys. Chem.*, 1996, **100**, 15483-15486.
33. D. Chakrabarty, P. Hazra and N. Sarkar, *J. Phys. Chem. A*, 2003, **107**, 5887-5893.
34. E. M. Kosower, H. Dodiuk, K. Tanizawa, M. Ottolenghi and N. Orbach, *J. Am. Chem. Soc.*, 1975, **97**, 2167-2178.
35. H. Ratajczak and W. J. Orville-Thomas, *Molecular interactions*, John Wiley & Sons, 1980.
36. M. Sowmiya, P. Purkayastha, A. K. Tiwari, S. S. Jaffer and S. K. Saha, *J. Photochem. Photobiol. A Chem.*, 2009, **205**, 186-196.
37. S. K. Saha, P. Purkayastha, A. B. Das and S. Dhara, *J. Photochem. Photobiol. A Chem.*, 2008, **199**, 179-187.
38. T. A. Fayed, *Colloids Surf. A Physicochem. Eng. Asp.*, 2004, **236**, 171-177.
39. K. Bhattacharyya, *Chem. Commun.*, 2008, 2848-2857.
40. J. R. Lakowicz, *Principles of fluorescence spectroscopy*, Springer, New York, 2006.
41. M. Maroncelli and G. R. Fleming, *J. Chem. Phys.*, 1987, **86**, 6221-6239.
42. A. Maciejewski, J. Kubicki and K. Dobek, *J. Phys. Chem. B*, 2003, **107**, 13986-13999.

43. V. G. Rao, C. Banerjee, S. Mandal, S. Ghosh and N. Sarkar, *Spectrochim. Acta A Mol. Biomol. Spectrosc.*, 2013, **102**, 371-378.
44. Š. Vajda, R. Jimenez, S. J. Rosenthal, V. Fidler, G. R. Fleming and E. W. Castner, *J. Chem. Soc. Faraday Trans.*, 1995, **91**, 867-873.
45. N. Nandi and B. Bagchi, *J. Phys. Chem. B*, 1997, **101**, 10954-10961.
46. R. Dutta, M. Chowdhury and M. A. Winnik, *Polymer*, 1995, **36**, 4445-4448.
47. S. Balasubramanian and B. Bagchi, *J. Phys. Chem. B*, 2001, **105**, 12529-12533.
48. S. Balasubramanian, S. Pal and B. Bagchi, *Phys. Rev. Lett.*, 2002, **89**, 115505.
49. A. Chakrabarty, P. Das, A. Mallick and N. Chattopadhyay, *J. Phys. Chem. B*, 2008, **112**, 3684-3692.
50. Y. Tamoto, H. Segawa and H. Shirota, *Langmuir*, 2005, **21**, 3757-3764.
51. R. Fee and M. Maroncelli, *Chem. Phys.*, 1994, **183**, 235-247.
52. P. A. Koya and Z. A. Khan, *J. Colloid Interface Sci.*, 2010, **342**, 340-347.
53. A. D. Headley and N. M. Jackson, *J. Phys. Org. Chem.*, 2002, **15**, 52-55.
54. S. Hesse-Ertelt, T. Heinze, B. Kosan, K. Schwikal and F. Meister, In *Solvent effects on the NMR chemical shifts of imidazolium-based ionic liquids and cellulose therein*, Macromolecular symposia, Wiley Online Library, 2010, pp 75-89.
55. D. C. Khara, J. P. Kumar, N. Mondal and A. Samanta, *J. Phys. Chem. B*, 2013, **117**, 5156-5164.
56. M. Kumbhakar, T. Goel, T. Mukherjee and H. Pal, *J. Phys. Chem. B*, 2004, **108**, 19246-19254.
57. K. Kinosita Jr, S. Kawato and A. Ikegami, *Biophys. J.*, 1977, **20**, 289.
58. D. Chakrabarty, D. Seth, A. Chakraborty and N. Sarkar, *J. Phys. Chem. B*, 2005, **109**, 5753-5758.
59. E. L. Quitevis, A. H. Marcus and M. D. Fayer, *J. Phys. Chem.*, 1993, **97**, 5762-5769.
60. L. B. Johansson and A. Niemi, *J. Phys. Chem.*, 1987, **91**, 3020-3023.

Effect of Urea on Solvation Dynamics and Rotational Relaxation of Coumarin 480 in Aqueous Micelles of Cationic Gemini Surfactants with Different Spacer Groups

Abstract: *The present work highlights the effect of urea on solvation dynamic and the rotational relaxation of Coumarin 480 (C-480) in the Stern layer of aqueous micelles of cationic gemini surfactants, 12-4(OH)$_n$-12 (n = 0, 1, 2). UV-Visible absorption, steady-state fluorescence and fluorescence anisotropy, time-resolved fluorescence and fluorescence anisotropy, and dynamic light scattering measurements have been carried out for this study. The formation of micelles becomes disfavored in presence of urea at high concentration. Solvation dynamics is bimodal in nature with fast solvation as a major component. Average solvation time increases, reaches a maximum and then decreases with increasing concentration of urea because the degree of counterion dissociation also follows the same order with the addition of urea in the micellar solution. With increased degree of counterion dissociation the extent of clustering of water molecules is increased resulting in slower solvation process. The –OH group present in the spacer group of gemini surfactant controls the rate of solvation by shielding the water molecules from the probe molecules forming hydrogen bond. The microviscosity of micelles is decreased with increasing concentration of urea as a result of it rotational relaxation process becomes faster. In presence of –OH group in the spacer group the microviscosity of micelles is enhanced resulting in longer rotational relaxation time. Rotational relaxation process is bimodal in nature with the major contribution from the fast component to the fluorescence depolarization. Slow rotational relaxation is mainly due to the lateral diffusion of C-480 molecules along the surface of the micelle. The tumbling motion of micelle as a whole is much slower than the lateral diffusion of C-480. Wobbling motion of C-480 becomes faster with increasing concentration of urea as a result of decreased microviscosity of micelles. The alignment of C-480 molecules in micelles might change with changing microviscosity.*

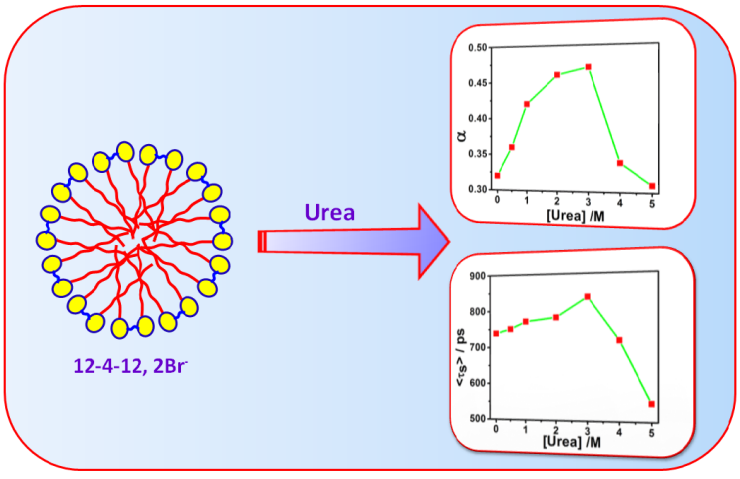

*Sunita Kumari, Sonu, Sayantan Halder, Rishika Aggrawal, G. Sundar and Subit K. Saha, *ACS Omega*, **2018**, *3*, 3079-3095.

3c.1 Introduction

Micelles, the assemblies of surfactant molecules, up to a certain extent, mimic the environment of lipid bilayers. The studies on micellar organization and dynamics pay special attention because the general principle for the micelles formation is related to other molecular assemblies such as bilayers, reverse micelles, liposomes, and biological membrane.[1-4] For biophysical or structure biological studies surfactants are used to maintain the purified protein in its native and functional states.[5, 6] Presence of an additive modifies various aggregating properties of the micellar solution of surfactant.[7-11] Urea, a well-known protein denaturant, present with ionic and nonionic surfactants increases the critical micellar concentration (*cmc*) values,[12-16] reduces the aggregation number of micelles[17, 18] etc. The solubility of hydrocarbons in the aqueous medium is enhanced in presence of urea. A mixture of surfactant and urea are used for various applications in membrane-protein research.[19-23] Urea facilitates the transfer of purified membrane protein from detergent micelles to lipid bilayers.[23] Two different mechanisms are proposed regarding urea-induced protein denaturation.[24-27] In one case urea acts as a water structure breaker or "chaotrope" facilitating the solvation of nonpolar solute. In another case, urea weakens the intramolecular proteinous bond while directly binding to proteins.[24-27] Various studies have been carried out to understand the properties of the urea-water system. Few studies reported that urea acts as water "structure breaker"[28, 29] while few others studies show that urea act as water "structure maker".[30, 31] Some other studies show the combination of these two effects.[32, 33] Hayashi *et al.*[34] have shown that urea retains the weakly associated water in the tetrahedral structure and thus, urea is not a strong structure breaker of water. Recently, Choudhury *et al.* have reported that urea is able to substitute for water in the hydrogen-bonded network without breaking the tetrahedral, hydrogen-bonded structure of water.[35]

Different groups have studied the effect of urea on various physical properties of conventional surfactants. Dey *et al.* have studied the effects of urea on aggregation properties of chiral surfactant.[36] Keller *et al*.[37] have reported the impact of urea on non-ionic sugar based surfactants. The effect of urea on the aggregation behavior of gemini surfactants and their mixed micelles with pluronic surfactant has been reported by Mahajan *et al*.[38]. Studies on the effect of urea concentration on the solvation dynamics in the micellar environment are scarcely available.

Considering the importance of gemini surfactants over conventional surfactants and urea in the protein denaturation process, it would be valuable to study the effect of urea on solvation and rotational relaxation dynamics in aqueous micelles of gemini surfactant. If there is any effect of urea on the micellization behavior of gemini surfactants with different spacer groups then how does it affect solvation dynamics and rotational relaxation processes of the probe molecule. Whether water structure breaker or maker properties of urea or some other factor(s) guide(s) the rate of solvation process? Is the effect of urea on the solvation dynamics and rotational relaxation and micellization behavior of gemini surfactant with different spacer group same or different? Answers to these questions are important as surfactant-urea mixtures are used in various membrane-protein research.[19-23]

In this chapter, we have investigated the effect of urea concentration on aggregation properties of gemini surfactants with different spacer groups (with and without –OH group(s)) [Scheme 3c.1] and also its effect on solvation dynamics and rotational relaxation of C-480 [Scheme 3c.1] in aqueous micelles of those surfactants. To probe the solvation dynamics the solute chosen should have zero or low dipole moment in the ground state and very high dipole moment in the excited state.[3639] C-480 is such kind of molecule. Moreover, because of the presence of several basic centers, it can also form hydrogen bonds.[40-45] There are arguments on the cleavage of hydrogen bond upon excitation.[42, 44] However, a more convincing report by Zhao *et al*.[45] says that the early time of photoexcitation of C-480 to the excited state is strengthened due to the intermolecular hydrogen bonding between C-480 and hydrogen bond donating solvents/groups. The surfactants used in the present study have been explored before to demonstrate the effect of –OH group(s) on solvation dynamics.[46] Microenvironmental properties around C-480 within the micelles of gemini surfactants with the variation of urea concentration have been studied. Two-step and wobbling-in-a-cone models have been explored to show the bimodal behavior of rotational relaxation processes and to demonstrate the wobbling motions in the micelles. Results obtained from this study could be useful to understand the water dynamics in biological systems in presence of urea.

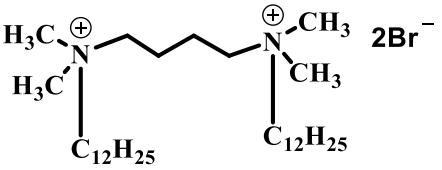

12-4-12 (Gemini-A)

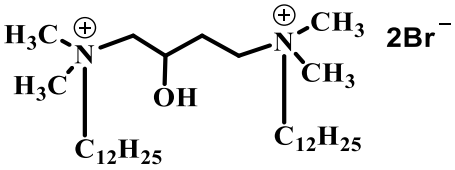

12-4(OH)-12 (Gemini-B)

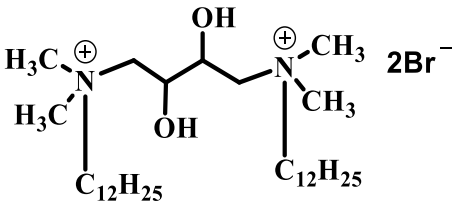

12-4(OH)$_2$-12 (Gemini-C)

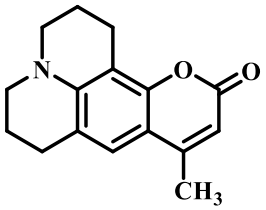

Coumarin 480 (C-480)

Scheme 3c.1: Molecular structures of gemini surfactants and Coumarin 480.

3c.2 Results and discussion

3c.2.1 Effect of urea on *cmc*

Cmc and degree of counter ion dissociation (α) values of all studied gemini surfactants in absence and in presence of various concentrations of urea have been determined by conductivity measurements performed at 298.15 K following Williams's method.[47] A plot of specific conductivity, κ versus concentration of surfactant with varying concentration of urea for Gemini-A is given in Figure 3c.1 as a representative one. Similar changes in κ with change in concentration of surfactant at varying concentration of urea have been noticed in cases of other two surfactants as well. While a *cmc* value has been calculated from the break point of two intersecting lines, a value of α has been calculated by taking the ratio of the slopes of the straight lines in post-micellar region to the pre-micellar region.[48] The values of *cmc* obtained are given in Table 3c.1 and the values of α are given later (Table 3c.6) where relevant discussion has been made. *Cmc* values of all the pure gemini surfactants are in good agreement with the reported values[46, 49] indicating the goodness of *cmc* values in presence of urea as well. It has been noticed that *cmc* value of gemini surfactants enhances with increasing the concentration of urea. It is reported in the literature that the solubility of a surfactant increases many fold in presence of urea.[50] Increased solubility of surfactant ions in the solution i.e. their reduced solvophobicity delays the aggregation process of surfactant molecules. In other words the hydrophobic interactions between surfactant molecules are decreased in presence of

urea.[51] Consequently, the concentration at which surfactant molecules start to form aggregates is increased.

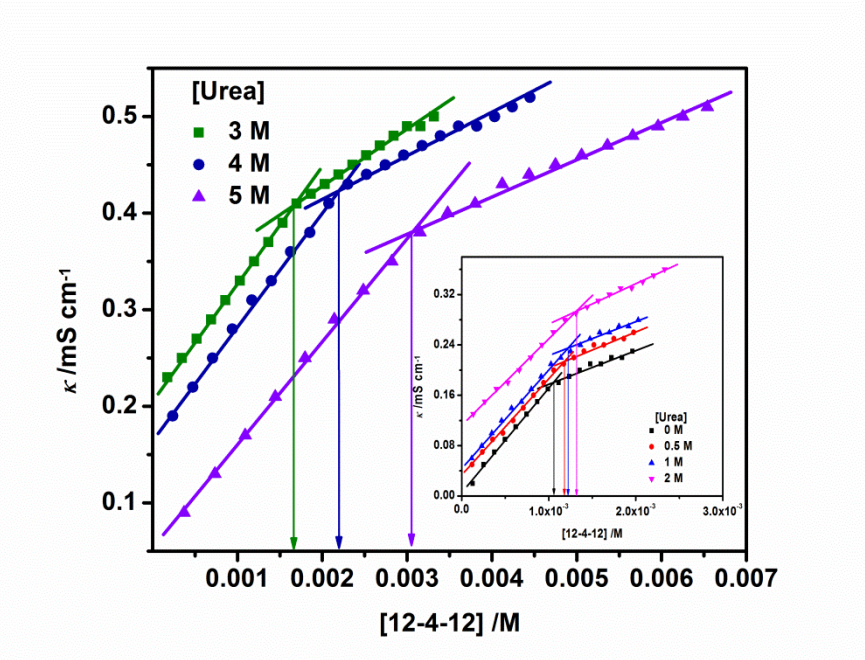

Figure 3c.1. Plot of κ versus concentration of Gemini-A with varying concentration of urea at 298.15 K.

Table 3c.1. Critical micelle concentration (*cmc*), mole fraction partition coefficient (K^{mic}), and standard molar Gibbs free energy of micellization ($\Delta G^{o,\,mic}$) of gemini surfactants in presence of urea.

Urea (M)	Gemini-A *Cmc* (mM)	Gemini-B *Cmc* (mM)	Gemini-C *Cmc* (mM)	Gemini-A K^{mic} (10^4)	Gemini-B K^{mic} (10^4)	Gemini-C K^{mic} (10^4)	Gemini-A $\Delta G^{o,\,mic}$ (kJ mol^{-1})	Gemini-B $\Delta G^{o,\,mic}$ (kJ mol^{-1})	Gemini-C $\Delta G^{o,\,mic}$ (kJ mol^{-1})
0.0	1.06 ±0.03	0.96 ±0.03	0.88 ±0.02	5.24 ±0.15	5.78 ±0.17	6.31 ±0.14	-26.93 ±0.07	-27.18 ±0.07	-27.40 ±0.05
0.5	1.18 ±0.04	1.07 ±0.03	0.96 ±0.03	4.70 ±0.15	5.19 ±0.14	5.78 ±0.17	-26.67 ±0.07	-26.91 ±0.07	-27.18 ±0.07
1.0	1.23 ±0.03	1.21 ±0.03	1.17 ±0.03	4.51 ±0.11	4.59 ±0.11	4.74 ±0.11	-26.57 ±0.06	-26.61 ±0.06	-26.69 ±0.05
2.0	1.31 ±0.05	1.47 ±0.07	1.67 ±0.09	4.24 ±0.16	3.78 ±0.18	3.32 ±0.17	-26.41 ±0.09	-26.12 ±0.12	-25.81 ±0.13
3.0	1.66 ±0.08	1.87 ±0.08	1.78 ±0.11	3.34 ±0.15	2.97 ±0.12	3.12 ±0.18	-25.82 ±0.11	-25.53 ±0.11	-25.65 ±0.15
4.0	2.19 ±0.10	2.12 ±0.11	2.02 ±0.12	2.53 ±0.11	2.62 ±0.13	2.75 ±0.16	-25.14 ±0.11	-25.22 ±0.13	-25.34 ±0.15
5.0	3.05 ±0.12	2.63 ±0.12	2.46 ±0.10	1.82 ±0.07	2.11 ±0.09	2.26 ±0.09	-24.31 ±0.09	-24.68 ±0.11	-24.85 ±0.11

To support the increment in *cmc* value with increasing the concentration of urea into aqueous phase, the mole fraction partition coefficient of gemini surfactants from aqueous phase to micellar phase (K^{mic}) has been determined by using the Equation 2.7 for all micellar systems.[37] K^{mic} values calculated are given in Table 3c.1. K^{mic} values are decreasing with increasing the urea concentration. In presence of urea because of depression in the water-to-micelles partition coefficient *cmc* value of a gemini surfactant

is increased. The values of standard molar Gibbs free energy of micellization have been calculated by the given Equation 2.8.[37] $\Delta G^{o,\ mic}$ values at 298.15 K at various urea concentrations are given in Table 3c.1. $\Delta G^{o,\ mic}$ values are increased with increasing the concentration of urea. This also indicates that micellization process becomes less favourable with increasing the concentration of urea.

3c.2.2 UV-visible absorption and steady-state fluorescence study

UV-visible absorption and steady state fluorescence spectra of C-480 have been obtained in presence of pure gemini surfactants and also in presence of gemini surfactant plus various concentrations of urea. Figure 3c.2a depicts the absorption spectra of C-480 in presence of 10 mM of Gemini-A and Gemini-A (10 mM) + varying concentration of urea as a representative. Figure 3c.2b demonstrates the fluorescence spectra of C-480 in presence of pure 10 mM Gemini-A and Gemini-A (10 mM) + varying concentration of urea. Similar absorption and fluorescence spectra are observed in presence of each of other two gemini surfactants plus urea systems as well.

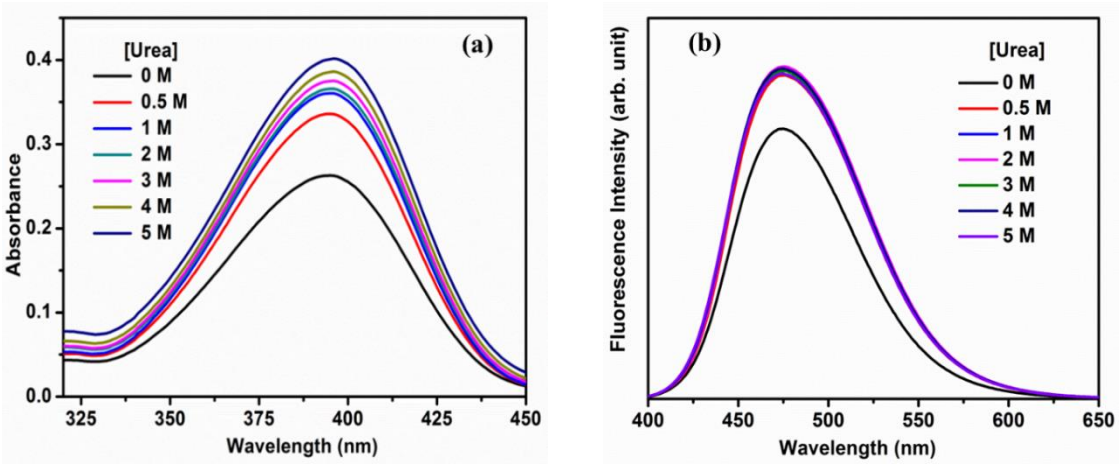

Figure 3c.2. (a) Absorption spectra and (b) fluorescence spectra (λ_{ex} = 375 nm) of C-480 in presence of pure Gemini-A and Gemini-A + varying concentration of urea. [C-480] = 5 μM.

In 10 mM of both Gemini-A and Gemini-B, the absorption and fluorescence peak maxima of C-480 are 395 nm and 475 nm, respectively. In 10 mM of Gemini-C, these values are 393 nm and 474 nm, respectively. There is no significant change in peak maxima values upon addition of urea. Absorption and fluorescence peak maxima values of C-480 in all the studied systems are given in Table 3c.2. It is noteworthy that an increase in absorbance and fluorescence intensity with increasing concentration of urea have been observed in pure water as well (spectra not shown). It could be because of either effect of

urea on hydrogen bonding between C-480 and water and/or salting-in effect of urea (a thorough study can be done later). However, this effect can be ruled out in presence of high concentration of surfactant (10 mM) where C-480 molecules are completely solubilized in micelles (excitation wavelength independent fluorescence peak maximum and very little change in absorption and fluorescence peak maxima in presence of urea noted). Figure 3c.3 shows absorption and fluorescence spectra of C-480 in pure water, methanol, cyclohaxane and 10 mM of Gemini-A. Absorption and fluorescence peak maxima of C-480 in pure water are observed at 389 nm and 489 nm, respectively and the same in cyclohaxane are appeared at 362 nm, 378 nm and 409 nm, respectively (Table 3c.2).

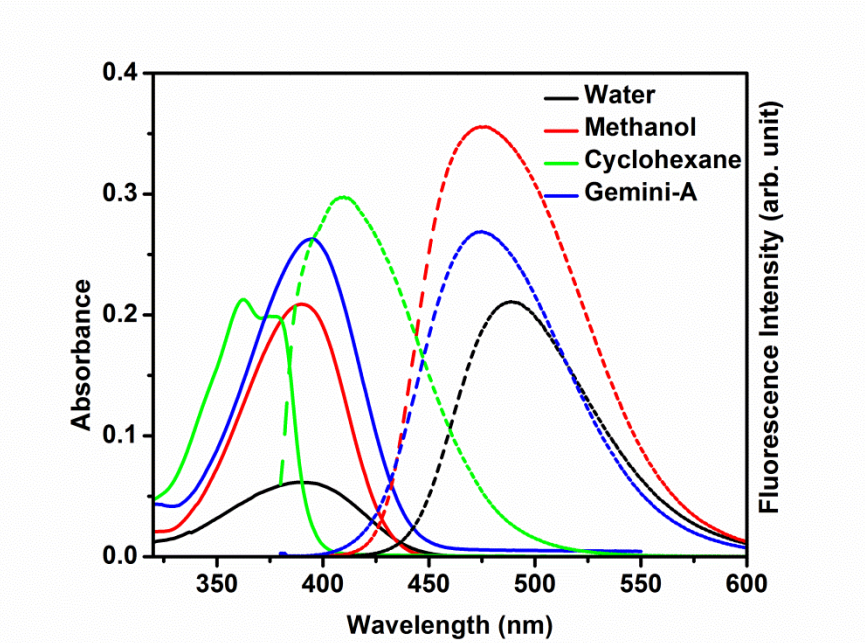

Figure 3c.3. Absorption (——) and fluorescence (– – –) spectra (λ_{ex} = 375 nm) of C-480 in pure water, methanol, cyclohexane and 10 mM of Gemini-A.

In water, fluorescence of C-480 occurs from the stabilized intramolecular charge transfer (ICT) state.[52-55] Low fluorescence intensity in a polar medium is because of high rate of non-radiative processes as triplet and ground states are very close to the ICT state. As compared to water, in a comparatively less polar medium like micelles fluorescence intensity increases with concomitant blue shift in peak maximum. This is because the emitting state now get destabilized and goes away from the triplet as well as ground states. The blue shift in absorption peak maximum in water with respect to that in micellar medium is because of intermolecular hydrogen bonding between C-480 and water molecules which generally observed for molecules with ICT characteristics.[52-55] The ICT

fluorescence of C-480 has also been demonstrated by recording fluorescence spectra in different % of dioxane-water mixtures. Figure 3c.4a represents fluorescence spectra and 3c.4b shows changes in fluorescence intensity and fluorescence peak maxima of C-480 with increasing % of water in dioxane-water mixtures. In presence of pure gemini surfactants and gemini surfactants plus urea absorption and fluorescence peak maxima of C-480 are different from that in presence of pure water.

Table 3c.2. Absorption peak maxima (λ_{max}^{abs}) and fluorescence peak maxima[a] (λ_{max}^{flu}) of C-480 in pure solvents and gemini surfactant-urea mixed systems.

Urea (M)	Gemini-A λ_{max}^{abs} (nm)	Gemini-A λ_{max}^{flu} (nm)	Gemini-B λ_{max}^{abs} (nm)	Gemini-B λ_{max}^{flu} (nm)	Gemini-C λ_{max}^{abs} (nm)	Gemini-C λ_{max}^{flu} (nm)
0.0	395	475	395	475	393	474
0.5	395	475	395	475	393	474
1.0	395	475	395	475	394	474
2.0	395	475	395	475	394	474
3.0	396	475	396	475	394	474
4.0	396	475	396	475	394	474
5.0	396	475	396	475	394	474
Water	389	489	-	-	-	-
Methanol	390	475	-	-	-	-
Cyclohexane	362, 378	409	-	-	-	-

[a] λ_{ex} = 375 nm.

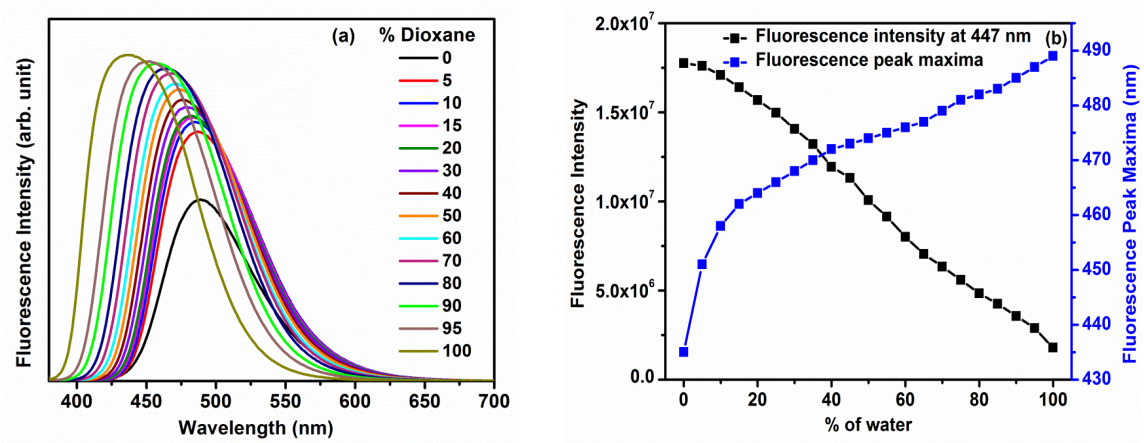

Figure 3c.4. (a) Fluorescence spectra and (b) variations in fluorescence intensity and fluorescence peak maxima of C-480 in different % dioxane-water mixtures. [C-480] = 5 μM, λ_{ex} = 375 nm.

These results indicate that microenvironment around C-480 in the micelles of pure gemini surfactant and that of gemini surfactant plus urea are different from that in presence of pure water. The blue shift in fluorescence peak maxima in a micellar medium as well as in a micelle plus urea mixed system as compared to pure water suggests that C-480 feels less polar environment in micelle and micelle-urea mixed media than that in bulk water.

3c.2.3 Study on microenvironment of micellar systems in presence and absence of urea

3c.2.3.1 Micropolarity

Determination of micropolarity value around the probe molecule gives valuable information about the location of the probe molecule inside the micellar environment. Fluorescence active probe molecules play an important role for the determination of micropolarity of biological and biologically related environment.[46, 56] In the present study, the micropolarity values expressed in terms of $E_T(30)$ which is an empirical solvent polarity parameter developed by Reichardt *et al*.[57] have been estimated to obtain the information about microenvironment surrounding the probe molecule inside the micelles. To determine the micropolarity around C-480 in various studied systems, the fluorescence behaviours of C-480 in absence and presence of various concentration of urea have been compared with that in different composition of dioxane-water mixture.[46] The values of ε_{max}^{fl} of C-480 in absence and presence of various concentration of urea have been estimated and $E_T(30)$ values have been estimated from the method in given Chapter 2, Section no. 2.2.5. The $E_T(30)$ values for all the systems are found to be vary between 53.8 - 55.8 kcal mol^{-1}. The calculated $E_T(30)$ value in the investigated systems indicating that micropolarity around C-480 in these systems is lesser than that of water ($E_T(30)$ = 63.1 kcal mol^{-1}).The $E_T(30)$ value in all the studied systems is similar to that of methanol (55.5 kcal mol^{-1}). It depicts that C-480 is neither present at the core of the micelles nor in the bulk water, but somewhere in between these two. Literature report says that the micropolarity of the Stern layer is similar to methanol.[46, 56, 58-60] Based on this literature report we state that C-480 molecules are mostly residing in the Stern layer. It is pertinent to note that C-480 being present in the Stern layer of micelles, microenvironment remains more or less same with the addition of urea in micellar systems. Consequently both fluorescence peak maximum and $E_T(30)$ values are found to be same in gemini micelles with varying concentration of urea.

3c.2.3.2 Microviscosity

Measurement of fluorescence anisotropy of a probe molecule in a microenvironment gives information about microviscosity around the molecule. As we were not getting proper trend of microviscosity using C-480 as a probe following our earlier method,[46] we explored 1,6-diphenyl-1,3,5-hexatriene (DPH) which is a well-known viscosity sensitive fluorescence probe molecule.[56] The absolute values of microviscosities of micelles, η_m using DPH have been estimated using Debye-Stokes-Einstein relation (Equation 2.2).[56, 61] The rotational correlation time, τ_R has been calculated using Perrin's equation (Equation 2.3, Chapter 2). [62] The values of r, $<\tau_f>$, τ_R and η_m are given in Table 3c.3. The data in Table 3c.3 show that in case of each micellar system the fluorescence anisotropy as well as microviscosity decrease with increasing concentration of urea. It further supports our above mentioned discussion based on K^{mic} and ΔG^o values (Table 3c.1) that urea disfavour the formation of micelles. As a result of that probe molecules get more and more exposed to the less viscous environment. Although this result does not provide the actual picture of microenvironment around C-480, but it serves our purpose to demonstrate the effect of urea concentration on the microviscosity of micelles.

Table 3c.3. Fluorescence anisotropy[a] (r), average excited singlet state lifetime[b] $<\tau_f>$, rotational correlation time (τ_R) of DPH, microviscosities (η_m) of micelles in presence of various gemini surfactants (10 mM) at various concentration of urea.

Urea (M)	Gemini-A				Gemini-B				Gemini-C			
	r	$<\tau_f>$ (ns)	τ_R (ns)	η_m (mPa s)	r	$<\tau_f>$ (ns)	τ_R (ns)	η_m (mPa s)	r	$<\tau_f>$ (ns)	τ_R (ns)	η_m (mPa s)
0.0	0.086	5.41	1.69 ±0.31	22.2 ±0.2	0.087 ±0.012	5.76	1.82 ±0.33	24.0 ±0.2	0.090 ±0.010	6.31	2.09 ±0.31	27.4 ±0.2
0.5	0.080	4.64	1.32 ±0.21	17.3 ±0.2	0.083 ±0.013	5.61	1.78 ±0.36	23.4 ±0.2	0.085 ±0.012	6.03	1.85 ±0.34	24.3 ±0.2
1.0	0.070	4.56	1.09 ±0.19	14.4 ±0.2	0.082 ±0.014	5.45	1.60 ±0.35	21.0 ±0.2	0.084 ±0.014	5.89	1.78 ±0.39	23.4 ±0.2
2.0	0.065	4.46	0.98 ±0.21	12.8 ±0.1	0.077 ±0.011	5.08	1.37 ±0.25	18.1 ±0.2	0.079 ±0.013	5.54	1.55 ±0.32	20.3 ±0.2
3.0	0.061	4.29	0.87 ±0.19	11.4 ±0.1	0.071 ±0.011	4.91	1.20 ±0.23	15.8 ±0.1	0.073 ±0.011	5.38	1.36 ±0.26	17.9 ±0.1
4.0	0.057 ±0.012	4.20	0.78 ±0.19	10.3 ±0.1	0.064 ±0.011	4.76	1.02 ±0.21	13.4 ±0.2	0.066 ±0.011	5.04	1.12 ±0.23	14.9 ±0.1
5.0	0.054 ±0.012	4.08	0.72 ±0.18	9.4 ±0.1	0.057 ±0.010	4.60	0.86 ±0.17	11.3 ±0.1	0.064 ±0.012	4.89	1.05 ±0.24	13.8 ±0.1

[a] λ_{ex} = 375 nm. [DPH] = 5 μM. A solution of DPH was prepared in tetrahydrofuran. [b] λ_{ex} = 375 nm, [b] λ_{em} = 429 nm.

To see whether there is any effect of nature of spacer group on the microviscosity of micelles, we have plotted η_m with varying concentration of urea for micelles of the all three surfactants. Figure 3c.5 shows that at a given concentration of urea, microviscosity increases on substitution of –OH group in the spacer group and it also increases with increasing number of –OH groups. This result could be depicting that hydroxyl group(s) protect(s) the probe molecules from their contact with the water molecules due to which the microviscosity of micelles increases. Further evidence in support of this phenomenon has been given later.

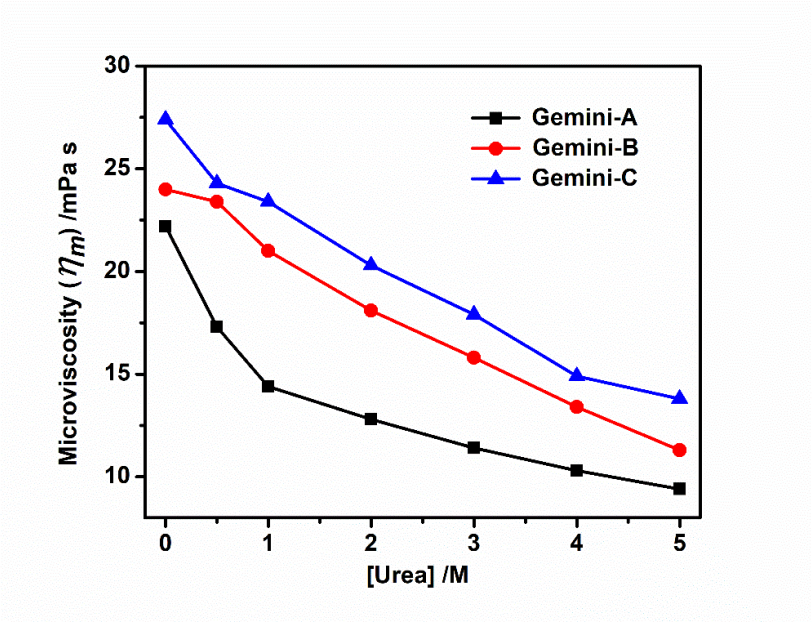

Figure 3c.5. Plot of variation of microviscosity of micelles with increasing concentration of urea in the micellar media of Gemini-A, -B and -C.

To further support the effect of urea concentration on the microviscosity of micelles the excited singlet state lifetime values of C-480 have been calculated using time-correlated single photon counting (TCSPC) method. Fluorescence decays in all micelles-urea mixed systems are bi-exponential in nature. The average lifetime has been calculated by using the Equation 1.8 in Chapter 1. The lifetime values of all components along with the average lifetime of C-480 and χ^2 values in all micelles-urea mixed systems are given in Table 3c.4a-c. The fact that all C-480 molecules are solubilized in micelles at 10 mM concentration of gemini, this biexponential decay could be because of two species: (1) locally excited (LE) and (2) intramolecular charge transfer (ICT) as it is known that C-480 has ICT characteristics.[41] At present we are not confirmed, a detailed study can be carried out later. Data in Table 3c.4a-c show that ICT species is mostly contributing to the decay.

It can be seen that average excited state lifetime values ($<\tau_f>$) are decreased with increasing urea concentration in all micellar systems. Figure 3c.6 shows the variation of average excited state lifetime values of C-480 in presence of all studied surfactants and urea mixed systems. Excited state lifetime values are decreased with microviscosity value of gemini surfactants. It has been mentioned (Table 3c.2) that fluorescence peak maxima of C-480 remains unchanged in presence and absence of urea. It infers that variation in excited singlet state lifetime is mostly due to change in microviscosity of the systems. Of course, a comparatively lesser effect due to the change in micropolarity cannot be ruled out.

Table 3c.4a. Excited-state lifetime[a] of C-480 in presence of pure Gemini-A and Gemini-A with various concentration of urea.

Urea (M)	a_1	τ_1 (ns)	a_2	τ_2 (ns)	$<\tau_f>$ (ns)	χ^2
0.0	0.17 ±0.02	4.39 ±0.03	0.83 ±0.02	6.00 ±0.03	5.73	1.05
0.5	0.09 ±0.01	3.11 ±0.02	0.91 ±0.01	5.91 ±0.03	5.66	1.03
1.0	0.08 ±0.01	2.80 ±0.02	0.92 ±0.01	5.86 ±0.04	5.62	1.06
2.0	0.25 ±0.02	4.29 ±0.04	0.75 ±0.02	5.99 ±0.04	5.57	1.00
3.0	0.12 ±0.01	3.44 ±0.03	0.88 ±0.01	5.73 ±0.03	5.46	1.06
4.0	0.16 ±0.01	3.89 ±0.04	0.84 ±0.01	5.72 ±0.01	5.43	1.11
5.0	0.31 ±0.02	4.38 ±0.04	0.69 ±0.01	5.77 ±0.02	5.34	1.07

[a] λ_{ex} = 375 nm, λ_{em} = 475 nm.

Table 3c.4b. Excited-state lifetime[a] of C-480 in presence of pure Gemini-B and Gemini-B with various concentration of urea.

Urea (M)	a_1	τ_1 (ns)	a_2	τ_2 (ns)	$<\tau_f>$ (ns)	χ^2
0.0	0.10 ±0.01	2.97 ±0.02	0.90 ±0.01	6.03 ±0.03	5.72	1.04
0.5	0.09 ±0.01	2.94 ±0.02	0.91 ±0.01	6.00 ±0.04	5.72	1.04
1.0	0.12 ±0.01	3.53 ±0.02	0.88 ±0.01	5.99 ±0.04	5.69	1.06
2.0	0.11 ±0.01	3.23 ±0.04	0.89 ±0.02	5.90 ±0.04	5.61	1.06
3.0	0.13 ±0.01	3.28 ±0.02	0.87 ±0.02	5.84 ±0.03	5.51	1.06
4.0	0.19 ±0.01	4.02 ±0.03	0.81 ±0.02	5.84 ±0.03	5.49	1.01
5.0	0.12 ±0.01	3.24 ±0.04	0.88 ±0.02	5.67 ±0.03	5.38	1.03

[a] λ_{ex} = 375 nm, λ_{em} = 475 nm.

Table 3c.4c. Excited-state lifetime[a] of C-480 in presence of pure Gemini-C and Gemini-C with various concentration of urea.

Urea (M)	a_1	τ_1 (ns)	a_2	τ_2 (ns)	$<\tau_f>$ (ns)	χ^2
0.0	0.10 ±0.01	3.06 ±0.02	0.90 ±0.01	6.00 ±0.03	5.71	1.07
0.5	0.24 ±0.01	4.32 ±0.02	0.76 ±0.01	6.17 ±0.04	5.73	1.03
1.0	0.14 ±0.02	3.62 ±0.02	0.86 ±0.01	6.02 ±0.04	5.68	1.07
2.0	0.14 ±0.02	3.54 ±0.03	0.86 ±0.02	5.95 ±0.03	5.61	1.05
3.0	0.27 ±0.02	4.35 ±0.03	0.73 ±0.02	5.98 ±0.02	5.54	1.07
4.0	0.20 ±0.01	4.13 ±0.03	0.80 ±0.01	5.87 ±0.02	5.52	1.05
5.0	0.17 ±0.01	3.85 ±0.03	0.83 ±0.02	5.72 ±0.03	5.40	1.07

[a] λ_{ex} = 375 nm, λ_{em} = 475 nm.

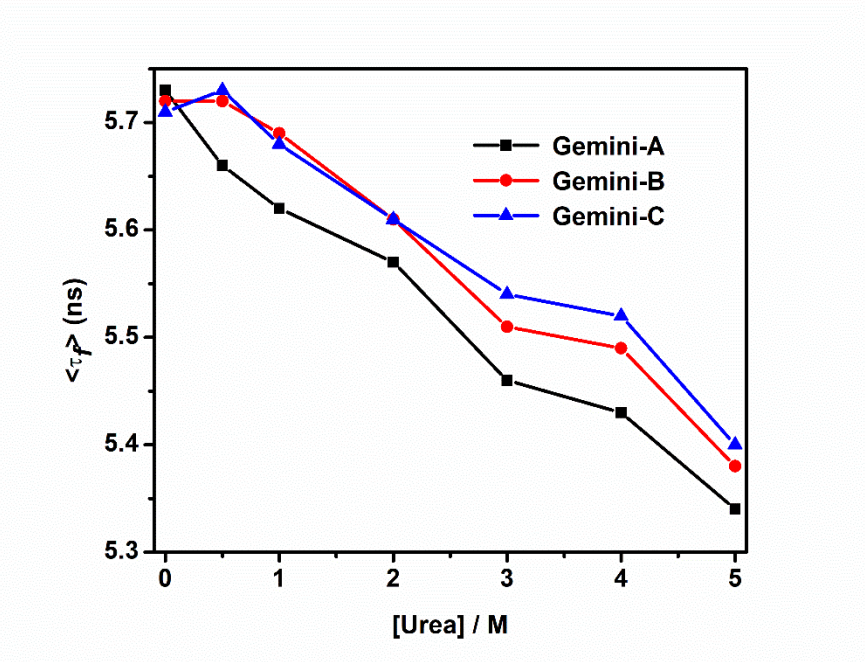

Figure 3c.6. Variation in average excited state lifetime ($<\tau_f>$) value of C-480 with increasing concentration of urea in presence of studied surfactants. [Surfactant] = 10 mM. λ_{ex} = 375 nm, λ_{em} = 475 nm.

3c.2.4 Solvation dynamics

Solvation dynamics of C-480 have been studied in presence of 10 mM of all three studied gemini surfactants and in presence of gemini surfactant with various concentrations of urea in the range mentioned above. Fluorescence decays of C-480 in 10 mM of all the three gemini surfactants with varying concentrations of urea have been recorded. In these systems emission wavelength dependent decays of C-480 have been

noted. Wavelengths are selected from the entire range of a steady-state fluorescence spectrum of C-480 (Figure 3c.2b). Figure 3c.7 shows the emission wavelength dependent decays of C-480 in surfactant (10 mM) + 5 M urea as a representative one. Similar behaviours have also been observed for all gemini surfactants and urea mixed systems. A fast decay is noticed at a short wavelength (say 430 nm). Fluorescence occurring from the unsolvated dipole generated at the excited state is responsible for fast decay. Of course there is a possibility of contribution of high % of solvated dipoles to the fast decay which could not be detected due to the shortcomings of our TCSPC setup. At a longer wavelength (say 565 nm) fluorescence decay shows a clear growth in the spectrum followed by the decay. The growth in the decay indicates the solvation of the probe molecule in the exited state [Chapter 3b]. While at a shorter wavelength decays were fitted tri-exponentially but at a longer wavelength decays were fitted bi-exponentially. It is mentioned above that most probable location of C-480 molecules is Stern layer. Therefore, the probe molecules located at the Stern layer of the micelles are mostly contributing to the said solvation process.[46, 56, 58, 63, 64] Because the solvation processes occur in the bulk are too fast to be measured by our instrumental set-up. On the other hand, the probe molecules located in the hydrocarbon core of the micelles are not supposed to contribute to any solvation process.[46, 56]

The time resolved emission spectra (TRES) have been constructed by following the method of Fleming and Maroncelli.[65] The dynamic Stokes shifts in the emission spectra of C-480 can be seen after constructing TRES. Figure 3c.8a shows the TRES of C-480 in presence of Gemini-A (10 mM) + varying concentration of urea. TRES for other systems are shown by Figures 3c.8b and 3c.8c. The peak wavenumber, $\bar{\upsilon}(t)$ for each TRES at different times was obtained after the fitting of TRES to a log-normal function.[55, 65] The peak wavenumber ($\bar{\upsilon}(t)$) values have been used to calculate the solvent response function (SRF), *C(t)* by using Equation 2.9 given by Fleming and Maroncelli[65] for the quantitative measurement of solvation dynamics. Figure 3c.9a represents the plot of *C(t)* versus time for the system of Gemini-A (10 mM) + varying concentration of urea. The *C(t)* decays for other systems are given as Figures 3c.9b and 3c.9c. The *C(t)* decays are generally bi-exponential in nature in all the studied systems. The bi-exponential fitting of decays of *C(t)* has been done by the Equation 2.14. The decay characteristic of *C*(*t*) are given in Tables 3c.5a-c for all the studied systems. The average solvation time, $\langle \tau_s \rangle$ for a bi-

exponential decay has been estimated by the Equation 2.15 and are also given in Tables 3c.5a-c.

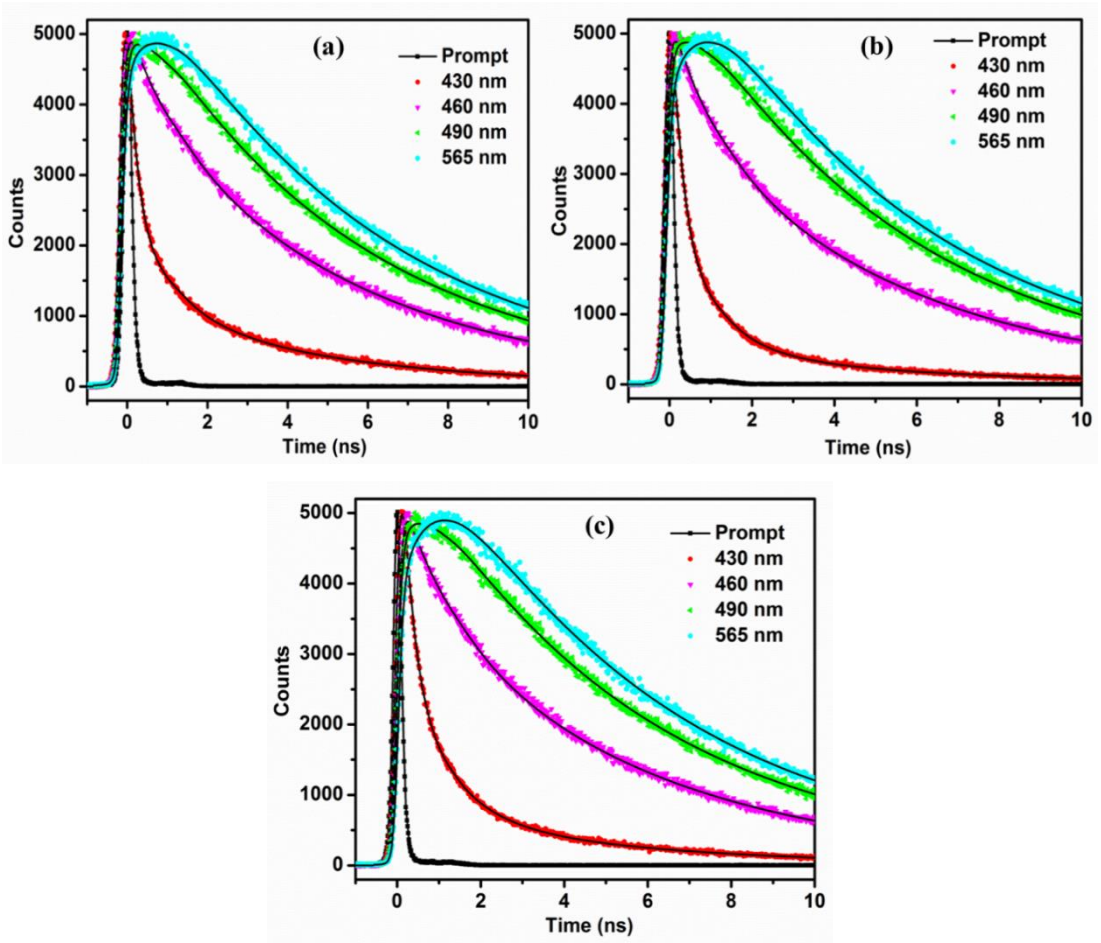

Figure 3c.7. Fluorescence decays of C-480 in (a) Gemini-A (10 mM) + 5 M urea, (b) Gemini-B (10 mM) + 5 M urea and (c) Gemini-C (10 mM) + 5 M urea. λ_{ex} = 375 nm.

As mentioned in the literature, the bimodal behavior of solvation in the microheterogeneous systems arises due to the presence of free and bound water molecules.[66] The strength of a hydrogen bonding between water molecule and polar headgroup is stronger than that between two water molecules.[60, 67, 68] The water molecules those are hydrogen bonded with the polar headgroups are called bound water. While free water molecules lead to the fast solvation, the bound water molecules are responsible for slow solvation.[69] In all micellar systems the fast components are the major components to contribute to the solvation processes. In case of gemini surfactant systems, polar headgroups, counterions and spacer group can also contribute to the solvation process. However, as decreased before for a gemini surfactant, essentially counterions and water molecules are responsible for the solvation processes.[46, 56, 58, 60, 63, 64]

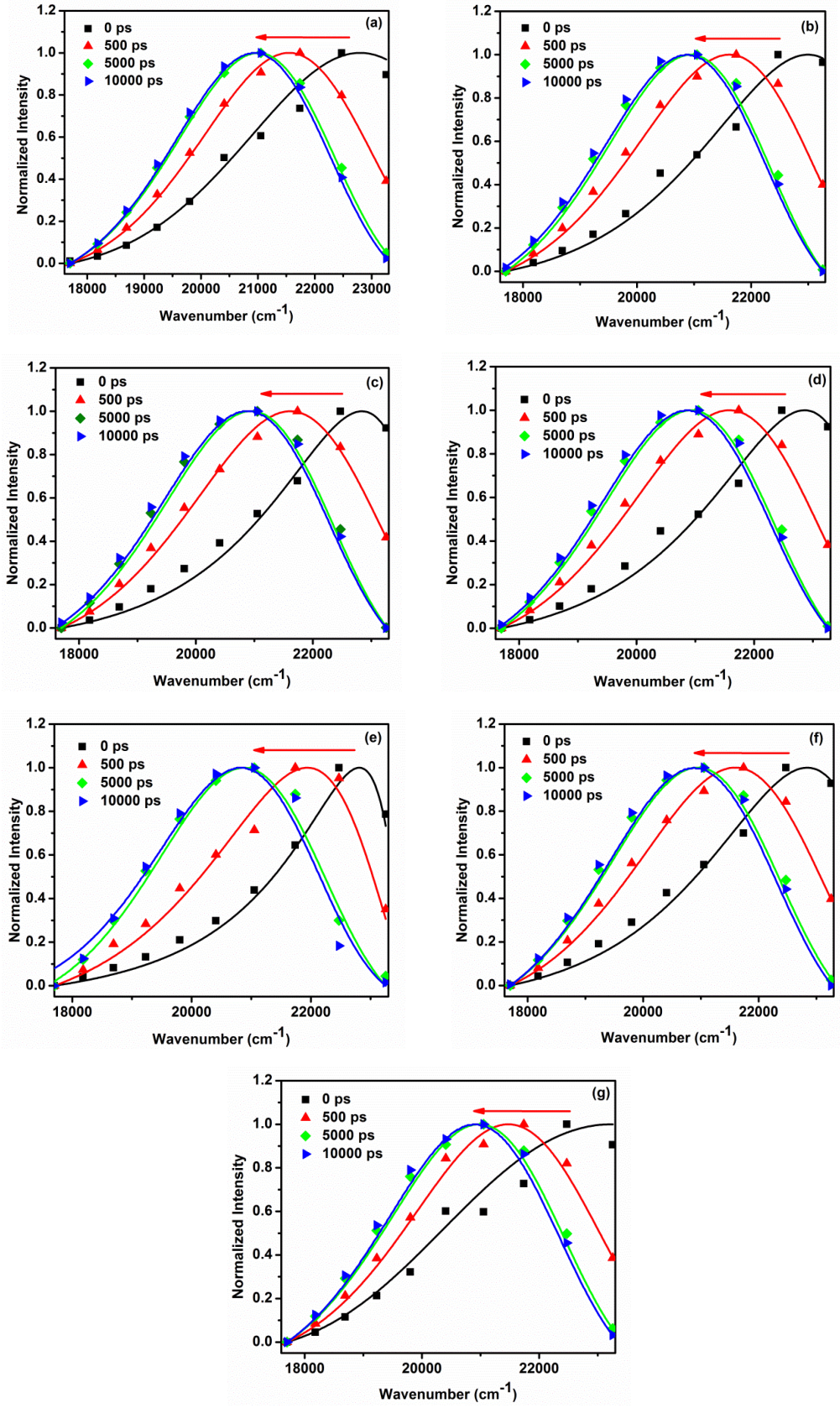

Figure 3c.8a. Time resolved emission spectra of C-480 in Gemini-A (10 mM) + X M urea (from right to left: 0ps, 500ps, 5000ps, and 10000 ps). X = 0 M (a), 0.5 M (b), 1.0 M (c), 2.0 M (d), 3.0 M (e), 4.0 M (f), 5.0 M (g).

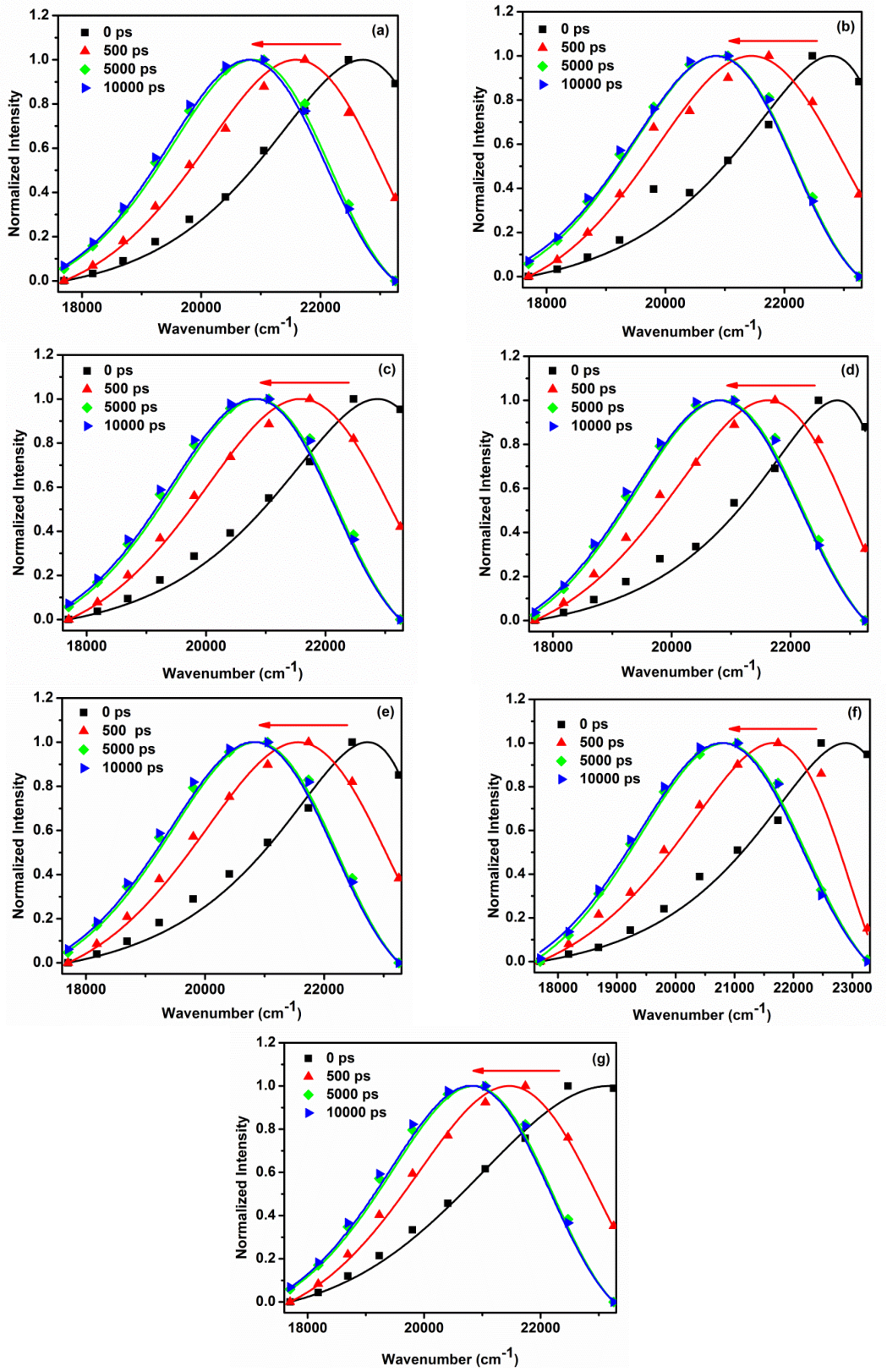

Figure 3c.8b. Time resolved emission spectra of C-480 in Gemini-B (10 mM) + X M urea (from right to left: 0ps, 500ps, 5000ps, and 10000 ps). X = 0 M (a), 0.5 M (b), 1.0 M (c), 2.0 M (d), 3.0 M (e), 4.0 M (f), 5.0 M (g).

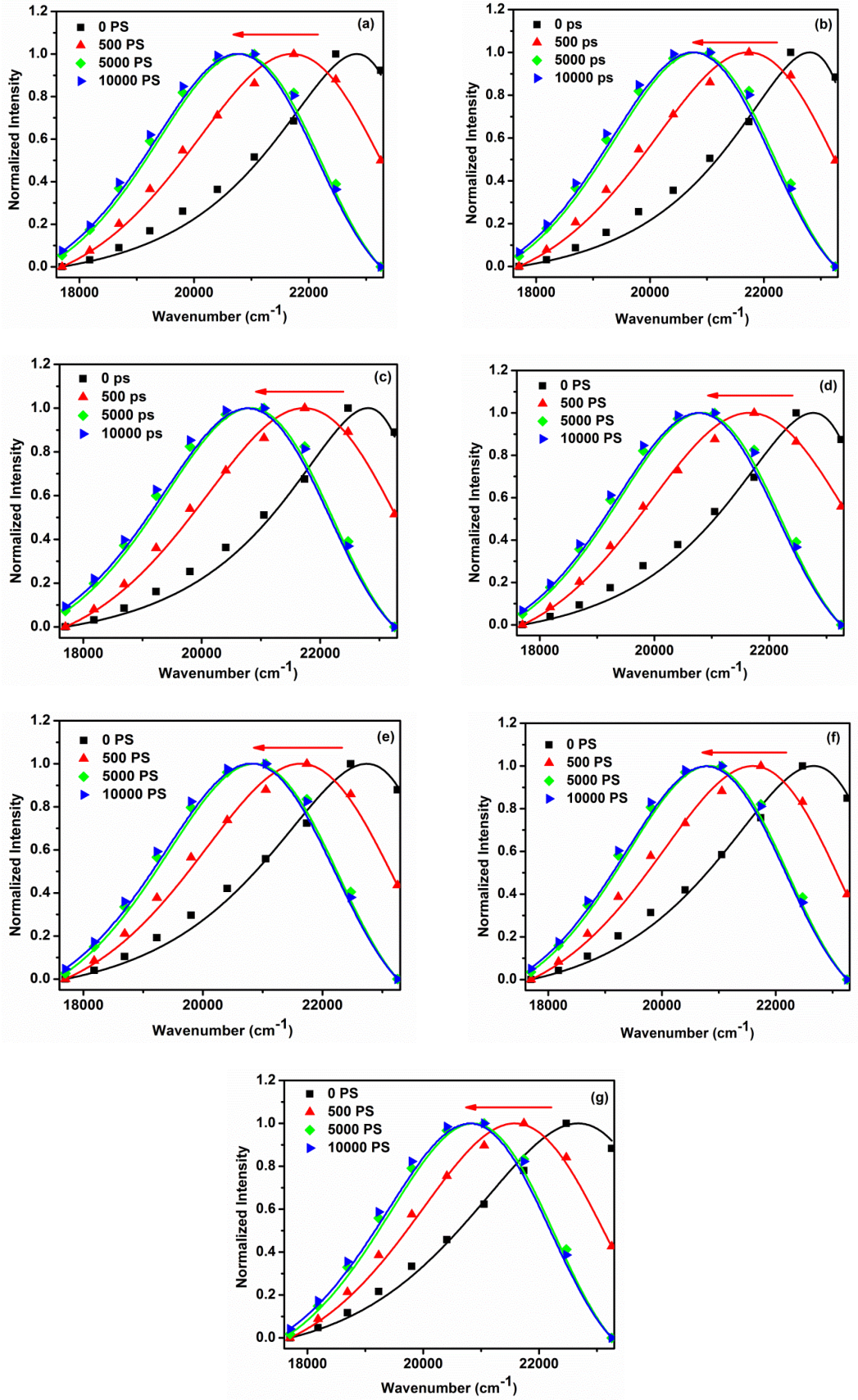

Figure 3c.8c. Time resolved emission spectra of C-480 in Gemini-C (10 mM) + X M urea (from right to left: 0ps, 500ps, 5000ps, and 10000 ps). X = 0 M (a), 0.5 M (b), 1.0 M (c), 2.0 M (d), 3.0 M (e), 4.0 M (f), 5.0 M (g).

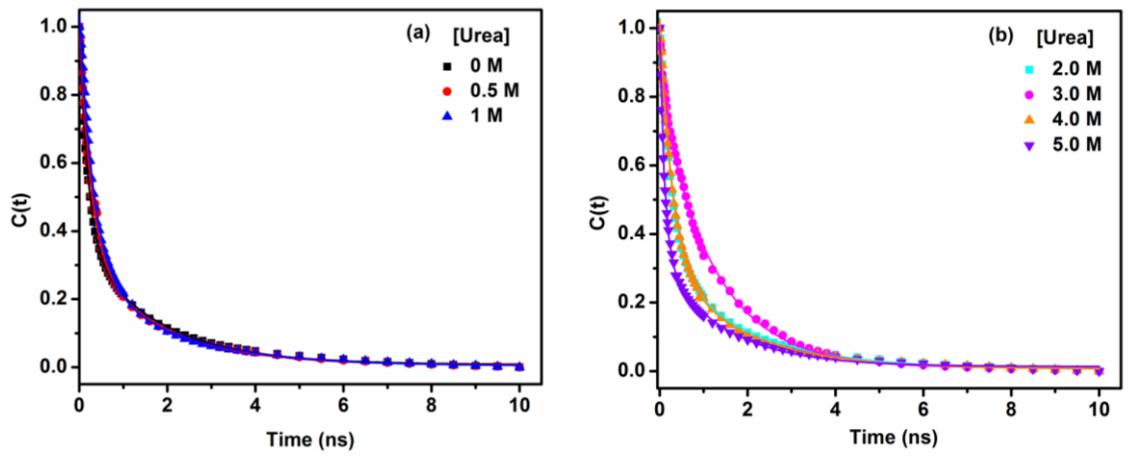

Figure 3c.9a. Decays of solvent response function, *C(t)* of C-480 in the micelles of Gemini-A and urea. (a) 0 M-1 M urea, (b) 2 M-5 M urea.

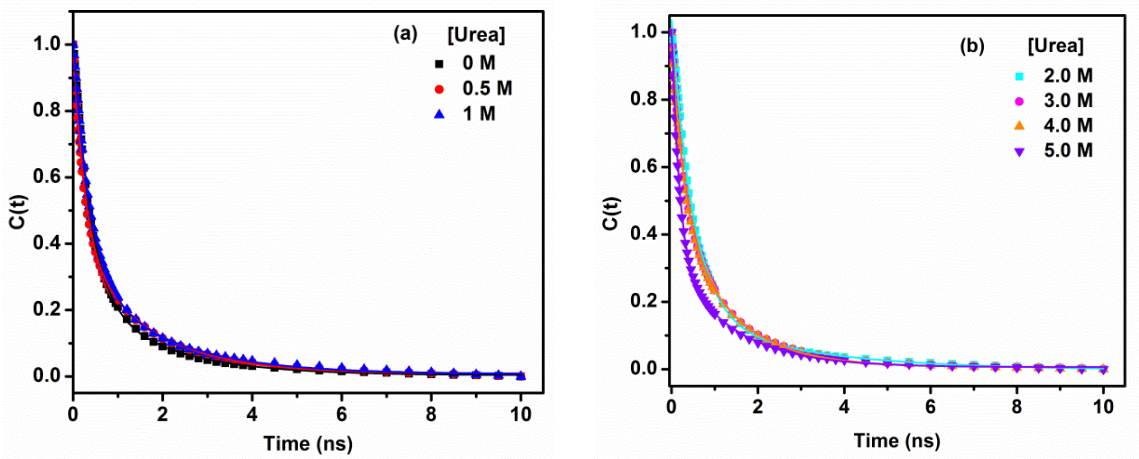

Figure 3c.9b. Decays of solvent response function, *C(t)* of C-480 in the micelles of Gemini-B and urea. (a) 0 M-1 M urea, (b) 2 M-5 M urea.

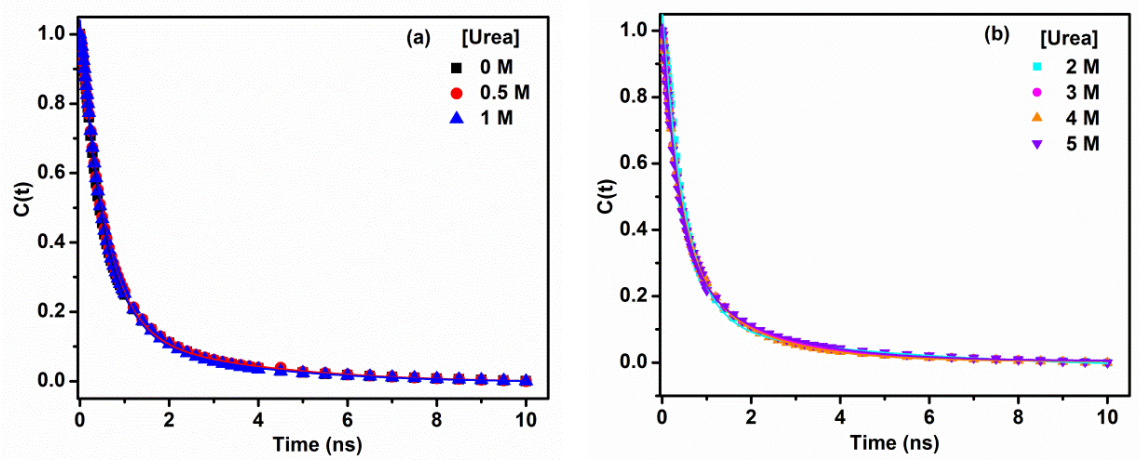

Figure 3c.9c. Decays of solvent response function, *C(t)* of C-480 in the micelles of Gemini-C and urea. (a) 0 M-1 M urea, (b) 2 M-5 M urea.

Table 3c.5a. Decay characteristic of solvent response function, $C(t)$ of C-480 in presence of pure Gemini-A and Gemini-A with various concentration of urea.

Urea (M)	a_{1s}	τ_{1s} (ps)	a_{2s}	τ_{2s} (ps)	$<\tau_s>$ (ps)	$\Delta\bar{\upsilon}$ cm^{-1}
0.0	0.64 ±0.01	193.15 ±0.01	0.36 ±0.01	1709.25 ±0.04	738.95	1855
0.5	0.66 ±0.02	258.12 ±0.01	0.34 ±0.02	1706.93 ±0.12	750.72	1917
1.0	0.73 ±0.02	321.99 ±0.01	0.27 ±0.02	1986.20 ±0.21	771.33	1956
2.0	0.69 ±0.01	270.65 ±0.01	0.31 ±0.01	1919.62 ±0.11	781.83	1995
3.0	0.69 ±0.01	373.04 ±0.01	0.31 ±0.01	1869.15 ±0.08	836.83	1989
4.0	0.71 ±0.01	285.66 ±0.01	0.29 ±0.01	1778.84 ±0.10	718.68	1957
5.0	0.67 ±0.01	115.14 ±0.01	0.33 ±0.01	1431.39 ±0.07	549.50	2314

$\Delta\bar{\upsilon} = \bar{\upsilon}(0) - \bar{\upsilon}(\infty)$.

Table 3c.5b. Decay characteristic of solvent response function, $C(t)$ of C-480 in presence of pure Gemini-B and Gemini-B with various concentration of urea.

Urea (M)	a_{1s}	τ_{1s} (ps)	a_{2s}	τ_{2s} (ps)	$<\tau_s>$ (ps)	$\Delta\bar{\upsilon}$ cm^{-1}
0.0	0.68 ±0.01	355.43 ±0.01	0.28 ±0.01	1861.01 ±0.08	762.76	1910
0.5	0.56 ±0.04	297.45 ±0.01	0.44 ±0.04	1409.21 ±0.25	786.62	1930
1.0	0.66 ±0.02	347.02 ±0.01	0.34 ±0.02	1735.24 ±0.17	819.01	2057
2.0	0.52 ±0.03	337.47 ±0.02	0.48 ±0.03	1498.59 ±0.13	894.81	1954
3.0	0.73 ±0.02	371.56 ±0.01	0.27 ±0.02	1768.15 ±0.16	748.64	1911
4.0	0.51 ±0.01	262.44 ±0.01	0.49 ±0.01	1230.69 ±0.02	736.88	2098
5.0	0.67 ±0.01	175.85 ±0.01	0.33 ±0.01	1350.64 ±0.03	563.53	2366

$\Delta\bar{\upsilon} = \bar{\upsilon}(0) - \bar{\upsilon}(\infty)$.

Table 3c.5c. Decay characteristic of solvent response function, $C(t)$ of C-480 in presence of pure Gemini-C and Gemini-C with various concentration of urea.

Urea (M)	a_{1s}	τ_{1s} (ps)	a_{2s}	τ_{2s} (ps)	$<\tau_s>$ (ps)	$\Delta\bar{\upsilon}$ cm^{-1}
0.0	0.80 ±0.04	493.77 ±0.02	0.20 ±0.03	2589.21 ±0.61	912.86	2075
0.5	0.82 ±0.03	521.95 ±0.02	0.18 ±0.03	2847.76 ±0.69	940.60	2050
1.0	0.82 ±0.04	535.06 ±0.02	0.18 ±0.03	2930.32 ±0.71	966.21	2030
2.0	0.86 ±0.03	515.85 ±0.03	0.14 ±0.02	4721.38 ±0.73	1104.62	1997
3.0	0.70 ±0.02	391.78 ±0.01	0.30 ±0.02	1743.48 ±0.11	797.29	1930
4.0	0.68 ±0.02	392.63 ±0.01	0.32 ±0.02	1580.51 ±0.07	772.75	1885
5.0	0.75 ±0.02	376.72 ±0.01	0.25 ±0.02	1867.86 ±0.13	749.51	1820

$\Delta\bar{\upsilon} = \bar{\upsilon}(0) - \bar{\upsilon}(\infty)$.

Average solvation time ($<\tau_s>$) of C-480 in presence of gemini surfactants and urea mixed systems have been calculated (Tables 3c.5a-c) using Equation 2.15 and the variations in the values with urea concentration are shown by Figure 3c.10. It can be observed from the data in Tables 3c.5a-c as well as from Figure 3c.10 that in the absence of urea and also upto 2.0 M concentration of urea the average solvation time increases on increasing the number of hydroxyl group in the spacer group of gemini surfactants.[46] As reported by us earlier,[46] the hydroxyl group(s) present in the spacer group of gemini surfactant might be forming hydrogen bonds with the water molecules. It protects the probe molecules from their contact with the water molecules and that is why solvation time is increased with increasing number of the hydroxyl group in the spacer of gemini surfactants.[46] In chapter 3b, we have discussed comparatively slower solvation processes in case the micelles of gemini surfactants containing diethyl ether spacer group causing similar effect. In case of micelles of Gemini-A i.e. 12-4-12 surfactant, due to the presence of hydrophobic spacer group the extent of free water molecules is greater than that in micelles of gemini surfactants possessing hydroxyl groups in the spacer. Evidence to this hypothesis has been discussed below.

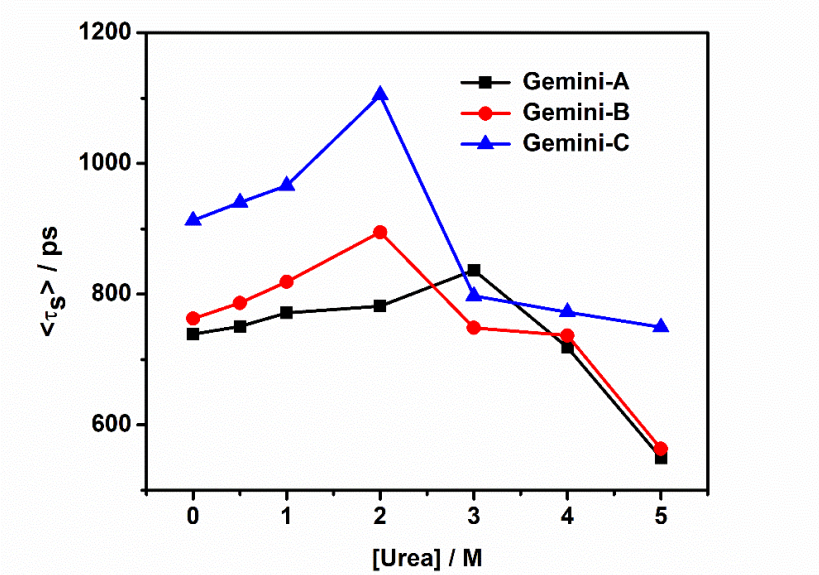

Figure 3c.10. Average solvation time of C-480 in presence of gemini surfactant and urea mixed systems.

We have carried out a separate fluorescence experiment to further support the fact that the hydroxyl group(s) present in the spacer group of gemini surfactants shields the probe molecules from their contact with a certain amount of water molecules [Chapter 3b]. It has been reported[48, 70] that the significant change in micelle size and *cmc* occurs only

when the percentage of organic co-solvent in water-organic solvent mixture is above 20%. In view of this fact, we have recorded fluorescence spectra of C-480 in aqueous micelles and also in micelles in presence of various % of organic co-solvent not exceeding 20%. By performing these experiments we wanted to demonstrate the extent of interactions between the hydroxyl group of methanol and C-480. For this purpose we have presented here Figure 3c.11(a) for Gemini-A which is same as Figure 3b.6a in Chapter 3b. This figure shows that in presence of 10 mM of Gemini-A the fluorescence peak maximum gets red-shifted from 477 nm to 480 nm on increasing % of methanol upto 20%. However, Figures 3c.11(b) and (c) show that there is no such change in fluorescence peak maximum in 10 mM of Gemini-B and Gemini-C, respectively in presence of same percentage of methanol. Thus these results depict that hydroxyl group(s) present in the spacer group of Gemini-B and Gemini-C protect molecules containing -OH groups from their contact with probe molecule. Also this experiment is an extra step as compared to our previous study[46] to support our hypothesis of protection of water molecules by –OH group(s) in the spacer groups.

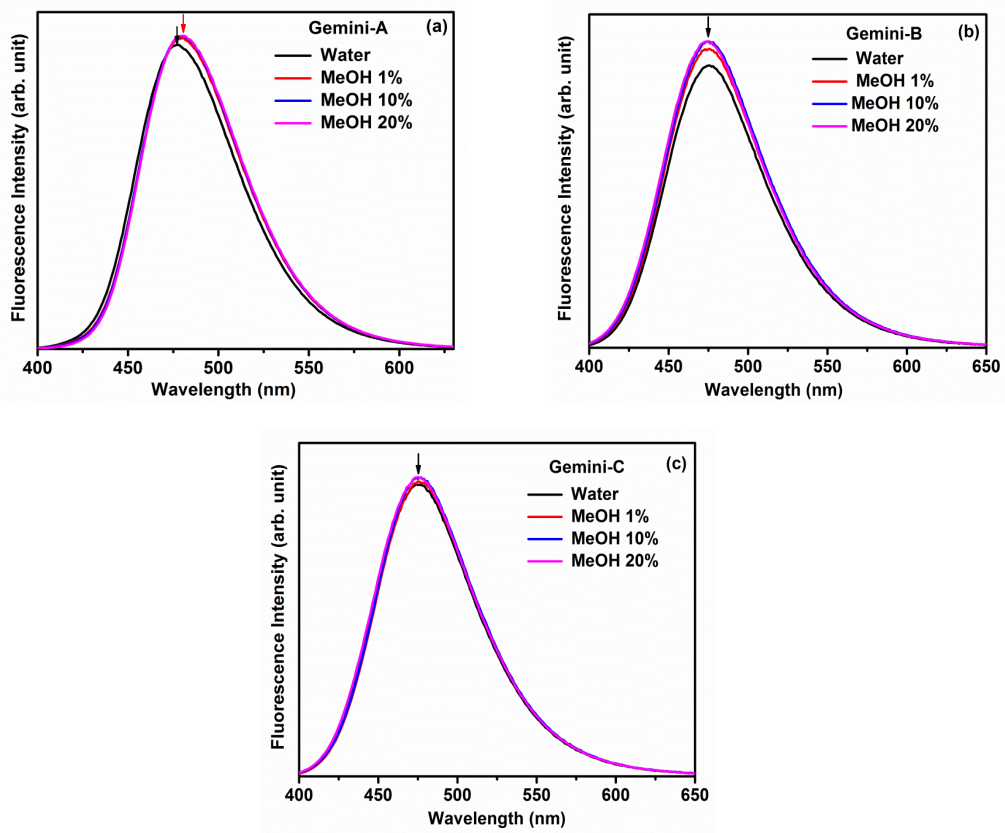

Figure 3c.11. Fluorescence spectra of C-480 in 10 mM of each of (a) Gemini-A, (b) Gemini-B and (c) Gemini-C in presence of various % of methanol in water-methanol mixture. λ_{ex} = 375 nm.

One can see in Figure 3c.10 that with increasing concentration of urea the average solvation time initially increases, reaches a maximum and then decreases for each of three gemini micellar systems. While for Gemini-B and Gemini-C the solvation time is maximum at 2.0 M of urea, but for Gemini-A the solvation time is maximum at 3.0 M of urea. While searching for the reason behind it we have found that concentration of urea has an effect on the degree of counterion dissociation (α) (Table 3c.6) as well.

Table 3c.6. Degree of counterion dissociation (α) for micelles of gemini surfactants.

Urea (M)	**Gemini-A** α	**Gemini-B** α	**Gemini-C** α
0.0	0.32 $\pm$0.03	0.29 $\pm$0.02	0.28 $\pm$0.02
0.5	0.36 $\pm$0.02	0.37 $\pm$0.03	0.29 $\pm$0.02
1.0	0.42 $\pm$0.04	0.38 $\pm$0.03	0.32 $\pm$0.02
2.0	0.46 $\pm$0.04	0.39 $\pm$0.03	0.37 $\pm$0.03
3.0	0.47 $\pm$0.04	0.36 $\pm$0.02	0.34 $\pm$0.02
4.0	0.34 $\pm$0.02	0.33 $\pm$0.02	0.32 $\pm$0.02
5.0	0.31 $\pm$0.02	0.30 $\pm$0.02	0.27 $\pm$0.02

Figure 3c.12 represents the variation of α with increasing concentrations of urea. α increases, reaches a maximum and then decreases with increasing concentrations of urea. The concentration of urea at which α is maximum is same as that of average solvation time. There is a good correlation between the variation of average solvation times and α with increasing concentration of urea in each case of gemini surfactant. These results show that counterions have effect on the solvation dynamics. In our previous study with gemini surfactants with polymethylene spacer group and also with mixed surfactant systems, we have found that the counterions have effect on solvation dynamics.[56, 58] With increasing α the extent of free counterions increases. It is known that water molecules can form hydrogen bonds with anions.[71] Thus upto a certain concentration of urea with increasing number of counter ions the clustering of water molecules increases.[72] With the greater degree of clustering of water molecules the number of free water molecules is expected to be decreased. That could be the reason that solvation process becomes slower. However, above a certain concentration of urea with decreasing α (decreasing number of free counter ions) the clustering of water molecules is reduced. Due to this the number of free water molecules probably starts increasing which results in an increase in the rate of solvation process i.e. the solvation time starts decreasing. Thus free counter ions indirectly control the solvation dynamics via the formation of water clusters.

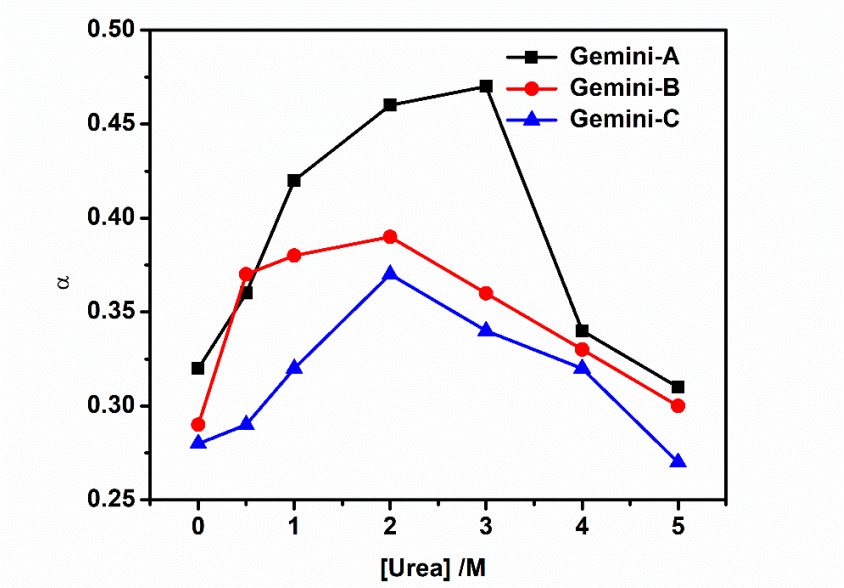

Figure 3c.12. Degree of counterion dissociation (α) versus concentration of urea for the micelles of Gemini-A, Gemini-B and Gemini-C.

It is noteworthy that the ascending order of α observed in the micelles of surfactants at a given concentration of urea is as follows: Gemini-C < Gemini-B < Gemini-A. However, the order is reversed as far as the average solvation times are concerned at a given concentration of urea. It is inferred that ultimately the net availability of free water molecules towards the solvation process of solute molecules probably controls the rate of solvation. Even if the clustering of water molecules is higher in case of Gemini-A due to comparatively greater α, but because of presence of hydrophobic spacer group the accessibility of free water molecules for effective solvation might be larger in this case. Thus spacer group of gemini surfactant plays an important role in solvation dynamics. It is to be mentioned here that even high concentration of urea has very less effect on the strength of hydrogen bonding interactions between water molecules.[73] Only a small fraction of water molecules gets immobilized by urea. Therefore, any significant direct effect of urea on the solvation dynamics can be ruled out.

3c.2.5 Time-resolved fluorescence anisotropy

To have further information about the microenvironment of micelles, the time-resolved fluorescence anisotropy, *r(t)* measurement in molecular assemblies has been carried out.[56, 58, 63] The *r(t)* values have been determined using Equation 2.16. Rotational relaxation behaviours of C-480 in micelles of gemini surfactants, and in presence of various concentration of urea have been characterized. Figures 3c.13a-c show the

fluorescence anisotropy decays of C-480 in Gemini-A, -B and -C, respectively in presence of various concentrations of urea. In pure water, the anisotropy decay of C-480 is monoexponential, whereas that in presence of pure gemini surfactants and also in presence of gemini surfactant with various concentration of added urea are bi-exponential in nature. The decay function represented by the Equation 2.17 has been applied to fit the bi-exponential anisotropy decay. The rotational relaxation times for fast and slow components have been obtained from the fitted decays. The average rotational relaxation time has been determined using Equation 2.18.

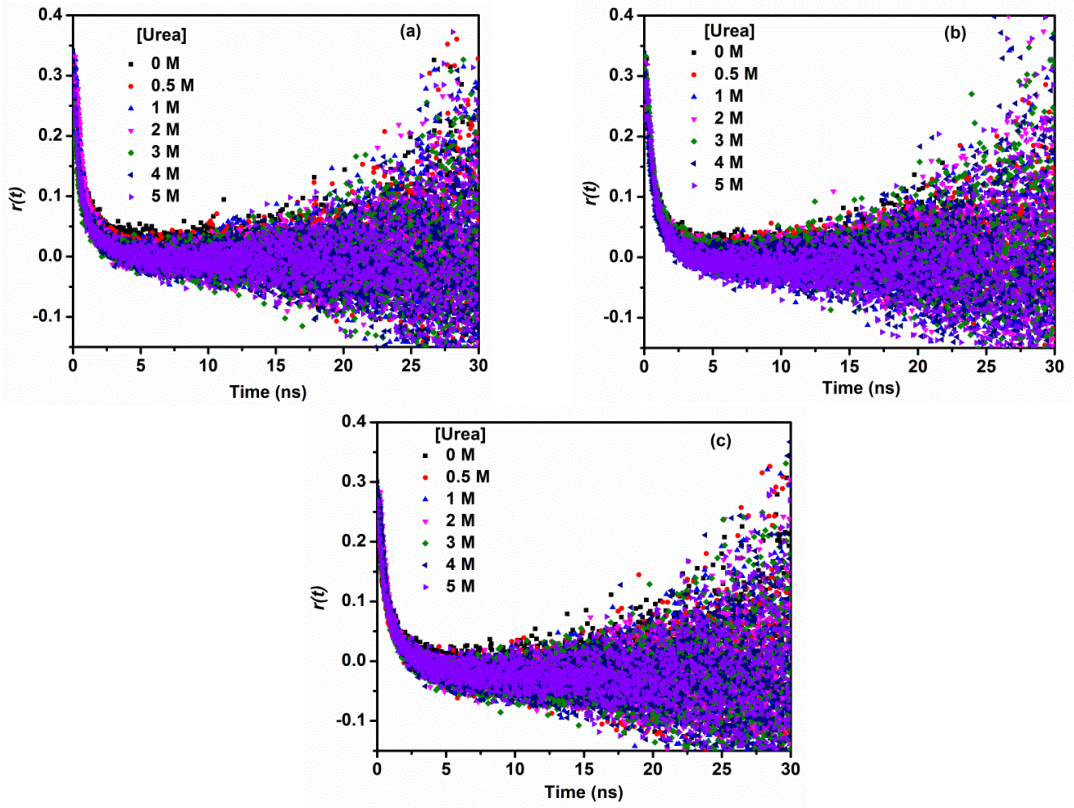

Figure 3c.13. Fluorescence anisotropy decays of C-480 in the micelles of gemini surfactants, (a) Gemini-A, (b) Gemini-B and (c) Gemini-C in presence of various concentrations of urea. λ_{ex} = 375 nm. λ_{em} = 470 nm.

Tables 3c.7a-c present the rotational relaxation parameters along with the average rotational relaxation times of C-480 in the micelles of Gemini-A, -B and –C, respectively in presence of various concentrations of urea. Rotational relaxation time of C-480 in presence of pure water is found to be 132 ps which is in well agreement with the reported value of 125 ps.[74] Rotational relaxation time of C-480 is many folds slower in micelles compared to that in pure water. This suggests that random motions of the probe molecules are restricted in a micellar medium. It can be seen that for each micellar system the fast

rotational relaxation component has major contribution to the fluorescence depolarization than that of the slow component. The fact that the fast motions are responsible for the loss of anisotropy is evidenced by the values of time-zero anisotropy, $r_o < 0.40$. It is known that the maximum possible value of $r_o = 0.40$.[40] The data in Tables 3c.7a-c show that fast as well as slow relaxation times along with the average relaxation time decrease with increasing concentration of urea in a given micelle.

The variations of $<\tau_r>$ of C-480 with increasing concentration of urea in all three micellar systems are shown by Figure 3c.14. The decreases in $<\tau_r>$ with increasing concentration of urea in a given micellar system is in the harmony of microviscosity of the systems. At a higher concentration of the urea the solvent molecules seep in the micelle. Urea molecules reduce the hydrophobic interaction between the surfactant molecules, causes the demicellization. As a result of it the microviscosity of micelles decreases with increasing concentration of urea which results in decrease in rotational relaxation time. This phenomenon is also evidenced by almost continuous decrease in r_o value with increasing concentration of urea in each micellar system. Mukherjee *et al.*[75] have found that the rotational relaxation process of the probe molecules became faster when concentration of the urea is increased in F127 micelles. It is also pertinent to note that at a given concentration of urea the increase in rotational relaxation time is as per the increasing order of microviscosity of micelles with the presence of more number of –OH group starting from 0 to 2.

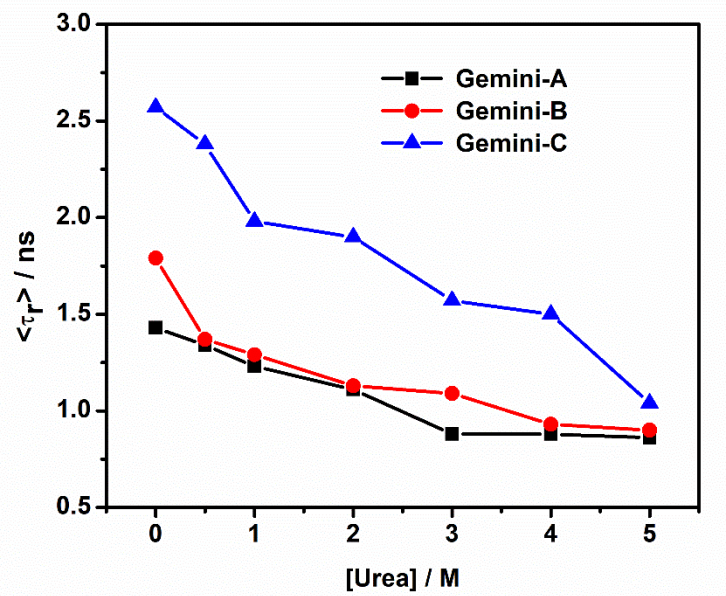

Figure 3c.14. Average rotational relaxation time of C-480 in presence of gemini surfactant and urea mixed systems.

From literature reports it can be stated that the observed bi-exponential behavior of the anisotropy decay is mainly because of the different types of rotational motions.[76, 77] The two-step and wobbling-in-a-cone model[77, 78] are very suitable to explain this kind of bimodal behaviour of anisotropy decay. According to the two-step model, the tumbling motion of the entire micelle (τ_m) and the lateral diffusion (τ_D) of the probe along the micelle surface contribute to the slow rotational relaxation (τ_{2r}). The time corresponding to the slow rotational relaxation is related to that of overall motion of micelle as a whole and lateral diffusion as Equation 2.19.

Table 3c.7a. Rotational relaxation parameters of C-480 in the micelles of Gemini-A and urea mixed systems.

Urea (M)	r_0	a_{1r}	τ_{1r} (ns)	a_{2r}	τ_{2r} (ns)	$\langle\tau_r\rangle$ (ns)	χ^2
0.0	0.34 ±0.04	0.87 ±0.02	0.61 ±0.06	0.13 ±0.02	6.91 ±0.53	1.43	1.06
0.5	0.33 ±0.05	0.90 ±0.02	0.67 ±0.07	0.10 ±0.02	7.41 ±0.61	1.34	1.06
1.0	0.31 ±0.03	0.92 ±0.01	0.66 ±0.06	0.08 ±0.01	7.74 ±0.63	1.23	1.02
2.0	0.29 ±0.03	0.93 ±0.01	0.67 ±0.07	0.07 ±0.01	6.96 ±0.56	1.11	1.09
3.0	0.28 ±0.04	0.62 ±0.02	0.36 ±0.04	0.38 ±0.01	1.73 ±0.12	0.88	0.99
4.0	0.27 ±0.03	0.74 ±0.02	0.45 ±0.05	0.26 ±0.01	2.09 ±0.14	0.88	1.01
5.0	0.27 ±0.03	0.70 ±0.02	0.39 ±0.04	0.30 ±0.01	1.96 ±0.13	0.86	0.99

λ_{ex} = 375 nm, λ_{em} = 470 nm

Table 3c.7b. Rotational relaxation parameters of C-480 in the micelles of Gemini-B and urea mixed systems.

Urea (M)	r_0	a_{1r}	τ_{1r} (ns)	a_{2r}	τ_{2r} (ns)	$\langle\tau_r\rangle$ (ns)	χ^2
0.0	0.33 ±0.05	0.91 ±0.02	0.67 ±0.07	0.09 ±0.01	13.13 ±0.98	1.79	1.01
0.5	0.32 ±0.04	0.93 ±0.02	0.69 ±0.07	0.07 ±0.01	10.39 ±0.87	1.37	1.03
1.0	0.33 ±0.05	0.91 ±0.01	0.63 ±0.06	0.09 ±0.01	7.97 ±0.65	1.29	1.02
2.0	0.32 ±0.03	0.89 ±0.01	0.62 ±0.05	0.11 ±0.01	5.29 ±0.44	1.13	1.02
3.0	0.31 ±0.03	0.90 ±0.01	0.65 ±0.06	0.10 ±0.01	5.09 ±0.43	1.09	1.04
4.0	0.30 ±0.03	0.78 ±0.01	0.49 ±0.05	0.22 ±0.01	2.51 ±0.15	0.93	1.03
5.0	0.27 ±0.03	0.78 ±0.01	0.52 ±0.05	0.22 ±0.01	2.25 ±0.14	0.90	1.00

λ_{ex} = 375 nm, λ_{em} = 470 nm.

Table 3c.7c. Rotational relaxation parameters of C-480 in the micelles of Gemini-C and urea mixed systems.

Urea (M)	r_0	a_{1r}	τ_{1r} (ns)	a_{2r}	τ_{2r} (ns)	$<\tau_r>$ (ns)	χ^2
0.0	0.30 ±0.04	0.85 ±0.01	0.76 ±0.08	0.15 ±0.02	12.82 ±0.97	2.57	1.05
0.5	0.28 ±0.03	0.86 ±0.02	0.75 ±0.08	0.14 ±0.01	12.38 ±0.89	2.38	1.10
1.0	0.28 ±0.03	0.90 ±0.02	0.79 ±0.08	0.10 ±0.01	12.68 ±0.98	1.98	1.02
2.0	0.27 ±0.03	0.91 ±0.01	0.78 ±0.08	0.09 ±0.01	13.25 ±0.99	1.90	1.08
3.0	0.27 ±0.03	0.87 ±0.02	0.73 ±0.07	0.13 ±0.01	7.19 ±0.59	1.57	1.09
4.0	0.26 ±0.03	0.89 ±0.02	0.72 ±0.07	0.11 ±0.01	7.84 ±0.63	1.50	1.05
5.0	0.26 ±0.03	0.57 ±0.02	0.39 ±0.05	0.43 ±0.02	1.89 ±0.12	1.04	1.03

λ_{ex} = 375 nm, λ_{em} = 470 nm.

Debye-Stokes-Einstein equation is used to calculate τ_m after estimating the hydrodynamic radii (r_h) of micelle (Equation 2.20, Chapter 2). The estimated r_h for all three micellar media in presence of urea are given in Tables 3c.8a-c. Figure 3c.15 represents the size distribution plot for Gemini-B as a representative one. The τ_m values at 298.15 K have been calculated by using the Equation 2.20. After knowing τ_m values, τ_D values have been calculated using Equation 2.19. Both τ_m and τ_D values have been tabulated in Tables 3c.8a-c. One can see that τ_D values (Tables 3c.8a-c) are almost same as slow rotational relaxation time (τ_{2r}) (Tables 3c.5a-c).Thus the lateral diffusion of the probe occurring along the surface of the micelle mainly contributes to the slow rotational relaxation. We have found that in case of Gemini-A there is an increasing tendency of the hydrodynamic radius of micelles with increasing concentration of urea. It is inferred that with increasing concentration of urea the micelles become less compact as the stabilization of micelles formation is reduced. As expected the time constant for the tumbling motion of the micelle (τ_m) increases with increasing size of micelles. However, we have not found any particular trend for hydrodynamic radii values of Gemini-B and Gemini-C with increasing concentration of urea although there is a relationship between the size of the micelle and τ_m value. There is a diminishing tendency of τ_D with increasing concentration of urea for a given micellar system. This trend is due to the decrease in the microviscosity of micelles with increasing concentration of urea. However, as τ_D is related to the τ_m, this correlation is also found to be comparatively better for Gemini-A than Gemini-B and Gemini-C. The lateral diffusion of probe molecule is much faster than the tumbling motion of the micelle as a whole. The time constants for the wobbling motion, τ_w of the probe

molecule, C-480 in all the micelles calculated using the Equation 2.25 are also tabulated in Tables 3c. 8a-c. As the wobbling motion gives an account of the relaxation of local structure in a micelle, there is a decreasing tendency of the value of τ_w with decreasing microviscosity of micelles.

Table 3c.8a. Hydrodynamic diameter (r_h), time for overall rotational motion of the micelle (τ_m), lateral diffusion time (τ_D), wobbling motion time (τ_w), wobbling diffusion coefficient (D_w), cone angle (θ_o) and order parameter ($|S|$) obtained from the anisotropy decays of C-480 in the micelles of Gemini-A and urea.

Gemini-A + Urea	r_h (nm)	τ_w (ns)	τ_m (ns)	τ_D (ns)	$D_w \times 10^{-8}$ (s^{-1})	θ_o (deg)	|S|	$^a\theta_o$ (deg)
0.0	1.25 ±0.06	0.67 ±0.06	221.46 ±0.53	7.13 ±0.53	4.93 ±0.77	61.0 ±0.9	0.36 ±0.03	58.1 ±0.9
0.5	1.10 ±0.03	0.74 ±0.07	150.91 ±0.61	7.79 ±0.61	4.87 ±0.78	63.7 ±0.9	0.32 ±0.03	53.1 ±0.9
1.0	1.38 ±0.07	0.72 ±0.06	297.99 ±0.63	7.95 ±0.63	5.44 ±0.69	66.4 ±0.8	0.28 ±0.02	48.5 ±0.8
2.0	1.44 ±0.08	0.74 ±0.07	338.57 ±0.56	7.11 ±0.56	5.52 ±0.76	67.8 ±0.8	0.26 ±0.02	46.1 ±0.8
3.0	2.07 ±0.12	0.46 ±0.04	1005.71 ±0.12	1.73 ±0.12	3.72 ±0.45	43.9 ±0.7	0.62 ±0.01	
4.0	2.13 ±0.14	0.57 ±0.05	1095.72 ±0.14	2.09 ±0.14	4.08 ±0.47	51.2 ±0.6	0.51 ±0.01	
5.0	2.14 ±0.15	0.49 ±0.04	1111.23 ±0.13	1.96 ±0.13	4.27 ±0.47	48.6 ±0.6	0.55 ±0.01	

$^a\theta_o$ is calculated using the Spinning-in-equatorial-band model.

Table 3c.8b. Hydrodynamic diameter (r_h), time for overall rotational motion of the micelle (τ_m), lateral diffusion time (τ_D), wobbling motion time (τ_w), wobbling diffusion coefficient (D_w), cone angle (θ_o) and order parameter ($|S|$) obtained from the anisotropy decays of C-480 in the micelles of Gemini-B and urea.

Gemini-B + Urea	r_h (nm)	τ_w (ns)	τ_m (ns)	τ_D (ns)	$D_w \times 10^{-8}$ (s^{-1})	θ_o (deg)	|S|	$^a\theta_o$ (deg)
0.0	1.30 ±0.06	0.71 ±0.07	249.11 ±0.98	13.86 ±0.98	5.29 ±0.75	65.0 ±0.8	0.30 ±0.02	50.8 ±0.8
0.5	1.50 ±0.07	0.74 ±0.07	382.68 ±0.87	10.68 ±0.87	5.52 ±0.81	67.8 ±0.8	0.26 ±0.02	46.1 ±0.8
1.0	1.28 ±0.06	0.68 ±0.06	237.79 ±0.65	8.25 ±0.65	5.53 ±0.74	65.0 ±0.8	0.30 ±0.02	50.8 ±0.8
2.0	1.38 ±0.06	0.71 ±0.05	297.99 ±0.44	5.39 ±0.44	4.96 ±0.58	63.0 ±0.8	0.33 ±0.02	54.3 ±0.8
3.0	1.78 ±0.08	0.75 ±0.06	639.47 ±0.43	5.13 ±0.43	4.81 ±0.51	63.7 ±0.6	0.32 ±0.01	53.1 ±0.7
4.0	1.58 ±0.08	0.61 ±0.05	447.23 ±0.15	2.52 ±0.15	4.21 ±0.45	53.8 ±0.6	0.47 ±0.01	75.8 ±0.9
5.0	1.34 ±0.07	0.68 ±0.05	272.82 ±0.14	2.27 ±0.14	3.78 ±0.37	53.8 ±0.6	0.47 ±0.01	75.8 ±0.9

$^a\theta_o$ is calculated using the Spinning-in-equatorial-band model**.**

Table 3c.8c. Hydrodynamic diameter (r_h), time for overall rotational motion of the micelle (τ_m), lateral diffusion time (τ_D), wobbling motion time (τ_w), wobbling diffusion coefficient (D_w), cone angle (θ_o) and order parameter ($|S|$) obtained from the anisotropy decays of C-480 in the micelles of Gemini-C and urea.

Gemini-C + Urea	r_h (nm)	τ_w (ns)	τ_m (ns)	τ_D (ns)	$D_w \times 10^{-8}$ (s^{-1})	θ_o (deg)	|S|	$^a\theta_o$ (deg)
0.0	1.28 ±0.05	0.81 ±0.08	237.79 ±0.97	13.55 ±0.97	3.82 ±0.56	59.0 ±0.8	0.39 ±0.02	62.0 ±0.9
0.5	1.28 ±0.05	0.79 ±0.08	237.79 ±0.89	13.06 ±0.89	4.09 ±0.59	60.3 ±0.8	0.37 ±0.02	59.3 ±0.9
1.0	1.15 ±0.02	0.84 ±0.08	172.45 ±0.98	13.69 ±0.98	4.29 ±0.51	63.7 ±0.7	0.32 ±0.01	53.1±0.7
2.0	1.22 ±0.04	0.83 ±0.08	205.89 ±0.99	14.16 ±0.99	4.53 ±0.64	65.0 ±0.6	0.30 ±0.02	50.8 ±0.8
3.0	0.88 ±0.02	0.81 ±0.07	77.27 ±0.59	7.93 ±0.59	4.08 ±0.45	61.0 ±0.7	0.36 ±0.01	58.1 ±0.7
4.0	1.05 ±0.03	0.79 ±0.07	131.26 ±0.63	8.34 ±0.63	4.46 ±0.59	63.0 ±0.8	0.33 ±0.02	54.3 ±0.8
5.0	1.34 ±0.06	0.49 ±0.05	272.82 ±0.12	1.91 ±0.12	3.07 ±0.29	41.1 ±0.6	0.66 ±0.01	

$^a\theta_o$ is calculated using the Spinning-in-equatorial-band model.

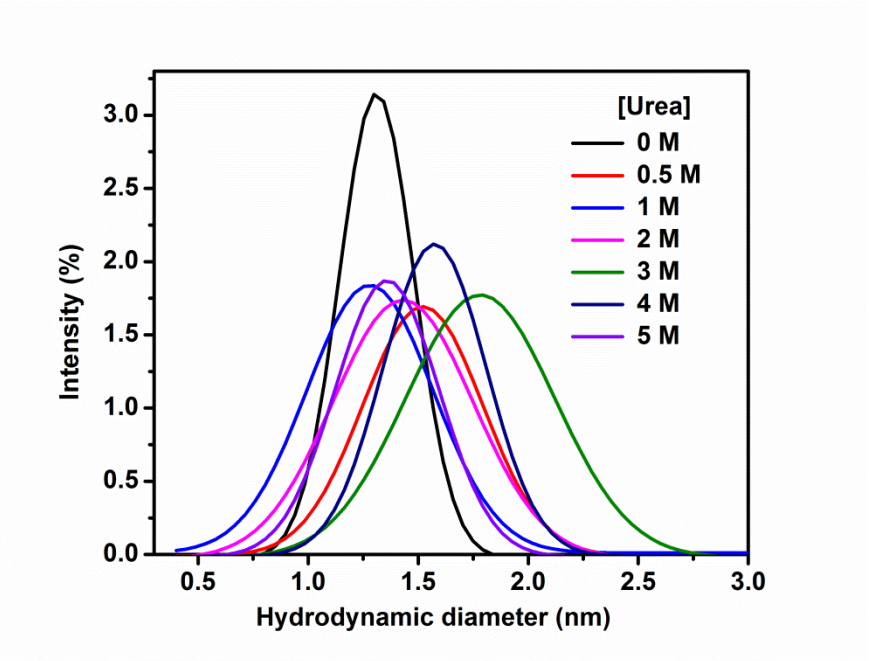

Figure 3c.15. The size distribution graph of the micelles of the Gemini-B obtained by dynamic light scattering (DLS) measurement.

The values of wobbling diffusion coefficient (D_w), order parameter ($|S|$) and cone angle (θ_o) have been calculated using Equations 2.26, 2.22 and 2.23, respectively upon application of wobbling-in-a-cone model[46, 77] to have more information about the motional restriction of the probe molecules within the micelles. These values are tabulated in Tables

3c.8a-c. Quite large values of spatial restriction parameter (|*S*|) show that the probe molecules are located in a restricted environment. The higher values of θ_o and lower values of (|*S*|) at lower concentration range of urea could be because of high microviscosity of micelles in this range. There is a possibility that wobbling-in-a-cone model is not appropriate for micelles with high microviscosity. To solve this apparent problem, sometimes the spinning-in-equatorial-band model[79, 80] is used. Spinning-in-equatorial-band model describes that the value of $|S|$ cannot exceed 0.5 and it is connected to θ_o by the following Equation 2.24. We have applied the spinning-in-equatorial-band model for micellar systems for which |*S*| < 0.5 which is the requirement to apply this model. After applying this model the calculated values of θ_o are also given in Tables 3c.8a-c. Thus possibly the probe molecule is oriented in such a way that the emission moment remains perpendicular to the long axis like that in spinning-in-equatorial-band model for micelles of high microviscosity. On the other hand for micelles of comparatively lower microviscosity the alignment of C-480 molecules would be such that the emission moment is parallel to the long axis like that is in the wobbling-in-a-cone model.

3c.3 Conclusions

Effect of added urea in the aqueous micelles of each of three cationic gemini surfactants with varying spacer groups on the micellization behaviour of surfactants, solvation dynamics and rotational relaxation of C-480 has been studied. With increasing concentration of urea the hydrophobic interactions between surfactant molecules are reduced due to lesser solvophobicity. This effect disfavors the formation of micelles so *cmc* is increased with increasing concentration of urea. The most probable location of C-480 molecules is the Stern layer of micelles. Solvation dynamics is found to be bimodal in nature. Average solvation time increases, reaches a maximum and then decreases with increasing concentration of urea. It has been observed that degree of counterion dissociation also increases, reaches a maximum and then decreases with more and more addition of urea in the micellar solution. With increasing concentration of free counterions the extent of clustering of water molecules is expected to be increased resulting in longer solvation times. Thus the rate of solvation process can be correlated with the degree of counterion dissociation. The presence of –OH group in the spacer group has effect on the rate of solvation process. The –OH groups protect the water molecules from their contact with the probe molecules through hydrogen bonding. As a result of it solvation process is slowed down. The microviscosity of micelles is decreased with increasing concentration

of urea as a result of it rotational relaxation process becomes faster. At a given concentration of urea the rotational relaxation process slows down with introduction of –OH group in the spacer group due to enhanced microviscosity of micelles. Rotational relaxation is bimodal in nature. The fast rotational relaxation component has major contribution to the fluorescence depolarization than that of the slow component. The lateral diffusion of the probe molecules along the surface of the micelle is mainly responsible for slow rotational relaxation. The tumbling motion of micelle as a whole is much slower than the lateral diffusion of the probe molecules. Wobbling motion also becomes faster with increasing concentration of urea as a result of decreased microviscosity of micelles. C-480 molecules might change its alignment in the micelles with changing microviscosity.

References

1. C. Tanford, *Science*, 1978, **200**, 1012-1018.
2. J. Israelachvili, S. Marčelja and R. G. Horn, *Q. Rev. Biophys.*, 1980, **13**, 121-200.
3. C. Tanford, *The hydrophobic effect: Formation of micelles and biological membranes 2d ed*, J. Wiley, 1980.
4. C. Tanford, *Biochem. Soc. Transac.*, 1987, **15**, 1S-7S.
5. R. M. Garavito and S. Ferguson-Miller, *J. Biol. Chem.*, 2001, **276**, 32403-32406.
6. G. G. Privé, *Methods*, 2007, **41**, 388-397.
7. M. Altschuler, D. Heddens, R. Diveley Jr and G. Kresheck, *BioTechniques*, 1994, **17**, 434, 436-434, 436.
8. G. C. Kresheck and J. Hwang, *Chem. Phys. Lipids*, 1995, **76**, 193-199.
9. S. K. Patra, A. Alonso and F. M. Goñi, *Biochim. Biophys. Acta Biomembranes*, 1998, **1373**, 112-118.
10. M. Kumbhakar, T. Goel, T. Mukherjee and H. Pal, *J. Phys. Chem. B*, 2005, **109**, 18528-18534.
11. R. Pramanik, S. Sarkar, C. Ghatak, V. G. Rao, S. Mandal and N. Sarkar, *J. Phys. Chem. B*, 2011, **115**, 6957-6963.
12. C. C. Ruiz and F. G. a. Sánchez, *J. Colloid Interface Sci.* , 1994, **165**, 110-115.
13. M. Schick, *J. Phys. Chem.*, 1964, **68**, 3585-3592.
14. S. Causi, R. De Lisi, S. Milioto and N. Tirone, *J. Phys. Chem.*, 1991, **95**, 5664-5673.
15. M. Abu-Hamdiyyah and K. Kumari, *J. Phys. Chem.*, 1990, **94**, 6445-6452.

16. H. Raghuraman, S. K. Pradhan and A. Chattopadhyay, *J. Phys. Chem. B*, 2004, **108**, 2489-2496.
17. M. Almgren and S. Swarup, *J. Colloid Interface Sci.* , 1983, **91**, 256-266.
18. E. Caponetti, S. Causi, R. De Lisi, M. Floriano, S. Milioto and R. Triolo, *J. Phys. Chem.*, 1992, **96**, 4950-4960.
19. J.-L. Baneres, J.-L. Popot and B. Mouillac, *Trends Biotechnol.*, 2011, **29**, 314-322.
20. S. K. Buchanan, *Curr. Opin. Struct. Biol.*, 1999, **9**, 455-461.
21. A. M. Stanley and K. G. Fleming, *Archiv. Biochem. Biophys.*, 2008, **469**, 46-66.
22. S. Fiedler, J. Broecker and S. Keller, *Cell. Mol. Life Sci.*, 2010, **67**, 1779-1798.
23. E. Udho, K. S. Jakes, S. K. Buchanan, K. J. James, X. Jiang, P. E. Klebba and A. Finkelstein, *Proc. Natl. Acad. Sci.*, 2009, **106**, 21990-21995.
24. A. Das and C. Mukhopadhyay, *J. Phys. Chem. B*, 2009, **113**, 12816-12824.
25. M. C. Stumpe and H. Grubmüller, *J. Phys. Chem. B*, 2007, **111**, 6220-6228.
26. M.-E. Lee and N. F. van der Vegt, *J. Am. Chem. Soc.*, 2006, **128**, 4948-4949.
27. N. F. van der Vegt, D. Trzesniak, B. Kasumaj and W. F. van Gunsteren, *Chem. Phys. Chem.*, 2004, **5**, 144-147.
28. E. Finer, F. Franks and M. Tait, *J. Am. Chem. Soc.*, 1972, **94**, 4424-4429.
29. X. Hoccart and G. Turrell, *J. Chem. Phys.*, 1993, **99**, 8498-8503.
30. F. Vanzi, B. Madan and K. Sharp, *J. Am. Chem. Soc.*, 1998, **120**, 10748-10753.
31. R. Chitra and P. E. Smith, *J. Phys. Chem. B*, 2000, **104**, 5854-5864.
32. B. J. Bennion and V. Daggett, *Proc. Natl. Acad. Sci.*, 2003, **100**, 5142-5147.
33. A. Caflisch and M. Karplus, *Structure*, 1999, **7**, 477-S472.
34. Y. Hayashi, Y. Katsumoto, S. Omori, N. Kishii and A. Yasuda, *J. Phys. Chem. B*, 2007, **111**, 1076-1080.
35. D. Bandyopadhyay, S. Mohan, S. K. Ghosh and N. Choudhury, *J. Phys. Chem. B*, 2014, **118**, 11757-11768.
36. S. Roy and J. Dey, *J. Colloid Interface Sci.* , 2005, **290**, 526-532.
37. J. Broecker and S. Keller, *Langmuir*, 2013, **29**, 8502-8510.
38. R. K. Mahajan, R. Kaur and V. K. Aswal, *Colloids Surf. A Physicochem. Eng. Asp.*, 2013, **419**, 61-68.
39. K. Bhattacharyya, *Chem. Commun.*, 2008, 2848-2857.
40. R. Yip, Y. Wen and A. Szabo, *J. Phys. Chem.*, 1993, **97**, 10458-10462.
41. G. Jones, W. R. Jackson, C. Y. Choi and W. R. Bergmark, *J. Phys. Chem.*, 1985, **89**, 294-300.

42. C. Chudoba, E. Nibbering and T. Elsaesser, *Phys. Rev. Lett.* , 1998, **81**, 3010.
43. Y. Liu, J. Ding, D. Shi and J. Sun, *J. Phys. Chem. A*, 2008, **112**, 6244-6248.
44. D. K. Palit, T. Zhang, S. Kumazaki and K. Yoshihara, *J. Phys. Chem. A*, 2003, **107**, 10798-10804.
45. G.-J. Zhao and K.-L. Han, *J. Phys. Chem. A*, 2007, **111**, 2469-2474.
46. A. K. Tiwari, Sonu and S. K. Saha, *J. Phys. Chem. B*, 2014, **118**, 3582-3592.
47. R. Williams, J. Phillips and K. Mysels, *Trans. Faraday Soc.*, 1955, **51**, 728-737.
48. A. K. Tiwari, M. Sowmiya, Sonu and S. K. Saha, *J. Mol. Liq.*, 2012, **167**, 18-27.
49. S. Wettig, P. Nowak and R. Verrall, *Langmuir*, 2002, **18**, 5354-5359.
50. A. F. de Moura, K. Bernardino, O. V. de Oliveira and L. C. G. Freitas, *J. Phys. Chem. B*, 2011, **115**, 14582-14590.
51. A. Idrissi, F. Sokolić and A. Perera, *J. Chem. Phys.*, 2000, **112**, 9479-9488.
52. B. K. Paul, A. Samanta, S. Kar and N. Guchhait, *J. Lumin.*, 2010, **130**, 1258-1267.
53. Z. R. Grabowski, K. Rotkiewicz and W. Rettig, *Chem. Rev.*, 2003, **103**, 3899-4032.
54. A. Maciejewski, J. Kubicki and K. Dobek, *J. Phys. Chem. B*, 2003, **107**, 13986-13999.
55. A. Mallick, P. Purkayastha and N. Chattopadhyay, *J. Photochem. Photobiol. C Photochem. Rev.*, 2007, **8**, 109-127.
56. Sonu, S. Kumari and S. K. Saha, *J. Phys. Chem. B*, 2015, **119**, 9751-9763.
57. C. Reichardt, *Chem. Rev.*, 1994, **94**, 2319-2358.
58. Sonu, S. Kumari and S. K. Saha, *Phys. Chem. Chem. Phys.*, 2016, **18**, 1551-1563.
59. A. Mallick, B. Haldar, S. Maiti, S. C. Bera and N. Chattopadhyay, *J. Phys. Chem. B*, 2005, **109**, 14675-14682.
60. N. Sarkar, A. Datta, S. Das and K. Bhattacharyya, *J. Phys. Chem.*, 1996, **100**, 15483-15486.
61. S. Roy, A. Mohanty and J. Dey, *Chem. Phys. Lett.*, 2005, **414**, 23-27.
62. J. R. Lakowicz, *Journal*.
63. Sonu, A. K. Tiwari, S. Kumari and S. K. Saha, *RSC Adv.*, 2014, **4**, 25210-25219.
64. R. Dutta, M. Chowdhury and M. A. Winnik, *Polymer*, 1995, **36**, 4445-4448.
65. M. Maroncelli and G. R. Fleming, *J. Chem. Phys.*, 1987, **86**, 6221-6239.
66. T. Asakawa, M. Hashikawa, K. Amada and S. Miyagishi, *Langmuir*, 1995, **11**, 2376-2379.
67. S. Balasubramanian and B. Bagchi, *J. Phys. Chem. B*, 2001, **105**, 12529-12533.
68. S. Balasubramanian, S. Pal and B. Bagchi, *Phys. Rev. Lett.* , 2002, **89**, 115505.

69. N. Nandi and B. Bagchi, *J. Phys. Chem. B*, 1997, **101**, 10954-10961.

70. P. A. Koya and Z. A. Khan, *J. Colloid Interface Sci.* , 2010, **342**, 340-347.

71. T. W. G. Solomons and C. B. *Fryhle*, *Organic Chemistry*. John Wiley & Sons, Singapore, 2004.

72. M. Kumbhakar, T. Goel, T. Mukherjee and H. Pal, *J. Phys. Chem. B*, 2005, **109**, 14168-14174.

73. Y. Rezus and H. Bakker, *Proc. Natl. Acad. Sci.*, 2006, **103**, 18417-18420.

74. D. Chakrabarty, A. Chakraborty, D. Seth, P. Hazra and N. Sarkar, *J. Chem. Phys.*, 2005, **122**, 184516.

75. U. Anand and S. Mukherjee, *Langmuir*, 2014, **30**, 1012-1021.

76. M. Kumbhakar, T. Goel, T. Mukherjee and H. Pal, *J. Phys. Chem. B*, 2004, **108**, 19246-19254.

77. K. Kinosita Jr, S. Kawato and A. Ikegami, *Biophys. J.*, 1977, **20**, 289.

78. D. Chakrabarty, D. Seth, A. Chakraborty and N. Sarkar, *J. Phys. Chem. B*, 2005, **109**, 5753-5758.

79. E. L. Quitevis, A. H. Marcus and M. D. Fayer, *J. Phys. Chem.*, 1993, **97**, 5762-5769.

80. L. B. Johansson and A. Niemi, *J. Phys. Chem.*, 1987, **91**, 3020-3023.

Chapter 4

Unfolding of Native Protein by Gemini Surfactants and Its Refolding Induced by β-Cyclodextrin and Sodium Dodecyl Sulfate in Aqueous Medium: Effect of Spacer Chain Length of Gemini Surfactants

---

Key Concepts:

- *The gemini surfactant-induced denaturation of the BSA through specific and nonspecific binding of surfactants has been explored.*

- *The present Chapter also demonstrates the step-by-step refolding of protein present in the form of protein-gemini surfactant complex using β-cyclodextrin (β-CD) and sodium dodecyl sulfate (SDS) as stripping agents.*

- *The spacer group of a gemini surfactant has an immense effect on the denaturation and renaturation of the BSA.*

Chapter 4

Unfolding of Native Protein by Gemini Surfactants and Its Refolding Induced by β-Cyclodextrin and Sodium Dodecyl Sulfate in Aqueous Medium: Effect of Spacer Chain Length of Gemini Surfactants

Abstract: *Several methods such as UV-visible absorption spectroscopy, steady-state and time-resolved fluorescence spectroscopy, circular dichroism spectroscopy (CD), dynamic light scattering (DLS) and field emitting scanning electron microscopy (FESEM) have been used to explore the interactions between protein, bovine serum albumin (BSA) and cationic gemini surfactants, 12-n-12 with varying number of –CH_2- group (n = 3, 6, 8, 12) in the spacer. At low concentration range of surfactants, the decrease in secondary structure (α-helix) of the protein is more with decreasing chain length of the spacer group due to the interaction of larger-sized pre-micellar aggregates with the protein. However, the unusual decrease in α-helix found in case of 12-12-12 is because of the greater extent of hydrophobic interactions between its long spacer chain and the protein. Present study also demonstrates the step-by-step refolding of protein present in the form of protein-gemini surfactant complex using β-cyclodextrin (β-CD)/sodium dodecyl sulfate (SDS) as stripping agents. This method is in contrast with the refolding of protein via artificial chaperone protocol. The mechanisms of interactions between β-CD/SDS and protein-gemini complex have been described. It has been observed that a gemini surfactant molecule with a long flexible spacer chain can more easily be captured by β-CD molecules forming simple inclusion complexes or nanotubes/rods depending on the concentration of β-CD. After the protein-micelles aggregates are dissociated, the gemini surfactant molecules with a short spacer chain are more easily stripped off by β-CD molecules and refolded proteins are formed. Gemini surfactant induced unfolded proteins are also refolded by SDS molecules through the formation of catanion (mixed micelles, vesicles etc.). The study of refolding of proteins induced by stripping agents and controlled by the spacer chain length of gemini surfactants and mechanisms of interactions involved has great impact. Because the refolding of non-native or misfolded proteins formed through different biological processes is a crucial step as these forms of proteins are believed to be the primary reasons for various neurodegenerative diseases in humans.*

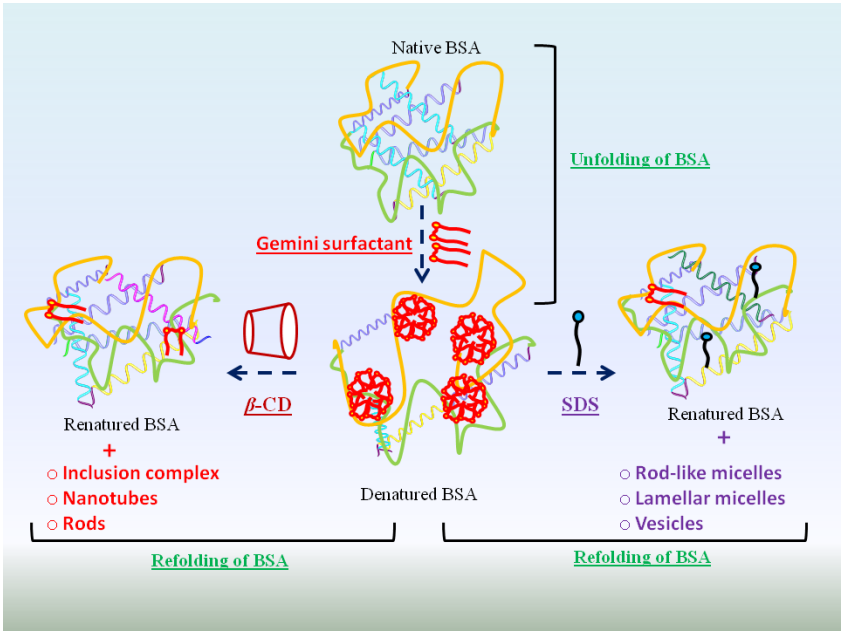

*Sunita Kumari, Sayantan Halder, Rishika Aggrawal, Vinod K. Aswal, G. Sundar and Subit K. Saha. (communicated for publication)

4.1 Introduction

Proteins are important molecules of living organisms and are involved in all life processes. To perform a certain biological function protein has to adopt the particular folded three-dimensional structure.[1, 2] This functional protein is called biologically active protein. Many works have been done to gain knowledge about the function-conformation relationship of protein.[3, 4] However, due to some unfavorable cellular conditions, proteins sometimes cannot gain proper folded structures on their own and assistance of a special type of ubiquitous protein called molecular chaperones is required.[5] Absence of function of molecular chaperones may result in the formation of misfolded proteins which unfortunately becomes the primary reasons for various neurodegenerative diseases such as Alzheimer, Perkinson etc. in humans.[6] Thus, the study of refolding of proteins has importance. Refolding study of proteins via artificial chaperones protocol using surfactants and cyclodextrins has been reported.[7] The present study is focused on two aspects: (i) unfolding of native protein, bovine serum albumin (BSA) by gemini surfactants with varying spacer chain length and mechanism of interactions, and (ii) refolding of BSA denatured by gemini surfactants with varying spacer chain using β-cyclodextrin and sodium dodecyl sulfate (SDS) as stripping agents and mechanism of interactions involved in it.

BSA protein used in the present study is the most abundant globular protein in blood plasma. BSA consists of 583 amino acids in a single polypeptide chain. It has high solubility in the aqueous media. BSA can interact with different types of amphiphilic biological molecules and has an important contribution to physiological function.[8, 9] The surfactant is generally an excellent agent to alter the protein conformation.[10-13] Protein-surfactant interaction performs an imperative role in various applications, such as foods, cosmetics, pharmaceuticals, biotechnology and physiological system. To control over the protein-surfactant interaction, intense research has been carried out in this area.[14-17] Many reports state that the denaturation of protein is possible due to the unfolding of proteins induced by ionic surfactants.[18-24] Mainly, two binding stages of an ionic surfactant and proteins are reported in the literature: (1) a specific binding stage, initially surfactant binds to ionic sites on the protein. This is driven by the ionic interaction of surfactant head groups with ionic sites on the proteins; (2) a nonspecific binding stage at the high concentration of surfactant; binding of alkyl chains of the surfactant to the protein through non-

cooperative and massive cooperative interactions. Surfactants used in the present study are a special class of surfactants called "Gemini", made up of two hydrophobic chains and two polar head groups, covalently associated via a spacer group at heads.[25-27] The unusual properties of aggregates of gemini surfactants are related to spacer structure because it influences the distances between head groups in the aggregate.[28] Gemini surfactants are more surface active and have higher affinity towards the protein than the conventional single chain counterparts.[15, 24, 29-32] The interactions of a gemini surfactant, 16-4-16 and its conventional counterpart, cetyltrimethylammonium bromide (CTAB) with the BSA show that significantly lower concentration of gemini is required as compared to CTAB to induce unfolding of BSA,[18, 33-35] and it is also noticed that at higher concentration of the gemini, refolding of protein can be happened.[29] Our recent report describes the effect of gemini surfactants, 12-4(OH)-12, 12-4-12, and 12-8-12 with different spacer group on the unfolding of the BSA in the buffer medium.[36] Circular dichroism (CD) spectra show that gemini surfactant with a hydroxyl group in the spacer is more capable in decreasing the α-helix of the BSA than that without hydroxyl group in the spacer. Gemini surfactant with a hydrophobic spacer group (12-8-12) gives more hydrophobic environment in the vicinity of Trp and Tyr residues in the protein by forming micelles.

Refolding of the BSA assisted by the artificial chaperones method is well reported.[7, 37-39] In these refolding processes, the surfactants are captured from the protein-surfactant complexes by the addition of cyclodextrin.[7, 37] Cyclodextrin is a special type of molecule which has a nonpolar cavity in their structure, thus they allow the formation of inclusion complexes with organic molecules, including surfactants.[40, 41] In recent reports,[42, 43] the effect of cyclodextrin on the interaction between BSA and the anionic surfactants, sodium dodecyl sulfate (SDS) and sodium dodecyl benzene sulfonate (SDBS) has been studied by means of different measurement techniques. The presence of cyclodextrins hinders the strong interactions between BSA and surfactants by the combined effect of electrostatic and hydrophobic interactions between them. The nonspecific interactions between BSA and surfactants are completely hindered by cyclodextrins. The hydrophobic interaction between cyclodextrin and surfactant is stronger than that between BSA and surfactant. The refolding of BSA by the use of gemini surfactants and β-CD and a comparison with a conventional surfactant has also been reported in the literature.[44]

Apart from cyclodextrin, the formation of mixed micelles of cationic-anionic surfactants is an appreciable method to refold the proteins. For these surfactants, the formation of micelles in the bulk solution is more favorable process than binding with proteins.[45] The equimolarly mixed micelles of catanion forms precipitates or turbid solution at very low concentration which limits the researchers to have an intense study on them.[46] These types of systems are especially used in protein separation.[47-49] It has been reported that cationic and anionic surfactants have noticeably strong synergistic interactions when they are mixed in aqueous solutions.[46] In addition to the hydrophobic interactions, there also exists the strong electrostatic attraction between the oppositely charged headgroups of surfactants. For these mixed systems, the formation of mixed micelles would compete with the binding process. The binding of surfactant molecules to BSA is restricted by the formation of mixed micelles and therefore, BSA can maintain its native structure even in a system containing mixed surfactants.

The first part of the chapter explores the gemini surfactant-induced denaturation of the BSA through specific and nonspecific binding of surfactants. Since the spacer group of a gemini surfactant has an immense effect on the aggregation behavior, a series of gemini surfactants with varying spacer chain length (Scheme 4.1) has been used to demonstrate the mechanisms of interactions between BSA and surfactants at various regions of binding isotherm. Study indicates that the larger-sized premicellar aggregates formed by the gemini surfactants with short spacer chain at low concentration has an effect on denaturation of the protein. The second part of the study is further divided into two parts, (i) interactions of β-CD molecules with gemini micelles-BSA complex thereby causing the refolding of the protein. Study demonstrates how this refolding process is controlled by the spacer chain length of the gemini surfactants. Here, denatured proteins get refolded as β-CD molecules strip off the surfactant molecules which is unlike the refolding of proteins via artificial chaperones protocol. Study reveals that β-CD molecules after stripping off the surfactant molecules form the simple inclusion complexes and also bigger structures (nanotubes or rods) depending on its concentration. There are some reports on the study of the interaction of BSA and gemini surfactants, but the effects of spacer groups of gemini surfactants are not investigated much.[15, 30, 36, 50-52] and (ii) study of SDS-induced refolding of BSA as an action of rather stronger binding and formation of catanion micelles/vesicles between the cationic gemini surfactants with varying spacer chain length and anionic SDS up to a certain molar ratio.[53] This chapter also describes how

the formation of catanion which is the cause for the refolding of the protein is dependent on the spacer chain length of gemini surfactants. This is a systematic study on β-CD and SDS induced refolding of proteins unfolded by gemini surfactants of varying spacer chain length. Even though it has immense significance, but little attention has been paid towards such type of study which could be useful for understanding the mechanism and developing new method for refolding of non-native or misfolded proteins.

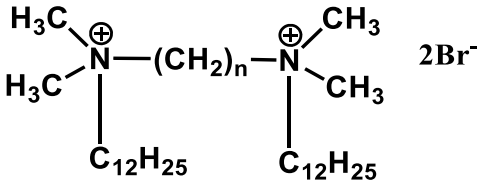

[12-*n*-12], *n* = 3, 6, 8 and 12

Scheme 4.1: Chemical structures of gemini surfactants.

4.2 Results and discussion

4.2.1 Binding interactions of gemini surfactants with BSA (unfolding of BSA)

4.2.1.1 UV- visible absorption spectra

The absorption spectrum of BSA is greatly responsive to the alteration in the microenvironment. Figure 4.1a-d display the absorption spectra of native BSA and BSA in presence of different concentrations of 12-3-12, 12-6-12, 12-8-12, and 12-12-12, respectively. Figure 4.1a clearly exhibits absorption bands with peak maxima at 210 nm and 279 nm. The details about these two bands are given elsewhere.[36] The band with peak maximum at 279 nm corresponds to $n \rightarrow \pi^*$ transition of the aromatic amino acids (Trp, Phe, and Tyr) present in the BSA. There is a red shift with a decrease in absorbance value for the band with peak maximum at 210 nm with increasing concentration of the gemini surfactants. However, very little changes are noted for the band with peak maximum at 279 nm. Observed ~14 nm bathochromic shift of the band with the peak position at 210 nm with the addition of the gemini surfactant, 12-3-12 (0 – 10 mM) is due to the exposure of amidic bond of BSA towards the more polar phase i.e. the bulk water phase.[36] Similar kinds of alterations are also noticed in the absorption spectra of the BSA in presence of other surfactants i.e. 12-6-12, 12-8-12, and 12-12-12; the corresponding figures are given as Figure 4.1b-d, respectively.

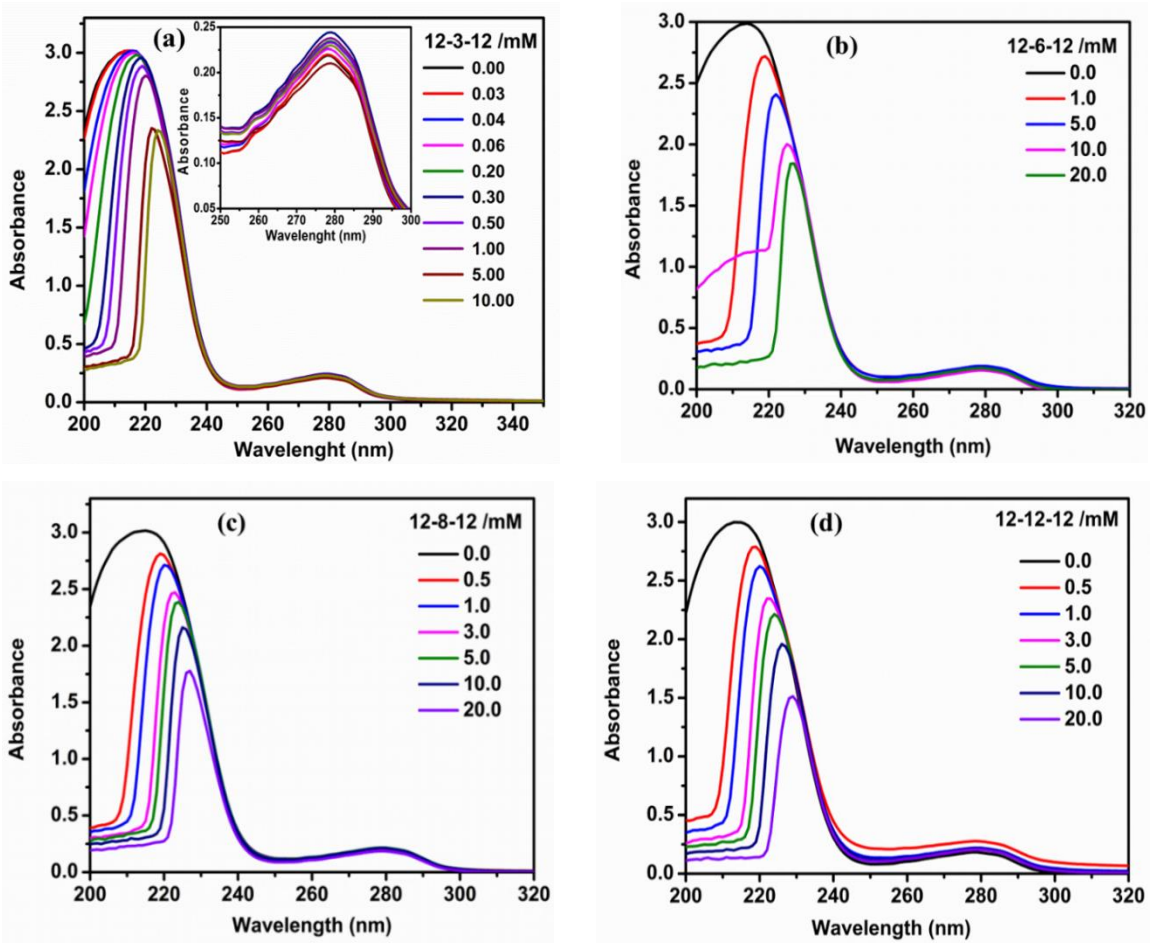

Figure 4.1. Absorption spectra of BSA at varying concentration of gemini surfactant: (a) 12-3-12, (b) 12-6-12, (c) 12-8-12, and (d) 12-12-12. [BSA] = 5.0 μM

4.2.1.2 Steady-state fluorescence spectra

Fluorescence spectroscopy is an excellent method to study the interactions of surfactants with protein. For this type of study, the intrinsic fluorescence (fluorophore(s) itself is(are) present in the protein and have fluorescence) is generally explored.[17, 30, 32, 54] In the present study also we have monitored the intrinsic fluorescence of the BSA i.e. the fluorescence due to the presence of aromatic amino acids *viz.* Trp, Phe, and Tyr. Earlier studies show that the fluorescence is mainly contributed by the Trp residues in BSA.[36, 55] Also, the fluorescence of Trp is affected more by gemini surfactant as compared to the fluorescence of Tyr.[36] In BSA, two types of domains, I and II are present. One of the two types of Trp amino acid residues i.e. Trp 134 is present in the domain I at the position of 134 in amino acid sequence, the other Trp residue, i.e. Trp 213 is present inside the hydrophobic pocket of domain II. Therefore, a slight change in the microenvironment of the intrinsic fluorophore can lead to the significant change in fluorescence properties.

Figure 4.2a-d represents the change in the fluorescence spectra of BSA with the variation in the concentration of the 12-3-12, 12-6-12, 12-8-12, and 12-12-12 surfactants, respectively. The peak maximum of the fluorescence band for pure BSA is located at 348 nm (Figure 4.2a). Upon addition of gemini surfactants, 12-*n*-12 to BSA solution, a decrease in the fluorescence intensity of BSA is occurred (Figure 4.3) which is accompanied by a blue shift of peak maximum by ~ 14 nm (Figure 4.4), suggesting that Trp residues are getting exposed to a more polar environment. Then, the fluorescence intensity increases gradually with a slight red shift (4 nm) in peak maximum. With a further increase in the concentration of gemini surfactants, the increase in fluorescence intensity is not much, with no change in the peak position (Figure 4.2). Similar trends are detected for all the 12-*n*-12 surfactants except for the difference in the concentration of the gemini surfactants at which the changes in various fluorescence properties take place. It has been reported that a similar trend is also noticed for a single-chain surfactant-BSA system such as cationic CTAC-BSA or zwitterionic HPS-BSA systems.[56]

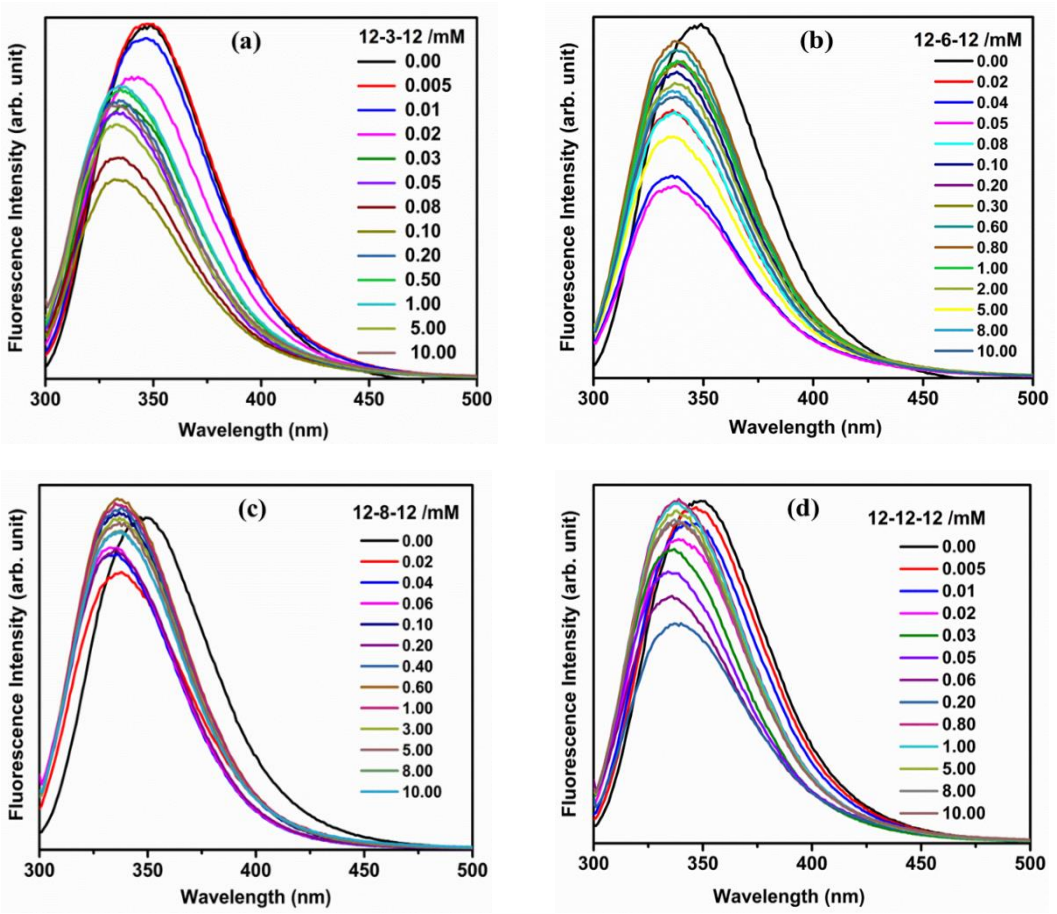

Figure 4.2. Fluorescence spectra of native BSA and BSA in presence of different concentrations of gemini surfactant, (a) 12-3-12, (b) 12-6-12, (c) 12-8-12, and (d) 12-12-12. λ_{ex} = 295 nm. [BSA] = 5.0 μM.

Detailed analysis of Figure 4.3 and Figure 4.4 are as follows. As the concentration of gemini surfactant in the solution of BSA is increased, the fluorescence intensity ratio (F/F_o, where F and F_o are intensities in presence and absence of surfactant, respectively) initially increases up to a very low concentration (0.04 mM). After that, intensity decreases up to 0.1 mM of surfactant with the blue shift in the peak maxima (348 nm to 334 nm) and then the intensity again rises up to 0.4 mM with red shift in peak maxima. Beyond 0.4 mM concentration of surfactant, there is a slight decrease in the fluorescence intensity with increasing concentration of a surfactant. At very low concentration range of a surfactant when the molar ratio of BSA and gemini surfactant is 1:1, the secondary structure of BSA is not change, however the tertiary structure is altered.[57] This conclusion can be drawn by an observation of enhancement in the fluorescence intensity in this range. The increase in fluorescence intensity is because of the binding of the gemini surfactant with very high energy binding sites of BSA, consequently, compactness of BSA is increased.[57, 58] This result indicates that the surrounding microenvironment of Trp is changed due to binding of the gemini surfactant with the protein.[59]

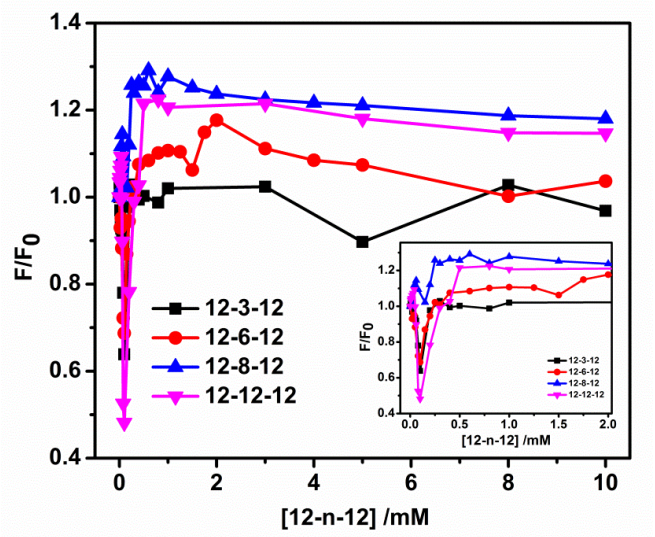

Figure 4.3. Fluorescence intensity ratio (F/F_o) of BSA at various concentrations of gemini surfactants, [12-*n*-12]. (Inset) clear view for the changes at low conc. range, λ_{ex} = 295 nm, fluorescence intensity is measured at 330 nm.

At a comparatively higher concentration of the gemini surfactant, the secondary structure of a protein is changed due to the non-co-operative binding between gemini and BSA.[30] When the BSA chain opens up, the fluorescence intensity starts to decrease due to the greater exposure of the fluorophore moiety of BSA towards the polar phase.[23] With further increasing concentration of the gemini surfactant the fluorescence intensity is

enhanced due to the comparatively nonpolar environment around the fluorophore moiety as a result of formation of micelles along the protein chain (co-operative binding) forming necklace-bead kind of structures.[54] Figure 4.4 shows variations in the fluorescence peak maxima of BSA at different concentrations of gemini surfactants. Table 4.1 represents the fluorescence peak maxima of BSA (5.0 µM) in presence of various concentrations of all four gemini surfactants, 12-*n*-12.

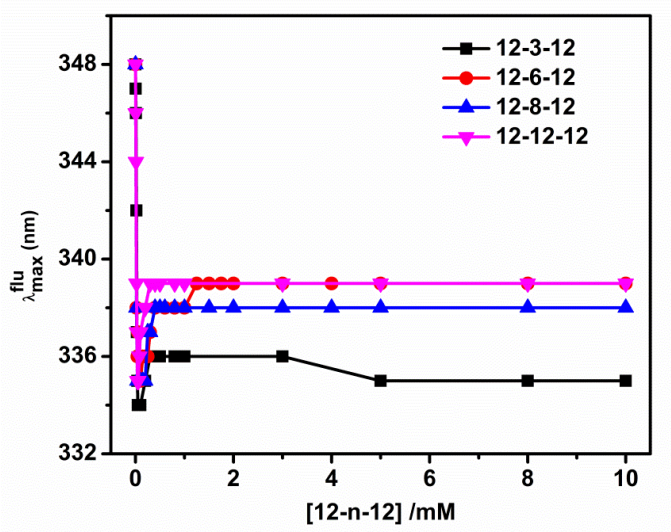

Figure 4.4. Change in fluorescence peak maxima of BSA (5.0 µM) with the variation in concentration of gemini surfactants, [12-*n*-12]. λ_{ex} = 295 nm.

At ~ 0.1 mM concentration of 12-*n*-12, the decrease in the fluorescence intensity follows the order as 12-8-12 < 12-6-12 < 12-3-12 < 12-12-12. For the first three surfactants, the order is as reported in the literature that the decrease in α-helix of protein is more with decrease in hydrophobicity (decrease in the chain length) of the spacer group.[60] The DLS measurements show that the sizes of the denatured protein particles associated with surfactant molecules in presence of 0.1 mM concentration of gemini surfactants, 12-8-12, 12-6-12, 12-3-12 and 12-12-12 are 8.7±1.0 nm, 10.5±1.8 nm, 11.0±0.8 nm, and 78.8±4.9 nm, respectively (See Figure 4.5 for size distribution graph). Zana *et al*. have reported that the extent of formation of micelles or extended micelles increases for gemini surfactants with short spacer chains.[28] Looking at the present results, we are proposing that in this concentration range of surfactants there is a possibility of formation of pre-micellar aggregates and the sizes of these aggregates are supposed to be in proportion to that of micelles or extended micelles. Thus the effect of pre-micellar aggregates of gemini surfactant with a short spacer chain like 12-3-12 would be more as

compared to gemini surfactants with longer spacer chain like 12-8-12. The bigger structures of protein-surfactant complexes in presence of the former than that of the latter are expected. In this respect, the interactions of BSA with gemini surfactants are different from that with conventional surfactants.

Table 4.1. Fluorescence peak maxima of BSA and BSA in presence of [12-*n*-12], *n* = 3, 6, 8 and 12. [BSA] = 5.0 μM, λ_{ex} = 295 nm.

Sr. No.	12-3-12 (mM)	λ_{max}^{flu} (nm)	12-6-12 (mM)	λ_{max}^{flu} (nm)	12-8-12 (mM)	λ_{max}^{flu} (nm)	12-12-12 (mM)	λ_{max}^{flu} (nm)
1	0.000	348	0.000	348	0.000	348	0.000	348
2	0.005	347	0.020	338	0.020	338	0.005	346
3	0.010	346	0.040	336	0.040	335	0.010	344
4	0.020	342	0.050	337	0.060	335	0.020	339
5	0.030	337	0.080	335	0.080	335	0.030	337
6	0.040	335	0.100	335	0.100	335	0.040	335
7	0.050	334	0.150	336	0.150	335	0.050	335
8	0.060	334	0.200	336	0.200	335	0.060	335
9	0.080	334	0.250	336	0.250	337	0.080	336
10	0.100	334	0.300	337	0.300	337	0.100	337
11	0.200	335	0.400	338	0.400	338	0.200	338
12	0.300	336	0.600	338	0.500	338	0.300	339
13	0.400	336	0.800	338	0.600	338	0.400	339
14	0.500	336	1.000	338	0.800	338	0.500	339
15	0.800	336	1.250	339	1.000	338	0.800	339
16	1.000	336	1.500	339	1.500	338	1.000	339
17	3.000	336	1.750	339	2.000	338	3.000	339
18	5.000	335	2.000	339	3.000	338	5.000	339
19	8.000	335	3.000	339	4.000	338	8.000	339
20	10.000	335	4.000	339	5.000	338	10.000	339
21			5.000	339	8.000	338		
22			8.000	339	10.000	338		
23			10.000	339				

In case of conventional surfactants there is no such report on formation of pre-micellar aggregates to the best of authors' knowledge. However, in case of 12-12-12 gemini surfactant, the maximum decrease in fluorescence intensity could be because of the fact that the effect of highly hydrophobic longer spacer group overcomes the other effect which is also supported by the particle size obtained from DLS measurements. Also the effect of formation of loop by a long spacer chain cannot be ruled out.[28] For 12-6-12, 12-8-12 and 12-12-12, at a concentration of 0.5 mM and greater than that, the fluorophores

feel comparatively less polar environment as compared to the native BSA (Figure 4.3). The reason is the formation of micelles along the BSA chain, which creates comparatively higher hydrophobicity around the fluorophores.[36]

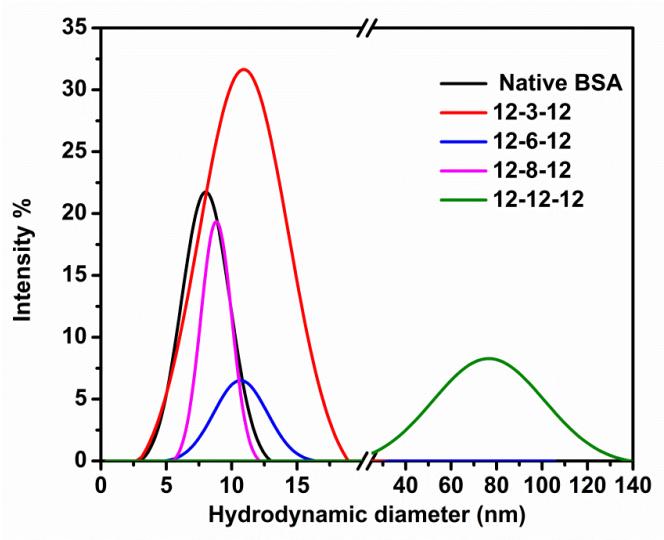

Figure 4.5. The size distribution graphs of the native BSA (5.0 μM) and BSA (5.0 μM) + [12-*n*-12] (0.1 mM), acquired by dynamic light scattering (DLS) measurement.

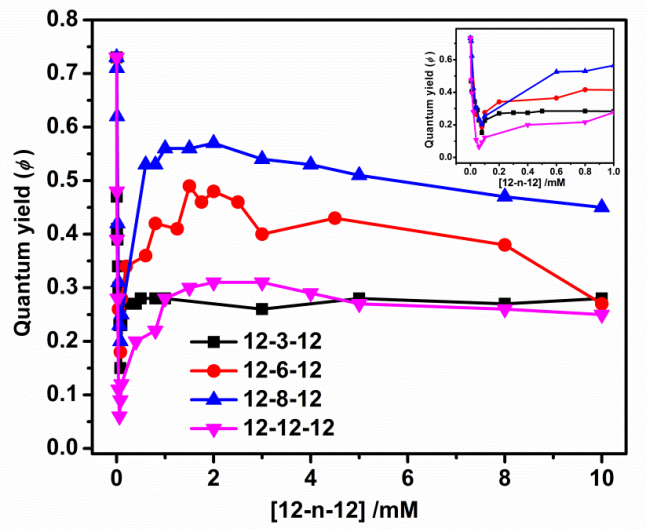

Figure 4.6. Variation in the quantum yield of BSA at different concentration of gemini surfactants, [12-*n*-12]. λ_{ex} = 295 nm.

Fluorescence quantum yields of BSA in absence and presence of various concentrations of gemini surfactants have been calculated and plotted in Figure 4.6. From Figure 4.6, it is clear that the trend for change in fluorescence quantum yields is in the same line with that of the fluorescence intensity ratio (F/F_o) given in Figure 4.3. It is well reported that the fluorescence quantum yield of Trp is reduced in a comparatively polar

solvent.[61] Upon denaturation of BSA the Trp moiety gets exposed to the water phase which results in the quenching of fluorescence. The quantum yield is found to be 0.73 for the native BSA. With the addition of a gemini surfactant to the native BSA the quantum yield starts to decrease, after reaching a minimum it increases and then becomes almost constant. Table 4.2 represents the quantum yield values for BSA in absence and presence of various concentrations of 12-*n*-12 surfactants.

Table 4.2. Quantum yield (ϕ_f) of BSA and BSA in presence of [12-*n*-12], *n* = 3, 6, 8 and 12. [BSA] = 5.0 μM, λ_{ex} = 295 nm

Sr. No.	12-3-12 (mM)	ϕ_f	12-6-12 (mM)	ϕ_f	12-8-12 (mM)	ϕ_f	12-12-12 (mM)	ϕ_f
1	0.000	0.73	0.00	0.73	0.000	0.73	0.000	0.73
2	0.005	0.47	0.04	0.26	0.005	0.71	0.005	0.48
3	0.010	0.41	0.08	0.18	0.010	0.62	0.010	0.39
4	0.020	0.39	0.10	0.28	0.020	0.42	0.020	0.28
5	0.030	0.34	0.20	0.34	0.040	0.31	0.040	0.11
6	0.040	0.30	0.60	0.36	0.060	0.23	0.060	0.06
7	0.050	0.29	0.80	0.42	0.080	0.20	0.080	0.09
8	0.060	0.23	1.25	0.41	0.100	0.25	0.100	0.12
9	0.080	0.15	1.50	0.49	0.600	0.53	0.400	0.20
10	0.100	0.23	1.75	0.46	0.800	0.53	0.800	0.22
11	0.200	0.27	2.00	0.48	1.000	0.56	1.000	0.28
12	0.300	0.27	2.50	0.46	1.500	0.56	1.500	0.30
13	0.400	0.27	3.00	0.40	2.000	0.57	2.000	0.31
14	0.500	0.28	4.50	0.43	3.000	0.54	3.000	0.31
15	0.800	0.28	8.00	0.38	4.000	0.53	4.000	0.29
16	1.000	0.28	10.00	0.27	5.000	0.51	5.000	0.27
17	3.000	0.26			8.000	0.47	8.000	0.26
18	5.000	0.28			10.000	0.45	10.000	0.25
19	8.000	0.27						
20	10.000	0.28						

4.2.1.3 Binding isotherm of gemini surfactants

Binding isotherm study provides with a better understanding of BSA-surfactant interaction by giving an idea about availability of binding positions in the protein, where the surfactants molecule can actually interact. Suppose, a protein has total binding positions, n_o, and at a particular concentration of surfactant, the surfactant molecules bind to *n* positions of protein, then the fraction of binding (α) of surfactant with protein has been

given by the Equation 2.28, Chapter 2.[17, 36, 62] At the saturated binding condition, the fractional alteration in the fluorescence of BSA (α) caused by the binding of gemini surfactant has been determined by Equation 2.29, Chapter 2.[17, 62, 63] Mainly, three binding regions have been reported earlier:[17, 60] (1) specific binding, (2) non-co-operative binding, and (3) co-operative binding. In the first binding region, binding isotherm shows very little rise because of specific ionic interaction between surfactant and BSA. In the second non-co-operative binding region, binding isotherm shows a very steep rise. And finally, in the third binding region, co-operative binding occurs between surfactant and BSA. After the third region, a flat terrain has been noticed, which shows saturation in the binding of surfactants with BSA. Das *et al.*[17] have reported and explained four regions of binding of surfactant with protein. Figure 4.7 shows binding isotherm plots for all gemini surfactants.

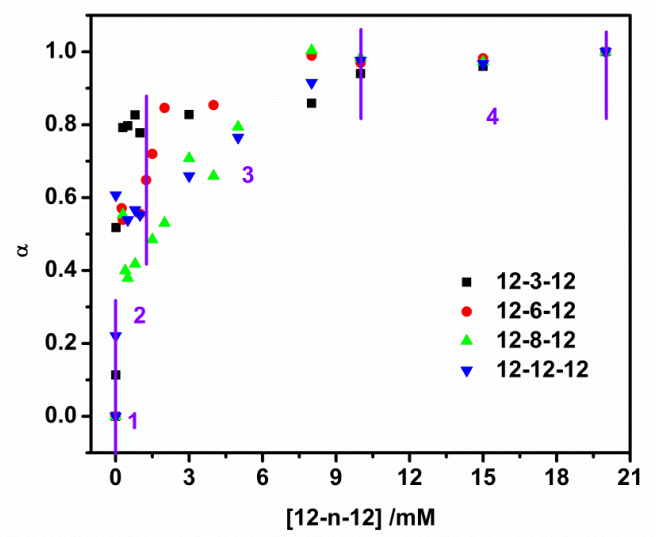

Figure 4.7. Binding isotherm of gemini surfactants, 12-*n*-12 with BSA, where *n* = 3, 6, 8, 12. [Fluorescence intensity measured at 348 nm].

4.2.1.4 Excited state lifetime

Fluorescence lifetime gives information about the rotational conformers of Trp and interconversion in their conformers with a change in protein conformation. Three rotational conformers of Trp are reported earlier, out of them, conformers 1 and 2 (Scheme 4.2) show the conformational exchange dynamics.[36, 64, 65] Fluorescence lifetime decays show bi-exponential fitting and corresponding lifetime decays are due to the conformers of Trp present in the BSA. Average excited state lifetime can be calculated by the help of following Equation (4.1)[62, 64]

$$\langle \tau_f \rangle = \frac{\sum_i a_i \tau_i^2}{\sum_i a_i \tau_i} \tag{4.1}$$

Here, a_i is a pre-exponential factor and τ_i is a lifetime of the *i*-th component. Figure 4.8 represents the fluorescence decay plots for native BSA and BSA in presence of different concentrations of 12-3-12 as a representative one. We observed bi-exponential fitting of lifetime decay with a good fitting parameter. Excited state lifetime of native BSA and BSA in presence of different concentrations of the 12-*n*-12 are given in the Tables 4.3a-d for 12-3-12, 12-6-12, 12-8-12, and 12-12-12, respectively. The longer component is appeared due to the rapid inter-conversion of conformers 1 and 2. The shorter component is due to the conformer 3 (Scheme 4.2).

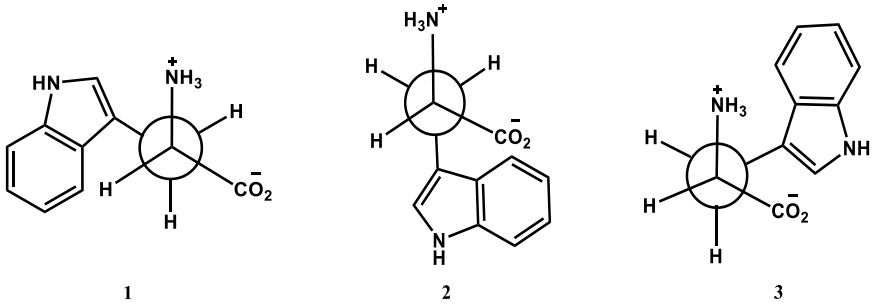

Scheme 4.2: Chemical structures of rotational conformers of tryptophan (trp).

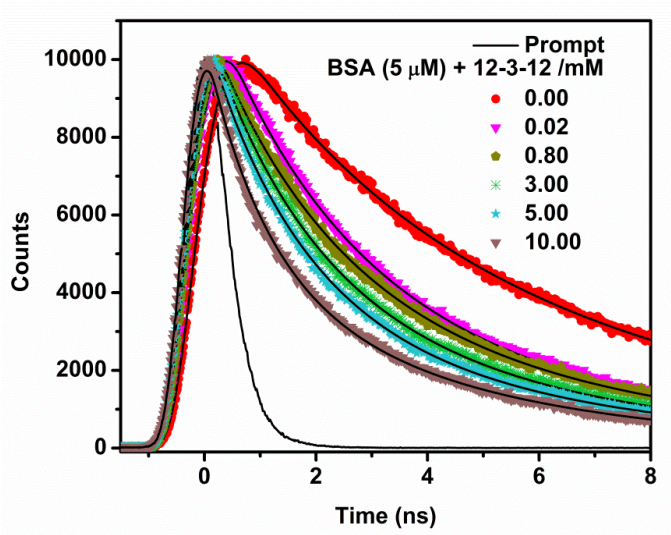

Figure 4.8. Fluorescence decays of native BSA and BSA in presence of different concentrations of 12-3-12. [BSA] = 5.0 μM, λ_{ex} = 300 nm, λ_{em} is the fluorescence peak maxima for each system.

Relative populations of conformers are assigned by their contributions in decay as decay components. The average excited state lifetime for native BSA is observed to be 6.21 ns which is in well corroborated with the reported values.[57, 58] Figure 4.9 shows changes in the average excited state lifetime of BSA as an action of varying concentration of gemini surfactants. Similar to our earlier report,[36] in the present study also we see that for less than 0.1 mM concentration of the gemini surfactant the lifetimes of BSA is decreased. This decrease in the lifetime infers that the conformation changes are occurred by the gemini surfactants. Due to this alteration in conformation of BSA, Trp is exposed to the more polar water phase and at the same time more surfactant molecules interact with Trp which results in disturbance of the planarity of indole ring that is present in Trp amino acid; consequently, contribute to the shortening of excited state lifetime.

Table 4.3a. Excited state lifetimes of BSA and in presence of different concentration of 12-3-12. [BSA] = 5.0 μM.

Sr. No.	**[12-3-12] (mM)**	a_1	τ_1 **(ns)**	a_2	τ_2 **(ns)**	$\langle\tau_f\rangle$ **(ns)**	χ^2
1	0.000	0.32	2.96	0.68	6.87	6.21	1.11
2	0.005	0.43	2.50	0.57	6.83	5.89	1.19
3	0.010	0.44	2.49	0.56	6.73	5.78	1.19
4	0.020	0.53	2.25	0.47	6.45	5.26	1.16
5	0.030	0.62	2.25	0.38	6.06	4.62	1.20
6	0.040	0.65	2.16	0.35	5.79	4.30	1.19
7	0.050	0.66	2.19	0.34	5.64	4.16	1.07
8	0.060	0.67	2.08	0.33	5.55	4.05	1.15
9	0.080	0.55	1.58	0.45	4.72	3.81	1.18
10	0.100	0.65	1.63	0.35	5.32	3.98	1.09
11	0.200	0.57	1.88	0.43	5.07	4.02	1.12
12	0.300	0.61	2.12	0.39	5.27	4.05	1.21
13	0.400	0.58	2.07	0.42	5.84	4.60	1.23
14	0.500	0.58	2.08	0.42	5.81	4.58	1.19
15	0.800	0.59	2.11	0.41	5.76	4.50	1.17
16	1.000	0.60	2.02	0.40	5.68	4.41	1.20
17	3.000	0.63	1.82	0.37	5.32	4.03	1.15
18	5.000	0.65	1.63	0.35	5.09	3.80	1.17
19	8.000	0.58	1.25	0.42	4.41	3.52	1.21
20	10.000	0.62	1.08	0.38	4.28	3.35	1.15

λ_{ex} = 300 nm, λ_{em} is the fluorescence peak maxima for each system.

Table 4.3b. Excited state lifetimes of BSA and in presence of different concentration of 12-6-12. [BSA] = 5.0 μM

Sr. No.	[12-6-12] (mM)	a_1	τ_1 (ns)	a_2	τ_2 (ns)	$<\tau_f>$ (ns)	χ^2
1	0.00	0.32	2.96	0.68	6.87	6.21	1.11
2	0.02	0.70	2.17	0.30	6.02	4.26	1.17
3	0.04	0.69	1.97	0.31	5.51	3.94	1.11
4	0.05	0.69	1.85	0.31	5.48	3.92	1.15
5	0.08	0.72	1.84	0.28	5.48	3.79	1.17
6	0.10	0.70	1.68	0.30	5.23	3.71	1.19
7	0.15	0.66	1.81	0.34	5.34	3.94	1.07
8	0.20	0.66	1.86	0.34	5.64	4.16	1.16
9	0.25	0.65	1.90	0.35	5.75	4.29	1.17
10	0.30	0.65	1.95	0.35	5.85	4.36	1.09
11	0.40	0.60	1.84	0.40	5.73	4.47	1.13
12	0.60	0.60	1.93	0.40	5.84	4.54	1.13
13	0.80	0.61	1.96	0.39	5.85	4.51	1.06
14	1.00	0.61	1.10	0.39	5.83	4.75	1.19
15	1.50	0.63	2.07	0.37	5.90	4.47	1.15
16	1.75	0.61	1.97	0.39	5.81	4.48	1.12
17	3.00	0.61	2.02	0.39	5.70	4.39	1.19
18	4.00	0.63	2.03	0.37	5.69	4.31	1.19
19	5.00	0.63	1.10	0.37	5.58	4.45	1.20
20	8.00	0.62	1.19	0.38	5.31	4.21	1.20
21	10.00	0.63	1.80	0.37	5.25	3.98	1.12

λ_{ex} = 300 nm, λ_{em} is the fluorescence peak maxima for each system.

However, on further increasing the concentration of 12-*n*-12, the excited state lifetime becomes longer and after a certain concentration it becomes constant. This decrement/increment in the lifetime is consistent with the decrement/increment in the fluorescence intensity as well as in the quantum yield at the same concentration range of gemini surfactants. The decrease in the lifetime is found to be more for the gemini surfactants with comparatively longer (more hydrophobic) spacer chain i.e. 12-8-12, 12-12-12. This result indicates that longer spacer is more effective to cause puckering of the indole ring of Trp by disturbing its planarity. Contrary to the earlier results, in the present

case we observe that at the higher concentration range of the 12-*n*-12 (beyond 1 mM), the increase in average excited state lifetime follows the order 12-3-12 < 12-6-12 < 12-8-12 < 12-12-12, which is in well agreement with the increasing order of hydrophobicity of the spacer group of gemini surfactants. This result reveals that Trp is feeling more hydrophobic microenvironment by increasing the methylene groups in the spacer. For all gemini surfactants, the overall contribution of the faster component increases and the contribution of shorter component decreases, as the concentration of gemini surfactant in the BSA system is increased.

Table 4.3c. Excited state lifetimes of BSA and in presence of different concentration of 12-8-12. [BSA] = 5.0 μM

Sr. No.	[12-8-12] (mM)	a_1	τ_1 (ns)	a_2	τ_2 (ns)	$<\tau_f>$ (ns)	χ^2
1	0.00	0.32	2.96	0.68	6.87	6.21	1.11
2	0.02	0.43	2.34	0.57	6.05	5.21	1.17
3	0.04	0.62	2.29	0.38	5.83	4.45	1.17
4	0.06	0.53	0.74	0.47	3.97	3.41	1.20
5	0.08	0.70	0.47	0.30	3.69	2.95	1.21
6	0.10	0.66	0.52	0.34	3.57	2.90	1.22
7	0.15	0.52	0.70	0.48	4.16	3.63	1.20
8	0.20	0.58	2.05	0.42	5.91	4.66	1.16
9	0.25	0.53	1.92	0.47	5.98	4.90	1.17
10	0.30	0.53	1.87	0.47	5.94	4.87	1.18
11	0.40	0.53	2.44	0.47	6.29	5.12	1.17
12	0.50	0.51	2.19	0.49	6.14	5.07	1.19
13	0.60	0.49	2.05	0.51	6.03	5.05	1.23
14	0.80	0.52	2.23	0.48	6.09	4.99	1.15
15	1.00	0.53	2.31	0.47	6.13	4.99	1.10
16	1.50	0.52	2.20	0.48	5.98	4.90	1.07
17	2.00	0.52	2.14	0.48	5.91	4.85	1.12
18	3.00	0.52	2.09	0.48	5.79	4.75	1.10
19	4.00	0.52	2.09	0.48	5.69	4.67	1.08
20	5.00	0.54	2.04	0.46	5.68	4.60	1.15
21	8.00	0.57	2.17	0.43	5.66	4.48	1.13
22	10.00	0.57	2.08	0.43	5.57	4.41	1.11

λ_{ex} = 300 nm, λ_{em} is the fluorescence peak maximum for each system.

Table 4.3d. Excited state lifetimes of BSA and in presence of different concentration of 12-12-12. [BSA] = 5.0 μM

Sr. No.	[12-12-12] (mM)	a_1	τ_1 (ns)	a_2	τ_2 (ns)	$<\tau_f>$ (ns)	χ^2
1	0.000	0.32	2.96	0.68	6.87	6.21	1.11
2	0.005	0.40	2.94	0.60	6.77	5.91	1.18
3	0.010	0.43	2.82	0.57	6.60	5.68	1.15
4	0.020	0.52	2.48	0.48	6.24	5.11	1.20
5	0.030	0.59	2.36	0.41	6.04	4.72	1.19
6	0.040	0.60	1.87	0.40	6.57	5.16	1.21
7	0.050	0.56	0.68	0.44	4.20	3.60	1.30
8	0.060	0.68	0.49	0.32	3.75	3.04	1.30
9	0.080	0.67	0.49	0.33	3.82	3.13	1.30
10	0.100	0.62	0.55	0.38	3.82	3.20	1.30
11	0.200	0.66	0.45	0.34	4.01	3.37	1.20
12	0.300	0.52	0.72	0.48	4.80	4.23	1.20
13	0.400	0.44	1.58	0.56	5.87	5.12	1.18
14	0.500	0.43	1.44	0.57	5.70	5.02	1.20
15	0.800	0.48	2.20	0.52	6.38	5.37	1.13
16	1.000	0.49	2.28	0.51	6.41	5.36	1.15
17	3.000	0.51	2.58	0.49	6.34	5.22	1.18
18	5.000	0.52	2.42	0.48	6.16	5.04	1.15
19	8.000	0.53	2.37	0.47	6.04	4.91	1.10
20	10.000	0.53	2.27	0.47	5.92	4.82	1.10

λ_{ex} = 300 nm, λ_{em} is the fluorescence peak maximum in each system.

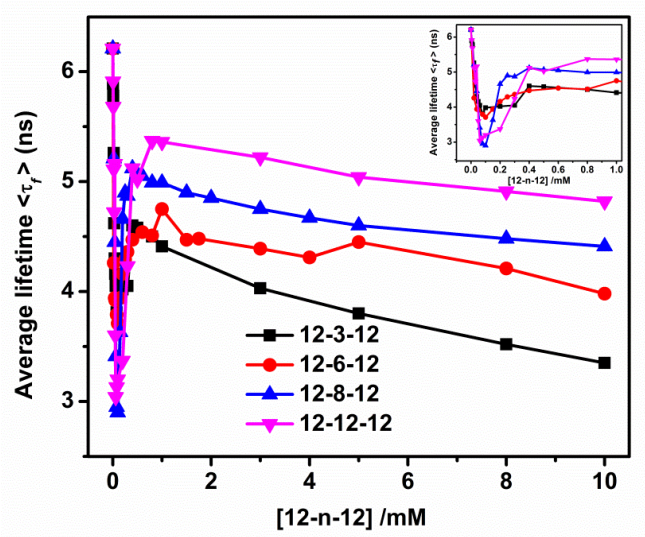

Figure 4.9. Variation in excited state lifetime of BSA (5.0 μM) in presence of varying conc. of gemini surfactants, 12-*n*-12. λ_{ex} = 300 nm, λ_{em} = 330 nm.

4.2.1.5 Circular dichroism (CD) spectra

CD spectral study is useful to probe the alteration in the secondary structure of the BSA caused by the action of surfactants.[66, 67] The far-UV CD spectra of the native BSA in absence and presence of the different concentrations of 12-3-12, 12-6-12, 12-8-12, and 12-12-12 are shown by Figure 4.10a-d, respectively. The α-helical, β-sheet and the random coil contents of the secondary structure of BSA were analyzed using a CDNN 2.1 software in the range of 200-260 nm and the data obtained are given in Table 4.4. Surfactants do not have any contribution in the range of 200-250 nm of CD spectra, hence, the observed CD spectra are only due to the peptide bonds of protein. It is clear from the Table 4.4 that for the all studied gemini surfactants, the content of α-helix decreases, however there are increasing tendency for other contents such as β-sheet, β-turn, and random coil. The CD spectra of the native BSA shows two negative bands in the far-UV region at 208 and 222 nm as characteristic of the α-helical structure.[68] Alterations of ellipticity at 222 nm ($-\theta_{222}$ nm) is helpful to probe the variation in the α-helical content.[69] We observe that as the concentration of a gemini surfactant in the BSA solution increases, the magnitude of ellipticity is decreased. It is well documented that the native BSA structure contains 60−67% of α-helix.[70, 71] Present results are in good resemblance with the previous reports as we find 60.2 % α-helix content in the pure BSA. Variation in the % of α-helix of BSA with increasing concentration of gemini surfactants has been shown in Figure 4.11. We have noticed that at very low concentrations of gemini surfactant, the magnitude of ellipticity is enhanced with an increase in α-helix content. Percentage of α-helix changes according to the same trend as observed in fluorescence properties. At the higher concentration of the surfactant, the α-helix content is decreased up to 6.4%, which exhibits that with the increase in the surfactant concentration, the unfolding of the BSA is obvious. If we compare the % α-helix of BSA in presence of 0.2 mM (from Table 4.4) of 12-*n*-12, then we observe that more decrease in the % α-helix occurs with the order as follows: 12-3-12 < 12-6-12 < 12-8-12 < 12-12-12. This result indicates that even at high concentration range of surfactants, the decrease in % α-helix depends on the spacer chain length. Longer the spacer chain length greater is the decrease in % α-helix observed in this concentration range. It is pertinent to note that the order of decrease in % α-helix noticed at low concentration range of surfactants (0.08-0.1 mM) is in good agreement with that of decrease in fluorescence intensity i.e. 12-8-12 < 12-6-12 < 12-3-12 < 12-12-12.

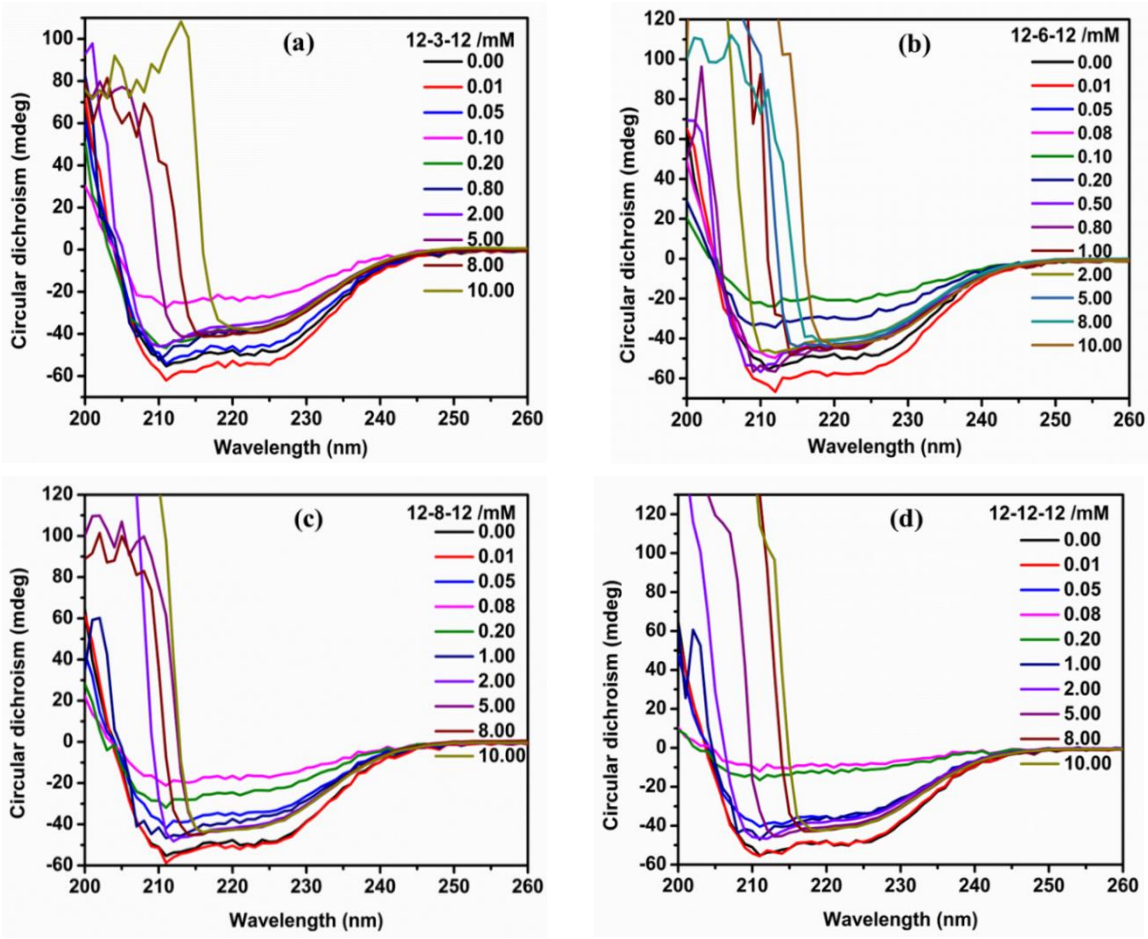

Figure 4.10. Circular dichroism (CD) spectra of BSA (5 µM) in absence and presence of gemini surfactant, (a) 12-3-12, (b) 12-6-12, (c) 12-8-12, and (d) 12-12-12.

Table 4.4. Various components of the secondary structure of BSA (5.0 µM) calculated from the CD spectra.

[12-*n*-12] (mM)	*α*-Helix	*β*-Sheet		*β*-turn	Random coil
		Anti-parallel	Parallel		
12-3-12					
0.00	60.2	3.4	4.5	12.4	21.1
0.01	68.0	2.5	3.6	11.3	17.8
0.05	57.5	3.7	4.8	12.8	22.3
0.08	23.2	12.1	12.6	18.8	42.5
0.20	49.1	5.0	5.9	14.2	25.1
0.50	54.3	4.2	5.2	13.4	22.8
0.80	57.3	3.8	4.9	13.0	22.3
2.00	56.6	3.8	5.5	12.9	25.7
5.00	22.6	9.6	16.0	16.5	58.2
8.00	15.9	12.8	20.9	18.0	66.7
10.00	6.4	24.0	37.1	21.9	82.5
12-6-12					

0.00	60.2	3.4	4.5	12.4	21.1
0.01	71.0	2.3	3.2	10.9	16.3
0.05	53.4	4.3	5.3	13.4	23.8
0.08	53.4	4.3	5.3	14.3	23.5
0.10	25.3	11.1	11.7	18.3	40.4
0.20	35.8	7.6	8.4	16.2	32.6
0.50	56.0	4.0	5.0	13.2	22.3
0.80	63.7	3.0	4.2	12.1	20.3
1.00	60.6	3.3	4.7	12.2	23.0
2.00	50.7	3.4	9.2	11.5	48.0
5.00	12.7	13.0	28.9	17.5	79.8
8.00	9.8	17.0	31.0	19.3	79.6
10.00	7.3	17.7	43.9	18.8	90.2
12-8-12					
0.00	60.2	3.4	4.5	12.4	21.1
0.01	62.4	3.1	4.2	12.1	20.2
0.05	41.9	6.2	7.3	15.1	29.9
0.10	29.1	9.6	10.5	17.4	37.9
0.20	31.3	9.0	9.6	17.1	35.4
0.50	56.8	3.9	4.9	13.2	21.8
1.00	50.1	4.7	6.1	13.8	27.1
2.00	32.9	5.4	15.7	13.2	65.6
5.00	13.0	13.8	26.0	18.1	75.2
8.00	17.8	11.10	20.30	17.0	67.4
10.00	12.2	12.2	33.8	16.8	85.5
12-12-12					
0.00	60.2	3.4	4.5	12.4	21.1
0.01	60.2	3.4	4.4	12.4	20.8
0.05	43.5	5.9	7.0	14.8.	29.1
0.08	17.1	16.0	15.8	20.6	48.4
0.20	19.5	14.4	14.2	19.9	45.1
0.50	40.1	6.7	7.5	15.6	29.8
1.00	48.0	5.0	6.5	14.1	28.3
2.00	63.5	2.7	5.2	11.4	27.7
5.00	23.2	8.3	18.2	15.4	66.3
8.00	9.7	14.8	37.3	17.9	87.0
10.00	7.5	17.3	44.0	18.6	90.4

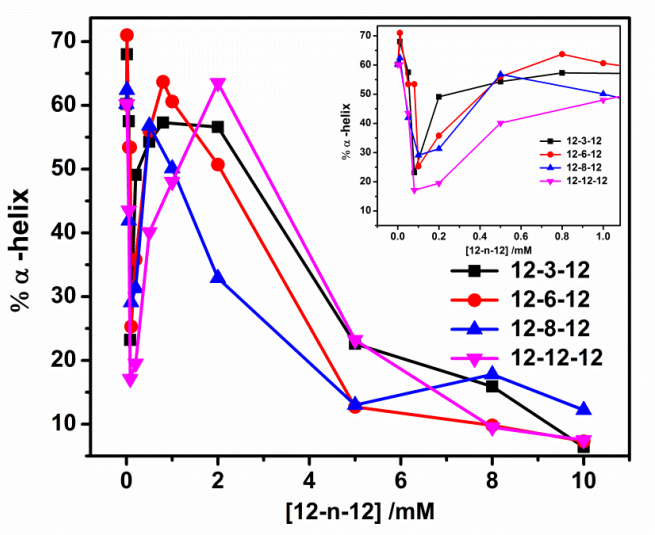

Figure 4.11. Variation in the % of α-helix of BSA (5.0 µM) with increasing concentration of gemini surfactants, [12-*n*-12].

4.2.2 Refolding of denatured BSA by the action of β-cyclodextrin (β-CD)

4.2.2.1 Steady-state fluorescence spectra

Even though the addition of β-CD leads to insignificant structural loss of the native protein but it is a very effective agent to refold the BSA.[57] β-CD molecules can effectively strip off the surfactant molecules those are bound to BSA molecules as a result of the fact that the hydrophobic interactions between tails of surfactant molecules and hydrophobic pocket of β-CD molecules are much stronger than that between BSA and surfactant molecules.[7, 37-39] The former interactions prevent the binding of surfactant molecules with BSA.[72] In the present case to study the efficiency of β-CD to refold the BSA denatured by a gemini surfactant, fluorescence spectra were recorded at a fixed concentration of BSA (5.0 µM) and gemini surfactant (0.5 mM) and with varying the concentrations of β-CD. The above mentioned fluorescence study states that at 0.5 mM concentration of a gemini surfactant, the protein molecules get completely unfolded where micelles are formed along the protein chain giving necklace-bead kind of structures.[18, 73-75] Figure 4.12 represents the change in the fluorescence spectra of BSA (5.0 µM) in presence of 0.5 mM of 12-3-12 with varying concentrations of β-CD as a representative one.

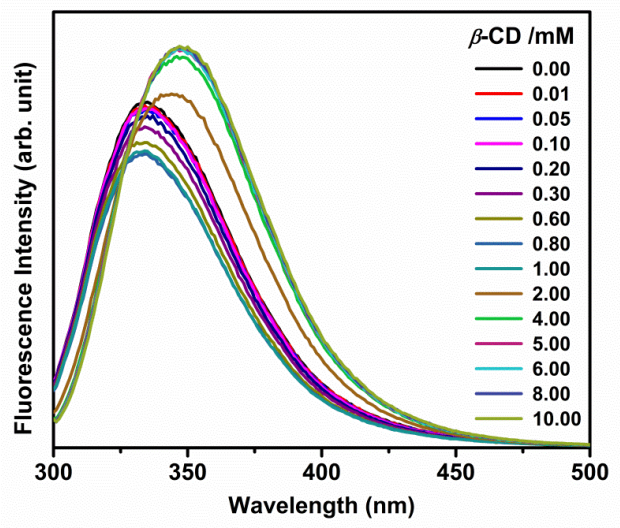

Figure 4.12. Change in fluorescence spectra of BSA (5.0 µM) in presence of 12-3-12 (0.5 mM) with varying concentrations of β-CD. λ_{ex} = 295 nm.

Figure 4.13 demonstrates the changes in fluorescence intensity ratios (F/F_o, where F and F_o are the fluorescence intensities in presence and absence of β-CD, respectively) with the variation in β-CD concentration. It is clear from the Figure 4.13 that with increasing concentration of the β-CD, F/F_o ratio initially increases, after reaching a maximum it decreases, reaches a minimum and then again starts to increase before reaching a saturation point. However, F/F_o ratio does not reach at 1.0 even at 10 mM concentration of β-CD. These results indicate that β-CD molecules can strip off the gemini molecules and the stripping efficiency of β-CD from the specific high energy binding sites of BSA is low even in presence of high concentration of β-CD.

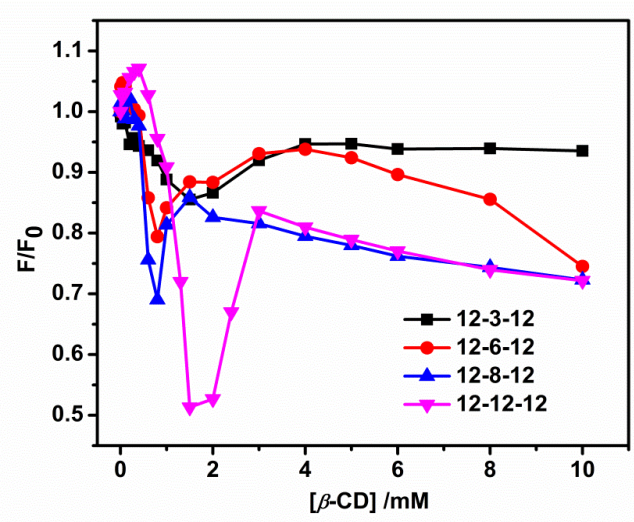

Figure 4.13. Change in fluorescence intensity ratio of BSA (5.0 µM) in presence of 0.5 mM of gemini surfactant, 12-*n*-12 with the variation of concentration of β-CD. λ_{ex} = 295 nm, fluorescence intensity measured at 330 nm.

The present study, however, says that these interactions depend on the hydrophobicity/chain length of the spacer group of the gemini surfactant molecules as described below. The *β*-CD molecules at a high concentration can be threaded on to the hydrophobic tails of the surfactant molecules.[76] The initial increase in F/F_o ratio at lower concentration range of *β*-CD (Figure 4.13) could be because of the binding of *β*-CD molecules with BSA-surfactant aggregates thereby providing with comparatively less polar environment around the Trp residues of BSA. However, at a comparatively higher concentration of *β*-CD, the BSA-surfactant aggregates get dissociated due to the binding of surfactant molecules with the *β*-CD molecules. The values of fluorescence peak maxima and fluorescence quantum yields are tabulated in Table 4.5 and 4.6, respectively. The changes in fluorescence peak maxima and fluorescence quantum yields are represented by Figure 4.14 and Figure 4.15, respectively. Fluorescence lifetime values with varying concentration of *β*-CD have also been estimated. Excited state lifetimes of BSA (5.0 µM) in presence of 12-*n*-12 (0.5 mM) at various concentration of *β*-CD are given in Tables 4.7a-d. Figure 4.16 represents the change in the average excited state lifetime of BSA in presence of 0.5 mM gemini surfactants, 12-*n*-12 with varying concentrations of *β*-CD. At the low concentration range of cyclodextrin lifetime shows a decreasing tendency, and after reaching a minimum, it shows the increasing tendency.

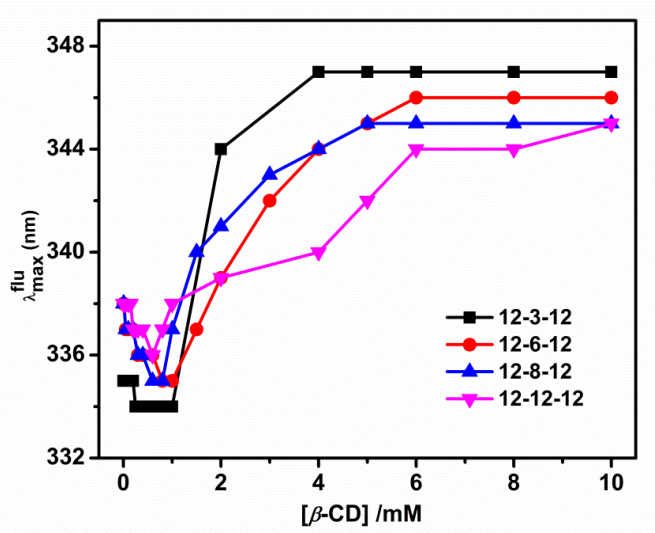

Figure 4.14. Change in the fluorescence peak maxima of BSA (5.0 µM) in presence of 0.5 mM gemini surfactant, 12-*n*-12 with varying concentration of *β*-CD. λ_{ex} = 295 nm.

Table 4.5. Fluorescence peak maxima of BSA (5.0 µM) in presence of 0.5 mM [12-*n*-12] and different concentrations of β-CD. λ_{ex} = 295 nm

Sr. No.	β-CD (mM)	12-3-12 λ_{max}^{flu} (nm)	12-6-12 λ_{max}^{flu} (nm)	12-8-12 λ_{max}^{flu} (nm)	12-12-12 λ_{max}^{flu} (nm)
1	0.00	335	338	338	338
2	0.01	335	338	338	338
3	0.05	335	337	337	338
4	0.10	335	337	337	338
5	0.20	335	337	337	338
6	0.30	335	336	336	337
7	0.40	334	336	336	337
8	0.60	334	336	335	337
9	0.80	334	335	335	337
10	1.00	334	335	337	336
11	1.50	334	337	340	337
12	2.00	334	339	341	338
13	3.00	344	342	343	339
14	4.00	347	344	344	340
15	5.00	347	345	345	342
16	6.00	347	346	345	344
17	8.00	347	346	345	344
18	10.00	347	346	345	345

Table 4.6. Quantum yield (ϕ_f) of BSA (5.0 µM) in presence of 0.5 mM [12-*n*-12] and different concentrations of β-CD. λ_{ex} = 295 nm.

Sr. No.	β-CD (mM)	12-3-12 ϕ_f	β-CD (mM)	12-6-12 ϕ_f	β-CD (mM)	12-8-12 ϕ_f	β-CD (mM)	12-12-12 ϕ_f
1	0.00	0.29	0.00	0.46	0.00	0.51	0.00	0.16
2	0.05	0.28	0.05	0.39	0.05	0.50	0.05	0.15
3	0.10	0.22	0.10	0.20	0.10	0.28	0.20	0.14
4	0.20	0.23	0.40	0.14	0.20	0.24	0.40	0.08
5	0.80	0.11	0.80	0.06	0.40	0.13	0.80	0.04
6	1.00	0.12	1.00	0.06	0.80	0.02	1.00	0.01
7	1.50	0.26	1.50	0.27	1.00	0.05	1.50	0.02
8	3.00	0.48	2.00	0.30	2.00	0.36	2.00	0.06
9	4.00	0.46	3.00	0.41	3.00	0.39	5.00	0.37
10	6.00	0.53	5.00	0.41	6.00	0.35	6.00	0.36
11	8.00	0.62	6.00	0.35	8.00	0.39	8.00	0.44
12	10.00	0.50	10.00	0.37	10.00	0.30	10.00	0.35

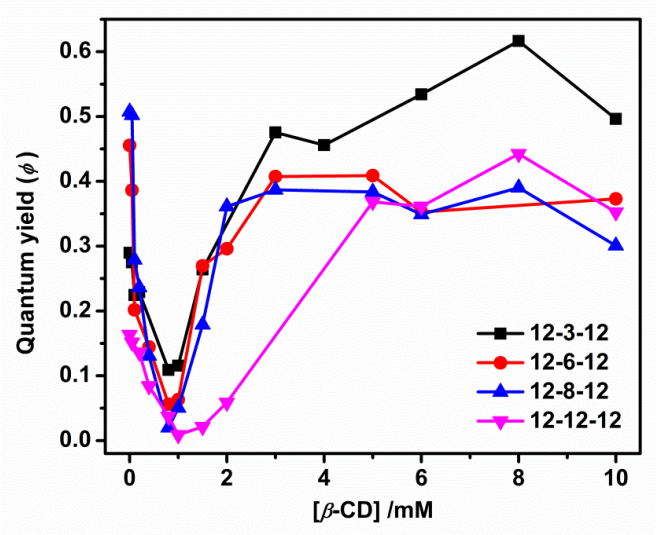

Figure 4.15. Change in the quantum yield of BSA (5.0 µM) in presence of 0.5 mM gemini surfactant [12-*n*-12] with varying concentration of *β*-CD. λ_{ex} = 295 nm.

Table 4.7a. Excited state lifetimes of BSA (5.0 µM) in presence of 12-3-12 (0.5 mM) at various concentration of *β*-CD.

Sr. No.	[*β*-CD] (mM)	a_1	τ_1 (ns)	a_2	τ_2 (ns)	$<\tau_f>$ (ns)	χ^2
1	0.00	0.58	2.06	0.42	5.75	4.53	1.11
2	0.01	0.58	2.10	0.42	5.76	4.53	1.10
3	0.05	0.58	2.03	0.42	5.70	4.49	1.14
4	0.10	0.57	1.98	0.43	5.65	4.49	1.12
5	0.15	0.60	2.22	0.40	5.88	4.56	1.09
6	0.20	0.59	2.21	0.41	5.86	4.58	1.06
7	0.25	0.60	2.22	0.40	5.86	4.54	1.11
8	0.30	0.63	2.32	0.37	5.98	4.52	1.07
9	0.40	0.64	2.33	0.36	5.99	4.49	1.12
10	0.60	0.64	2.19	0.36	5.77	4.33	1.08
11	0.80	0.66	2.04	0.34	5.59	4.12	1.13
12	1.00	0.65	1.89	0.35	5.39	4.01	1.13
13	2.00	0.51	2.42	0.49	6.43	5.30	1.10
14	4.00	0.42	2.81	0.58	6.74	5.83	1.10
15	5.00	0.38	2.70	0.62	6.71	5.92	1.17
16	6.00	0.37	2.69	0.63	6.68	5.92	1.13
17	8.00	0.36	2.43	0.64	6.59	5.88	1.13
18	10.00	0.36	2.25	0.64	6.55	5.85	1.19

λ_{ex} = 300 nm, λ_{em} is the fluorescence peak maxima for each system.

Table 4.7b. Excited state lifetimes of BSA (5.0 µM) in presence of 12-6-12 (0.5 mM) at various concentration of *β*-CD.

Sr. No.	[*β*-CD] (mM)	a_1	τ_1 (ns)	a_2	τ_2 (ns)	$<\tau_f>$ (ns)	χ^2
1	0.00	0.62	1.90	0.38	5.9	4.52	1.14
2	0.01	0.62	2.05	0.38	6.01	4.59	1.17
3	0.05	0.61	1.89	0.39	5.79	4.47	1.10
4	0.10	0.62	1.93	0.38	5.85	4.48	1.16
5	0.15	0.64	1.97	0.36	5.86	4.40	1.16
6	0.20	0.65	1.91	0.35	5.79	4.32	1.17
7	0.25	0.66	1.88	0.34	5.70	4.21	1.11
8	0.30	0.64	1.71	0.36	5.21	3.92	1.12
9	0.40	0.69	1.79	0.31	5.42	3.88	1.15
10	0.60	0.69	1.71	0.31	5.27	3.78	1.23
11	0.80	0.71	2.00	0.29	5.75	4.03	1.13
12	1.00	0.67	1.93	0.33	5.86	4.29	1.13
13	2.00	0.64	2.06	0.36	6.22	4.68	1.12
14	4.00	0.64	2.04	0.36	6.32	4.76	1.13
15	5.00	0.60	2.02	0.40	6.28	4.89	1.15
16	6.00	0.61	2.05	0.39	6.33	4.89	1.17
17	8.00	0.61	2.06	0.39	6.36	4.91	1.13
18	10.00	0.60	2.00	0.40	6.31	4.92	1.18

λ_{ex} = 300 nm, λ_{em} is the fluorescence peak maxima for each system.

Table 4.7c. Excited state lifetimes of BSA (5.0 µM) in presence of 12-8-12 (0.5 mM) at various concentration of *β*-CD.

Sr. No.	[*β*-CD] (mM)	a_1	τ_1 (ns)	a_2	τ_2 (ns)	$<\tau_f>$ (ns)	χ^2
1	0.00	0.50	2.28	0.50	6.26	5.20	1.19
2	0.01	0.50	2.19	0.50	6.21	5.16	1.17
3	0.05	0.51	2.21	0.49	6.21	5.13	1.18
4	0.10	0.51	2.22	0.49	6.21	5.13	1.19
5	0.15	0.52	2.07	0.48	6.10	5.02	1.19
6	0.20	0.52	2.00	0.48	6.06	4.99	1.20
7	0.25	0.53	1.99	0.47	6.04	4.94	1.19
8	0.30	0.48	1.29	0.52	5.05	4.33	1.20
9	0.40	0.50	0.77	0.50	4.16	3.63	1.22
10	0.60	0.62	0.65	0.38	4.14	3.43	1.20
11	0.80	0.62	2.24	0.38	5.89	4.49	1.15
12	1.00	0.54	2.45	0.46	6.34	5.13	1.15
13	2.00	0.51	2.55	0.49	6.46	5.32	1.15
14	4.00	0.51	2.44	0.49	6.45	5.32	1.13
15	5.00	0.49	2.14	0.51	6.29	5.27	1.11
16	6.00	0.50	1.98	0.50	6.25	5.22	1.18
17	8.00	0.51	1.73	0.49	6.08	5.09	1.18
18	10.00	0.51	1.69	0.49	6.13	5.14	1.20

λ_{ex} = 300 nm, λ_{em} is the fluorescence peak maxima for each system.

Table 4.7d. Excited state lifetimes of BSA (5.0 µM) in presence of 12-12-12 (0.5 mM) at various concentration of *β*-CD.

Sr. No.	[*β*-CD] (mM)	a_1	τ_1 (ns)	a_2	τ_2 (ns)	$<\tau_f>$ (ns)	χ^2
1	0.00	0.56	1.91	0.44	6.33	5.10	1.12
2	0.01	0.51	1.99	0.49	6.33	5.26	1.14
3	0.05	0.50	1.87	0.50	6.27	5.26	1.20
4	0.10	0.48	1.79	0.52	6.12	5.20	1.20
5	0.15	0.44	1.38	0.56	5.64	4.95	1.21
6	0.20	0.43	1.29	0.57	5.49	4.86	1.21
7	0.25	0.44	0.91	0.56	4.97	4.46	1.21
8	0.30	0.53	0.73	0.47	5.06	4.45	1.20
9	0.40	0.55	0.63	0.45	4.63	4.06	1.20
10	0.60	0.68	0.50	0.32	4.45	3.69	1.21
11	0.80	0.65	0.63	0.35	4.55	3.74	1.22
12	1.00	0.51	0.73	0.49	4.32	3.78	1.20
13	2.00	0.52	0.50	0.48	4.85	4.41	1.20
14	4.00	0.55	2.43	0.45	6.28	5.04	1.16
15	5.00	0.53	2.43	0.47	6.30	5.13	1.15
16	6.00	0.52	2.22	0.48	6.23	5.11	1.13
17	8.00	0.53	2.31	0.47	6.27	5.11	1.18
18	10.00	0.55	1.96	0.45	6.08	4.92	1.09

λ_{ex} = 300 nm, λ_{em} is the fluorescence peak maxima for each system.

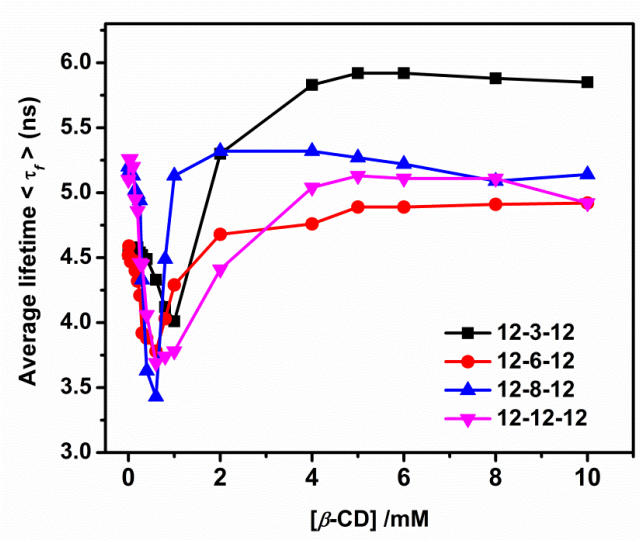

Figure 4.16. Change in average excited state lifetime of BSA (5.0 µM) in presence of 0.5 mM gemini surfactant, 12-*n*-12 with varying concentration of *β*-CD. λ_{ex} = 300 nm.

Circular dichroism (CD) measurements were also performed to examine the stripping process of surfactant molecules from BSA-gemini complexes upon addition of *β*-CD in the system. The addition of 0.5 mM of gemini surfactant leads to change in the CD spectrum for BSA and then *β*-CD was added to monitor whether the CD spectrum of

BSA corresponds to its native state. Far-UV CD spectra for BSA-12-3-12 gemini complexes before and after the addition of β-CD are shown by Figure 4.17. It has been noted that even in the presence of high concentration of β-CD the spectrum is not exactly similar to that of the native BSA, but is closer to the spectrum of BSA in the presence of very less amount of a gemini surfactant. During the stripping process, the unfolded protein molecule gets refolded step-by-step, and tries to refold in native form before the surfactant molecules are finally removed. Variation in the % of α-helix of BSA in presence of 0.5 mM of 12-*n*-12 at varying concentrations of β-CD is given in Figure 4.18.

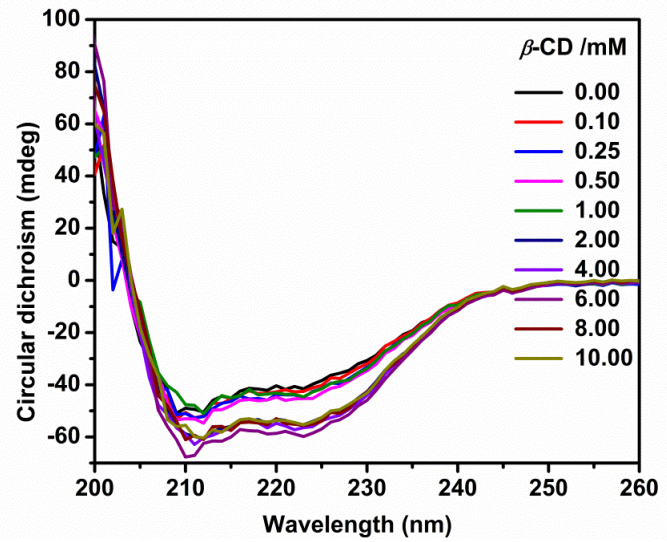

Figure 4.17. Far-UV circular dichroism spectra for BSA–12-3-12 complexes before and after addition of β-CD.

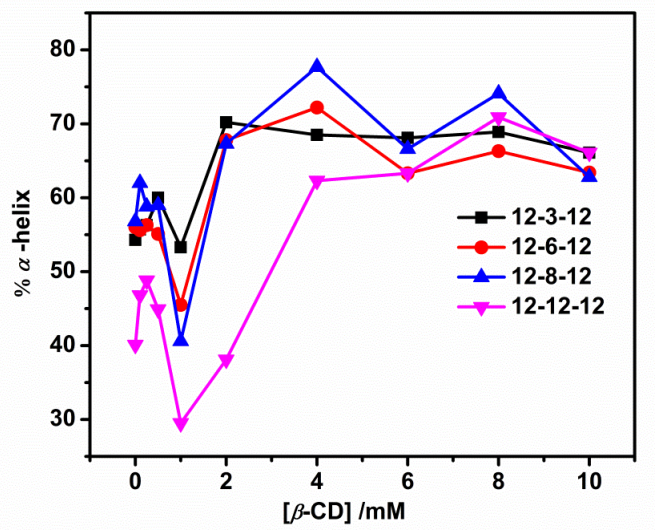

Figure 4.18. Variation in the % of α-helix of BSA (5.0 µM) in presence of 0.5 mM of 12-*n*-12 at varying concentrations of β-CD.

Table 4.8. Various components of the secondary structure of BSA (5.0 μM) in presence of 0.5 mM of 12-*n*-12 at varying concentrations of *β*-CD calculated from the CD spectra.

***β*-CD /mM**	**α-Helix**	***β*-Sheet**		***β*-turn**	**Random coil**
		Anti-parallel	**Parallel**		
			12-3-12		
0.00	54.3	4.2	5.2	13.4	22.8
0.10	55.7	4.0	5.0	13.2	22.6
0.25	56.3	3.9	4.9	13.1	22.1
0.50	60.0	3.4	4.3	12.5	20.2
1.00	53.3	4.3	5.4	13.4	24.4
2.00	70.2	2.4	3.3	11.1	16.9
4.00	68.5	2.5	3.5	11.3	17.3
6.00	68.1	1.9	2.8	10.3	15.0
8.00	68.9	2.4	3.5	11.2	17.9
10.00	66.1	2.7	3.8	11.6	18.6
			12-6-12		
0.00	56.0	4.0	5.0	13.2	22.3
0.10	55.6	4.1	5.0	13.3	22.5
0.25	56.3	3.9	4.9	13.1	22.1
0.50	55.1	4.0	5.2	13.2	23.7
1.00	45.5	5.5	6.7	14.5	28.2
2.00	67.8	2.5	3.7	11.3	18.5
4.00	72.2	2.1	3.2	10.7	16.9
6.00	63.3	3.0	4.2	11.9	20.4
8.00	66.3	2.7	3.8	11.5	19.2
10.00	63.4	3.0	4.1	11.9	20.1
			12-8-12		
0.00	56.8	3.9	4.9	13.2	21.8
0.10	62.0	3.3	4.4	12.4	20.5
0.25	58.8	3.6	4.7	12.7	21.9
0.50	59.0	3.6	4.7	12.8	21.7
1.00	40.6	6.4	7.6	15.3	31.0
2.00	67.3	2.6	3.7	11.4	18.8
4.00	77.7	1.7	2.7	9.9	14.5
6.00	66.6	2.7	3.7	11.6	18.0
8.00	74.1	2.0	2.9	10.5	15.3
10.00	62.8	3.0	4.2	12.0	20.6
			12-12-12		
0.00	40.1	6.7	7.5	15.6	29.8
0.10	46.8	5.5	6.3	14.6	26.0
0.25	48.8	5.1	6.1	14.3	25.8
0.50	44.9	5.7	6.7	14.7	27.8
1.00	29.5	9.6	10.2	17.4	36.8
2.00	38.1	7.0	8.0	15.7	31.9
4.00	62.3	3.1	4.3	12.1	20.9
6.00	63.3	3.0	4.2	11.9	20.9
8.00	70.9	2.3	3.4	10.9	17.4
10.00	66.1	2.7	3.8	11.6	18.6

It has been observed that the capability of *β*-CD to start the recovery of the protein depends on the molar ratio between the surfactant and *β*-CD. When the surfactant-*β*-CD

ratio is 1:1, recovery of the protein is not achieved. Table 4.8 expresses the various components of the secondary structure of BSA in presence of 0.5 mM of 12-*n*-12 at varying concentrations of *β*-CD, calculated from the CD spectra.

Above mentioned fluorescence study on denaturation of protein states that at 0.5 mM of a gemini surfactant, the dependence of efficiency to create a less polar environment around Trp residues on spacer group through the formation of micelles along the protein chain follows the order: 12-3-12 < 12-6-12 < 12-8-12 ~ 12-12-12. Thus it depicts that Trp residues feel more hydrophobic environment with increasing spacer chain length of gemini surfactants taking part in micelles formation. As described above the refolding study has been done at 0.5 mM of a gemini surfactant with varying concentration of *β*-CD. As far as refolding study is concerned, the initial decrease in F/F_o, quantum yield and % of *α*-helix values due to the addition of *β*-CD in presence of different gemini surfactants follows the order: 12-3-12 < 12-6-12 < 12-8-12 < 12-12-12. Therefore, the dissociation of protein-micelle aggregates by the use of a particular concentration of *β*-CD is found to be more in case of a gemini surfactant with highly hydrophobic spacer group or spacer group with a long chain. It indicates that gemini surfactant molecules taking part in micelle formation along the protein chain can easily be taken out by *β*-CD molecules when they have got a long spacer chain. It could be due to the fact that the tail(s) of a gemini surfactant molecule with a long flexible spacer chain can more easily be entered into the hydrophobic pocket of a *β*-CD molecule. Our earlier study says that *β*-CD molecules at high concentration form nanotubes/rods in presence of hydrophobic guest molecules which in this case are surfactant molecules.[77]

DLS measurements show that the sizes of these particles in presence of 0.5 mM of each of 12-3-12, 12-6-12, 12-8-12 and 12-12-12 in a system containing 5.0 μM of BSA and 2.0 mM of *β*-CD are 256±21 nm, 887±111 nm, 981±162 nm and 1021±192 nm, respectively (Figure 4.19). Thus when surfactant molecules are stripped off by *β*-CD molecules, the complexes formed between *β*-CD molecules and surfactant molecules are mostly secondary aggregates of nanotubes (rods) where in each nanotube, *β*-CD molecules are threaded onto the hydrophobic tail(s) of a gemini molecule depending on the concentration of *β*-CD.[76, 78] The sizes of these rods are in support of the fact that the gemini molecules with a longer spacer chain are more easily stripped off by *β*-CD molecules forming bigger structures. On the other hand the gain of native state of BSA by stripping off the remaining surfactant molecules after the protein-micelle aggregates have got

dissociated is occurred with an order as follows: 12-12-12 < 12-8-12 < 12-6-12 < 12-3-12 which is opposite to that of the stripping process from the protein-micelle aggregates. F/F_o value can reach up to 0.95 in presence of 12-3-12, while for the rest of the gemini surfactants, 12-6-12, 12-8-12, and 12-12-12 it has not been obtained up to that extent. The trend in the change in fluorescence peak maxima in this case is just opposite to that in the unfolding process of BSA. In presence of 12-3-12, the recovery of peak maximum is up to 347 nm, which is very close to the peak maximum of native BSA i.e. 348 nm. At the higher concentration of the *β*-CD, maximum regain in the excited state lifetime of Trp occurs in presence of 12-3-12 which is also in support of the fact that maximum gain in native state occurs in case of binding with 12-3-12. The trends in changes in fluorescence quantum yield, fluorescence lifetime as well as % of *α*-helix with increasing concentration of *β*-CD are also similar to that of fluorescence intensity ratio, F/F_o.

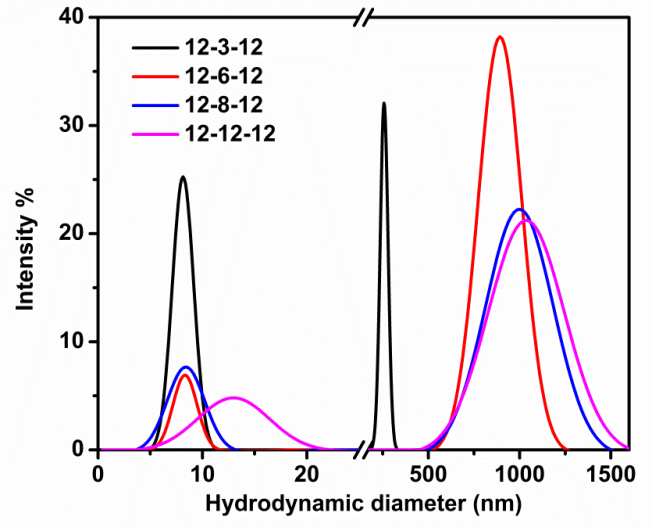

Figure 4.19. The size distribution plot of the BSA (5.0 µM) + 12-*n*-12 (0.5 mM) + *β*-CD (2.0 mM) acquired by dynamic light scattering (DLS) measurement.

Zana *et al*. have reported that 12-3-12 molecules can form wormlike micelles.[28, 79, 80] Present study shows that 12-3-12 micelles provide with less polar environment to Trp residues of protein chain. 12-3-12 molecules, at low concentration range, denature protein molecules most effectively due to the formation of larger-sized pre-micellar aggregates. However, at high concentration range they might form wormlike micelles those remain in the bulk. Thus smaller number of 12-3-12 gemini surfactant molecules those are bound to the protein molecules can easily be taken out by *β*-CD molecules. As a result of that in case of 12-3-12 surfactant the refolding of the protein occurs more easily as compared to gemini surfactant with comparatively longer spacer group. To further support this we have

collected DLS data. As per DLS data the sizes of aggregates formed by 5.0 μM of BSA and 0.5 mM of each of 12-3-12, 12-6-12, 12-8-12 and 12-12-12 (i.e. BSA-micelles aggregate) are 19.8±7.2 nm, 13.0±3.8 nm, 13.9 ±5.8 nm and 23.6±4.6 nm, respectively (Figure 4.20). Except for 12-12-12, for each of the other surfactants, the size is larger than that with 0.1 mM of a surfactant. From these results it is noteworthy that (i) 12-12-12 micelles-BSA aggregate is smaller than 12-12-12-BSA aggregate i.e. the binding of individual 12-12-12 surfactant molecules makes the protein structure more open as compared to binding of 12-12-12 micelles; (ii) the particle of size of 19.8 nm in presence of 0.5 mM of 12-3-12 could be the aggregate of BSA-wormlike micelles rather than BSA-spherical micelles as it may be the cases for other three surfactants. After addition of 2.0 mM of β-CD the sizes of protein particles are found to be 8.1±0.9 nm, 8.2±1.0 nm, 8.3±1.6 nm and 12.6±3.2 nm for gemini surfactants, 12-3-12, 12-6-12, 12-8-12 and 12-12-12, respectively (Figure 4.19). The size of the native BSA (5 μM) is 8.1 nm (Figure 4.5). Thus, the sizes of the protein particles in presence of each of 12-3-12, 12-6-12 and 12-8-12 are similar to that of native protein or protein with a very low concentration of surfactant. However, larger size with 12-12-12 as compared to other three surfactants indicate that in presence of the former the protein is still in denatured state and re-naturation is faster in presence of the latter. The data obtained from fluorescence as well as CD-spectra measurements with comparatively higher concentration of β-CD infer that the added β-CD cannot remove the gemini molecules bound to high energy binding sites of BSA via specific interactions. Thus, the secondary structure of the native BSA is only partially recovered.

Figure 4.21 represents FESEM images of native BSA (Figure 4.21a), BSA with 0.5 mM of 12-3-12 (Figure 4.21b) and BSA with 0.5 mM of 12-3-12 and varying concentrations of β-CD (Figure 4.21c-e). In presence of 0.5 mM of 12-3-12 in BSA, although the denatured proteins are not clearly visible, but the micellar structures can be seen in Figure 4.21b. After addition of different concentrations of β-CD to the protein denatured by 0.5 mM of 12-3-12, the changes in the systems are shown by Figure 4.21c-e as representatives. With increasing concentration of β-CD more and more surfactants molecules are stripped off from the protein-micelle complexes. As a result of it progressively bigger structures like nanotubes and secondary aggregates of nanotubes are formed by β-CD and surfactant molecules with greater extent of efficiency. It is noteworthy that none of these FESEM images would be the actual representation of what

is happening in the solution phase discussed above as the images are taken in the solid phase. However, it is expected that the representation may not be completely different from that in the solution phase.

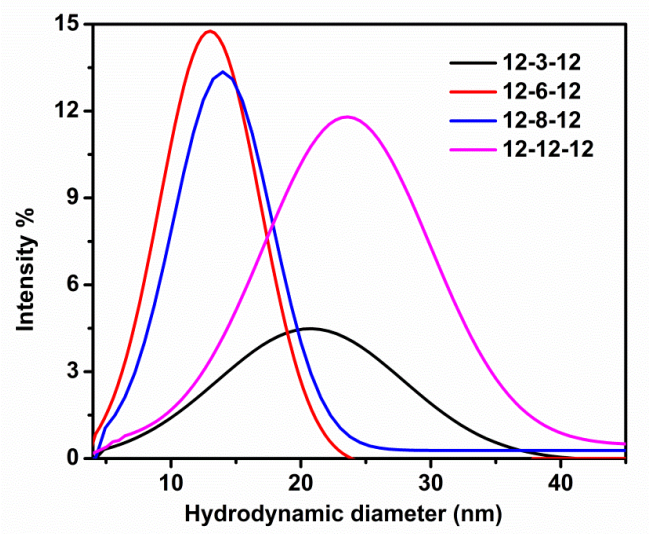

Figure 4.20. The size distribution graph of the BSA (5.0 µM) + 12-*n*-12 (0.5 mM), acquired by dynamic light scattering (DLS) measurement.

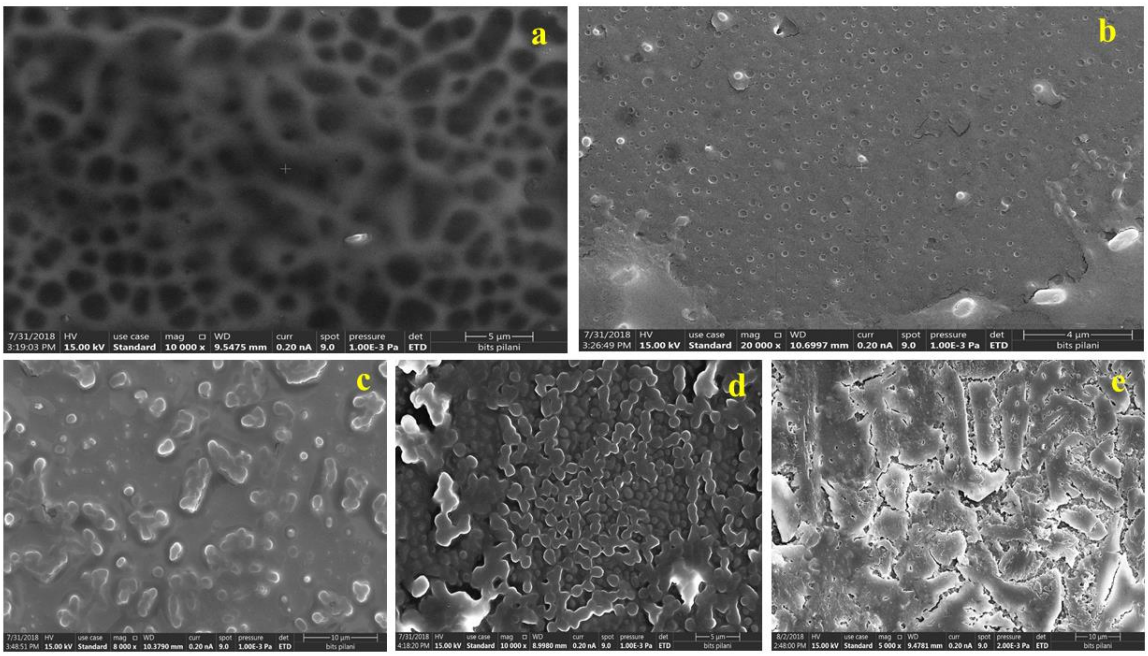

Figure 4.21. FESEM images of native BSA (5.0 µM) and BSA in presence of 12-3-12 and *β*-CD: (a) native BSA, (b) BSA + 0.5 mM 12-3-12, (c) BSA + 0.5 mM 12-3-12 + 0.2 mM *β*-CD, (d) BSA + 0.5 mM 12-3-12 + 1.0 mM *β*-CD, (e) BSA + 0.5 mM 12-3-12 + 8.0 mM *β*-CD.

4.2.3 Refolding of denatured BSA by using SDS through formation of catanion (mixed micelles, vesicles etc.)

4.2.3.1 Steady-state fluorescence

Cationic–anionic mixtures of surfactants form a clear homogeneous solution at all concentration range except for equimolar mixture which gives a heterogeneous system. This type of phase behavior has been explained in terms of distinct composition of micelles with different concentrations.[48, 81] It has been observed that for non-equimolar mixtures, mixed micelles formed because of strong electrostatic attraction between oppositely charged head groups remain in the solution due to the residual charge. However, for an equimolar mixture, mixed micelles formed are uncharged resulting in the formation of particles of large size those get precipitated out.[48]

SDS molecules form mixed micelles with cationic gemini surfactant molecules since they have got negatively charged headgroups, opposite to the charges on the headgroups of gemini surfactants. Protein molecules in presence of gemini surfactants get unfolded. SDS molecules added to this BSA-gemini system should extract gemini surfactant molecules through the formation of mixed micelles, consequently, BSA molecules would be free from gemini surfactants and should move to its native form. Keeping this phenomenon in mind, the present study has been carried out by the addition of varying concentration of SDS to a system of a fixed concentration of BSA (5 μM) and 0.5 mM of each of gemini surfactants, 12-*n*-12, at which aggregates are formed between micelles and unfolded BSA molecules. Figure 4.22 represents the changes in fluorescence spectra of the BSA (5.0 μM) with 12-3-12 gemini surfactant (0.5 mM) with the addition of varying concentrations of SDS as representative one. Figure 4.23 illustrates the plot of fluorescence intensity ratio, F/F_o versus SDS concentration. It has been found that with the variation in the concentration of the SDS in this system, the fluorescence intensity ratio, F/F_o is first increased (0.05-0.3 mM depending on the type of gemini surfactants) and then decreased, after reaching a minimum (0.8-1.0 mM depending on gemini surfactants) again it (1.0-2.5 mM depending on the type of gemini surfactants) starts to increase. This profile is similar to that as observed in case of refolding by β-CD molecules. Thus results indicate that SDS molecules are capable of refolding BSA denatured by gemini surfactants. However, beyond the concentration range of 2.0-2.5 mM, continuous decrease in the F/F_o ratio has been noticed. It depicts that at this high concentration, the

SDS molecules themselves act as a protein denaturant.[18, 21] It is noteworthy that the efficiency of SDS molecules to strip the gemini molecules out from the BSA-gemini aggregates is maximum with molar ratio of Gemini:SDS as 1:2. However, we are unable to study the stripping process at this molar ratio of gemini and SDS due to the occurrence of precipitation. Fluorescence peak maxima data are given in Table 4.9.The trend in variation of fluorescence peak maxima is just the reverse of the unfolding process of BSA which is shown by Figure 4.24. This trend corroborates well with the fluorescence intensity change.

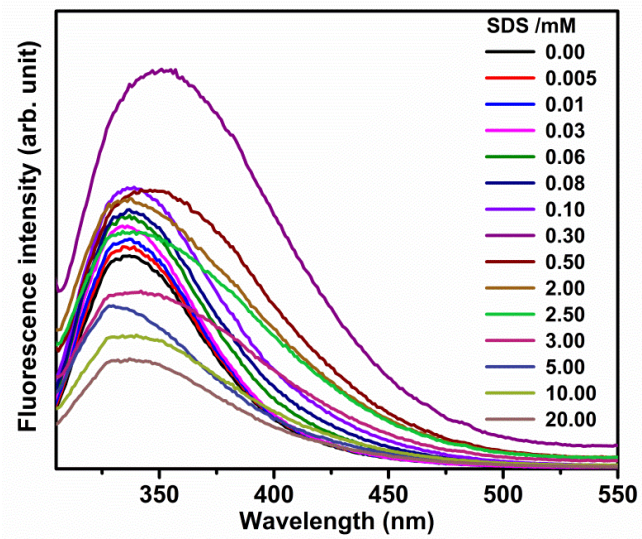

Figure 4.22. Changes in the fluorescence spectra of BSA (5.0 µM) in 12-3-12 surfactant (0.5 mM) with the addition of varying concentrations of SDS. λ_{ex} = 295 nm

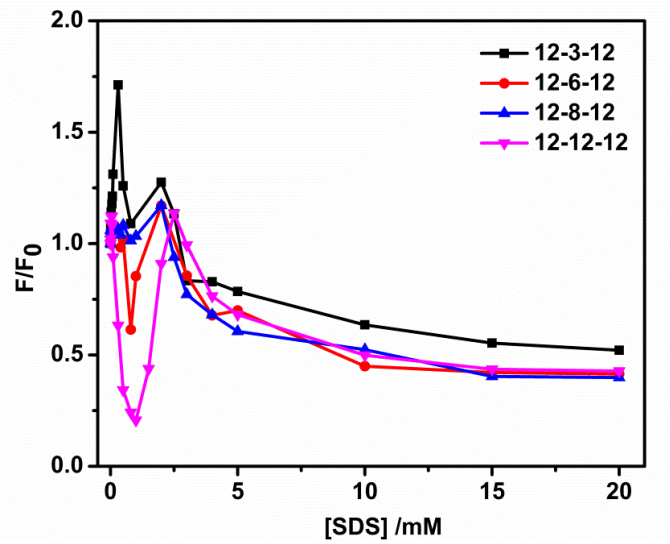

Figure 4.23. Changes in the fluorescence intensity of BSA (5.0 µM) in presence of 0.5 mM gemini surfactant, 12-*n*-12 with increasing concentration of SDS. λ_{ex} = 295 nm.

Table 4.9. Fluorescence peak maxima of BSA (5.0 µM) in presence of 0.5 mM of 12-*n*-12 and different concentrations of SDS. λ_{ex} = 295 nm

Sr. No.	SDS (mM)	12-3-12 λ_{max}^{flu} (nm)	SDS (mM)	12-6-12 λ_{max}^{flu} (nm)	SDS (mM)	12-8-12 λ_{max}^{flu} (nm)	SDS (mM)	12-12-12 λ_{max}^{flu} (nm)
1	0.000	336	0.000	337	0.000	337	0.000	339
2	0.005	336	0.005	337	0.005	337	0.005	339
3	0.010	336	0.010	337	0.010	337	0.010	339
4	0.030	336	0.030	338	0.030	337	0.030	338
5	0.060	337	0.060	338	0.060	337	0.060	338
6	0.080	337	0.080	338	0.080	339	0.080	338
7	0.100	338	0.100	338	0.100	339	0.100	339
8	0.300	347	0.200	339	0.300	337	0.300	339
9	0.500	346	0.300	339	0.500	340	0.500	340
10	2.000	335	0.400	338	0.800	338	0.800	343
11	2.500	335	0.500	338	1.500	348	2.500	334
12	4.000	332	0.800	341	2.500	333	3.000	333
13	5.000	332	1.000	349	3.000	333	4.000	334
14	10.000	335	2.000	338	4.000	333	5.000	334
15	15.000	336	3.000	335	5.000	333	10.000	334
16	20.000	336	4.000	332	10.000	333	15.000	335
17			5.000	332	15.000	334	20.000	336
18			10.000	332	20.000	334		
19			15.000	333				
20			20.000	334				

To further support the refolding process of BSA, the CD spectra have also been recorded. The CD spectra for BSA + 12-12-12 (0.5 mM) system in presence of different concentrations of SDS are shown by Figure 4.25 as a representative. Table 4.10 indicates the various components of the secondary structure of BSA in presence of 0.5 mM of 12-*n*-12 at varying concentrations of SDS calculated from the CD spectra. Figure 4.26 exhibits the variation in the % of α-helix of BSA in presence of 0.5 mM of 12-*n*-12 at varying concentrations of SDS. % of α-helix data show the reverse trend of the BSA unfolding process and the trend is same as that for change in F/F_o versus SDS concentration. Both the plots of F/F_o versus SDS concentration (Figure 4.23) and % α-helix versus SDS concentration (Figure 4.26) show that SDS molecules have greatest affinity towards 12-12-12 and least affinity towards 12-3-12. The increasing order with which the SDS molecules strip the gemini molecules out from the Gemini-BSA aggregates is as follows:

12-3-12 < 12-8-12 < 12-6-12 < 12-12-12. The average sizes of BSA-SDS aggregates in presence of SDS in the range of 0.06 mM to 0.1 mM obtained from DLS measurements are found to be 8.2±0.6 nm, 12.2±0.8 nm, 11.9±1.4 nm and 22.2±3.6 nm for 12-3-12, 12-6-12, 12-8-12 and 12-12-12, respectively.

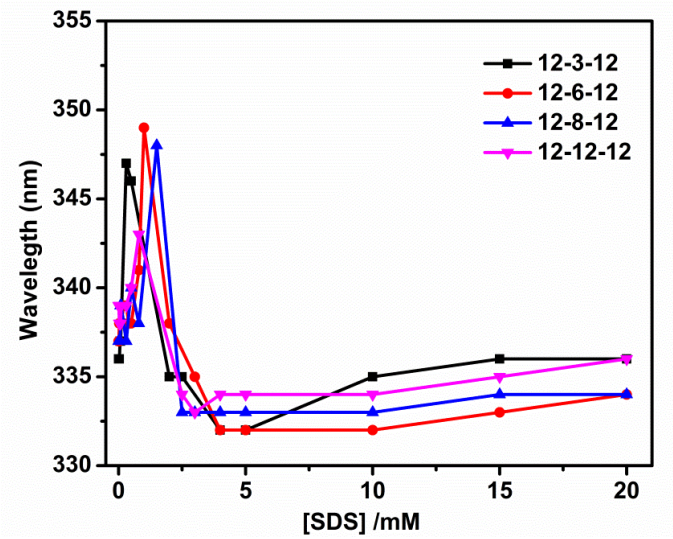

Figure 4.24. Change in the fluorescence peak maxima of BSA (5.0 µM) in presence of 0.5 mM gemini surfactant, 12-*n*-12 at varying concentrations of SDS. λ_{ex} = 295 nm.

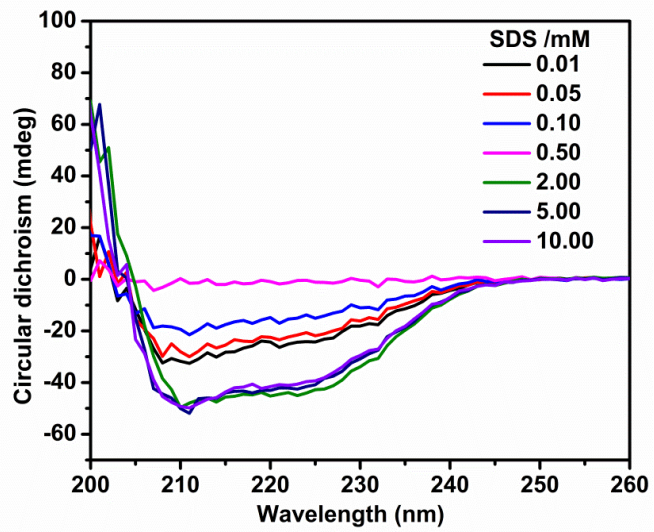

Figure 4.25. Far-UV CD spectra for BSA (5.0 µM) in presence of 0.5 mM of 12-12-12 at varying concentrations of SDS.

This is the concentration range at which SDS molecules strip off some of the gemini molecules from BSA-gemini micelles aggregates. In addition, Gemini-SDS aggregates are also formed. The average sizes of these Gemini-SDS aggregates are found to be 104±13 nm, 253±42 nm, 300±47 nm and 620±68 nm in presence of 12-3-12, 12-6-

12, 12-8-12 and 12-12-12, respectively. The average sizes are reported here because the particle sizes are not reproducible. As per literature report in absence of protein these aggregates of SDS and gemini surfactants could be rod-like micelles, lamellar micelles, vesicles, etc.[82-85] In fact the existence of these kind of structures even at very low concentration of catanion is reported in the literature.[86] The efficiency of SDS molecules to strip off the gemini molecules in some way must be correlated with the sizes of the partially denatured protein and Gemini-SDS aggregates which is evidenced by the above mentioned DLS data. The increasing order of sizes of these partially denatured protein particles and Gemini-SDS aggregates (except for SDS-12-6-12 micelles) are same as the increasing order of efficiency with which SDS molecules strip off the gemini molecules (discussed above based on fluorescence and CD data). Higher the affinity of SDS molecules towards gemini molecules for the formation of mixed micelles kind of structures greater would the efficiency of SDS molecules to strip off the gemini molecules from BSA-gemini micelles complexes.

As mentioned above the trend for changes in % α-helix with SDS concentration is same as that of fluorescence data. It is expected that when SDS molecules will have high affinity towards gemini molecules associated with the BSA protein (eg. 12-12-12), due to a great extent of stripping, the system will contain unfolded protein chains without any micelles associated with them. This is the state at which the unfolding of protein molecules would be maximum giving minimum % of α-helix (minima in Figure 4.26). It is noteworthy that although at this state no micelles formation is there along the protein chain, however, some surfactant molecules are still bound with the protein chain as it happened during the denaturation process. At this stage, as a result of the maximum exposure of the Trp residues of the protein chain the fluorescence intensity would be minimum (Figure 4.23). With further increasing concentration of SDS beyond the minimum, more mixed micelles, vesicles etc. would be formed between SDS and gemini surfactant molecules which will lead to the re-naturation of protein through the refolding of protein chain. During this process protein molecules move to their native state as a result of that % α-helix increases (Figure 4.26). Also, the Trp residues feel more hydrophobic environment and because of that fluorescence intensity increases.

Results show that once the protein molecules attain the saturation of their native state, with the addition of further surfactant molecules again the denaturation of protein is

started. It is to be noted from Figure 4.23 that initially at very low concentration range of SDS there is a little increase in the fluorescence intensity without any change in % α-helix. This could be because of the fact that SDS molecules form mixed micelles with the gemini molecules even in the binding state along the protein chain. Thus, Trp residues feel comparatively more nonpolar environment, which results in increase in fluorescence intensity. This increase is comparatively more significant in case of 12-3-12. It further supports the fact that in case of 12-3-12 there are interactions between wormlike micelles and BSA which was evidenced by DLS data as well. This kind of binding of SDS molecules at low concentration with BSA, however, does not change any secondary structure of protein showing no change in % α-helix.

Table 4.10. Various components of the secondary structure of BSA (5.0 µM) in presence of 0.5 mM of 12-*n*-12 at varying concentrations of SDS calculated from the CD spectra.

SDS /mM	α-Helix	β-Sheet		β-turn	Random coil
		Anti-parallel	Parallel		
		12-3-12			
0.05	53.2	4.4	5.5	13.7	23.8
0.10	47.0	5.4	6.3	14.5	26.5
0.50	54.7	4.1	5.3	13.2	23.9
5.00	53.9	4.2	5.3	13.4	23.7
10.00	49.8	5.0	5.6	14.2	23.9
		12-6-12			
0.05	47.0	5.3	6.3	14.5	26.4
0.10	46.4	5.5	6.4	14.6	26.6
0.50	31.8	8.8	9.5	16.9	35.3
2.00	60.5	3.3	4.6	12.3	22.2
5.00	56.8	3.8	5.0	13.0	22.8
10.00	53.1	4.4	5.4	13.6	23.6
		12-8-12			
0.01	47.5	5.3	6.3	14.4	26.6
0.05	46.8	5.4	6.4	14.5	27.1
0.50	50.7	4.8	5.8	14.0	25.1
5.00	60.2	3.3	4.6	12.3	22.3
10.00	35.9	7.7	8.4	16.3	32.4
		12-12-12			
0.01	30.3	9.4	9.7	17.3	35.2
0.05	28.6	10.0	10.3	17.7	36.8
0.10	23.4	12.2	12.3	18.9	41.3
0.50	13.3	19.8	18.8	22.1	53.0
2.00	54.7	4.0	5.4	13.0	25.0
5.00	56.8	3.9	5.0	13.0	22.6
10.00	54.9	4.2	5.1	13.4	22.7

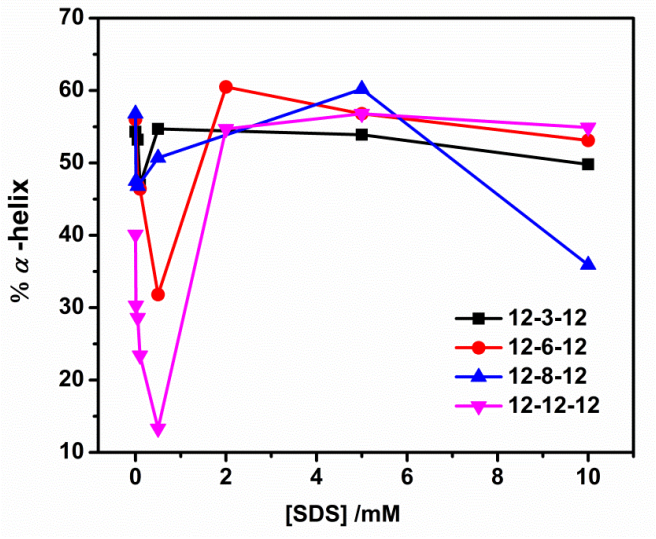

Figure 4.26. Variation in the % of α-helix of BSA (5.0 µM) in presence of 0.5 mM of 12-*n*-12 at varying concentrations of SDS.

To monitor the morphological changes occurring after adding different concentrations of SDS in the system containing 5 µM of BSA and 0.5 mM of 12-3-12 as representatives, the FESEM images have been recorded and are presented by Figure 4.27a-c. One can see that both the size and the number of particles increase with increasing concentration of SDS. It depicts that more the number of SDS molecules present in the system greater would be the stripping of gemini molecules from BSA-gemini complexes. As a result of that larger would be the size of a particles and also number of particles formed by SDS and gemini surfactant molecules. These particles seem to be vesicles, multi-lamellar micelles, multi-lamellar vesicles *etc.* depending on the concentration of SDS which are in accordance with the literature report.[100-101]

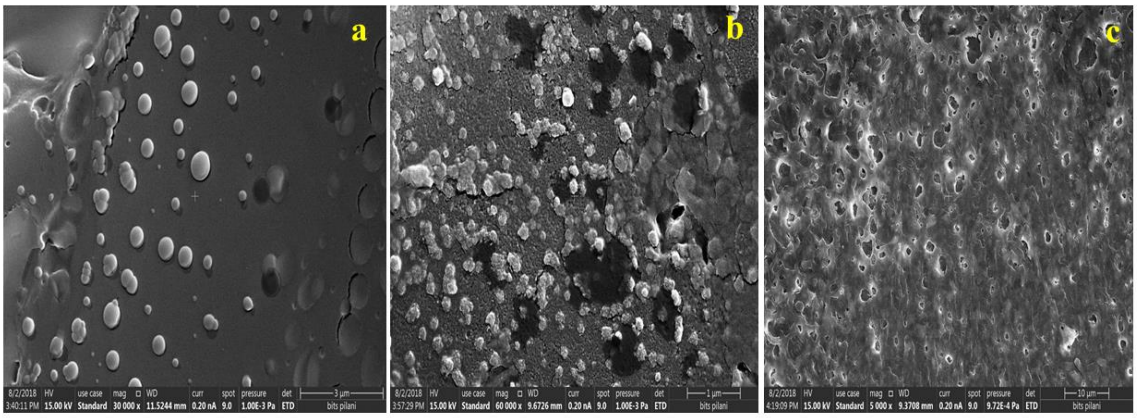

Figure 4.27. FESEM images of BSA (5.0 µM) in presence of 12-3-12 and SDS: (a) BSA + 0.5 mM 12-3-12 + 0.1 mM SDS, (b) BSA + 0.5 mM 12-3-12 + 0.5 mM SDS, and (c) BSA + 0.5 mM 12-3-12 + 10.0 mM SDS.

4.3 Conclusions

Gemini surfactants, 12-*n*-12, each with two hydrophobic tails, one polymethylene spacer group and double charges (headgroups), can interact intensely with BSA via electrostatic and hydrophobic forces, which leads to change in the fluorescence spectra of proteins due to changes in the polarity of microenvironments of Trp residues. At low concentration range of surfactants (~ 0.1 mM), the decrease in the fluorescence intensity follows the order as 12-8-12 < 12-6-12 < 12-3-12 < 12-12-12. The decrease in α-helix of the protein is more with decreasing hydrophobicity/chain length of the spacer group. It could be due to the interaction between the protein and larger-sized pre-micellar aggregates formed by gemini molecules with short spacer chains. However, the unusual decrease in α-helix found in case of 12-12-12 could be because of highly hydrophobic interaction between protein and long hydrophobic spacer chain and also could be due to the formation of a loop by the long flexible spacer chain in it. At comparatively higher concentration range of surfactants (~0.5 mM), micelles are formed along the protein chain creating comparatively higher hydrophobicity around the Trp residues. The dependence of efficiency to create hydrophobic environment on spacer group via the formation of micelles along the protein chain is found to follow the order: 12-3-12 < 12-6-12 < 12-8-12~12-12-12 i.e. with increasing hydrophobicity of the spacer group the environment around Trp residues becomes less polar. This result supports the formation of necklace-bead kind of structures. Fluorescence lifetime data reveal that at low concentration range of surfactants, during denaturation of the protein, the Trp residues get exposed to the more polar water phase and at the same time more surfactant molecules interact with Trp which results in disturbance of the planarity of indole ring that is present in Trp amino acid. The unfolded protein molecule can get refolded step-by-step by the stripping process with β-CD as well as with SDS. The efficiency of β-CD to strip the different gemini surfactant molecules follows the order: 12-3-12 < 12-6-12 < 12-8-12 < 12-12-12 which is an increasing order of chain length of the spacer group. Therefore, with increasing chain length of the spacer group of a gemini surfactant molecule, the binding efficiency with β-CD molecules is increased. It could be due to the fact that the tail(s) of a gemini surfactant molecule containing a long flexible spacer chain can more easily be entered into the hydrophobic pocket of a β-CD molecule forming simple inclusion complexes or nanotubes/rods where β-CD molecules are threaded onto the tails. However, once the protein-micelles aggregates are dissociated, the gemini surfactant molecules with a short

spacer chain like 12-3-12 can more easily be taken out by β-CD molecules. This could be due to less effective binding of wormlike micelles formed by 12-3-12 with the protein. Initially at a low concentration, probably β-CD molecules bind with the BSA-micelle aggregates thereby providing with comparatively less polar environment around the Trp residues of BSA. Results show that β-CD cannot remove the gemini surfactant molecules bound to high energy binding sites of BSA through specific interactions. The secondary structure of the native BSA is only partially recovered. The refolding of the protein unfolded by gemini surfactants has also been done by SDS through the formation of catanion (mixed micelles, vesicles etc.). The increasing efficiency of SDS molecules to strip the gemini molecules out from the Gemini-BSA aggregates follows the order: 12-3-12 < 12-8-12 < 12-6-12 < 12-12-12. At a low concentration range of SDS, a marginal structural regain to the native BSA through the formation of catanion micelles, vesicles etc. are occurred. However, SDS again unfolds the BSA at a comparatively higher concentration. Initially at a very low concentration, SDS molecules form mixed micelles with gemini molecules those are bound along the protein chain without making any change in secondary structure of the protein. Results show that the mechanism of unfolding and subsequent refolding is reversible in nature, although, the protein does not regain its full native structure. β-CD and SDS induced refolding of protein tuned by the polymethylence spacer chain length of gemini surfactants can find some useful applications in various filelds.

References

1. A. Latnikova, S.-Y. Lin, G. Loglio, R. Miller and B. Noskov, *J. Phys. Chem. C*, 2008, **112**, 6126-6131.
2. S.-C. Wang and C. T. Lee, *Biochemistry*, 2007, **46**, 14557-14566.
3. A. Liljas, *Science*, 1999, **285**, 2077-2078.
4. Q. Xu and T. A. Keiderling, *Proteins*, 2006, **63**, 571-580.
5. A. R. Kinjo and S. Takada, *Biophys. J.*, 2003, **85**, 3521-3531.
6. T. K. Chaudhuri and S. Paul, *FEBS J.*, 2006, **273**, 1331-1349.
7. D. Rozema and S. H. Gellman, *J. Am. Chem. Soc.*, 1995, **117**, 2373-2374.
8. A. Tobitani and S. B. Ross-Murphy, *Macromolecules*, 1997, **30**, 4845-4854.
9. S. Gani, D. Mukherjee and D. Chattoraj, *Langmuir*, 1999, **15**, 7139-7144.
10. L.-T. Lee, B. K. Jha, M. Malmsten and K. Holmberg, *J. Phys. Chem. B*, 1999, **103**, 7489-7494.

11. A. Stenstam, G. Montalvo, I. Grillo and M. Gradzielski, *J. Phys. Chem. B*, 2003, **107**, 12331-12338.
12. K. K. Andersen, P. Westh and D. E. Otzen, *Langmuir*, 2008, **24**, 399-407.
13. M. F. Engel, A. J. Visser and C. P. van Mierlo, *Langmuir*, 2003, **19**, 2929-2937.
14. A. Stenstam, D. Topgaard and H. Wennerström, *J. Phys. Chem. B*, 2003, **107**, 7987-7992.
15. Y. Li, X. Wang and Y. Wang, *J. Phys. Chem. B*, 2006, **110**, 8499-8505.
16. J.-M. Jung, G. Savin, M. Pouzot, C. Schmitt and R. Mezzenga, *Biomacromolecules*, 2008, **9**, 2477-2486.
17. R. Das, D. Guha, S. Mitra, S. Kar, S. Lahiri and S. Mukherjee, *J. Phys. Chem. A*, 1997, **101**, 4042-4047.
18. N. J. Turro, X.-G. Lei, K. Ananthapadmanabhan and M. Aronson, *Langmuir*, 1995, **11**, 2525-2533.
19. A. D. Nielsen, K. Borch and P. Westh, *Biochim. Biophys. Acta Protein Struct. Mol. Enzymol.*, 2000, **1479**, 321-331.
20. E. Gelamo, C. Silva, H. Imasato and M. Tabak, *Biochim. Biophys. Acta Protein Struct. Mol. Enzymol.*, 2002, **1594**, 84-99.
21. S. F. Santos, D. Zanette, H. Fischer and R. Itri, *J. Colloid Interface Sci.*, 2003, **262**, 400-408.
22. D. Kelley and D. McClements, *Food Hydrocoll.*, 2003, **17**, 73-85.
23. S. De, A. Girigoswami and S. Das, *J. Colloid Interface Sci.*, 2005, **285**, 562-573.
24. N. Gull, S. Chodankar, V. Aswal, P. Sen and R. H. Khan, *Colloids Surf. B Biointerfaces*, 2009, **69**, 122-128.
25. F. M. Menger and C. Littau, *J. Am. Chem. Soc.*, 1991, **113**, 1451-1452.
26. M. J. Rosen, *J. Chemtech.*, 1993, 30-30.
27. F. Menger and C. Littau, *J. Am. Chem. Soc.*, 1993, **115**, 10083-10090.
28. R. Zana, *J. Colloid Interface Sci.*, 2002, **248**, 203-220.
29. N. Gull, P. Sen and R. H. Khan, *Langmuir*, 2009, **25**, 11686-11691.
30. D. Wu, G. Xu, Y. Sun, H. Zhang, H. Mao and Y. Feng, *Biomacromolecules*, 2007, **8**, 708-712.
31. D. Wu, G. Xu, Y. Feng and Y. Li, *Int. J. Biol. Macromol.*, 2007, **40**, 345-350.
32. Y. Pi, Y. Shang, C. Peng, H. Liu, Y. Hu and J. Jiang, *Biopolymers*, 2006, **83**, 243-249.
33. M. Jones, *Chem. Soc. Rev.s*, 1992, **21**, 127-136.

34. M. N. Jones, *Biochem. J.*, 1975, **151**, 109.
35. K. K. Andersen, C. L. Oliveira, K. L. Larsen, F. M. Poulsen, T. H. Callisen, P. Westh, J. S. Pedersen and D. Otzen, *J. Mol. Biol.*, 2009, **391**, 207-226.
36. Sonu, S. Halder, S. Kumari, R. Aggrawal, V. K. Aswal and S. K. Saha, *J. Mol. Liq.*, 2017, **243**, 369-379.
37. D. Rozema and S. H. Gellman, *Biochemistry*, 1996, **35**, 15760-15771.
38. R. Yazdanparast, M. A. Esmaeili and F. Khodagholi, *Int. J. Biol. Macromol.*, 2007, **40**, 126-133.
39. R. Yazdanparast, F. Khodagholi and R. Khodarahmi, *Int. J. Biol. Macromol.*, 2005, **35**, 257-263.
40. L. García-Río and A. Godoy, *J. Phys. Chem. B*, 2007, **111**, 6400-6409.
41. J. Szejtli, *Chem. Rev.*, 1998, **98**, 1743-1754.
42. Y. Liu, Y. Liu and R. Guo, *J. Sol. Chem.*, 2011, **40**, 1140-1152.
43. Y. Liu, Y. Liu and R. Guo, *J. Colloid Interface Sci.*, 2010, **351**, 180-189.
44. N. Gull, M. A. Mir, J. M. Khan, R. H. Khan, G. M. Rather and A. A. Dar, *J. Colloid Interface Sci.*, 2011, **364**, 157-162.
45. E. D. Goddard, *Interactions of Surfactants with Polymers and Proteins*, CRC press, 2017.
46. G. Zhao and B. Zhu, *J Dispersion Sci. Technol.*, 1995, **16**, 305-332.
47. G.-X. Zhao and J.-X. Xiao, *J. Colloid Interface Sci.*, 1996, **177**, 513-518.
48. J.-X. Xiao, U. Sivars and F. Tjerneld, *J. Chromatog. B Biomed. Sci. Appl.*, 2000, **743**, 327-338.
49. C. Tondre and C. Caillet, *Adv. Colloid Interface Sci.*, 2001, **93**, 115-134.
50. Y. Pi, Y. Shang, C. Peng, H. Liu, Y. Hu and J. Jiang, *Biopolymers*, 2006, **83**, 243-249.
51. M. Hu, X. Wang, H. Wang, Y. Chai, Y. He and G. Song, *Luminescence*, 2012, **27**, 204-210.
52. M. U. H. Mir, J. K. Maurya, S. Ali, S. Ubaid-Ullah, A. B. Khan and R. Patel, *Process Biochemistry*, 2014, **49**, 623-630.
53. R.-C. Lu, A.-N. Cao, L.-H. Lai, B.-Y. Zhu, G.-X. Zhao and J.-X. Xiao, *Colloids and Surfaces B: Biointerfaces*, 2005, **41**, 139-143.
54. V. I. Martín, A. Rodríguez, A. Maestre and M. L. Moyá, *Langmuir*, 2013, **29**, 7629-7641.
55. W. G. Liu, K. De Yao, G. C. Wang and H. X. Li, *Polymer*, 2000, **41**, 7589-7592.

56. E. Gelamo and M. Tabak, *Spectrochim. Acta A Mol. Biomol. Spectrosc.*, 2000, **56**, 2255-2271.
57. U. Anand and S. Mukherjee, *Phys. Chem. Chem. Phys.*, 2013, **15**, 9375-9383.
58. U. Anand, C. Jash and S. Mukherjee, *Phys. Chem. Chem. Phys.*, 2011, **13**, 20418-20426.
59. Y. Shu, M. Liu, S. Chen, X. Chen and J. Wang, *J. Phys. Chem. B*, 2011, **115**, 12306-12314.
60. S. Sinha, D. Tikariha, J. Lakra, T. Yadav, S. Kumari, S. K. Saha and K. K. Ghosh, *J. Mol. Liq.*, 2016, **218**, 421-428.
61. L. D'Alfonso, M. Collini and G. Baldini, *Biochemistry*, 2002, **41**, 326-333.
62. J. Hierrezuelo and C. C. Ruiz, *Mater. Sci. Eng. C*, 2015, **53**, 156-165.
63. J. M. Andreu and J. A. Munoz, *Biochemistry*, 1986, **25**, 5220-5230.
64. J. R. Lakowicz, in *Principles of fluorescence spectroscopy*, Springer, New York, 2006.
65. A. Szabo and D. Rayner, *J. Am. Chem. Soc.*, 1980, **102**, 554-563.
66. N. Sreerama and R. W. Woody, *Anal. Biochem.*, 2000, **287**, 252-260.
67. C. Sun, J. Yang, X. Wu, X. Huang, F. Wang and S. Liu, *Biophys. J.*, 2005, **88**, 3518-3524.
68. J. Corbin, N. Méthot, H. H. Wang, J. E. Baenziger and M. P. Blanton, *J. Biol. Chem.*, 1998, **273**, 771-777.
69. R. F. Chen, *Archiv. Biochem. Biophys.*, 1974, **160**, 106-112.
70. P. Bharmoria, K. S. Rao, T. J. Trivedi and A. Kumar, *J. Phys. Chem. B*, 2013, **118**, 115-124.
71. J. Mandeville and H. Tajmir-Riahi, *Biomacromolecules*, 2010, **11**, 465-472.
72. X. Shen, M. Belletête and G. Durocher, *Langmuir*, 1997, **13**, 5830-5836.
73. K. Shirahama, K. Tsujii and T. Takagi, *J. Biochem.*, 1974, **75**, 309-319.
74. J. A. Reynolds and C. Tanford, *J. Biol. Chem.*, 1970, **245**, 5161-5165.
75. K. Ananthapadmanabhan, in *Interactions of surfactants with polymers and proteins*, CRC Press, 2017, pp. 319-366.
76. A. J. Valente and O. Söderman, *Adv. Colloid Interface Sci.*, 2014, **205**, 156-176.
77. M. Sowmiya, P. Purkayastha, A. K. Tiwari, S. S. Jaffer and S. K. Saha, *J. Photochem. Photobiol. A Chem.*, 2009, **205**, 186-196.
78. R. Carvalho, H. Correia, A. Valente, O. Söderman and M. Nilsson, *J. Colloid Interface Sci.*, 2011, **354**, 725-732.

79. D. Danino, Y. Talmon and R. Zana, *Langmuir*, 1995, **11**, 1448-1456.
80. R. Zana, *Curr. Opin. Colloid Interface Sci.*, 1996, **1**, 566-571.
81. Z.-J. Yu and G.-X. Zhao, *J. Colloid Interface Sci.*, 1989, **130**, 421-431.
82. Y. Shang, H. Liu, Y. Hu and J. M. Prausnitz, *Colloids Surf. A Physicochem. Eng. Asp.*, 2007, **294**, 203-211.
83. Y. Shang, Y. Xu, H. Liu and Y. Hu, *J. Dispersion Sci. Technol.*, 2006, **27**, 105-108.
84. Y. Shang, Q. Chen and H. Liu, *J. Dispersion Sci. Technol.*, 2007, **28**, 854-859.
85. Y. Wang, G. Bai, E. F. Marques and H. Yan, *J. Phys. Chem. B*, 2006, **110**, 5294-5300.
86. D. Jurašin, I. Weber and N. Filipović-Vinceković, *J. Dispersion Sci. Technol.*, 2009, **30**, 622-633.

Chapter 5

Binding Interactions of Gemini Surfactants with Nanotubes of β-Cyclodextrin and Controlled Release of Guest Molecules: Effect of Spacer Chain Length and Concentration of Surfactants

---

Key Concepts:

- *Guest molecule (C-485) induced formation of nanotubes and secondary aggregates of β-cyclodextrin.*

- *Interaction of gemini surfactants with nanotubes of β-CD: Effect of spacer chain length, hydrophobic tails length and concentration of gemini surfactants on controlled release of the guest molecule.*

Binding Interactions of Gemini Surfactants with Nanotubes of β-Cyclodextrin and Controlled Release of Guest Molecules: Effect of Spacer Chain Length and Concentration of Surfactants

Abstract: *The formation of guest molecule (Coumarin 485, C-485) induced nanotubes by β-cyclodextrin (β-CD) and their interactions with cationic gemini surfactants (12-n-12, where n = 3, 6, and 12) have been explored by means of UV-visible absorption, steady-state fluorescence and fluorescence anisotropy, time-resolved fluorescence and fluorescence anisotropy, and dynamic light scattering (DLS) measurements. β-CD at its high concentration forms extended nanotubes and secondary aggregates of nanotubes. A gemini surfactant has a role on binding between C-485 and nanotubes of β-CD. At a low concentration range, surfactant molecules are co-associated with the guest molecules, C-485, however at high concentrations they are capable of pushing C-485 out of the nanotubular cavities. A gemini molecule with a comparatively longer spacer chain is more efficient in removing the guest molecules out of the nanotubular cavities. Also, rate of release of guest molecules increases with increasing concentration of surfactants. Release of guest molecules from the nanotubes can be tuned by changing the spacer chain length and concentration of gemini surfactants. Guest molecules after coming out of the nanotubular cavities, get solubilized in the micelles formed by surfactant molecules in the solution. The results of the present work suggest potential application in the development of promising drug delivery systems.*

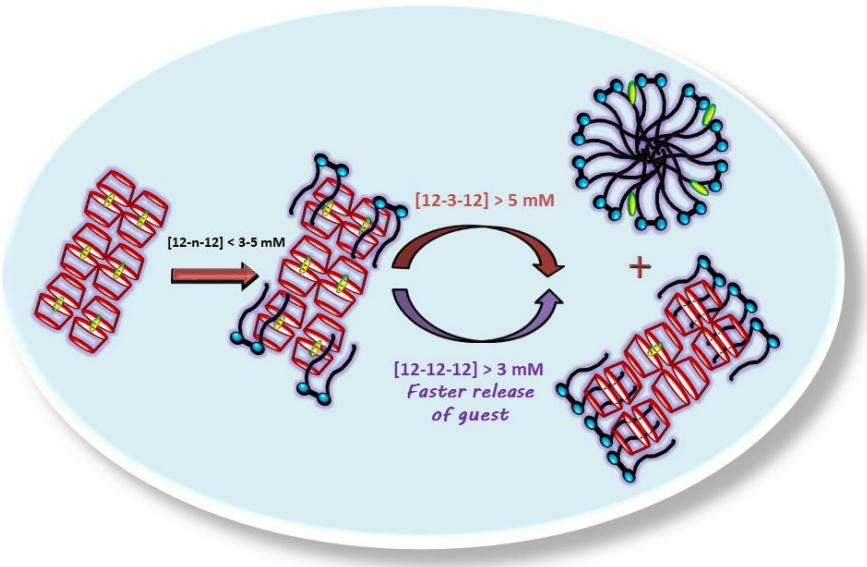

*Sunita Kumari, G. Sundar, and Subit K. Saha, *ChemistrySelect*, **2019**, *4*, 4190-4202.

5.1 Introduction

Controlled drug delivery process is being developed as an important area of research in last few years.[1-4] The toxicity arises because of the concentration of drug itself can be avoided by the controlled release of drugs.[5] Different drug carriers have been developed to overcome the problems of carrying a drug to the target site.[4, 6, 7] Cyclodextrins (CDs) are cyclic carbohydrates of different sizes, i.e., amylase-derived oligomers in which glucose units are linked via α-1-4 bonds, arranged in a cyclic fashion and form hollow, truncated cone-like structures. Based on the number of glucose units (i.e. 6, 7, or 8) present in the ring, these are called α–, β– and γ–cyclodextrin, respectively.[8] CDs constitute a class of carrier systems that have found a range of applications in drug delivery because of their unique characteristic of possessing a hydrophobic interior and hydrophilic exterior.[9] Due to their hydrophobic cavity, CDs serve as hosts for appropriate sized organic molecules (guest). The hydroxyl groups containing hydrophilic rims give a platform for hydrogen bonding.[10] Hashimoto *et al*. have found inclusion complexation between pyrene and β-CD, because of the strong hydrophobic interaction between them in the aqueous solution.[11] The cavity size of γ–CD is enough for the formation of excimer of pyrenes in the aqueous solution, which is noticed by an enhancement in the fluorescence intensity as well as fluorescence lifetime (77 ns). This dimer formation did not happen in an aqueous solution of α– and β–CDs because of their comparatively smaller cavity sizes.[12] There are reports on the formation of rotaxanes,[13] polyrotaxanes,[14] catenanes,[15] supramolecular tape,[16] and threaded cyclodextrins[17] types of supramolecular assemblies which are potential scaffold molecular devices as well. Of these assemblies, the formation of nanotubes of CDs in the presence of guest molecules[18-22] and their applications[23-27] is of particular interest. The formation of nanotubes depends on the concentration and cavity size of CDs and also on the size of the guest molecules.[18-22, 28-30] At a low concentration of CD, small inclusion complexes with a stoichiometric ratio of either 1:1 or 1:2 are formed depending on the nature of host and guest molecules.[20-22, 29, 31, 32] Upon further increasing the concentration of CD, nanotubes are formed governed by van der Waals, hydrophobic and hydrogen bonding interactions.[18-22, 29, 31, 33, 34] Not only the nanotubes but the secondary aggregates of nanotubes in the form of micrometer-sized rods have also been reported.[20, 21, 32] Secondary aggregates are formed by inter nanotubular hydrogen bonding interactions. Secondary aggregates of nanotubes are grown mostly in 2D fashion, but aggregation in 3D fashion has also been found.[16]

Formation of inclusion complexes between polymer molecules and CDs, depending on their inner cavity size (4-8 Å diameter), has also been reported.[33, 35-38] *α*–, *β*– and *γ*–CD form complexes with appropriately sized polymers such as PEG (poly(ethylene glycol)), PPG (poly(propylene glycol)) and poly (methyl vinyl ether), respectively, by threading action of the tail of polymers through the inner cavity of CDs.[38, 39] Both hydrophilic and hydrophobic polymers form inclusion complexes with CDs.[15] The formation of inclusion complexes of *β*–CD with the hydrophobic tail of a conventional surfactant molecule is well documented.[40-43] This type of complex formation delays the micellization process of surfactants and enhances the critical micellar concentration (*cmc*). The *cmc* in presence of a CD is called apparent critical micellar concentration (*cmc**).[42, 44-46] Mehta *et al.*[47] have recently observed the delay in the micellization of dodecyldimethylammonium (DDA) and tetradecyltrimethylammonium (TDA) with different counterions such as bromide and chloride, in the presence of different concentration range of various CDs (*α*– and *β*–CD, and hydroxypropyl-*β*–, and *γ*–CD). Delay in micellization is due to the greater magnitude of the hydrophobic interactions between the surfactant and CD cavities rather than that between surfactant molecules to form micelles. Petek *et al.*[48] have also studied the micelle formation of alkyltrimethylammonium bromide with different chain lengths such as C_{12}, C_{14}, and C_{16} in presence of *β*–CD. They have, however, observed that once micellization starts in presence of *β*–CD, the standard Gibbs free energy of micellization is more negative than the standard Gibbs free energy of complexation. Because of this reason the concentration of surfactants in micellar state continuously increases even some uncomplexed *β*–CD molecules (i.e. free *β*–CD) are present in the system. Huang and co-workers have done extensive study on host-guest inclusion complexes forming supramolecular structures of the amphiphilic molecules (including nonionic, anionic and cationic/anionic mixed surfactants) and alkanes with the CDs.[49-55]

Saha *et al.* have reported[32, 56, 57] earlier the guest molecule induced formation of nanotubes and the secondary aggregates of nanotubes giving micrometer size rods. We have seen that the extent of nanotubes formation, and of their secondary aggregation, depends on the concentration of the guest molecule.[32] We have also sudied[58] the concentration dependent binding of a conventional cationic surfactant, cetylpyridinium chloride (CPyCl) with the nanotubes of *β*–CD and the release of the guest molecule, trans-2-[4-(dimethylamino)styryl]benzothiazole (DMASBT) from the nanotubular cavities.

Gemini surfactants have found a range of applications in diverse fields of sciences.[59-63] A gemini surfactant is an amphiphilic molecule containing two hydrophobic tails joined by a spacer group at their hydrophilic headgroups. Gemini surfactants have greater surface activity as compared to their conventional counterparts.[64] Properties of gemini surfactants depend on various parts of surfactants such as hydrophobic tails, hydrophilic headgroups, counterions and spacer groups.[65-72] Spacer groups play a very important role in the aggregation behaviour of gemini surfactants. Studies with gemini surfactants with rigid, flexible, hydrophilic or hydrophobic spacer groups have been reported.[64, 73, 74] As far as new drug carriers and drug releasing systems are concerned, it is largely conventional surfactant based systems that have been studied. Currently, there is considerable interest in the design and construction of various CDs based systems, and tailoring of such systems for optimum drug loading and drug release.

This chapter is focused on the concentration and spacer chain length dependent binding of a series of gemini surfactants, 12-*n*-12, $2Br^-$ (where n = 3, 6, 12) (Scheme 5.1) with the nanotubes, and secondary aggregates of nanotubes of β–CD and release of guest molecules from the nanotubular cavities. A fluorescent guest molecule, Coumarin-485 (C-485) (Scheme 5.1), has been used to induce the formation of nanotubes, and their secondary aggregates. β–CD has been chosen for its medium cavity size which allows for effective binding of various guest molecules, and for binding of C-485 as well. We have also studied how the binding of a surfactant with the nanotubular systems and the release of guest molecules take place with time. Our observation is there is a controlled release of guest molecules from the nanotubular cavities.

In the current scenario, pharmaceutical research is focused on how can be a drug molecule released at the site of action effectively? To fulfill this purpose, several advance nanostimuli-responsive drug delivery systems are developed.[75, 76] Stimuli-responsive systems can be exogenous such as thermoresponsive, magnetically responsive, ultrasound triggered, photoresponsive, electroresponsive etc. and can be endogenous such as pH-sensitive systems, enzyme sensitive systems, redox-sensitive systems etc. Despite the benefits of these systems, these stimuli-responsive systems are too complicated to apply *in vitro* and *in vivo* condition, especially the second ones. Endogenous systems are indeed difficult to control because they may vary with the patient. Apart from this, these systems have sophisticated designs, that make the potential pharmaceutical process more complex as far as reproducibility and modification in drug/drug safety/quality control are

concerned. It is true that CDs have versatile applications in pharmaceutical industry and drug delivery for their complexation ability and other attractive physical and chemical properties. However, there is a need of research to find out any suitable additives which impart important interactions to these CDs based complexation systems and adversely affect the performance. It is also noteworthy that in the earlier studies on CDs based drug delivery systems, there was no mention about the formation of nanotubes of CDs/secondary aggregates of nanotubes of CDs. However, it is a fact that above a certain conc. CDs form nanotubes in presence of a guest.

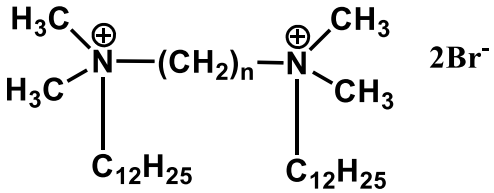

[12-*n*-12], *n* = 3, 6, and 12

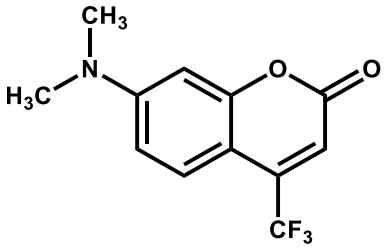

C-485

Scheme 5.1: Structure of gemini surfactants and C-485.

5.2 Results and discussion

5.2.1 UV–visible absorption spectra of C-485 in presence of *β*–CD

5.2.1.1 Binding of C-485 with *β*–cyclodextrin

Figure 5.1a represents the absorption spectra of C-485 (5.0 μM) in aqueous solutions with varying concentration of *β*–CD at pH = 7.4. Spectra have been recorded up to 9.5 mM concentration of *β*–CD. Absorption peak maximum of C-485 in pure aqueous solution of pH 7.4 occurs at 405 nm which matches well with earlier reports (403 nm in pure water).[77, 78] Figure 5.1b shows the variation in absorbance and absorption peak maxima of C-485 with increasing concentration of *β*–CD (0 mM to 9.5 mM). As the concentration of *β*–CD increases the absorbance increases continuously up to 4.0 mM with blue shift of 6 nm of the absorption peak maximum. Above this concentration of *β*–CD, a comparatively slower rise in absorbance was noticed. From 4.0 mM to 9.5 mM the absorption peak maximum was constant at 399 nm. This variation in absorption spectra of C-485 shows the binding of the C-485 molecule with *β*–CD. The absence of any isosbestic point in absorption spectra indicates the progressive formation of big molecular structures

like nanotubes starting from small inclusion complexes with increasing concentration of *β*–CD.

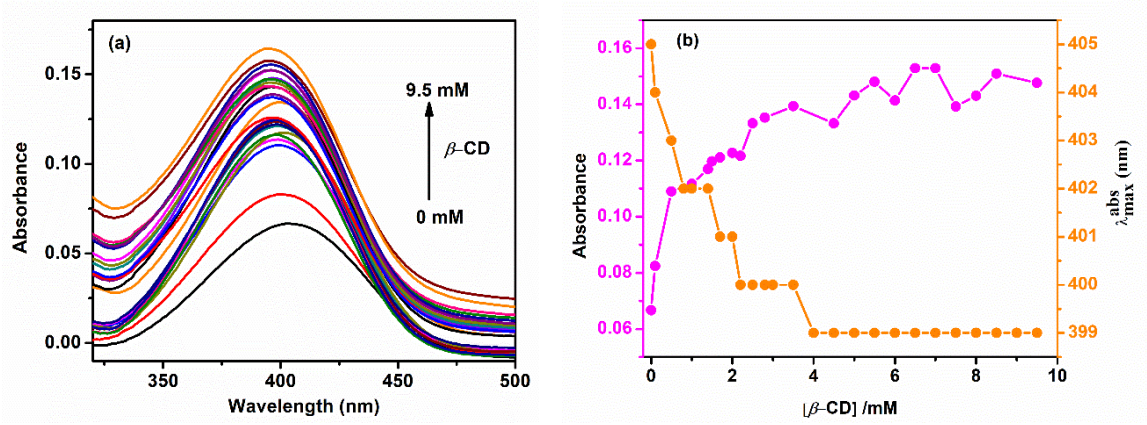

Figure 5.1. (a) Absorption spectra of C-485 (5.0 µM), (b) variation in absorbance (at 404 nm), and absorption peak maxima of C-485 as a function of the concentration of *β*–CD (pH = 7.4).

5.2.2 Steady-state fluorescence spectra of C-485 in presence of *β*–CD

5.2.2.1 Formation of nanotubes of *β*–CD in presence of C-485

The fluorescence spectra along with absorption spectra of C-485 in different solvents are given in Figure 5.2. The fluorescence peak maxima in pure solvents like water (at pH 7.4), methanol, acetone, ethyl acetate, cyclohexane, and hexane are 536 nm, 521 nm, 497 nm, 489 nm, 461 nm, and 457 nm, respectively and fluorescence quantum yields are 0.05, 0.11, 0.28, 0.50, 0.52, and 0.54, respectively. With increasing concentration of *β*–CD, the fluorescence intensity increases with concomitant blue shift in fluorescence peak maximum (Figure 5.3a). These results suggest that with increasing concentration of *β*–CD, the C-485 molecules progressively get transferred from the polar to the nonpolar environment. In a polar medium, fluorescence occurs from the ICT state. ICT to non-fluorescent TICT state conversion is feasible. So, in the polar medium it follows the ICT-TICT-ground state non-radiative de-excitation pathway.[79-81] In a polar environment, the charge transfer state being closer to the ground state as well as to the triplet state, the rates of non-radiative processes are high. As a result, the fluorescence intensity is low (Figures 5.3a and 5.2). However, with increasing concentration of *β*–CD more and more C-485 molecules move to the comparatively less polar environment of the hydrophobic pocket of *β*–CD, which leads to the destabilization of ICT state, is now away from the triplet and

ground states. This phenomenon is evidenced by the blue shift in fluorescence peak maximum with concomitant increase in fluorescence intensity.

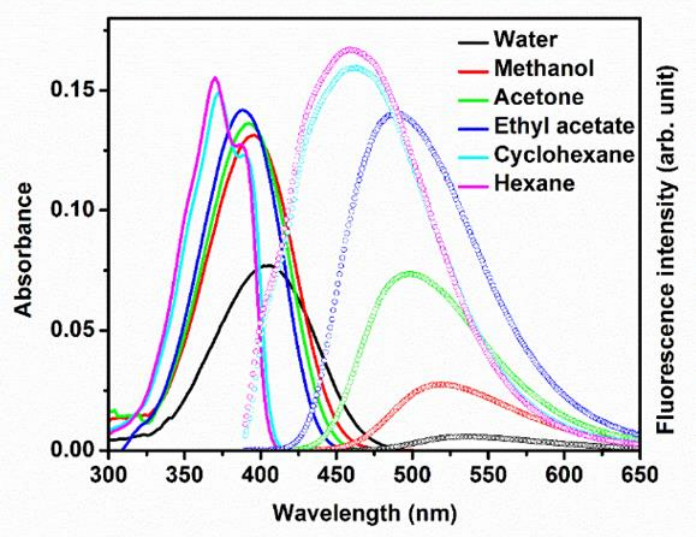

Figure 5.2. Absorption (solid lines) and fluorescence (symbol lines) spectra of C-485 in pure solvents. [λex = 375 nm].

Figure 5.3b represents the variation in fluorescence intensity ratio (F/F_o) and peak maximum of C-480 with the change in concentration of *β*–CD. At 9.5 mM concentration of *β*–CD, fluorescence peak maximum of C-485 is blue shifted by 17 nm and fluorescence intensity is increased by 1.9 times (at 520 nm) with respect to those in pure water. According to literature report very high increase in fluorescence intensity of C-485 in presence of *β*–CD is a result of formation of nanotubes, and also secondary aggregation of nanotubes of *β*–CD.[32, 58] Like absorption spectra, the significant changes in fluorescence intensity and fluorescence peak maximum are observed up to 4.0 mM concentration of *β*–CD. Therefore, the growth of nanotubes and secondary aggregation of nanotubes mainly takes place up to 4.0 mM concentration of *β*–CD. The variation noted in absorption as well as in fluorescence spectra of C-485 could be because of the formation of various kinds of aggregated structures like simple inclusion complex, nanotubes of various lengths, secondary aggregates of nanotubes etc. with increasing concentration of *β*–CD.

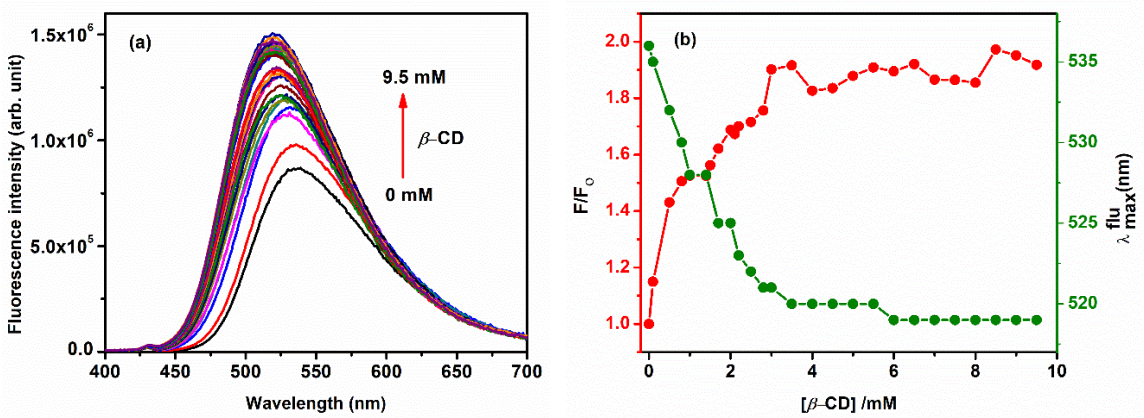

Figure 5.3. (a) Fluorescence spectra of C-485 (5.0 µM), (b) variation in the fluorescence intensity ratio (F/F_o) and peak maximum of C-485 as a function of the concentration of *β*–CD. [λ_{ex} = 375 nm, λ_{em} = 520 nm].

At low concentration of *β*–CD, small inclusion complexes are formed which are then converted to the extended nanotubes, followed by secondary aggregation of nanotubes by internanotubular hydrogen bonding interactions, at a high concentration of *β*–CD.[32] The stoichiometry of the inclusion complex at a low concentration of *β*-CD was determined by analyzing the fluorescence data using Benesi–Hildebrand plots[32, 82-84] for 1:1 and 1:2 stoichiometries following the given Equations 1.1 and 1.2, respectively (Chapter 1). The analysis has been confined to values of [*CD*], the concentration of *β*–CD, up to 2.0 mM, since at high concentration nanotubes are formed and the equations are not applicable. *K* and *K′* are the association constants, which were determined from the slope and intercept values of the Benesi-Hildebrand plot. For the Benesi-Hildebrand plot, the intensity of fluorescence has been measured at 525 nm. Figure 5.4 represents the best fitting of Benesi-Hildebrand plot for 1:1 stoichiometry with regression coefficient = 0.998. The Benesi–Hildebrand double reciprocal plot for 1:2 stoichiometry deviates from the linearity (figure not shown). This result shows that at low concentration of *β*–CD it forms simple inclusion complex of 1:1 stoichiometric ratio with C-485 with an association constant (*K*) value of 5221 M^{-1}. Further evidence to support the formation of nanotubes and other structures of *β*–CD has been obtained from steady-state fluorescence anisotropy measurements. Fluorescence anisotropy is a directional property, which depends upon the environment. It gives precise information about the microenvironment. Because of the high sensitivity of fluorescence anisotropy of a probe molecule towards shape, size, rigidity, and viscosity of microenvironment, it has a wide range of applications in biological fields.

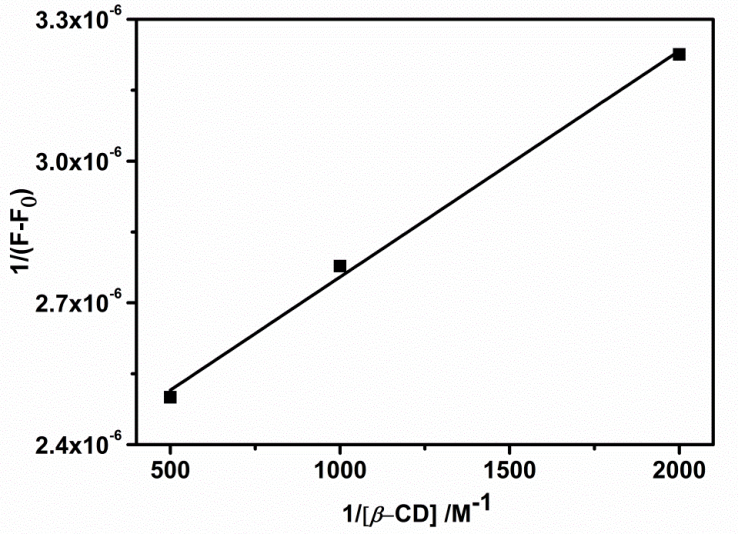

Figure 5.4. Benesi-Hildebrand plot of C-485 (5.0 µM) in *β*–CD for a 1:1 stoichiometry.

5.2.3 Steady-state fluorescence anisotropy of C-485 as a function of the concentration of *β*–CD

Figure 5.5 represents the variation in fluorescence anisotropy with change in the concentration of *β*–CD in the aqueous solution of C-485. There is a sharp increment in anisotropy (0.12) up to 2.0 mM concentration of *β*–CD. After that, a slow rise in anisotropy is noted with a value of 0.14 at 9.5 mM concentration of *β*–CD. This high value of fluorescence anisotropy is only possible when the C-485 molecule goes inside the cavity of *β*–CD.

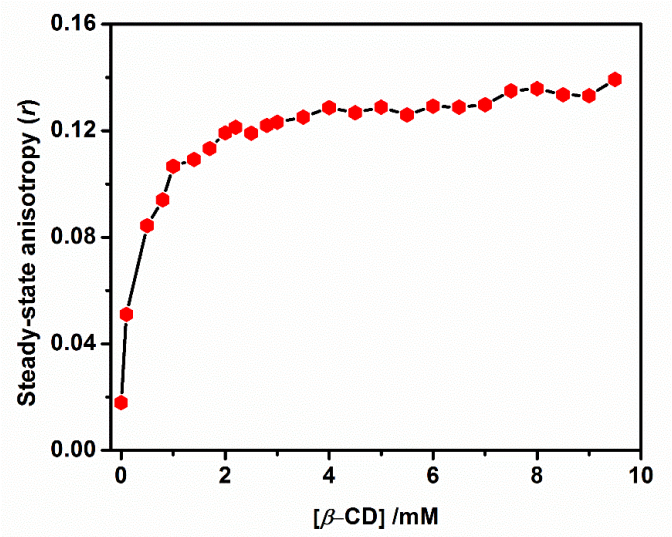

Figure 5.5. Variation in the steady-state fluorescence anisotropy of C-485 (5.0 µM) (intensities have measured at λ_{em} = 510 nm) as a function of the concentration of *β*–CD.

The high anisotropy value indicates the restricted movement of C-485 molecules when present as guest molecules in the cavity of *β*–CD. Many reports have confirmed that guest molecules exhibit this high anisotropy value only after the formation of nanotubes of CDs.[18-21, 32] This result confirms the formation of nanotubes of *β*–CDs in presence of C-485 as a guest at a high concentration of *β*–CD.

5.2.4 Fluorescence lifetime and rotational relaxation time of C-485 as a function of the concentration of *β*–CD

Some representative fluorescence intensity decays of C-485 in water and in presence of different concentrations of *β*–CD at pH 7.4 are shown by Figure 5.6a. Fluorescence intensity decays of C-485 have been measured at λ_{em} = 510 nm upon excitation at 375 nm. Fluorescence decay is found to be bi-exponential with $<\tau_f>$ = 85 ps in water at pH = 7.4. Decays are bi-exponential in presence of *β*–CD as well. Average lifetime has been calculated using Equation 1.8 (given in Chapter 1). Figure 5.7 shows that average excited state lifetime of C-485 increases with increasing concentration of *β*–CD with very sharp initial increase. C-485 molecules are transferred from the bulk aqueous phase to the hydrophobic pocket of *β*–CD forming inclusion complexes and nanotubes. As a result of transfer to the comparatively nonpolar environment, the ICT state of C-485 gets destabilized.[80, 81] Thus the rates of non-radiative processes decrease and fluorescence lifetime increases. Fluorescence anisotropy decays also have been measured at λ_{em} = 510 nm after excitation at 375 nm. Some representative fluorescence anisotropy decays of C-485 in water and in presence of different concentrations of *β*–CD at pH 7.4 are also shown by Figure 5.6b. Anisotropy decay is mono-exponential with rotational relaxation time = 118 ps in water at pH = 7.4. Anisotropy decays are mono-exponential with much slower relaxation process in *β*–CD system as well. Table 5.1 represents the rotational relaxation time (τ_r) (calculated by Equation 2.18, Chapter 2). and limiting anisotropy (r_o) values at different conc. of *β*–CD. The lower r_o values as compared to $(r_o)_{max}$ = 0.4 over a large range of concentrations of *β*–CD indicate the contribution of fast motions to the loss of anisotropy. These motions might occur on a time scale faster than the resolution of our instrumental set-up and that perhaps is why mono-exponential decays were observed.[85] Sarkar *et al.* have reported the slower rotational relaxation of C-485 in the micelles (τ_r = 435 ps) and in protein-surfactant system (τ_r = 550 ps) as compared to pure water (τ_r = 120 ps).[78] The rotational relaxation time of C-485 also increases with increasing concentration

of β–CD (Figure 5.7). Initially both lifetime and rotational relaxation time increase very sharply (Figure 5.7). The changes observed in both excited state lifetime and rotational relaxation time with increasing concentration of β–CD are in consistent with that of steady-state fluorescence anisotropy. These results are again in support of the fact that C-485 molecules are present inside the nanotubes of β–CD. Comparatively higher values of r_o (close to 0.4) at higher concentration range of β–CD also indicates rigid environment around C-485.

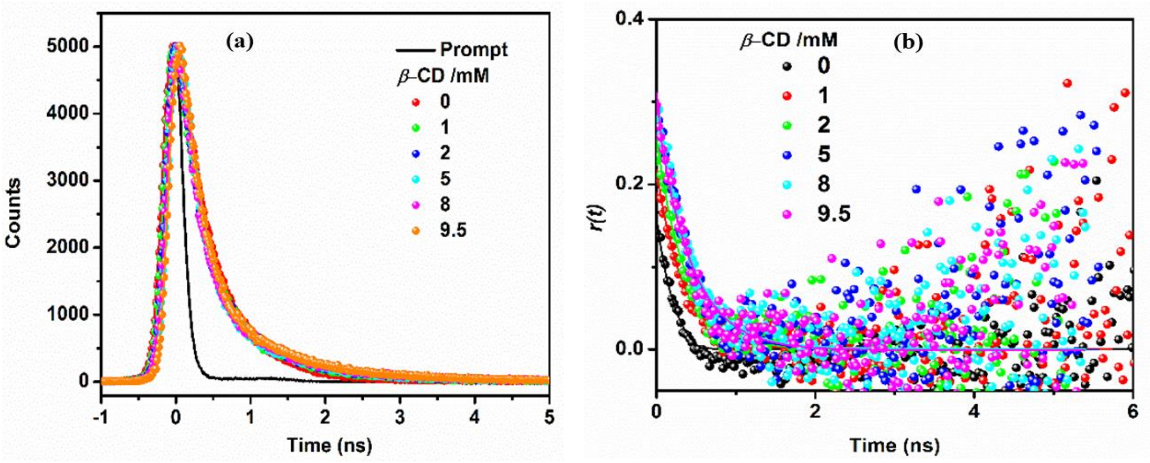

Figure 5.6. (a) Fluorescence intensity decays and (b) anisotropy decays of C-485 in water and in presence of different concentration of β–CD at pH = 7.4. [λ_{ex} = 375 nm, λ_{em} = 510 nm].

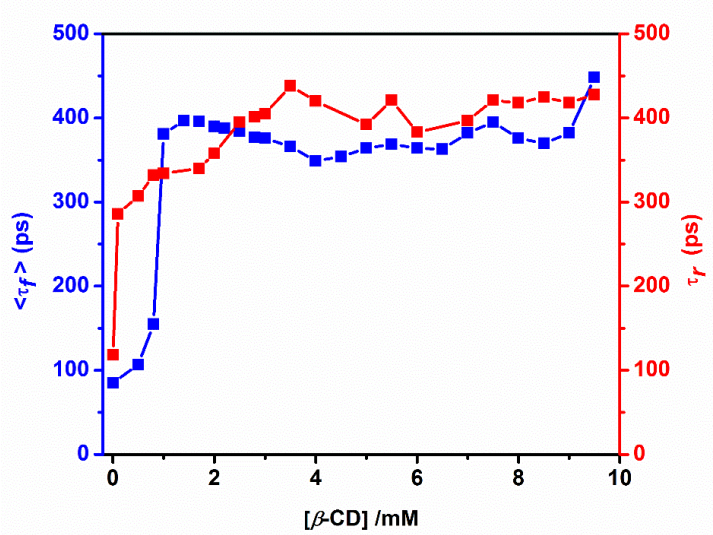

Figure 5.7. Variations in the average excited state lifetime ($<\tau_f>$) and rotational relaxation time (τ_r) of C-485 (5.0 µM) (λ_{em} = 510 nm) as a function of the concentration of β–CD. λ_{ex} = 375 nm.

Table 5.1. Rotational relaxation time (τ_r), limitting anisotropy (r_0) of C-485 (5.0 μM) in the aqueous solution of different concentration of *β*–CD. [λ_{ex} = 375 nm, λ_{em} = 510 nm].

***β*–CD mM**	**τ_r ps**	***a***	**r_o**	**χ^2**
0	118	1.00	0.15	1.20
0.1	286	1.00	0.20	1.06
0.5	307	1.00	0.29	1.09
0.8	332	1.00	0.22	1.15
1.0	334	1.00	0.25	1.05
1.7	340	1.00	0.30	1.15
2.0	358	1.00	0.27	1.16
2.5	395	1.00	0.28	1.23
2.8	401	1.00	0.29	1.17
3.0	405	1.00	0.28	1.09
3.5	438	1.00	0.29	1.11
4.0	420	1.00	0.37	1.20
5.0	392	1.00	0.38	1.22
5.5	421	1.00	0.40	1.19
6.0	383	1.00	0.37	1.20
7.0	397	1.00	0.34	1.24
7.5	421	1.00	0.38	1.22
8.0	418	1.00	0.37	1.12
8.5	425	1.00	0.37	1.11
9.0	418	1.00	0.39	1.17
9.5	428	1.00	0.36	1.20

5.2.5 Interactions of gemini surfactants, 12-*n*-12 with C-485-*β*–CD system

5.2.5.1 UV-visible absorption spectra of C-485 in presence of *β*–CD (8.0 mM) with varying concentration of 12-*n*-12

To see the effect of gemini surfactants on the binding of C-485 with the nanotubes of *β*–CD and also its secondary aggregates, gemini surfactant has been added in the C-485-*β*–CD system with 8.0 mM concentration of *β*–CD and various spectroscopic techniques have been used. The absorption spectra of C-485-*β*–CD system have been recorded with various concentrations of each of gemini surfactants, [12-*n*-12]. Absorbance of C-485 initially increases up to 0.8 mM concentration of each of gemini surfactants, [12-*n*-12] (Figure 5.8a). Beyond 0.8 mM concentration, the absorbance decreases up to the concentration range of 3-5 mM of surfactants, the specific value depending on the spacer group of gemini surfactants. With further increase in the concentration of surfactant in the

system, the absorbance increases and then becomes constant at ~10.0 mM of the surfactant. Figure 5.8b shows the change in absorption peak maxima with increasing concentration of a gemini surfactant. The blue shift at a low concentration of a gemini surfactant (1 nm) followed by a red shift (11 nm) at a comparatively higher conc. of surfactant has been noted. This result indicates that initially a surfactant tail provides more nonpolar environment around C-485 inside the nanotube and then it pushes the C-485 out of the nanotube. A detailed discussion of this aspect has been presented below.

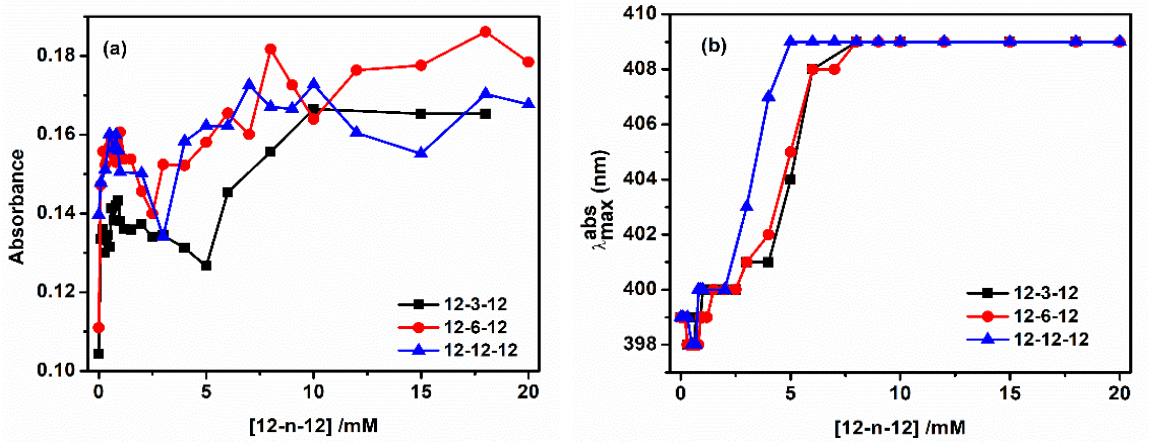

Figure 5.8. (a) Variation in the absorbance at 404 nm of C-485 (5.0 µM), (b) variation in the peak maxima of absorption spectra (λ_{max}^{abs}) of C-485 (5.0 µM) in the aqueous solution of *β*–CD (8.0 mM) with the addition of gemini surfactants, 12-*n*-12.

5.2.5.2 Fluorescence properties of C-485 in presence of *β*–CD (8.0mM) as a function of conc. of gemini surfactants, [12-*n*-12]

To monitor the change in microenvironment around C-485 upon addition of gemini surfactant in the system, the fluorescence spectra have also been recorded. Figure 5.9a represents the variation in the fluorescence intensity ratio, F/F_o (where, F and F_o are the fluorescence intensities at 510 nm of the band in presence and absence of 12-*n*-12 surfactants, respectively) with increasing concentration of each of the surfactants, [12-*n*-12]. In the concentration range, 0–1.0 mM (first concentration range) of surfactants, the fluorescence intensity increases on addition of the surfactants. After that, from 1.0 mM to ~5.0 mM (second concentration range), the fluorescence intensity initially remains almost constant followed by a small decrease in fluorescence intensity towards the end. Beyond this concentration range (> 5 mM) (third concentration range), the fluorescence intensity again starts to rise followed by saturation at a high concentration of a surfactant. Figures 5.9b and 5.10 display the changes in fluorescence peak maxima and steady-state

fluorescence anisotropy, respectively with increasing concentration of each of gemini surfactants. Initially, at low concentrations of surfactants, there is an increase in fluorescence intensity with blue shift in fluorescence peak maximum by 3 nm along with an increase in fluorescence anisotropy. This indicates that surfactant tail(s) has/have entered into the nanotubular cavities thereby providing comparatively less polar and more rigid environment around C-485 molecules.[34] Thus there is a co-association of tails and C-485 in the cavities up to a certain concentration of surfactants. It has been reported in the literature that C-485 is a planner molecule and its width is 5.675 Å.[86, 87] The width of the tail part of dodecyltrimethylammonium bromide (DTAB) (conventional counterpart of a gemini surfactant) is reported to be 3.065Å[88] which should not be very much different from that of gemini surfactant. Therefore, the width of each of C-485 and a gemini tail is lesser than the inner cavity diameter of *β*-CD (7.8 Å). Thus both of them can be accommodated inside the cavity of nanotubes of *β*-CD. Scheme 5.2 represents such type of co-association in a part of the nanotubular cavity.

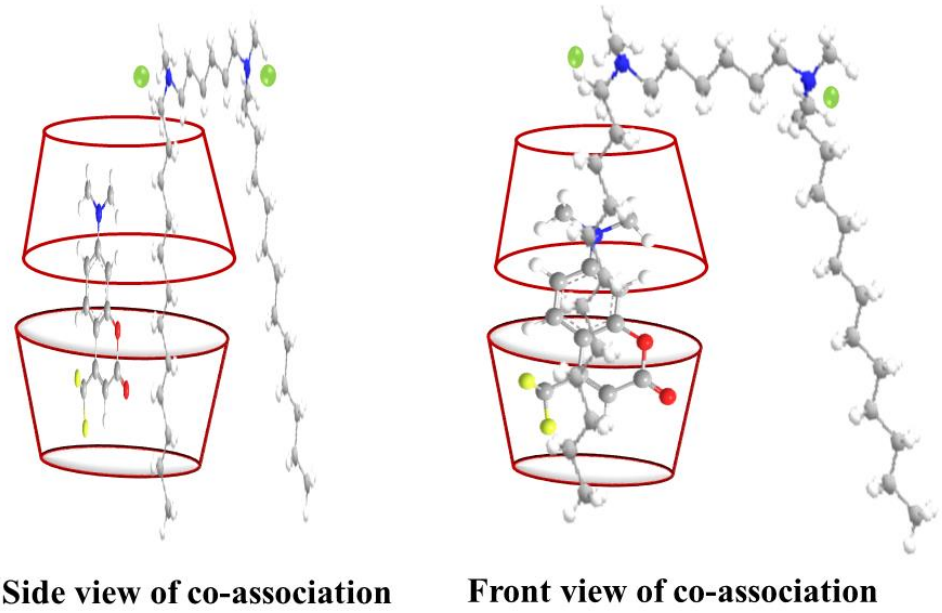

Scheme 5.2: Side and front views of possible co-association of the tail of gemini surfactant and C-485 inside the part of the cavity of a nanotube of *β*-CD.

A minimum in peak maxima and a maximum in intensity as well as anisotropy are noted in Figures 5.9b, 5.9a and 5.10, respectively at a comparatively lower conc. (0.7 mM) of 12-12-12 than that of other two surfactants. This could be due to the presence of a more flexible spacer group in 12-12-12 surfactant, the tail can easily enter into the nanotubular cavity. There is also the possibility that two tails of a given surfactant molecule can enter

at the same time into two different nanotubes, therefore the effective concentration required to provide rigid/nonpolar environment around C-485 molecules inside the nanotubes would be comparatively less in case of 12-12-12 surfactant. In the second concentration range of surfactant (1.0 mM – max. 5 mM), the fluorescence intensity initially remains constant followed by a drop in intensity which is accompanied by a red shift (~10 nm) as well as decrease in fluorescence anisotropy. This result indicates that at a certain concentration, the surfactant tails can push out the C-485 molecules from the nanotubular cavities. As a result of that C-485 molecules feel polar and free environment evidenced by the above mentioned fluorescence data. It is noteworthy that a minimum in fluorescence intensity and anisotropy and a maximum in fluorescence peak occurred at a comparatively lower concentration for 12-12-12 than that for 12-3-12 and 12-6-12. While the minima in fluorescence intensity and anisotropy values appear at 3.0 mM concentration of 12-12-12, the same appear at 5.0 mM concentration of each of 12-3-12 and 12-6-12. Since the tails of 12-12-12 surfactant molecules can more easily be entered into the nanotubular cavities, they are comparatively more effective to push the C-485 molecules out of the cavities. Therefore, the flexibility of a spacer group of a gemini surfactant has a role on how easily the guest molecules can be released from the *β*-CD nanotubular cavities. In the third concentration range (> min. 3.0 mM – max. 5.0 mM depending on the surfactant), the fluorescence intensity starts increasing with a blue shift in peak maximum and increase in fluorescence anisotropy values up to ~10.0 mM of surfactant. Beyond this concentration, all fluorescence properties remain almost constant.

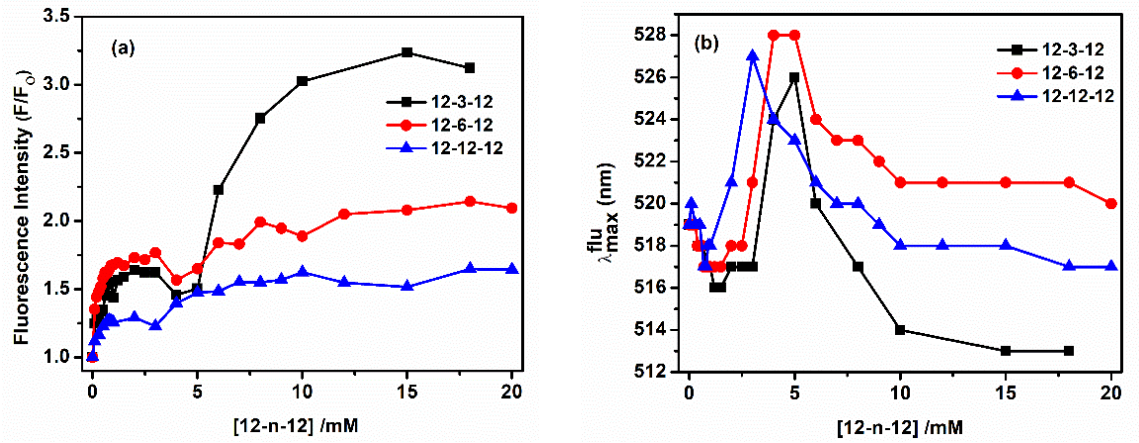

Figure 5.9. (a) Variation in the fluorescence intensity at 515 nm of C-485 (5.0 µM), (b) variation in fluorescence peak maxima of C-485 (5.0 µM) in the aqueous solution of *β*–CD (8.0 mM) as function of concentration of gemini surfactants [12-*n*-12]. [λ_{ex} = 375 nm].

These fluorescence results indicate that the C-485 molecules that are released from the nanotubes are getting solubilized in the micelles formed by surfactant molecules present in the aqueous phase. One can see that at a high concentration of surfactant when C-485 molecules are mostly present in the micelles, the increasing order of fluorescence intensities is as follows: 12-12-12 < 12-6-12 < 12-3-12. Zana *et al.*[89, 90] have reported, and we have also seen in one of our earlier studies,[75] that the microviscosity of gemini micelles decreases with increasing polymethylene spacer chain length. Thus, the above mentioned trend in fluorescence intensity could be due to increasing microviscosity of micelles with decreasing spacer chain length.

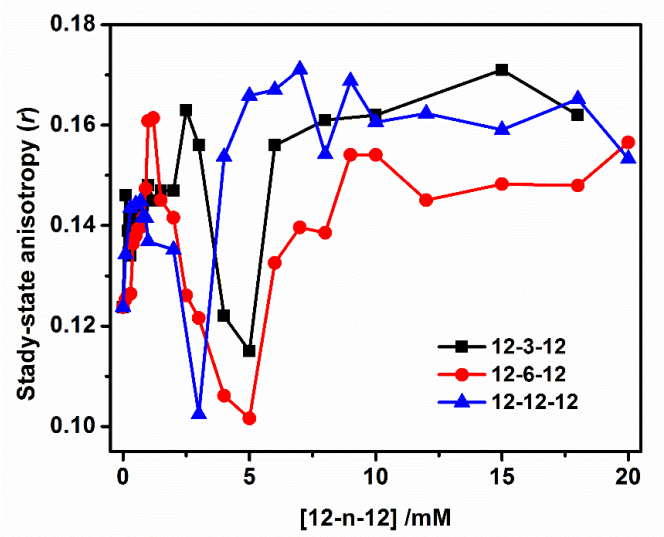

Figure 5.10. Steady-state anisotropy of C-485 (5.0 µM) in the aqueous solution of *β*-CD (8.0 mM) as function of concentration of gemini surfactants [12-*n*-12]. [λ_{ex} = 375 nm, λ_{em} = 510 nm].

5.2.5.3 Fluorescence lifetime and rotational relaxation time of C-485 in 8.0 mM aqueous solution of *β*–CD as a function of conc. of gemini surfactants, [12-*n*-12]

To gather further evidence for the binding of surfactants with the C-485-*β*–CD nanotubular systems, the fluorescence lifetimes and the rotational relaxation times of C-485 have been measured with a fixed concentration of *β*–CD (8.0 mM) and different concentration of each of surfactants. All fluorescence intensity decays are bi-exponential in nature with the fast component as a major component (80-98%). Tables 5.2a-c represent the lifetimes of both the components along with average lifetimes at various concentrations of each of 12-3-12, 12-6-12 and 12-12-12, respectively. All fluorescence anisotropy decays are mono-exponential in nature. In these systems also we find r_o values lower than

$(r_o)_{max}$ = 0.4 (data not shown), indicating that fast motion which could not be detected with our present instrumental set-up, along with slow motion, are responsible for loss of anisotropy. Figures 5.11 and 5.12 represent the variation in average lifetime and rotational relaxation times with increasing concentration of surfactants. Like other fluorescence properties shown above, both the fluorescence lifetime and rotational relaxation time increase initially, reach a maximum value, and then decrease to a minimum followed by an increase with further increasing concentration of a surfactant. In a comparatively less polar environment (when C-485 resides inside the tube along with surfactant tail and also when C-485 gets solubilized in the micelles), due to the destabilization of polar emitting state of C-485, the rate of non-radiative processes is decreased, and as a result the lifetime is increased. In this comparatively rigid environment, the rotational relaxation process is hindered, resulting in longer relaxation time. When C-485 molecules come out from the nanotubes into the bulk, the polar emitting state of C-485 gets stabilized which leads to faster rate of non-radiative processes thereby reducing the excited state lifetime. In this case the rotational relaxation process becomes faster, giving shorter relaxation time. Thus these results are also in support of the process of surfactant induced release of guest molecules from the nanotubes followed by their solubilization in the micelles at higher concentration of surfactant. Further analysis of insets of Figures 5.11 and 5.12 infer that minimum occurs at comparatively lesser conc. of 12-12-12 as compared to other two surfactants. Thus 12-12-12 is more efficient to push the guest molecules out of the nanotubes as discussed above based on results of other fluorescence properties. Moreover, at a given high concentration of surfactant both average lifetime and rotational relaxation time increase with decreasing spacer chain length. Thus these results are also in same line with the fact that microviscosity/rigidity of microenvironment of micelles increases and micropolarity decreases with decreasing spacer chain length of gemini surfactants.

A detailed analysis of data on fluorescence lifetimes of two components and their weightage gives more information about the binding of the probe, C-485 with the nanotubes and also with micelles. In all three cases of surfactants the fast components have major contribution towards the decays. We suggest that the fast components are for the C-485 molecules present in an environment where they can freely move and slow components are for the molecules present in a rigid environment. C-485 molecules present deep inside the nanotubes could be contributing towards slow components. C-485 molecules present near to the ends of tubes might be contributing towards fast components.

We also find that the weightage of fast components for 12-3-12, 12-6-12 and 12-12-12 at their low concentration range are 81-89%, 82-95% and 83-97%, respectively. Thus, the minimum weightage for slow components for these surfactants are 11%, 5% and 3%, respectively. Therefore, these results are also in accordance with the fact that 12-12-12 surfactant is more efficient to get the C-485 molecules out of the nanotubes thereby contributing towards greater extent of fast components and lesser extent of slow components. For all three surfactants, the lifetimes of fast components become longer at their high concentrations range when C-485 molecules are present in their micelles. It indicates that the rigidity of microenvironment of micelles is greater than that of nanotubes which is supported by the higher values of $<\tau_f>$, τ_r, r and fluorescence intensity of C-485 in micelles than that in nanotubes. Figures 5.13a and 5.13b represent fluorescence intensity decays and anisotropy decays, respectively of C-485 in presence of 8 mM concentration of β–CD and 10 mM concentration of 12-*n*-12 to demonstrate the effect of spacer chain length.

Table 5.2a. Excited-state lifetime of C-485 (5.0 μM) in presence of 8.0 mM aqueous solution of β–CD at various concentration of [12-3-12]. [λ_{ex} = 375 nm, λ_{em} = 510 nm].

Sr. no.	[12-3-12] mM	τ_1 ps	a_1	τ_2 ps	a_2	$<\tau_f>$ ps	$\chi 2$
1	0.00	275	0.89	1162	0.11	373	1.12
2	0.10	295	0.83	1103	0.17	432	1.16
3	0.20	295	0.83	1133	0.17	437	1.20
4	0.30	314	0.88	1303	0.12	433	1.19
5	0.40	298	0.83	1184	0.17	449	1.14
6	0.50	320	0.88	1377	0.12	447	1.16
7	0.60	297	0.85	1313	0.15	449	1.13
8	0.70	295	0.84	1281	0.16	453	1.16
9	0.80	278	0.82	1262	0.17	443	1.17
10	0.90	283	0.81	1240	0.19	465	1.21
11	1.00	289	0.83	1356	0.17	470	1.13
12	1.20	290	0.82	1350	0.18	481	1.15
13	1.50	308	0.82	1409	0.18	506	1.14
14	2.00	298	0.82	1459	0.18	507	1.16
15	2.50	316	0.81	1529	0.19	546	1.15
16	3.00	387	0.81	1669	0.18	614	1.16
17	4.00	372	0.84	1540	0.16	559	1.17
18	5.00	396	0.88	1567	0.12	537	1.16
19	6.00	547	0.82	1521	0.18	722	1.14
20	8.00	612	0.77	1480	0.23	812	1.13
21	10.0	731	0.82	1672	0.18	900	1.15
22	15.00	749	0.81	1697	0.19	929	1.07
23	18.00	726	0.82	1732	0.18	907	1.05

Table 5.2b. Excited-state lifetime of C-485 (5.0 μM) in presence of 8.0 mM aqueous solution of *β*–CD at various concentration of [12-6-12]. [λ_{ex} = 375 nm, λ_{em} = 510 nm].

Sr. no.	[12-6-12] mM	τ_1 ps	a_1	τ_2 ps	a_2	$<\tau_f>$ ps	$\chi 2$
1	0.00	275	0.89	1162	0.11	373	1.12
2	0.10	229	0.85	973	0.15	371	1.02
3	0.20	239	0.86	1043	0.14	352	1.18
4	0.30	245	0.87	1095	0.13	356	1.12
5	0.40	239	0.82	1077	0.18	390	1.13
6	0.50	267	0.88	1215	0.12	381	1.15
7	0.60	261	0.88	1249	0.12	380	1.12
8	0.80	272	0.87	1322	0.13	409	1.14
9	0.90	275	0.88	1367	0.12	406	1.10
10	1.00	286	0.88	1401	0.12	420	1.05
11	1.20	287	0.84	1412	0.16	467	1.16
12	1.50	304	0.87	1546	0.13	465	1.11
13	2.00	314	0.86	1641	0.14	500	1.16
14	2.50	329	0.86	1696	0.14	520	1.12
15	3.00	339	0.87	1707	0.13	517	1.12
16	4.00	417	0.89	1784	0.11	567	1.21
17	5.00	434	0.95	1727	0.05	499	1.04
18	6.00	456	0.94	1409	0.06	513	1.02
19	7.00	465	0.94	1326	0.06	516	0.97
20	8.00	466	0.94	1150	0.06	507	0.99
21	9.00	472	0.95	1186	0.05	508	0.98
22	10.00	475	0.93	1191	0.07	525	1.00
23	12.00	455	0.86	950	0.14	524	1.16
24	15.00	455	0.84	879	0.16	523	0.98
25	18.00	464	0.86	898	0.14	525	0.95
26	20.00	446	0.78	852	0.22	535	1.16
27	25.00	453	0.76	846	0.24	547	1.15
28	30.00	464	0.78	857	0.22	550	1.11

Table 5.2c. Excited-state lifetime of C-485 (5.0 µM) in presence of 8.0 mM aqueous solution of *β*–CD at various concentration of [12-12-12]. [λ_{ex} = 375 nm, λ_{em} = 510 nm].

Sr. no.	[12-12-12] mM	τ_1 ps	a_1	τ_2 ps	a_2	$<\tau_f>$ ps	$\chi 2$
1	0.00	275	0.89	1162	0.11	373	1.12
2	0.10	221	0.83	965	0.17	347	1.13
3	0.60	256	0.88	1123	0.12	360	1.19
4	0.70	265	0.88	1260	0.12	384	1.12
5	0.90	284	0.88	1356	0.12	413	1.19
6	1.00	346	0.85	1402	0.15	504	1.14
7	2.00	327	0.89	1590	0.11	466	1.16
8	3.00	395	0.92	1777	0.08	506	1.14
9	4.00	451	0.96	1787	0.04	504	1.20
10	5.00	458	0.96	1603	0.04	504	1.20
11	6.00	466	0.96	1479	0.04	507	1.13
12	7.00	480	0.96	1378	0.04	516	1.20
13	8.00	488	0.94	1374	0.04	514	1.13
14	9.00	496	0.94	1322	0.04	519	1.21
15	10.00	492	0.97	1270	0.03	515	1.13
16	12.00	493	0.97	1156	0.03	513	1.15
17	15.00	533	0.96	1484	0.04	571	1.19
18	18.00	538	0.97	1341	0.03	562	1.20
19	20.00	544	0.96	1360	0.04	577	1.20
20	25.00	579	0.98	1617	0.02	600	1.20
21	30.00	559	0.95	1086	0.05	585	1.13

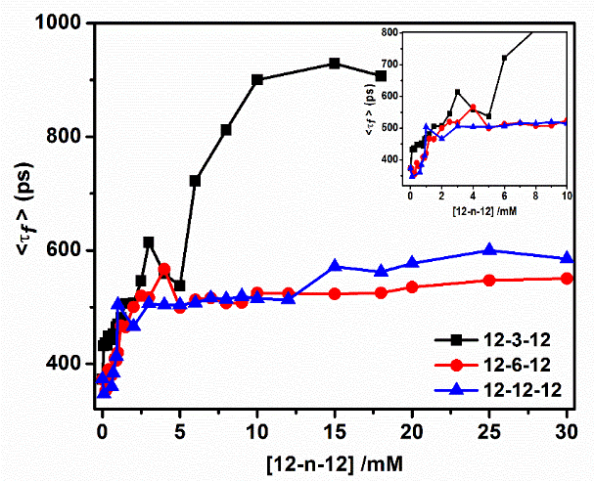

Figure 5.11. Average lifetime of C-485 (5.0 µM) in the aqueous solution of *β*–CD (8.0 mM) as a function of concentration of gemini surfactants [12-*n*-12]. Inset is for more clear view of changes at low conc. range [λ_{ex} = 375 nm, λ_{em} = 510 nm].

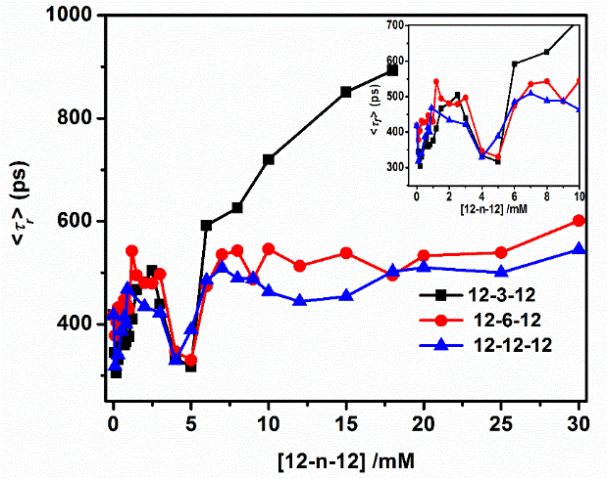

Figure 5.12. Rotational relaxation time of C-485 (5.0 µM) in the aqueous solution of *β*–CD (8.0 mM) as function of concentration of gemini surfactants [12-*n*-12]. Inset is for more clear view of changes at low conc. range [λ_{ex} = 375 nm, λ_{em} = 510 nm].

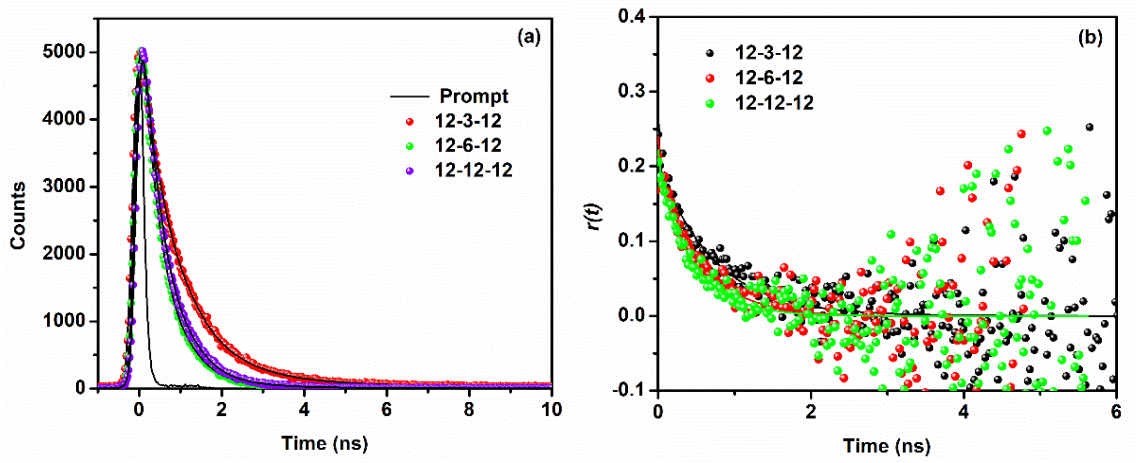

Figure 5.13. (a) Fluorescence intensity decays and (b) anisotropy decays of C-485 in presence of 8.0 mM concentration of *β*–CD and 10 mM of 12-*n*-12 at pH = 7.4. [λ_{ex} = 375 nm, λ_{em} = 510 nm].

To gather support for the conclusion that C-485 molecules are getting solubilized in the micelles after they are released from the nanotubular cavities at a given concentration of surfactant, we have done some controlled experiments by recording absorption and fluorescence spectra of C-485. The absorption and fluorescence spectra of C-485 have been recorded at 10.0 mM conc. of each of gemini surfactants and are shown by Figure 5.14a and Figure 5.14b, respectively. The absorption peak maximum of C-485 in each of three micellar system (10 mM) is 409 nm which is exactly same as that noted in presence of *β*–CD and high concentration of surfactants.

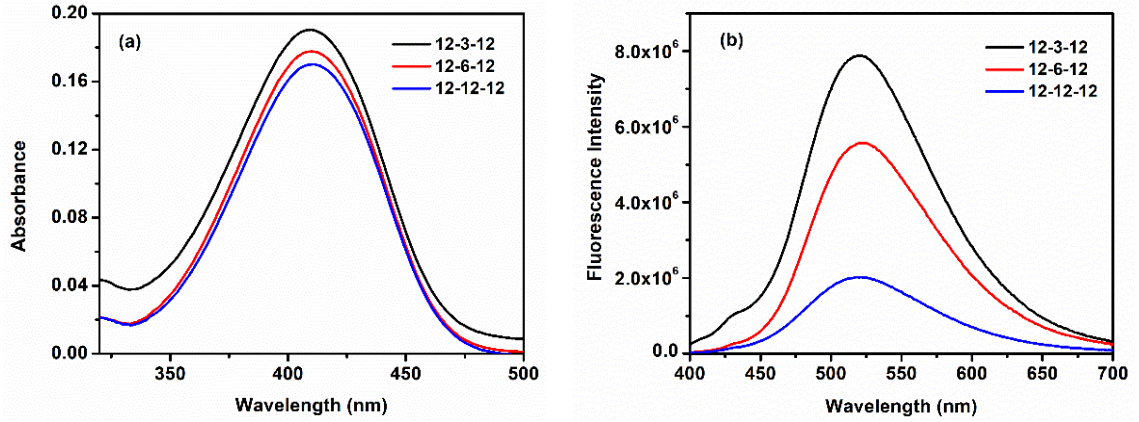

Figure 5.14. (a) Absorption spectra, (b) fluorescence spectra of C-485 (5.0 µM) in the aqueous micellar solutions of gemini surfactants ([12-*n*-12] = 10 mM). [λ_{ex} = 375 nm].

Fluorescence peak maxima of C-485 are observed at 520 nm, 520 nm, and 519 nm in micelles of 10.0 mM of each of 12-3-12, 12-6-12, and 12-12-12, respectively which are also quite similar to that in presence of *β*–CD and high concentration of surfactants. The λ_{max}^{abs} and λ_{max}^{flu} of C-485 are reported to be 407 nm, and 514 nm, respectively in micelles of 50 mM of DTAB by Sarkar *et al.*[78] In addition to these results, one can also see from Figure 5.14b that the increasing order of fluorescence intensity in the micelles of surfactants is 12-12-12 < 12-6-12 < 12-3-12, which is same as that in presence of *β*–CD at a high concentration of surfactant (Figure 5.9a). There are also similarities between the values of steady-state anisotropy (*r*), average fluorescence lifetime ($<\tau_f>$) and rotational relaxation time (τ_r) in micelles, and those in C-485-*β*–CD-[12-*n*-12] (high concentration) system (Table 5.3). All these results support our conclusion that C-485 molecules, after being released from nanotubes get solubilized in micelles at a high concentration of surfactant.

Table 5.3. *Cmc*, experimental concentration of [12-n-12], and *β*–CD, peak maxima of absorption (λ_{max}^{abs}) band, peak maxima of fluorescence (λ_{max}^{flu}) bands, steady-state anisotropy (*r*), average excited state lifetime ($<\tau_f>$) and rotational relaxation time (τ_r) of C-485 (5.0 µM) in the aqueous micellar solution. [λ_{ex} = 375 nm, λ_{em} = 510 nm].

System	*cmc* mM	Conc. mM	*β*–CD mM	λ_{max}^{abs} nm	λ_{max}^{flu} nm	*r*	$<\tau_f>$ ps	τ_r ps
12-3-12	0.93	10	-	409	520	0.160	749	615
12-6-12	1.03	10	-	409	520	0.160	595	577
12-12-12	0.41	10	-	409	519	0.140	549	467
12-3-12	-	10	8	409	514	0.162	899	720
12-6-12	-	10	8	409	518	0.154	510	546
12-12-12	-	10	8	409	521	0.160	569	463

5.2.6 Study of time dependent release of guest upon binding of gemini surfactants with nanotubes

Time dependent release of guest molecules upon binding of a surfactant with the nanotubes has been studued by monitoring the changes in fluorescence intensities of C-485 (present as a guest in the nanotubes). To perform this experiment, initially after addition of C-485 in 8.0 mM solution of β–CD, the solution has been kept for overnight to have an equilibrium system of C-485 induced nanotubes. After that a gemini surfactant of a suitable concentration has been added to the solution containing nanotubes. This experiment has been done with 5 mM, 10 mM, 15 mM, and 20 mM of each of gemini surfactants. Figure 5.15 represents how the guest molecules are released with time by showing the changes in fluorescence intensities with time in presence of 20 mM of each of gemini surfactants.

Essentially, after addition of surfactant to the solution, the fluorescence intensity increases over a period of about 30 minutes, as a result of co-association of surfactant tail(s) with C-485 inside the nanotubes, thereby providing a comparatively hydrophobic environment around C-485 molecules. After ~ 30 minutes, fluorescence intensity starts to decrease for about 1.5 hrs with a red shift of fluorescence band by 2 nm. This indicates that surfactant molecules need a total of about 2 hrs time to get the guest molecules out of nanotubes i.e the release of guest molecules is not an instantaneous process, rather it takes place in a controlled way. Thus this observation could be used for surfactant induced controlled release of drug from the nanotubes. After this the fluorescence intensity remains almost constant up to ~3.5 hrs followed by an increase in intensity for about 2.5 hrs. This indicates that the total time needed for the equilibrium state of formation of micelles and solubilization of released C-485 molecules in the micelles to be attained, is about 2.5 hrs.

We have also studied this time dependent binding with different concentrations of each of surfactants. Similar trends in results as described above have been noted. Table 5.4 represents the time at which maximum amount of C-485 molecules has been released from the nanotubular cavities. For a given surfactant, the rate of release increases with increaseg concentration of the surfactant. The rate of release of guest molecules also depends on the spacer chain length of gemini surfactants. At lower concentration range of gemini surfactants (up to ~ 15 mM), gemini surfactant with comparatively longer spacer chain (e.g. 12-12-12) is more effective in releasing the C-485 molecules from the cavities.

However, beyond this concentration range of surfactants, effect of chain length is not very significant. In fact, the short spacer chain (e. g. 12-3-12) is found to be slightly more effective. Thus at low concentration range, the flexible spacer chain of a surfactant allows its tail(s) to effectively enter into the cavities. However, at a high concentration, because of availability of large number of surfactant molecules to push the guest molecules out of cavities, the effect of spacer chain length becomes insignificant. This study thus reveals that binding of a guest molecule which can be a drug molecule with the nanotubes of *β*-CD and its release from the nanotubular cavities depend on the conc. and spacer chain length of gemini surfactants. The study has been carried out at a physiological pH (~7.4). The release of the guest molecule is mostly controlled which can be tuned by conc. and spacer chain length of gemini surfactants. As compared to stimuli-responsive exogenous and endogenous drug delivery systems the present system is much simpler which might provide a new direction for the development of promising drug delivery systems.

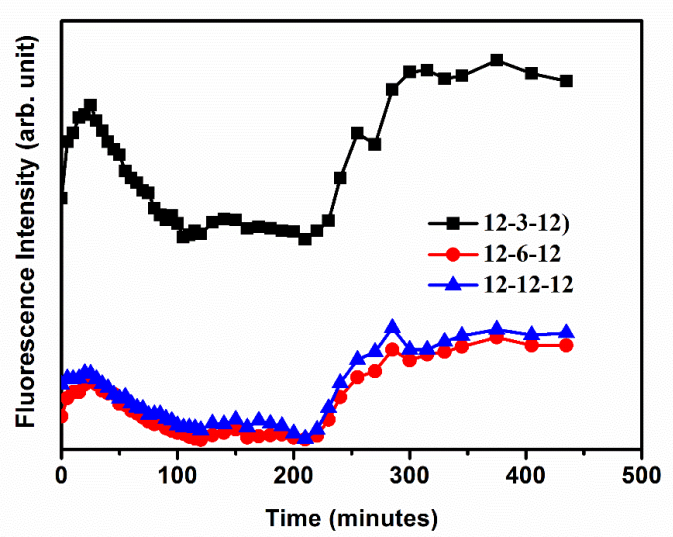

Figure 5.15. Variation in the steady-state fluorescence intensity of C-485 at 514 nm in 8.0 mM of *β*–CD with time after addition of a surfactant ([12-*n*-12] = 20 mM).

Table 5.4. Time needed to release the C-485 molecules from the nanotubular cavities by the gemini surfactants with varying spacer groups at their different concentrations.

Concentration of [12-n-12] (mM)	12-3-12 (mints)	12-6-12 (mints)	12-12-12 (mints)
5	200	200	200
10	200	180	160
15	150	130	120
20	110	120	120

5.2.3.7 Dynamic light scattering study

With increasing concentration of *β*–CD starting from a low value, the sequential formations of inclusion complexes, then nanotubes, followed by secondary aggregation of nanotubes giving rods, is seen from dynamic light scattering (DLS) measurements. The size distribution graphs obtained from DLS experiments are shown by Figures 5.16a-c and hydrodynamic diameter data are presented by Table 5.5. It is known that *β*–CD molecules in absence of guest molecules form spherical aggregates in aqueous medium.[21, 91] In the present case the size of this aggregates at 8.0 mM concentration of *β*–CD is found to be 269 nm (Table 5.5). In presence of 5.0 μM of C-485 as guest, the *β*–CD molecules at 1.5 mM concentration form small inclusion complexes of sizes 1.47 nm and 74.28 nm. On further increasing concentration of *β*–CD with same concentration of C-485, initially nanotubes are formed, the sizes of which are seen to be ~141 nm and ~150 nm with smaller inclusion complexes of sizes 1.10 nm and 1.48 nm at 4 mM and 5 mM of *β*–CD, respectively. The size of the rods formed through secondary aggregation of nanotubes is found to be ~287 nm at 8.0 mM of *β*–CD. The structural changes of these rods upon addition of surfactant has also been studied with DLS measurements. As discussed above at a low concentration of surfactant there is coassociation of the guest molecule and surfactant tail(s) inside the tubes. DLS data shows that at a low concentration of surfactant longer rodlike structures are formed than that in absence of a surfactant. The sizes of rods are found to be ~659, ~594, and ~357 nm in presence of 0.5 mM of each of 12-3-12, 12-6-12 and 12-12-12, respectively. Thus surfactant molecules at a low concentration favor the formation of longer rod structures. The spacer chain length also has an effect on the formation of rods. Gemini surfactant molecules with comparatively smaller spacer chain form longer rods. With increasing concentration of surfactant, the structures of rods become shorter. For 12-3-12, 12-6-12, and 12-12-12, the sizes of rods are ~413, ~562, ~330 nm, respectively at their 1.0 mM concentration and ~237, ~185 and ~177 nm, respectively at their 5.0 mM concentration. These results show that with increasing concentration of a surfactant the structures of rods become shorter as a result of release of guest molecules from the nanotubular cavities. At 5.0 mM concentration of each of three surfactants, the sizes of rods are shorter than that in absence of these surfactants. This is a concentration at which a large portions of guest molecules come out from the nanotubular cavities. The rod structures do exist in presence of surfactant molecules as well. Of course, there is a possibility that some C-485 molecules may be present deep inside the tubes.

Micelles formed by a portion of surfactant molecules not participating in tube formation begin to appear along with the big stuctures at a higher concentration of surfactants. Bigger micelles are observed at 10 mM concentration of surfactants. At this concentration the increasing order of size of micelles is as follows: 12-12-12 < 12-6-12 < 12-3-13. These results are consistent with our above mentioned observations that the fluorescence intensity, fluorescence lifetime, and rotational relaxation time of C-485 in the micelles of gemini surfactants increase with decreasing spacer chain length. Zana *et al*. also have reported that gemini surfactants with small spacer chain form bigger micelles.[92]

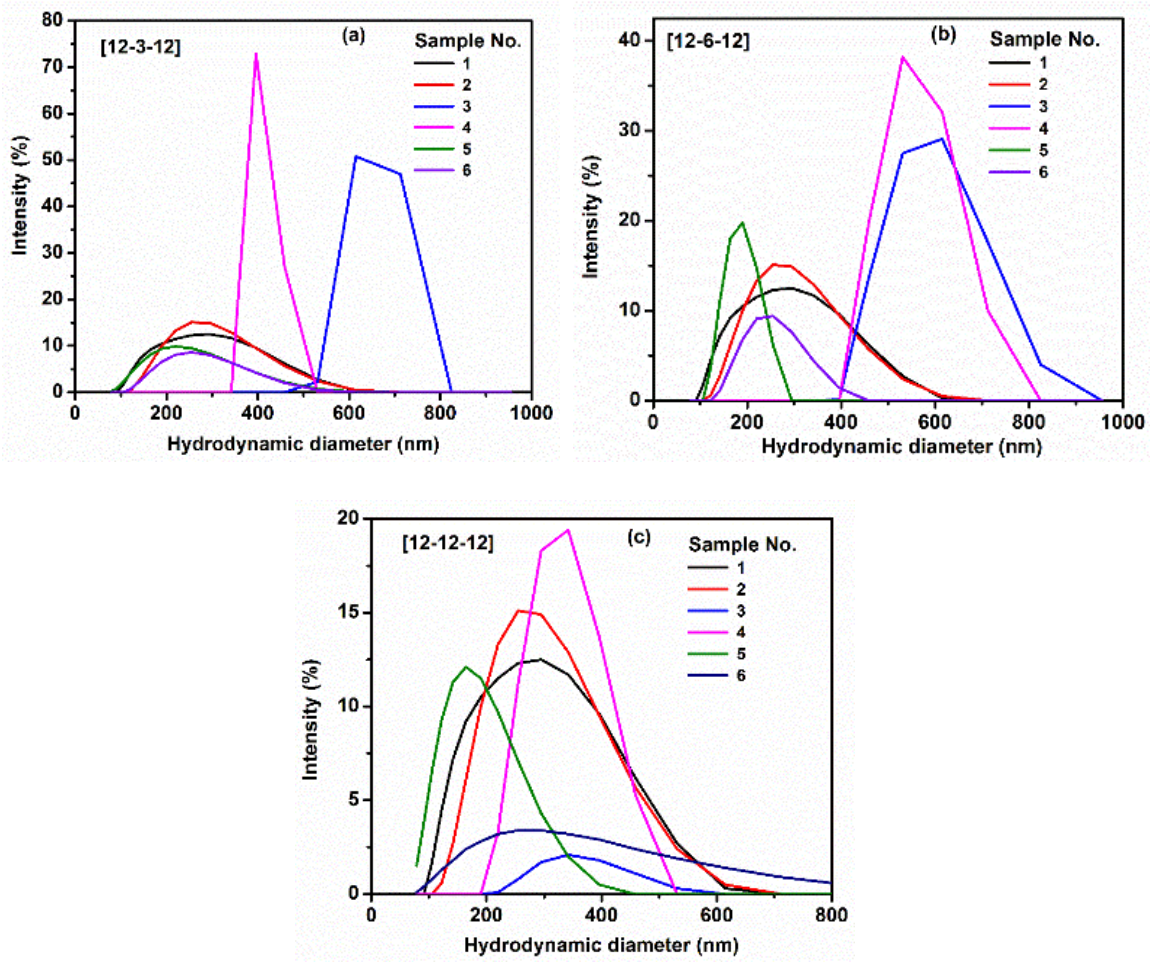

Figure 5.16. Size distribution graphs for C-485-*β*–CD-[12-*n*-12] systems for (a) 12-3-12, (b) 12-6-12, and (c) 12-12-12 obtained from dynamic light scattering (DLS) measurement. (Details of samples are given in Table 5.5)

From DLS data it is also noted that at 10 mM concentration of surfactant the sizes of rods are bigger as compared to 5 mM concentration. Thus in presence of very high concentration of surfactant molecules again big rod like structures are fomed. Our above mentioned observation of easy release of guest molecules by gemini surfactants with

longer spacer is also evidenced by the DLS data. Up to 5.0 mM concentration (concentration required for release of good portion of guest molecules), 12-12-12 surfactant molecules have formed smallest rod structures. Therefore, while gemini surfactant with a small spacer chain can form bigger rod structures, a gemini surfactant with a long spacer chain is more easily able to get guest molecules out of nanotubes. Scheme 5.3 is a pictorial representation of the formation of nanotubes and secondary aggregation of nanotubes, and the effect of the concentration of a gemini surfactant on the binding interaction of C-485 with the nanotubes.

Ganzalez Gaitano *et al.*[91] have studied the aggregation behaviour of the cyclodextrins, and found aggregates of *β*–CD with hydrodynamic radius of 174 nm even after the filtration with 0.2 μM pore sized filter paper without presence of any guest molecules. They concluded these large aggregates of *β*–CD after the filtration are due to the aggregation of cyclodextrins. The stability of the aggregates of *β*–CD is greater than those of *α*– and *γ*–CD.

Table 5.5. Hydrodynamic diameter of various particles: *β*–CD, C-485-*β*–CD and C-485-*β*–CD-[12-n-12] in aqueous solutions at various compositions. All samples were filtered through a 0.22 μM filter.

Sample	[*β*–CD] (mM)	[C-485] (μM)	[12-n-12] (mM)	Diam. (nm)	12-3-12 Diam. (nm)	12-6-12 Diam. (nm)	12-12-12 Diam. (nm)
1.	8.0	-	-	269 ±26	-	-	-
2.	8.0	5.0	-	287 ±19	-	-	-
3.	8.0	5.0	0.5		659 ±45	594 ±41	357 ±32
4.	8.0	5.0	1.0		413 ±28	562 ±39	330 ±31, 1.2 ±0.3
5.	8.0	5.0	5.0		237 ±23, 0.9 ±0.2	185±15, 3.1 ±0.6, 0.7 ±0.1	177 ±13, 1.4 ±0.9
6.	8.0	5.0	10.0		265 ±25, 7.8 ±3.0, 2.6 ±0.8	248 ±29, 2.8 ±0.9, 0.6 ±0.1	323 ±27, 1.5 ±0.7

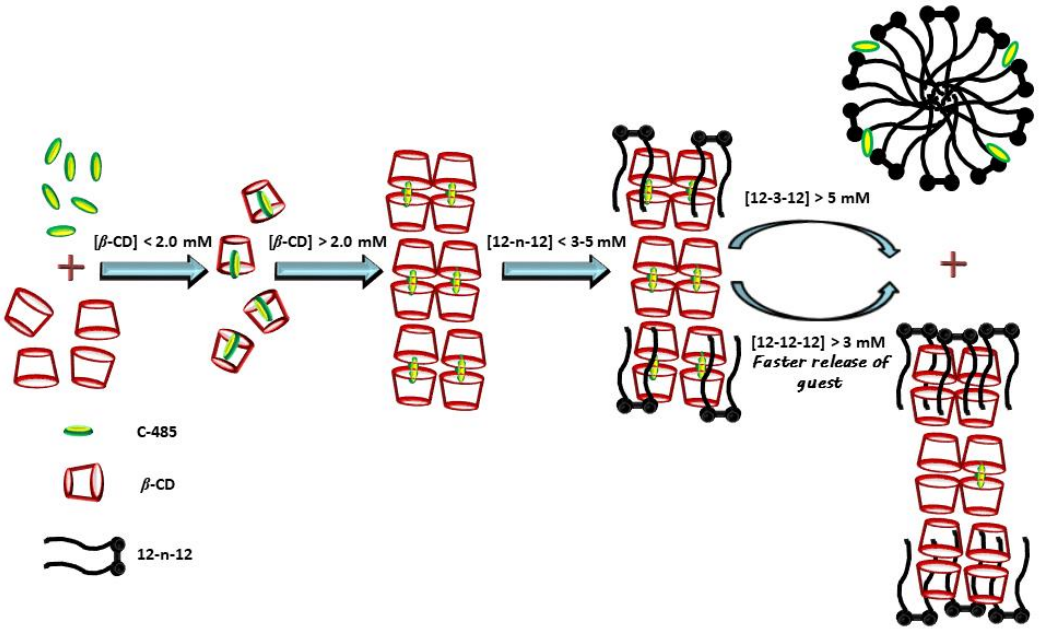

Scheme 5.3: Pictorial representation of the formation of nanotubes and secondary aggregation of nanotubes, and effect of concentration of a gemini surfactant on the binding interaction of C-485 with the nanotubes.

5.3 Conclusions

β–CD molecules at low concentration range form simple 1:1 inclusion complexes with C-485 molecules. However, at a high concentration, *β*–CD molecules form extended nanotubes, which further leads to the secondary aggregates by internanotubular hydrogen bonding making rod-like structures. Gemini surfactant molecules affects the binding of C-485 molecules with the nanotubes of *β*–CD molecules. Studies have been carried out with three different gemini surfactants, 12-3-12, 12-6-12 and 12-12-12 with 3, 6, and 12 $–CH_2-$ units, respectively present in the spacer group. At low concentration of surfactants, there is a co-association of tail(s) of a gemini surfactant molecule with C-485 molecule inside the nanotubular cavities. Gemini surfactant molecules at low concentration favor the guest molecules induced formation of nanotubes, and secondary aggregates of nanotubes of *β*–CD molecules giving bigger rodlike structures. However, with increasing concentration of gemini surfactant, the sizes of rods are reduced. Both fluorescence and DLS data show that gemini surfactant molecules at high concentrations, are capable of releasing the guest molecules i.e. C-485 molecules from the cavities of nanotubes. The release of guest molecules is not instantaneous but controlled which is affected by the length of spacer group and concentration of gemini surfactant molecules. A gemini molecule with a

comparatively longer spacer chain is more efficient in taking the guest molecules out of the nanotubular cavities. Evidently, tails attached to a longer spacer group can more easily enter into the cavities, and at the same time, two tails can enter into two different nanotubes due to the flexible nature of spacer group. With increasing concentration of surfactant, less time is required for release of the guest molecules. At very high concentration of a surfactant, however, the dependence of release time on the length of spacer group becomes less significant probably due to the availability of large number of surfactant molecules to push the guest molecules out of the cavities. Study also shows that the guest molecules those come out of the nanotubular cavities get solubilized in the micelles formed by surfactant molecules. The physical properties like micropolarity and microviscosity of the micelles, are not affected by the presence of β–CD molecules in the system. Even in presence of β–CD, the microviscosity of micelles decreases and micropolarity of micelles increases with increasing spacer chain length, which is similar to the behaviour observed in the absence of β–CD. In case of micelles of each of 12-6-12 and 12-12-12 surfactants, the environment around guest molecules (i.e. C-485) in the micelles, is similar to that inside the nanotubular cavities. However, in the case of micelles of 12-3-12 the free rotation of guest is more restricted than that in nanotubular cavities because 12-3-12 form comparatively bigger micelles with greater microviscosity. The present work suggests that drug delivery systems may be designed, with controlled release of drug molecules which can be tuned by changing the spacer chain length and concentration of gemini kind of surfactant molecules.

References

1. P. Gupta, K. Vermani and S. Garg, *Drug Discov. Today* , 2002, **7**, 569-579.
2. Q. He and J. Shi, *J. Mater. Chem.*, 2011, **21**, 5845-5855.
3. H. Yan, C. Teh, S. Sreejith, L. Zhu, A. Kwok, W. Fang, X. Ma, K. T. Nguyen, V. Korzh and Y. Zhao, *Angew. Chem.*, 2012, **124**, 8498-8502.
4. Y. Bae, N. Nishiyama, S. Fukushima, H. Koyama, M. Yasuhiro and K. Kataoka, *Bioconjugate Chem.*, 2005, **16**, 122-130.
5. O. Tacar, P. Sriamornsak and C. R. Dass, *J. Pharm. Pharmacol.* , 2013, **65**, 157-170.
6. F. Masood, *Mater. Sci. Eng. C* , 2016, **60**, 569-578.
7. K. Kataoka, A. Harada and Y. Nagasaki, *Adv. Drug Deliv. Rev.*, 2001, **47**, 113-131.

8. M. L. Bender and M. Komiyama, *Cyclodextrin chemistry*, Springer Science & Business Media, 2012.
9. S. Aggarwal, P. Singh and B. Mishra, *Die Pharmazie*, 2002, **57**, 191-193.
10. A. Ohira, M. Sakata, I. Taniguchi, C. Hirayama and M. Kunitake, *J. Am. Chem. Soc.*, 2003, **125**, 5057-5065.
11. S. Hashimoto and J. Thomas, *J. Am. Chem. Soc.*, 1985, **107**, 4655-4662.
12. T. Yorozu, M. Hoshino and M. Imamura, *J. Phys. Chem.*, 1982, **86**, 4426-4429.
13. R. S. Wylie and D. H. Macartney, *J. Am. Chem. Soc.*, 1992, **114**, 3136-3138.
14. A. Harada, J. Li and M. Kamachi, *Nature*, 1992, **356**, 325.
15. A. Harada, *Acc. Chem. Res.*, 2001, **34**, 456-464.
16. B. J. Ravoo, R. Darcy, A. Mazzaglia, D. Nolan and K. Gaffney, *Chem. Commun.*, 2001, 827-828.
17. A. Harada, J. Li and M. Kamachi, *Nature*, 1993, **364**, 516.
18. G. Li and L. B. McGown, *Science*, 1994, **264**, 249-252.
19. G. Pistolis and A. Malliaris, *J. Phys. Chem.*, 1996, **100**, 15562-15568.
20. A. Wu, X. Shen and Y. He, *J. Colloid Interface Sci.*, 2006, **297**, 525-533.
21. A. Wu, X. Shen and Y. He, *J. Colloid Interface Sci.*, 2006, **302**, 87-94.
22. R. A. Agbaria and D. Gill, *J. Photochem. Photobiol. A Chem.*, 1994, **78**, 161-167.
23. P. Das, A. Chakrabarty, B. Haldar, A. Mallick and N. Chattopadhyay, *J. Phys. Chem. B*, 2007, **111**, 7401-7408.
24. L. Tormo, J. A. Organero and A. Douhal, *J. Phys. Chem. B*, 2005, **109**, 17848-17854.
25. M. El-Kemary, J. A. Organero, L. Santos and A. Douhal, *J. Phys. Chem. B*, 2006, **110**, 14128-14134.
26. A. Douhal, *Chem. Rev.*, 2004, **104**, 1955-1976.
27. T. Shimomura, T. Akai, T. Abe and K. Ito, *J. Chem. Phys.*, 2002, **116**, 1753-1756.
28. E. Engeldinger, D. Armspach and D. Matt, *Chem. Rev.*, 2003, **103**, 4147-4174.
29. K. A. Agnew, T. D. McCarley, R. A. Agbaria and I. M. Warner, *J. Photochem. Photobiol. A Chem.*, 1995, **91**, 205-210.
30. C. Zhang, X. Shen and H. Gao, *Chem. Phys. Lett.*, 2002, **363**, 515-522.
31. R. A. Agbaria and D. Gill, *J. Phys. Chem.*, 1988, **92**, 1052-1055.
32. M. Sowmiya, P. Purkayastha, A. K. Tiwari, S. S. Jaffer and S. K. Saha, *J. Photochem. Photobiol. A Chem.*, 2009, **205**, 186-196.
33. T. E. Girardeau, J. Leisen and H. W. Beckham, *Macromol. Chem. Phys.*, 2005,

206, 998-1005.

34. C. Zhang, X. Shen and H. Gao, *Chem. Phys. Lett.*, 2002, **363**, 515-522.
35. A. Harada and M. Kamachi, *Macromolecules*, 1990, **23**, 2821-2823.
36. A. Harada, J. Li and M. Kamachi, *Nature*, 1994, **370**, 126.
37. A. Harada, M. Okada, J. Li and M. Kamachi, *Macromolecules*, 1995, **28**, 8406-8411.
38. S. A. Nepogodiev and J. F. Stoddart, *Chem. Rev.*, 1998, **98**, 1959-1976.
39. A. Harada, *Adv. Polym. Sci.* , 1997, 141-191.
40. R. Palepu and V. C. Reinsborough, *Can. J. Chem.*, 1988, **66**, 325-328.
41. U. R. Dharmawardana, S. D. Christian, E. E. Tucker, R. W. Taylor and J. F. Scamehorn, *Langmuir*, 1993, **9**, 2258-2263.
42. R. Palepu, J. E. Richardson and V. C. Reinsborough, *Langmuir*, 1989, **5**, 218-221.
43. A. A. Rafati, A. Bagheri, H. Iloukhani and M. Zarinehzad, *J. Mol. Liq.*, 2005, **116**, 37-41.
44. E. Junquera, G. Tardajos and E. Aicart, *Langmuir*, 1993, **9**, 1213-1219.
45. A. J. Valente and O. Söderman, *Adv.Colloid Interface Sci.*, 2014, **205**, 156-176.
46. N. Funasaki, H. Yodo, S. Hada and S. Neya, *Bull. Chem. Soc. Jpn* , 1992, **65**, 1323-1330.
47. S. Mehta, K. Bhasin, S. Dham and M. Singla, *J. Colloid Interface Sci.*, 2008, **321**, 442-451.
48. A. Petek, M. Krajnc and A. Petek, *J. Incl. Phenom. Macrocyl. Chem.*, 2016, **86**, 221-229.
49. L. Zhao, L. Jiang, Y. Han, Z. Xian, J. Huang and Y. Yan, *Soft Matter*, 2013, **9**, 7710-7717.
50. C. Zhou, X. Cheng, Q. Zhao, Y. Yan, J. Wang and J. Huang, *Langmuir*, 2013, **29**, 13175-13182.
51. L. Jiang, Y. Peng, Y. Yan and J. Huang, *Soft Matter*, 2011, **7**, 1726-1731.
52. L. Jiang, Y. Peng, Y. Yan, M. Deng, Y. Wang and J. Huang, *Soft Matter*, 2010, **6**, 1731-1736.
53. L. Jiang, M. Deng, Y. Wang, D. Liang, Y. Yan and J. Huang, *J. Phys. Chem. B*, 2009, **113**, 7498-7504.
54. C. Zhou, J. Huang and Y. Yan, *Soft matter*, 2016, **12**, 1579-1585.
55. C. Zhou, X. Cheng, Q. Zhao, Y. Yan, J. Wang and J. Huang, *Scientific reports*, 2014, **4**, 7533.

56. S. S. Jaffer, S. K. Saha and P. Purkayastha, *J. Colloid Interface Sci.*, 2009, **337**, 294-299.
57. S. S. Jaffer, S. K. Saha, G. Eranna, A. K. Sharma and P. Purkayastha, *J. Phys. Chem. C*, 2008, **112**, 11199-11204.
58. S. Muthusubramanian, A. K. Tiwari and S. K. Saha, *Soft Matter*, 2012, **8**, 11072-11084.
59. Y. Han and Y. Wang, *Phys. Chem. Chem. Phys.*, 2011, **13**, 1939-1956.
60. S. He, H. Chen, Z. Guo, B. Wang, C. Tang and Y. Feng, *Colloids Surf. A Physicochem. Eng. Asp.*, 2013, **429**, 98-105.
61. S. Bhattacharya and J. Biswas, *Nanoscale*, 2011, **3**, 2924-2930.
62. C. McGregor, C. Perrin, M. Monck, P. Camilleri and A. J. Kirby, *J. Am. Chem. Soc.*, 2001, **123**, 6215-6220.
63. L. Caillier, E. T. de Givenchy, R. Levy, Y. Vandenberghe, S. Geribaldi and F. Guittard, *J. Colloid Interface Sci.*, 2009, **332**, 201-207.
64. F. M. Menger and J. S. Keiper, *Angew. Chem. Int. Ed.*, 2000, **39**, 1906-1920.
65. M. Borse, V. Sharma, V. Aswal, N. K. Pokhriyal, J. V. Joshi, P. S. Goyal and S. Devi, *Phys. Chem. Chem. Phys.*, 2004, **6**, 3508-3514.
66. M. Borse, V. Sharma, V. Aswal, P. Goyal and S. Devi, *J. Colloid Interface Sci.*, 2005, **284**, 282-288.
67. M. S. Borse and S. Devi, *Adv.Colloid Interface Sci.*, 2006, **123**, 387-399.
68. X. Wang, J. Wang, Y. Wang, H. Yan, P. Li and R. K. Thomas, *Langmuir*, 2004, **20**, 53-56.
69. M. Pisárčik, J. Jampílek, F. Devínsky, J. Drábiková, J. Tkacz and T. Opravil, *J. Surfactants Deterg.*, 2016, **19**, 477-486.
70. P. X. Li, C. C. Dong, R. K. Thomas, J. Penfold and Y. Wang, *Langmuir*, 2011, **27**, 2575-2586.
71. S. Manet, Y. Karpichev, D. Bassani, R. Kiagus-Ahmad and R. Oda, *Langmuir*, 2010, **26**, 10645-10656.
72. S. Zhang, J. Yu, J. Wu, W. Tong, Q. Lei and W. Fang, *J. Chem. Eng. Data*, 2014, **59**, 2891-2900.
73. R. Zana, *Adv.Colloid Interface Sci.*, 2002, **97**, 205-253.
74. A. K. Tiwari, M. Sowmiya and S. K. Saha, *J. Mol. Liq.*, 2012, **167**, 18-27.
75. S. Mura, J. Nicolas and P. Couvreur, *Nature Mater.*, 2013, **12**, 991.
76. R. Challa, A. Ahuja, J. Ali and R. Khar, *Aaps Pharmscitech*, 2005, **6**, E329-E357.

77. S. Bairu and G. Ramakrishna, *J. Phys. Chem. B*, 2013, **117**, 10484-10491.
78. A. Chakraborty, D. Seth, P. Setua and N. Sarkar, *J. Chem. Phys.*, 2006, **124**, 074512.
79. G. Jones, W. R. Jackson, C. Y. Choi and W. R. Bergmark, *J. Phys. Chem.*, 1985, **89**, 294-300.
80. P. Dahiya, M. Kumbhakar, T. Mukherjee and H. Pal, *Chem. Phys. Lett.*, 2005, **414**, 148-154.
81. S. Nad, M. Kumbhakar and H. Pal, *J. Phys. Chem. A*, 2003, **107**, 4808-4816.
82. H. A. Benesi and J. Hildebrand, *J. Am. Chem. Soc.*, 1949, **71**, 2703-2707.
83. S. K. Saha and A. Kanchanmala, *group*, 2006, **3**, 2.
84. J. Dey, E. L. Roberts and I. M. Warner, *J. Phys. Chem. A*, 1998, **102**, 301-305.
85. J. A. Ross, C. J. Schmidt and L. Brand, *Biochemistry*, 1981, **20**, 4369-4377.
86. K. Chinnakali, K. Sivakumar and S. Natarajan, *Acta Crystallogr. Sect. C*, 1990, **46**, 833-835.
87. J. Jasinski and E. Paight, *Acta Crystallogr. Sect. C*, 1994, **50**, 1928-1930.
88. S. Kamitori, Y. Sumimoto, K. Vongbupnimit, K. Noguchi and K. Okuyama, *Mol. Cryst. Liq. Cryst. Sci. Technol. Sect. A.*, 1997, **300**, 31-43.
89. R. Zana, M. In, H. Lévy and G. Duportail, *Langmuir*, 1997, **13**, 5552-5557.
90. M. In, V. Bec, O. Aguerre-Chariol and R. Zana, *Langmuir*, 2000, **16**, 141-148.
91. G. González-Gaitano, P. Rodriguez, J. Isasi, M. Fuentes, G. Tardajos and M. Sánchez, *J. Incl. Phenom. Macrocyl. Chem.*, 2002, **44**, 101-105.
92. R. Zana, *J. Colloid Interface Sci.*, 2002, **248**, 203-220.

Chapter 6

Gemini Surfactant Induced Release of Coumarin 485 (C-485) From the Nanotubes of β-CD Followed by Binding of C-485 with ctDNA

Key Concepts:

- *Binding of C-485 with Calf Thymus DNA (ctDNA) in a groove binding mode.*

- *Binding of the guest molecule (C-485) with ctDNA after being released from the cavity of nanotubes induced by gemini surfactants.*

Gemini Surfactant Induced Release of Coumarin 485 (C-485) From the Nanotubes of β-CD Followed by Binding of C-485 with ctDNA

Abstract: *Present study is focused on the binding of a dye, Coumarin 485 (C-485) with Calf Thymus DNA (ctDNA), explored using the spectroscopic tools such as UV-visible absorption, steady-state fluorescence and fluorescence anisotropy and time-resolved fluorescence spectroscopy and dynamic light scattering measurements. The hyperchromic shifts in absorbance and fluorescence intensity bands show that the C-485 binds with ctDNA. Ethidium bromide displacement assay and iodide ion quenching experiment confirm that C-485 binds with ctDNA through the groove binding mode. The binding of C-485 with β–CD is reduced in presence of ctDNA. β–CD molecules in presence of C-485 form the nanotubes and secondary aggregates of nanotubes, which has been explored for the carrier for C-485. Gemini surfactants, m-4-m induced the release of C-485 from the cavity of nanotubes of the β–CD. After being released from the cavity, C-485 molecules interact with ctDNA at low concentration of the gemini surfactants. The efficiency to release of C-485 from the cavity is higher for gemini with longer tails due to the favored interaction between the hydrophobic cavity of β–CD and tails of gemini surfactants. The releasing efficiency of gemini surfactants increases in the order as 12-4-12 < 14-4-14 < 16-4-16, which is according to the hydrophobicity order of their tails. The present system is useful for controlled release and binding of a drug with ctDNA.*

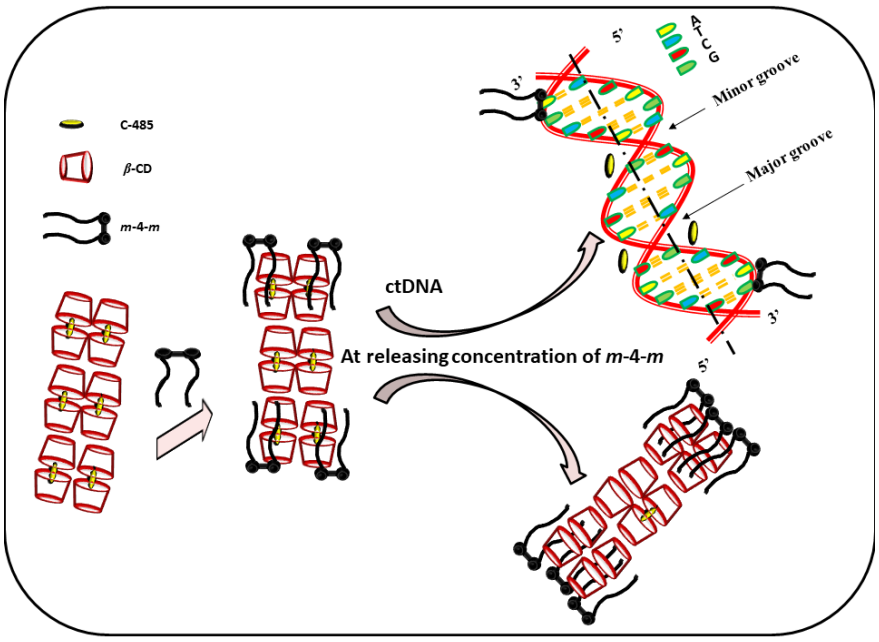

*Sunita Kumari, Sayantan Halder, Rishika Aggrawal, G. Sundar and Subit K. Saha. (communicated for publication)

6.1 Introduction

In recent times, the interactions of biological supramolecules with the drugs entities are in limelight to endorse the various structural and functional features of biomacromolecules in biophysical simulation processes.[1] The characterizations of these interactions are very much cooperative to build up effective therapeutic drugs and to have control over the gene expression.[2] Binding interaction of small molecules leads to design of the active drug against chronic and malignant diseases, biosensors, biochips and fabrication of nano-materials with the help of DNA template and DNA machines.[2-4] The biological processes are mainly controlled by the nucleic acids via relay of the instructions or message for the synthesis of functional proteins, which respond to the biological process. Further, the nucleic acid splits into deoxyribonucleic acid and ribonucleic acid based on the absence and presence of oxygen at 2^{nd} position of the ribose sugar. The deoxyribonucleic acid, DNA, is a biopolymer, controls the hereditary character of one's life, and is explored most. DNA is involved in nature's most essential processes such as gene transcription,[5] gene expression,[6, 7] mutagenesis,[8] etc.

Calf thymus DNA, abbreviated as ctDNA, is a polymer of nucleotides. Its backbone contains the sugar-phosphate sequence in the alternate form. The protein contents are very low in ctDNA. The drug-DNA interactions show mainly three types of binding modes *viz.* (i) electrostatic binding between the negatively charged DNA phosphate backbone, which is along the external DNA double helix and the positively charged part of drug, (ii) groove binding, which involves hydrogen bonding or van der Waals interaction with the nucleic acid bases in deep major groove or shallow minor groove of the DNA helix, and (iii) intercalative binding, in which the drug intercalates itself within the nucleic acid base pairs.[9, 10] Out of all three binding modes, intercalative binding is mainly effective for targeted drugs DNA interaction and are investigated using sensitive spectroscopic techniques.[11] However, groove binding is also well studied and are important in antitumor activity.[12, 13] Structural design and electronic distribution of the small molecules affect their binding affinities towards the specific sequence of biomacromolecules.[14] To design and develop the effective drug molecule against diseases,[15] which are controlling the gene expression,[16] the interaction of the small molecules with DNA gives the useful information. Thus, the efficient fluorescent probe

molecules are helping us in the fluorometric detection of DNA-drug interaction and are getting attention for the several biological target[1]

Coumarins, a family of benzo-α-pyrones, are well known fluorescent molecules with a wide range of emission for the biological applications.[17-21] Coumarins have been used clinically for the treatment of many diseases.[22, 23] Coumarin derivatives exhibit interesting fluorescence properties, which include a high degree of sensitivity to their local environment, including polarity and viscosity and are used in the heterogeneous inclusion system.[24] Reports are available on the binding of some coumarin derivatives with DNA.[25-27] Among CDs, α-CD, β-CD and γ-CD, with six, seven and eight D-glucopyranose units of cavity size 5.6, 7.8 and 9 Å, respectively, the β-CD is the most used because of its suitable size for encapsulation of aromatic molecules. Mostly available pharmaceutical products with β-CD are Cetirizine/β-CD, Flunarizine/β-CD, Thiomersal/β-CD, Meloxicam/β-CD, Voriconazole/sulfobutyl ether-β-CD.[28]

Not only the aromatic molecules but also some polymers are reported to form inclusion complexes with CDs.[29] The formation of inclusion complexes of the β–CD with the hydrophobic tail of a conventional surfactant molecule is explored well[30-33] and observed that this type of complex formation delays the micellization process of surfactants, consequently, enhances the apparent critical micellar concentration (*cmc**).[32, 34-36].[37, 38] There are also other reports on the binding of amphiphilic molecules with the CDs.[39, 40] Recently, we have studied guest molecule induced formation of the nanotubes and secondary aggregates of nanotubes of β–CD and release of guest in presence of conventional[41] as well as gemini surfactants [Chapter 5].

Nowadays, gemini surfactants have been displayed to be highly effective in delivering genetic material to cells, and also have been shown talented as synthetic additives in liposome formulations for drug delivery.[42] Because of the negative charge of the phosphate backbone, DNA can bind with the cationic surfactants easily.[43-47] Cationic surfactants have the capability to compact/condense and decompact/decondense the DNA by their electrostatic interactions.[47] These types of interactions in DNA-cationic surfactants are useful in the transfer the DNA across the cell membranes for the gene delivery.

In this chapter, we have explored C-485-*β*–CD host-guest system as a possible drug carrier, which has been discussed in Chapter 5. Gemini surfactants, *m*-4-*m*, where *m* [*m* = 12, 14, and 16] [Scheme 6.1] represents the number of carbon atoms in a hydrocarbon tail, are used for this study These gemini surfactants are used to release the guest molecule, C-485 [Scheme 6.1] from the cavity of the nanotubes of *β*–CD. Effectiveness of the gemini surfactants to release C-485 from the cavity of nanotubes of *β*–CD increases on increase in the tail length of gemni surfactants. After being released from the cavity of nanotubes of *β*–CD, C-485 molecules bind with ctDNA. The binding of the C-485 with ctDNA depends on the concenration of the gemini surfactants. Thus for the binding of C-485 with ctDNA, a certain concentration of gemini surfactant is required, which is capable of release of guest C-485 from the cavity of *β*–CD. If a high concentration of gemini surfactant is used, then the surfactants form micelles and the released C-485 solublized in the micelles. Study shows that the groove binding is the mode of the binding of C-485 with ctDNA. The binding of C-485 with *β*–CD is restricted to some extent in presence of ctDNA.

The investigation of the interactions between drugs and DNA, especially some antifungal, antiviral, antibacterial, and antitumor drugs targeting the tumor and infected cells, has grown to be an imperative center in life sciences, medicine and chemistry. Small molecules with fluorescent entity with precisely known mode of binding can result in DNA-binding based leads in the development of drugs. The release of drug molecule is does not depends on the exogenous and endogenous stimuli as these are required in the stimuli-responsive drug releasing systems. Therefore, studied system can be applied in the effective drug carrier and release system in pharmaceutics and biomedical science.

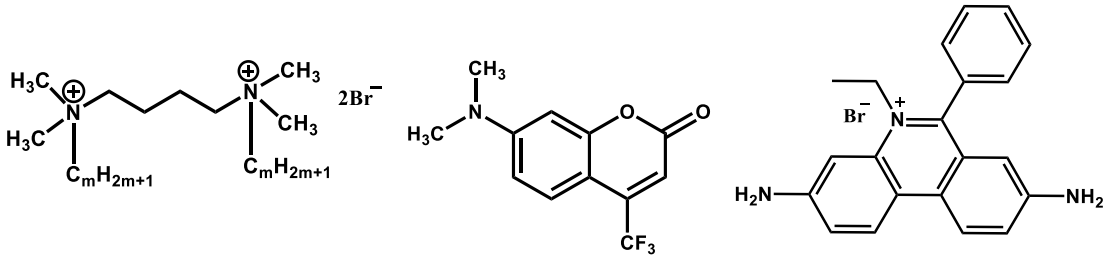

m-4-*m*, *m* = 12, 14, and 16 C-485 Ethidium bromide (EB)

Scheme 6.1: Structure of gemini surfactants, Coumarin 485 (C-485) and ethidium bromide (EB).

6.2 Results and discussion

6.2.1 Binding of C-485 with ctDNA

6.2.1.1 UV-visible absorption and fluorescence properties

The UV-Vis absorption spectra of C-485 (5.0 μM) in aqueous HEPES buffer solution shows a λ_{max}^{abs} of low energy broad band at 405 nm. The absorption spectra and A/A_o plot of C-485 with variation in the concentration of ctDNA is shown in Figure 6.1. Absorption peak maxima are given in Table 6.1. Additions of ctDNA (0-15 μM) to the buffered solution of C-485 trigger the significant increase in the absorbance with 1 nm blue shift in λ_{max}^{abs}. The increase in absorbance with the addition of ctDNA reveals the binding interaction between both ctDNA and C-485. Beyond 15 μM, absorbance exhibits decreasing tendency because at this concentration of ctDNA binding between ctDNA and C-485 reach a saturation level with a very little (1 nm) blue shift in λ_{max}^{abs} suggesting a non-intercalative binding of C-485 with the ctDNA. Generally, as a result of intercalative binding of small molecules with ctDNA there should be a large shift in the absorption peak maxima.[48] It is well documented that the groove binding of small molecules with ctDNA does not alter the absorption peak maxima or causes an insignificant change in absorption maxima[8, 49-51] is well corroborated with the present results. Thus, the present mode of binding of C-485 with ctDNA is groove binding. The weaker interactions between the small molecules and ctDNA cause only hypochromic or hyperchromic shift without significant changes in the wavelength in their spectral profiles.[52]

Figure 6.2a displays the changes in the fluorescence spectra of C-485 in presence of different concentrations of ctDNA. To illustrate the interactions of C-485 with ctDNA, the ratio of its fluorescence intensities in presence and in absence of ctDNA (F/F_o), is displayed in Figure 6.2b. Figure 6.2b reveals that with an increase in the concentration of ctDNA the fluorescence intensity of C-485 increases and then decreases after a certain high concentration of ctDNA. The fluorescence peak maxima, however, remain unaffected with an increase in the concentration of ctDNA (data are given in Table 6.1). The increase in fluorescence intensity describes the binding of C-485 with ctDNA. The hyperchromic shifts in the fluorescence intensity of C-485 in presence of ctDNA suggests that C-485 is experiencing comparatively rigid microenvironment due to binding interactions with

ctDNA. To check the motional restrictions of C-485 after binding with ctDNA, the steady-state fluorescence anisotropy measurements have been carried out.[53-56]

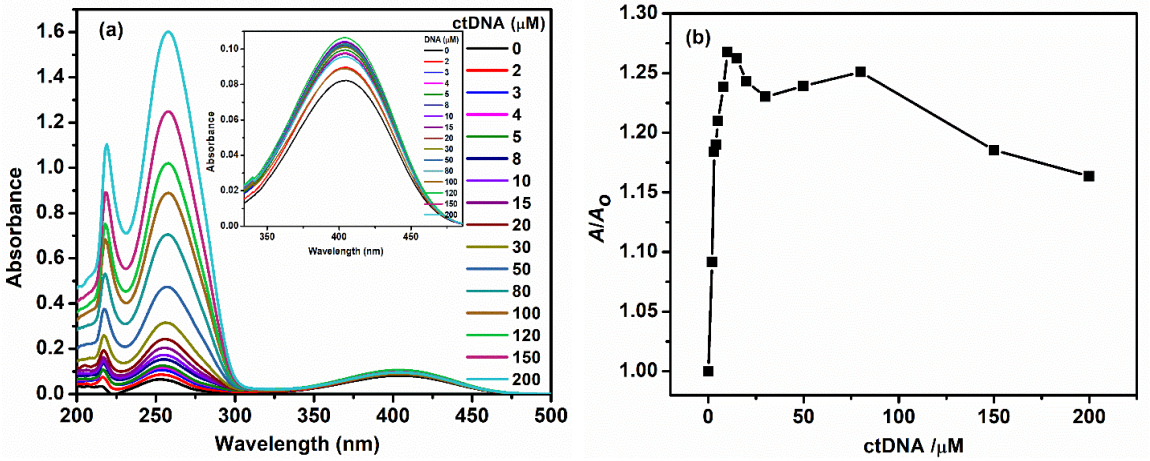

Figure 6.1. (a) Absorption spectra of C-485 (5.0 μM), (b) A/A_o at the wavelength of 404 nm, with varying concentrations of ctDNA.

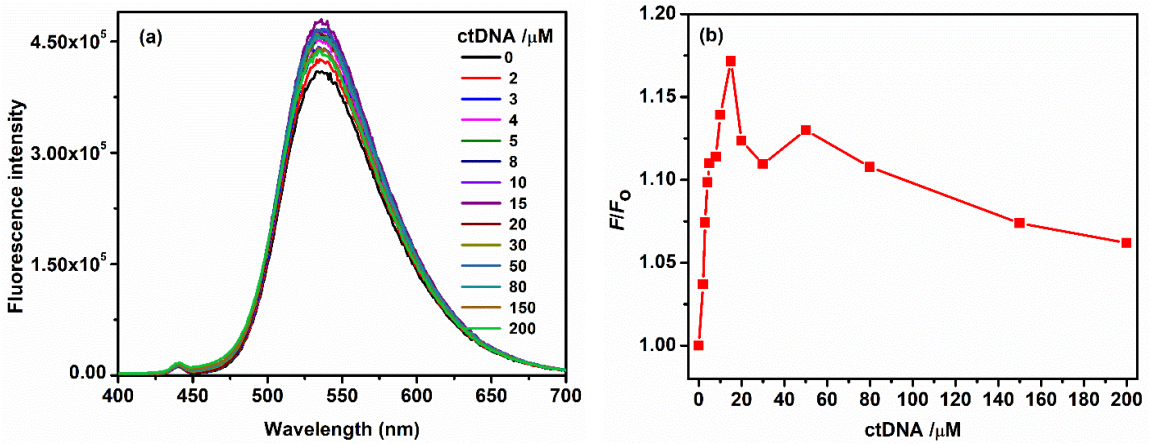

Figure 6.2. (a) Fluorescence spectra of C-485 (5 μM), (b) F/F_o at the wavelength of 526 nm, with varying concentrations of ctDNA. [λ_{ex} = 375 nm].

The fluorescence anisotropy values of C-485 at different concentrations of ctDNA are given in Table 6.1 and are plotted in Figure 6.3. The increase in fluorescence anisotropy with an increasing concentration of ct-DNA suggests that the tumbling motions of C-485 are restricted after binding with ctDNA. Therefore, on binding with ctDNA the rates of nonradiative processes are reduced resulting in the fluorescence enhancement.[57] Thus, the fluorescence properties depict that C-485 is residing in the comparatively less polar and more rigid environment in ctDNA as compared to the buffer solution.[58, 59]

Table 6.1. Variation in the peak maxima of absorption (λ_{max}^{abs}) band, peak maxima of fluorescence (λ_{max}^{flu}) band, steady-state anisotropy (r), and average excited state lifetime ($<\tau_f>$) of C-485 (5.0 μM) in the HEPES buffer solution with addition of ctDNA (0-200 μM). [λ_{ex} = 375 nm, λ_{em} = 510 nm].

Sr. No.	ctDNA (μM)	λ_{max}^{abs} (nm)	λ_{max}^{flu} (nm)	r	a_1	τ_1 (ps)	a_2	τ_2 (ps)	$<\tau_f>$ (ps)	χ^2
1	0	405	536	0.026	0.55	70	0.45	470	250	1.29
2	2	405	536	0.028	0.53	74	0.47	473	262	0.95
3	3	405	536	0.030	0.99	405	0.01	1501	416	1.07
4	4	404	536	0.029	0.99	407	0.01	1360	417	1.18
5	5	404	536	0.030	0.99	411	0.01	1203	419	1.18
6	8	404	536	0.034	0.99	409	0.01	1427	419	1.14
7	10	404	536	0.034	0.99	410	0.01	1518	421	1.19
9	15	404	536	0.034	0.99	422	0.01	1721	435	1.07
10	20	404	536	0.038	0.99	416	0.01	2728	440	1.08
11	50	404	536	0.039	0.99	417	0.01	2931	456	0.95
12	80	404	536	0.046	0.99	426	0.01	3426	454	0.98
13	100	404	536	0.044	0.99	422	0.01	3650	454	1.01
14	150	404	536	0.047	0.99	418	0.01	4011	456	1.03
15	200	404	536	0.053	0.99	416	0.01	4121	459	1.11

Fluorescence lifetime decays are highly sensitive and responsive towards the changes in microenvironment around the probe.[49, 50, 60, 61] Therefore, decay components obtained from the fluorescence lifetime measurements provide important information about the interaction of the fluorophore in the microheterogeneous environment. In HEPES buffer, C-485 shows bi-exponential decay with a fast component of 70 ps (55 %) and a slow component of 470 ps (45 %) (average lifetime of 250 ps) (Table 6.1). In presence of ctDNA, C-485 exhibits bi-exponential decays with very nominal slow component. On increase in the concentration of ctDNA in the solution, the average lifetime of C-485 is increased (Table 6.1), because on addition of ctDNA more and more C-485 molecules bind with ctDNA. After binding with ctDNA, the fast decay component is found to be ~ 400 ps. However, the lifetime of slow component (1%) becomes longer with increasing concentration of ctDNA. The multiexponential decays of a polarity sensitive fluorophore in the microheterogeneous environment are due to the different location of the fluorophore. [62-64] The fast and slow components might be corresponding to binding of C-485 with ctDNA with a groove binding mode (discussed later) and a mode with comparatively stronger binding interactions.

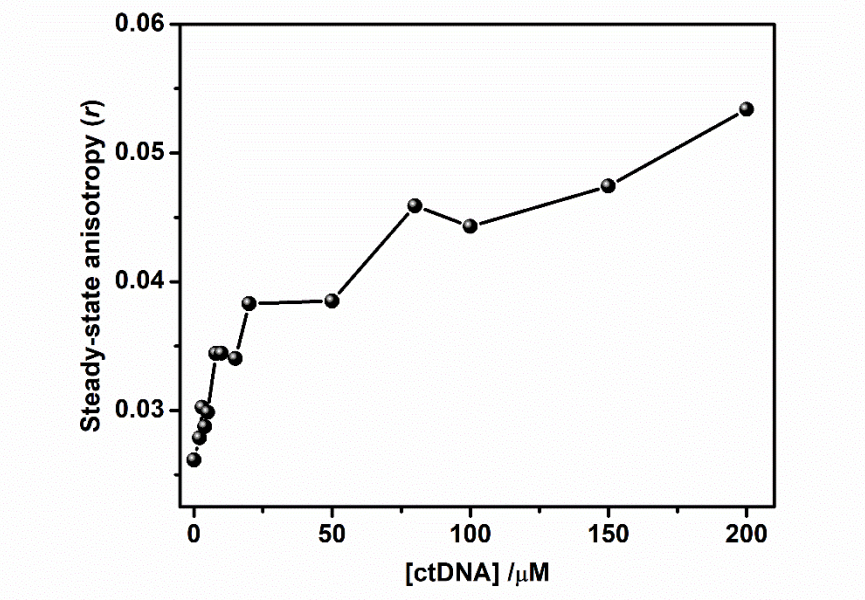

Figure 6.3. Variation of the steady-state fluorescence anisotropy of C-485 (5.0 μM) as a function of the concentration of ctDNA (intensities have been measured at 525 nm).

6.2.2 Competitive displacement analysis between ethidium bromide and C-485

Ethidium bromide (EB) [Scheme 6.1] is a well-known planar fluorophore that binds to ct-DNA in an intercalative mode.[65] EB have less emission intensity in the buffer solution due to quenching by the solvent molecules. The fluorescence of EB is drastically enhanced in presence of ct-DNA with a blue shift in the peak maxima as shown by the Figure 6.4. This change in the fluorescence properties confirmed that the EB molecules are strongly intercalated within the base pairs of DNA double helix.[66] Due to this type of binding, the EB is highly applicable in DNA binding investigations to confirm the binding mode.

The fluorescence properties of DNA bound EB depend on other added intercalative or groove binder. If the added molecule is intercalated strongly within base pairs of DNA as compared to the EB, consequently, the fluorescence intensity of EB decreases because the newly added molecule replaces the EB from the ctDNA. However, if the added molecule has a groove mode of binding with DNA, then in that case EB molecule is not replaced and no change in the fluorescence properties should be observed. Thus, the fluorescence quenching of EB bound to ct-DNA can be used to estimate the extent of binding between a new molecule and ct-DNA.[67-69] Herein, to confirm the binding mode of C-485 with ctDNA, the EB displacement experiment has been performed in which, C-485

have been added to the EB-ctDNA solution. Insignificant change has been observed in the fluorescence spectra of EB on the addition of C-485 (represented by Figure 6.4) which indicates that C-485 molecule does not have an intercalative mode of binding rather it binds with ctDNA through groove mode of binding (discussed below).

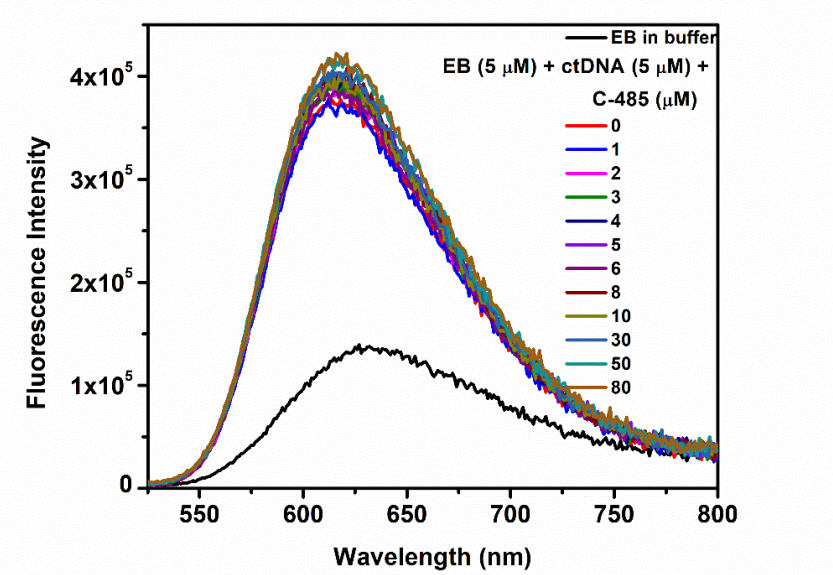

Figure 6.4. Fluorescence spectra of the EB (5.0 μM) in the buffer and in presence of the ct-DNA (5 μM), and in presence of the ct-DNA (5 μM) and EB with varying concentration of the C-485 (0-80 μM). (λ_{ex} = 515 nm, both excitation, and emission slit widths are kept at 3 nm).

6.1.3 Iodide quenching

Further, to prove that the C-485 molecule binds with ctDNA through groove binding mode instead of intercalative mode, the quenching experiment has been performed with KI. Iodide ion is good quencher for the small molecules. Since the DNA molecule has the phosphate backbone, which is negatively charged, so, the small molecules, which are interacting with DNA, are protected from the anionic quencher molecules. The extent of protection is lesser for the groove binder as compared to the intercalated binders.[70] Therefore, the fluorescence of groove binder molecule would be quenched effectively due to ease of access by the anionic quencher. Quenching has been studied by using following Stern-Volmer Equation:

$$\frac{F_0}{F} = 1 + K\mathrm{sv}[Q] \qquad (6.1)$$

where F_o and F are the fluorescence intensities of C-485 in the absence and presence of the quencher molecule, Q. K_{sv} is the Stern-Volmer quenching constant. Figure 6.5 represents the Stern-Volmer plots for the quenching of C-485 by I^- ions in absence and presence of the ctDNA. K_{sv} values calculated from the slope of the plots for the free C-485 and bound C-485 are found to be 3.75 M^{-1} and 2.38 M^{-1}, respectively. The regression coefficient for these two plots are noted to be 0.999 and 0.996. We find that the quenching constant of C-485 bound with ctDNA is comparatively lesser than that of free C-485 which again supports the binding of C-485 with ctDNA. Quenching results indicate that C-485 molecules bind with ctDNA through the groove binding mode.

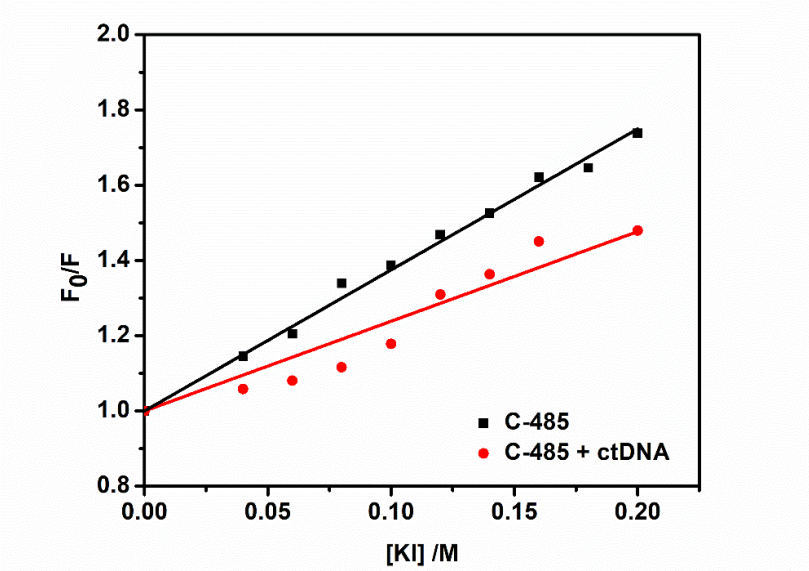

Figure 6.5. Fluorescence quenching plot of C-485 (5.0 µM) in the absence and presence of ctDNA (5.0 µM) with varied concentration of KI.

6.1.4 Binding of C-485 with *β*-CD in presence of ctDNA (5.0 µM)

The effect of *β*-CD on the absorption spectra of C-485 has been studied by keeping the concentrations of C-485 and ctDNA fixed (both 5.0 µM) and changing the concentration of *β*-CD. Absorption spectra and A/A_o of C-485 with different concentration of *β*-CD are shown in Figure 6.6a and 6.6b, respectively, absorption peak maxima are tabulated in Table 6.2. The addition of *β*-CD increases the absorbance of C-485 up to 2.5 mM, with a blue shift of 2 nm, and above 2.5 mM, the absorbance becomes constant. Blue shift indicates the complexation of C-485 with *β*-CD. Since, the complexation between the C-485 with *β*-CD is more stronger than that between C-485 and ctDNA, consequently, more and more C-485 molecules bind with *β*-CD with increasing concentration of *β*-CD.

The fluorescence spectra and F/F_o of C485 with various concentrations of β-CD are shown in Figure 6.7 and spectral data are summarized in Table 6.2. Upon addition of β-CD, the fluorescence of C-485 is enhanced, with a larger magnitude initially up to 4 mM of β-CD and above this concentration, fluorescence intensity becomes constant. Fluorescence peak maxima are blue shifted from 536 to 520 nm. This data also support that C-485 molecules are encapsulated in β-CD even in presence of ctDNA.

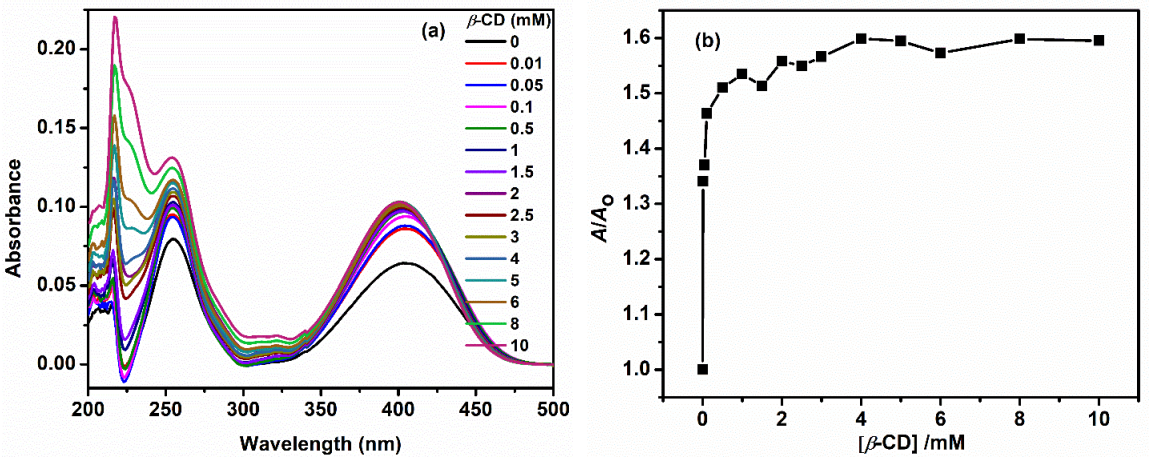

Figure 6.6 (a) Absorption spectra of C-485 (5 µM), (b) A/A_o at the wavelength of 404 nm, at a fixed concentration of ctDNA (5 µM) with varying concentrations of β-CD.

In presence of ctDNA, at the low concentration of β-CD simple inclusion complexes are formed followed by formation of nanotubes at further higher concentration of β-CD. The stoichiometry of inclusion complexes is determined by Benesi-Hildebrand Equations, 1.1 and 1.2 (Chapter 1).[71-74] The concentration of β-CD is restricted only up to 2.0 mM knowing the fact that at high concentration nanotubes are formed and the equations are not applicable. *K* and *K′* are the association constants, were determined from the slope and intercept values of Benesi–Hildebrand plot. Figure 6.8 depicts the best fitting of the Benesi-Hildebrand plot for 1:1 stoichiometry. The reciprocal plot for 1:2 stoichiometry deviates from the linearity (figure has not given). This result shows that at low concentration of β-CD, it forms inclusion complex of 1:1 stoichiometric ratio with C-485 with an association constant (*K)* value of 4624 M^{-1} in presence of ctDNA. Earlier we have shown that the association constant (1:1 stoichiometry) value is 5221 M^{-1} in absence of ctDNA (Chapter 5). This result depicts that the binding of C-485 with β-CD is restricted up to certain extent in presence of ctDNA, which further confirms the interaction of C-485 with ctDNA even in presence of β-CD.

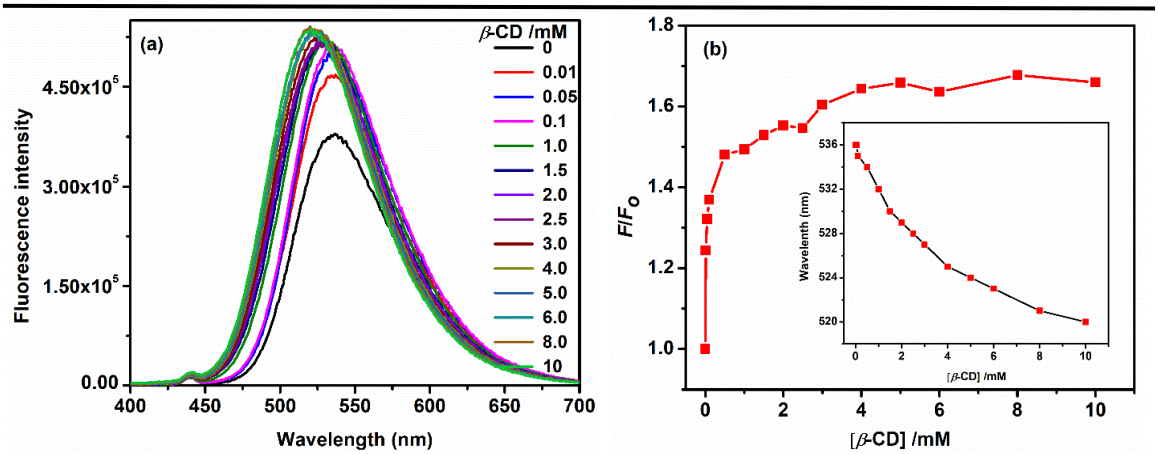

Figure 6.7. (a) Fluorescence spectra, (b) F/F_o at 536 nm wavelength of C-485 (5 µM) at a fixed concentration of ctDNA (5 µM) with varying concentrations of β-CD. [λ_{ext}= 375 nm]. [Inset shows the variations of fluorescence peak maxima on the addition of β-CD.]

Table 6.2. Variation in the peak maxima of absorption (λ_{max}^{abs}) band, peak maxima of fluorescence (λ_{max}^{flu}) band, steady-state anisotropy (r), and average excited state lifetime ($<\tau_f>$) of C-485 (5.0 µM) in the presence of ctDNA (5.0 µM) with addition of β-CD (0-10 mM) in the HEPES buffer. [λ_{ex} = 375 nm, λ_{em} = 510 nm].

Sr. No.	β-CD (mM)	λ_{max}^{abs} (nm)	λ_{max}^{flu} (nm)	r	a_1	τ_1 (ps)	a_2	τ_2 (ps)	$<\tau_f>$ (ps)	χ^2
1	0.00	404	536	0.030	0.99	411	0.01	1203	419	1.18
2	0.01	404	536	0.032	0.98	409	0.02	1363	428	1.27
3	0.05	404	536	0.034	0.99	416	0.01	2074	433	1.02
4	0.10	404	535	0.047	0.98	418	0.02	1319	436	1.03
5	0.50	403	534	0.052	0.84	362	0.16	829	437	1.27
6	1.00	403	532	0.070	0.85	358	0.15	904	440	1.10
7	1.50	403	530	0.094	0.85	351	0.15	958	442	1.20
9	2.00	402	529	0.095	0.87	367	0.13	1036	454	1.12
10	2.50	401	528	0.118	0.85	358	0.15	1007	455	1.15
11	3.00	401	527	0.112	0.84	353	0.16	1000	457	1.23
12	4.00	401	525	0.111	0.84	353	0.16	1016	459	1.20
13	5.00	400	524	0.111	0.84	343	0.16	1044	455	1.22
14	6.00	400	523	0.122	0.86	352	0.14	1076	453	1.30
15	8.00	400	521	0.128	0.80	325	0.20	959	452	1.25
16	10.00	400	520	0.136	0.85	338	0.15	1099	452	1.30

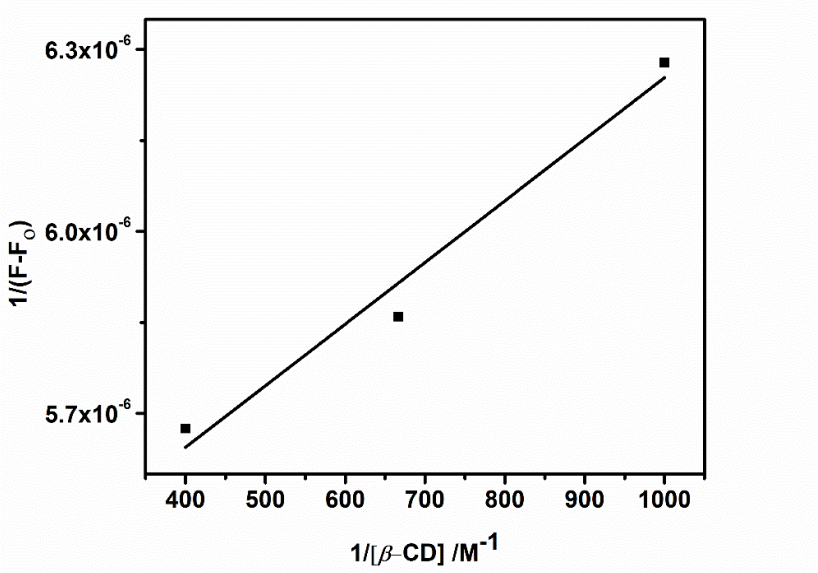

Figure 6.8. Benesi-Hildebrand plot of C-485 (5 µM) in *β*-CD in presence of ctDNA for a 1:1 stoichiometry with regression coefficient (r) = 0.987. (Fluorescence intensity is measured at 525 nm).

To have the intense knowledge about the microenvironment of C-485, the steady-state fluorescence anisotropy values have been estimated in presence of ctDNA with varying the concentration of *β*–CD and the change in anisotropy is represented by Figure 6.9 and corresponding data are given in Table 6.2. The formation of nanotubes and other structures of the *β*–CD in presence of ctDNA is confirmed by high value (~0.14) of steady-state fluorescence anisotropy. At low concentration of *β*–CD (< 2.5 mM), there is a rapid enhancement in anisotropy and above that a comparatively lesser increment has been observed. Thus, the high value of anisotropy indicates that C-485 molecules go inside the cavity of *β*–CD and formation the nanotubes and their secondary aggregates.[74-78] This result also confirms the form of nanotubes of *β*–CDs at its high concentration in presence of C-485 as a guest and ctDNA as an additive.

Fluorescence decays of C-485 are found to be bi-exponential in presence of ctDNA with varying the concentration of *β*–CD. Average lifetime values have been determined using Equation 1.8 in Chapter 1 and are tabulated in Table 6.2. It is clear from the data in Table 6.2 that average excited state lifetime of C-485 increases with increasing concentration of *β*–CD with the very sharp initial increase, which suggests that ctDNA bound C-485 molecules are transferred to the hydrophobic pocket of the *β*–CD and are forming inclusion complexes and nanotubes. Due to transfer in a comparatively nonpolar

environment, the ICT state of C-485 gets destabilized.[79, 80] Thus, the rates of non-radiative transitions decrease and fluorescence lifetime increases. The changes observed in excited state lifetime with increasing concentration of *β*–CD are in consistent with other fluorescence properties. Thus, lifetime data further supports the presence of C-485 molecules inside the nanotubes of the *β*–CD. It is to be noted here that the weightage of the fast component decreases and that of slow component increases. Also there is a gradual decrease in the lifetime of the fast component with increasing *β*–CD concentration. However, weightage of the fast component has decreased from 99 % at zero concentration of *β*–CD to 85 % at 10.0 mM of *β*–CD. It infers that even at a very higher concentration of *β*–CD, a large amount of C-485 still bind with ctDNA.

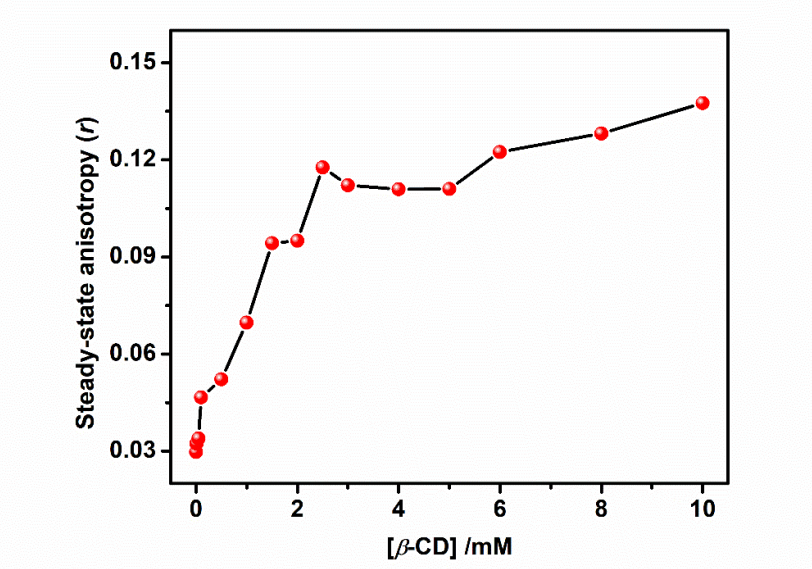

Figure 6.9. Variation in the steady-state fluorescence anisotropy of C-485 (5.0 µM) in presence of ctDNA (5.0 µM) (intensities have measured at λ_{em} = 525 nm) as a function of the concentration of *β*–CD.

6.2.5 Gemini surfactant induced release of C-485 from nanotubes and binding with ctDNA

6.1.5.1 Steady-state absorption and fluorescence studies

To monitor the surfactant induced release of C-485 from the nanotubes of *β*-CD in presence of ctDNA, the gemini surfactants with different tails length, *m*-4-*m*, [*m* =12, 14, and 16] have been added in the C-485-*β*-CD-ctDNA system. Figures 6.10, 6.11 and 6.12 represent the absorption and fluorescence spectra of C-485 in presence of ctDNA (5 µM)

and β-CD (5.0 mM) with varying concentrations of gemini surfactants, 12-4-12, 14-4-14 and 16-4-16, respectively. The absorbance of C-485 initially enhances for each of gemini surfactants, *m*-4-*m*. After that, the absorbance starts to decrease each case. With further increasing concentration of a surfactant in the system, the absorbance is found to be increased continuously. At the same time, the absorption peak maximum also varies as the polarity of the environment changes on the addition of surfactant (Figures 6.10a, 6.11a, and 6.12a.)

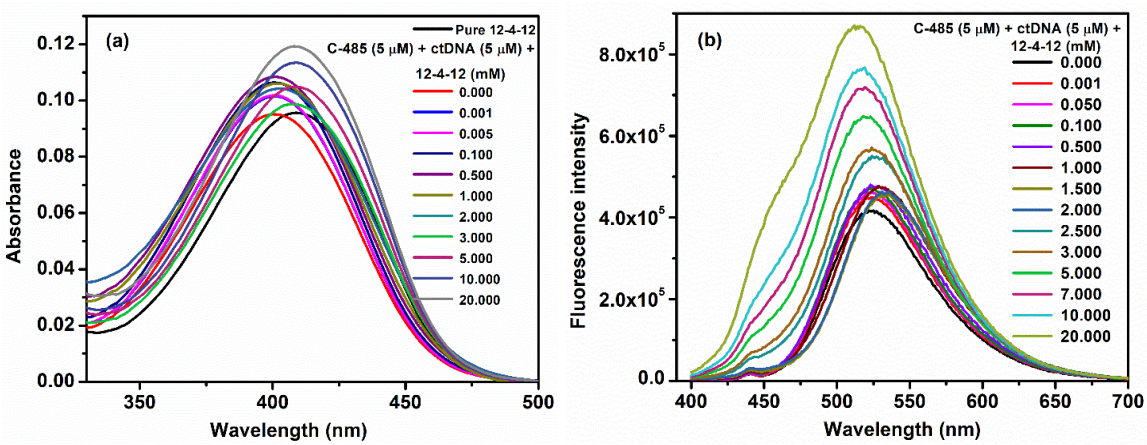

Figure 6.10. (a) Absorption spectra and (b) Fluorescence spectra of C-485 (5 μM), at the fixed concentration of ctDNA (5 μM) and β-CD (5.0 mM) with varying concentrations of 12-4-12. [λ_{ex} = 375 nm].

Fluorescence spectroscopic properties reflect the surrounding microenvironment of the fluorophore. Figure 6.13a and 6.13b represent change in fluorescence intensity ratio, F/F_o (where, F and F_o are the fluorescence intensities at 525 nm in presence and absence of *m*-4-*m* surfactants, respectively) and peak maxima of fluorescence bands of C-485 with the variation in concentration of the surfactants, [*m*-4-*m*], respectively. Depending on the tail length, initially in the concentration range of 0.05 – 0.5 mM of surfactants, the fluorescence intensity increases. After that, in the concentration range of 0.05 – 2.0 mM, the fluorescence intensity remains almost constant followed by a small decrease in intensity with red shift in peak position. Beyond the concentration range 0.2 – 2.0 mM, the fluorescence intensity gradually rises with a blue shift in peak position. Fluorescence properties of C-485 are changing according to the change in rigidity and polarity of the microenvironment around the C-485[Chapter 5]. At low concentration range, co-association of tails and C-485 in the cavities of β-CD has been discussed [Chapter 5].

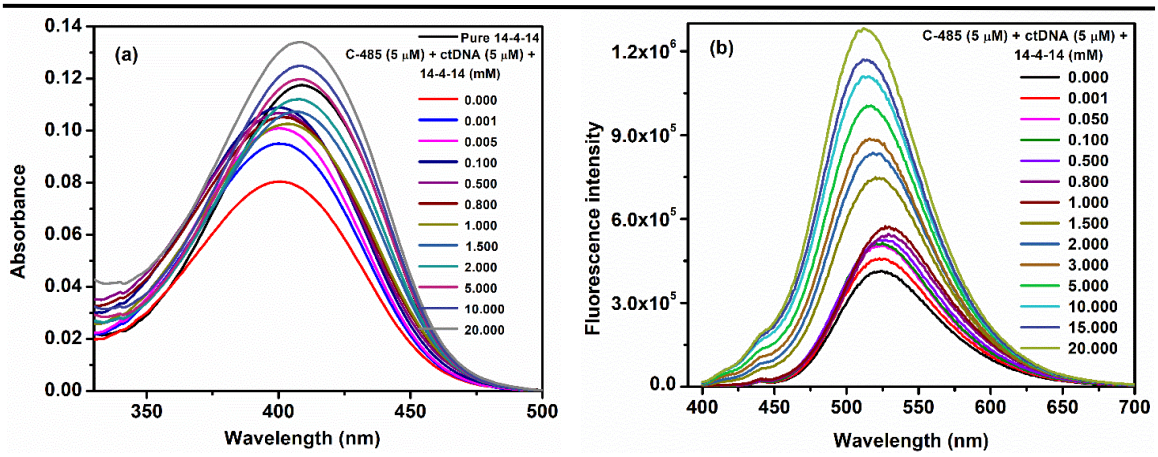

Figure 6.11. (a) Absorption spectra and (b) Fluorescence spectra of C-485 (5 μM), at the fixed concentration of ctDNA (5 μM) and *β*-CD (5 mM) with varying concentrations of 14-4-14. [λ_{ex} = 375 nm].

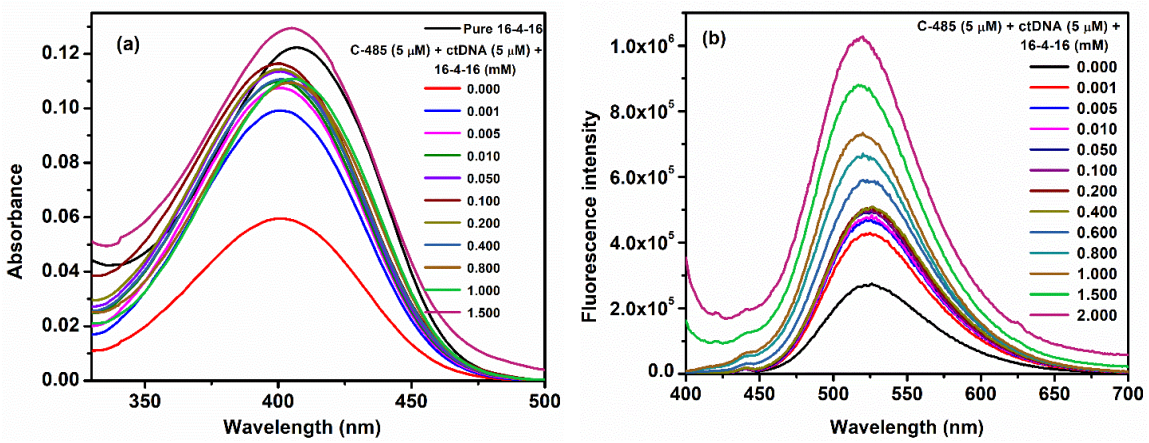

Figure 6.12. (a) Absorption spectra and (b) fluorescence spectra of C-485 (5 μM), at the fixed concentration of ctDNA (5 μM) and *β*-CD (5 mM) with varying concentrations of 16-4-16. [λ_{ex} = 375 nm].

Fluorescence anisotropy values are also following the similar trend as the fluorescence intensity as given in Figure 6.14. When C-485 is released from the cavity of nanotubes and come out in the buffer solution, at that condition the anisotropy is minimum. For example anisotropy is 0.06 at 2.00 mM concentration of 12-4-12 which is near to the anisotropy value of C-485 when binds with ctDNA (Table 6.1). This anisotropy value is also close to that of C-485 binding with *β*–CD forming simple inclusion complex (Table 6.2). It has been discussed above that at lower concentration range of *β*-CD (less then 2.0 mM), C-485 molecules form 1:1 inclusion complexes with the *β*-CD in presence of ctDNA.

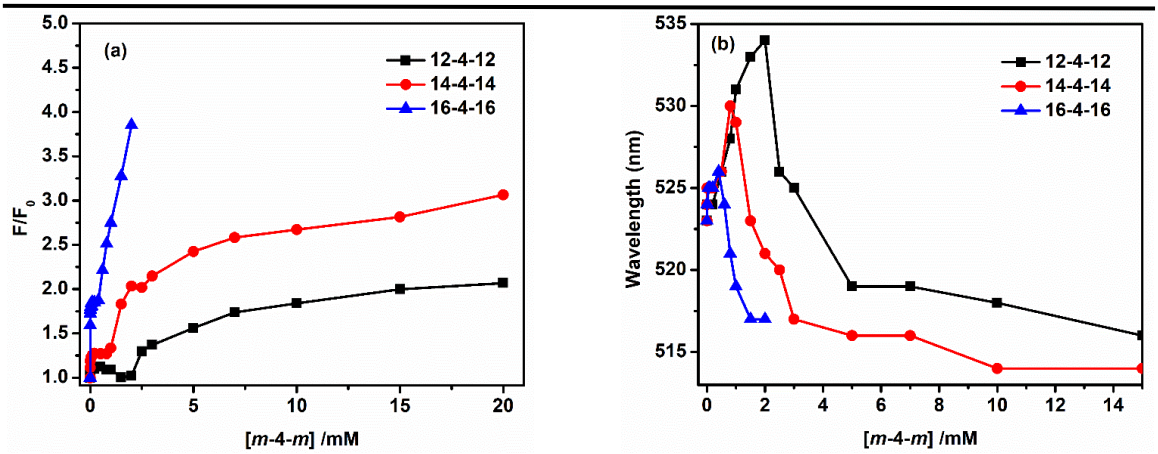

Figure 6.13. (a) Fluorescence intensity ratio (F/F_o) at 520 nm, and (b) fluorescence peak maxima of C-485 (5.0 µM), at the fixed concentration of ctDNA (5.0 µM) and *β*-CD (5.0 mM) with varying concentrations of *m*-4-*m*. [λ_{ex} = 375 nm].

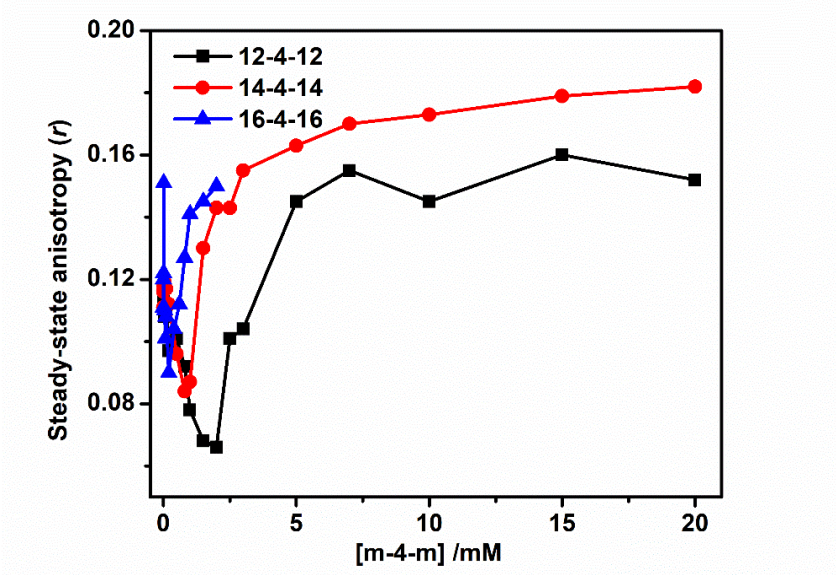

Figure 6.14. Steady-state fluorescence anisotropy of C-485 (5 µM) at the fixed concentration of ctDNA (5.0 µM) and β-CD (5.0 mM) with varying concentrations of *m*-4-*m*. [λ_{ex} = 375 nm, λ_{em} =520 nm].

It has been reported that binding constant of C-314 to ctDNA is lowed in presence of *β*-CD. Therefore, there is competition between ctDNA and *β*-CD to bind with C-314. Thus, *β*-CD forms the inclusion complex with C-314 and then that complex binds with ctDNA with a groove binding mode.[26] In the present study also, there is a possibility that C-485 forms the inclusion complex with *β*-CD and the complex then binds with ctDNA through the groove binding mode, because some of the fluorescence properties of C-485 (after being released from cavity) are matching with the fluorescence properties in

presence of low concentration of the *β*-CD (Table 6.2). At a higher concentration of the gemini surfactants, the fluorescence properties of C-485 are well resembled with the properties in the pure micellar system (given in Table 6.3). For 14-4-14 and 16-4-16 gemini surfactants, the anisotropy values are not decreased as those are in case of 12-4-12 due to their lower *cmc* or higher extent of aggregation ability.

Therefore, it can be concluded that C-485 molecules bind with ctDNA instead of getting solubilized in micelles after being released from the cavity of nanotubes. The order of the increasing efficiency to release the C-485 from nanotubes is as follows 12-4-12 < 14-4-14 < 16-4-16. For the 16-4-16, studies have been carried out up to 2 mM concentration because beyond this concentration surfactant has less solubility.

Table 6.3. *Cmc*, the experimental concentration of *m*-4-*m*, and *β*–CD, peak maxima of absorption (λ_{max}^{abs}) bands, peak maxima of fluorescence (λ_{max}^{flu}) bands, steady-state anisotropy (*r*), and average excited state lifetime ($<\tau_f>$) of C-485 (5.0 μM) in the aqueous micellar solution. [λ_{ex} = 375 nm, λ_{em} = 520 nm].

System	*cmc* (mM)	Conc. (mM)	*β*–CD (mM)	ctDNA (μM)	λ_{max}^{abs} (nm)	λ_{max}^{flu} (nm)	*r*	$<\tau_f>$ (ps)
12-4-12	0.93	10	-	-	408	517	0.134	638
14-4-14	0.152	10	-	-	408	516	0.166	706
16-4-16	0.024	10	-	-	407	513	0.171	946
12-4-12	-	10	5	5	408	518	0.145	899
14-4-14	-	10	5	5	408	514	0.145	739
16-4-16	-	2	5	5	407	517	0.150	760

Further, to confirm that after being released from the cavity of nanotubes, some of C-485 molecules bind with ctDNA, four controlled experiments on the fluorescence spectra of C-485 have been performed: (a) C-485 (5.0 μM) in the presence of *β*-CD (5.0 mM), (b) C-485 (5.0 μM) in the presence of *β*-CD (5.0 mM) and ctDNA (5.0 μM), (c) C-485 (5.0 μM) in the presence of *β*-CD (5.0 mM) and 12-4-12 (2.0 mM), and (d) C-485 (5.0 μM) in the presence of *β*-CD (5.0 mM), ctDNA (5.0 μM) and 12-4-12 (2 .0 mM). All fluorescence spectra are given in Figure 6.15. By comparing the fluorescence properties of C-485 in first two solutions, we can see that in presence of ctDNA fluorescence intensity is decreased. It indicates that the binding of C-485 with *β*-CD is reduced in presence of ctDNA because some of the C-485 molecules bind with ctDNA even in presence of *β*-CD. By comparison of fluorescence properties in last two solutions, it can

be stated that after coming out from the cavity, C-485 binds with ctNDA that could be the reason for the increase in the fluorescence intensity in presence of ctDNA. Although, this much enhancement in fluorescence intensity does not occur for binding of C-485 with ctDNA in pure condition. It is noteworthy that because ctDNA also interacts with the surfactants that causes the more compact form of ctDNA resulting in greater extent of increase in fluorescence intensity. Compact form of ctDNA is confirmed by measurement of hydrodynamic diameter (r_h). r_h for pure ctDNA (5.0 µM) is 288 ±8 nm, which is reduced to 137 ±6 nm. Along with the bigger size particle of r_h = 443 ±13 nm is also obtained which is for nanotubes/secondary aggregates of nanotubes of β-CD (Chapter 5) in a system containing C-485 (5.0 µM), β-CD (5.0 mM), 12-4-12 (2.0 mM) and ctDNA (5.0 µM).

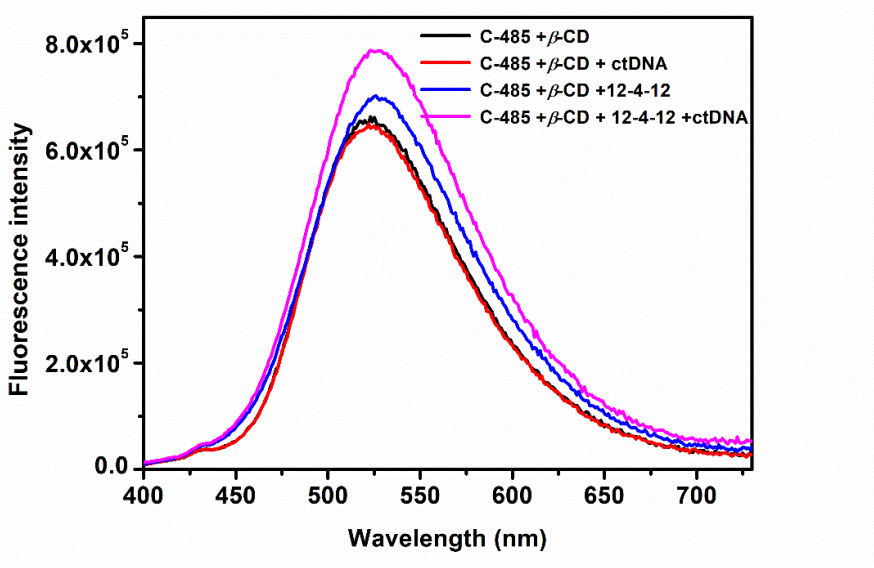

Figure 6.15. Fluorescence spectra of C-485 (5.0 µM) in the presence of β-CD (5.0 mM), ctDNA (5.0 µM) and 12-4-12 (2 .0 mM) at different controlled conditions.

6.2.5.2 The time-resolved fluorescence measurements

Fluorescence lifetime measurements have also helped us to explore the binding interactins of gemini surfactants with the C-485-β–CD nanotubular systems and release of C-485 from the same system as a function of concentration of surfactants followed by binding of the released C-485 with ctDNA. For this, the lifetimes of C-485 have been determined at a fixed concentration of β–CD (5.0 mM) and ctDNA (5.0 µM) with varying concentration of each of surfactants. Fluorescence intensity decays are bi- or tri-exponential in nature, which represents the microheterogeneous environment of C-485. Tables 6.4a-c represent the fluorescence lifetimes of various components along with

average lifetimes at various concentrations of each of 12-4-12, 14-4-14 and 16-4-16, respectively. Figures 6.16 depicts the variation in an average lifetime with varying concentration of surfactants.

Table 6.4a. Excited state lifetimes of C-485 in presence of different concentration of 12-4-12 in a system containing β-CD and ctDNA. [C-485] = 5.0 μM, [β-CD] = 5.0 mM and [ctDNA] = 5.0 μM.

Sr. No.	[12-4-12] (mM)	a_1	τ_1 (ps)	a_2	τ_2 (ps)	a_3	τ_3 (ps)	$<\tau_f>$ (ps)	χ^2
1	0.000	0.84	343	0.16	1044	-	-	455	1.22
2	0.001	0.79	329	0.21	948	-	-	459	1.04
3	0.005	0.80	330	0.20	938	-	-	452	1.25
4	0.050	0.80	329	0.20	933	-	-	450	1.34
5	0.100	0.80	328	0.20	933	-	-	449	1.10
6	0.200	0.78	318	0.22	902	-	-	446	1.20
7	0.500	0.75	293	0.24	823	0.01	2470	442	0.97
8	0.800	0.69	275	0.30	722	0.01	2350	430	1.24
9	1.000	0.62	258	0.37	654	0.01	2356	426	0.94
10	1.500	0.49	226	0.50	576	0.01	2594	425	0.94
11	2.000	0.46	233	0.53	570	0.01	2942	439	0.96
12	2.500	0.98	548	0.02	243	-	-	542	1.08
13	3.000	0.99	579	0.01	267	-	-	576	1.14
14	5.000	0.99	618	0.01	308	-	-	615	1.09
15	7.000	0.99	637	0.01	322	-	-	634	1.07
16	10.000	0.99	656	0.01	362	-	-	653	1.10
17	15.000	0.98	670	0.02	390	-	-	664	1.13
18	20.000	0.98	695	0.02	414	-	-	689	1.15

Average fluorescence lifetimes are varied in the same way as other fluorescence properties do. The values of the average lifetimes depend on the micropolarity and microviscosity of the environment as discussed in the previous chapter [Chapter 5]. Lifetime data also support that the efficiency to release the guest depends on the tail length of surfactants. This increasing order is 12-4-12 < 14-4-14 < 16-4-16. Figure 6.16 shows that at higher concentration range of surfactant average lifetime gradually increases with increasing concentration of surfactants as a result of more and more solubilization of C-485 in the micelles of surfactants. Moreover, at a given high concentration of surfactant average lifetime increases with increasing lengths of tails. Thus these results are also in the same line with the fact that microviscosity/rigidity of microenvironment of micelles

increases and micropolarity decreases with increasing tail length of gemini surfactants [Chapter 3b].

Table 6.4b. Excited state lifetimes of C-485 in presence of different concentration of 14-4-14 in a system containing β-CD and ctDNA. [C-485] = 5.0 μM, [β-CD] = 5.0 mM and [ctDNA] = 5.0 μM.

Sr. No.	[14-4-14] (mM)	a_1	τ_1 (ps)	a_2	τ_2 (ps)	a_3	τ_3 (ps)	$<\tau_f>$ (ps)	χ^2
1	0.000	0.84	343	0.16	1044	-	-	455	1.22
2	0.001	0.79	334	0.21	934	-	-	460	1.33
3	0.005	0.81	335	0.19	948	-	-	451	1.34
4	0.050	0.76	309	0.24	891	-	-	449	1.04
5	0.100	0.78	294	0.21	866	0.01	3.290	444	1.19
6	0.200	0.74	283	0.25	829	0.01	2.617	443	1.10
7	0.500	0.62	252	0.36	665	0.02	2.197	440	1.10
8	0.800	0.63	256	0.35	679	0.02	2.281	445	0.96
9	1.000	0.57	271	0.42	673	0.01	2.482	462	1.11
10	1.500	0.35	219	0.63	677	0.02	2.101	545	1.06
11	2.000	0.29	226	0.69	694	0.02	2.001	584	0.97
12	2.500	0.91	547	0.09	1439	-	-	627	1.19
13	3.000	0.91	583	0.09	1461	-	-	662	1.21
14	5.000	0.88	595	0.12	1418	-	-	694	1.11
15	7.000	0.88	611	0.12	1464	-	-	713	1.08
16	10.000	0.87	625	0.13	1503	-	-	739	0.98
17	15.000	0.85	626	0.15	1505	-	-	758	1.05
18	20.000	0.86	655	0.14	1586	-	-	785	1.07

We have further analyzed the decay components at varying concentration of surfactants (Tables 6.4a-c). While at low and high concentrations of the gemini surfactants, the fluorescence decays are bi-exponential, at middle concentration range the decays are tri-exponential. At low, middle and high concentration ranges C-485 molecules mostly reside inside the nanotube, outside the nanotubes and in micelles, respectively. These concentration ranges depend on the type of surfactants. In the middle range, when C-485 molecules come out of the nanotubes, they may interact with micelles, ctDNA and again with β-CD. That is the reason that decays are tri-exponential. Moreover, data also show that out of these surfactants used 16-4-16 is most efficient to get out C-485 molecules from the nanotubes at low concentration range. In the middle concentration range, the values of average fluorescence lifetimes of C-485 are near to that of C-485 bound with ctDNA (Table 6.1), and also of C-485 present in solutions containing low concentration of β–CD

where inclusion complexes are formed (Table 6.2). These values are different from the lifetimes of C-485 present in micelles, nanotubes and in pure buffer. These data infer that after coming out from the nanotubes, C-485 molecules bind with ctDNA, or form the inclusion complexes with *β*–CD which bind with ctDNA to some extent even in presence of micelles.

Table 6.4c. Excited state lifetimes of C-485 in presence of different concentration of 16-4-16 in a system containing *β*-CD and ctDNA. [C-485] = 5.0 µM, [*β*-CD] = 5.0 mM and [ctDNA] = 5.0 µM.

Sr. No.	[16-4-16] (mM)	a_1	τ_1 (ps)	a_2	τ_2 (ps)	a_3	τ_3 (ps)	$<\tau_f>$ (ps)	χ^2
1	0.000	0.84	343	0.16	1044	-	-	455	1.22
2	0.001	0.84	352	0.16	1042	-	-	462	1.36
3	0.005	0.79	335	0.21	929	-	-	460	1.16
4	0.050	0.73	285	0.26	854	0.01	2680	457	1.40
5	0.100	0.77	298	0.22	884	0.01	2885	453	1.12
6	0.200	0.75	296	0.24	846	0.01	2521	450	0.97
7	0.500	0.75	325	0.24	880	0.01	2498	480	1.18
8	0.800	0.87	551	0.13	1370	-	-	657	1.28
9	1.000	0.88	626	0.12	1460	-	-	726	1.21
10	2.000	0.90	673	0.10	1542	-	-	760	1.17

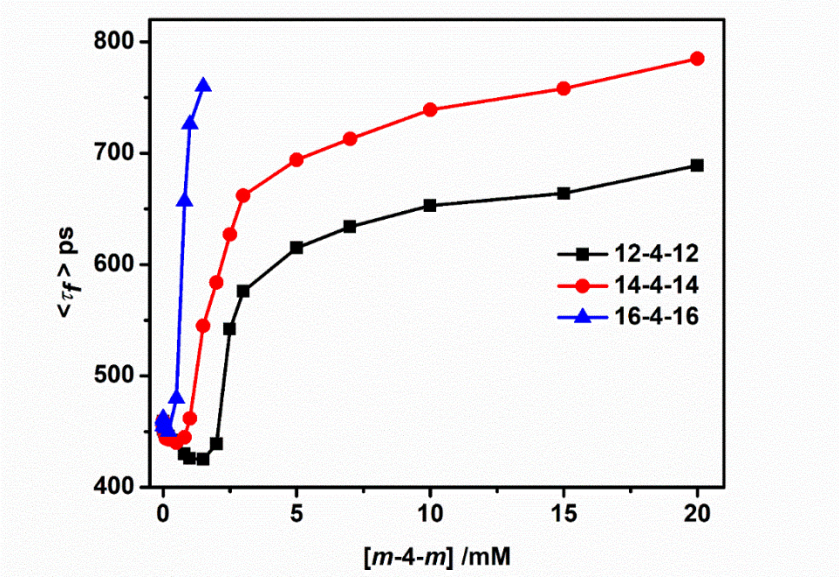

Figure 6.16. Average lifetime of C-485 (5.0 µM) in the aqueous solution of ctDNA (5.0 µM) and *β*–CD (5.0 mM) as a function of concentration of gemini surfactants, *m*-4-*m*. [λ_{ex} = 375 nm, λ_{em} = 520 nm].

6.3 Conclusions

The absorption and fluorescence spectra of C-485 show the enhancement in absorbance and fluorescence intensity up to a certain concentration of ctDNA with insignificant change in their peak positions, respectively. The changes in absorption and fluorescence spectra profiles confirm the binding of C-485 with ctDNA. Fluorescence lifetime data further support the binding of C-485 with ctDNA. Ethidium bromide displacment experiment and iodide ion quenching study confirm the groove binding mode of C-485 with ctDNA. The lower value of binding constant in presence of ctDNA than that in absence of ctDNA suggest that the binding of C-485 with *β*–CD is reduced in presence of ctDNA. It further depicts that some of C-485 bind with ctDNA even in presence of *β*–CD. The presence of a gemini surfactant in the system induces the release of C-485 molecules from the cavity of nanotubes. The efficiency of gemini surfactants to push the guest molecules out of the cavities increases in the order as 12-4-12 < 14-4-14 < 16-4-16. By comparing the fluorescence properties such as steady-state anisotropy and lifetime of C-485 at a low concentration of a gemini surfactant with that of C-485 binds with ctDNA and with *β*–CD forming inclusion complexes, we concluded that C-485 molecules released from the nanotubular cavities interact or bind with ctDNA either in the form of inclusion complex with *β*–CD and/or as in the uncomplexed form.

References

1. S. E. Osborne and A. D. Ellington, *Chem. Rev.*, 1997, **97**, 349-370.
2. P. B. Dervan, *Bioorg. Med. Chem.*, 2001, **9**, 2215-2235.
3. K. Gopidas and P. V. Kamat, *J. Photochem. Photobiol. A Chem.*, 1989, **48**, 291-301.
4. M. Ganguli, K. N. Jayachandran and S. Maiti, *J. Am. Chem. Soc.*, 2004, **126**, 26-27.
5. Y. Ma, G. Zhang and J. Pan, *J. Agricul. Food Chem.*, 2012, **60**, 10867-10875.
6. X.-L. Li, Y.-J. Hu, H. Wang, B.-Q. Yu and H.-L. Yue, *Biomacromolecules*, 2012, **13**, 873-880.
7. L. Zhou, J. Yang, C. Estavillo, J. D. Stuart, J. B. Schenkman and J. F. Rusling, *J. Am. Chem. Soc.*, 2003, **125**, 1431-1436.
8. Y. Fei, G. Lu, G. Fan and Y. Wu, *Anal. Sci.*, 2009, **25**, 1333-1338.
9. B. Armitage, *Chem. Rev.*, 1998, **98**, 1171-1200.

10. K. E. Erkkila, D. T. Odom and J. K. Barton, *Chem. Rev.*, 1999, **99**, 2777-2796.
11. Y. Cao and X.-w. He, *Spectrochim. Acta A Mol. Biomol. Spectrosc.*, 1998, **54**, 883-892.
12. L. H. Hurley and D. R. Needham-VanDevanter, *Acc. Chem. Res.*, 1986, **19**, 230-237.
13. J. Mann, A. Baron, Y. Opoku-Boahen, E. Johansson, G. Parkinson, L. R. Kelland and S. Neidle, *J. Med. Chem.*, 2001, **44**, 138-144.
14. R. P. Haugland, *Handbook of fluorescent probes and research products*, Molecular Probes, 2002.
15. G. J. Mohr, *Chem. A Eur. J.*, 2004, **10**, 1082-1090.
16. M. Wahl, F. Koberling, M. Patting and E. H. Rahn, *Curr. Pharma. Biotechnol.*, 2004, **5**, 299-308.
17. M. R. Webb and J. E. Corrie, *Biophys. J.*, 2001, **81**, 1562-1569.
18. M. P. Brun, L. Bischoff and C. Garbay, *Angew. Chem. Int. Ed.*, 2004, **43**, 3432-3436.
19. K. Komatsu, Y. Urano, H. Kojima and T. Nagano, *J. Am. Chem. Soc.*, 2007, **129**, 13447-13454.
20. M. S. Dillingham, K. L. Tibbles, J. L. Hunter, J. C. Bell, S. C. Kowalczykowski and M. R. Webb, *Biophys. J.*, 2008, **95**, 3330-3339.
21. A. R. Katritzky, J. Cusido and T. Narindoshvili, *Bioconjug. Chem. Biochem. Pharm.*
22. G. J. Finn, B. S. Creaven and D. A. Egan, *Biochemical pharmacology*, 2004, **67**, 1779-1788.
23. T. Sarwar, S. U. Rehman, M. A. Husain, H. M. Ishqi and M. Tabish, *Int. J. Biol. Macromol*, 2015, **73**, 9-16.
24. B. D. Wagner, *Molecules*, 2009, **14**, 210-237.
25. S. Chandrasekaran, Y. Sameena and I. V. Enoch, *J. Mol. Recog.*, 2014, **27**, 640-652.
26. C. Sowrirajan, S. Yousuf and I. V. Enoch, *Aust. J. Chem.*, 2014, **67**, 256-265.
27. S. Chandrasekaran, Y. Sameena and I. V. Enoch, *J. Incl. Phenom. Macrocycl. Chem.*, 2015, **81**, 225-236.
28. A. Astakhova and N. Demina, *Pharma. Chem. J.*, 2004, **38**, 105-108.
29. A. Harada, *Acc. Chem. Res.*, 2001, **34**, 456-464.
30. R. Palepu and V. C. Reinsborough, *Can. J. Chem.*, 1988, **66**, 325-328.

31. U. R. Dharmawardana, S. D. Christian, E. E. Tucker, R. W. Taylor and J. F. Scamehorn, *Langmuir*, 1993, **9**, 2258-2263.
32. R. Palepu, J. E. Richardson and V. C. Reinsborough, *Langmuir*, 1989, **5**, 218-221.
33. A. A. Rafati, A. Bagheri, H. Iloukhani and M. Zarinehzad, *J. Mol. Liq.*, 2005, **116**, 37-41.
34. E. Junquera, G. Tardajos and E. Aicart, *Langmuir*, 1993, **9**, 1213-1219.
35. A. J. Valente and O. Söderman, *Adv. Colloid Interface Sci.*, 2014, **205**, 156-176.
36. N. Funasaki, H. Yodo, S. Hada and S. Neya, *Bull. Chem. Soc. Jpn*, 1992, **65**, 1323-1330.
37. S. Mehta, K. Bhasin, S. Dham and M. Singla, *J. Colloid Interface Sci.*, 2008, **321**, 442-451.
38. A. Petek, M. Krajnc and A. Petek, *J. Incl. Phenom. Macrocycl. Chem.*, 2016, **86**, 221-229.
39. L. Jiang, Y. Yan and J. Huang, *Adv. Colloid Interface Sci.*, 2011, **169**, 13-25.
40. X. Du, X. Chen, W. Lu and J. Hou, *J. Colloid Interface Sci.*, 2004, **274**, 645-651.
41. S. Muthusubramanian, A. K. Tiwari and S. K. Saha, *Soft Matter*, 2012, **8**, 11072-11084.
42. C. Bombelli, L. Giansanti, P. Luciani and G. Mancini, *Curr. Med. Chem.*, 2009, **16**, 171-183.
43. M. C. Morán, M. G. Miguel and B. Lindman, *Soft Matter*, 2011, **7**, 2001-2010.
44. S. Marchetti, G. Onori and C. Cametti, *J. Phys. Chem. B*, 2005, **109**, 3676-3680.
45. V. Jadhav, S. Maiti, A. Dasgupta, P. K. Das, R. S. Dias, M. G. Miguel and B. Lindman, *Biomacromolecules*, 2008, **9**, 1852-1859.
46. X. Guo, B. Cui, H. Li, Z. Gong and R. Guo, *J. Polym. Sci. A Polym. Chem.*, 2009, **47**, 434-449.
47. T. Zhou, G. Xu, M. Ao, Y. Yang and C. Wang, *Colloids Surf. A Physicochem. Eng. Asp.*, 2012, **414**, 33-40.
48. D. Sarkar, P. Das, S. Basak and N. Chattopadhyay, *J. Phys. Chem. B*, 2008, **112**, 9243-9249.
49. D. Sahoo, P. Bhattacharya and S. Chakravorti, *J. Phys. Chem. B*, 2010, **114**, 2044-2050.
50. S. S. Mati, S. S. Roy, S. Chall, S. Bhattacharya and S. C. Bhattacharya, *J. Phys. Chem. B*, 2013, **117**, 14655-14665.
51. S. Bhattacharya, G. Mandal and T. Ganguly, *J. Photochem. Photobiol. B Biol.* ,

2010, **101**, 89-96.

52. V. González-Ruiz, A. I. Olives, M. A. Martín, P. Ribelles, M. T. Ramos and J. C. Menéndez, in *Biomedical engineering, trends, research and technologies*, InTech, 2011.
53. J. R. Lakowicz, in *Principles of fluorescence spectroscopy*, Springer, New York, 2006.
54. A. Mallick, B. Haldar and N. Chattopadhyay, *J. Photochem. Photobiol. B Biol.* , 2005, **78**, 215-221.
55. D. Sahoo and S. Chakravorti, *J. Photochem. Photobiol. A Chem.*, 2009, **205**, 129-138.
56. A. Mallick, B. Haldar, S. Maiti and N. Chattopadhyay, *J. Colloid Interface Sci.*, 2004, **278**, 215-223.
57. R. Ramadass and J. Bereiter-Hahn, *J. Phys. Chem. B*, 2007, **111**, 7681-7690.
58. M. Mohapatra and A. K. Mishra, *Langmuir*, 2013, **29**, 11396-11404.
59. D. Sarkar, D. Ghosh, P. Das and N. Chattopadhyay, *J. Phys. Chem. B*, 2010, **114**, 12541-12548.
60. A. Mallick, B. Haldar and N. Chattopadhyay, *J. Phys. Chem. B*, 2005, **109**, 14683-14690.
61. B. K. Paul and N. Guchhait, *J. Phys. Chem. B*, 2011, **115**, 11938-11949.
62. D. Sarkar, A. Mahata, P. Das, A. Girigoswami, D. Ghosh and N. Chattopadhyay, *J. Photochem. Photobiol. B Biol.* , 2009, **96**, 136-143.
63. A. Chakrabarty, A. Mallick, B. Haldar, P. Das and N. Chattopadhyay, *Biomacromolecules*, 2007, **8**, 920-927.
64. A. Mahata, D. Sarkar, D. Bose, D. Ghosh, A. Girigoswami, P. Das and N. Chattopadhyay, *J. Phys. Chem. B*, 2009, **113**, 7517-7526.
65. Y. Song, J. Kang, J. Zhou, Z. Wang, X. Lu, L. Wang and J. Gao, *Spectrochim. Acta A Mol. Biomol. Spectrosc.*, 2000, **56**, 2491-2497.
66. J. Olmsted III and D. R. Kearns, *Biochemistry*, 1977, **16**, 3647-3654.
67. N. Li, Y. Ma, C. Yang, L. Guo and X. Yang, *Biophys. Chem.*, 2005, **116**, 199-205.
68. H.-L. Wu, K. Li, T. Sun, F. Kou, F. Jia, J.-K. Yuan, B. Liu and B.-L. Qi, *Trans. Metal Chem.*, 2011, **36**, 21-28.
69. H. Wu, F. Jia, F. Kou, B. Liu, J. Yuan and Y. Bai, *Trans. Metal Chem.*, 2011, **36**, 847-853.
70. S. Kashanian, M. M. Khodaei and P. Pakravan, *DNA Cell Biol.*, 2010, **29**, 639-646.

71. H. A. Benesi and J. Hildebrand, *J. Am. Chem. Soc.*, 1949, **71**, 2703-2707.

72. S. K. Saha and A. Kanchanmala, *group*, 2006, **3**, 2.

73. J. Dey, E. L. Roberts and I. M. Warner, *J. Phys. Chem. A*, 1998, **102**, 301-305.

74. M. Sowmiya, P. Purkayastha, A. K. Tiwari, S. S. Jaffer and S. K. Saha, *J. Photochem. Photobiol. A Chem.*, 2009, **205**, 186-196.

75. G. Li and L. B. McGown, *Science*, 1994, **264**, 249-252.

76. G. Pistolis and A. Malliaris, *J. Phys. Chem.*, 1996, **100**, 15562-15568.

77. A. Wu, X. Shen and Y. He, *J. Colloid Interface Sci.*, 2006, **297**, 525-533.

78. A. Wu, X. Shen and Y. He, *J. Colloid Interface Sci.*, 2006, **302**, 87-94.

79. P. Dahiya, M. Kumbhakar, T. Mukherjee and H. Pal, *Chem. Phys. Lett.*, 2005, **414**, 148-154.

80. S. Nad, M. Kumbhakar and H. Pal, *J. Phys. Chem. A*, 2003, **107**, 4808-4816.

Chapter 7

Summary and Future Approaches of Thesis Work

Key Concepts:

- *This chapter includes the summary of each Chapter.*
- *Future works are suggested from the present thesis.*

Chapter 7

Summary and Future Approaches of Thesis Work

Summary

Chapter 1:

This chapter covers generalized introduction of surfactants, types of surfactants, process of micellization, structure and shape of micelles, factors affecting the micellization of surfactant, types of micelles, solubilization of solute in micelles, mixed micelles, cyclodextrin, inclusion complex formation of cyclodextrin, protein (BSA), interactions of BSA with surfactants, deoxyribonucleic acid (DNA), drug-DNA interactions and their mode of binding, and steady-state fluorescence and time-resolved fluorescence spectroscopic methods used to carry out the research work.

Chapter 2:

This chapter includes details of chemicals, synthesis and characterization method of surfactants, preparation of samples, instrumentation and different spectroscopic techniques used for research work.

Chapter 3:

This chapter is on the study of solvation dynamics and rotational relaxation and is divided into three parts Chapter 3a, Chapter 3b, and Chapter 3c.

Chapter 3a:

This chapter demonstrates the effect of counterions on the solvation dynamics and rotational relaxation of C-480 in the Stern layer of aqueous micelles of hexadecyltrimethylammonium surfactants ($C_{16}TAX$, X = *p*-TS^-, NO_3^-, Br^- and SO_4^{-2}) and found that the solvation time decreases in the order $C_{16}TABr > C_{16}TANO_3 > (C_{16}TA)_2SO_4 > C_{16}TAp\text{-}TS$ and rotational relaxation time decreases in the order $C_{16}TAp\text{-}TS >> C_{16}TABr > C_{16}TANO_3 > (C_{16}TA)_2SO_4$.

Chapter 3b:

This chapter explores the solvation dynamics and rotational relaxation of C-480 in aqueous micelles of cationic gemini surfactants with diethyl ether (*EE*) spacer group (*m*–

EE–m) and tails with varying tail lengths (*m* = 12, 14 and 16). Rotational relaxation time increases with increasing tail length of surfactant because of increasing microviscosity of micelles. With increasing hydrophobicity of tails of surfactants water molecules in the Stern layer become progressively more rigid resulting in a decrease in the rate of solvation process. With increasing hydrophilicity of the spacer group of gemini surfactant, the extent of free water molecules is decreased thereby making the duration of solvation process longer.

Chapter 3c:

This chapter describes the effect of added urea on solvation dynamic and rotational relaxation of C-480 in the Stern layer of aqueous micelles of cationic gemini surfactants, 12-4$(OH)_n$-12 (*n* = 0, 1, 2). Solvation time increases, reaches a maximum and then decreases with increasing concentration of urea, which is similar to the order of degree of counterion dissociation with the addition of urea in the micellar solution. With increased degree of counterion dissociation, the extent of clustering of water molecules is increased resulting in slower solvation process. The –OH group present in the spacer group of gemini surfactant controls the rate of solvation by shielding the water molecules from the probe molecules forming hydrogen bond. The microviscosity of micelles is decreased with increasing concentration of urea as a result of it rotational relaxation process becomes faster.

Chapter 4:

This chapter explores the interactions between protein, bovine serum albumin (BSA) and cationic gemini surfactants, 12-*n*-12 with varying number of $–CH_2-$ group (*n* = 3, 6, 8, 12) in the spacer. At low concentration range of surfactants, the decrease in the fluorescence intensity follows the order as 12-8-12 < 12-6-12 < 12-3-12 < 12-12-12. The decrease in α-helix of the protein is more with decreasing hydrophobicity/chain length of the spacer group. However, the unusual decrease in α-helix found in case of 12-12-12 could be because of highly hydrophobic interaction between protein and long hydrophobic spacer chain. This chapter also demonstrates the step-by-step refolding of protein present in the form of protein-gemini surfactant complex using β-CD)/SDS as capturing agents. The refolding of BSA is induced by capturing agents and controlled by the spacer chain length of gemini surfactants.

Chapter 5:

This chapter illustrates the formation of the guest molecule (C-485) induced nanotubes by *β*-cyclodextrin (*β*-CD) and their interactions with cationic gemini surfactants (12-*n*-12, where *n* = 3, 6, and 12). Gemini surfactants have an effect on binding between C-485 and nanotubes of *β*-CD. At a low concentration range, surfactant molecules are co-associated with the C-485, however, at high concentrations, they are capable of pushing C-485 out of the nanotubular cavities. After being released from the nanotubular cavities, C-485 get solubilized in the micelles. The rate of release of C-485 increases with increasing spacer chain length and concentration of surfactants.

Chapter 6:

This chapter describes the binding of a dye, C-485 with ctDNA through the groove binding mode. C-485-*β*–CD system includes the nanotubes and secondary aggregates of nanotubes, which has been explored for the carrier for C-485. Gemini surfactants, *m*-4-*m* are act as releasing agent for C-485 from the cavity of nanotubes of the *β*–CD. After being released from the cavity, C-485 molecules interact with ctDNA at a low concentration of the gemini surfactants, but at the high concentration of gemini surfactants, released C-485 solubilized in the micelles. The releasing efficiency of gemini surfactants increases in the order of 12-4-12 < 14-4-14 < 16-4-16, which is according to the increasing order of hydrophobicity of their tails.

Suggested Future Works from Present Thesis:

1. The effect of counterions on the solvation dynamics and rotational relaxation of probe molecule in the Stern layer of aqueous micelles of conventional surfactant can be extended with various organic counterions of gemini surfactants, which will provide further informations about the role of counterions in the solvation dynamics.
2. The hydrophobicity of tails and hydrophilicity of the spacer group has a great impact on the solvation dynamics and rotational relaxation of C-485 in the aqueous micelles of gemini surfactants. The use of gemini surfactants having peptide spacer group to form micelles can mimic the solvation dynamics on the surface of the biomolecules like proteins.
3. Urea is a denaturing agent of proteins. Urea has effect on degree of counterion dessociation of micelles which indirectally affects the solvation dynamics and

rotational relaxation of C-485. This idea could help the study of solvation dynamics in systems containing biomolecules, urea and salts.

4. The refolding of unfolded proteins induced by stripping agents β-CD and SDS has a great importance. The refolding of non-native or misfolded proteins formed through different biological processes is a crucial step as these forms of proteins are believed to be the primary reasons for various neurodegenerative diseases in humans. So, the process of refolding of proteins using in presence of biosurfactants can be further explored in the same direction.
5. The binding interaction of the gemini surfactants with the nanotubes of the β-CD suggest potential application in the development of promising drug delivery systems without any stimuli-responsive drug releasing agents as it is required in most of the drug delivery processes. Further study can be carried out using different biosurfactants.
6. Interactions of the gemini surfactants with ctDNA further can be explored for the gene delivery through the cell membrane because the interactions between these two cause the compaction of the ctDNA. A systematic study on the interactions of a series of surfactants of various chemical nature and also biosurfactants with β–CD and release of drug molecules followed by binding with ctDNA may help in delivering the mechanisms of interactions and developing potential drug delivery systems.

Appendices

List of publications [A-1]

From thesis work

Published

1. **Sunita Kumari**, Sonu, G. Sundar, and Subit K. Saha. "Effect of organic and a Hofmeister series of inorganic counterions on the solvation dynamics and rotational relaxation in aqueous micelles of hexadecyltrimethylammonium surfactants." *J. Photochem. Photobiol. A Chem.*, **2017**, *345*, 98-108.

2. **Sunita Kumari**, Rishika Aggrawal, Sonu, Sayantan Halder, G. Sundar, and Subit K. Saha. "Effect of hydrophobicity of tails and hydrophilicity of spacer group of cationic gemini surfactants on solvation dynamics and rotational relaxation of coumarin 480 in aqueous micelles." *ACS Omega*, **2017**, *9*, 5898-5910.

3. **Sunita Kumari**, Sonu, Sayantan Halder, Rishika Aggrawal, G. Sundar, and Subit K. Saha. "Effect of urea on solvation dynamics and rotational relaxation of Coumarin 480 in aqueous micelles of cationic gemini surfactants with different spacer groups" *ACS Omega*, **2018**, *3*, 3079-3095.

4. **Sunita Kumari**, G. Sundar, and Subit K. Saha. "Binding interaction of gemini surfactants with nanotubes of *β*-cyclodextrin and controlled release of guest molecules: Effect of spacer chain length and concentration of surfactants." *ChemistrySelect*, **2019**, *4*, 4190-4202.

Communicated

1. **Sunita Kumari**, Sayantan Halder, Rishika Aggrawal, Vinod K. Aswal, G. Sundar, and Subit K. Saha. "Unfolding of native protein by gemini surfactants and its refolding induced by *β*-cyclodextrin and sodium dodecyl sulfate in aqueous medium: Effect of spacer chain length of gemini surfactants."

2. **Sunita Kumari**, Sayantan Halder, Rishika Aggrawal, G. Sundar, and Subit K. Saha. "Gemini surfactant induced release of Coumarin 485 (C-485) from the nanotubes of *β*-CD followed by binding of C-485 with ctDNA."

Publications other than thesis work

1. Sonu, Amit K. Tiwari, **Sunita Kumari**, and Subit K. Saha. "Study on intramolecular charge transfer processes, solvation dynamics and rotational relaxation of coumarin 490 in reverse micelles of cationic gemini surfactant." *RSC Adv.*, **2014**, *48*, 25210-25219.

2. Sonu, **Sunita Kumari**, and Subit K. Saha. "Effect of polymethylene spacer of cationic Gemini surfactants on solvation dynamics and rotational relaxation of coumarin 153 in aqueous micelles." *J. Phys. Chem. B,* **2015,** *119*, 9751-9763.

3. Srishti Sinha, Deepti Tikariha, Jyotsna Lakra, Toshikee Yadav, **Sunita Kumari**, Subit K. Saha, and Kallol K. Ghosh. "Interaction of bovine serum albumin with cationic monomeric and dimeric surfactants: A comparative study." *J. Mol. Liq.,* **2016**, *218*, 421-428.

4. Sonu, **Sunita Kumari**, and Subit K. Saha. "Solvation dynamics and rotational relaxation of coumarin 153 in mixed micelles of Triton X-100 and cationic gemini surfactants: effect of composition and spacer chain length of gemini surfactants." *Phys. Chem. Chem. Phys.,* **2016**, *18*, 1551-1563.

5. Sonu, Sayantan Halder, **Sunita Kumari**, Rishika Aggrawal, Vinod K. Aswal, and Subit K. Saha. "Study on interactions of cationic gemini surfactants with folded and unfolded bovine serum albumin: Effect of spacer group of surfactants." *J. Mol. Liq.*, **2017**, *243*, 369-379.

6. Sayantan Halder, **Sunita Kumari**, Sugam Kumar, Vinod K. Aswal, and Subit K. Saha. "Fluorescence resonance energy transfer, small-angle neutron scattering, and dynamic light scattering study on interactions of gemini surfactants having different spacer groups with protein at various regions of binding isotherms." *ACS Omega*, **2018,** *9*, 11192–11204.

List of National/International Conferences [A-2]

1. **Sunita Kumari**, Sonu, Amit K. Tiwari and Subit K. Saha. "Study on Intramolecular Charge Transfer Processes, Solvation Dynamics and Rotational Relaxation of Coumarin 490 in Reverse Micelles of Cationic Gemini Surfactant" National Conference on Nano and Functional Materials (NFM-2014), held at Department of Chemistry, BITS Pilani, Pilani Campus. November 7-8, 2014. (**Poster**)

2. **Sunita Kumari**, Sonu, G. Sundar and Subit K. Saha, "Solvation Dynamics and Rotational Relaxation of Coumarin 480 in Aqueous Micelles: Effect of Polar Spacer Group and Hydrophobic Tails of Cationic Gemini Surfactants" in National Conference on Frontiers at the Chemistry- Allied Sciences Interface (FCASI-2015), held at University of Rajasthan, Jaipur. March 13-14, 2015.

3. **Sunita Kumari**, Sonu, G. Sundar and Subit K. Saha, "Aggregation Behavior of Hexadecyltrimethylammonium Surfactants with Various Counterions: A Solvation Dynamics and Rotational Relaxation Study" in National Conference on Recent Advancements in Chemical Sciences (RACIS-2015), held at Malaviya national institute of technology, Jaipur. August 21 - 23, 2015. (**Best Poster Award**)

4. **Sunita Kumari**, Sonu, G. Sundar and Subit K. Saha, "Effect of Counterions on Solvation Dynamics and Rotational Relaxation of Coumarin 480 in Aqueous Micelles of Hexadecyltrimethylammonium Surfactants" in International Conference on Nascent Developments in Chemical Sciences: Opportunities for Academia-Industry Collaboration (NDCS-2015), held at Department of Chemistry, BITS Pilani, Pilani Campus. October 16-18, 2015. **(Poster)**

5. **Sunita Kumari**, Sonu, G. Sundar and Subit K. Saha, "Aggregation Behavior of Hexadecyltrimethylammonium Surfactants with Various Counterions: Effect of Counterions on Solvation Dynamics and Rotational Relaxation Study" in National Conference on Organic Chemistry in Sustainable Development: Recent Advances and Future Challenges (OCSD-2016), held at Department of Chemistry, BITS Pilani, Pilani Campus. August 29-30, 2016. **(Poster)**

6. **Sunita Kumari**, G. Sundar and Subit K. Saha , "Interaction of Cationic Gemini Surfactants with Nanotubes of β-Cyclodextrin: Effect of Spacer Chain Length of Gemini Surfactants" in National Conference on New Frontiers in Chemistry from Fundamentals to Applications II (NFCFA-2017), held at Department of Chemistry, BITS Pilani, KK Birla Goa Campus. January 28-29, 2017. **(Poster)**

7. **Sunita Kumari**, G. Sundar and Subit K. Saha, "Study on Interaction of Cationic Gemini Surfactants with Guest Induced Nanotubes of β-Cyclodextrin and the Role of Spacer Chain Length of Gemini Surfactants to Release the Guest" in National Conference on Advanced Physical Methods in Chemical Sciences (NCAPMCS-2017), held at Department of Chemistry, Guru Jambheshwar University of Science and Technology, Hisar, Haryana. February 22-23, 2017. **(Poster)**

8. **Sunita Kumari**, Sonu, G. Sundar and Subit K. Saha, "Effect of Organic and a Hofmeister Series of Inorganic Counterions on the Solvation Dynamics and Rotational Relaxation in Aqueous Micelles of Hexadecyltrimethylammonium Surfactants" in North West Meeting on Spectroscopy, Structure and Dynamics (SSD-2017), held at Department of Chemistry, BITS Pilani, Pilani Campus. March 18-19, 2017. **(Poster)**

9. **Sunita Kumari**, Rishika Aggrawal, Sonu, Sayantan Halder, G. Sundar and Subit K. Saha, "Effect of Hydrophobicity of Tails and Hydrophilicity of Spacer Group of Cationic Gemini Surfactants on Solvation Dynamics and Rotational Relaxation of Coumarin 480 in Aqueous Micelles" in International conference on Frontiers at the Chemistry- Allied Sciences Interface (FCASI-2017), held at University of Rajasthan, Jaipur. July 22-23, 2017. **(Oral)**

Brief Biography of Candidate [A-3]

Ms. Sunita Kumari

Research Scholar

Department of Chemistry

BITS-Pilani, Pilani Campus

Pilani, Rajasthan-333031, India

Ms. S. Kumari obtained her B.Sc. degree (B.Sc. Chemistry) in 2009, M.Sc. degree (M.Sc. Organic Chemistry) in 2011, and B.Ed. degree (Science) in 2012 from the University of Rajasthan, Jaipur, Rajasthan, India. She joined the Department of Chemistry, Birla Institute of Technology & Science (BITS) Pilani, Pilani Campus, Pilani, Rajasthan in 2013, to pursue her Doctorate with the Prof. Subit Kumar Saha (Supervisor) and Prof. G. Sundar (Co-supervisor). To the Date, she has published ten papers in peer-reviewed international journals and has presented nine papers in various international/national conferences. She qualified Graduate Aptitude Test in Engineering (GATE) twice in GATE-2013, and GATE-2014 conducted jointly by the Indian Institute of Science (IISc) and Indian Institute of Technologies (IITs) on the behalf of the National Co-ordination Board-GATE, Department of Higher Education, MHRD, Govt. of India.

Brief Biography of the Supervisor [A-4]

Prof. Subit Kumar Saha

Professor

Department of Chemistry

BITS-Pilani, Pilani Campus

Pilani, Rajasthan-333031, India

Prof. S. K. Saha attained his B.Sc. degree (B.Sc., Chemistry Honours) in 1988 and M.Sc. degree (M.Sc., Specialization in Physical Chemistry) in 1990 from University of Kalyani, Kalyani, West Bengal. He obtained his Ph.D. in the year 1998 from IIT Kanpur. His title of thesis is "Spectroscopic study of new molecular probes for micelles using steady-state and nanosecond fluorescence spectroscopy". Later, he worked as a CSIR Research Associate till November 1999 in IIT Kanpur. He joined Department of Chemistry, BITS, Pilani in December, 1999 as Lecturer. He became Assistant Professor in December, 2003 and Associate Professor in August 2010. Currently, he is working as Professor in the same institute. His research interests are in the areas of characterization of ICT/TICT fluorescent probes and their application in the characterization of micelles, mixed micelles, reverse micelles, proteins, DNA, cyclodextrins and their supramolecular structures, synthesis and study of thermodynamics and aggregation behaviour of different Gemini surfactants etc. He successfully completed major research projects financially supported by CSIR, Aditya Birla Groups and UGC. Two major research projects supported by the UGC-DAE Consortium for Scientific Research, Mumbai Centre and CSIR, New Delhi are going on in his laboratory. As a result of his research accomplishment, he has published number of research articles in various national and international journals. He has acted as an Associate Editor of "Global Journal of Physical Chemistry". He is also a co-author of a book 'Thermodynamics – A Core Course'. He is a reviewer of a number of reputed national and international journals. Currently, Prof. Saha is guiding three Ph.D. students.

Email Id: *sksaha@pilani.bits-pilani.ac.in*

Brief Biography of the Co-Supervisor [A-5]

Prof. G. Sundar
Senior Professor & Director
BITS-Pilani, Hyderabad Campus
Hyderabad, Telangana-500078, India

Prof. G. Sundar did his M.Sc. in Chemistry from IIT Kanpur (1977-79), and Ph.D. (Chemistry) from Cornell University in 1987. He joined the Department of Chemistry at BITS Pilani in 1987, was designated Professor in 2000, and is now Senior Professor. Prof. G. Sundar has been with BITS Pilani for close to three decades. Prof. Sundar has held various positions at BITS over the years, all of which he has served with distinction, and left a mark with. He has been Group Leader; Dean, Student Welfare Division; Chief Warden; Dean, Practice School; Deputy Director, Off-campus Programmes and Director, Off-campus Programmes and Industry Engagement. Prof. G. Sundar currently serving as Director, BITS Pilani, Hyderabad Campus since July 2016. His academic interests are in Thermodynamics, Statistical Mechanics, Quantum Chemistry and Chemical Instrumentation, and he is well respected as a teacher by students and faculty colleagues. His tenure as Chief Warden and Dean Student welfare has given him a deep understanding of student motivations and aspirations. In 2013, he led a programme to improve and transform our Work Integrated Learning Programme (WILP), and the programme is being implemented with excellence.

Email Id: *sundar@hyderabad.bits-pilani.ac.in*